
Hydrogen and Halogen Bonding as Enabling Concepts for the Synthesis of Unprecedented Halogen Compounds and a More Sustainable Chlorine Technology

Inaugural-Dissertation
to obtain the academic degree
Doctor rerum naturalium (Dr. rer. nat.)

submitted to the
Department of Biology, Chemistry, Pharmacy
of Freie Universität Berlin

by

Patrick Voßnacker

2023

The work for the present dissertation has been conducted between July 2018 and August 2023 under the guidance of Prof. Dr. Sebastian Hasenstab-Riedel at the Institute of Chemistry and Biochemistry (Department of Biology, Chemistry, Pharmacy) of Freie Universität Berlin.

Herewith I certify that I have prepared and written my thesis independently and that I have not used any sources and aids other than those indicated by me. All intellectual property of other authors used as references has been marked accordingly. I also certify that I have not applied for an examination procedure at any other institution and that this dissertation has not been submitted in this or any other form to another faculty.

Berlin, 08.01.2024

Patrick Voßnacker

1 st referee:	Prof. Dr. Sebastian Hasenstab-Riedel
2 nd referee:	Prof. Dr. Christian Müller
Day of Disputation:	08.12.2023

*„Ideen an und für sich haben nur einen sehr geringen Wert.
Der Wert einer Erfindung liegt in ihrer praktischen Durchführung.“*

- Werner von Siemens

Acknowledgements

First, I want to express my sincere gratitude to my doctoral advisor Prof. Dr. Sebastian Hasenstab-Riedel for the possibility to work in his research group, for convincing me to work on the very interesting topic of polychloride chemistry and for motivating me to finish my projects.

I also want to thank Prof. Dr. Christian Müller for accepting the position as second referee.

I would like to thank all my cooperation partners for their help with my projects: Prof. Dr. Konrad Seppelt and Dr. Moritz Malischewski for their help with the structural characterization of novel polychloride compounds, Dr. Yuliya Schiesser, Dr. Sivathmeehan Yogendra, Dr. Rainer Weber from Covestro for introducing me into industrial chemistry and Dr. Marc Reimann, Dr. Robert Müller, Dr. Martin Kaupp for their quantum-chemical support.

I want to thank Dr. Merlin Kleoff for helping me out with writing my publications and all the scientific and philosophical discussions we had over the last eleven years. Even though we don't always agree and sometimes have different perspectives on life I think we always have been a great team when it comes to solving problems.

I like to thank all my students Alisa, Thomas, Haralds, Helen, Sophie, Fabio, André, Friedrich for their excellent work and their motivation. I also want to thank Gesa and Merlin for proof-reading this thesis.

A big thanks goes to the whole AG Riedel with all their former and current members. I always had a great time with you since the first time I joined the group more than eight years ago. I will always remember all the workgroup trips, the BBQs and the Feierabendbiere. A special thanks goes to my lab mates Tyler, Benny, Jonas. We always had a great time working together. During my time at the university, I made many friends who helped me a lot during my time as a doctoral candidate. Many thanks to Karsten, Benny, Jan, Gene, Freddy, Marlon, Tyler, Paul, Maite, Gesa, Luise, Thomas, Jonas, Lili and Niklas.

Finally, I would like to thank my family and friends who have supported me throughout my entire time at the university.

List of Abbreviations

3c-4e	Three-center-four-electron
Alk	Alkyl
B3LYP	Becke, three-parameter, Lee-Yang-Parr
BASIL	Biphasic acid scavenging utilizing ionic liquids
BOVB	Breathing-orbital valance bond
btmgn	1,8-bis(tetramethylguanidinylnaphthalene
Bu	Butyl
[C₄MPyr]⁺	<i>N</i> -butyl- <i>N</i> -methyl-pyrrolidinium
[C₁₀MPyr]⁺	<i>N</i> -decyl- <i>N</i> -methyl-pyrrolidinium
Cat	Cation
CC BY-SA 4.0	Creative common share alike 4.0
CCDC	Cambridge crystallographic data center
CCSD(T)	Coupled cluster with single, double and perturbative triple excitations
CD	Compact disc
D3	Dispersion correction (Grimme)
DBPs	Disinfectant by-products
DBU	1,8-Diazobicyclo[5.4.0]undec-7-en
DDT	Dichloro-diphenyl-trichloroethane
DVD	Digital video/versatile disc
Et	Ethyl
EU	European Union
HOMO	Highest occupied molecular orbital
IL	Ionic liquid
IRS	Indore residual spraying
LC	Lethal concentration
LED	Light-emitting diode
Me	Methyl
MO	Molecular orbital
NMR	Nuclear magnetic resonance
NPA	Natural population analysis

NPSP	<i>N</i> -(phenylseleno)phtalimide
NXS	<i>N</i> -Chloro/Bromo/Iodosuccinimide
ODC	Oxygen depolarized cathode
[OTf]⁻	Trifluoromethanesulfonate
[P_{444,10}]⁺	Tributyl-decylphosphonium
[P_{444,14}]⁺	Tributyl-tetradecylphosphonium
[P_{666,14}]⁺	Trihexyl-tetradecylphosphonium
PC	Polycarbonate
PCDDs	Polychlorinated dibenzo- <i>p</i> -dioxins
PCDFs	Polychlorinated dibenzofurans
Ph	Phenyl
POP	Persistent organic pollutants
[PNP]⁺	Bis(triphenylphosphine)iminium
Pr	Propyl
PTFE	Polytetrafluorethylene
PU	Polyurethane
PVC	Polyvinyl chloride
RI	Resolution of identity
RTIL	Room-temperature ionic liquid
SCS-MP2	Spin-component scaled second-order Møller-Plesset perturbation
SI	Supporting information
TFE	Tetrafluoroethylene
TMS	Trimethylsilyl
[Tf₂N]⁻	Bis(trifluoromethanesulfonyl)azanide
ttmgn	1,2,4,5-tetrakis(tetramethylguanidinylnaphthalene
VB	Valance bond
WHO	World Health Organization
XRD	X-ray diffraction
X, Y	Halogen atoms

Abstract

In this work, novel poly(hydrogen halide) halogenates ($-I$) and polychlorides have been prepared while also new applications for polychlorides have been investigated. The reaction of $[Cat]X$ ($Cat = PPh_4, PNP; X = Cl, Br, I$) with HF and HCl yielded in the formation of various novel $[Cat][X(HCl)_n]$ and $[Cat][X(HX)(HF)_2]$ salts. A thorough characterization by X-ray diffraction, Raman spectroscopy and quantum-chemical calculations resulted in a better understanding of the hydrogen bonding within poly(hydrogen halide) halogenates. Furthermore, the $[Cl(Cl_2)_4]^-$ and $[Cl_2]^{2-}$ anion have been prepared for the first time by the reaction of Cl_2 with $[NPr_4]Cl$ and decamethylferrocene, respectively. Structural characterization by X-ray diffraction revealed a distorted tetrahedral structure for the $[Cl(Cl_2)_4]^-$ anion while the structure of the $[Cl_2]^{2-}$ is best described as two pyramidal $[Cl(Cl_2)_4]^-$ units which are connected by a Cl_2 molecule. Additionally, $[FeCp^*_2][Cl(Cl_2)_4(HF)]$, which is the first example of polychloride-HF network stabilized by strong hydrogen and halogen bonding, was obtained when traces of HF were present in the reaction mixture of $[FeCp^*_2]$ and Cl_2 .

A series of ammonium chloride salts have been tested towards their capability to act as a chlorine storage medium. $[NEt_3Me]Cl$ was chosen to be the most promising candidate since it has a high storage capacity of 0.79 kg Cl_2 / kg storage material and is readily prepared from the abundant starting materials MeCl and NEt_3 while the loaded storage is stable for extended times. A release of chlorine from the storage material can be achieved by heating, applying vacuum or by the addition of water. However, as polychlorides were already shown to be efficient chlorination reagents, a combined process was envisioned in which the loaded storage is directly used for chlorination. To further develop this approach, $[NEt_3Me][Cl_3]$ was used for the synthesis of industrial important chemicals. For instance, Phosgene, which is an important intermediate chemical, is obtained by the reaction of $[NEt_3Me][Cl_3]$ with CO without activation by heat or light. Additionally, also catalytic amounts of $[NEt_3Me]Cl$ result in a full conversion of Cl_2 and CO to $COCl_2$. Quantum-chemical calculations revealed that this reaction can be understood as an insertion of CO into the weakened Cl-Cl bond of a $[Cl_3]^-$ anion which proceeds with an activation barrier of only 56.9 to 77.6 kJ mol $^{-1}$.

The reaction of $[NEt_3Me][Cl_3]$ with elemental sulfur yielded in the formation of the unknown $[SCl_6]^{2-}$ dianion. It has an octahedral structure in the solid state while co-crystallization of

CH_2Cl_2 results in a distortion yielding a C_{4v} symmetric structure for the $[\text{SCl}_6]^{2-}$ anion. Quantum-chemical calculations showed that the lone pair at the sulfur atom is stereochemically inactive for both structures and the distortion is a result of strong hydrogen bonding interactions to the CH_2Cl_2 molecules. Furthermore, Raman spectroscopic investigations showed that $[\text{NEt}_3\text{Me}]_2[\text{SCl}_6]$ decomposes above $40\text{ }^\circ\text{C}$ into $[\text{NEt}_3\text{Me}][\text{Cl}_3]$ and various sulfur chlorine compounds making it significantly more stable than SCl_4 which already decomposes at $-30\text{ }^\circ\text{C}$.

Kurzzusammenfassung

In dieser Arbeit wurden neuartige Poly(halogenwasserstoff)halogenate ($-I$) und Polychloride hergestellt und gleichzeitig neue Anwendungen für Polychloride untersucht. Die Reaktion von $[Kat]X$ ($Kat = PPh_4, PNP; X = Cl, Br, I$) mit HF bzw. HCl führte zur Bildung verschiedener neuer $[Kat][X(HCl)_n]$ und $[Kat][X(HX)(HF)_2]$ Salze. Eine gründliche Charakterisierung durch Röntgenbeugung, Raman-Spektroskopie und quantenchemische Berechnungen führte zu einem besseren Verständnis der Wasserstoffbrückenbindungen in Poly(halogenwasserstoff)halogenaten ($-I$). Darüber hinaus wurden die Anionen $[Cl(Cl_2)_4]^-$ und $[Cl_{20}]^{2-}$ erstmalig durch die Reaktion von Cl_2 mit $[NPr_4]Cl$ bzw. Decamethylferrocen hergestellt. Die strukturelle Charakterisierung durch Röntgenbeugung ergab eine verzerrte tetraedrische Struktur für das $[Cl(Cl_2)_4]^-$ Anion, während die Struktur von $[Cl_{20}]^{2-}$ am besten als zwei pyramidale $[Cl(Cl_2)_4]^-$ -Einheiten beschrieben werden kann, die durch ein Cl_2 -Molekül verbunden sind. Darüber hinaus wurde $[FeCp^*_2][Cl(Cl_2)_4(HF)]$, welches das erste Beispiel für ein Polychlorid-HF-Netzwerk, das durch starke Wasserstoff- und Halogenbindungen stabilisiert ist, erhalten, wenn Spuren von HF in der Reaktionsmischung von $[FeCp^*_2]$ und Cl_2 vorhanden waren.

Eine Reihe von Ammoniumchloridsalzen wurde auf ihre Eignung als Chlorspeichermedium getestet. $[NEt_3Me]Cl$ wurde als der vielversprechendste Kandidat ausgewählt, da es eine hohe Speicherkapazität von 0,79 kg Cl_2 / kg Speichermaterial aufweist und leicht aus den verfügbaren Ausgangsstoffen $MeCl$ und NEt_3 hergestellt werden kann, während der beladene Speicher für längere Zeit stabil ist. Eine Freisetzung von Chlor aus dem Speichermaterial kann durch Erhitzen, Anlegen von Vakuum oder durch Zugabe von Wasser erreicht werden. Da sich Polychloride jedoch bereits als effiziente Chlorierungsreagenzien erwiesen haben, wurde ein kombinierter Prozess ins Auge gefasst, bei dem der beladene Speicher direkt zur Chlorierung verwendet wird. Um diesen Ansatz weiterzuentwickeln, wurde $[NEt_3Me][Cl_3]$ für die Synthese von industriell wichtigen Chemikalien verwendet. So wurde beispielsweise Phosgen, ein wichtiges chemisches Zwischenprodukt, durch die Reaktion von $[NEt_3Me][Cl_3]$ mit CO ohne Aktivierung durch Wärme oder Licht gewonnen. Außerdem führen auch katalytische Mengen von $[NEt_3Me]Cl$ zu einer vollständigen Umwandlung von Cl_2 und CO zu $COCl_2$. Quantenchemische Berechnungen ergaben, dass diese Reaktion als eine Insertion

von CO in die geschwächte Cl-Cl-Bindung eines $[\text{Cl}_3]^-$ Anions verstanden werden kann, die mit einer Aktivierungsbarriere von lediglich 56,9 bis 77,6 kJ mol⁻¹ abläuft.

Die Reaktion von $[\text{NEt}_3\text{Me}][\text{Cl}_3]$ mit elementarem Schwefel führte zur Bildung des unbekanntes $[\text{SCl}_6]^{2-}$ Dianions. Im festen Zustand weist es eine oktaedrische Struktur auf, während die Co-Kristallisation von CH_2Cl_2 zu einer Verzerrung führt, die dem $[\text{SCl}_6]^{2-}$ Dianion eine C_{4v} -symmetrische Struktur verleiht. Quantenchemische Berechnungen ergaben, dass das freie Elektronenpaar am Schwefelatom für beide Strukturen stereochemisch inaktiv ist und die Verzerrung das Ergebnis starker Wasserstoffbrückenbindungen zu den Co-kristallisierten CH_2Cl_2 Molekülen ist. Darüber hinaus zeigten Raman-spektroskopische Untersuchungen, dass sich $[\text{NEt}_3\text{Me}]_2[\text{SCl}_6]$ oberhalb von 40 °C in $[\text{NEt}_3\text{Me}][\text{Cl}_3]$ und verschiedene Schwefel-Chlor-Verbindungen zersetzt und damit wesentlich stabiler ist als SCl_4 , das sich bereits bei -30 °C zersetzt.

Table of Content

1. Introduction.....	1
1.1 Chlorine	1
1.1.1 Properties and Danger of Chlorine	1
1.1.2 Uses of Chlorine	3
1.1.3 Industrial Production of Chlorine	7
1.1.4 Achievements and Responsibilities of the Chlorine Industry.....	12
1.2 Polyhalides	16
1.2.1 Bonding Situation of Polyhalides	16
1.2.2 Polyfluorides	19
1.2.3 Polychlorides	20
1.2.4 Polybromides.....	26
1.2.5 Applications of Polyhalides	30
1.3 Poly(hydrogen halide) Halogenates (-I)	38
1.3.1 Synthesis and Structural Characterization of $[X(HX)_n]^-$ Anion.....	38
1.3.2 Applications of Poly(hydrogen halide) Halogenates (-I)	41
2. Objective	44
3. Publications	45
3.1 Synthesis and Characterization of Poly(hydrogen halide) Halogenates (-I).....	45
3.2 From Missing Links to New Records: A Series of Novel Polychlorine Anions	54
3.3 Alkyl Ammonium Chloride Salts for Efficient Chlorine Storage at Ambient Conditions	62
3.4 Novel Synthetic Pathway for the Production of Phosgene	70
3.5 Synthesis of a Hexachloro Sulfate(IV) Dianion Enabled by Polychloride Chemistry	78
3.6 The Rise of Trichlorides Enabling an Improved Chlorine Technology	84
4. Conclusion and Outlook.....	94
4.1 Conclusion.....	94
4.2 Outlook	100
5. References.....	102
6. Publications, Patents and Conference Contributions.....	113
6.1. Publications	113
6.2. Patents	115
6.3. Conference Contributions – Oral and Poster Presentations.....	115
7. Curriculum Vitae.....	116
8. Appendix	117
8.1 SI of Synthesis and Characterization of Poly(hydrogen halide) Halogenates (-I).....	117

8.2 SI of From Missing Links to New Records: A Series of Novel Polychlorine Anions....	195
8.3 SI of Alkyl Ammonium Chloride Salts for Efficient Chlorine Storage at Ambient Conditions	271
8.4 SI of Novel Synthetic Pathway for the Production of Phosgene	310
8.5 SI of Synthesis of a Hexachloro Sulfate(IV) Dianion Enabled by Polychloride Chemistry	358

1. Introduction

Chlorine is produced on a scale of 96 million tons per year worldwide,^[1] making it one of the most important base chemicals. It is involved in the synthesis of approximately 50% of all industrial compounds, 20% of all small molecule drugs and 30% of all active compounds in agrochemistry. However, elemental chlorine is a highly reactive and toxic gas which can oxidize many materials and causes severe damage to the skin, eyes and the respiratory system.^[2] Furthermore, chlorine is primarily produced by the highly energy demanding chloralkali process. For instance, 12 million MWh of electrical power are used for chlorine production in Germany corresponding to ~2.5% of its total electrical energy consumption.^[3-5] Due to its high toxicity, reactivity and vapor pressure, chlorine cannot be easily stored in large amounts. Therefore, in Europe 95.7% of the produced chlorine is used in follow-up reactions directly at the production sites.^[4]

Polyhalides were already shown to be suitable replacements for elemental halogens being safer and significantly easier to handle. Accordingly, their potential application in important industrial processes is of interest for today's research.

1.1 Chlorine

1.1.1 Properties and Danger of Chlorine

At ambient conditions elemental chlorine is a yellowish gas with a boiling point of $-34\text{ }^{\circ}\text{C}$ and a melting point of $-101\text{ }^{\circ}\text{C}$. It has a vapor pressure of 7.7 bar and a liquid density of 1.38 g cm^{-3} at $25\text{ }^{\circ}\text{C}$. As a gas it has a 2.48 times higher density compared to air and persists to the ground, which, combined with its toxicity, resulted in its use as a war gas in the World War I.^[2] Chlorine has the highest dissociation energy of 239 kJ mol^{-1} among the halogens which is still significantly lower than that of other element chlorine bonds like, e.g., C-Cl ($267\text{-}436\text{ kJ mol}^{-1}$), Si-Cl (464 kJ mol^{-1} in SiCl_4) and H-Cl (431 kJ mol^{-1}).^[6] Additionally, it has the highest electron affinity ($364.25\text{ kJ mol}^{-1}$) among all elements as well as a standard electrode potential of 1.36 V explaining the high reactivity and oxidation power of elemental chlorine. An overview of some physical properties of chlorine is given in Table 1.

Table 1. Overview of some properties of elemental chlorine^[2]

Property	Value
Boiling point	-34 °C
Melting point	-101 °C
Vapor pressure at 25 °C	7.7 bar
Liquid density at 25 °C	1.38 g cm ⁻³
Density (gas) relative to air	2.48 g cm ⁻³
Enthalpy of dissociation	239.44 kJ mol ⁻¹
Electron affinity	364.25 kJ mol ⁻¹
Standard electrode potential	1.359 V
LC ₅₀	300-400 ppm · 30 min

The toxicity of chlorine is mostly caused by its strong oxidation power. Additionally, it is converted into hypochlorous acid under physiological conditions, which is a cytotoxic substance. At low concentrations of 1-2 ppm, chlorine irritates the eyes and respiratory tract while for expositor concentrations above 30 ppm nausea, vomiting, oppressive feeling, shortness of breath, fits of coughing and sometimes bronchial spasms are classical symptoms. The LC₅₀ value of chlorine is estimated to 300-400 ppm in 30 min.^[2,7] Apart from the toxicity of chlorine, many downstream products of the chlorine industry degrade slowly and are harmful to humans and the environment (see 1.1.4).^[8,9]

1.1.2 Uses of Chlorine

Even though chlorine is a highly toxic chemical it found numerous industrial applications making our modern life hardly possible without it. Roughly 50% of all industrial chemicals and polymers, 20% of small molecule pharmaceuticals and 30% of agrochemicals depend on chlorine chemistry.^[10] An overview of the various applications and their share of European chlorine consumption is given in Figure 1.

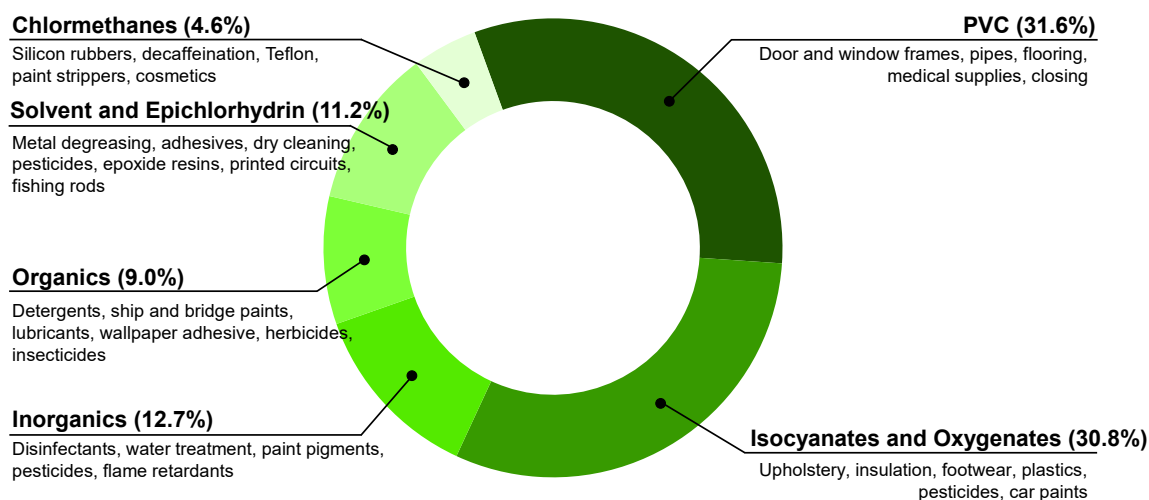
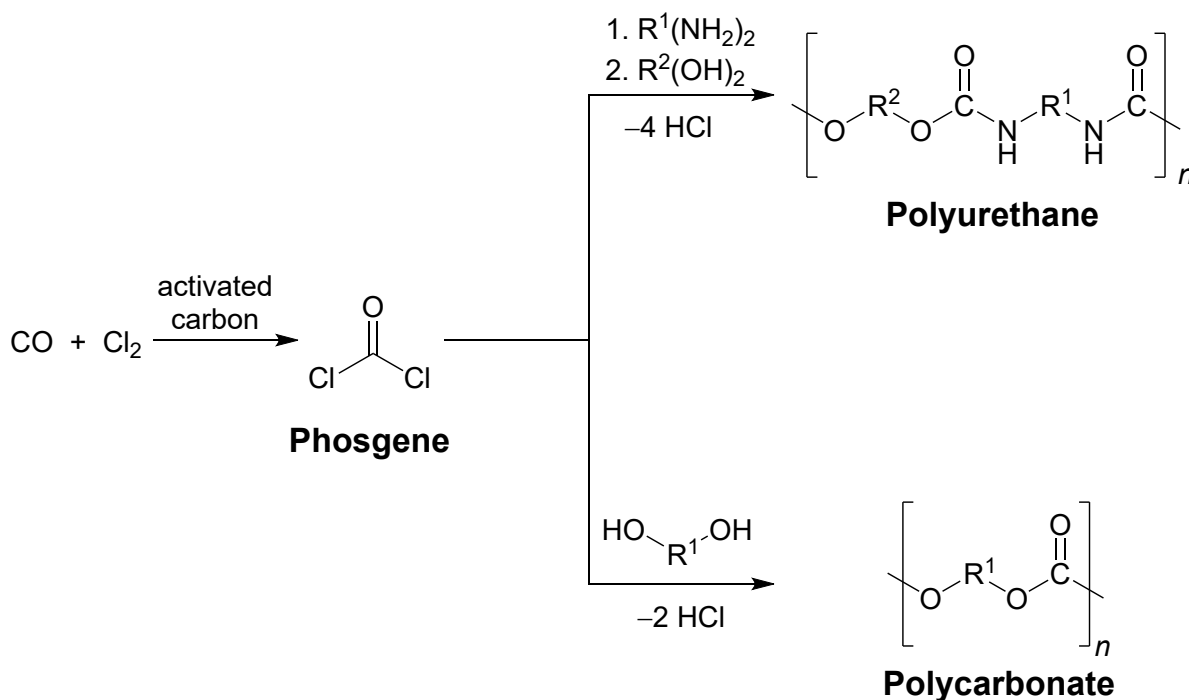


Figure 1. Uses of chlorine and their share of the European chlorine consumption.^[4,11] Reproduced from Ref. 11 with permission from the Royal Society of Chemistry.

One of the oldest applications for elemental chlorine is its utilization for the disinfection of drinking water which can be achieved either by the direct use of elemental chlorine or by using chlorine derivatives like calcium hypochlorite, chlorine dioxide or chloramines.^[12,13] This possible usage of elemental chlorine was already described in 1910 by Darnall and is commonly used today.^[12,14] For instance, in 2007, 61% of all municipal water systems in the United States were disinfected with elemental chlorine, while another 30% used chloramines.^[15] When water is treated with chlorine, hypochlorous acid is formed which rapidly destroys bacteria as well as other micro-organisms also preventing the growth of algae and slime in pipes.^[12]

Most of the time, chlorine is further processed to yield valuable intermediate chemicals. While in some cases the end product still contains chlorine atoms, roughly one-third of all products manufactured by the chlorine industry, are free of chlorine. The most prominent examples for this class of compounds are polyurethanes (PU) and polycarbonates (PC) accounting for 30.8%

of the European chlorine consumption.^[11] Both polymers are made using phosgene as an intermediate which is prepared by the reaction of chlorine with carbon monoxide over an activated carbon catalyst on a scale of 12 million tons per year.^[16] During the synthesis of polyurethanes, phosgene reacts at first with diamines to yield diisocyanates which react further with diols to give the polymer, while in the production of polycarbonates phosgene is directly reacted with a diol (Scheme 1).^[17,18]



Scheme 1. Synthesis of polyurethanes and polycarbonates using phosgene.

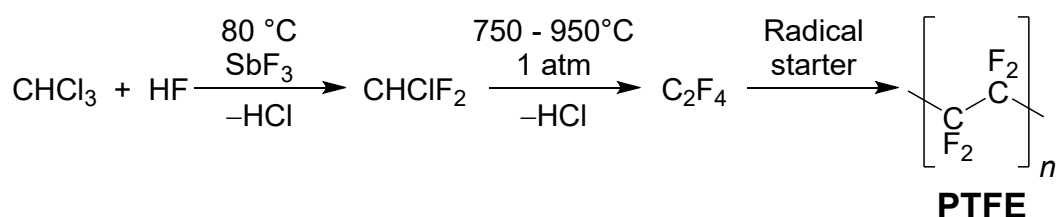
Polycarbonates have outstanding electrical insulation properties, e.g., good flame retardance, high heat resistance, good fracture toughness, and are transparent. Therefore, they are used in electronics, as in housings of mobile devices or in optics for LEDs, for data storage media like CDs, DVDs and Blu-rays, in building and construction for window panes and roofing, as well as for protection equipment like protection glasses or helmet visors.^[18] On the other hand polyurethanes are highly diverse in their properties depending on the monomers and additives used as well as their processing. They are mostly used as foams in mattresses, sponges as well as in upholstery of furniture and car seats, as fibers in swimsuits and cycling uniforms and as two-component reactive adhesives.^[17]

Poly vinyl chloride (PVC) was produced in a quantity of 37.5 million tons in 2012 making it the most important product of the chlorine industry as well as the third most used plastic in the EU after polyethylene and polypropylene.^[19,20] It is estimated that its production will

further increase to 58 million tons per year till 2027.^[21] PVC is produced by the polymerization of vinyl chloride which is obtained from 1,2-dichloroethane by the elimination of HCl at higher temperatures while dichloroethane is produced by the direct chlorination of ethylene.^[19] PVC has various applications, e.g., in pipes, window frames, cable insulation, flooring as well as medical equipment.^[19]

Chloromethanes are another major product of the chlorine industry and were produced on a scale of 6.7 million tons in 2017 consisting of 50% chloromethane, 25% dichloromethane, 22% chloroform and 3% tetrachloromethane.^[22] While the higher chlorinated chloromethanes are produced by radical chlorination of methane or chloromethane, chloromethane itself is nowadays usually prepared by the hydrochlorination of methanol using HCl.

The main application of chloromethane is its usage in the so-called Müller-Rochow process where it is reacted with silicon to yield dimethyldichlorosilane, a precursor for silicone production. Additionally, it is used as a methylating agent in the synthesis of cellulose ethers, which are wall paper adhesives, and for the synthesis of cationic polymers and ammonium salts.^[23] Dichloromethane and tetrachloromethane are mostly used as solvents in industry and laboratories while chloroform is the starting material for the production of PTFE. Chloroform can be fluorinated with HF and catalytic amounts of SbF₃ yielding CHClF₂ which is then pyrolyzed to give tetrafluoroethene (TFE), the monomer of PTFE. The polymerization of TFE is achieved by radical polymerization (Scheme 2)^[24]



Scheme 2. Synthesis of PTFE from chloroform.^[24]

Other chlorinated alkanes are produced in significantly smaller amounts and are mostly used as alkylation reagents and as solvents.^[25,26] However, some chlorinated alkenes possess industrial applications and are therefore produced in larger amounts. For instance, tetrachloroethene was produced by the chlorination of acetylene, ethylene, or C1-C3 hydrocarbons on a scale of 410 000 t in 2012 and is used for dry cleaning and metal degreasing.^[25] A total of 800 000 t of allyl chloride were prepared by radical chlorination of propene at 500 °C in 1997.^[12] Most of it is further processed to epichlorohydrin which is then

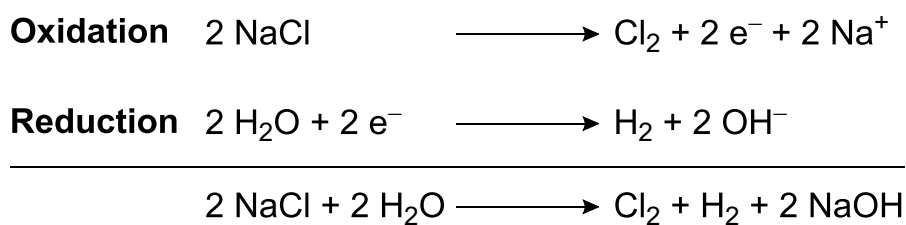
used to make epoxy resin.^[27] Chlorinated aromatic compounds are the last important class of organic substances produced by using chlorine. Monochlorobenzene is obtained by the Lewis acid catalyzed reaction of benzene with chlorine and was produced on a scale of 365 000 t in 1993. It is used as a solvent and as a precursor for other aromatic compounds like nitrochlorobenzene. In general, ring chlorinated aromatic compounds are important intermediates in the synthesis of dyes, pharmaceuticals and fungicides.^[12] Also, side chain chlorinated aromatic compounds are of interest with benzyl chloride, with a production of 320 000 t in 2015, being the most important one. It is prepared by radical chlorination initiated by heat or light and is used for the production of benzyl alcohol, benzyl butyl phthalate (a plasticizer in PVC), phenylacetic acid (for penicillin synthesis), as well as quaternary ammonium salts.^[28]

There are also several inorganic chlorine compounds which are produced by using chlorine. Phosphorous trichloride is produced by the combustion of white phosphorous in a chlorine stream on a scale of 350 000 t per year.^[29] It is further processed to phosphorous pentachloride and phosphor oxychloride. Phosphorous chloride compounds are important intermediates in the synthesis of pesticides, and flame retardants, as well as in the pharmaceutical industry for the production of antibiotics.^[29,30]

Additionally, titanium tetrachloride plays a major role in the purification of titanium dioxide, which is the most important inorganic pigment with a production of 5 million tons per year, as well as in the production of titanium sponge.^[31-33] Crude titanium dioxide is reacted with carbon and chlorine yielding titanium tetrachloride, which can be purified by distillation, and carbon dioxide. The titanium tetrachloride can then either be burned with oxygen to give highly pure titanium dioxide or reduced with magnesium to give titanium sponge (Kroll process).^[32,33]

1.1.3 Industrial Production of Chlorine

Chlorine was first synthesized by C. W. Scheele in 1774 by chemical oxidation of hydrochloric acid with manganese dioxide.^[34] Based on this outcome, Weldon developed a first process for chlorine production which had a low yield of only 35%. Therefore, in 1868, Deacon developed and patented a new method based on the oxidation of gaseous HCl using atmospheric oxygen and a CuCl₂ catalyst resulting in an increased yield of 65%.^[12,35] Since the end of the 19th century the chloralkali process has become the most important method for the industrial chlorine production accounting for more than 95% of the annual produced chlorine to date.^[12] During the chloralkali process an aqueous sodium chloride solution is electrolyzed resulting in the oxidation of chloride ions to chlorine as well as the reduction of water to hydrogen and hydroxide ions (Scheme 3).



Scheme 3. General reaction scheme of the chloralkali process.

To avoid the reaction of the Cl₂, formed at the anode, with hydrogen or hydroxide, formed at the cathode, the two electrodes must be separated. This was achieved in different ways by the development of three processes namely the mercury cell process, the diaphragm cell process and the membrane cell process, which all have been used in the industrial production of chlorine.^[12]

In the mercury cell process the separation of Cl₂ from NaOH and H₂ is achieved by using a mercury cathode. During the electrolysis, chloride ions are oxidized to chlorine at the anode while at the mercury cathode sodium cations are reduced to elemental sodium. Thus, the formation of H₂ is suppressed because of the high overpotential of hydrogen at the mercury electrode and the significantly reduced standard potential for the Na⁺/Na redox couple due to the formation of sodium amalgam. The liquid amalgam is then removed from the electrolysis cell and transferred to the amalgam decomposer where it is reacted with water

at a graphite catalyst yielding highly pure sodium hydroxide, hydrogen and mercury which is pumped back into the electrolysis cell (Figure 2).^[12]

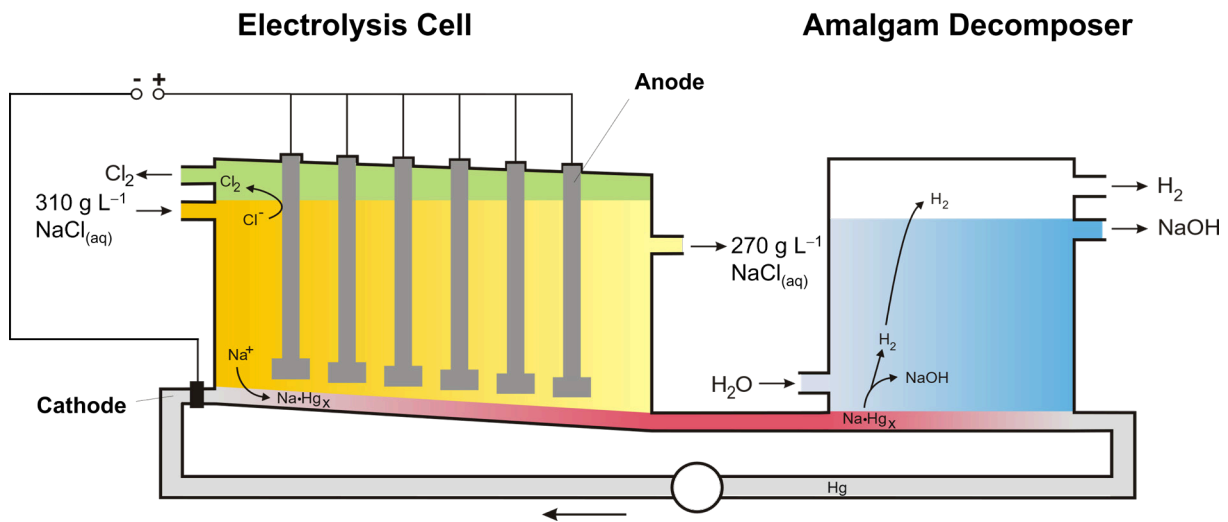


Figure 2. Schematic representation of the mercury cell process. Scheme was taken from reference [36] with data added from reference [12].

In contrast to the mercury cell process, during the diaphragm and membrane cell processes water is directly reduced to hydrogen and hydroxide at the cathode of the electrolysis cell. In a diaphragm cell there is a flow of a sodium chloride solution from the anode compartment through a permeable asbestos or PTFE diaphragm, which prevents the chlorine from passing into the cathode compartment, where hydrogen and hydroxide are produced (Figure 3). The resulting aqueous mixture of NaOH and NaCl is removed from the cathode compartment and is further processed by removal of excess water.^[12]

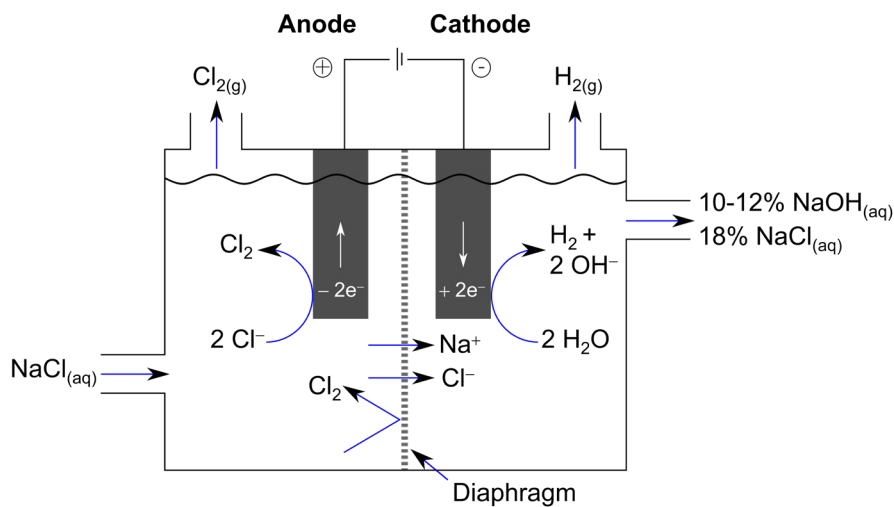


Figure 3. Schematic representation of diaphragm cell process. Scheme was taken and modified from reference [37] under CC BY-SA 4.0 with data added from reference [12].

The membrane process was developed 1970 and is based on the separation of anode and cathode compartments by a cation-exchange membrane which can only be passed by the sodium cations but not by chloride or hydroxide ions (Figure 4). Therefore, the anode compartment of the cell is fed with a stream of sodium chloride solution of which the chloride ions are oxidized to chlorine while the sodium ions pass the membrane into cathode compartment. On the other hand, the cathode compartment is fed with a 30% NaOH solution which is concentrated by the reduction of water to H_2 and OH^- .^[12]

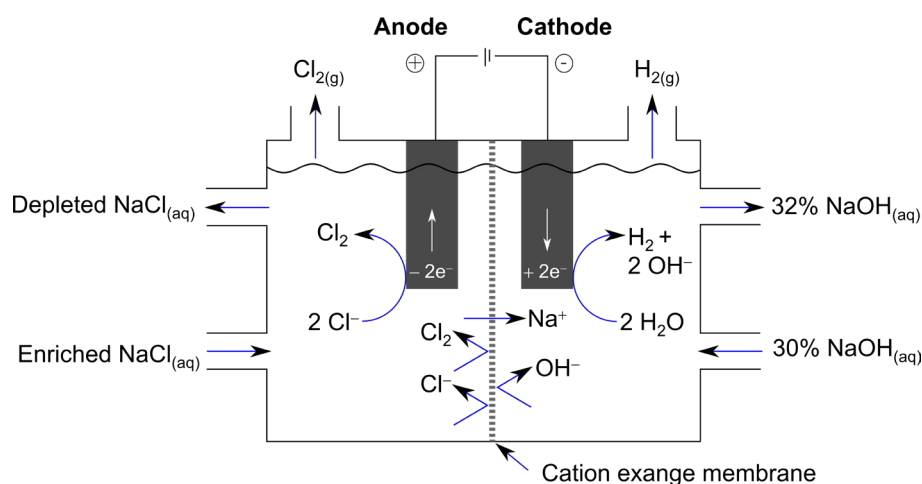
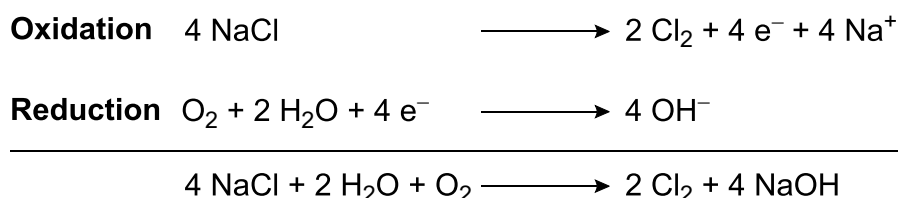


Figure 4. Schematic representation of mercury cell process. Scheme was taken and changed from reference [38] under CC BY-SA 4.0 with data added from reference [12].

All of the described methods have been used for the industrial production of chlorine and come along with advantages as well as disadvantages. The mercury cell process give rise to highly pure chlorine and hydrogen while also a chloride-free, highly concentrated NaOH solution can directly be obtained from the amalgam decomposer. On the other hand, it requires the highest amount of electrical energy for the electrolysis and requires costly environmental protection to minimize the release of mercury. Therefore, the mercury cell process is almost faced out today. For the diaphragm process, lower quality NaCl solutions can be used as a starting material while the obtained NaOH has to be concentrated and separated from NaCl using steam which result in an even higher total energy consumption compared to the mercury cell. The membrane cell process is the most state of the art having the lowest total energy consumption also yielding highly pure NaOH. However, the membranes are relatively costly and the obtained chlorine has a high oxygen content.^[12] Nowadays, all new build plants use membrane cells while the other production methods are slowly phased out with the membrane cell process already being responsible for 85% of the total production capacity in Europe^[4,11,12]

For all described electrochemical processes of chlorine production there is a physicochemical limit for the lowest amount of voltage needed for electrolysis which is given by the Nernst equation and the standard potentials of the Cl⁻/Cl₂ and H₂O/H₂ redox couples. Recently, a new process for chlorine production was developed in which instead of H₂O, O₂ is reduced to OH⁻ at an oxygen depolarized cathode (ODC, Scheme 4).^[39]



Scheme 4. Reaction scheme for the chlor-alkali process using an oxygen depolarized cathode (ODC).

The cell voltage of this system is 1 V lower compared to the conventional membrane cell process, saving 30% electrical energy. In contrast to the classical methods for the chloralkali process, no hydrogen is obtained when ODCs are used which is a valuable raw material for further chemical reactions. Additionally, pure oxygen is needed for this process which is obtained by the energy intensive air liquification method. Due to this two disadvantages the chloralkali electrolysis using ODCs is only economical under some conditions, for example if the hydrogen produced by the conventional chloralkali process is not required for chemical reactions or if the price of electrical energy is high.^[39,40] Nevertheless, the first large scale chlorine production plant using this technology was put into operation by Covestro at the start of 2023.^[41]

Even after more than a century of optimization, chlorine production is still a very energy-intensive process, with energy costs accounting for about 50% of production costs.^[11] To meet the demand of chlorine, needed for the production of many valuable compounds (see 1.1.2), a total of 260 million MWh of electrical power is needed to globally produce 96 million tons per year while a further increase of the production capacities to 123 million tons until 2029 is anticipated (Figure 5).^[1,4]

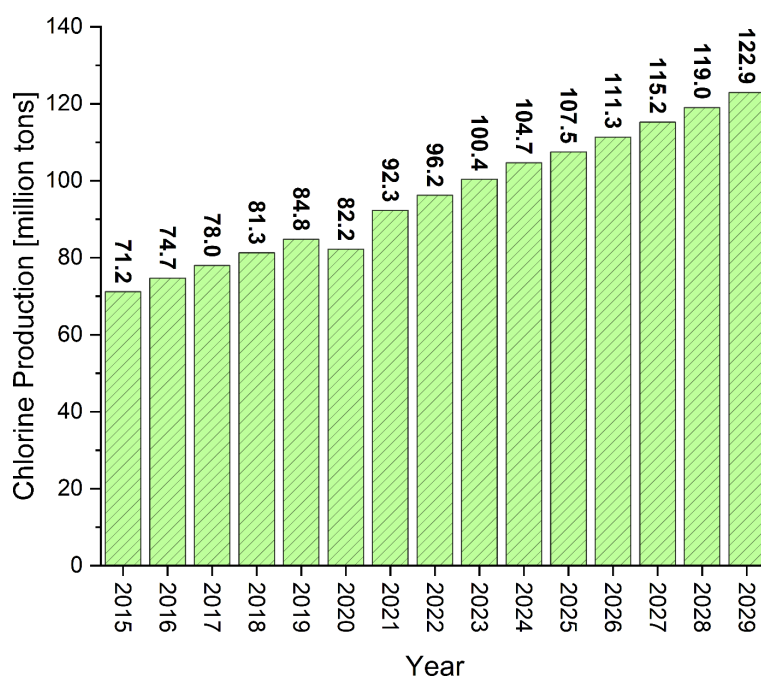


Figure 5. Market volume of chlorine worldwide from 2015 to 2029.^[1]

To put these numbers into perspective, in Germany, which has a chlorine production capacity of 5.4 million tons per year, the chlorine production is responsible for ~2.5 % of the total electrical energy consumption and therefore has a significant influence on the electrical grid.^[3-5] To reduce the environmental impact of chlorine production, it would be advantageous to rely on renewable energy sources which is however difficult due to their fluctuating power supply depending on the current weather circumstances. Even though the chloralkali electrolysis itself was shown to be relatively adaptable to electrical fluctuation, most of its downstream processes are not.^[42] Therefore, a flexible operation of the chloralkali electrolysis is only possible if there is a safe and efficient way of chlorine storage to provide a constant supply of chlorine for follow up processes.

Currently, chlorine is usually stored in its liquid form either by pressure liquefaction at 7 bar or by cooling below the boiling point of $-34\text{ }^{\circ}\text{C}$.^[12] This is, however, only done if unavoidable and with particularly high safety requirements, due to the danger of chlorine leakage when the storage systems fail.^[42] Hence, Euro Chlor, the association of chlor-alkali plant operators in Europe, concluded in their latest review on the chlor-alkali industry that: “[The adoption to renewable energies] requires more support solutions to maintain stability in the electrical grid to prevent black-outs. Chlor-alkali production units can partly contribute to this, but this capability is limited by [...] the limited ability to store chlorine”.^[4]

1.1.4 Achievements and Responsibilities of the Chlorine Industry

In the public perception, chlorine is often seen exclusively as a dangerous, toxic chemical and the products of the chlorine industry are often associated with environmental disasters such as the one in Seveso in 1976 where large amounts of the toxic 2,3,7,8-tetrachlordibenzo-*p*-dioxin (TCDD) have been released into the environment.^[43] This is somewhat understandable as many products of the chlorine industry do can be hazardous when handled without care. Additionally, some properties which make chlorinated compounds useful, for example the stability of chlorinated insecticides which allow a less frequent use of them, can lead to environmental problems, for instance due to their persistent nature. Therefore, there is a large responsibility by the chlorine industry to continuously evaluate their products and to minimize their environmental impact or to find suitable replacements when a safe utilization is impossible. On the other hand, chlorine, when used in a responsible manner, can have a great benefit to society. In this chapter, some examples for achievements of the chlorine industry as well as the responsible evaluation and the improvement of chlorinated products are given.

The availability of clean drinking water is of major importance for human health as there are many waterborne diseases which are transmitted by the consumption of contaminated water, e.g., cholera, typhoid fever as well as hepatitis A and E.^[44] Even today, a total of 1.2 billion people lack access to safe drinking water resulting in the death of 3.4 million people per year, most of them children, as reported by the World Health Organization (WHO).^[45] Therefore the *“ensure availability and sustainable management of water and sanitation for all”* is one of 17 sustainable development goals of the United Nations.^[46] Within the United States and Europe, water treatment by using chlorine was introduced at the start of the 20th century and since then cases of waterborne diseases have been drastically reduced in these countries.^[47] Today, chlorine or chlorinated compounds are used for water disinfection in most developed countries and the Life Magazine concluded that *“The filtration of drinking water plus the use of chlorine is probably the most significant public health advancement of the millennium.”*^[48] Nevertheless, there are concerns regarding disinfectant by-products (DBPs) like trihalomethanes or trichloroacetic acid which are potentially carcinogenic. Therefore, the concentration of these compounds is monitored and reduced by the combination

of chlorination with conventional water treatment methods like coagulation, sedimentation or filtration lowering the level of organic precursors and consequently the level of DBPs.^[44] Overall, the use of chlorine for water treatment has greatly benefited humanity and the gain by preventing the transmittance of waterborne diseases highly outweighs the risks from DBPs which was also acknowledged by the WHO.^[44,49]

An example which illustrates the responsibility of the chlorine industry, is the release of dioxins into the environment. This class of compounds include the toxic and carcinogenic polychlorinated dibenzo-*p*-dioxins (PCDDs) and dibenzofurans (PCDFs) which are persistent organic pollutants meaning they are poorly degradable in the environment and can accumulate in the food chain due to their lipophilicity (Figure 6).^[50]

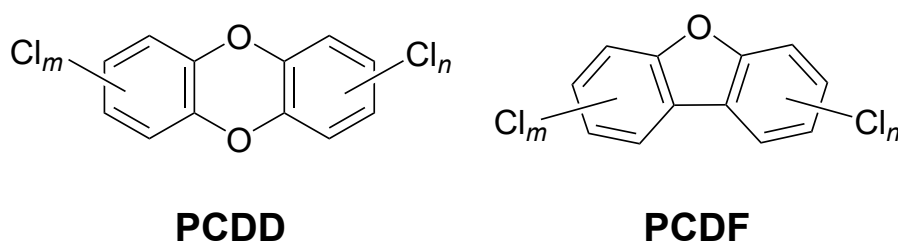


Figure 6. Structure of polychlorinated dibenzo-*p*-dioxins (PCDDs) and dibenzofurans (PCDFs) ($m + n = 1-8$).

Dioxins are formed as unintentional byproducts of chemical processes, for example chlorine-bleaching of wood pulp, in the synthesis of chlorinated phenols (fungicides), and during metal smelting, refining, and processing. However, the most important source of dioxins is the combustion of organic materials in the presence of chlorine sources like in municipal and medical waste incineration.^[12,51] Since 1985, the release of dioxins in Europe and the United States was drastically reduced by up to 90%.^[51,52] This was achieved by phasing out some processes for example the previous mentioned bleaching of wood pulp with chlorine or the use of leaded gasoline as well as by optimizing the waste burning process by including waste gas cleaning.^[12,51] This indicates that a combination of strict legal regulations with voluntary actions of industry can yield a significant reduction of risks associated with chemical industry.

The last example illustrating the ambivalence of some chlorinated products, is the insecticide dichloro-diphenyl-trichloroethane (DDT) which was first synthesized by Othmar Zeidler in 1874.^[53] It can easily be prepared by the condensation of chlorobenzene with chloral accessible from ethanol and chlorine.^[54] The insecticidal properties of this compound were discovered by Paul H. Müller in 1939 for which he was awarded with the Nobel Prize for medicine in

1948.^[12,55] Since then, DDT was heavily used in agricultural pest control as well as in fighting mosquito-borne diseases such as dengue fever and filariasis.^[54] In addition, using DDT for indoor residual spraying (IRS) was highly effective to fight malaria and for instance, reduced the cases of malaria in India by 99% from 100 million in 1933 to 150000 in 1966. This was a major factor for the increased life expectancy from 32 years in 1948, to 52 years in 1970.^[54] Furthermore until 1967, malaria was eradicated in developed countries as well as in many subtropical Asian and Latin American countries.^[56] Overall, it is estimated that the use of DDT saved approximately 5 million human lives and prevented 100 million illnesses in the first ten years after its introduction.^[57] However, the same factors which makes DDT an efficient insecticide, like its low vapor pressure, its lipophilicity as well as its stability towards photooxidation, lead to environmental problems. Like PCDDs and PCDFs, it was also shown for DDT, that it is persistent in nature and accumulates in the food chain leading.^[54] One of its most severe impacts was the eggshell thinning and population decline of several bird of prey species in North America and Europe.^[58] Consequently, DDT was banned for agricultural use in many countries starting in the 1970s ultimately leading to the Stockholm convention on persistent organic pollutants (POPs) which banned or restricted the use of DDT and eleven other POPs in 2004 and was signed by 152 countries.^[56,59] Despite all concerns regarding the environmental impact as well as the toxicity of DDT, in 2006 the WHO released a position paper in which they promote the application of DDT for malaria vector control as a low-cost insecticide which is why it is still used in 18 countries worldwide.^[60,61] This highlights the dilemma as DDT is highly efficient and can prevent the death of many people while there are rising concerns regarding the potential risk to human health.^[56,62] Ultimately, a complete abandonment of DDT can only be achieved through further research on new, safer insecticides or by the introduction of other effective measures for malaria control for example by vaccination, which is presumably reachable as a malaria vaccine with an efficiency of 75% was developed recently.^[63]

In conclusion, products of the chlorine industry have a great impact on the society for the last 150 years. While byproducts of the chlorine industry such as dioxins are harmful, the insecticide DDT has despite its disadvantages for the environment an enormous potency for malaria pest control. For the degemination of tap water with chlorine, the advantages significantly outweigh the disadvantages. However, the save storage of chlorine is still a major problem of the chlorine industry which has not been resolved so far. In recent years,

polyhalides were already shown to be efficient substitutes for elemental halogens raising the question of their storage properties. Additionally, further research on chlorine chemistry still offers the possibility to deal with central problems of humanity.

1.2 Polyhalides

The ability of halide ions to interact with halogen molecules to form polyhalides is already known since the discovery of strychnine triiodide by Pelletier and Caventou in 1819.^[64] Since then, the field of polyhalide chemistry has significantly advanced and a lot of research towards their bonding situation, their structural diversity, and their possible applications have been carried out.^[65-67] This is especially true for polyiodides of which a variety of mono, di, tri and tetra anions are known for a long time.^[67] Over the last years, also the lighter polyhalides received much attentions as they could potentially be used as easy to handle replacements for the toxic and volatile chlorine or bromine. The following section summarizes the chemistry of the lighter polyhalides including their structural diversity, their applications as well as their bonding situation.

1.2.1 Bonding Situation of Polyhalides

Trihalides tests the limits of molecular bonding by having 22 valance electrons and therefore cannot be represented in one simple Lewis formular obeying the octet rule. Consequently, their bonding situation has been the topic of research for a long time as one of the simplest examples for hypervalent compounds. After initial research by Pauling^[68] and Kimball^[69], which suggested hybridization involving higher energy d and s orbitals, Rundle and Pimentel presented an MO theoretic approach in 1951.^[70,71] They recommended that within linear $D_{\infty h}$ symmetric $[X_3]^-$ the three p orbitals along the bond axes combine yielding three delocalized orbitals of which one is bonding (Ψ_1), one is non-bonding (Ψ_2) and one is antibonding (Ψ_3) with the former two being occupied (Figure 7 left). This three-center-four-electron (3c-4e) bond corresponds to a bond order of 0.5 for the X-X bonds, which explains the relatively long X-X distance compared to free halogens (Figure 7 right). Additionally, also the charge distribution within the $[X_3]^-$ anion (mostly on the outer X atoms) is in accordance to this simple MO picture since there is a node through the central X atom in the HOMO of the molecule.

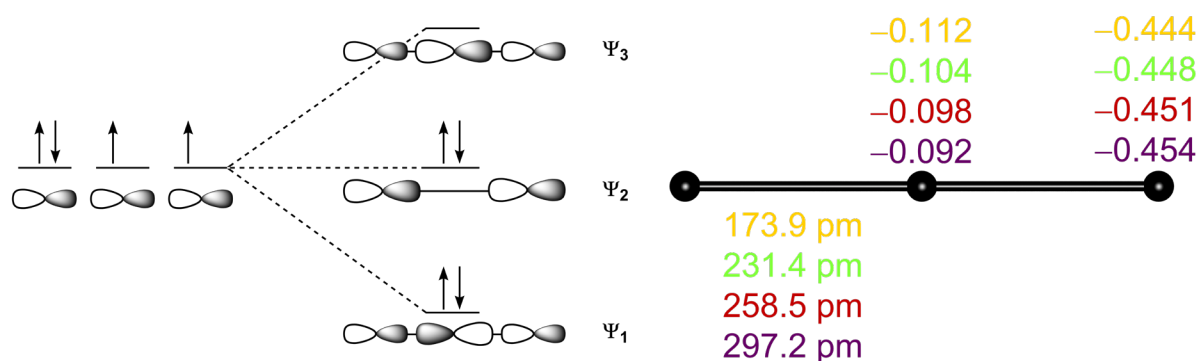
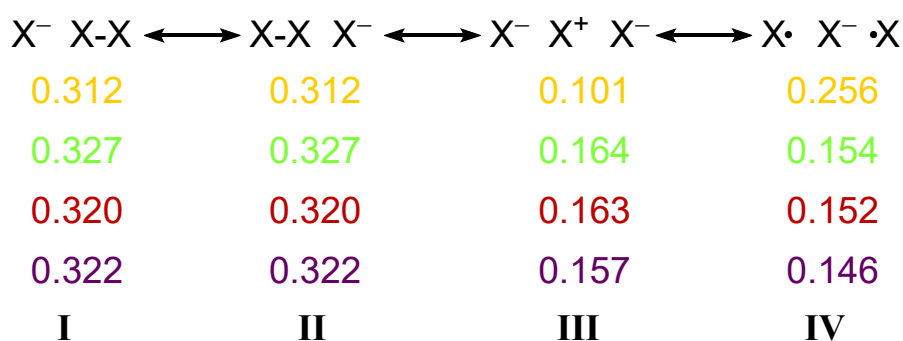


Figure 7. Rundle-Pimentel scheme for the bonding situation in a three-center-four-electron bond (left) and bond length as well as NPA charges of the $[X_3]^-$ anion ($X = \text{F}$ (yellow), Cl (green), Br (red), I (violet)) calculated on CCSD(T) level of theory.^[65,72-74]

In recent years, it has been outlined that this MO theoretic approach is oversimplified as according to the Rundle-Pimentel scheme, all 3c-4e systems should be stable which is not the case since many exceptions, e.g. $[\text{H}_3]^-$, ArF_2 and NF_5 , are known in the literature.^[75-77] Therefore, a valence bond (VB) theoretic approach was chosen by Coulsen to describe this bonding situation in more detail. He showed that the Rundle Pimentel model can be transformed into a VB-theoretical description of a $X-X-X$ (3c-4e) system by using four main resonance structures I to IV (Scheme 5).^[78]



Scheme 5. Main resonance structures of the $[X_3]^-$ anion $X = \text{F}$ (yellow), Cl (green), Br (red), I (violet) and their weights calculated at BOVB level of theory.^[76]

Breathing-Orbital Valence Bond (BOVB) calculations showed that all four resonance structures significantly contribute to the overall electronic structure (Scheme 5) resulting in a stabilization of the system by a large resonance energy.^[76] This type of bonding, in which the covalent-ionic resonance energy is the major contribution to the total bonding energy, is called charge-shift bonding.^[79,80] Similar to the MO theoretical description, the VB approach can be used to explain the charge distribution of the $[X_3]^-$ by considering the charges within as well as the weight of the respective resonance structures. Furthermore, this approach can be used to rationalize why

certain 3c-4e systems are stable while others are not by considering the influence that results in high resonance energies. If the energy levels and weights of the individual resonance structures are comparable, a high resonance energy is expected. In VB structure III the central atom has a positive charge (for neutral 3c-4e systems 2+). Therefore, low ionization potentials of the central atom stabilize this resonance structure while high ionization potentials destabilize it, resulting in less resonance energy. This explains the instability of compounds like ArF_2 , NF_5 and OF_4 in which the central atom has a relatively high first and especially high second ionization potential.^[77] To understand the instability of $[\text{H}_3]^-$, the resonance energy of the two covalently bound structures ($\text{H}\cdots\text{H}-\text{H}$) **I** and ($\text{H}-\text{H}\cdots\text{H}$) **II** must be considered. Within these resonance structures, the H-H bond can be classified as a classic covalent bond. For systems involving covalent bonds the resonance energy is about one-half of the H-H bond energy or less.^[81] On the other hand, if the X-X bond itself is a charge-shift bond, as for example in $[\text{Cl}_3]^-$ or $[\text{XeF}_2]$, the resonance stabilization can be as large as twice the X-X bond energy, which significantly stabilizes those systems.^[75] Therefore, it was concluded that the 3c-4e bond can only be stable if the normal valent X-X bond is a charge-shift bond itself. This is true for, e.g., $X = \text{Cl}$, making $[\text{Cl}_3]^-$ stable, but not for $X = \text{H}$ making $[\text{H}_3]^-$ a transition state.^[77,79]

The presence of a charge-shift bond can be deduced from the experimental observable electron density using tools like the electron localization functions (ELF) and the Laplacian in the quantum theory of atoms in molecules.^[79,80] Recent electron density measurements on the symmetric $[\text{Cl}_3]^-$ within $[\text{NPr}_4][\text{Cl}_3]$ revealed a value of 0.48 for the ELF at the bond critical point, which shows the delocalized character of the electrons, in addition to a positive Laplacian. Both reflect the charge shift nature of these bonds.^[82]

Hoffmann and co-worker further investigated the trihalide system using the transition state energy decomposition procedure which breaks down the bonding energy between fragments of a molecule into chemically intuitive contributions, namely Pauli repulsion, electrostatic interaction and orbital interaction.^[83] According to their results, all energy contributions are of major importance for the bonding in trihalide systems while the orbital interaction is the main reason for the linear geometry of the $[\text{X}_3]^-$ anion. It was shown that nearly 40% of the orbital energy is lost when the angle within a $[\text{I}_3]^-$ is changed from 180° to 120° while for the other energy contributions only a small change is observed. This orbital interaction within the trihalides can be understood as a charge transfer from the lone pair of the X^- fragment into the

σ^* orbital of the X-X bond. Shaik, Mo, and co-worker showed that this type of covalent donor acceptor interaction is also the dominant contribution to the bonding in larger polyhalides $[X(X_2)_n]^-$ while the covalent character of the bond decreases with an increasing number of n .^[74] This is rationalized by the weakening of the Lewis basicity of the central halide ion with an increasing number of coordinated halogen molecules. The impact of the charge transfer can be seen in the structure of the polyhalides since the partial occupation of the σ^* orbital results in an elongation of the X-X bond which is most prominent for the $[X_3]^-$ and gradually decreases for larger polyhalides.^[84] The electrostatic interaction, which is the second important contribution to the binding in larger polyhalides, can be rationalized using the σ -hole concept.^[85] Even though dihalogens do not have a dipole moment, their electrostatic potential is anisotropic and shows an area of higher charge accumulating perpendicular to the molecule's main axis while a region of more positive potential is located at the extension of the bonding axes, the so called σ -hole (Figure 8).^[66]

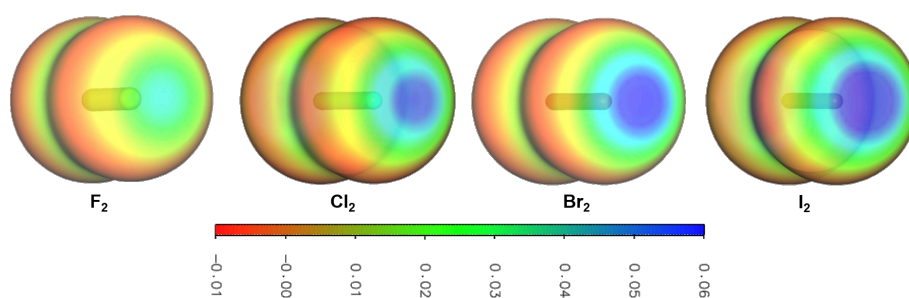


Figure 8. The electrostatic potentials of the halogens F_2 , Cl_2 , Br_2 , and I_2 in the range of -0.01 a.u. (red) to 0.06 a.u. (blue) have been mapped onto their electron densities (isosurface value 0.0035 a.u.); calculated at the B3LYP-D3/def2-TZVPP level of theory.^[66] Reproduced from Ref. 66 with permission from Wiley-VCH Verlag GmbH & Co. KGaA.

Electron rich molecular entities, in this case the halide ions, can interact with this more positive region forming a halogen bond.

1.2.2 Polyfluorides

Fluorine has the smallest σ -hole among all halogens making it the worst halogen bond donor.^[66,86] Additionally, its high reactivity significantly limits the choice of cations for the synthesis of polyfluorides while strict safety precautions and a specialized experimental setup are required when working with F_2 . This explains why only the $[F_3]^-$ as well as the $[F(F_2)_2]^-$ anions have been described in the literature yet.^[87-89]

The $[\text{F}_3]^-$ anion was first observed by Ault and Andrews in matrix isolation experiments. They obtained the ion pairs $\text{M}[\text{F}_3]$ ($\text{M} = \text{K}, \text{Rb}, \text{Cs}$) by thermally evaporation of alkali metal fluorides and co-deposition of a fluorine/argon gas mixture under cryogenic conditions. The formed species were characterized by IR and Raman spectroscopy showing one band at 550 cm^{-1} , corresponding to the antisymmetric stretching mode of the $\text{Cs}[\text{F}_3]$ in the IR spectrum, and two bands at 461 cm^{-1} (symmetric stretch of $\text{Cs}[\text{F}_3]$) and 389 cm^{-1} (higher CsF/F_2 complex) in the Raman spectrum.^[87,88] In 2015, Riedel and co-worker also observed the combination band of the two modes ($\nu_{\text{as}} + \nu_{\text{s}}$) by using laser ablation of alkali metal fluorides to prepare $\text{Cs}[\text{F}_3]$.^[90] Mass spectroscopic experiments were used to observe the free $[\text{F}_3]^-$ anion for the first time and also to determine its bond dissociation energy to be $98 \pm 11 \text{ kJ mol}^{-1}$.^[91,92] This value is in good agreement to the calculated bond dissociation energy of 97 kJ mol^{-1} on CCSD(T)/aug-cc-pV5Z level of theory.^[93] An isolated $[\text{F}_3]^-$ anion was also detected by vibrational spectroscopy (metal independent IR band at 525 cm^{-1}) after co-deposition of laser-ablated transition metals with F_2 in neon matrixes. This was rationalized by the breaking of the F-F bond generating fluorine radicals, initialized by UV light generated from the metal plasma, and subsequent capture of free electrons, also generated by the laser ablation of a metal, yielding the formation of fluoride ions. The formed fluoride ions combine with F_2 forming the $[\text{F}_3]^-$ anion.^[89] If an excess of fluorine is present, an additional fluorine molecule can coordinate to the $[\text{F}_3]^-$ yielding the only other known polyfluorides the $[\text{F}(\text{F}_2)_2]^-$. This anion was calculated to be stable against elimination of F_2 by 17.4 kJ mol^{-1} on CCSD(T)/aug-cc-pVQZ and has a hockey stick-like minimum structure in the gas phase which is favored over the V-shaped structure usually observed for polyhalides by 6.2 kJ mol^{-1} .^[89,93] Spectroscopic evidence for a $[\text{F}(\text{F}_2)_2]^-$ was obtained after co-deposition of laser-ablated transition metals with F_2 in neon matrixes yielding an additional metal independent band at 850 cm^{-1} which was assigned to the antisymmetric stretching mode of a $[\text{F}(\text{F}_2)_2]^-$ anion.^[89]

1.2.3 Polychlorides

The first evidence for the formation of a $[\text{Cl}_3]^-$ anion was given by Chattaway and Hoyle in 1923. They treated solid $[\text{NEt}_4]\text{Cl}$ with elemental chlorine and observed a rapid gas absorption resulting in the formation of a pale yellow, hygroscopic solid with the composition $[\text{NEt}_4][\text{Cl}_3]$.^[94] First information on the structure of the $[\text{Cl}_3]^-$ anion were obtained by vibrational

spectroscopy. Evans and Lo concluded that within $[\text{NPr}_4][\text{Cl}_3]$ the trichloride has a linear, centrosymmetric $D_{\infty h}$ -structure since they only observed one band at 268 cm^{-1} in the Raman spectrum corresponding to the antisymmetric stretching mode, and one band at 242 cm^{-1} in the IR spectrum for the symmetric stretching mode.^[95] On the other hand, Ault and Andrews investigated alkali metal trichlorides in matrix isolation experiments and observed both stretching modes in the Raman spectrum indicating an asymmetric structure of the $[\text{Cl}_3]^-$. This is likely due to a stronger interaction between the metal cation and the $[\text{Cl}_3]^-$ compared to the larger $[\text{NPr}_4]^+$ cation.^[96] In recent years also the free linear trichloride could be observed in neon and argon matrixes after co-deposition of laser ablated alkali metal chlorides and Cl_2 confirming the centrosymmetric structure of the free ion.^[97]

Bogaard and co-workers reported the molecular structure of $[\text{AsPh}_4][\text{Cl}_3]$ in 1981 which corresponds to the first molecular structure of a $[\text{Cl}_3]^-$ anion. In $[\text{AsPh}_4][\text{Cl}_3]$, the trichloride exists as a discrete anion with an almost linear but asymmetric geometry and Cl-Cl bond lengths of $222.7(1)$ and $230.6(1)$ pm.^[98] Since then, eight additional molecular structures of trichloride salts were published containing $[\text{Cl}_3]^-$ anions with a wide range of Cl-Cl distances.^[98-101] $[\text{NPr}_4][\text{Cl}_3]$ is the only known compound containing a completely symmetric $[\text{Cl}_3]^-$ anion with two equal Cl-Cl distances of $228.3(1)$ pm (Figure 9A right). For all other examples, two different Cl-Cl distances were observed with $[\text{NMe}_3(\text{C}_2\text{H}_4\text{Cl})][\text{Cl}_3]$ being the most asymmetric one having Cl-Cl bond lengths of 210.7 and $258.2(1)$ pm (Figure 9A left).^[82] The reason for the asymmetric structure of the $[\text{Cl}_3]^-$ in most trichloride salts is the interaction with the cation in the solid state. For $[\text{NMe}_3(\text{C}_2\text{H}_4\text{Cl})][\text{Cl}_3]$ the Hirshfeld surface shows strong hydrogen bonding interaction between one chlorine atom and three cations while for $[\text{NPr}_4][\text{Cl}_3]$ significantly weaker and also symmetric interactions between the anion and the cation are observed (Figure 9B).

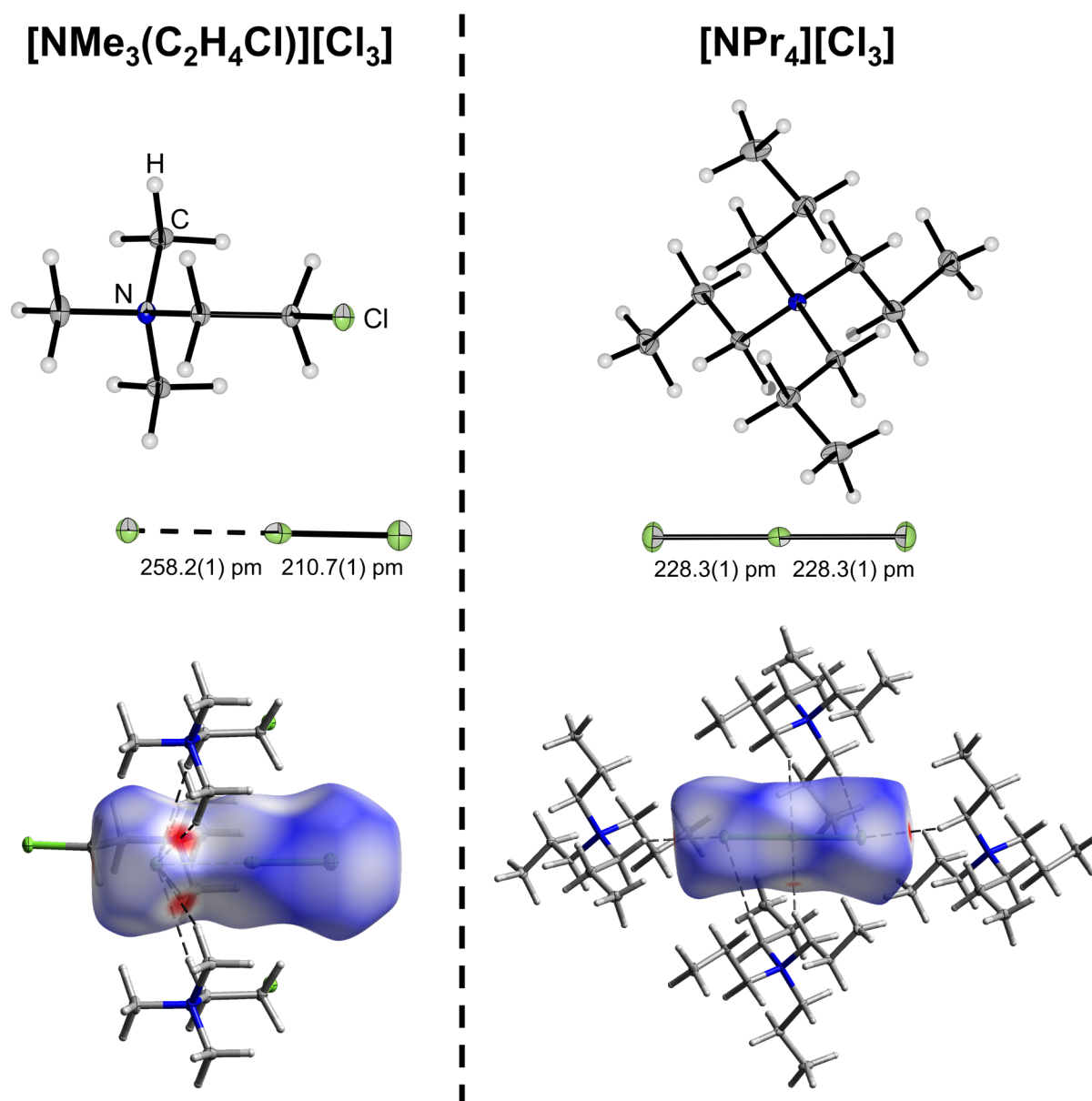
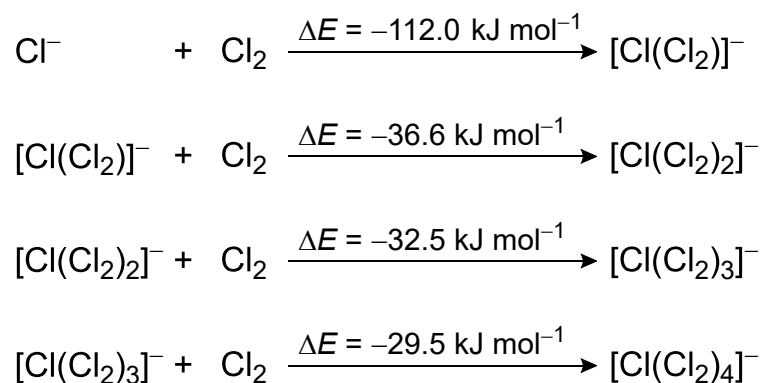


Figure 9. Molecular structures in the solid state (top) and Hirshfeld surfaces (bottom) of $[\text{NMe}_3(\text{C}_2\text{H}_4\text{Cl})][\text{Cl}_3]$ (left) and $[\text{NPr}_4][\text{Cl}_3]$ (right).^[82] The Hirshfeld surface of $[\text{NMe}_3(\text{C}_2\text{H}_4\text{Cl})][\text{Cl}_3]$ indicates short contacts between the $[\text{Cl}_3]^-$ anion and the surrounding cations (red areas) indication strong hydrogen bonding interaction.

First evidence for the existence of polychlorides with a higher chlorine content were obtained by Evans and Lo by investigation of an acetonitrile solution of $[\text{NPr}_4]\text{Cl}$ with different amounts of Cl_2 . For a 2:1 mixture of chlorine and $[\text{NPr}_4]\text{Cl}$ they observed an intense Raman band at 482 cm^{-1} , besides two bands for the $[\text{Cl}_3]^-$ at 275 cm^{-1} and for dissolved chlorine at 538 cm^{-1} . After further increasing the chlorine content, the band corresponding to the $[\text{Cl}_3]^-$ vanished. They assigned the new Raman band to the highest-frequency stretching mode of a $[\text{Cl}(\text{Cl}_2)_2]^-$ ion since the molecular structure of the corresponding $[\text{I}(\text{I}_2)_2]^-$ was already known at this time.^[95,102] Subsequently, Riedel and co-workers used a combined quantum chemical and Raman spectroscopical approach to investigate higher polychlorides.^[84] First, they optimized

the geometries of different possible isomers of $[\text{Cl}_{2n+1}]^-$ ($n = 2-4$) and observed that for all n symmetric structures (C_{2v} ($n = 2$), C_{3v} ($n=3$) and T_d ($n=4$)) with a central chloride and coordinating Cl_2 molecules ($[\text{Cl}(\text{Cl}_2)_n]^-$) are the most stable. Additionally, quantum chemical calculations on the SCS-MP2/def2-TZVPP level of theory predicted all $[\text{Cl}(\text{Cl}_2)_n]^-$ anions ($n = 1-4$) to be stable towards the loss of Cl_2 , which is the preferred decomposition channel for polychlorides (Scheme 6).



Scheme 6. Reaction energies for the formation of $[\text{Cl}(\text{Cl}_2)_n]^-$ calculated on SCS-MP2/def2-TZVPP level of theory.^[84]

When the optimized structures of the polychlorides $[\text{Cl}(\text{Cl}_2)_n]^-$ are compared, it can be seen that with increasing n the distance between the chloride and the coordinating Cl_2 molecules increases while the Cl-Cl bond length of the coordinated Cl_2 molecule decreases. This can also be observed in the calculated Raman spectra of these ions where the bands for the Cl-Cl stretching modes are shifted to higher wavenumbers with increasing n . Therefore, Raman spectroscopy was claimed to be a good tool to investigate polychloride systems. However, as shown above, the molecular environment in the solid state can have a significant influence on the structure of polychlorides. Bond length of 210.7(1) – 228.3(1) pm were observed in the solid state for different $[\text{Cl}_3]^-$ anions in dependency of the cation which also leads to a large shift of the Raman band for the Cl-Cl stretching mode (270 cm^{-1} for $[\text{NPr}_4][\text{Cl}_3]$, 370 and 351 cm^{-1} for $[\text{NMe}_3(\text{C}_2\text{H}_4\text{Cl})][\text{Cl}_3]$).^[82] Thus, Raman spectra of polychlorides can often not be assigned to a certain $[\text{Cl}(\text{Cl}_2)_n]^-$ anion and for indisputable assignment the determination of the molecular structure in the solid state is necessary.

The first structural proof for a polychloride with a higher chlorine content than the trichloride was given by Taraba and Zak in 2003 who obtained single crystals of $[\text{PPh}_2\text{Cl}_2][\text{Cl}_3\cdot\text{Cl}_2]$.^[103] The solid-state structure consists of anionic layers build up by $[\text{Cl}_3]^-$ and Cl_2 units which are arranged in a system of connected parallelograms (Figure 10). The trichloride unit, which is

rather asymmetric ($R(\text{Cl}-\text{Cl}) = 214.4(3)$ and $241.9(3)$ pm), has contacts to the Cl_2 units ($317.1(3)$ and $330.0(3)$ pm) which are shorter than the sum of the van der Waals radii (350 pm)^[104] and therefore indicate halogen bonding interactions. The anionic layers are interconnected by additional short contacts to the $[\text{PPh}_2\text{Cl}_2]^+$ cations.

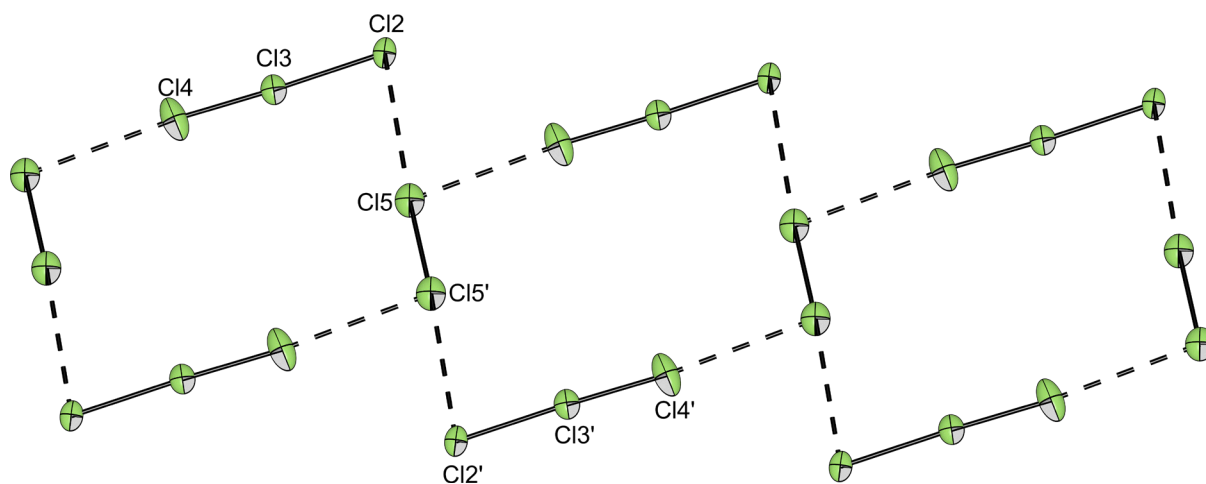


Figure 10. Anionic layer within the structure of $[\text{PPh}_2\text{Cl}_2][\text{Cl}_3-\text{Cl}_2]$.^[103] Ellipsoids are shown at the 50% probability level.

In recent years, Riedel and co-workers significantly increased the number of structurally characterized polychlorides.^[105–107] Single crystals of $[\text{NPr}_3\text{Me}][\text{Cl}(\text{Cl}_2)_3]$ could be obtained by slowly cooling a solution of $[\text{NPr}_3\text{Me}]\text{Cl}$ in liquid chlorine to -40 °C.^[106] The structure contains isolated $[\text{Cl}(\text{Cl}_2)_3]^-$ anions which strongly interact with the cations via hydrogen bonding. The distance between the central chloride and the coordinated Cl_2 molecules is significantly lower than the sum of the van der Waals radii ($R(\text{Cl}-\text{Cl}) = 276.0(1)$ – $277.4(1)$ pm, $\sum_{\text{vdW}}(\text{Cl}-\text{Cl}) = 350$ pm) and the bond length within the coordinated Cl_2 molecules is significantly elongated ($202.7(1)$ to $203.8(1)$ pm) compared to solid chlorine ($198.5(2)$ pm)^[108].

While the $[\text{Cl}(\text{Cl}_2)_4]^-$ has not been structurally characterized yet, for $[\text{Cl}(\text{Cl}_2)_5]^-$ two different motives have been observed in the solid state.^[105] Within $[\text{PPh}_4][\text{Cl}(\text{Cl}_2)_5]$ and $[\text{AsPh}_4][\text{Cl}(\text{Cl}_2)_5]$ the $[\text{Cl}(\text{Cl}_2)_5]^-$ units are connected to form one-dimensional chains yielding an octahedral coordination for the central chloride. On the other hand, within $[\text{PNP}][\text{Cl}(\text{Cl}_2)_5] \cdot \text{Cl}_2$ the $[\text{Cl}(\text{Cl}_2)_5]^-$ anion are isolated and have a square-pyramidal structure with an additional co-crystallized chlorine molecule which only weakly interacts with the $[\text{Cl}(\text{Cl}_2)_5]^-$ unit.

$[\text{PNP}][\text{Cl}(\text{Cl}_2)_6]$ (Figure 11), which is the polychloride with the highest chlorine content known, was obtained by condensing an excess of Cl_2 onto a solution of $[\text{PNP}]\text{Cl}$ in acetonitrile. In this salt the $[\text{Cl}(\text{Cl}_2)_6]^-$ anion has an octahedral structure with distances of $277.6(1)$ – $290.2(1)$ pm

between the central chloride and the chlorine ligands and Cl-Cl bond lengths of 201.7(1)-202.2(1) pm for the coordinated Cl₂ molecules. Due to the high coordination number, less electron density is donated from the central chloride into the antibonding σ^* orbitals of the Cl-Cl bonds. Therefore, the weakening of the Cl-Cl bond is least pronounced for the [Cl(Cl₂)₆]⁻ anion when comparing all [Cl(Cl₂)_{*n*}]⁻ anions.

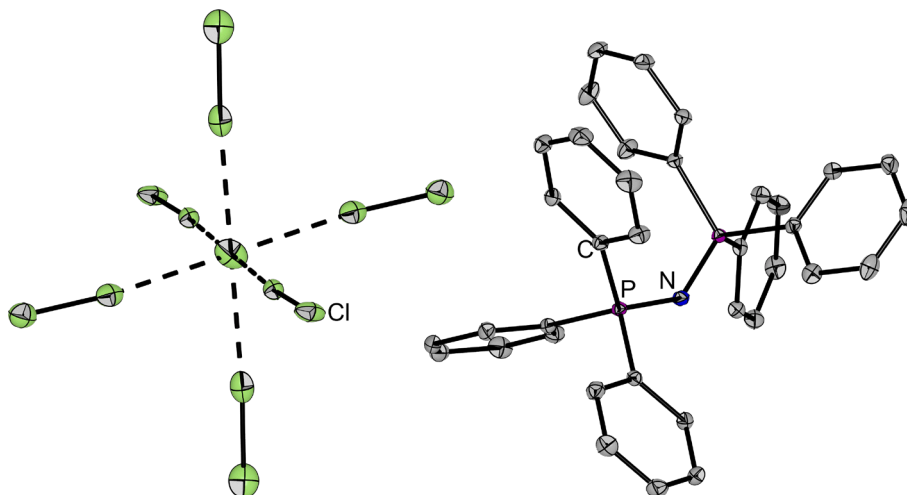


Figure 11. Molecular structure in the solid state of [PNP][Cl(Cl₂)₆].^[105] Ellipsoids are shown at the 50% probability level and hydrogen atoms are omitted for clarity.

The first example for a polychloride dianion was the [Cl₈]²⁻ dianion.^[107] It was obtained from a solution of tetramethylchloroamidinium chloride [CCl(NMe₂)₂]Cl and Cl₂ in [BMP][OTf]. In [CCl(NMe₂)₂][Cl₈] the [Cl₈]²⁻ dianions are isolated and can best be described as two asymmetric trichloride units which are connected by an additional Cl₂ molecule in a Z-shaped structure. This structural motive is also observed for the heavier homologues [Br₈]²⁻ and [I₈]²⁻.^[109–112] Additionally, there is a two-dimensional polychloride network with the same chlorine content ([NEt₄]₂[(Cl₃)₂-Cl₂]) known in the literature.^[113] The only other known polychloride dianion is [Cl₁₂]²⁻ which was obtained by exposing [NMe₃Ph]Cl to an excess of Cl₂.^[105] The structure of the [Cl₁₂]²⁻ dianion can be described as two [Cl(Cl₂)₂]⁻ units which are connected by a Cl₂ molecule (Figure 12). Within [NMe₃Ph]₂[Cl₁₂] the [Cl₁₂]²⁻ units are further connected by strong halogen bonding interactions forming a honeycomb-like three-dimensional network.

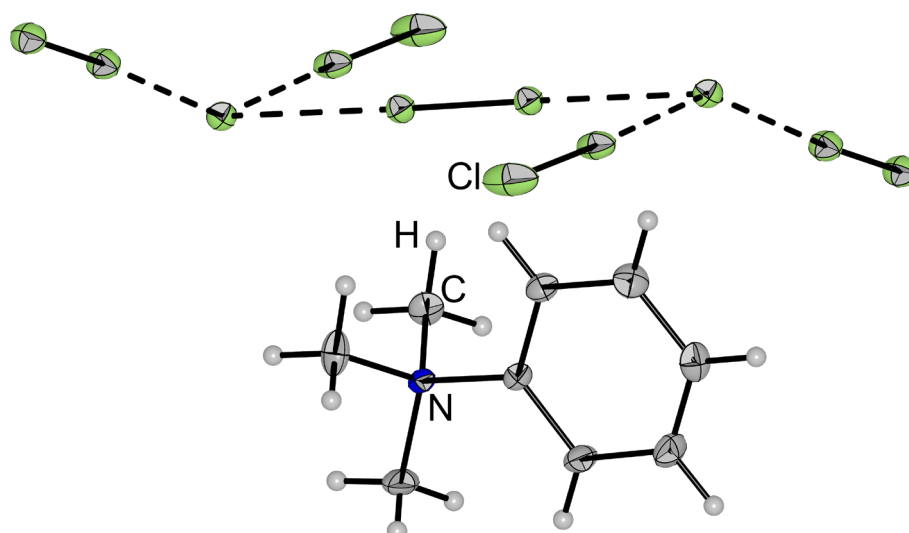


Figure 12. Molecular structure in the solid state of $[\text{NMe}_3\text{Ph}][\text{Cl}_{12}]$.^[105] Ellipsoids are shown at the 50% probability level.

1.2.4 Polybromides

In recent years, a large number of polybromide anions have been synthesized, far exceeding the number of known polychlorides and polyfluorides. This can be rationalized by the more pronounced σ -hole of bromine leading to stronger halogen bonding as well as the easier handling of liquid bromine in comparison to gaseous chlorine and fluorine. A complete row of polybromine monoanions $[\text{Br}(\text{Br}_2)_n]^-$ ($n = 1-5$) as well as eight polybromine dianions, the largest being $[\text{Br}_{24}]^{2-}$, are known in the literature.^[66]

More than 100 $[\text{Br}_3]^-$ salts have been characterized by X-ray diffraction and their structures can be found in the CCDC. Pichierri analyzed this data in 2011 and found, similar to the $[\text{Cl}_3]^-$ anion, that with an amount of 71%, most $[\text{Br}_3]^-$ anions are asymmetric in the solid state.^[114] He performed a relaxed potential energy surface scan on this system and found that although the symmetric structure with two equivalent Br-Br bonds ($R(\text{Br}-\text{Br}) = 254.2$ pm) corresponds to the energy minimum, the elongation of one Br-Br bond by 30 pm results in an energy increase of only 10 kJ mol^{-1} .^[114] This small energy difference can easily be compensated by weak interactions within the crystal, e.g. by hydrogen or halogen bonding. Indeed, the two most asymmetric $[\text{Br}_3]^-$ anions, found within $[\text{DBUH}][\text{Br}_3]$ ($R(\text{Br}-\text{Br}) = 242.7, 274.4$ pm)^[115] and $[(\text{H}_2\text{N})(\text{Me}_2\text{N})\text{CBr}]_5[\text{SeBr}_6][\text{Se}_2\text{Br}_9][\text{Br}_3]$ ($R(\text{Br}-\text{Br}) = 242.3$ and 274.0 pm)^[116], interact strongly with their environment within the crystal.

The first structural prove for a $[\text{Br}(\text{Br}_2)_2]^-$ anion was given by Himmel and co-worker in 2012 by investigating single crystals of $[(\text{ttmgn}-\text{Br}_4(\text{BF}_2)_2)[\text{Br}(\text{Br}_2)_2]_2 \cdot 0.65\text{Br}_2]$ as well as $[(\text{btmgn}-\text{Br}_3)\text{BF}_2][\text{Br}(\text{Br}_2)_2]^-$ using X-ray diffraction.^[117] Within these salts, V-shaped as well as hockeystick-like geometries were observed for the $[\text{Br}(\text{Br}_2)_2]^-$ unit. Quantum chemical calculations as well as previously reported Raman spectroscopic investigations^[118,119] predicted a C_{2v} symmetric V-shaped structure to be the most stable.

Simoncic and co-worker systematically investigated mixtures of $[\text{NEt}_4]\text{Br}$ and bromine using Raman spectroscopy and compared their result to calculated spectra on MP2/6-31G(d) level of theory. For a 1:3 mixture only one signal at 270 cm^{-1} was observed in the Raman spectra which they assigned to a C_{3v} symmetric, pyramidal $[\text{Br}(\text{Br}_2)_3]^-$ anion which was also calculated to be the minimum structure for this ion.^[119] Feldman and co-worker were able to structurally characterize $[\text{PPh}_3\text{Br}][\text{Br}(\text{Br}_2)_3]$ by growing single crystals from a 1:5 mixture of PPh_3 and bromine using an eutectic mixture of the ionic liquids $[\text{C}_{10}\text{MPyr}]\text{Br}$ and $[\text{C}_4\text{MPyr}][\text{OTf}]$ as a solvent.^[120] The obtained $[\text{Br}(\text{Br}_2)_3]^-$ anion has a pyramidal structure and has short contacts to the next $[\text{Br}(\text{Br}_2)_3]^-$ units ($R(\text{Br}-\text{Br}) = 331.7\text{-}339.5\text{ pm}$) as well as to the cation ($R(\text{Br}-\text{Br}) = 349.9\text{ pm}$) which are below the sum of the van der Waals radii (370 pm)^[104].

The molecular structure of the next higher polybromide, $[\text{Br}(\text{Br}_2)_4]^-$, was first reported by Riedel and co-workers by characterizing $[\text{NPr}_4][\text{Br}(\text{Br}_2)_4]$, which contains $[\text{Br}(\text{Br}_2)_4]^-$ anions with a slightly distorted tetrahedral structure (Figure 13).^[121] To investigate the influence of the cation, they further prepared a complete series of $[\text{NAlk}_4][\text{Br}(\text{Br}_2)_4]$ (Alk = Me, Et, Pr, Bu) salts and found that within $[\text{NPr}_4][\text{Br}(\text{Br}_2)_4]$ the anions are the most isolated and are only loosely connected to the next anion by halogen bonding interactions. Polybromide networks are obtained for the $[\text{NMe}_4]^+$ (chains), $[\text{NEt}_4]^+$ (layers) and $[\text{NBu}_4]^+$ (3D-network) salts.^[122]

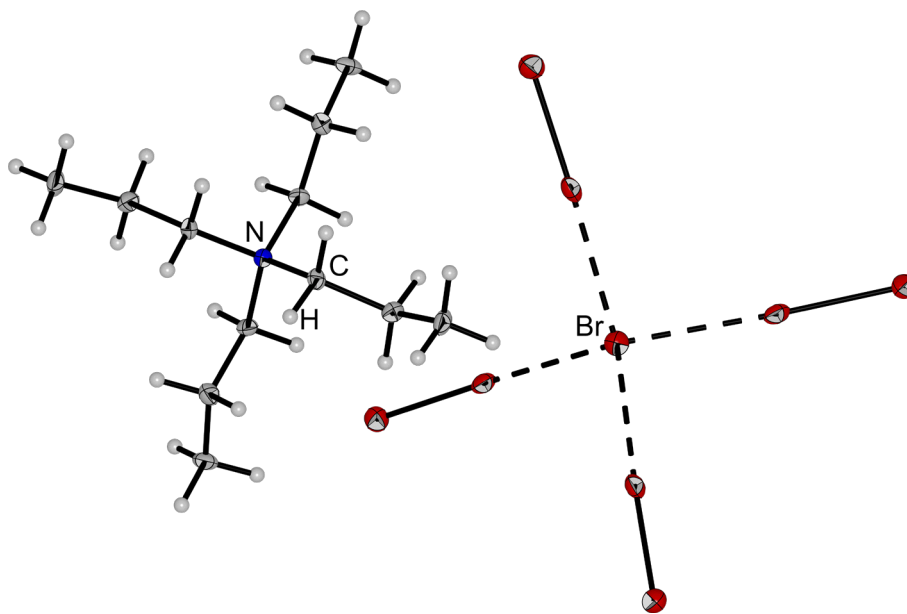


Figure 13. Molecular structure in the solid state of $[\text{NPr}_4][\text{Br}(\text{Br}_2)_4]$.^[121] Ellipsoids are shown at the 50% probability level.

The largest known polybromine monoanion is $[\text{Br}(\text{Br}_2)_5]^-$ which was observed in the salt $[\text{PNP}][\text{Br}(\text{Br}_2)_5] \cdot \text{Br}_2$.^[123] It has a square pyramidal structure with only slightly elongated Br-Br bond length of 232.0 to 233.5 pm for the coordinated Br_2 molecules compared to 229.5 pm for solid Br_2 .^[108] In the solid state, it is further connected by the co-crystallized Br_2 molecule to form a weakly bound three-dimensional network.

In contrast to the polychlorides, where only two examples of polychlorine dianions are known, a variety of polybromine dianions have been described.^[124–129] The first example which was structurally characterized was the $[\text{Br}_4]^{2-}$ which was obtained by adding diluted Br_2 to a solution of $[\text{NMe}_2\text{H}_2]\text{Br}$ in chloroform.^[124] It has an almost linear geometry ($\alpha(\text{Br}-\text{Br}-\text{Br}) = 173^\circ$) with symmetric Br-Br distances of 303 pm (outer) and 242 pm (inner). Therefore, it is best described as two bromide ions coordinating to one Br_2 molecule.

The $[\text{Br}_6]^{2-}$ was recently observed by Riedel and co-workers and is best described as two $[\text{Br}_3]^-$ units which are connected yielding a L-shaped geometry.^[125] This L-shaped geometry is surprising as according to quantum-chemical calculations the negative charge of the $[\text{Br}_3]^-$ anion is mostly located on the outer two Br atoms, which is in line with the simple MO description (see 1.2.1). Therefore, an L-shaped geometry should result in significant coulomb repulsion between the $[\text{Br}_3]^-$ units. Further quantum chemical investigations indicated that the $[\text{Br}_3]^-$ also has a weak σ -hole which explains the interaction between the two anions. The

dianion is further stabilized by halogen bond interactions to the $[\text{C}_5\text{H}_{10}\text{N}_2\text{Br}]^+$ cation reducing the negative charge of the anion.

The $[\text{Br}_8]^{2-}$ anion was first prepared by Knop and co-workers in 1997^[111] and has a Z-shaped structure in all known crystal structures.^[112,120,130] It consists of two tribromide units which are connected by a Br_2 unit. The structure of the next larger polybromine dianion, $[\text{Br}_{10}]^{2-}$, prepared as a tetrazolium salt by McKee and co-workers in 1990, is closely related. It is best described as two $[\text{Br}_3]^-$ units which are connected by two Br_2 molecules giving a rectangular polybromine anion.^[129]

Furthermore, Riedel and co-worker tested a series of fluorinated phosphonium cations $[(\text{C}_6\text{H}_5-n\text{F}_n)_3\text{PBr}]^+$ ($n=0-3$) in the synthesis of new polybromide anions.^[127] While the reaction of a 1:10 mixture of PPh_3 and Br_2 without an additional solvent (see above for comparison with $[\text{PPh}_3\text{Br}][\text{Br}(\text{Br}_2)_3]$ ^[120]) gave $[\text{PPh}_3\text{Br}]_2[\text{Br}_{14}]$ containing an anion which is best seen as two $[\text{Br}(\text{Br}_2)_3]^-$ units connected by halogen bonding, the use of a $[(\text{C}_6\text{H}_4\text{F})_3\text{PBr}]^+$ cation yielded the $[\text{Br}_{14}]^{2-}$ anion which is better described as a network consisting of a bromide ion which is octahedrally coordinated by Br_2 molecules as well as a $[\text{Br}_3]^-$ unit.^[127] Further increasing the degree of fluorination of the cation resulted in the formation of $[(\text{C}_6\text{H}_2\text{F}_3)_3\text{PBr}]_2[\text{Br}_{16}]$ which consists of two $[\text{Br}(\text{Br}_2)_3]^-$ units that are connected by a Br_2 molecule (Figure 14).^[127]

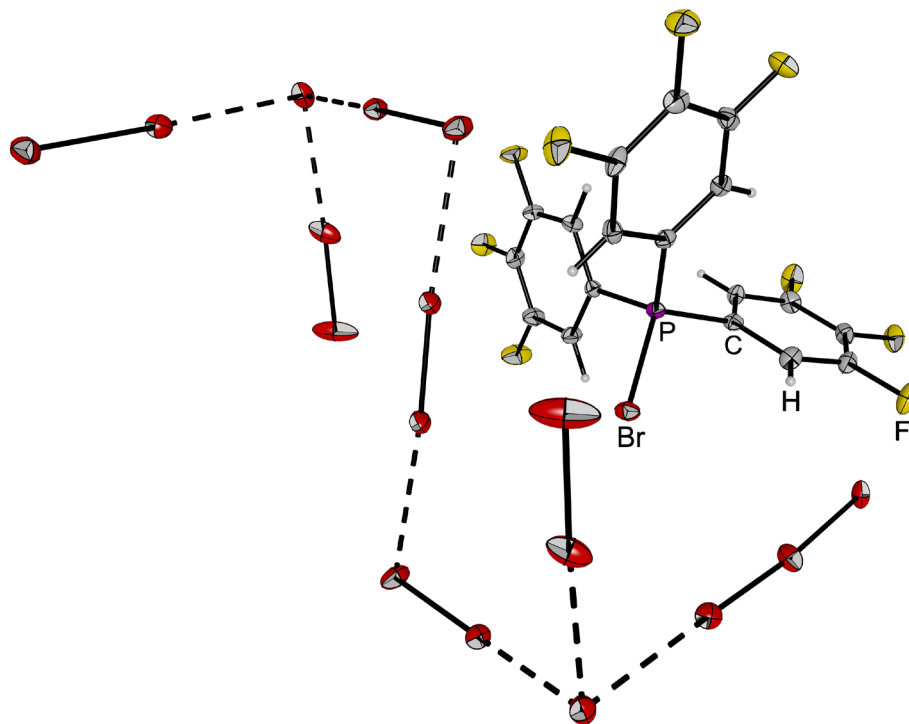


Figure 14. Molecular structure in the solid state of $[(\text{C}_6\text{H}_2\text{F}_3)_3\text{PBr}]_2[\text{Br}_{16}]$.^[127] Ellipsoids are shown at the 50% probability level.

The two largest polybromine dianions are $[\text{Br}_{20}]^{2-}$, first prepared by Feldmann and co-workers,^[126] as well as $[\text{Br}_{24}]^{2-}$ which was synthesized by Maschmeyer and co-workers.^[128] For both anions strong interactions between the anions forming 3D-networks are observed. Within $[\text{C}_4\text{MPyr}]_2[\text{Br}_{20}]$ the bromide ions are distorted, octahedrally coordinated by Br_2 molecules and the network is formed by corner-sharing as well as an interlinking bromine molecule, while within $[\text{PBu}_4]_2[\text{Br}_{24}]$ the $[\text{Br}_{24}]^{2-}$ anion can be described as two $[\text{Br}(\text{Br}_2)_4]^- \cdot \text{Br}_2$ units which are connected by an additional Br_2 molecule.

1.2.5 Applications of Polyhalides

Polyhalide salts are usually solids or low viscous ionic liquids with significantly reduced vapor pressures compared to the neat halogens (Figure 15).

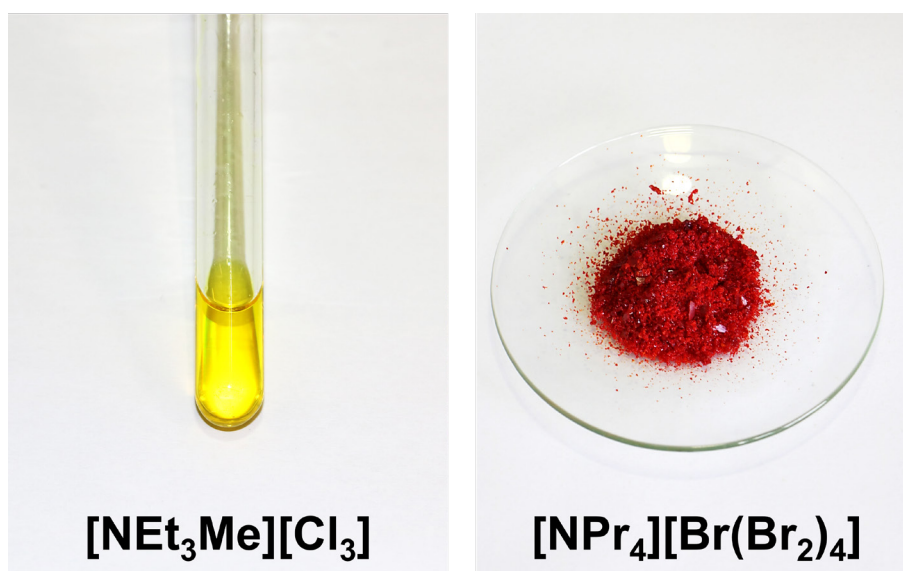
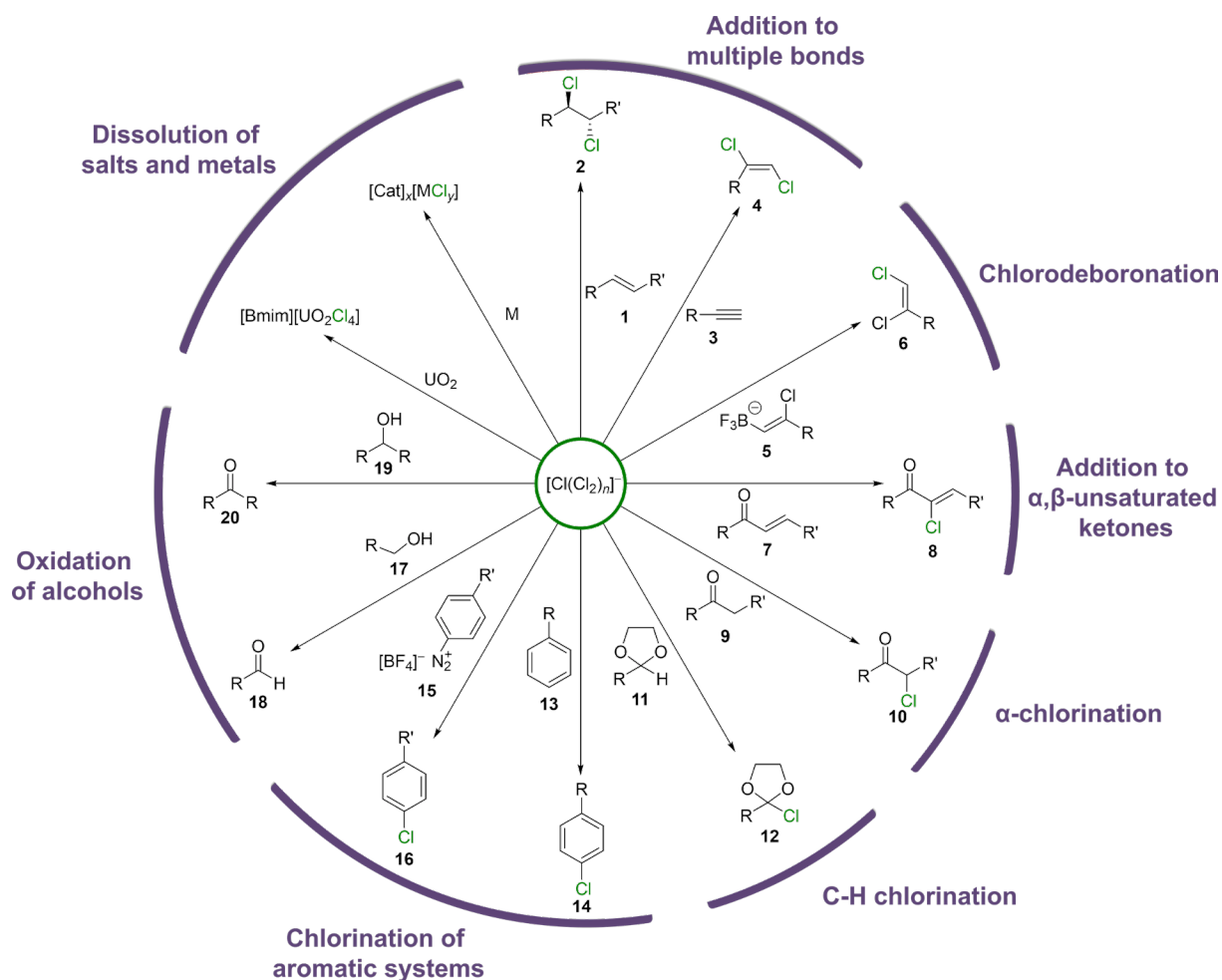


Figure 15. Examples of a liquid ($[\text{NEt}_3\text{Me}][\text{Cl}_3]$, left) and a solid ($[\text{NPr}_4][\text{Br}(\text{Br}_2)_4]$, right) polyhalide salt.

Therefore, polyhalides have become useful reagents in various fields over the last 25 years, combining the strong oxidizing power of elemental halogens with significantly improved handling properties. This is especially true for polychlorides which can replace the gaseous and toxic Cl_2 . In 1997, Mioskowski and co-worker prepared $[\text{NEt}_4][\text{Cl}_3]$ by saturating a solution of $[\text{NEt}_4]\text{Cl}$ in DCM with chlorine and removing the solvent afterwards. The obtained yellow solid is stable for months under an argon atmosphere and can be used for chlorination reactions.^[131] Since then, many different reactions using $[\text{Cl}(\text{Cl}_2)_n]^-$ anions as reagents have been

developed and also have been applied in the total synthesis of complex molecules (Scheme 7).^[131–135]

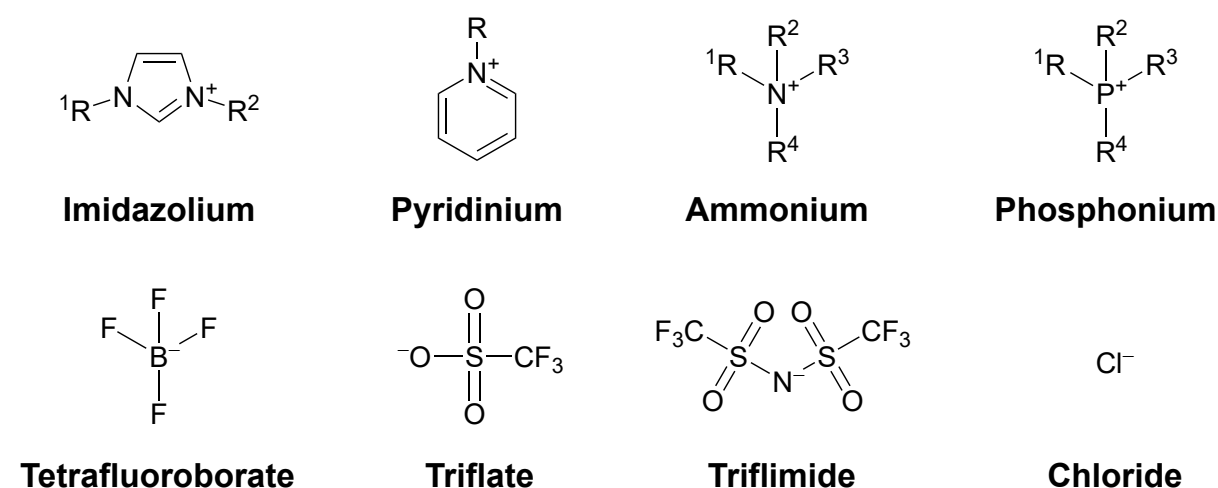


Scheme 7. Overview of the reactivity of $[\text{Cl}(\text{Cl}_2)_n]^-$ with various substrates. R = alkyl, aryl, OR, NR₂.

The reaction of alkenes **1** or alkynes **3** with polychlorides results in an anti-addition of Cl_2 to the multiple bond yielding vicinal dichlorinated alkanes **2** or *E*-alkenes **4**, respectively.^[131] *Z*-1,2-dichloroalkenes **6** are accessible from chlorovinyl trifluoroborates **5** by chlorodeboronation.^[136] Trichlorides also react with α,β -unsaturated ketones **7** yielding the α,β -unsaturated α -chloroketones **8**, presumably by dichlorination of the double bond and subsequent elimination of HCl. While for aldehydes dichlorination in the α -position is observed even without an excess of $[\text{Cl}(\text{Cl}_2)_n]^-$, ketones **9** selectively form the mono α -chlorinated product **10**. Surprisingly, even the tertiary C-H bond of acetals **11** are chlorinated by polychlorides yielding the 2-chloro-1,3-dioxolane **12**. Additionally, aromatic compounds with electron donating groups **13**, e.g., ethers^[131] and amines,^[137] are chlorinated yielding chloroarenes **14**. To achieve the chlorination of electron deficient aromatic systems, Gooßen and co-worker recently developed a photochemical Sandmeyer-type chlorination reaction of

aryldiazonium salts **15**.^[138] They isolated a series of substituted chloroarenes **16** with electron withdrawing functional groups ($R = \text{CN}, \text{NO}_2, \text{CO}_2\text{Me}$). Due to its high oxidation potential, $[\text{Cl}(\text{Cl}_2)_n]^-$ can also be applied in oxidation reactions. For instance, primary alcohols **17** are selectively oxidized to the corresponding aldehydes **18**, while secondary alcohols **19** are oxidized to ketones **20**.^[131] Polybromides show a similar reactivity compared to the $[\text{Cl}(\text{Cl}_2)_n]^-$ anion and have been used for the bromination of alkenes^[139-141] and alkynes^[142], α -bromination of ketones^[143,144] as well as aromatic^[145,146] and benzylic^[145] bromination reactions.

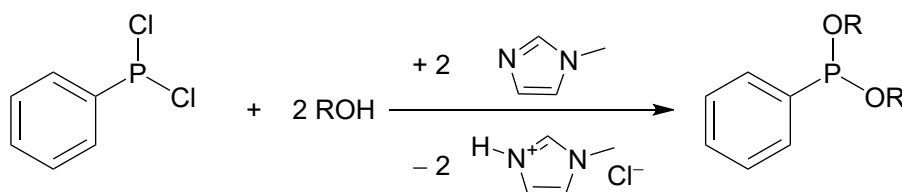
For industrial applications, liquid reagents are often advantageous over solids as they can easily be pumped through plants. Polyhalide salts with asymmetric cations are often liquids at room temperature and therefore can be classified as room-temperature ionic liquids (RTIL).^[66] In general, ionic liquids (ILs) are defined as compounds completely composed of ions with a melting point below 100 °C. This class of compounds has received significant attention in the last 25 years, while the number of publications regarding this topic have increased from only a few in 1996 to over 5000 in 2016.^[147,148] ILs usually consist of bulky, asymmetric, organic cations (e.g., imidazolium, pyridinium, ammonium or phosphonium) and inorganic, often polyatomic anions (e.g., tetrafluoroborate, triflate, triflimide but also halides, Scheme 8).^[148,149] This combination of large asymmetric ions with high charge delocalization leads to a decreased lattice energy and therefore to low melting salts.^[149]



Scheme 8. Example of cations and anions used in common ionic liquids. R^1 - R^4 = alkyl or aryl.

Ionic liquids have some unique properties such as low volatility, low flammability, a large temperature span between melting and boiling point, high thermal stability, high conductivity and a wide electrochemical window.^[148] Additionally, some features, as their polarity, can be

tailored by permutation of the cation and the anion, resulting in solvents with exceptional solvation properties. Therefore, ionic liquids are often regarded as so-called “designer” solvents and found many academic and industrial applications like in the electrodeposition of metals, for processing biomass and for gas storage.^[148,150-153] The first industrial process relying on the use of ionic liquids, is the BASIL (Biphasic Acid Scavenging utilizing Ionic Liquids) process and was introduced by BASF in 2002.^[153,154] In the production of $\text{PPh}(\text{OR})_2$ from PPhCl_2 and an alcohol, HCl is released which has to be captured to prevent side reactions (Scheme 9). To do so, 1-methylimidazole is added to the reaction mixture to form the corresponding imidazolium chloride salt which has a melting point of $75\text{ }^\circ\text{C}$ and forms a second phase which can be separated from the reaction product. Afterwards, the 1-methylimidazole can be regenerated by treatment of the obtained ionic liquid with a base like NaOH . Due to the introduction of the BASIL process, the space-time yield of the reaction could be increased by a factor of 80000 in comparison to the previously used process relying on acid scavenging using tertiary amines.^[153]



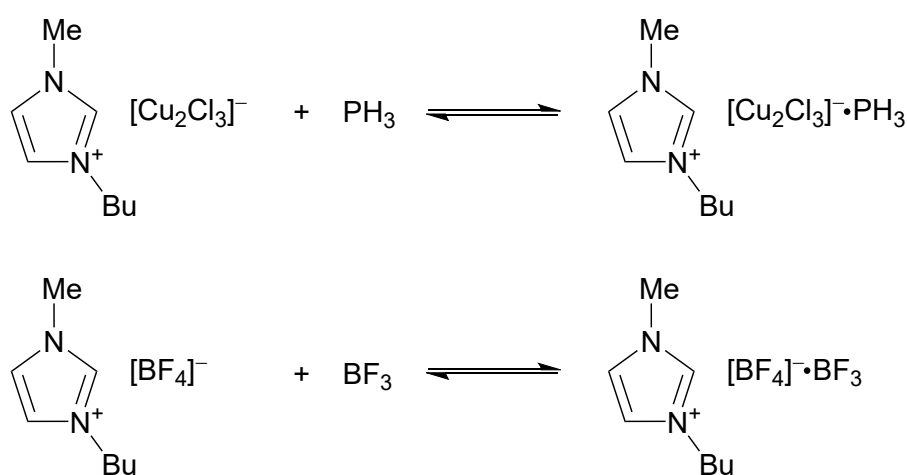
Scheme 9. Synthesis of dialkoxyphenylphosphines by the BASIL process. R = alkyl.

The chlorination of alcohols is industrially performed using reagents such as phosgene, SOCl_2 or PCl_3 . In general, HCl would be the most efficient chlorination reagent but cannot always be used due to the formation of side products. For instance, if diols are treated with HCl gas, the main products are usually cyclic or open chain ethers. This can be changed by using imidazolium or pyridinium chloride based ionic liquids as solvents for the reaction resulting in the formation of dichlorinated alkanes as main product. While the diols are soluble in the ionic liquid, the corresponding dichlorinated alkanes are not and therefore form a second phase which can easily be separated. The ionic liquid can be recycled by distilling of the water formed during the reaction.^[148,155]

Due to their large electrochemical window and high conductivity ionic liquids also found many electrochemical applications.^[156-159] For instance, Abbott and co-worker developed a method for the electroplating of chromium from an ionic liquid containing $\text{Cr}(\text{III})$ salts. This

process is superior over previously used aqueous systems as those systems require more toxic Cr(VI) salts and have lower current efficiencies. Additionally, the formation of hydrogen is avoided, when ionic liquids are used as solvents resulting in crack-free, highly corrosion resistant deposits.^[148,159]

The safe storage and transport of toxic, pyrophoric or corrosive gases is very challenging and is ideally realized under low pressure to overcome the risk of a fulminating gas release. Therefore, Tempel and co-worker developed a method to reversibly store PH_3 and BF_3 , which are both important intermediates in the semiconductor industry, within imidazolium based ionic liquids (Scheme 10).^[160] The Lewis base PH_3 forms an acid-base adduct with the Lewis acidic ionic liquid $[\text{BMIM}][\text{Cu}_2\text{Cl}_3]$ which explains its high solubility of 7.6 mol L^{-1} . In the same way, BF_3 can be bound within $[\text{BMIM}][\text{BF}_4]$. Since the reaction energy for the adduct formation is relatively low, the reaction is reversible and the gases can be released by heating or by applying vacuum.^[148,160]



Scheme 10. Storage of BF_3 and PH_3 in ionic liquids.

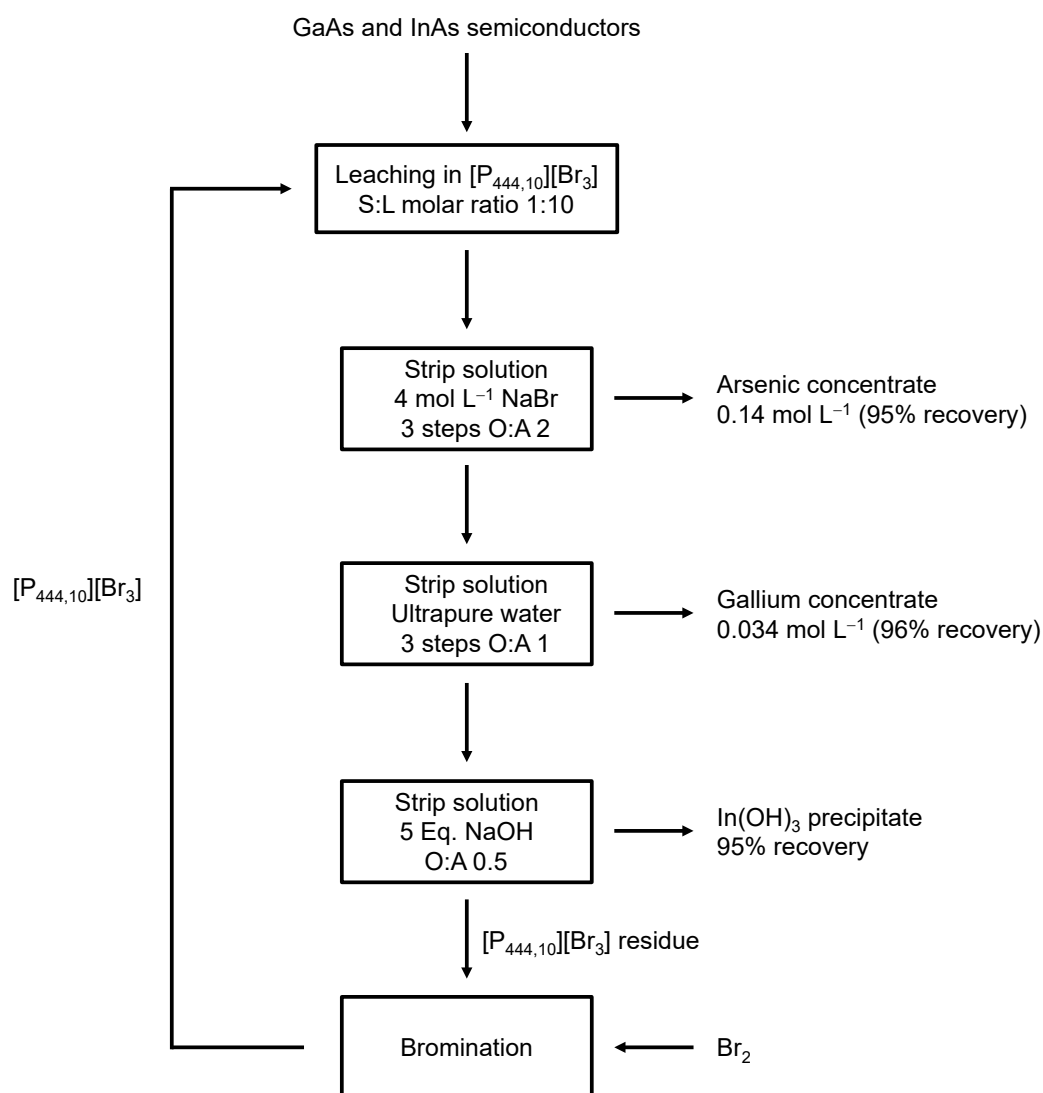
Furthermore, ionic liquids based on polyhalides are an interesting class of compounds which have been used as reactive ILs in metal recycling processes.^[161-167] In 2018, Binnemans and co-worker prepared and characterized a series of ionic liquids with the reactive $[\text{Cl}_3]^-$ anion and tested their oxidation properties by dissolving a total of eight metals (Fe, Cu, In, Zn, Ga, Au, Ge, Sb) as well as two alloys (InAs, GaAs) (Figure 16).^[161]



Figure 16. Metals and Alloys dissolved in $[P_{444,14}][Cl_3]$.^[161] $[P_{444,14}]$ = Tributyl-tetradecylphosphonium. Reproduced from Ref. [161] with permission from the Royal Society of Chemistry.

Additionally, they tested other polyhalide and polyinterhalide based ionic liquids ($[P_{444,10}][An]$, $An = [Cl_3]^-$, $[Br_3]^-$, $[I_3]^-$, $[BrCl_2]^-$, $[ClBr_2]^-$, $[IBr_2]^-$, $[BrI_2]^-$) and observed that all of them are able to dissolve copper. Hence, they concluded that the properties of these reactive ILs can be tailored for specific tasks by the choice of the anion.^[165] For instance, polychlorides are prepared using Cl_2 , which is the cheapest halogen, and have the highest oxidation potential^[168] while the $[I_3]^-$ based ILs are the safest to use since iodine is less volatile. Based on this initial results, processes for the metal recovery from phased out magnets,^[162,167] semiconductors and LEDs^[164] as well as automotive catalysts^[163] have been developed.

Metal recycling is of major importance since it can lower the supply risk as well as reduce environmental issues during mining.^[169] Therefore, Binnemans and co-worker developed also a procedure for the recycling of gallium, indium and arsenic from semiconductors and LEDs by oxidative leaching of those elements using $[P_{444,10}][Br_3]$ and successive stripping using NaBr solutions for As, water for Ga and NaOH solutions for In. The residue $[P_{444,10}][Br_3]$ can be regenerated by treatment with Br_2 resulting in a closed cycle recycling process (Scheme 11).^[164]



Scheme 11. Proposed flowsheet for the recycling of As, Ga and In from semiconductors.^[164] $[P_{444,10}]^+$ = tributyldecylphosphonium. Reproduced from Ref. [164] with permission from the American Chemical Society.

Additionally, procedures for the recycling of SmCo and NdFeB magnets by dissolving them in $[P_{666,14}][Cl_3]$ and a method for the selective leaching of palladium from automotive catalysts have been developed.^[162,163,167] Chu and co-worker showed that polychloride based ionic liquids can also be used to separated uranium from other lanthanides by the selective crystallization of $[BMIM]_2[UO_2Cl_4]$ from a mixture of dissolved uranium and lanthanide oxides in $[BMIM][Tf_2N]$ and $[BMIM][Cl_3]$.^[166]

Besides their application as useful reagents in organic chemistry and as reactive ionic liquids, polyhalides also show some useful electrochemical properties, which lead to some technical applications. For instance, the conductivity of ionic liquids based on polyhalides anions is surprisingly high being sometimes three orders of magnitude larger compared to the corresponding halide salt (conductivity $[HMIM][Br(Br_2)_4] = 52.1 \text{ mS cm}^{-1}$,

[HMIM]Br) = $54.1 \mu\text{S cm}^{-1}$).^[170] This was explained by a Grotthuss-type hopping mechanism.^[171] Additionally, organic bromide salts are used as complexing agents in zinc bromine redox flow batteries. They bind bromine forming polybromide ionic liquids which are insoluble in the aqueous electrolyte yielding an emulsion. The formation of the polybromide results in a reduced vapor pressure, less corrosion as well as an increased coulombic efficiency.^[172] More recent studies showed that the polybromide ionic liquid not only acts as a complexing agent but also plays a vital role in the electro-oxidation of Br^- .^[173] Another example for application of polyhalides is the use of $[\text{I}_3]^-$ in dye-sensitized solar cells. The $\text{I}^-/[\text{I}_3]^-$ redox couple is used as a redox mediator due to its good solubility, suitable redox potential, rapid dye regeneration as well as a slow recombination kinetics with the electrons of the TiO_2 electrode.^[174] The $\text{Br}^-/[\text{Br}_3]^-$ redox couple can also be used and shows a higher open-circuit photovoltage as well as a higher energy conversion efficiency while the more corrosive nature of Br_2 , compared to I_2 , is problematic.^[175–177]

In several previously mentioned chlorination reactions, HCl is formed as a byproduct. This leads to a class of compounds closely related to polyhalides, the poly(hydrogen halide) halogenides ($-\text{I}$) which can be described as anions containing a halide ion bonded to hydrogen halide molecules by strong hydrogen bonding interactions with the formula $[\text{X}(\text{HX})_n]^-$ ($\text{X}=\text{F}, \text{Cl}, \text{Br}, \text{I}$). These species are of interest as they might be suitable replacements for the neat hydrogen halides similar to polyhalides being substitutes for the neat halogens.

1.3 Poly(hydrogen halide) Halogenates (-I)

The bifluoride ion, $[\text{FHF}]^-$, as well as $\text{NEt}_3 \cdot 3\text{HF}$ and $[\text{C}_5\text{H}_5\text{NH}][\text{F}(\text{HF})_n]$ (Olah reagent) are the most prominent examples for poly(hydrogen halide) halogenides (-I). $[\text{FHF}]^-$ has the highest hydrogen bond energy of 160 kJ mol^{-1} ^[178] and shows some promising applications for example as efficient catalyst in the evolving field of sulfur(VI) fluoride exchange (SuFEx) reactions^[179] while $\text{NEt}_3 \cdot 3\text{HF}$ and $[\text{C}_5\text{H}_5\text{NH}][\text{F}(\text{HF})_n]$ are convenient fluorination reagents in organic chemistry which can replace highly toxic anhydrous HF.^[180-184] Many other examples of $[\text{X}(\text{HX})_n]^-$ are known in the literature and their structural characterizations as well as further applications will be presented in the following chapter.

1.3.1 Synthesis and Structural Characterization of $[\text{X}(\text{HX})_n]^-$ Anion

In general, poly(hydrogen halide) halogenides (-I) can be prepared using three different synthetic routes (Scheme 12).^[185-192] As all hydrogen halides are strong acids, they can protonate suitable bases like pyridine, tertiary amines or dimethyl sulfide forming salts of the type $[\text{BH}][\text{X}(\text{HX})_{n-1}]$. Within these salts, strong interactions between the cation and the anion are observed in the solid state since protonated bases are often strong hydrogen bond donors as well.^[186,187] To obtain poly(hydrogen halide) halogenides (-I) with less coordinating cations also halide salts can directly be treated with halogen halides to give salts of the type $[\text{Cat}][\text{X}(\text{HX})_n]$. As many organic fluoride salts are unstable due to the high basicity of the naked fluoride^[193], another approach was developed for the synthesis of $[\text{Cat}][\text{F}(\text{HF})_n]$. When a chloride salt is treated with HF, HCl is formed in an equilibrium reaction. The HCl can be removed from the equilibrium by purging the reaction mixture with nitrogen, since HCl is more volatile than HF, yielding the desired species $[\text{Cat}][\text{F}(\text{HF})_n]$.^[192]



Scheme 12. Synthetic routes for the preparation of poly(hydrogen halide) halogenates. B = base, Cat = Cation.

While for the $[\text{FHF}]^-$ anion many molecular structures in the solid state are known,^[194-198] larger poly(hydrogen fluoride) fluorates ($-I$) ($[\text{F}(\text{HF})_n]^-$ ($n = 2-6$)) were mainly prepared and structurally characterized by the group of Mootz. They obtained single crystals suitable for X-ray diffraction of $[\text{Cat}][\text{F}(\text{HF})_n]$ ($[\text{Cat}] = [\text{NEt}_3\text{H}]^+$ ($n = 2, 3$),^[190] $[\text{NMe}_3\text{H}]^+$ ($n = 2, 3, 4, 6$),^[190] $[\text{NMe}_4]^+$ ($n = 2, 3, 5$),^[185] NO ($n = 4, 5$)^[189] and $[\text{C}_5\text{H}_5\text{NH}]^+$ ($n = 5$)^[190]) using a miniature zone-melting technique with focused head ration. For $[\text{F}(\text{HF})_2]^-$ and $[\text{F}(\text{HF})_3]^-$, the structure of the anion in the obtained salts can be described as a central fluoride which is coordinated by two (V-shaped, Figure 17 left) or three (trigonal pyramidal or trigonal planar) HF molecules. On the other hand, the structures of poly(hydrogen fluoride) fluorates ($-I$) with higher HF content are more complex. In the compound $[\text{NO}][\text{F}(\text{HF})_4]$, the anion has a tetrahedral geometry with four HF molecules bound to the central fluoride while the anion in $[\text{NMe}_3\text{H}][\text{F}(\text{HF})_4]$ is better described as a $[\text{FHF}]^-$ which is further coordinated by three additional HF molecules (two on one side and one on the other). For a $\text{F}^-:\text{HF}$ ratio of 1:5, also two isomers were observed which can either be described as a $[\text{FHF}]^-$ coordinated by four HF molecules (two on each side, $[\text{Cat}] = [\text{NMe}_4]^+$) or as a $[\text{F}(\text{HF})_3]^-$ unit which has an additional HF molecules attached to two of the three HF ligands ($[\text{Cat}] = [\text{C}_5\text{H}_5\text{NH}]^+$, Figure 17 right). The poly(hydrogen fluoride) fluorate with the highest HF content crystallographically characterized, is $[\text{NMe}_3\text{H}][\text{F}(\text{HF})_6]$. It is best described as a $[\text{F}(\text{HF})_3]^-$ unit where an additional HF molecule is bound to every HF ligand.

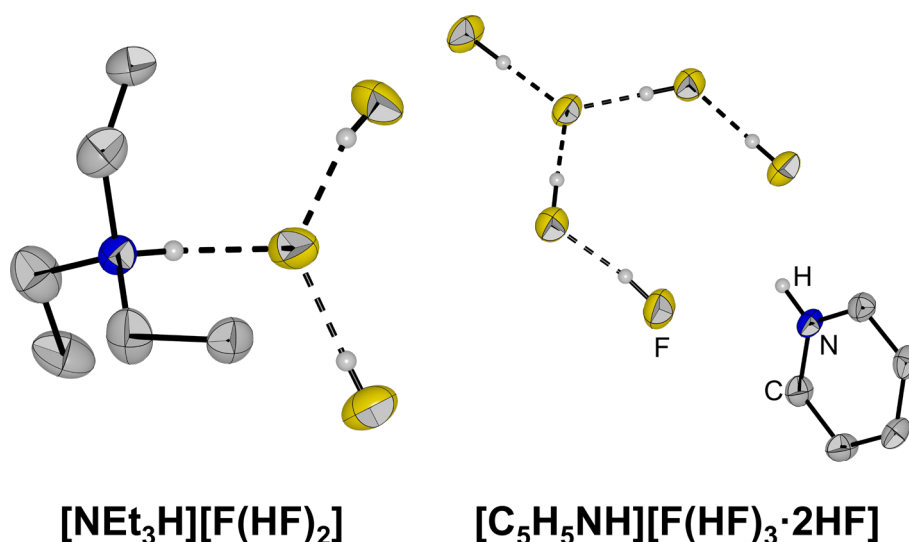


Figure 17. Molecular structure in the solid state of $[\text{NEt}_3\text{H}][\text{F}(\text{HF})_2]$ ($\text{NEt}_3 \cdot 3\text{HF}$) and $[\text{C}_5\text{H}_5\text{NH}][\text{F}(\text{HF})_3 \cdot 2\text{HF}]$ (Olah reagent).^[190] Hydrogen atoms bound to carbon are omitted for clarity.

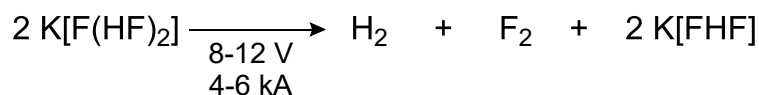
For the class of poly(hydrogen chloride) chlorates ($[\text{Cl}(\text{HCl})_n]^-$), anions with $n = 1 - 5$ have been structurally characterized. The bichloride ion $[\text{ClHCl}]^-$, which is the most stable among them^[194], can be obtained by, e.g., treating pyridine with two equivalents of HCl .^[188] A V-shaped $[\text{Cl}(\text{HCl})_2]^-$ anion was observed in the structure of adamantylideneadamantanechloronium di(hydrogen chloride) chlorate ($-\text{I}$).^[199] Additionally, it was found that the compound $[\text{C}_5\text{H}_5\text{NH}]_2[\text{Cl}(\text{HCl})_2][\text{Cl}(\text{HCl})_4]$ contains a $[\text{Cl}(\text{HCl})_2]^-$ unit which strongly interacts with two pyridinium cations as well as an isolated $[\text{Cl}(\text{HCl})_4]^-$ anion yielding a distorted tetrahedral coordination geometry for both Cl^- ions in this structure.^[188] The salt $[\text{SMe}_2\text{H}][\text{Cl}(\text{HCl})_3]$ contains a trigonal pyramidal $[\text{Cl}(\text{HCl})_3]^-$ anion which strongly interacts with the cation also yielding a tetrahedral geometry for the central chloride ion.^[187] A $[\text{Cl}(\text{HCl})_4]^-$ anion was observed in $[\text{SMe}_2\text{H}][\text{Cl}(\text{HCl})_4]$ ^[187] where the central chloride is coordinated by four HCl units and one cation in a tetragonal pyramidal way. In contrast, in the compound $[\text{NMe}_3\text{H}][\text{Cl}(\text{HCl})_4]$ the $[\text{Cl}(\text{HCl})_4]^-$ anion possesses a trigonal bipyramidal structure.^[186] An octahedral coordination of the chloride anions was observed in the species $[\text{C}_5\text{H}_5\text{NH}]_2[\text{Cl}(\text{HCl})_5]$ which is the largest known poly(hydrogen chloride) chlorate.^[188]

The polarization of the H-X bond is decreasing when going from iodine to fluorine which leads to weaker hydrogen bonding interactions. This is likely the reason why for the heavier homologues only $[\text{BrHBr}]^-$ ^[200] and $[\text{Br}(\text{HBr})_2]^-$ ^[201] have been structurally characterized while for $[\text{IHI}]^-$ no molecular structure is reported in the literature so far.

Since many poly(hydrogen halide) halogenates, commonly used as reagents, are liquids at room temperature,^[180,191] their behavior in the liquid form as well as in solution is of interest. Campbell and Johnson performed NMR experiments with neat [Im][Cl(HCl)_n] ([Im]⁺ = 1-ethyl-3-methyl-1H-imidazolium, *n* = 0 – 2) at room temperature. They only observed one broad signal for the [Cl(HCl)_n]⁻ anions in the ¹H NMR which shifts to higher field when the HCl contented increases. This is rationalized by a fast equilibrium between different [Cl(HCl)_n]⁻ ions in solution.^[202] Low temperature NMR experiments at 110 to 150 K on the [F(HF)_n]⁻ systems confirm this assumption as signals belonging to [F(HF)_n]⁻ (*n* = 2 - 4) were detected in the ¹H NMR spectra of a 1:2 mixture of [NBu₄]F and HF.^[203]

1.3.2 Applications of Poly(hydrogen halide) Halogenates (-I)

Poly(hydrogen halide) halogenates are often used as easy to handle replacements for the gaseous, corrosive and toxic hydrogen halides which sometimes even have improved properties. For instance, the industrial production of elemental fluorine relies on the electrolysis of K[F(HF)₂] at temperatures between 70 and 130 °C, the so-called middle-temperature method, to avoid the low conductivity of anhydrous HF (Scheme 13).^[204,205]

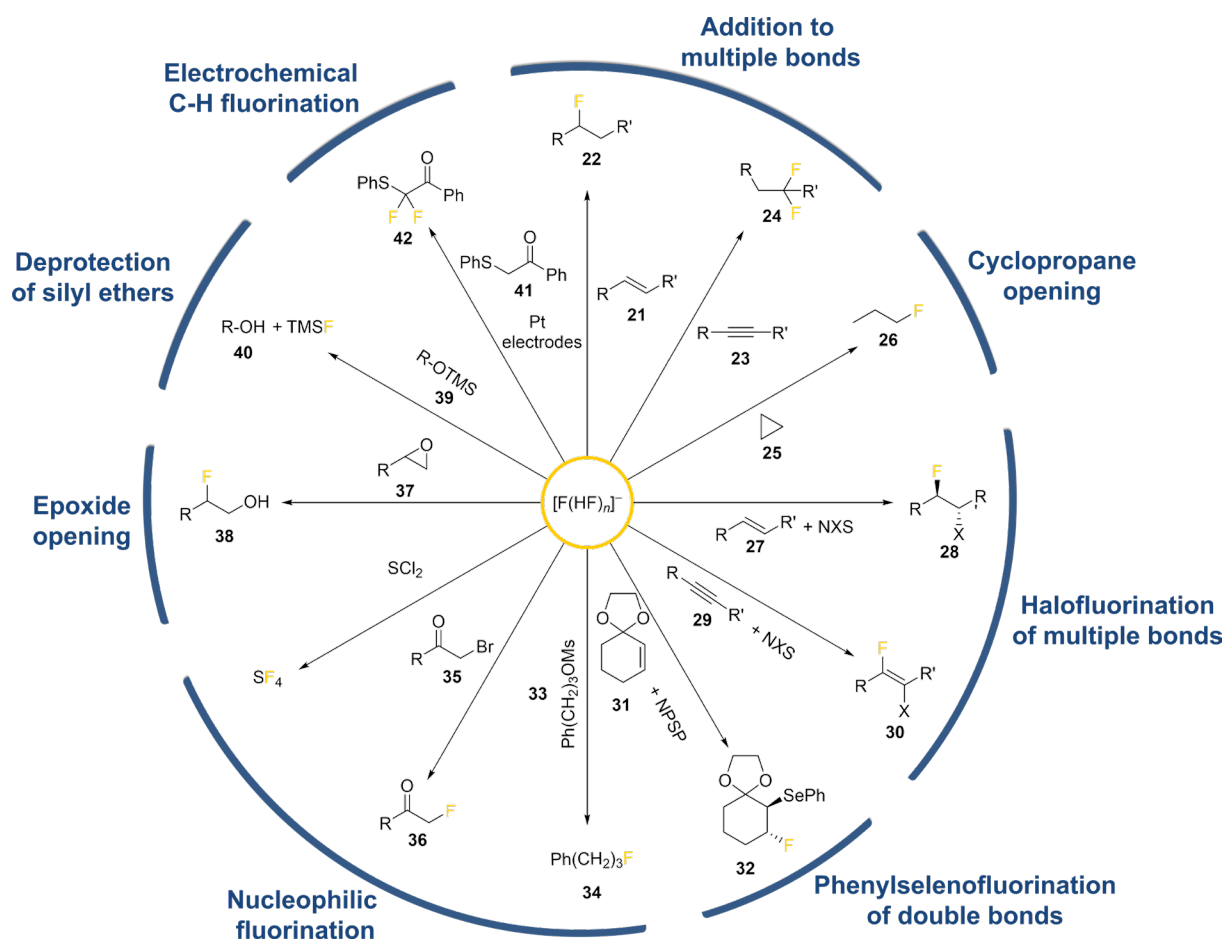


Scheme 13. Synthesis of F₂ by electrolysis of K[F(HF)₂].

Additionally, many nucleophilic fluorination reagents based on [F(HF)_n]⁻ were developed and have been used in a variety of reactions.^[180,182–184,192] Olah's reagent, which is a complex of pyridine with 9 HF molecules (70% HF by weight), was the first example described in the literature.^[182–184] This mixture is strongly acidic and etches glass but has a significantly lower vapor pressure compared to anhydrous HF which makes it much safer and easier to handle.^[205] Over time, other reagents with lower HF content like NEt₃·3HF have been developed.^[180,205] These reagents are less acidic and can also be handled in glass even at elevated temperatures. More recently, ionic liquids containing [F(HF)_n]⁻ anions and larger, organic cations like [EMIM]⁺ (EMIM = 1-ethyl-3-methylimidazolium) have been described.^[192] The advantage of these systems is their immiscibility with organic solvent and thus they can be used in

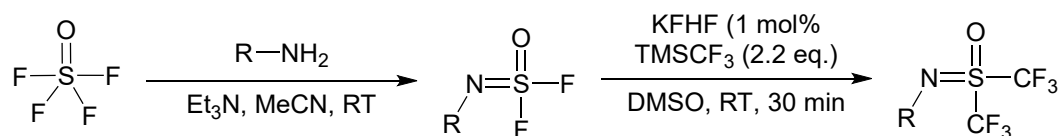
a biphasic fluorination reaction not requiring an aqueous work-up. Therefore the fluorinated product can be separated by decantation of the organic phase while the ionic liquid can be recycled in further reactions.^[192]

Poly(hydrogen fluoride) fluorate based reagents are mostly used to generate carbon fluorine bonds (Scheme 14). They react with alkanes **21** yielding the Markovnikov addition products **22** while reactions with alkynes **23** yield 1,1-difluorinated compounds **24**.^[182,206] Additionally, they react with cyclopropane **25** to the corresponding 1-fluoropropane **26**.^[182] When alkanes **27** or alkynes **29** are treated with $[F(HF)_n]^-$ in the presence of electrophilic sources of halogens (NXS = *N*-Chloro/Bromo/Iodosuccinimide) the halofluorination products **28** or **30** are obtained.^[181,183,192,206] Additionally, protected α,β -unsaturated carbonyls **31** can be reacted with *N*-(phenylseleno)phtalimide) (NPSP) and $[F(HF)_n]^-$ yielding the phenylselenofluorination product **32**.^[206] Poly(hydrogen fluoride) fluorates can also act as a fluoride source allowing the substitution of labile leaving groups. For instance, alkyl methanesulfonates **33** and α -bromo ketones **35** can be treated with $NEt_3 \cdot 2HF$ yielding the alkyl fluorides **34** and the α -fluoro ketones **36**.^[180,207] Vayron and co-worker observed that the nucleophilicity of $NEt_3 \cdot 3HF$ can be enhanced by adding NEt_3 , likely due to a reduced stabilization of the F^- ion by hydrogen bonding interactions.^[207] While $K[HF_2]$ is used for the synthesis of organotrifluoroborates (RBF_3K)^[208], which are convenient precursors for Suzuki-Miyaura type coupling reactions since they are stable, can easily be purified and withstand many reaction conditions,^[209] $[F(HF)_n]^-$ can also be applied in the synthesis of inorganic, fluorinated compounds. For example, Franz described an efficient synthesis of SF_4 starting from SCl_2 and $NEt_3 \cdot 3HF$.^[180] Furthermore, epoxides **37** can be opened using poly(hydrogen fluoride) fluorate giving 1,2 fluoro alcohols **38**^[192] and, due to the strong Si-F bond, the $[F(HF)_n]^-$ anion can also be used as a mild reagent for the deprotection of silyl ethers **39** yielding the free alcohol **40** and TMSF.^[192] At last, Poly(hydrogen fluoride) fluorates have been used in the electrochemical fluorination of activated C-H bonds, e.g., for the conversion of thioether **41** to difluoro-thioether **42**.^[210]



Scheme 14. Overview of the reactivity of $[F(HF)_n]^-$ with various substrates. R = alkyl or aryl; X = Cl, Br, I; NXS = N-chloro/bromo/iodosuccinimide, NPSP = N-(phenylseleno)phtalimide).

Beside its applications as fluorination reagent, the $[F(HF)_n]^-$ anion has also been used as a highly efficient catalyst in sulfur(VI) fluoride exchange (SuFEx) reactions. Sharpless and co-worker revisited the field of SuFEx reactions in 2014 and described them as new kind of “click chemistry”.^[211] This type of reaction can be used in the synthesis of pharmaceutically important triflones and bis(trifluoromethyl)sulfur oxyimines (Scheme 15)^[212] as well as in the synthesis of polysulfates and sulfonates.^[179]



Scheme 15. Bifluoride catalyzed trifluoromethylation using a SuFEx reaction.^[212]

While many applications are known for the $[F(HF)_n]^-$ anions, the heavier poly(hydrogen halide) halogenates are mostly of academic interest as examples for strongly hydrogen bonded systems. Their only application described in the literature is the use of $[Hmim][Br(HBr)_n]$ for the cleavage of ethers.^[213]

2. Objective

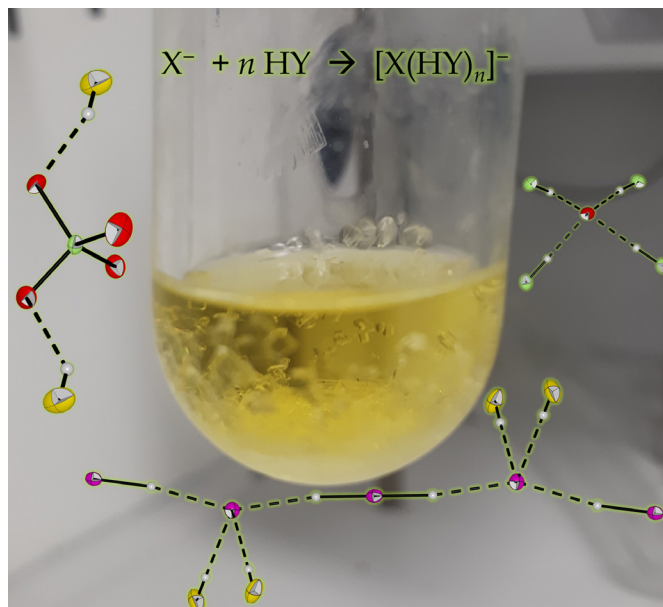
Polyhalides and poly(hydrogen halide) halogenates are structural diverse classes of compounds and many examples are already known for a long time. However, there are only a few poly(hydrogen halide) halogenates containing two different halogen atoms known. These compounds are of interest to investigate and thus to understand the hydrogen bonding properties of the different halide ions. Therefore the first objective of this work was to synthesize and characterize poly(hydrogen halide) halogenates of the type $[X(HY)_n]^-$. Additionally, the structural diversity of polychlorides is significantly lower compared to their heavier homologues while no examples of anions of the type $[Cl(Cl_2)_n(HX)_m]^-$ are known. Thus, different approaches for the synthesis of polychlorides and $[Cl(Cl_2)_n(HX)_m]^-$ anions should be explored in this work.

Besides their structural characterization, polychlorides have already been applied as reagents in organic synthesis to replace elemental chlorine. The storage, transportation and handling of elemental chlorine is challenging due to its toxicity and corrosiveness. Therefore, the second objective of this work was to screen various chloride salts towards their capability to act as chlorine storage medium. The chlorine storage medium should have a high storage capacity, a high long-term stability and needs to be accessible from cheap raw materials. Additionally, efficient ways for releasing the chlorine from the storage media needs to be found.

Within polychlorides, the Cl-Cl bond is weakened due to charge transfer into the σ^* orbital which might result in an enhanced reactivity. In accordance with this, the third objective of this work was to further explore the reactivity of polychlorides and compare it to the reactivity of elemental chlorine. The reaction of polychlorides with CO is of major interest as phosgene is an important intermediate chemical of the chlorine industry. Moreover, polychloride salts could be used for the synthesis of unprecedented chlorinated anions. The $[SCl_6]^{2-}$ ion is not known to the literature even though the heavier homologues $[SeCl_6]^{2-}$ and $[TeCl_6]^{2-}$ have been prepared a long time ago. This type of anions are of interest as they belong to the class of 14 valance electron (VE) systems which have structures sometimes differing from the structures predicted by the VSEPR model. A structural characterization of the $[SCl_6]^{2-}$ dianion would be the first example for a 14 VE system from the third period and the first example of a chlorosulfate anion at all.

3. Publications

3.1 Synthesis and Characterization of Poly(hydrogen halide) Halogenates (-I)



Patrick Voßnacker, Simon Steinhauer, Julia Bader, Sebastian Riedel*

Chem. Eur. J. **2020**, *26*, 13256.

<https://doi.org/10.1002/chem.202001864>

© 2020 Wiley-VCH Verlag GmbH. This is an open-access article distributed under the terms of the [Creative Commons Attribute 4.0 International license](https://creativecommons.org/licenses/by/4.0/).

Author contributions

Patrick Voßnacker designed the project, performed the experiments and wrote the manuscript. Simon Steinhauer performed the XRD measurements, provided scientific guidance, and revised the manuscript. Julia Bader revised the manuscript. Sebastian Riedel managed the project and revised the manuscript.

■ Poly(hydrogen halide) Halogenates

Synthesis and Characterization of Poly(hydrogen halide) Halogenates (–I)

Patrick Voßnacker, Simon Steinhauer, Julia Bader, and Sebastian Riedel*^[a]

Abstract: Herein, we report the synthesis and characterization of a variety of novel poly(hydrogen halide) halogenates (–I). The bifluoride ion, which is known to have the highest hydrogen bond energy of $\approx 160 \text{ kJ mol}^{-1}$, is the most famous among many examples of $[\text{X}(\text{HX})_n]^-$ anions ($\text{X} = \text{F}, \text{Cl}$) known in the literature. In contrast, little is known about poly(hydrogen halide) halogenates containing two different halogens, $[\text{X}(\text{HY})_n]^-$. In this work we present the synthesis

of anions of the type $[\text{X}(\text{HY})_n]^-$ ($\text{X} = \text{Br}, \text{I}, \text{ClO}_4$; $\text{Y} = \text{Cl}, \text{Br}, \text{CN}$) stabilized by the $[\text{PPh}_4]^+$ and $[\text{PPN}]^+$ cation. The obtained compounds have been characterized by single-crystal X-ray diffraction, Raman spectroscopy and quantum-chemical calculations. In addition, the behavior of halide ions in hydrogen fluoride was investigated by using experimental and quantum-chemical methods in order to gain knowledge on the acidity of hydrogen halides in HF.

Introduction

Polyhalides ($[\text{X}(\text{X}_2)_n]^-$), which are prominent examples for halogen-bonded systems, show a large structural diversity as well as a variety of possible applications.^[1] A related class of compounds, the poly(hydrogen halide) halogenates (–I) ($[\text{X}(\text{HY})_n]^-$), consists of a central halide (X^-) that is coordinated to hydrogen halide molecules (HY). This combination of halide anions with hydrogen halides, which has a large positive charge on the hydrogen atom, yields compounds with quite strong hydrogen-bonding interactions. The most prominent example for this class of compounds, the bifluoride ion $[\text{FHF}]^-$, has the highest known hydrogen bond energy of 160 kJ mol^{-1} .^[2] To gain knowledge on strongly hydrogen-bonded systems, the synthesis of novel compounds containing $[\text{X}(\text{HY})_n]^-$ anions, while X and Y are halogens, is of interest.

Three different synthetic routes have been used to synthesize a variety of different $[\text{X}(\text{HX})_n]^-$ anions (Scheme 1).^[3–9]

Mootz' group prepared and characterized salts containing $[\text{X}(\text{HX})_n]^-$ anions ($\text{X} = \text{F}$ ($n = 1–6$), Cl ($n = 2–5$)). Crystal structures of $[\text{Cat}][\text{F}(\text{HF})_n]$ ($[\text{Cat}] = [\text{NO}]^+$ ($n = 3, 4$),^[8] $[\text{NMe}_3\text{H}]^+$ ($n = 2–6$),^[6] $[\text{NMe}_4]^+$ ($n = 2, 3, 5$)^[3]) as well as $[\text{Cat}][\text{Cl}(\text{HCl})_n]$ ($\text{Cat} = [\text{SMe}_2\text{H}]^+$ ($n = 3, 4$),^[7] $[\text{C}_3\text{H}_5\text{NH}]^+$ ($n = 1, 4, 5$)^[5]) were determined by X-ray

diffraction (XRD) using a miniature zone-melting technique for crystallization. Structures containing a protonated base as a cation, like $[\text{NMe}_3\text{H}]^+$, show strong hydrogen bonding between anion and cation, whereas less coordinating cations, for example, $[\text{NMe}_4]^+$, yield more isolated anions. For the heavier homologues only $[\text{BrHBr}]^{-[10]}$ and $[\text{Br}(\text{HBr})_2]^{-[11]}$ have been characterized by X-ray diffraction while no molecular structure in the solid state is known for $[\text{I}(\text{HI})_n]^-$ anions. The behavior of $[\text{X}(\text{HX})_n]^-$ anions in solution was investigated using NMR spectroscopy by several groups. The group of Limbach performed ^1H and ^{19}F NMR experiments on a 1:2 mixture of $[\text{NBu}_4]\text{F}$ and HF in the temperature range between 110 and 150 K and was able to identify $[\text{F}(\text{HF})_n]^-$ ($n = 1–4$) which coexist in solution.^[12] Campbell and Johnson conducted ^1H NMR experiments on the $[\text{Im}][\text{Cl}(\text{HCl})_n]$ ($[\text{Im}]^+ = 1\text{-ethyl-3-methyl-1H-imidazolium}$) system at room temperature, and only observed one signal, which shifts to a higher field when the concentration of HCl is increased. They explained this finding with a fast equilibrium between different $[\text{Cl}(\text{HCl})_n]^-$ species.^[13] Further studies on the ternary $\text{HCl}:[\text{Im}]\text{Cl}:\text{AlCl}_3$ systems have shown that various species of the type $[\text{X}(\text{HCl})_n]^-$ are present in solution ($\text{X} = \text{Cl}^-$, $[\text{ClHCl}]^-$, $[\text{Cl}(\text{HCl})_2]^-$, $[\text{AlCl}_4]^-$, $[\text{Al}_2\text{Cl}_7]^-$). By changing the ratios between the components solutions with various acidities from weakly acidic solutions (high concentration of $[\text{Im}]\text{Cl}$; $[\text{ClHCl}]^-$ as dominant acidic species) to super-acidic solutions (high concentrations of AlCl_3 ; $[\text{Al}_2\text{Cl}_7]^- \cdot \text{HCl}$ as dominant acidic species)

[a] P. Voßnacker, Dr. S. Steinhauer, Dr. J. Bader, Prof. Dr. S. Riedel
Fachbereich Biologie, Chemie, Pharmazie
Institut für Chemie und Biochemie–Anorganische Chemie
Freie Universität Berlin
Fabeckstrasse 34/36, 14195 Berlin (Germany)
E-mail: s.riedel@fu-berlin.de

Supporting information and the ORCID identification numbers for the authors of this article can be found under:
<https://doi.org/10.1002/chem.202001864>.

© 2020 The Authors. Published by Wiley-VCH GmbH. This is an open access article under the terms of the Creative Commons Attribution License, which permits use, distribution and reproduction in any medium, provided the original work is properly cited.



Scheme 1. Synthetic routes for the synthesis of poly(hydrogen halide) halogenates (–I).

can be obtained.^[14] Electrochemical studies suggests that upon dissolution of HCl in chloride free ionic liquids also $[\text{Cl}(\text{HCl})]^-$ is formed.^[15] Enthalpies, entropies and free energies for the formation of poly(hydrogen halide) halogenates (–I) ($[\text{X}(\text{HY})_{n-1}]^- + \text{HY} \rightarrow [\text{X}(\text{HY})_n]^-$) have been determined using high pressure mass spectrometry. In general, the free energies of formation are highest for the combination of the most basic hydrogen bond acceptor (F^-) with the best hydrogen bond donor (HF). Vice versa, the weakest hydrogen bond is formed by the least basic hydrogen bond acceptor (I^-) with the worst hydrogen bond donor (HI). This tendency is observed for all possible combinations of X and Y.^[16,17]

Poly(hydrogen halide) halogenates (–I), especially $[\text{F}(\text{HF})_n]^-$, show some useful properties which lead to a variety of applications. $[\text{K}(\text{F}(\text{HF})_2)]$ is electrolyzed in the synthesis of elemental fluorine to avoid the low conductivity of anhydrous HF (aHF).^[18] In addition $[\text{Cat}][\text{F}(\text{HF})_n]$ (Cat = for example, $[\text{NET}_3\text{H}]^+$,^[19,20] $[\text{C}_5\text{H}_5\text{NH}]^+$,^[21–23] $[\text{EMIM}]^+$ (1-ethyl-3-methylimidazolium)^[9,11]) have been used as a reagent in organic chemistry which are safer and more convenient to handle when compared to highly toxic anhydrous HF with its boiling point at 19.5 °C. They can be used to perform hydro- and halofluorination reactions as well as epoxide ring openings and deprotection of silyl ethers.^[9,19–23] Recently Sharpless et al. proposed the sulfur(VI) fluoride exchange (SuFEx) as a new kind of “click chemistry”.^[24] Since then, the reaction has been used in the synthesis of pharmaceutically important triflones and bis(trifluoromethyl)sulfur oxyimines^[25] as well as in the synthesis of polysulfates and sulfonates.^[26] For many SuFEx reactions bifluoride anions as well as higher poly(hydrogen fluoride) fluorates (–I) have been tested as catalysts and it was shown that they have a significantly higher activity compared to previously used organosuperbases.^[26]

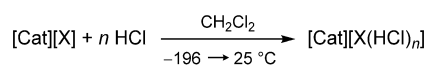
Even though poly(hydrogen halide) halogenates have been studied in detail over the last decades little is known about the $[\text{X}(\text{HY})_n]^-$ anion. In addition the known $[\text{Cl}(\text{HCl})_n]^-$ ($n > 2$) compounds exhibit low melting points and in general a low stability. Therefore, they were only characterized by X-ray diffraction. Herein we present the synthesis of more stable $[\text{Cat}][\text{Cl}(\text{HCl})_4]$ salts (Cat = $[\text{PPN}]^+$ (bis(triphenylphosphoranylidene)iminium), $[\text{PPh}_4]^+$, $[\text{AsPh}_4]^+$) which allow further investigation by low temperature Raman spectroscopy. In addition a variety of $[\text{Cat}][\text{X}(\text{HY})_n]$ ($[\text{Cat}] = [\text{PPh}_4]^+$, $[\text{PPN}]^+$; X = Cl, Br, I, ClO_4 ; Y = F, Cl, Br, CN) compounds were synthesized and characterized by X-ray diffraction and Raman spectroscopy.

Results and Discussion

Tetraphenylphosphonium salts $[\text{PPh}_4][\text{X}(\text{HCl})_4]$

Poly(hydrogen chloride) halogenates (–I) were prepared by condensing stoichiometric amounts of hydrogen chloride onto a dichloromethane solution of the respective halide salts (Scheme 2).

By slowly cooling saturated solutions of the reaction mixture to –40 °C single crystals of the respective poly(hydrogen chloride) halogenate (–I) salts were obtained. The obtained crystals



Scheme 2. Synthesis of poly(hydrogen chloride) halogenates (–I) ($[\text{Cat}] = [\text{PPN}]^+$, $[\text{PPh}_4]^+$; X = Cl, Br, I).

are stable at –40 °C under a hydrogen chloride atmosphere but show a noticeable loss of hydrogen chloride when handled under a nitrogen stream of –40 °C.

Using $[\text{PPh}_4]\text{X}$ (X = Cl, Br, I) as a starting material single crystals of $[\text{PPh}_4][\text{Cl}(\text{HCl})_4]$, $[\text{PPh}_4][\text{Br}(\text{HCl})_4]$ and $[\text{PPh}_4][\text{I}(\text{HCl})_3]$ were obtained by using the method described above. $[\text{PPh}_4][\text{Cl}(\text{HCl})_4]$ and $[\text{PPh}_4][\text{Br}(\text{HCl})_4]$ are isostructural and crystallize in the tetragonal space group $P4/n$ while $[\text{PPh}_4][\text{I}(\text{HCl})_3]$ crystallizes in the monoclinic space group $P2_1/c$ (Figure 1)

Since the position of hydrogen atoms cannot be determined accurately by XRD only halogen–halogen distances will be discussed. $[\text{Cl}(\text{HCl})_4]^-$ as well as $[\text{Br}(\text{HCl})_4]^-$ show a square pyramidal structure with $R(\text{Cl}–\text{Cl}) = 340.1(1)$ pm and $R(\text{Br}–\text{Cl}) = 353.4(1)$ pm. Those values are in good agreement with the halogen–halogen distances from quantum-chemical calculations in the gas phase on the B3LYP(D3BJ)/def2-TZVPP (SCS-MP2/def2-TZVPP) level of theory ($R(\text{Cl}–\text{Cl}) = 341.1$ pm (342.0 pm) and $R(\text{Cl}–\text{Br}) = 358.1$ pm (358.5 pm)). The observed increase of the halogen–halogen distance going from $[\text{Cl}(\text{HCl})_4]^-$ to $[\text{Br}(\text{HCl})_4]^-$ also correlates well with the increase in ion radii when going from chlorine to bromine ($\Delta R_{\text{ion}}(\text{Br}, \text{Cl}) = 13.3$ pm, $\Delta R_{\text{ion}}(\text{Br}, \text{Cl}) = 15$ pm^[27]).

When $[\text{PPh}_4]\text{I}$ is used as starting material the reaction with four equivalents of HCl yields $[\text{PPh}_4][\text{I}(\text{HCl})_3]$. $[\text{PPh}_4][\text{I}(\text{HCl})_4]$ could not be obtained with this cation even when higher amounts of HCl were used. Quantum-chemical calculations on the B3LYP(D3BJ)/def2-TZVPP (SCS-MP2/def2-TZVPP) level of theory show that the addition of the fourth HCl molecule to $[\text{I}(\text{HCl})_3]^-$ is only by –8.8 (–4.5) kJ mol^{-1} exergonic in the gas phase. In comparison the formation of $[\text{Cl}(\text{HCl})_4]^-$ (–13.6 (–8.8) kJ mol^{-1}) and $[\text{Br}(\text{HCl})_4]^-$ (–11.6 (–8.4) kJ mol^{-1}) is more favored. Free reaction energies were calculated for the formation of the most favorable geometry which is a tetrahedral structure for all $[\text{X}(\text{HCl})_4]^-$ anions (Figure 4). These calculations indicate a lower stability of the $[\text{I}(\text{HCl})_4]^-$ anion which might explain why it could not be isolated as a $[\text{PPh}_4]^+$ salt. The $[\text{I}(\text{HCl})_3]^-$ anion shows a distorted trigonal pyramidal structure with $R(\text{I}–\text{Cl}) = 374.1(1)–377.2(1)$ pm that are in good agreement

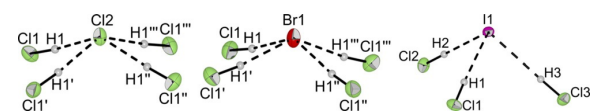


Figure 1. Molecular structure of the anions in $[\text{PPh}_4][\text{Cl}(\text{HCl})_4]$, $[\text{PPh}_4][\text{Br}(\text{HCl})_4]$ and $[\text{PPh}_4][\text{I}(\text{HCl})_3]$ in the solid state with thermal ellipsoids shown at 50% probability. Cations and disordered atoms have been omitted for clarity (see Figures S1–S3 for representations including cations and disordered atoms). Selected interatomic distances [pm]: Cl1–Cl2 340.1(1), Cl1–Cl2–Cl1' 144.3(1), Cl1–Br1 353.4(1), Cl1–Br1–Cl1'' 145.1(1), Cl1–I1 374.1(1), Cl2–I1 374.1(1), Cl3–I1 377.2(1), Cl1–I1–Cl3 70.7(1), Cl1–I1–Cl2 89.1(1), Cl2–I1–Cl3 113.0(1).

with the values obtained from quantum-chemical calculations of $R(\text{I}–\text{Cl}) = 375.8 \text{ pm}$ (377.9 pm).

The most important contributions to the binding energy for strong hydrogen bonding are charge transfer, electrostatic and Pauli repulsion. For hydrogen bonding between halide ions and hydrogen halides the charge transfer contribution can be described as a donation of electron density from the lone pair of the halide ion into the σ^* orbital of the HX bond. The partial occupation of the σ^* orbital leads to a weakening of the HX bond. This results in an increase of the H–X distance as well as a shift of the H–X stretching frequency to lower wavenumbers which can be observed in the Raman spectrum.^[28] The experimental Raman spectra recorded at -196°C as well as the calculated spectra (B3LYP/def2-TZVPP and MP2/def2-TZVPP) of $[\text{PPh}_4][\text{Cl}(\text{HCl})_4]^-$, $[\text{PPh}_4][\text{Br}(\text{HCl})_4]^-$ and $[\text{PPh}_4][\text{I}(\text{HCl})_3]^-$ are shown in Figure 2. For the C_{4v} symmetric $[\text{Cl}(\text{HCl})_4]^-$ and $[\text{Br}(\text{HCl})_4]^-$ anions three H–Cl stretching modes are expected (A_1 , B_2 , E). In the experimental spectra, two bands are observed. The bands at 2517 cm^{-1} ($[\text{Br}(\text{HCl})_4]^-$) and 2523 cm^{-1} ($[\text{Cl}(\text{HCl})_4]^-$) can be assigned to the symmetric stretching mode of the HCl molecules (A_1) while the bands at 2370 cm^{-1} ($[\text{Br}(\text{HCl})_4]^-$) and 2318 cm^{-1} ($[\text{Cl}(\text{HCl})_4]^-$) can be assigned to one antisymmetric H–Cl stretching mode (B_1). The second antisymmetric stretching mode (E) is calculated to have a significantly lower intensity and to be in close proximity to the B_1 symmetric stretching mode. This might explain why only one band is visible for the antisymmetric stretching modes. In general the calculated spectra on the B3LYP(D3BJ) level of theory agree well with the experimental ones even though the calculation predicts the symmetric and asymmetric stretching bands to be closer together. As known for calculations at the MP2 level of theory, the HCl bond strength is overestimated and therefore the calculated wavenumbers for the HCl stretching vibration are significantly too high.

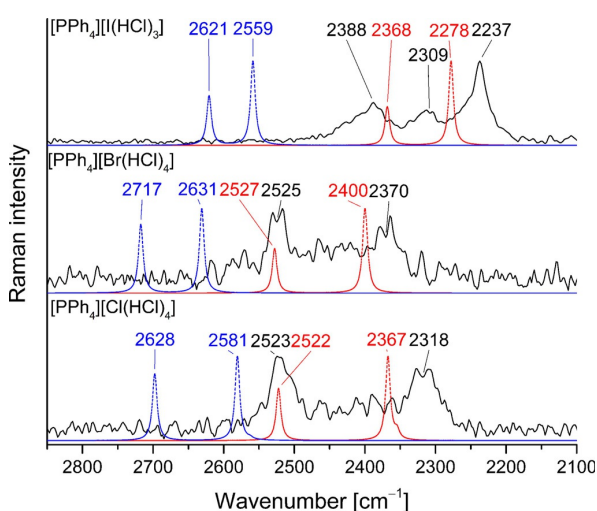


Figure 2. Raman spectra of single crystals of $[\text{PPh}_4][\text{X}(\text{HCl})_n]^-$ recorded at -196°C (black) as well as calculated gas phase spectra (B3LYP/def2-TZVPP (red) and MP2/def2-TZVPP (blue)) of $[\text{X}(\text{HCl})_n]^-$ ($n = 4$ for $\text{X} = \text{Cl}, \text{Br}$ and $n = 3$ for $\text{X} = \text{I}$).

For $[\text{PPh}_4][\text{I}(\text{HCl})_3]^-$ three bands at $2390, 2312, 2237 \text{ cm}^{-1}$ are observed in the H–Cl stretching region. This can be explained by a reduced symmetry of the $[\text{I}(\text{HCl})_3]^-$ anion within the crystal when compared to the C_{3v} symmetric optimized gas-phase structure. Therefore the degeneracy of the asymmetric stretching mode (E) is removed and the three crystallographically independent HCl molecules in the crystal and contribute each, one band in the vibrational spectrum. The experimental spectra again agree well with the calculated spectra on the B3LYP level of theory.

All observed bands are significantly shifted to lower wavenumbers compared to crystalline HCl at 2705 and 2748 cm^{-1} (measured at -196°C)^[29] which indicates hydrogen bond interactions. Three major trends can be emphasized in the recorded Raman spectra:

- 1) The splitting between the symmetric and asymmetric stretching modes is larger for $[\text{Cl}(\text{HCl})_4]^-$ compared to $[\text{Br}(\text{HCl})_4]^-$. This tendency is observed in the experiment as well as in the calculations.
- 2) The average wavenumber for the H–Cl stretching is lower for $[\text{Cl}(\text{HCl})_4]^-$ compared to $[\text{Br}(\text{HCl})_4]^-$. This is expected since chloride is the stronger base and can donate more electron density into the LUMO of the H–Cl bond. Quantum-chemical calculations (B3LYP(D3BJ)/def2-TZVPP (SCS-MP2/def2-TZVPP)) show a decrease of the H–Cl bond length from 132.3 pm (130.3 pm) for $[\text{Cl}(\text{HCl})_4]^-$ to 132.0 pm (130.0 pm) for $[\text{Br}(\text{HCl})_4]^-$ which matches the observed shift of the H–Cl stretching vibration.
- 3) For $[\text{I}(\text{HCl})_3]^-$ the shift towards lower wavenumbers is more pronounced compared to the four times coordinated $[\text{Cl}(\text{HCl})_4]^-$ and $[\text{Br}(\text{HCl})_4]^-$. This indicates that the coordination number has a stronger influence on the weakening of the H–Cl bond than the change of the central halide. Quantum-chemical calculations (B3LYP(D3BJ)/def2-TZVPP (SCS-MP2/def2-TZVPP)) predict a shortening of the H–Cl bond by 2.1 pm (1.6 pm ; $\text{X} = \text{Cl}$), 1.7 pm (1.2 pm ; $\text{X} = \text{Br}$) and 1.3 pm (0.9 pm ; $\text{X} = \text{I}$) going from $[\text{X}(\text{HCl})_4]^-$ to $[\text{X}(\text{HCl})_3]^-$ ($\text{X} = \text{Cl}, \text{Br}, \text{I}$). In contrast the difference in the H–Cl bond length is calculated to be 0.3 pm (0.3 pm) between $[\text{Cl}(\text{HCl})_4]^-$ and $[\text{Br}(\text{HCl})_4]^-$ and 0.2 pm (0.4 pm) between $[\text{Br}(\text{HCl})_4]^-$ and $[\text{I}(\text{HCl})_3]^-$. These calculations support the experimental results.

Bis(triphenylphosphoranylidene)iminium salts $[\text{PPN}][\text{X}(\text{HCl})_4]$

The weakly coordinating $[\text{PPN}]^+$ cation has been used to stabilize large anions like $[\text{Cl}_{13}]^-$,^[30] $[\text{Cl}(\text{BrCl})_6]^-$ ^[31] and $[\text{Br}(\text{BrCN})_3]^-$.^[32] Therefore $[\text{PPN}]\text{X}$ was used as a starting material to investigate whether higher coordinated poly(hydrogen halide) halogenates (–I) can be stabilized. Single crystals of $[\text{PPN}][\text{X}(\text{HCl})_4]$ ($\text{X} = \text{Cl}, \text{Br}, \text{I}$) were obtained using the method described above. The three isostructural salts crystallize in the monoclinic space group $C2/c$ (Figure 3).

In contrast to the $[\text{PPh}_4][\text{X}(\text{HCl})_4]$ ($\text{X} = \text{Cl}, \text{Br}$) salts the $[\text{X}(\text{HCl})_4]^-$ ($\text{X} = \text{Cl}, \text{Br}, \text{I}$) anions show a distorted tetrahedral ge-

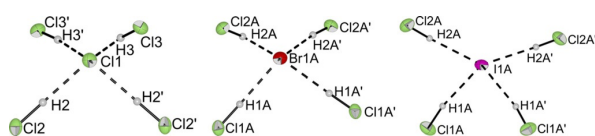


Figure 3. Molecular structure of [PPN][Cl(HCl)₄], [PPN][Br(HCl)₄], and [PPN][I(HCl)₄] in the solid state with thermal ellipsoids shown at 50% probability. Cation and disorders have been omitted for clarity (see Figures S5–S9 for representation including cations and disorders). Selected interatomic distances [pm]: Cl2–Cl1 334.8(1), Cl3–Cl1 341.6(1), Cl1A–Br1A 347.7(1), Cl2A–Br1A 354.0(2), Cl1A–I1A 370.4(2), Cl2A–I1A 374.8(2).

ometry when [PPN]⁺ is used as a cation. The halogen–halogen distances of 334.8(1)–341.6(1) pm (X=Cl), 347.7(1)–354.0(2) pm (X=Br) and 370.4(2)–374.8(2) pm (X=I) are comparable with those obtained for [PPh₄][X(HCl)₄] (X=Cl, Br) and are again in good agreement with the calculated distances. Quantum-chemical calculations show that the tetrahedral structure is the global minimum in the gas phase while the C_{4v} symmetric pyramidal structure is only 3.46 kJ mol^{–1} (for X=I) to 6.03 kJ mol^{–1} (for X=Cl) higher in energy (Figure 4).

The Raman spectra of the single crystals of [PPN][I(HCl)₄] show three bands in the HCl stretching region (2472, 2415, 2301 cm^{–1}, Figure S17). The bands at 2472 and 2415 cm^{–1} are in good agreement with the calculated bands at the B3LYP(D3BJ)/def2-TZVPP level of theory for the [I(HCl)₄][–] anion (Table S33). Within the crystal the position of the [I(HCl)₄][–] anion is sometimes occupied by a [I(HCl)₃][–] anion due to a disorder (ratio [I(HCl)₄][–]/[I(HCl)₃][–] = 78:22; Figure S9). This explains a third broad band at 2301 cm^{–1}. For [PPN][Cl(HCl)₄] and [PPN][Br(HCl)₄] no bands are observed in the HCl stretching region which might be due to the low intensity of these bands (Figure S17).

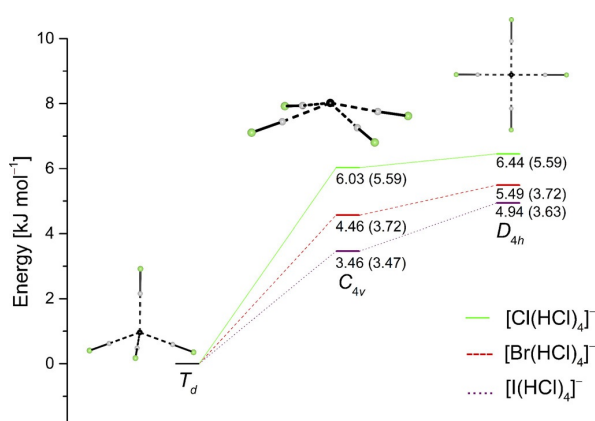


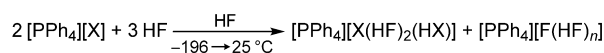
Figure 4. Relative energies of possible geometries for [X(HCl)₄][–] calculated at the B3LYP(D3BJ)/def2-TZVPP (SCS-MP2/def2-TZVPP) level of theory. The pyramidal structures (C_{4v}) are transition states (one imaginary frequency) between tetrahedral structures, while the planar structures (D_{4h}) are saddle points (two imaginary frequencies) at the B3LYP level of theory and either transition states ([Cl(HCl)₄][–]) or minima ([Br(HCl)₄][–], [I(HCl)₄][–]) at the MP2 level of theory.

Halides in aHF

Even though poly(hydrogen fluoride) fluorates (–I) have been extensively characterized and applied in various fields of chemistry^[6,12,20,24] little is known about adducts between the heavier halide ions and HF. Slowly cooling a solution of [PPh₄]⁺X[–] (X=Br, I) in anhydrous HF to –80 °C yields single crystals of [PPh₄][X(HF)₂(HX)] (Scheme 3).

The two isostructural salts crystallize in the monoclinic space group P2₁/n (Figure 5).

Analyzing the molecular structure of [PPh₄][I(HF)₂(HI)] (Figure 5. 1) in detail reveals that there are different possibilities to describe the structure of the anion. The position of H1 can only have an occupation number of 0.5 to obtain an overall neutral compound. Different occupations of the H1 positions lead to two possible descriptions of the anion structure. An alternating occupation of H1 (1: H1, H1'' occupied, H1', H1''' unoccupied) leads to isolated [I(HF)₂(HI)][–] units (2). In comparison, when two neighboring H1 positions are occupied (1: H1, H1' occupied, H1'' and H1''' unoccupied) alternating [I(HF)₂][–] and [I(HF)₂(HI)₂][–] anions are present (3). Vibrational spectroscopy is the method of choice for a further analysis of



Scheme 3. Synthesis of poly(hydrogen fluoride) halogenates (–I) (X=Cl, Br, I).

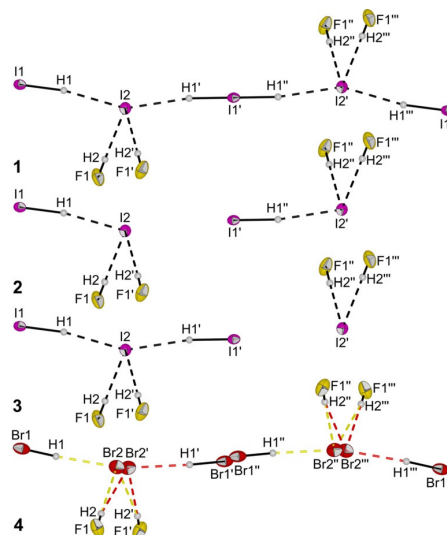
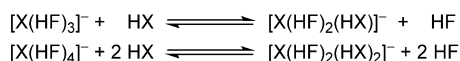


Figure 5. Molecular structure of [PPh₄][I(HF)₂(HI)] (1) and [PPh₄][Br(HF)₂(HBr)] (4) in the solid state with thermal ellipsoids shown at 50% probability. Cations have been omitted for clarity (see Figures S10 and S11 for representation including cations). The positions of Br1, Br2 and H1 (in both structures) have an occupation number of 0.5. Compounds 2 and 3 show two possible descriptions of the anion in [PPh₄][I(HF)₂(HI)] as either isolated [I(HF)₂(HI)][–] anions (2) or alternating [I(HF)₂][–] and [I(HF)₂(HI)₂][–] anions (3). Selected interatomic distances [pm]: Br2–F1 300.0(3), Br2–F1' 320.2(3), Br2–Br1 371.9(3), Br2–Br1' 416.1(3), I1–I2 422.1(1), I2–F1 323.7(2).

the described compound. The Raman spectrum of a single crystal of $[\text{PPh}_4][\text{I}(\text{HF})_2(\text{HI})]$ shows three bands (2017, 1963 and 1904 cm^{-1}) in the region of the HI stretching mode (Figure S18). The position of these bands correlates well with the calculated bands (MP2/def2-TZVPP) for the $[\text{I}(\text{HF})_2(\text{HI})]^-$ anion while the number of bands indicates a mixture of $[\text{I}(\text{HF})_2(\text{HI})]^-$ and $[\text{I}(\text{HF})_2(\text{HI})_2]^-$ anions within the crystal.

$[\text{PPh}_4][\text{Br}(\text{HF})_2(\text{HBr})]$ is isostructural to $[\text{PPh}_4][\text{I}(\text{HF})_2(\text{HI})]$. Besides the occupational disorder of H1, the molecular structure of $[\text{PPh}_4][\text{Br}(\text{HF})_2(\text{HBr})]$ exhibits a positional disorder of Br1 and Br2. The disorder of the bromine atoms results in two symmetry-equivalent, pyramidal anions (Figure 5. 4, red and yellow lines). Due to the disorder of Br2 a $[\text{Br}(\text{HF})_2(\text{HBr})_2]^-$ anion is conceivable which would have two Br-Br distances of $R(\text{Br1}-\text{Br2}) = 371.9(3)\text{ pm}$ and $R(\text{Br2}-\text{Br1}') = 416.1(3)\text{ pm}$ which differ by 45 pm. The calculated (B3LYP(D3BJ)/def2-TZVPP (SCS-MP2/def2-TZVPP)) distances of 358.7 (355.2) pm for $[\text{Br}(\text{HF})_2(\text{HBr})]^-$ and 367.8 (369.5) pm for $[\text{Br}(\text{HF})_2(\text{HBr})_2]^-$ are significantly shorter than the Br2-Br1' distance which might indicate only a weak bonding interaction. Therefore the pyramidal description as $[\text{Br}(\text{HF})_2(\text{HBr})]^-$ anions seems to be more reasonable. Unfortunately, no bands for the HBr stretching modes were observed in the Raman spectrum of $[\text{PPh}_4][\text{Br}(\text{HF})_2(\text{HBr})]$ which might be due to the low Raman intensity of these bands (Figure S20). Therefore, there is no clear evidence whether isolated $[\text{Br}(\text{HF})_2(\text{HBr})]^-$ anions or alternating $[\text{Br}(\text{HF})_2(\text{HBr})_2]^-$ and $[\text{Br}(\text{HF})_2]^-$ units are present within the crystal.

The formation of heteroleptic adducts between halides and halogen halides is unexpected as the hydrogen bond donor strength of the halogen halides decreases from HF to HI due to the decreasing polarization of the HX bond. An adduct between the halide ion and the strongest hydrogen bond donor should be most favorable which should favor the formation of homoleptic complexes. The exchange of one HF against one HX molecule ($X = \text{Cl}, \text{Br}, \text{I}$) was calculated to be 2 to 7 kJ mol^{-1} endergonic for $[\text{X}(\text{HF})_3]^-$ while the exchange of two HF against two HX in $[\text{X}(\text{HF})_4]^-$ was calculated to be 10 to 24 kJ mol^{-1} endergonic (Scheme 4, Table S12 and S13). This indicates that in solution the most stable anions are of the $[\text{X}(\text{HF})_n]^-$ type while the small energy differences between the homoleptic and heteroleptic complexes can be compensated by small interactions within the crystal.



Scheme 4. Equilibrium between the homoleptic $[\text{X}(\text{HF})_n]^-$ and the heteroleptic $[\text{X}(\text{HF})_{n-m}(\text{HX})_m]^-$.

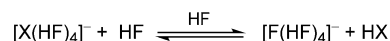
When halide salts are dissolved in aHF there are in general three possible scenarios depending on the relative acidities of the hydrogen halide and HF:

- 1) *HF is a stronger acid than the hydrogen halide:* The halide will be completely protonated forming HX and F^- . Therefore, ions of the type $[\text{F}(\text{HF})_n]^-$ should be the domi-

nant anionic species in solution; HX is also present in solution.

- 2) *HF is a weaker acid than the hydrogen halide:* The halide will not be protonated but solvated by the HF molecules. Ions of the type $[\text{X}(\text{HF})_n]^-$ should be the dominant anionic species in solution; no HX is present.
- 3) *HF and HX in HF have similar acidities:* The halide ion will be partially protonated forming HX and F^- . As a consequence, ions of the type $[\text{X}(\text{HF})_n]^-$ and $[\text{F}(\text{HF})_n]^-$ should be present in solution; HX is present as well.

The obtained molecular structure of $[\text{PPh}_4][\text{X}(\text{HF})_2(\text{HX})]$ ($X = \text{Br}, \text{I}$) indicates that scenario 3 is the preferred one for HBr and HI. To enable the crystallization of $[\text{PPh}_4][\text{X}(\text{HF})_2(\text{HX})]$ ($X = \text{Br}, \text{I}$) sufficient quantities of X^- , HX and HF have to be present in solution. When $[\text{PPh}_4]\text{X}$ and HF are used as starting materials this can only be the case when there is an equilibrium between X^- and HX in solution. Because the concentration of the salt in HF is very large (8 equiv HF per X^-) the influence of the concentration on the equilibrium should be rather small. The formed HX is mostly dissolved in HF and since the reaction is performed in a closed reaction vessel the shift of the equilibrium by removal of HX by evaporation can also be neglected. Therefore, it can be concluded that HBr/HI in aHF should have similar acidities as aHF. To further verify this hypothesis the free reaction energies and equilibrium constants for the protonation reaction of X^- in HF were calculated (Tables S7–S10). Gas-phase calculations on the B3LYP(B3BJ)/def2-TZVPP (SCS-MP2/def2-TZVPP) level of theory predict a free reaction energy of 171.81 (173.96) kJ mol^{-1} ($X = \text{Cl}$) to 266.50 (270.64) kJ mol^{-1} ($X = \text{I}$) for the protonation reaction of X^- with HF (see Table S 9). This large discrepancy from the expected $\approx 0\text{ kJ mol}^{-1}$ for an equilibrium reaction can be explained by not taking solvation into account. The high acidity of aHF results from the high solvation energy of the fluoride ion in HF, which is formed during the protonation reaction. Therefore, a proper consideration of solvation effects is essential for a correct description of this system. The solvation of the molecules was therefore modeled by an explicit calculation of the first solvation shell of the halide ions, which was estimated to consist of four HF molecules, and solvation was additionally treated using the Cosmo model (Scheme 5).



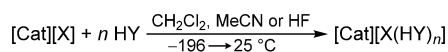
Scheme 5. Equilibrium between solvated X^- and F^- in HF.

Free reaction energies of 3.0 kJ mol^{-1} for $X = \text{Cl}$ ($K_{\text{eq}} = 0.29$, ratio $\text{HCl}/\text{Cl}^- = 0.54$ for $c_0(\text{HF}) = c_0(\text{Cl}^-)$, Scheme S1), 14.8 kJ mol^{-1} for $X = \text{Br}$ ($K_{\text{eq}} = 0.0025$, ratio $\text{HBr}/\text{Br}^- = 0.05$ for $c_0(\text{HF}) = c_0(\text{X}^-)$) and 7.4 kJ mol^{-1} for $X = \text{I}$ ($K_{\text{eq}} = 0.050$, ratio $\text{HI}/\text{I}^- = 0.22$ for $c_0(\text{HF}) = c_0(\text{X}^-)$) have been calculated (SCS-MP2(COSMO)/def2-TZVPP) for the protonation reactions in HF. The calculated free reaction energies are decently close to 0; this supports the thesis that all hydrogen halides have similar

acidities in HF. In addition, the calculated ratios between HX and X^- indicate that in solution sufficient quantities of X^- , HF and HX should be present to enable the crystallization of $[\text{PPh}_4][\text{X}(\text{HF})_2(\text{HX})]$.

Further investigations on hydrogen bond donors and acceptors

Besides the halide-HCl and halide-HF systems, further investigations have been carried out on weaker hydrogen bond donors and acceptors. Therefore, hydrogen bromide and hydrogen cyanide have been tested as hydrogen bond donors. In addition, the hydrogen bond acceptor abilities of the perchlorate anion have been investigated (Scheme 6).



Scheme 6. Synthesis of hydrogen-bonded adducts between anions ($X = \text{Br}, \text{I}, \text{ClO}_4$) and HY ($Y = \text{F}, \text{Br}, \text{CN}$). $[\text{Cat}] = [\text{PPh}_4]^+, [\text{PPN}]^+$.

The molecular structures of $[\text{PPh}_4][\text{I}(\text{HBr})_2]$ (Cc), $[\text{PPN}][\text{Br}(\text{HCN})]$ (Pca2₁) and $[\text{PPh}_4][\text{ClO}_4(\text{HF})_2]$ (C2/c) have been determined by XRD (Figure 6).

Hydrogen bromide is a weaker hydrogen bond donor compared to HCl and HF and only two examples of halide HBr adducts are known in the literature ($[\text{BrHBr}]^{-[10]}$ and $[\text{Br}(\text{HBr})_2]^{-[11]}$). The reaction of bromide salts with over-stoichiometric amounts of HBr leads to the formation of rather instable compounds which could not be characterized while the reaction of $[\text{PPh}_4]$ with four equivalents of HBr and slowly cooling to -40°C led to the crystallization of $[\text{PPh}_4][\text{I}(\text{HBr})_2]$. In the crystal the $[\text{I}(\text{HBr})_2]^-$ anion shows an asymmetrically V-shaped structure. The obtained Br–I distances of 373.4(2) and 387.1(1) pm are in good agreement with the distance calculated on the B3LYP(D3BJ)/def2-TZVPP (SCS-MP2/def2-TZVPP) level of theory of 379.5 pm (381.7 pm).

Recently it was shown that BrCN forms adducts with bromide to form $[\text{Br}(\text{BrCN})_n]^-$ anions ($n = 1, 3$) by halogen bonding interactions.^[32] Therefore it was tested whether similar hydrogen-bonded compounds can be synthesized. $[\text{PPN}][\text{Br}(\text{HCN})]$ was obtained by the reaction of $[\text{PPN}]\text{Br}$ with four equivalents of HCN. The nearly linear geometry of the anion is in agree-

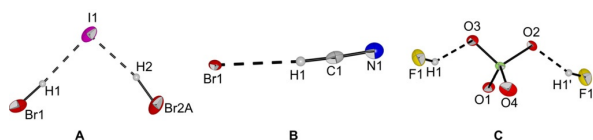
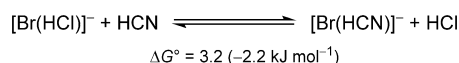


Figure 6. Molecular structures of A) $[\text{PPh}_4][\text{I}(\text{HBr})_2]$, B) $[\text{PPN}][\text{Br}(\text{HCN})]$ and C) $[\text{PPh}_4][\text{ClO}_4(\text{HF})_2]$ in the solid state with thermal ellipsoids shown at 50% probability. Cations and disorders have been omitted for clarity (see Figures S13 to S15 for representations including cations and disorders). Selected interatomic distances [pm]: Br1–I1 387.1(1), Br2A–I1 373.4(2), Br1–C1 340.5(6), F1–O3 256.1(4), F1'–O2 255.7(5), Cl1–O1 143.2(6), Cl1–O2 145.9(7), Cl1–O3 145.0(6), Cl1–O4 143.6(4), F1–Cl1 353.3(4), F1'–Cl1 352.3(4).

ment with a strong hydrogen bond interaction. This observation is also supported by quantum-chemical calculations (B3LYP(D3BJ)/def2-TZVPP (SCS-MP2/def2-TZVPP)) which show that the bromide HCN adduct has a similar stability as $[\text{BrHCl}]^-$ (Scheme 7) of which the hydrogen bond energy was experimentally determined to be 54 kJ mol^{-1} .^[16]



Scheme 7. Comparison of the stabilities of $[\text{Br}(\text{HCN})]^-$ and $[\text{Br}(\text{HCl})]^-$.

The equilibrium constant for the protonation reaction of the perchlorate ion in HF forming bifluoride and perchloric acid was determined to be $K_{\text{eq}} = (7.5 \pm 1.5) \cdot 10^{-5} \text{ L mol}^{-1}$ by Raman spectroscopy.^[33] Therefore perchlorate is a promising candidate to act as a hydrogen bond acceptor in HF without forming higher amounts of fluoride ions. When $[\text{PPh}_4][\text{ClO}_4]$ was treated with 8 equivalents of HF and cooled to -80°C single crystals of $[\text{PPh}_4][\text{ClO}_4(\text{HF})_2]$ were obtained. The short F–O distances of 255.7(5) to 256.1(4) pm are in good agreement with the calculated distances (B3LYP/def2TZVPP and MP2/def2-TZVPP) of 259.6 (261.5) pm and indicate a strong hydrogen bond interaction. This is also in agreement with thermochemical calculations on the B3LYP(D3BJ)/def2-TZVPP (SCS-MP2/def2-TZVPP) level of theory which predict $[\text{ClO}_4(\text{HF})_2]^-$ to be -75.5 (-61.1) kJ mol^{-1} more stable with respect to the decomposition into HF and ClO_4^- .

Conclusions

By using weakly coordinating cations ($[\text{PPh}_4]^+$, $[\text{PPN}]^+$) eight hitherto unknown poly(hydrogen halide) halogenate (–I) anions ($[\text{X}(\text{HCl})_n]^-$ ($X = \text{Br}, \text{I}$), $[\text{I}(\text{HCl})_3]^-$, $[\text{I}(\text{HBr})_2]^-$, $[\text{X}(\text{HF})_2(\text{HX})]^-$ ($X = \text{Br}, \text{I}$), $[\text{Br}(\text{HCN})]^-$ and $[\text{ClO}_4(\text{HF})_2]^-$) were synthesized and thoroughly characterized by X-ray diffraction, Raman spectroscopy, and quantum-chemical calculations. The measured Raman spectra of $[\text{PPh}_4][\text{X}(\text{HCl})_n]$ ($X = \text{Cl}, \text{Br}$ ($n = 4$), I ($n = 3$)) were used to investigate the influence of the central base and the coordination number on the hydrogen bond strength. It was observed that the hydrogen bond energy decreases from chloride to iodide as a central base, and with increasing coordination number. In addition, quantum-chemical calculations on halide ions in aHF were carried out. These calculations show that HF and HX ($X = \text{Cl}, \text{Br}, \text{I}$) have a similar acidity in aHF, which explains why mixed poly(hydrogen halide) halogenate anions $[\text{X}(\text{HF})_2(\text{HX})]^-$ ($X = \text{Br}, \text{I}$) were obtained starting from $[\text{PPh}_4][\text{X}]$ and HF. Furthermore, it was shown that weaker hydrogen-bond donors, like HBr and HCN can form adducts with halide ions. Additionally, it was observed that even the perchlorate anion, which is often used as a weakly coordinating anion, forms hydrogen-bonded adducts with HF.

Experimental Section

Apparatus and materials: All substances sensitive to water and oxygen were handled under an argon atmosphere using standard Schlenk techniques and oil pump vacuum up to 10^{-3} mbar. Reactions with HF, HCl and HBr were performed on a stainless steel vacuum line in self-built reactors consisting of 8 mm o. d. PFA (perfluoroalkoxy alkanes) tubing which were heat sealed on one end and connected to a steel valve on the other end. Dry MeCN and CH_2Cl_2 were obtained by distillation from P_4O_{10} . *n*-Pentane was dried over molecular sieves. All solvents were stored over activated 3 Å molecular sieves. Commercially available $[\text{AsPh}_4]\text{Cl}$, $[\text{PPh}_4]\text{X}$ ($\text{X} = \text{Cl}, \text{Br}, \text{I}$), $[\text{PPN}]\text{Cl}$ (PPN = bis(triphenylphosphoranylidene)iminium), HF, HCl and HBr were used without further purification. $[\text{PPN}]\text{Br}$,^[34] $[\text{PPN}]\text{I}$,^[35] $[\text{PPh}_4][\text{ClO}_4]$ ^[36] and HCN ^[37] were prepared according to literature procedures. All salts were dried in vacuo at 100°C for 10 min prior to use. Raman spectra were recorded on a Bruker MultiRAM II equipped with a low-temperature Ge detector (1064 nm, 100–180 mW, resolution of 4 cm^{-1}). Spectra of single crystals were recorded at -196°C using the Bruker RamanScope III (see part g of the Supporting Information for a description of the method used). X-ray diffraction data were collected on a Bruker D8 Venture CMOS area detector (Photon 100) diffractometer with MoK_α radiation. Single crystals were coated with perfluoroether oil at low temperature ($-40/-80^\circ\text{C}$) and mounted on a 0.1–0.2 mm Micromount. The structures were solved with the ShelXT^[38] structure solution program using intrinsic phasing and refined with the ShelXL^[39] refinement package using least squares on weighted F^2 values for all reflections using OLEX2.^[40] For quantum chemical calculations (structure optimization (with and without solvent model COSMO^[41]) and frequency calculations (including Raman intensities)) the program package TURBOMOLE 7.3^[42] was used. Functionals (B3LYP(D3BJ)^[43] and SCS-MP2^[44]) and the basis set (def2-TZVPP)^[45] were used as implemented in TURBOMOLE. Minima on the potential energy surface were characterized by harmonic vibrational frequency analysis. Thermochemistry was provided with zero-point vibration correction, ΔG values were calculated at 298.15 K and 1.0 bar.

$[\text{Cat}][\text{X}(\text{HCl})_n]$: In a typical experiment 0.4 mmol $[\text{Cat}]\text{X}$ ($\text{Cat} = \text{PPN}^+$, PPh_4^+ , AsPh_4^+ (only for $\text{X} = \text{Cl}^-$); $\text{X} = \text{Cl}^-, \text{Br}^-, \text{I}^-$) were dissolved in 0.2 mL CH_2Cl_2 . 1.6 mmol HCl were condensed onto the obtained suspension and the reaction mixture was allowed to warm to room temperature. A clear solution was obtained after carefully heating to a maximum of 40°C and mechanically agitating. Colorless single crystals of $[\text{PPN}][\text{X}(\text{HCl})_n]$ ($\text{X} = \text{Cl}^-, \text{Br}^-, \text{I}^-$), $[\text{PPh}_4][\text{X}(\text{HCl})_n]$ ($\text{X} = \text{Cl}^-, \text{Br}^-$), $[\text{PPh}_4][\text{I}(\text{HCl})_3]$ and $[\text{AsPh}_4][\text{Cl}(\text{HCl})_4]$ were obtained by slowly cooling the reaction mixture to -40°C .

$[\text{AsPh}_4][\text{Cl}(\text{HCl})_4]$: CCDC number: 1995595

$[\text{PPh}_4][\text{Cl}(\text{HCl})_4]$: Raman (-196°C): $\tilde{\nu} = 3083$ (w), 3068 (m), 3059 (m), 2523* (w), 2318* (w), 1589 (m), 1576 (w), 1187 (w), 1164 (w), 1114 (w), 1102 (w), 1024 (w), 1001 (s), 727 (w), 682 (w), 615 (w), 295 (w), 251 (w), 200 cm^{-1} (w). CCDC number: 1995600.

$[\text{PPh}_4][\text{Br}(\text{HCl})_4]$: Raman (-196°C): $\tilde{\nu} = 3081$ (w), 3068 (m), 3059 (m), 2525* (w), 2370* (w), 1589 (m), 1577 (w), 1186 (w), 1164 (w), 1114 (w), 1102 (w), 1025 (w), 1001 (s), 728 (w), 702 (w), 682 (w), 616 (w), 296 (w), 252 (w), 199 cm^{-1} (w). CCDC number: 1995596.

$[\text{PPh}_4][\text{I}(\text{HCl})_3]$: Raman (-196°C): $\tilde{\nu} = 3084$ (w), 3063 (s), 2388* (m), 2309* (m), 2232* (m), 1588 (m), 1575 (w), 1184 (w), 1164 (w), 1112 (w), 1102 (w), 1028 (w), 1000 (s), 681 (w), 292 (w), 253 (w), 198 cm^{-1} (w). CCDC number: 1995597.

$[\text{PPN}][\text{Cl}(\text{HCl})_4]$: Raman (-196°C): $\tilde{\nu} = 3067$ (m), 3057 (m), 1589 (m), 1114 (w), 1027 (w), 1001 (s), 669 (w), 616 (w), 240 cm^{-1} (w). CCDC number: 1995602.

$[\text{PPN}][\text{Br}(\text{HCl})_4]$: Raman (-196°C): $\tilde{\nu} = 3065$ (s), 3056 (s), 1590 (m), 1576 (w), 1114 (w), 1026 (w), 1001 (s), 701 (w), 669 (w), 617 (w), 287 (w), 269 (w), 240 cm^{-1} (w). CCDC number: 1995603.

$[\text{PPN}][\text{I}(\text{HCl})_4]$: Raman (-196°C): $\tilde{\nu} = 3058$ (s), 2472 (w), 2415 (w), 2301 (w), 1590 (m), 1575 (w), 1182 (w), 1114 (w), 1026 (w), 1001 (s), 809 (w), 751 (w), 668 (w), 617 (w), 238 cm^{-1} (w). CCDC number: 1995604.

Bands marked with an asterisk belong to the $[\text{X}(\text{HCl})_n]^-$ species.

$[\text{PPh}_4][\text{I}(\text{HBr})_2]$: In a typical experiment $[\text{PPh}_4]\text{I}$ (0.4 mmol, 186 mg, 1 equiv) was dissolved in 0.2 mL CH_2Cl_2 . HBr (1.6 mmol, 4 equiv) was condensed onto the obtained suspension and the reaction mixture was allowed to warm to room temperature. A clear solution was obtained after carefully heating to a maximum of 40°C and mechanically agitating. Colorless single crystals of $[\text{PPh}_4][\text{I}(\text{HBr})_2]$ and $[\text{AsPh}_4][\text{Cl}(\text{HCl})_4]$ were obtained by slowly cooling the reaction mixture to -40°C . CCDC number: 1997012.

$[\text{PPN}][\text{BrHBr}]\cdot\text{CH}_2\text{Cl}_2$: In a typical experiment $[\text{PPN}]\text{Br}$ (0.4 mmol, 246 mg, 1 equiv) was dissolved in 2 mL CH_2Cl_2 . HBr (1.6 mmol, 4 equiv) was condensed onto the obtained solution, and the reaction mixture was allowed to warm to room temperature. Colorless single crystals of $[\text{PPN}][\text{BrHBr}]\cdot\text{CH}_2\text{Cl}_2$ were obtained by vapor diffusion of *n*-pentane into the CH_2Cl_2 solution at room temperature. CCDC number: 1995599.

$[\text{PPh}_4][\text{X}(\text{HX})(\text{HF})_2]$: In a typical experiment 0.4 mmol $[\text{PPh}_4]\text{X}$ ($\text{X} = \text{Cl}^-, \text{Br}^-, \text{I}^-$) were filled into an 8 mm o.d. PFA tubing which was heat sealed on one end. The PFA tube was connected to a steel valve and HF (3.2 mmol, 64 mg, 8 equiv) was condensed onto the solid. The reactor was flame-sealed and mechanically agitated until a clear solution was obtained. Colorless single crystals of $[\text{PPh}_4][\text{X}(\text{HX})(\text{HF})_2]$ ($\text{X} = \text{Cl}^-, \text{Br}^-, \text{I}^-$) were obtained by slowly cooling the reaction mixture to -80°C .

$[\text{PPh}_4][\text{I}(\text{HF})_2(\text{HI})]$: Raman (-196°C): $\tilde{\nu} = 3065$ (m), 2017* (m), 1963* (m), 1904* (m), 1589 (m), 1575 (w), 1189 (w), 1165 (w), 1103 (w), 1028 (w), 1001 (s), 671 (w), 616 (w), 329 (w), 252 (w), 199 (w), 164 cm^{-1} (w). CCDC number: 1995598.

$[\text{PPh}_4][\text{Br}(\text{HF})_2(\text{HBr})]$: Raman (-196°C): $\tilde{\nu} = 3070$ (m), 1590 (s), 1577 (w), 1487 (vw), 1439 (vw), 1382 (w), 1343 (vw), 1319 (vw), 1305 (vw), 1215 (vw), 1191 (w), 1166 (vw), 1112 (w), 1101 (m), 1028 (m), 1002 (vs.), 733 (s), 681 (w), 616 (w), 576 (vw), 385 (w), 294 (m), 250 (m), 198 (m). CCDC number: 1995605.

Bands marked with an asterisk belong to the $[\text{X}(\text{HF})_2(\text{HX})]^-$ species.

$[\text{PPh}_4][\text{ClO}_4(\text{HF})_2]$: In a typical experiment $[\text{PPh}_4][\text{ClO}_4]$ (0.4 mmol, 175 mg, 1 equiv) was filled into an 8 mm o.d. PFA tubing which was heat sealed on one end. The PFA tube was connected to a steel valve and HF (3.2 mmol, 64 mg, 8 equiv) was condensed onto the solid. The reactor was flame-sealed and mechanically agitated until a clear solution was obtained. Colorless single crystals of $[\text{PPh}_4][\text{ClO}_4(\text{HF})_2]$ were obtained by slowly cooling the reaction mixture to -80°C . CCDC number: 1995606.

$[\text{PPN}][\text{Br}(\text{HCN})]$: In a typical experiment $[\text{PPN}]\text{Br}$ (0.4 mmol, 246 mg, 1 equiv) was dissolved in 0.4 mL MeCN. HCN (1.6 mmol, 4 equiv) was condensed onto the obtained suspension and the reaction mixture was allowed to warm to room temperature. Colorless single crystals of $[\text{PPN}][\text{Br}(\text{HCN})]$ were obtained by slowly cooling to -40°C . CCDC number: 1995601.

Crystallographic data: Deposition numbers 1995595 (for $[\text{AsPh}_4][\text{Cl}(\text{HCl})_4]$), 1995596 (for $[\text{PPh}_4][\text{Br}(\text{HCl})_4]$), 1995597 (for $[\text{PPh}_4][\text{I}(\text{HCl})_3]$), 1995598 (for $[\text{PPh}_4][\text{I}(\text{HF})_2(\text{HI})]$), 1995599 (for $[\text{PPN}][\text{BrHBr}]\cdot\text{CH}_2\text{Cl}_2$), 1995600 (for $[\text{PPh}_4][\text{Cl}(\text{HCl})_4]$), 1995601 (for $[\text{PPN}][\text{Br}(\text{HCN})]$), 1995602 (for $[\text{PPN}][\text{Cl}(\text{HCl})_4]$), 1995603 (for $[\text{PPN}][\text{Br}(\text{HCl})_4]$), 1995604 (for $[\text{PPN}][\text{I}(\text{HCl})_4]$), 1995605 (for $[\text{PPh}_4]$

[Br(HF)₂(HBr)], 1995606 (for [PPh₄][ClO₄(HF)₂]), and 1997012 (for [PPh₄][I(HBr)₂]) contain the supplementary crystallographic data for this paper. These data are provided free of charge by the joint Cambridge Crystallographic Data Centre and Fachinformationszentrum Karlsruhe Access Structures service www.ccdc.cam.ac.uk/structures.

Acknowledgements

We gratefully acknowledge the Zentraleinrichtung für Datenverarbeitung (ZEDAT) of the FU Berlin for computational resources. We also thank the priority program SPP 1708 for financial support as well as the DFG, CRC 1349 Fluorine Specific Interactions (Project-ID 387284271) for support. Open access funding enabled and organized by Projekt DEAL.

Conflict of interest

The authors declare no conflict of interest.

Keywords: acidity · hydrogen bonds · hydrogen halide · quantum-chemical calculations · X-ray structures

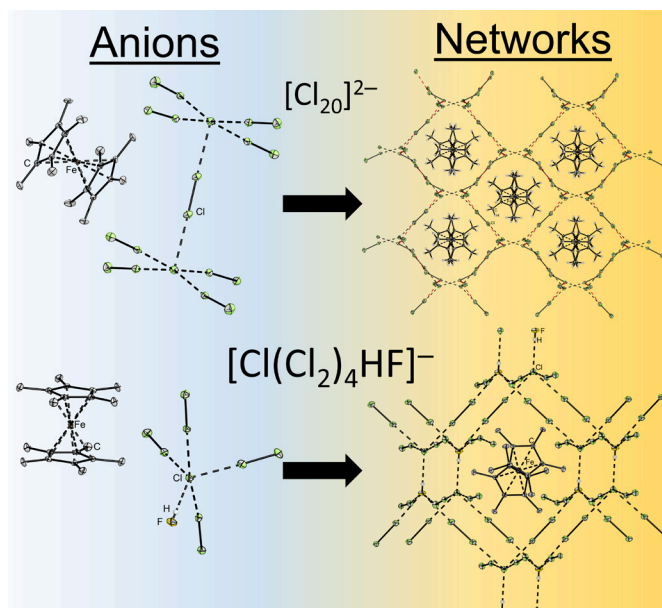
- [1] K. Sonnenberg, L. Mann, F. A. Redeker, B. Schmidt, S. Riedel, *Angew. Chem. Int. Ed.* **2020**, *59*, 5464; *Angew. Chem.* **2020**, *132*, 5506.
- [2] a) T. Steiner, *Angew. Chem. Int. Ed.* **2002**, *41*, 48–76; *Angew. Chem.* **2002**, *114*, 50–80; b) N. E. Klepeis, A. L. L. East, A. G. Császár, W. D. Allen, T. J. Lee, D. W. Schwenke, *J. Chem. Phys.* **1993**, *99*, 3865.
- [3] D. Mootz, D. Boenigk, *Z. Anorg. Allg. Chem.* **1987**, *544*, 159.
- [4] a) D. Mootz, J. Hocken, *Angew. Chem. Int. Ed. Engl.* **1989**, *28*, 1697; *Angew. Chem.* **1989**, *101*, 1713; b) A. Deeg, Th. Dahlems, D. Mootz, Z. *Kristallogr. New Cryst. Struct.* **1997**, *212*, 401; c) R. Hagiwara, T. Hirashige, T. Tsuda, Y. Ito, *J. Electrochem. Soc.* **2002**, *149*, D1–D6.
- [5] D. Mootz, J. Hocken, *Z. Naturforsch. B* **1989**, *44*, 1239.
- [6] D. Wiechert, D. Mootz, R. Franz, G. Siegemund, *Chem. Eur. J.* **1998**, *4*, 1043.
- [7] D. Mootz, A. Deeg, *Z. Anorg. Allg. Chem.* **1992**, *615*, 109.
- [8] D. Mootz, W. Poll, *Z. Naturforsch. B* **1984**, *39*, 1300.
- [9] H. Yoshino, K. Matsumoto, R. Hagiwara, Y. Ito, K. Oshima, S. Matsubara, *J. Fluorine Chem.* **2006**, *127*, 29.
- [10] J. L. Atwood, S. G. Bott, C. M. Means, A. W. Coleman, H. Zhang, M. T. May, *Inorg. Chem.* **1990**, *29*, 467.
- [11] G. W. Driver, I. Mutikainen, *Dalton Trans.* **2011**, *40*, 10801.
- [12] I. G. Shenderovich, S. N. Smirnov, G. S. Denisov, V. A. Gindin, N. S. Golubev, A. Dunger, R. Reibke, S. Kirpekar, O. L. Malkina, H.-H. Limbach, *Ber. Bunsenges. Phys. Chem.* **1998**, *102*, 422.
- [13] J. L. E. Campbell, K. E. Johnson, *Inorg. Chem.* **1993**, *32*, 3809.
- [14] J. L. E. Campbell, K. E. Johnson, *J. Am. Chem. Soc.* **1995**, *117*, 7791.
- [15] L. Aldous, D. S. Silvester, W. R. Pitner, R. G. Compton, Lagunas, M. Cristina, C. Hardacre, *J. Phys. Chem. C* **2007**, *111*, 8496.
- [16] G. Caldwell, P. Kebarle, *Can. J. Chem.* **1985**, *63*, 1399.
- [17] R. Yamdagni, P. Kebarle, *Can. J. Chem.* **1974**, *52*, 2449.
- [18] a) P. Kirsch, *Modern Fluoroorganic Chemistry. Synthesis Reactivity, Applications*, Wiley-VCH, Weinheim, **2004**; b) M. Jaccaud, R. Faron, D. Devilliers, R. Romano, H. Pernice, S. Riedel, “Fluorine” in *Ullmann Encyclopedia of Industrial Chemistry* **2020**, 1–19.
- [19] R. Franz, *J. Fluorine Chem.* **1980**, *15*, 423.
- [20] G. Alvernhe, A. Laurent, G. Haufe, *Synthesis* **1987**, *6*, 562.
- [21] G. A. Olah, M. Nojima, I. Kerekes, *Synthesis* **1973**, *12*, 779.
- [22] G. A. Olah, M. Nojima, I. Kerekes, *Synthesis* **1973**, *12*, 780.
- [23] G. A. Olah, J. T. Welch, Y. D. Vankar, M. Nojima, I. Kerekes, J. A. Olah, *J. Org. Chem.* **1979**, *44*, 3872.
- [24] J. Dong, L. Krasnova, M. G. Finn, K. B. Sharpless, *Angew. Chem. Int. Ed.* **2014**, *53*, 9430; *Angew. Chem.* **2014**, *126*, 9584.
- [25] C. J. Smedley, Q. Zheng, B. Gao, S. Li, A. Molino, H. M. Duivenvoorden, B. S. Parker, D. J. D. Wilson, K. B. Sharpless, J. E. Moses, *Angew. Chem. Int. Ed.* **2019**, *58*, 4552; *Angew. Chem.* **2019**, *131*, 4600.
- [26] B. Gao, L. Zhang, Q. Zheng, F. Zhou, L. M. Klivansky, J. Lu, Y. Liu, J. Dong, P. Wu, K. B. Sharpless, *Nat. Chem.* **2017**, *9*, 1083.
- [27] R. D. Shannon, *Acta Crystallogr. A Cryst. Phys. Diffraction. Gen. Crystallogr.* **1976**, *32*, 751.
- [28] G. A. Landrum, N. Goldberg, R. Hoffmann, *J. Chem. Soc. Dalton Trans.* **1997**, 3605.
- [29] R. Savoie, A. Anderson, *J. Chem. Phys.* **1966**, *44*, 548.
- [30] K. Sonnenberg, P. Pröhm, N. Schwarze, C. Müller, H. Beckers, S. Riedel, *Angew. Chem. Int. Ed.* **2018**, *57*, 9136; *Angew. Chem.* **2018**, *130*, 9274.
- [31] B. Schmidt, K. Sonnenberg, H. Beckers, S. Steinhauer, S. Riedel, *Angew. Chem. Int. Ed.* **2018**, *57*, 9141; *Angew. Chem.* **2018**, *130*, 9279.
- [32] B. Schmidt, B. Schröder, K. Sonnenberg, S. Steinhauer, S. Riedel, *Angew. Chem. Int. Ed.* **2019**, *58*, 10340; *Angew. Chem.* **2019**, *131*, 10448.
- [33] L. Stein, E. H. Appelman, *Inorg. Chem.* **1983**, *22*, 3017.
- [34] F. J. Lalor, S. Chaona, *J. Organomet. Chem.* **1988**, *344*, 163.
- [35] A. Schulz, A. Villinger, *Chem. Eur. J.* **2015**, *21*, 3649.
- [36] B. V. Lebedev, N. N. Smirnova, L. Y. Tsvetkova, Y. Marcus, G. T. Hefter, *J. Chem. Thermodyn.* **2001**, *33*, 485.
- [37] K. Bläsing, J. Bresien, R. Labbow, A. Schulz, A. Villinger, *Angew. Chem. Int. Ed.* **2018**, *57*, 9170; *Angew. Chem.* **2018**, *130*, 9311.
- [38] G. M. Sheldrick, *Acta Crystallogr. A Found. Crystallogr.* **2008**, *64*, 112.
- [39] G. M. Sheldrick, *Acta Crystallogr. C Struct. Chem.* **2015**, *71*, 3.
- [40] O. V. Dolomanov, L. J. Bourhis, R. J. Gildea, J. A. K. Howard, H. Puschmann, *J. Appl. Crystallogr.* **2009**, *42*, 339.
- [41] A. Klamt, G. Schüürmann, *J. Chem. Soc. Perkin Trans. 2* **1993**, 799.
- [42] TURBOMOLE GmbH, TURBOMOLE V7.3. a development of University of Karlsruhe and Forschungszentrum Karlsruhe GmbH, **2018**.
- [43] a) A. D. Becke, *J. Chem. Phys.* **1993**, *98*, 5648; b) C. Lee, W. Yang, R. G. Parr, *Phys. Rev. B* **1988**, *37*, 785; c) S. H. Vosko, L. Wilk, M. Nusair, *Can. J. Phys.* **1980**, *58*, 1200; d) P. J. Stephens, F. J. Devlin, C. F. Chabalowski, M. J. Frisch, *J. Phys. Chem.* **1994**, *98*, 11623; e) S. Grimme, J. Antony, S. Ehrlich, H. Krieg, *J. Chem. Phys.* **2010**, *132*, 154104; f) A. D. Becke, E. R. Johnson, *J. Chem. Phys.* **2005**, *123*, 154101; g) E. R. Johnson, A. D. Becke, *J. Chem. Phys.* **2006**, *124*, 174104.
- [44] S. Grimme, *J. Chem. Phys.* **2003**, *118*, 9095.
- [45] F. Weigend, R. Ahlrichs, *Phys. Chem. Chem. Phys.* **2005**, *7*, 3297.

Manuscript received: April 17, 2020

Accepted manuscript online: May 7, 2020

Version of record online: September 16, 2020

3.2 From Missing Links to New Records: A Series of Novel Polychlorine Anions



Patrick Voßnacker, Thomas Keilhack, Nico Schwarze, Karsten Sonnenberg, Konrad Seppelt, Moritz Malischewski*, Sebastian Riedel*

Eur. J. Inorg. Chem. **2021**, 2021, 1034.

<https://doi.org/10.1002/ejic.202001072>

© 2020 European Journal of Inorganic Chemistry published by Wiley-VCH GmbH. This is an open-access article distributed under the terms of the [Creative Commons Attribute 4.0 International license](https://creativecommons.org/licenses/by/4.0/)

Author contributions

Patrick Voßnacker designed the project, performed the experiments and wrote the manuscript. Thomas Keilhack and Nico Schwarze performed some of the experiments. Karsten Sonnenberg and Konrad Seppelt performed the XRD measurements. Moritz Malischewski performed some of the experiments, revised the manuscript and provided scientific guidance. Sebastian Riedel managed the project and revised the manuscript.

VIP Very Important Paper



From Missing Links to New Records: A Series of Novel Polychlorine Anions

Patrick Voßnacker,^[a] Thomas Keilhack,^[a] Nico Schwarze,^[a] Karsten Sonnenberg,^[a] Konrad Seppelt,^[a] Moritz Malischewski,^{*,[a]} and Sebastian Riedel^{*,[a]}

Herein we report the synthesis and structural characterization of four novel polychloride compounds. The compounds $[\text{CCl}(\text{NMe}_2)_2][\text{Cl}(\text{Cl}_2)_3]$ and $[\text{NPr}_4][\text{Cl}(\text{Cl}_2)_4]$ have been obtained from the reaction of the corresponding chloride salts with elemental chlorine at low temperature. They are the missing links in the series of polychloride monoanions $[\text{Cl}(\text{Cl})_n]^-$ ($n = 1-6$). Additionally, the reaction of dexamethylferrocene with

elemental chlorine was studied yielding $[\text{Cp}^*_2\text{Fe}]_2[\text{Cl}_{20}]$, which contains the largest known polychloride $[\text{Cl}_{20}]^{2-}$ to date, and $[\text{Cp}^*_2\text{Fe}][\text{Cl}(\text{Cl}_2)_4(\text{HF})]$, which is the first example of a polychloride-HF network stabilized by strong hydrogen and halogen bonding. All compounds have been characterized by single-crystal X-ray diffraction, Raman spectroscopy and quantum-chemical calculations.

Introduction

In recent years, polyhalides have received much attention due to various possible applications.^[1] They exist as either solids or low viscous ionic liquids with significantly lower vapor pressure compared to the neat halogens.^[2] Therefore, trihalides as well as higher polyhalides have been applied as easy-to-handle halogenation reagents which react with ketones,^[3] alkenes^[4] and alkynes.^[5] Additionally, polychlorides have shown to be efficient and safe materials for the storage of elemental chlorine.^[5] Recently it was shown that ionic liquids based on polyhalogen- and polyinterhalogen anions can be used for the oxidative dissolution of metals and alloys. Since even noble elements can be dissolved, an application in metal recycling and urban mining might be possible.^[6] Besides their potential as oxidation reagents, ionic liquids based on polyhalogen anions possess a surprisingly high conductivity^[2] and it was shown that polybromides are present in zinc-bromine (redox flow) batteries.^[7]

Polybromides and polyiodides display a structurally rich and diverse chemistry and large anions up to $[\text{Br}_{24}]^{2-}$, $[\text{I}_{26}]^{4-}$ and $[\text{I}_{29}]^{3-}$ can be isolated (Figure 1).^[8] In contrast, the more

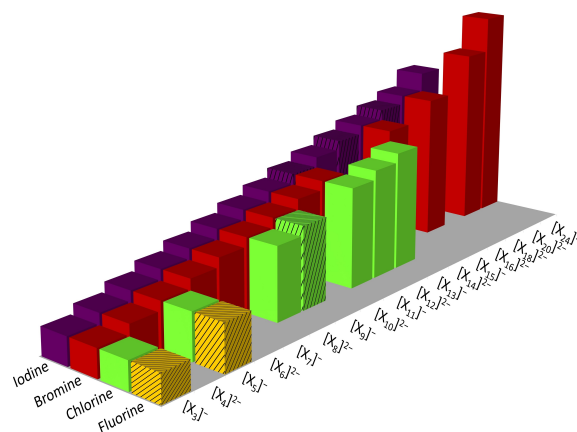


Figure 1. Overview of experimentally known homoatomic polyhalogen mono- and dianions. These anions have been crystallographically characterized except for the shaded ones, which have only been observed spectroscopically. Reproduced from ref.^[1]

challenging handling of gaseous chlorine as well as the lower stability of polychlorides have so far hampered the exploration of the structural chemistry of polychlorides.^[9] Polyfluorides have only been detected under matrix conditions.^[10] So far, the only structurally characterized polychlorine monoanions were $[\text{Cl}_3]^-$, $[\text{Cl}(\text{Cl}_2)_2]^{-[11]}$ and only very recently crystal structures of $[\text{Cl}(\text{Cl}_2)_5]^-$ and $[\text{Cl}(\text{Cl}_2)_6]^-$ were reported.^[12] The $[\text{Cl}_3]^-$ anion possesses a nearly linear structure in the solid state while the structure of the $[\text{Cl}(\text{Cl}_2)_2]^-$ within $[\text{PPh}_2\text{Cl}_2][\text{Cl}(\text{Cl}_2)_2]$ ($[\text{PPh}_2\text{Cl}_2]^+$ = diphenyldichlorophosphonium) can best be described as a hockey stick structure.^[11,1b] $[\text{Cl}(\text{Cl}_2)_5]^-$ exists as either isolated square pyramidal structure $([\text{PPN}][\text{Cl}(\text{Cl}_2)_5] \cdot \text{Cl}_2$, $[\text{PPN}]^+$ = bis(triphenylphosphine)iminium) or as square pyramidal $[\text{Cl}(\text{Cl}_2)_5]^-$ unit which are connected by one Cl_2 molecule (octahedral coordination for the central halide) forming infinite chains ($[\text{PPh}_4][\text{Cl}(\text{Cl}_2)_5]$, $[\text{AsPh}_4][\text{Cl}(\text{Cl}_2)_5]$; $[\text{PPh}_4]^+$ = tetraphenylphosphonium, $[\text{AsPh}_4]^+$ = tetraphenylarsonium). The polychloride with

[a] P. Voßnacker, T. Keilhack, Dr. N. Schwarze, Dr. K. Sonnenberg, Prof. Dr. K. Seppelt, Dr. M. Malischewski, Prof. Dr. S. Riedel
Fachbereich Biologie, Chemie, Pharmazie
Institut für Chemie und Biochemie – Anorganische Chemie
Fabeckstr. 34/36, 14195 Berlin, Germany
E-mail: moritz.malischewski@fu-berlin.de
s.riedel@fu-berlin.de

<https://www.bcp.fu-berlin.de/chemie/chemie/forschung/InorgChem/ag-malischewski>
www.fluorinechemistry.de

Supporting information for this article is available on the WWW under <https://doi.org/10.1002/ejic.202001072>

Part of the joint "German Chemical Society ADUC Prizewinner" Collection with EurJOC.

© 2020 The Authors. European Journal of Inorganic Chemistry published by Wiley-VCH GmbH. This is an open access article under the terms of the Creative Commons Attribution License, which permits use, distribution and reproduction in any medium, provided the original work is properly cited.

the highest chlorine content, $[\text{Cl}(\text{Cl}_2)_6]^-$, has an octahedral geometry in the solid state.^[12] So far, only two polychlorine dianions are known in the literature. The $[\text{Cl}_8]^{2-}$ ($[\text{CCl}(\text{NMe}_2)_2][\text{Cl}_8]^{13}$, $[\text{CCl}(\text{NMe}_2)_2]^+$ = tetramethylchloroamidinium) which shows a discrete, Z-shaped structure and the $[\text{Cl}_{12}]^{2-}$ ($[\text{NMe}_3\text{Ph}]_2[\text{Cl}_{12}]^{12}$, $[\text{NMe}_3\text{Ph}]^+$ = trimethylphenylammonium) which possesses inversion symmetry and can be described as two $[\text{Cl}(\text{Cl}_2)_2]^-$ units which are connected by a Cl_2 molecule. The $[\text{Cl}_{12}]^{2-}$ units are further connected to form a three-dimensional network resembling a honeycomb. In 2015 the molecular structure of a 2D layered infinite polychlorine structure consisting of $[\text{Cl}_3]^-$ and Cl_2 building blocks ($[\text{NEt}_4][\text{Cl}_3]_2 \cdot \text{Cl}_2$, $[\text{NEt}_4]^+$ = tetraethylammonium) was described.^[14]

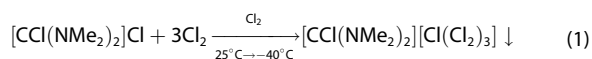
The bonding situation of such higher polyhalogen anions can be described as a Lewis acid-base interaction between the halide (Lewis base) and the dihalogen (Lewis acid). Two major interactions contribute to the bonding: First there is charge transfer from the HOMO of the halide ion (lone pair) into the LUMO of the dihalogen ($\sigma^*(\text{X}-\text{X})$) which leads to an elongation of the $\text{X}-\text{X}$ bond. Additionally, the electrostatic potential of the dihalogen is anisotropic. This results in a belt of higher electron density perpendicular to the molecule's bonding axis and an area of lower electron density along the extension of the covalent bond, the so called σ -hole. Between the negatively charged halide ion and the positive σ -hole there is an attractive electrostatic interaction.^[15] Very recently the bonding situation of the $[\text{Cl}_3]^-$ has been studied by experimental and computed electron densities determination. It was shown that a genuine $\text{pp}\sigma$ bond is formed if a chlorine molecule interacts with a "naked" chloride ion. Furthermore, it appears to be a smooth transition from the asymmetric to the symmetric compound which is a crucial property for its chemical reactivity.^[16]

Herein, we report the synthesis and characterization of four hitherto unknown polychloride compounds. It was possible to obtain the first molecular structures of a heptachloride ($[\text{CCl}(\text{NMe}_2)_2][\text{Cl}(\text{Cl}_2)_3]$) and a nonachloride ($[\text{NPr}_4][\text{Cl}(\text{Cl}_2)_4]$). In addition, the first polychloride-HF network was synthesized ($[\text{Cp}^*_2\text{Fe}]_2[\text{Cl}(\text{Cl}_2)_4(\text{HF})]$) and the largest known polychloride, the $[\text{Cl}_{20}]^{2-}$ could be obtained by oxidation of Cp^*_2Fe with a large excess of chlorine.

Results and Discussion

The Heptachloride $[\text{Cl}(\text{Cl}_2)_3]^-$

An anion, which can formally be described as a $[\text{Cl}(\text{Cl}_2)_3]^-$, was obtained by the reaction of the Vilsmeier salt $[\text{CCl}(\text{NMe}_2)_2]\text{Cl}$ with a large excess of chlorine without additional solvent (Equation 1).



By slowly cooling the reaction mixture to -40°C single crystals of $[\text{CCl}(\text{NMe}_2)_2][\text{Cl}(\text{Cl}_2)_3]$ were obtained which crystallize in the orthorhombic space group $P2_12_12_1$ (Figure 2).

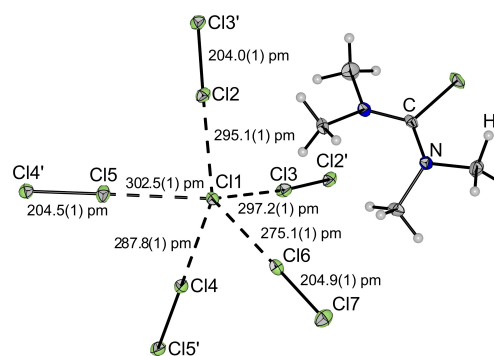


Figure 2. Molecular structure of $[\text{CCl}(\text{NMe}_2)_2][\text{Cl}(\text{Cl}_2)_3]$ in the solid state with thermal ellipsoids shown at 50% probability.

The anion within $[\text{CCl}(\text{NMe}_2)_2][\text{Cl}(\text{Cl}_2)_3]$ is best described as a polychloride network in which the central chloride is coordinated by five chlorine molecules, four of them are bridging to the next chloride ion while one is terminal. Four chloride ions connected by four chlorine molecules form a bent rectangle, with the fifth chlorine alternatingly pointing up and downwards. The bent rectangles are connected by all four edges to form an extended network (Figure 3).

The distance between the central halide and the terminal Cl_2 unit (275.1(1) pm) as well as the Cl_2 bond length (204.9(1) pm) are in good agreement to the bond length calculated on SCS-MP2/def2-TZVPP for a square pyramidal $[\text{Cl}(\text{Cl}_5)]^-$ anion (277.8–282.2 pm, 203.9–204.8 pm). In comparison to crystalline Cl_2 ($R(\text{Cl}-\text{Cl})=198.4(1)$ pm) the Cl_2 bond length is elongated by 6.5(2) pm which can be explained by the aforementioned donation of electron density into the σ^* -orbital of the $\text{Cl}-\text{Cl}$ bond which leads to a bond weakening effect. The distance between the central halide and the bridging Cl_2 units is significantly longer (287.8(1)–302.5(1) pm). Nevertheless, the

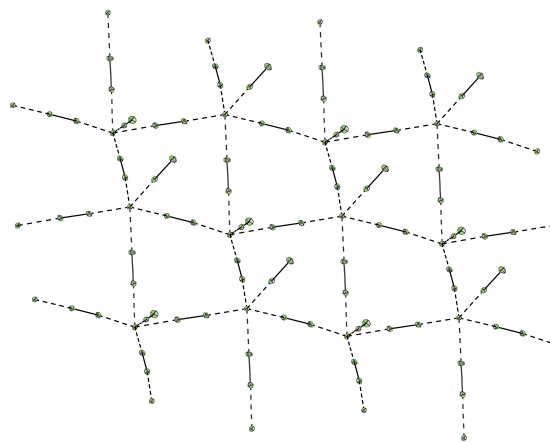


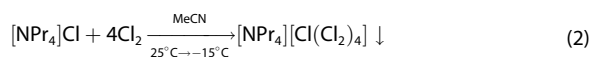
Figure 3. Structure of the polychlorine monoanion within the solid state structure of $[\text{CCl}(\text{NMe}_2)_2][\text{Cl}(\text{Cl}_2)_3]$. Thermal ellipsoids are shown at 50% probability. Cations are omitted for clarity.

weakening of the Cl–Cl bond is comparable for the bridging Cl₂ units ($R(\text{Cl}–\text{Cl}) = 204.0(1)–204.5$ pm) which is due to a charge transfer from two chloride ions. The shortest distances between cation and anion are a Cl–H distance of 274.0(3) pm and a Cl–Cl distance of 339.1(1) pm which indicate moderate hydrogen and halogen bonding interactions.

The Raman spectrum of the single crystal of $[\text{C}(\text{Cl}_2)_3]$ shows three bands at 471, 451 and 430 cm^{-1} (see Figure S8). Those bands correspond to the stretching modes of the three crystallographic independent Cl₂ units in the crystal. The experimentally obtained spectra is rather similar to the computed spectra at SCS-MP2/def2-TZVPP level for a C_{4v} symmetric $[\text{Cl}(\text{Cl}_2)_3]^-$ anion in the gas phase while no exact match can be expected due to the network structure in the solid state (see Figure S9).

The Nonachloride $[\text{Cl}(\text{Cl}_2)_4]^-$

$[\text{NPr}_4][\text{Cl}(\text{Cl}_2)_4]$ ($[\text{NPr}_4]^+$ = tetrapropylammonium) was prepared by condensing stoichiometric amounts of chlorine onto an acetonitrile (MeCN) solution of $[\text{NPr}_4]\text{Cl}$ (Equation 2).



By slowly cooling to -15 °C single crystals of $[\text{NPr}_4][\text{Cl}(\text{Cl}_2)_4]$ were obtained which crystallize in the tetragonal space group $\bar{I}4$. (Figure 4). The structure of the anion can best be described as a distorted tetrahedron. Quantum-chemical calculations (B3LYP(D3BJ)/def2-TZVPP and SCS-MP2/def2-TZVPP (value in parentheses) predicted the tetrahedral structure to be the minimum in the gas phase. In comparison the pyramidal structure (C_{4v}) is 8.54 (4.29) kJ mol^{-1} higher in energy and shows one imaginary frequency (transition state between two tetrahedral structures) while the planar structure (D_{4h}) is 9.7 (4.4) kJ mol^{-1} higher in energy and shows one (MP2) or two (B3LYP) imaginary frequencies (transition between tetrahedral as well as pyramidal structures). The bond length of the coordinated Cl₂ is elongated by 8.1(6) pm when compared to crystalline Cl₂ ($R(\text{Cl}–\text{Cl}) = 198.4(1)$ pm)^[17] which agrees well with the computed bond length on MP2 level of theory ($R(\text{Cl}–\text{Cl}) = 205.6$ pm). In the Raman spectrum of the single crystal two bands at 477 and 450 are observed in the Cl₂ region. Those bands are in good agreement to the calculated bands on SCS-MP2 level at 472 and 438 cm^{-1} (Figure S9).

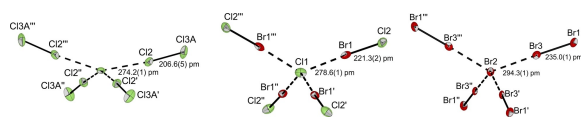


Figure 4. Comparison of the molecular structure of $[\text{NPr}_4][\text{Cl}(\text{Cl}_2)_4]$, $[\text{NPr}_4][\text{Cl}(\text{BrCl})_4]$ and $[\text{NPr}_4][\text{Br}(\text{Br}_2)_4]$ in the solid state. Thermal ellipsoids are shown at 50% probability. Disorders are omitted for clarity (see Figure S2 for structure including disorder). Bond angles in []: Cl2–Cl1–Cl2' 93.2(1), Cl2–Cl1–Cl2'' 152.6(1), Br1–Cl1–Br1' 100.3(1), Br1–Cl1–Br1'' 130.1(1), Br3–Br2–Br3' 99.8(1), Br3–Br2–Br3'' 131.2(1).

Two isostructural compounds, $[\text{NPr}_4][\text{Cl}(\text{BrCl})_4]^{[18]}$ and $[\text{NPr}_4][\text{Br}(\text{Br}_2)_4]^{[19]}$, are known in the literature. When the structures of the polyhalogen anions are compared it can be seen that the distortion of the tetrahedra is most pronounced for the $[\text{Cl}(\text{Cl}_2)_4]^-$ anion (bond angles of 93.2(1) and 152.6(1), compared to 100.3(1), 130.1(1) for $[\text{Cl}(\text{BrCl})_4]^-$ and 99.8(1), 131.2(1) for $[\text{Br}(\text{Br}_2)_4]^-$). This can be explained by inter-molecular interactions. Within the molecular structure of $[\text{NPr}_4][\text{Br}(\text{Br}_2)_4]$ there are short Br3–Br1 distances of 339.5(1) pm ($\Sigma_{\text{vdW radii}} = 370$ pm)^[20] yielding a connection between the $[\text{Br}(\text{Br}_2)_4]^-$ units by forming eight-membered folded rectangles (see Figure 5B). When going from Br₂ to BrCl the structure of the anion does not change much but the inter-molecular interactions get weaker (Br1–Cl2 distances of 350.8(2) pm, $\Sigma_{\text{vdW radii}} = 360$ pm)^[20] due to the shorter Br–Cl bonds which increases the distance between the $[\text{Cl}(\text{BrCl})_4]^-$ units (see Figure 5A). Due to the even shorter Cl–Cl bond lengths the distances between the $[\text{Cl}(\text{Cl}_2)_4]^-$ units would become so large that there would be no inter-molecular interactions. Therefore, for the $[\text{Cl}(\text{Cl}_2)_4]^-$ unit, a stronger distortion is observed which allows inter-molecular interaction by short Cl3A–Cl3A distances of 319(1) pm ($\Sigma_{\text{vdW radii}} = 350$ pm)^[20] forming four-membered folded rectangles (see Figure 5A).

Reactions of $[\text{Cp}^*_2\text{Fe}]$ with Cl₂

The reactions of ferrocene with dihalogens are known for a long time.^[21] Ferrocenium is well known to form a series of polyiodide complexes, from the triiodide $[\text{Cp}_2\text{Fe}][\text{I}_3]^{[21]}$, $[\text{Cp}_2\text{Fe}][\text{I}_7]^{[22]}$, $[\text{Cp}_2\text{Fe}_2][\text{I}_{16}]^{[23]}$ to $[\text{Cp}_2\text{Fe}_3][\text{I}_{29}]^{[8c]}$ (Cp₂Fe = ferrocene, Cp₂*Fe = dexamethylferrocene). However, elemental bromine or chlorine are so reactive, that they partially or completely destroy the ferrocene moiety, leading to either $[\text{Cp}_2\text{Fe}][\text{FeX}_4]$ or pentahalocyclopentane C₅H₅X₅ (X=Cl, Br).^[24] Only a small number of ferrocenium derivatives with tribromide counter anions have been isolated so far.^[25]

Recently it was shown that ferrocene derivatives can be oxidized twice to form stable compounds containing tetravalent iron ($[\text{Cp}^*_2\text{Fe}]^{2+}$, $[\text{Cp}^*_2\text{FeCO}]^{2+}$ and $[\text{Cp}_2\text{FeH}^+]$).^[26] Therefore it was attempted to oxidize $[\text{Cp}^*_2\text{Fe}]$ using an excess of the strong oxidizer Cl₂ to form either $[\text{Cp}^*_2\text{Fe}]^{2+}$ or the unknown

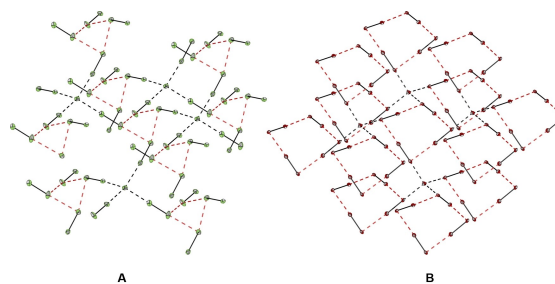
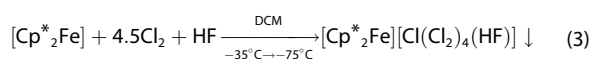


Figure 5. Anion network within the solid state structures of $[\text{NPr}_4][\text{Cl}(\text{Cl}_2)_4]$ (A) and $[\text{NPr}_4][\text{Br}(\text{Br}_2)_4]$ (B). Intermolecular interactions are indicated by red dotted lines.

$[\text{Cp}^*_2\text{FeCl}]^+$. Although oxidation to $[\text{Cp}^*_2\text{Fe}]^+$ occurs rapidly in dichloromethane, longer reaction times at room temperature (especially in the sunlight) lead to chlorination or cleavage of the Cp^* ligand. A two-electron oxidation of the $[\text{Cp}^*_2\text{Fe}]$ was not observed. Slowly cooling the reaction mixture to -75°C yields green single crystals of $[\text{Cp}^*_2\text{Fe}][\text{Cl}(\text{Cl}_2)_4(\text{HF})]$ (Equation 3).



Co-crystallized HF is most likely a result of adventitious traces of HF which were present since the reaction was performed in a PFA reactor on a steel line which was previously used for reactions involving HF. To rule out a contamination with water (differentiation between HF and H_2O is not always possible by XRD) the reaction was repeated, and stoichiometric amounts of HF and H_2O were added, respectively. The addition of milligram amounts of HF led to the formation of the same crystals, while addition of water was inconclusive.

$[\text{Cp}^*_2\text{Fe}][\text{Cl}(\text{Cl}_2)_4(\text{HF})]$ crystallizes in the monoclinic space group $C2/m$ (Figure 6).

The structure of the anion can be described as an intermediate between a square pyramidal structure with HF on the top of the pyramid (C_{4v}) and a trigonal bipyramidal (C_{2v}) structure with HF in an equatorial position. This interpretation is further supported by the structural parameter τ which was calculated to be 0.56 ($\tau = (\beta - \alpha)/60$, α and β are the largest angle in the coordination sphere; $\tau = 0$ for perfect square-pyramidal structure and 1 for perfect bipyramidal symmetric structure)^[27]. Quantum-chemical calculations in the gas-phase predict both structures to be very close in energy. On B3LYP(D3BJ)/def2-TZVPP level of theory the C_{2v} structure is favored by 0.5 kJ mol^{-1} with the C_{4v} being a transition state while on SCS-MP2 level of theory the C_{4v} symmetric structure is equal in energy both being minima, indicating a very shallow potential energy surface. The bond length of the coordinated Cl_2 is only slightly elongated by 2.7(2) to 4.3(2) pm when compared to crystalline Cl_2 ($R(\text{Cl}-\text{Cl}) = 198.4(1) \text{ pm}$)^[17] while the short F1–Cl1 distance of 289.1(2) pm indicate strong hydrogen bonding interaction. A comparison with the molecular structure of $[\text{PPN}][\text{Cl}(\text{Cl}_2)_5] \cdot \text{Cl}_2$, in which the central chloride also has a coordination number of five, shows a comparable weakening of the Cl–Cl bond with

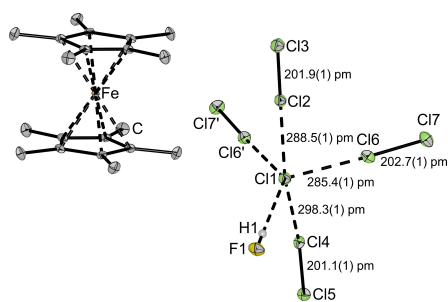


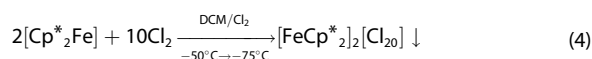
Figure 6. Molecular structure of $[\text{Cp}^*_2\text{Fe}][\text{Cl}(\text{Cl}_2)_4(\text{HF})]$ in the solid state with thermal ellipsoids shown at 50% probability. The F1–Cl1 distance is 289.1(2) pm. Hydrogen atoms are omitted for clarity.

bond length of 201.5(1) to 202.6(1) pm.^[12] This indicates that the Lewis acidity of the HF molecule is at least comparable to the Lewis acidity of Cl_2 . Quantum-chemical calculations support this observation since the addition of a HF molecule to $[\text{Cl}(\text{Cl}_2)_4]^-$ was calculated (B3LYP(D3BJ)/def2-TZVPP and SCS-MP2/def2-TZVPP (value in parentheses) to be 8.6 (13.3) kJ mol^{-1} exergonic while the exchange of one Cl_2 unit from $[\text{Cl}(\text{Cl}_2)_5]^-$ against one HF molecule is 17.2 (32.0) kJ mol^{-1} exergonic (Scheme 1).

This also explains why a mixed anion containing HF and Cl_2 is obtained even when an excess of chlorine was used. Further quantum-chemical calculations show that in principle all exchange reactions of Cl_2 against HF are exergonic for the system $[\text{Cl}(\text{Cl}_2)_{5-n}(\text{HF})_n]^- + \text{HF} \rightarrow [\text{Cl}(\text{Cl}_2)_{5-n-1}(\text{HF})_{n+1}]^- + \text{Cl}_2$ ($n = 0-4$, see Table S6) while an exchange of Cl_2 in $[\text{Cl}(\text{Cl}_2)_5]^-$ against HCl is also exergonic (Table S7).

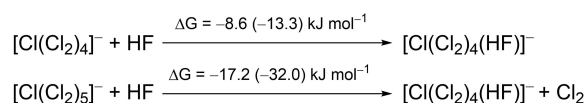
The Raman spectrum of the single crystal of $[\text{Cp}^*_2\text{Fe}][\text{Cl}(\text{Cl}_2)_4(\text{HF})]$ shows three bands at 507, 488 and 477 cm^{-1} . Those bands agree well to the bands calculated on SCS-MP2/def2-TZVPP level of theory for a C_{2v} symmetric $[\text{Cl}(\text{Cl}_2)_4(\text{HF})]^-$ (499, 480, 477 cm^{-1}) while again no exact match can be expected due to the reduced symmetry in the crystal and the formation of the polyhalide network (see Figure S9).

When an even larger excess of Cl_2 (21 equiv.) is used in absence of HF slow cooling of the reaction mixture to -75°C yields single crystals of $[\text{Cp}^*_2\text{Fe}]_2[\text{Cl}_{20}]$ which represents the largest known polychloride today. (Equation 4).



$[\text{Cp}^*_2\text{Fe}]_2[\text{Cl}_{20}]$ crystallizes in the monoclinic space group $C2/c$ (Figure 7).

The structure of the anion is interpreted as two $[\text{Cl}(\text{Cl}_2)_4]^-$ units which are connected by a single bridging Cl_2 molecule. Overall, the structure of the anion is rather asymmetric with large differences in the distance between the central halide and the coordinated Cl_2 unit ($R(\text{Cl}-\text{Cl}) = 271.4(1)$ to 299.2(1) pm). This might be due to further inter-molecular interactions to other $[\text{Cl}_{20}]^{2-}$ units. The Cl_2 bond length of the coordinated Cl_2 units correlates well to the distance to the central halide. It increases when the distance is shorter which can be explained by a stronger interaction and therefore more donation of electron density into the σ^* orbital of the Cl–Cl bond. The only exception is the bridging Cl_2 which has a significantly elongated bond (203.6(1) pm) even though the distance to the chloride ion is rather large (299.2(1) pm). This is due to the interaction with two Cl^- ions. The Raman spectrum shows five bands between 490 and 419 cm^{-1} (see Figure S8). This is in agreement with the symmetry of the anion as the $[\text{Cl}_{20}]^{2-}$ exhibits inversion



Scheme 1. Free reaction energies for the reaction of $[\text{Cl}(\text{Cl}_2)_4]^-$ with HF and for the substitution of one Cl_2 against one HF in $[\text{Cl}(\text{Cl}_2)_5]^-$.

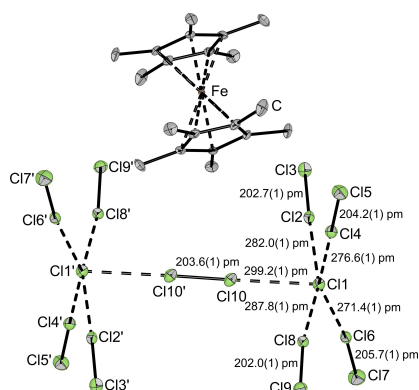


Figure 7. Molecular structure of $[\text{Cp}^*_2\text{Fe}]_2[\text{Cl}_{20}]$ in the solid state with thermal ellipsoids shown at 50% probability. Only one cation and no hydrogen atoms are shown for clarity.

symmetry (C_i). Therefore, the rule of mutual exclusion holds, and only vibrations of g symmetry are visible in the Raman spectrum. For a C_i symmetric $[\text{Cl}_{20}]^{2-}$, five bands with A_g symmetry are computed on B3LYP(D3BJ)-COSMO/def2-TZVPP and SCS-MP2-COSMO/def2-TZVPP ($\epsilon_{\text{rel}}=100$) level of theory (see Figure S9). The broad area of wavenumbers over which the bands are spread can be explained by the rather large differences in the Cl–Cl bond length ($R(\text{Cl}–\text{Cl})=202.0(1)–205.7(1)$ pm).

Both the $[\text{Cl}(\text{Cl}_2)_4(\text{HF})]^-$ and the $[\text{Cl}_{20}]^{2-}$ form three-dimensional networks in the solid state. The $[\text{Cl}(\text{Cl}_2)_4(\text{HF})]^-$ forms hexagonal prisms via short inter-molecular F–Cl distances of F1–Cl3 273.9(2) pm, F1–Cl5 287.8(2) pm and F1–Cl7 283.2(2) pm ($\sum_{\text{vdW radii}}=322$ pm^[20], see Figure 8). This gives a coordination number of five for the central fluoride as well as for the fluorine of the HF molecule. In this case the fluorine acts as a halogen bond acceptor (Lewis base) to connect the $[\text{Cl}(\text{Cl}_2)_4(\text{HF})]^-$ units. The center of the hexagonal prism is occupied by a $[\text{Cp}^*_2\text{Fe}]^+$ cation with the prisms being connected via all eight phases to translate in all three

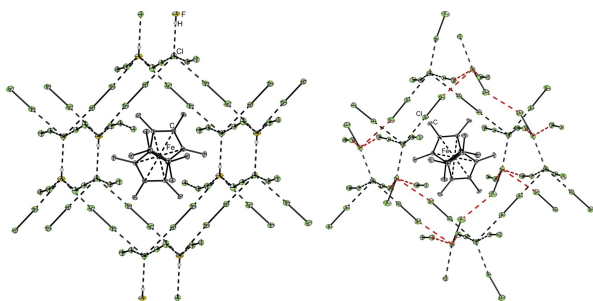


Figure 8. Anion network within the solid state structure of $[\text{Cp}^*_2\text{Fe}][\text{Cl}(\text{Cl}_2)_4(\text{HF})]$ and $[\text{Cp}^*_2\text{Fe}]_2[\text{Cl}_{20}]$. Thermal ellipsoids are shown at 50% probability. Hydrogen atoms are omitted for clarity. Intramolecular interactions between the $[\text{Cl}_{20}]^{2-}$ units are indicated by red dotted lines.

dimensions (see Figure S5.) For the $[\text{Cl}_{20}]^{2-}$ the same hexagonal prismatic arrangement is observed in the solid state, even though the prism is heavily distorted (See Figure 8). The Hirshfeld surface of the $[\text{Cl}_{20}]^{2-}$ unit shows significant interactions between the anions while only weak interactions with the cations are observed (See Figure S7). Nevertheless, a description as discrete $[\text{Cl}_{20}]^{2-}$ units is reasonable since the inter-molecular distances of $R(\text{Cl6}–\text{Cl3})=326.9(1)$ pm, $R(\text{Cl6}–\text{Cl5})=336.9(1)$ pm, $R(\text{Cl6}–\text{Cl9})=324.8(1)$ pm and $R(\text{Cl7}–\text{Cl7})=321.8(2)$ pm ($\sum_{\text{vdW radii}}=350$ pm^[20]) are significantly longer than the longest intramolecular distance (at least 22.6 pm).

Conclusion

In this work the synthesis of the four hitherto unknown polychlorides compounds, $[\text{CCl}(\text{NMe}_2)_2][\text{Cl}(\text{Cl}_2)_3]$, $[\text{NPr}_4][\text{Cl}(\text{Cl}_2)_4]$, $[\text{Cp}^*_2\text{Fe}][\text{Cl}(\text{Cl}_2)_4(\text{HF})]$ and $[\text{Cp}^*_2\text{Fe}]_2[\text{Cl}_{20}]$ was reported. All compounds have been thoroughly characterized by single-crystal X-ray diffraction, single crystal Raman spectroscopy as well as quantum-chemical calculations. With the syntheses of $[\text{Cl}(\text{Cl}_2)_3]^-$ and $[\text{Cl}(\text{Cl}_2)_4]^-$ the row of polychloride monoanions $[\text{Cl}(\text{Cl}_2)_n]^-$ ($n=1–6$) was completed while with $[\text{Cp}^*_2\text{Fe}]_2[\text{Cl}_{20}]$ we succeeded in the synthesis of the largest known polychloride. Additionally, the $[\text{Cl}(\text{Cl}_2)_4(\text{HF})]^-$ anion is the first example for a polychloride-HF network which is stabilized by strong hydrogen and halogen bonding interaction. Overall, it could be shown that polychloride chemistry shows a surprising structural diversity, which is comparable to that of the heavier polyhalogen anions.

Experimental Section

Apparatus and Materials

All substances sensitive to water and oxygen were handled under an argon atmosphere using standard Schlenk techniques and oil pump vacuum up to 10^{-3} mbar. Some reactions were performed on a stainless steel vacuum line in self-built reactors consisting of 8 mm o. d. PFA (perfluoroalkoxy alkanes) tubing which were heat sealed on one end and connected to a steel valve on the other end. Dry DCM was obtained by storage over activated 3 Å molecular sieves. Commercially available $[\text{NPr}_4]\text{Cl}$ and Cp^*_2Fe were used without further purification. Chlorine (Linde, purity 2.8) was passed through calcium chloride to remove traces of water. $[\text{CCl}(\text{NMe}_2)_2]\text{Cl}^{[28]}$ was prepared according to literature procedures. All salts were dried *in vacuo* at 100 °C for 10 min prior to use. Raman spectra were recorded on a Bruker (Karlsruhe, Germany) MultiRAM II equipped with a low-temperature Ge detector (1064 nm, 100–180 mW, resolution of 4 cm⁻¹). Spectra of single crystals were recorded at -196 °C using the Bruker RamanScope III (see supporting information part g for description of the used method). X-ray diffraction data were collected on a Bruker D8 Venture CMOS area detector (Photon 100) diffractometer with $\text{Mo}_{K\alpha}$ radiation. Single crystals were coated with perfluoroether oil at low temperature ($-40/–80$ °C) and mounted on a 0.1–0.2 mm Micro-mount. The structures were solved with the ShelXT^[29] structure solution program using intrinsic phasing and refined with the ShelXL^[30] refinement package using least squares on weighted F2

values for all reflections using OLEX2^[31]. For quantum chemical calculations (structure optimization (with and without solvent model COSMO^[32]) and frequency calculations (including Raman intensities)) the program package TURBOMOLE 7.3^[33] was used. Functionals (B3LYP(D3BJ)^[34] and SCS-MP2^[35]) and the basis set (def2-TZVPP)^[36] were used as implemented in TURBOMOLE. Minima on the potential energy surface were characterized by harmonic vibrational frequency analysis. Thermochemistry was provided with zero-point vibration correction, ΔG values were calculated at 298.15 K and 1.0 bar. Representations of Hirshfeld surfaces were generated using CrystalExplorer17^[37]

[CCl(NMe₂)₂][Cl(Cl₂)₃]

1.57 g (22.45 mmol, 15.4 equiv.) Cl₂ were condensed onto 250 mg (1.46 mmol) [CCl(NMe₂)₂] Cl at –196 C. Warming to room temperature yields a clear yellow solution. Yellow single crystals of [CCl(NMe₂)₂][Cl(Cl₂)₃] were obtained within several days by slowly cooling to –40 C.

[CCl(NMe₂)₂][Cl(Cl₂)₃] Raman (–196 C): $\tilde{\nu}$ = 2950 (vw), 2985 (vw), 1456 (vw), 1389 (vw), 618 (vw), 471 (vs), 451 (vs), 430 (m), 272 (m), 146 cm^{–1} (vw).

CCDC number: 2031714

[NPr₄][Cl(Cl₂)₄]

601 mg (2.7 mmol) [NPr₄]Cl was dissolved in 1.4 mL MeCN. 766 mg (10.9 mmol, 4.0 equiv.) Cl₂ are condensed onto the solution at –196 C. The reaction mixture was warmed to room temperature and a clear yellow solution was obtained. Yellow single crystals of [NPr₄][Cl(Cl₂)₄] were obtained within several days by slowly cooling to –15 C.

[NPr₄][Cl(Cl₂)₄] Raman (–196 C): $\tilde{\nu}$ = 3003 (vw), 2982 (vw), 2954 (vw), 2937 (vw), 2872 (vw), 1458 (vw), 1445 (vw), 1315 (vw), 477 (vs), 450 (vs), 151 cm^{–1} (w).

CCDC number: 2031713

[Cp*₂Fe][Cl(Cl₂)₄(HF)]

Inside a 8 mm PFA tube connected to a stainless steel valve, 32 mg (0.1 mmol) Cp*₂Fe were dissolved in 1.5 ml dichloromethane. 90 mg Cl₂ (1.25 mmol) were condensed in at –196 C. The mixture was warmed to –70 C and mechanically agitated resulting in a dark green suspension. After some minutes 3 mg anhydrous hydrogen fluoride were condensed in at –196 C. The mixture was warmed to approximately –35 C, resulting in a clear dark-green solution. The mixture was frozen at –196 C, and the PFA tube was flame-sealed in vacuum. The sealed-off tube was placed inside a Dewar filled with 1–2 liters of –35 C cold ethanol and placed in a –75 C freezer. After one day, dark-green crystals had formed.

[Cp*₂Fe][Cl(Cl₂)₄(HF)] Raman (–196 C): $\tilde{\nu}$ = 2931 (m), 1423 (w), 735 (w), 588 (w), 507 (s), 488 (s), 477 (vs), 367 (w), 292 (vw).

CCDC number: 2031710

[Cp*₂Fe]₂[Cl₂₀]

Inside a 8 mm PFA tube connected to a stainless steel valve, 32 mg (0.1 mmol) Cp*₂Fe were dissolved in 1.5 ml dichloromethane. 180 mg Cl₂ (2.5 mmol) were condensed in at –196 C. The mixture was warmed to –70 C and mechanically agitated resulting in a dark green suspension. After some minutes, the mixture was

warmed to –50 C, resulting in a clear dark-green solution. The mixture was frozen at –196 C, and the PFA tube was flame-sealed in vacuum. The sealed-off tube was placed inside a Dewar filled with 1–2 liters of –50 C cold ethanol and placed in a –75 C freezer. After one day, dark-green crystals had formed.

[Cp*₂Fe]₂[Cl₂₀] Raman (–196 C): $\tilde{\nu}$ = 2986 (vw), 2965 (vw), 2914 (w), 1480 (vw), 1442 (vw), 1425 (vw), 1025 (vw), 700 (vw), 591 (vw), 490 (s), 473 (vs), 450 (vs), 417 (m), 366 (w), 291 (m), 242 (vw), 223 (vw), 182 cm^{–1} (vw).

CCDC number: 2031711.

Deposition Numbers 2031714 (for [CCl(NMe₂)₂][Cl(Cl₂)₃]), 2031713 (for [NPr₄][Cl(Cl₂)₄]), 2031710 (for [Cp*₂Fe][Cl(Cl₂)₄(HF)]), and 2031711 (for [Cp*₂Fe]₂[Cl₂₀]) contain the supplementary crystallographic data for this paper. These data are provided free of charge by the joint Cambridge Crystallographic Data Centre and Fachinformationszentrum Karlsruhe Access Structures service www.ccdc.cam.ac.uk/structures.

Acknowledgements

We gratefully acknowledge the Zentraleinrichtung für Datenverarbeitung (ZEDAT) of the FU Berlin for computational resources. We thank the priority program SPP 1708 for financial support. We thank Tyler Andrew Gully for helping prepare the table of contents graphic. Open access funding enabled and organized by Projekt DEAL.

Conflict of Interest

The authors declare no conflict of interest.

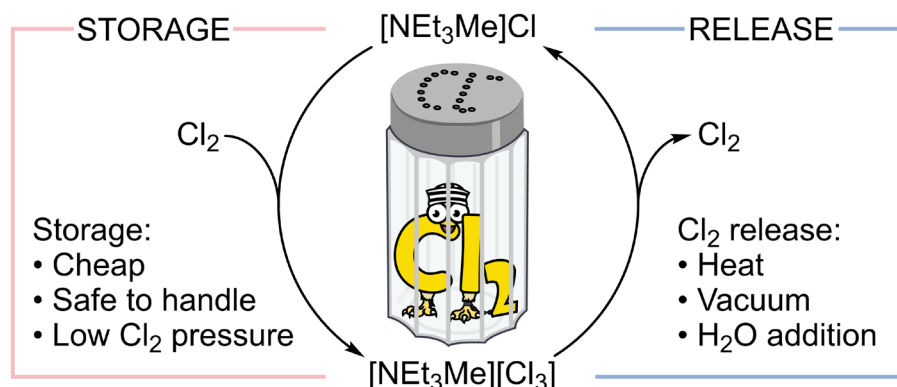
Keywords: Halogens · Polychlorides · Quantum-chemical calculations · Halogen-bonding · Structure elucidation

- [1] K. Sonnenberg, L. Mann, F. A. Redeker, B. Schmidt, S. Riedel, *Angew. Chem. Int. Ed.* **2020**, *59*, 5464–5493, *Angew. Chem.* **2020**, *132*, 5506–5535.
- [2] H. Haller, M. Hog, F. Scholz, H. Scherer, I. Krossing, S. Riedel, *Z. Naturforsch.* **2013**, *68b*, 1103–1107.
- [3] T. Schlama, K. Gabriel, V. Gouverneur, C. Mioskowski, *Angew. Chem. Int. Ed.* **1997**, *36*, 2342–2344, *Angew. Chem.* **1997**, *109*, 2440–2442.
- [4] a) T. M. Beck, H. Haller, J. Streuff, S. Riedel, *Synthesis* **2014**, *46*, 740–747; b) S. S. Tartakoff, C. D. Vanderwal, *Org. Lett.* **2014**, *16*, 1458–1461; c) C. V. Vogel, H. Pietraszkiewicz, O. M. Sabry, W. H. Gerwick, F. A. Valeriote, C. D. Vanderwal, *Angew. Chem. Int. Ed.* **2014**, *53*, 12205–12209, *Angew. Chem.* **2014**, *126*, 12401–12405; d) W.-j. Chung, J. S. Carlson, C. D. Vanderwal, *J. Org. Chem.* **2014**, *79*, 2226–2241; e) Z. A. Könst, A. R. Szklarski, S. Pellegrino, S. E. Michalak, M. Meyer, C. Zanette, R. Cencic, S. Nam, V. K. Vora, D. A. Horne, J. Pelletier, D. L. Mobley, G. Yusupova, M. Yusupov, C. D. Vanderwal, *Nat. Chem.* **2017**, *9*, 1140–1149.
- [5] a) M. Paven, Y. Schiesser, R. Weber, G. Langstein, V. Trieu, S. Riedel, N. Schwarze, S. Steinhauer, **2018**, WO 2019215037 A1; b) A. N. Usoltsev, S. A. Adonin, B. A. Kolesov, A. S. Novikov, V. P. Fedin, M. N. Sokolov, *Chem. Eur. J.* **2020**, *26*, 13776–13778.
- [6] a) A. van den Bossche, E. de Witte, W. Dehaen, K. Binnemans, *Green Chem.* **2018**, *20*, 3327–3338; b) X. Li, A. van den Bossche, T. Vander Hoogerstraete, K. Binnemans, *Chem. Commun.* **2018**, *54*, 475–478; c) X. Li, Z. Li, M. Orefice, K. Binnemans, *ACS Sustainable Chem. Eng.* **2019**, *7*, 2578–2584; d) B. Schmidt, B. Schröder, K. Sonnenberg, S. Steinhauer, S. Riedel,

- Angew. Chem. Int. Ed.* **2019**, *58*, 10340–10344, *Angew. Chem.* **2019**, *131*, 10448.
- [7] G. Bauer, J. Drobts, C. Fabjan, H. Mikosch, P. Schuster, *J. Electroanal. Chem.* **1997**, *427*, 123–128.
- [8] a) M. E. Easton, A. J. Ward, T. Hudson, P. Turner, A. F. Masters, T. Maschmeyer, *Chem. Eur. J.* **2015**, *21*, 2961–2965; b) K.-F. Tebbe, R. Buchem, *Z. Anorg. Allg. Chem.* **1998**, *624*, 671–678; c) K.-F. Tebbe, R. Buchem, *Angew. Chem. Int. Ed. Engl.* **1997**, *36*, 1345–1346.
- [9] H. Haller, S. Riedel, *Z. Anorg. Allg. Chem.* **2014**, *640*, 1281–1291.
- [10] a) S. Riedel, T. Köchner, X. Wang, L. Andrews, *Inorg. Chem.* **2010**, *49*, 7156–7164; b) T. Vent-Schmidt, F. Brosi, J. Metzger, T. Schlöder, X. Wang, L. Andrews, C. Müller, H. Beckers, S. Riedel, *Angew. Chem. Int. Ed.* **2015**, *54*, 8279–8283, *Angew. Chem.* **2015**, *127*, 8397.
- [11] a) M. P. Bogaard, J. Peterson, A. D. Rae, *Acta Crystallogr. Sect. B* **1981**, *37*, 1357–1359; b) J. Taraba, Z. Zak, *Inorg. Chem.* **2003**, *42*, 3591–3594.
- [12] K. Sonnenberg, P. Pröhm, N. Schwarze, C. Müller, H. Beckers, S. Riedel, *Angew. Chem. Int. Ed.* **2018**, *57*, 9136–9140, *Angew. Chem.* **2018**, *130*, 9274.
- [13] R. Brückner, P. Pröhm, A. Wiesner, S. Steinhauer, C. Müller, S. Riedel, *Angew. Chem. Int. Ed.* **2016**, *55*, 10904–10908, *Angew. Chem.* **2016**, *128*, 11064.
- [14] R. Brückner, H. Haller, S. Steinhauer, C. Müller, S. Riedel, *Angew. Chem. Int. Ed.* **2015**, *54*, 15579–15583, *Angew. Chem.* **2015**, *127*, 15800.
- [15] a) G. Cavallo, P. Metrangolo, R. Milani, T. Pilati, A. Priimägi, G. Resnati, G. Terraneo, *Chem. Rev.* **2016**, *116*, 2478–2601; b) T. Clark, M. Hennemann, J. S. Murray, P. Politzer, *J. Mol. Model.* **2007**, *13*, 291–296.
- [16] H. Keil, K. Sonnenberg, C. Müller, R. Herbst-Irmer, H. Beckers, S. Riedel, D. Stalke, *Angew. Chem. Int. Ed.* **2021**, *60*, 2569–2573, *Angew. Chem.* **2021**, *133*, 2600–2604.
- [17] B. M. Powell, K. M. Heal, B. H. Torrie, *Mol. Phys.* **1984**, *53*, 929–939.
- [18] B. Schmidt, S. Ponath, J. Hannemann, P. Voßnacker, K. Sonnenberg, M. Christmann, S. Riedel, *Chem. Eur. J.* **2020**, *26*, 15183–15189.
- [19] H. Haller, M. Ellwanger, A. Higelin, S. Riedel, *Z. Anorg. Allg. Chem.* **2012**, *638*, 553–558.
- [20] A. Bondi, *J. Phys. Chem.* **1964**, *68*, 441–451.
- [21] T. Bernstein, F. H. Herbststein, *Acta Crystallogr.* **1968**, *B24*, 1640–1645.
- [22] K.-F. Tebbe, R. Buchem, *Z. Kristallogr. Cryst. Mater.* **1995**, *210*, 438–441.
- [23] K.-F. Tebbe, R. Buchem, *Z. Kristallogr. Cryst. Mater.* **1996**, *211*, 689–694.
- [24] A. N. Nesmeyanov, L. P. Yur'eva, R. B. Materikova, B. Y. Getnarski, *Russ. Chem. Bull.* **1965**, *14*, 711–713.
- [25] a) S. Zürcher, J. Petrig, V. Gramlich, M. Wörle, C. Mensing, D. von Arx, A. Togni, *Organometallics* **1999**, *18*, 3679–3689; b) J. Pickardt, H. Schumann, R. Mohtachemi, *Acta Crystallogr.* **1990**, *C46*, 39–41.
- [26] a) M. Malischewski, M. Adelhardt, J. Sutter, K. Meyer, K. Seppelt, *Science* **2016**, *353*, 678–682; b) M. Malischewski, K. Seppelt, J. Sutter, F. W. Heinemann, B. Dittrich, K. Meyer, *Angew. Chem. Int. Ed.* **2017**, *56*, 13372–13376, *Angew. Chem.* **2017**, *129*, 13557–13561; c) M. Malischewski, K. Seppelt, J. Sutter, D. Munz, K. Meyer, *Angew. Chem. Int. Ed.* **2018**, *57*, 14597–14601, *Angew. Chem.* **2018**, *130*, 14806–14810.
- [27] A. W. Addison, T. N. Rao, J. Reedijk, J. van Rijn, G. C. Verschoor, *J. Chem. Soc. Dalton Trans.* **1984**, 1349–1356.
- [28] V. Štrukil, E. Lekšič, E. Meštrović, M. Eckert-Maksić, *Aust. J. Chem.* **2014**, *67*, 1129–1133.
- [29] G. M. Sheldrick, *Acta Crystallogr.* **2008**, *A64*, 112–122.
- [30] G. M. Sheldrick, *Acta Crystallogr.* **2015**, *C71*, 3–8.
- [31] O. V. Dolomanov, L. J. Bourhis, R. J. Gildea, J. A. K. Howard, H. Puschmann, *J. Appl. Crystallogr.* **2009**, *42*, 339–341.
- [32] A. Klamt, G. Schüürmann, *J. Chem. Soc. Perkin Trans. 2* **1993**, 799–805.
- [33] TURBOMOLE GmbH, *TURBOMOLE V7.3: a development of University of Karlsruhe and Forschungszentrum Karlsruhe GmbH*, **2018**.
- [34] a) A. D. Becke, *J. Chem. Phys.* **1993**, *98*, 5648–5652; b) C. Lee, W. Yang, R. G. Parr, *Phys. Rev. B* **1988**, *37*, 785–789; c) S. H. Vosko, L. Wilk, M. Nusair, *Can. J. Phys.* **1980**, *58*, 1200–1211; d) P. J. Stephens, F. J. Devlin, C. F. Chabalowski, M. J. Frisch, *J. Phys. Chem.* **1994**, *98*, 11623–11627; e) S. Grimme, J. Antony, S. Ehrlich, H. Krieg, *J. Chem. Phys.* **2010**, *132*, 154104; f) A. D. Becke, E. R. Johnson, *J. Chem. Phys.* **2005**, *123*, 154101; g) E. R. Johnson, A. D. Becke, *J. Chem. Phys.* **2005**, *123*, 24101; h) E. R. Johnson, A. D. Becke, *J. Chem. Phys.* **2006**, *124*, 174104.
- [35] S. Grimme, *J. Chem. Phys.* **2003**, *118*, 9095–9102.
- [36] F. Weigend, R. Ahlrichs, *Phys. Chem. Chem. Phys.* **2005**, *7*, 3297–3305.
- [37] M. J. Turner, J. J. McKinnon, S. K. Wolff, D. J. Grimwood, P. R. Spackman, D. Jayatilaka, M. A. Spackman, *CrystalExplorer17*; University of Western Australia, **2017**.

Manuscript received: November 25, 2020
 Revised manuscript received: December 22, 2020
 Accepted manuscript online: December 28, 2020

3.3 Alkyl Ammonium Chloride Salts for Efficient Chlorine Storage at Ambient Conditions



Patrick Voßnacker, Nico Schwarze, Thomas Keilhack, Merlin Kleoff, Simon Steinhauer, Yuliya Schiesser, Maxime Paven, Sivathmeehan Yogendra, Rainer Weber, Sebastian Riedel*

ACS Sustainable Chem. Eng. **2022**, 29, 9525.

<https://doi.org/10.1021/acssuschemeng.2c02186>

© 2022 American Chemical Society. Modified and reproduced with permission

Author contributions

Patrick Voßnacker designed the project, performed most of the experiments and wrote the manuscript. Thomas Keilhack and Nico Schwarze and Merlin Kleoff performed some of the experiments. Merlin Kleoff and Simon Steinhauer revised the manuscript and provided scientific guidance. Yuliya Schiesser, Maxime Paven, Sivathmeehan Yogendra and Rainer Weber provided scientific guidance. Sebastian Riedel managed the project and revised the manuscript.

Alkyl Ammonium Chloride Salts for Efficient Chlorine Storage at Ambient Conditions

Patrick Voßnacker, Nico Schwarze, Thomas Keilhack, Merlin Kleoff, Simon Steinhauer, Yuliya Schiesser, Maxime Paven, Sivathmehaan Yogendra, Rainer Weber, and Sebastian Riedel*

Cite This: ACS Sustainable Chem. Eng. 2022, 10, 9525–9531

Read Online

ACCESS |

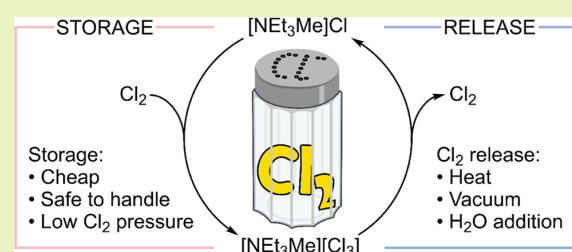
Metrics & More

Article Recommendations

Supporting Information

ABSTRACT: Herein, we report the use of alkyl ammonium chloride salts as safe and sustainable chlorine storage media. The most promising candidate, $[\text{NEt}_3\text{Me}]\text{Cl}$, stores up to 0.79 kg chlorine/kg storage material, is readily prepared, and stable against chlorination for extended times. Chlorine release can be achieved by applying heat or vacuum, or, alternatively, by the addition of water. The combination of these properties emphasizes $[\text{NEt}_3\text{Me}]\text{Cl}$ as a suitable storage medium to facilitate the flexibilization of industrial chlorine production. As polychlorides can be used for various chlorination reactions, a combined industrial process is envisaged utilizing $[\text{NEt}_3\text{Me}]\text{Cl}$ as the storage medium and the loaded system, $[\text{NEt}_3\text{Me}][\text{Cl}(\text{Cl}_2)_n]$ ($n = 1.68$), as the reagent for industrial chlorinations.

KEYWORDS: chlorine, polychlorides, halogen bonding, sustainable chemistry, ionic liquid, industrial chemistry



INTRODUCTION

With a production of 75 million tons per year, chlorine is one of the most important base chemicals. It is used in numerous reactions and involved in the synthesis of roughly 50% of all industrial compounds, 20% of small-molecule pharmaceutical products, and 30% of agrochemicals.¹ Primarily, chlorine is applied in the synthesis of precursors for polymers, e.g., vinyl chloride for PVC and phosgene for polyurethanes and polycarbonates.²

However, the production of chlorine by chloralkali electrolysis is an extremely energy-demanding process requiring, for instance, 2% of the entire electrical energy production in Germany.³ To realize the vision of an exit of coal and nuclear energy, the production of renewable energy (e.g., solar and wind energy) is currently expanded, which results in a more inconsistent energy supply depending on local weather circumstances. Therefore, achieving higher flexibility for energy-intensive processes is a key challenge.⁴ Currently, the flexibilization of chlorine production is mainly limited by the lack of techniques for efficient chlorine storage.^{5,6}

Typically, chlorine is stored either by pressure liquefaction at 7 bar or by cooling below the boiling point of $-34\text{ }^\circ\text{C}$.² Both methods are energy-intensive and require circumstantial corrosion protection and safety concepts in case of a failure of the storage system, resulting in the expansion of toxic chlorine gas.⁷ This is of particular importance for the transport of large quantities of chlorine.⁸ In this context, porous silicon dioxide particles have been investigated by the Polarz group in cooperation with Covestro for chlorine storage at milder

conditions still requiring relatively high pressures (3.5 bar at $30\text{ }^\circ\text{C}$ for 0.4 kg Cl_2 stored on 1 kg SiO_2) or low temperatures (1 bar at $-26\text{ }^\circ\text{C}$ for 1.1 kg Cl_2 stored on 1 kg SiO_2).⁹ This indicates that the main challenges of chlorine storage are only partially solved thus far. Therefore, safe chlorine storage materials, which allow the storage of chlorine at ambient pressure and temperature, are highly desirable.

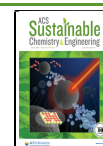
In general, the storage of chlorine by liquefaction and consecutive chlorine release for further reactions is an energy-demanding process (Figure 1A). Thus, we aimed for a medium that is able to store chlorine under ambient conditions without requiring additional energy. To further pursue the idea of sustainability, we envisioned to develop a storage medium that is not only able to store chlorine gas but ideally also to serve directly as a reagent for chlorination reactions. In this way, an industrial process could be realized, combining chlorine storage and chlorination reactions in an energetic “downhill process” (Figure 1B).

At the outset of this work, we anticipated that organic chloride salts can reversibly bind chlorine by forming polychlorides (also known as polychlorine anions). Due to their large structural diversity and possible applications,

Received: April 13, 2022

Revised: June 30, 2022

Published: July 14, 2022



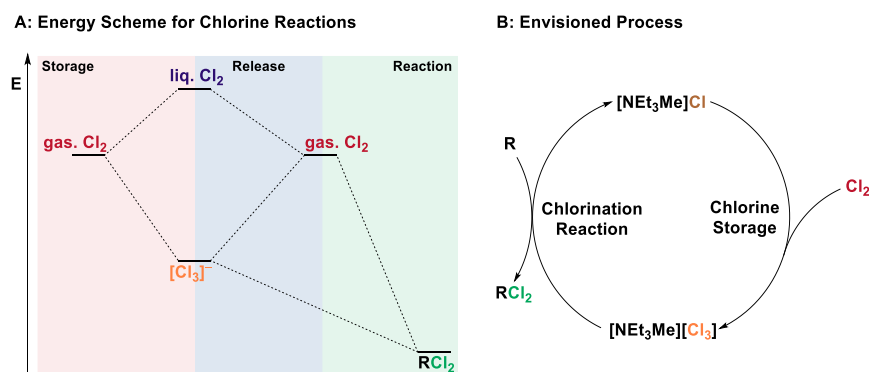


Figure 1. (A) Comparison of the energy profile for conventional chlorine storage as well as chlorine storage as polychlorides and (B) proposed scheme for the direct use of $[\text{NEt}_3\text{Me}][\text{Cl}_3]$ as a chlorination reagent.

polychloride salts received much attention in recent years.¹⁰ It was shown that a complete row of polychlorine monoanions $[\text{Cl}(\text{Cl}_2)_n]^-$ with $n = 1-6$ ¹¹⁻¹⁵ can be stabilized using weakly coordinating cations (e.g., PPh_4 or NPr_4), while the recently reported $[\text{Cl}_{20}]^{2-}$ represents the largest known polychloride.¹⁵ Polychlorides with lower chlorine content exist either as solids or as low viscous ionic liquids (Figure 2) with a significantly

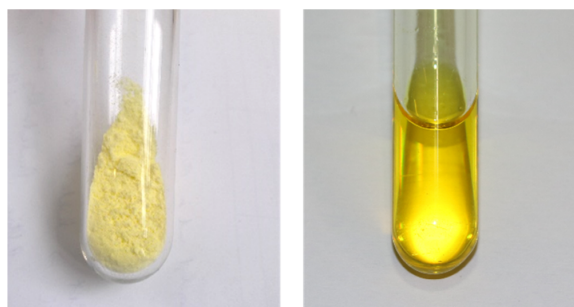


Figure 2. Examples of a solid ($[\text{NEt}_4][\text{Cl}_3]$, left) and a liquid organic trichloride system ($[\text{NEt}_3\text{Me}][\text{Cl}_3]$, right) at ambient temperature.

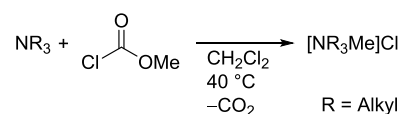
reduced vapor pressure compared to Cl_2 gas. This makes them easy-to-handle chlorination reagents that have been used in numerous organic transformations.¹⁶ Very recently, we found that $[\text{NEt}_3\text{Me}][\text{Cl}_3]$ can directly react with CO , without further activation by light or heat, to form phosgene (COCl_2), a major intermediate in the synthesis of polyurethanes and polycarbonates.¹⁷ Additionally, trichloride ionic liquids are useful for the oxidative dissolution of metals and alloys for metal recycling applications, as demonstrated by the group of Binnemans and others.¹⁸⁻²⁰

In this work, we show that ammonium chlorides are an enabling technique for an efficient chlorine storage at ambient pressure and temperature, as some of them have a high storage capacity, are accessible from cheap raw materials, are stable against undesired chlorination, and the formed polychlorides have a low viscosity. As the application of polychlorides for industrial transformations has been demonstrated, ammonium chlorides could be used as storage media and the obtained polychlorides as versatile reagents to enable flexible production of chlorinated materials in a combined process.

RESULTS AND DISCUSSION

Synthesis of Storing Materials and Their Physical Properties. To find suitable candidates, we determined the storage capacities of various alkyl ammonium chloride salts and investigated the physical properties of the corresponding polychlorides. These chloride salts are either commercially available or can readily be prepared by methylation of amines using, e.g., methyl chloroformate or inexpensive methyl chloride (Scheme 1).

Scheme 1. Preparation of Ammonium Chlorides by Methylation of Amines



To determine the chlorine storage capacities of these chloride salts, an excess of Cl_2 gas was condensed onto a defined amount of the chloride salt. Warming the reaction mixture to room temperature and allowing unreacted chlorine gas to evaporate until the system reaches atmospheric pressure yields polychloride salts as the loaded chlorine storages.

Alternatively, the system can be loaded by exposing the chloride salt to an atmosphere of chlorine gas. This procedure is more convenient for large-scale preparations and is applied for the synthesis of 1 kg of $[\text{NEt}_3\text{Me}][\text{Cl}(\text{Cl}_2)_{1.68}]$ (Scheme 2 and Video S1).²¹

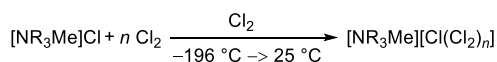
The amount of stored chlorine was determined by gravimetric analysis. Additionally, the melting points, densities, and viscosities (for selected systems) of the obtained polychlorides $[\text{NR}_3\text{Me}][\text{Cl}(\text{Cl}_2)_n]$ were determined. The results for selected ammonium salt systems are summarized in Table 1 (see Table S2 for full data).

The physicochemical properties of symmetric and asymmetric ammonium polychlorides show significant differences. In general, polychlorides with symmetric cations have higher melting points and viscosities compared to asymmetric cations.

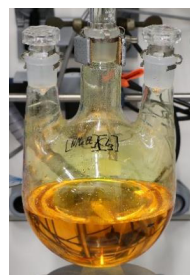
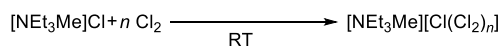
Notably, ammonium salts with short alkyl chains, e.g., methyl or ethyl, have the lowest viscosities rendering them advantageous candidates for industrial applications as they can be more easily pumped and transferred within a plant. The amount of chlorine, which can be stored per mole of chloride, is highest for asymmetric cations with propyl and butyl groups.

Scheme 2. Reaction of Organic Chlorides with Chlorine to the Corresponding Polychlorides

Screening



Large Scale

Table 1. Storage Capacities of $[\text{NR}_3\text{Me}]\text{Cl}$ and Physical Properties of $[\text{NR}_3\text{Me}][\text{Cl}(\text{Cl}_2)_n]$

substrate	melting point polychloride [$^\circ\text{C}$]	density at 25 $^\circ\text{C}$ [kg L^{-1}]	dynamic viscosity [mPa s]	storage capacity by amount of substance [mol mol^{-1}] ^a	storage capacity by mass [kg kg^{-1}] ^b	storage capacity by volume [kg L^{-1}] ^c
Cl_2 ²	-101, -35 ^d	1.38				1.38
$[\text{NBu}_4]\text{Cl}$	5	1.30	684	2.18	0.55	0.46
$[\text{NEtMe}_3]\text{Cl}$	8	1.24	low viscosity	1.44	0.82	0.56
$[\text{NEt}_2\text{Me}_2]\text{Cl}$	-19	1.20	16	1.57	0.8	0.54
$[\text{NEt}_3\text{Me}]\text{Cl}$	1 (-10) ^e	1.21	19	1.68	0.79	0.53
$[\text{NBuMe}_3]\text{Cl}$	21	1.25	low viscosity	2.57	1.19	0.68
$[\text{NBuEt}_2\text{Me}]\text{Cl}$	-19	1.30	46	2.72	1.06	0.67
$[\text{NMePr}_3]\text{Cl}$	9	1.23	141	2.13	0.77	0.54
$[\text{NBu}_3\text{Me}_2]\text{Cl}$	-27	1.17	low viscosity	2.29	0.83	0.53
$[\text{NBu}_3\text{Me}]\text{Cl}$	8	1.19	low viscosity	2.46	0.73	0.51

^aStorage capacity by the amount of substance is equal to the amount of substance of Cl_2 that can be stored on 1 mol of the chloride salt. ^bStorage capacity by mass is equal to the mass of Cl_2 that can be stored on 1 kg of the chloride salt. ^cStorage capacity by volume is equal to the mass of Cl_2 that is stored in 1 L of $[\text{Cat}][\text{Cl}(\text{Cl}_2)_n]$. ^db.p. of elemental chlorine. ^eDetermined by cooling liquid $[\text{NEt}_3\text{Me}][\text{Cl}(\text{Cl}_2)_{1.68}]$.

This is likely due to a weaker interaction between the cation and the chloride ion. The storage capacity by mass is only slightly larger for asymmetric cations with propyl and butyl groups compared to cations with ethyl groups due to their higher molar mass. For example, $[\text{NBuEt}_2\text{Me}]\text{Cl}$ has a higher storage capacity by the amount of substance than $[\text{NEt}_3\text{Me}]\text{Cl}$ (2.72 vs 1.68 mol mol^{-1}), while the difference of the storage capacity by mass is significantly smaller (1.06 vs 0.79 kg kg^{-1}).

To allow a comparison to liquefied chlorine, we investigated how much chlorine can be stored in a certain volume of $[\text{Cat}][\text{Cl}(\text{Cl}_2)_n]$. Values between 0.5 and 0.7 kg Cl_2 per L polychloride are obtained for the best candidates compared to 1.38 kg L^{-1} for liquefied chlorine at 7 bar and 25 $^\circ\text{C}$. Even though the storage capacity by volume for liquefied chlorine is higher, these results are promising since chlorine storage at ambient conditions allows for a more efficient design of the storage containers and holds enormous advantages in terms of safety and handling.

Then, we tested the long-term stabilities of $[\text{NBu}_4][\text{Cl}(\text{Cl}_2)_n]$ and $[\text{NEt}_3\text{Me}][\text{Cl}(\text{Cl}_2)_n]$ as we expected that ammonium salts with butyl groups could undergo possible chlorination over prolonged time. When we stored a sample of $[\text{NBu}_4][\text{Cl}(\text{Cl}_2)_n]$ and measured Raman spectra after 6 month, we found that the bands for polychloride species disappeared (Figure 3 top), while further investigations by electrospray ionization (ESI)-mass spectrometry revealed signals for the chlorinated cation with up to four hydrogen atoms substituted by chlorine (Figures S18 and S19). In the case of $[\text{NEt}_3\text{Me}][\text{Cl}(\text{Cl}_2)_n]$, no changes in the Raman spectra were observed even after more than 2 years (Figure 3 bottom). Additional experiments with $[\text{NEt}_3\text{Me}][\text{Cl}_3]$ and $[\text{NEt}_3\text{Me}][\text{Cl}(\text{Cl}_2)_{1.6}]$

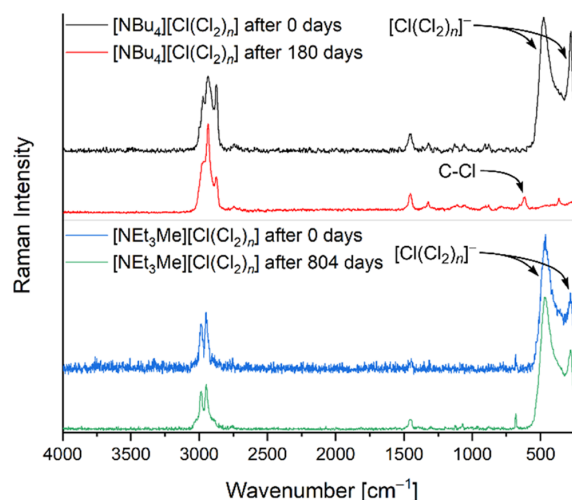


Figure 3. Comparison of the long-term stabilities of $[\text{NEt}_3\text{Me}][\text{Cl}(\text{Cl}_2)_n]$ and $[\text{NBu}_4][\text{Cl}(\text{Cl}_2)_n]$.

showed that even storing at 50 $^\circ\text{C}$ or in the sunlight for 2 months did not lead to any decomposition (see Figures S10–S17).

By evaluating all collected data, we selected $[\text{NEt}_3\text{Me}]\text{Cl}$ as the most promising candidate for chlorine storage as it shows a high stability against chlorine, has one of the highest storage capacities, and the lowest viscosities. Additionally, it can be

prepared from cheap and abundant starting materials, e.g., NEt_3 and MeCl .

Methods of Chlorine Release. The efficiency of chloride salts as chlorine storage media can be explained by two different bonding situations, namely, the multicentered bonding as $3c4e$ bonding in $[\text{Cl}_3]^-$ and the strong halogen-bonding interaction between $[\text{Cl}_3]^-$ and additional Cl_2 . This is supported by experimentally determined dissociation energies of $99 \pm 5 \text{ kJ mol}^{-1}$ for $[\text{Cl}_3]^-$ in the gas phase.²² In the condensed phase, there is an attractive interaction between the chloride and the organic cations that reduces the basicity of the chloride ion, resulting in a lower dissociation energy of $[\text{Cl}_3]^-$. This leads to an equilibrium between $[\text{NEt}_3\text{Me}][\text{Cl}(\text{Cl}_2)_n]$ and free chlorine gas and, consequently, a chlorine vapor pressure. Therefore, chlorine release can be performed by shifting this equilibrium using heat, vacuum, or a gas stream (Figure 4A).

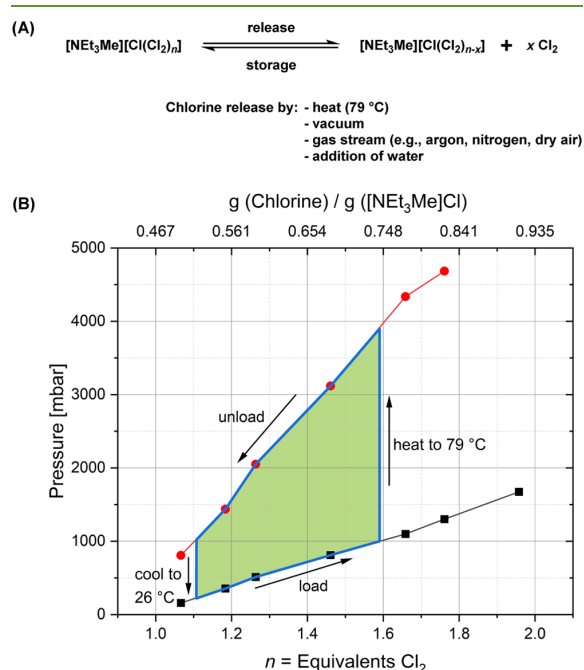


Figure 4. (A) Release of x equiv of chlorine by shifting the equilibrium between polychloride species $[\text{NEt}_3\text{Me}][\text{Cl}(\text{Cl}_2)_n]$ with various chlorine contents n . (B) Envisioned storage–release process based on vapor pressure curves measured for $[\text{NEt}_3\text{Me}][\text{Cl}(\text{Cl}_2)_n]$ at 26 and 79 °C.

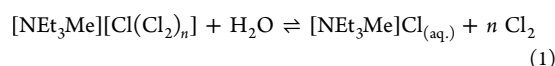
As we aimed for the development of an industrial chlorine storage, we envisioned a simple storage–release process for a liquid system that maintains ambient pressure and utilizes abundant process heat at ~ 80 °C to release chlorine gas. Therefore, we measured vapor pressure curves of $[\text{NEt}_3\text{Me}][\text{Cl}(\text{Cl}_2)_n]$ at 26 and 79 °C in dependency of n (see Figure S22). Based on these results, starting from liquid $[\text{NEt}_3\text{Me}][\text{Cl}(\text{Cl}_2)_n]$ with $n = 1.1$ chlorine is stored until a vapor pressure of $p = 1$ bar is achieved at $n = 1.6$, keeping the system at ambient pressure (Figure 4B). By heating to 79 °C, the chlorine vapor pressure is increased to $p = 3.9$ bar, resulting in the release of chlorine gas until the system reaches its equilibrium at $p = 1$ bar with $n = 1.1$. By cooling to ambient

temperature (26 °C), the storage can again be loaded with chlorine gas.

For many applications, a mobile chlorine storage is required that does not build up an overpressure at higher ambient temperatures on warm days. Given these considerations, chlorine storage has to be utilized in a range with a limited vapor pressure translating to a lower chlorine load (e.g., $p = 70$ mbar at $n = 1.0$; see Figure S21). However, in this range, chlorine release by physicochemical methods as described above is less effective (see Figures S25 and S26). Therefore, we aimed for an alternative method, enabling a simple and complete chlorine release from the storage, leading back to $[\text{NEt}_3\text{Me}]\text{Cl}$. As this chlorine-free system is significantly less hazardous than the loaded system, it could be easily disposed, rendering the sustainable of chlorine storage.

To realize this idea, we took advantage of the higher solvation energy of $[\text{NEt}_3\text{Me}]\text{Cl}$ compared to $[\text{NEt}_3\text{Me}][\text{Cl}(\text{Cl}_2)_n]$ in polar solvents such as H_2O due to a more localized charge of the chloride compared to the polychloride. Indeed, the addition of 10 equiv of H_2O led to a release of 70% Cl_2 from $[\text{NEt}_3\text{Me}][\text{Cl}_3]$ ($n = 1$) in an endothermic reaction. The obtained aqueous solution of $[\text{NEt}_3\text{Me}]\text{Cl}$ can be recycled by evaporation of the solvent yielding pure $[\text{NEt}_3\text{Me}]\text{Cl}$ as shown by ^1H NMR spectroscopy (Figure S27). Since the evaporation of H_2O requires energy, we tried to limit the amount of H_2O to the lowest possible amount. Therefore, H_2O was added portionwise to $[\text{NEt}_3\text{Me}][\text{Cl}_3]$ until the stored Cl_2 was completely released, which was achieved after the addition of 5 equiv of H_2O (Figure S28).

The phenomenon why a smaller amount of H_2O results in an increased chlorine release can be explained by taking the contrary equilibria of chlorine release and chlorine solvation into account (see eqs 1 and 2). According to Le Chatelier's principle, an excess of water should shift the equilibrium from $[\text{NEt}_3\text{Me}][\text{Cl}(\text{Cl}_2)_n]$ to solvated $[\text{NEt}_3\text{Me}]\text{Cl}$ and free Cl_2 (eq 1). On the other hand, the dissolution of chlorine is also increased with the amount of water (eq 2). Therefore, it can be assumed that solvation of $[\text{NEt}_3\text{Me}]\text{Cl}$ with 5 equiv of water is sufficient to release chlorine completely, while increasing the water content above this point results in the dissolution of chlorine



The observed value for the optimal amount of water correlates well to the determined maximal solubility of $[\text{NEt}_3\text{Me}]\text{Cl}$ in water of 2152 g L^{-1} , which corresponds to 4 equiv of water per equivalent $[\text{NEt}_3\text{Me}]\text{Cl}$. Therefore, by adding 5 equiv of water, an almost saturated solution of $[\text{NEt}_3\text{Me}]\text{Cl}$ is obtained, resulting in a minimal solubility of chlorine. A similar behavior was observed for the solubility of chlorine in aqueous solutions of sodium chloride (see Table S1).²³ In fact, the addition of 5 equiv of water to $[\text{NEt}_3\text{Me}][\text{Cl}(\text{Cl}_2)_1]$ led to the release of 97% Cl_2 after 40 min. Thus, the release of chlorine from the storage by the simple addition of water is a useful alternative to the industrial methods applying heat or vacuum, allowing a substantial liberation of chlorine within minutes (see Video S2). Several other solvents for releasing chlorine gas from polychloride-based storage media have been patented as well.²⁴

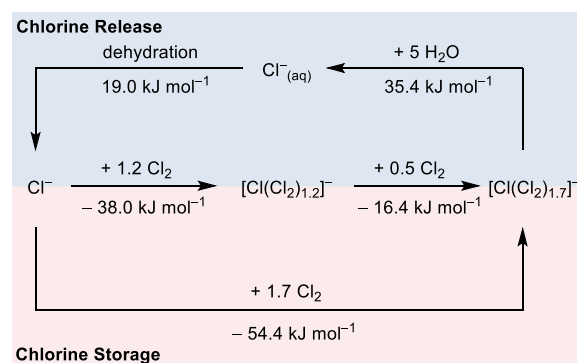
Investigation of Process Enthalpies. As an industrial application of $[\text{NET}_3\text{Me}]\text{Cl}$ as chlorine storage is envisioned, we investigated the thermodynamic parameters of the storage–release cycle by heat flow calorimetry. First, the enthalpy of chlorine release from $[\text{NET}_3\text{Me}][\text{Cl}(\text{Cl}_2)_{1.7}]$ by the addition of 5 equiv of water was elucidated to be endothermic with $H_{\text{release}} = 35.4 \text{ kJ mol}^{-1}$. In this reaction, chlorine is completely released, while the formed $[\text{NET}_3\text{Me}]\text{Cl}$ is hydrated, leading to $[\text{NET}_3\text{Me}]\text{Cl}_{(\text{aq})}$. Therefore, the formation enthalpy ($H_{\text{formation}}$) of $[\text{NET}_3\text{Me}][\text{Cl}(\text{Cl}_2)_{1.7}]$ from $[\text{NET}_3\text{Me}]\text{Cl}$ and Cl_2 can be estimated by correcting the enthalpy of chlorine release (H_{release}) by the hydration enthalpy of $[\text{NET}_3\text{Me}]\text{Cl}$ (H_{solv}) (eq 3)

$$\begin{aligned} H_{\text{formation}}([\text{NET}_3\text{Me}][\text{Cl}(\text{Cl}_2)_{1.7}]) \\ = H_{\text{solv}}([\text{NET}_3\text{Me}]\text{Cl}) - H_{\text{release}}([\text{NET}_3\text{Me}][\text{Cl}(\text{Cl}_2)_{1.7}]) \end{aligned} \quad (3)$$

The hydration enthalpy was determined to be $H_{\text{solv}} = -19.0 \text{ kJ mol}^{-1}$ yielding $H_{\text{formation}}([\text{NET}_3\text{Me}][\text{Cl}(\text{Cl}_2)_{1.7}]) = -54.4 \text{ kJ mol}^{-1}$. In the same way, the formation enthalpy ($H_{\text{formation}}$) of $[\text{NET}_3\text{Me}][\text{Cl}(\text{Cl}_2)_{1.2}]$ was determined to be $-38.0 \text{ kJ mol}^{-1}$. The energy required for chlorine release from $[\text{NET}_3\text{Me}][\text{Cl}(\text{Cl}_2)_{1.7}]$ to $[\text{NET}_3\text{Me}][\text{Cl}(\text{Cl}_2)_{1.2}]$ is the difference of these formation enthalpies and is calculated to be 16.4 kJ mol^{-1} .

These experimentally determined enthalpies can be summarized in a thermodynamic cycle representing the energetic pathways of chlorine storage and release (Scheme 3). This could streamline the upscaling of this chlorine storage technique for industrial applications.

Scheme 3. Thermodynamic Cycle for Chlorine Storage and Release^a



^aThe cation was neglected for clarity.

CONCLUSIONS

In this work, we investigated alkyl ammonium chlorides as sustainable chlorine storages at ambient pressure and temperature. Several alkyl ammonium chlorides have been prepared and the physical properties of the corresponding trichlorides have been studied. As $[\text{NET}_3\text{Me}]\text{Cl}$ is readily prepared from abundant starting materials, is essentially nontoxic, and is stable against chlorination over a prolonged period of time, we selected this system for further studies. Up to 0.79 kg kg^{-1} chlorine can be stored on $[\text{NET}_3\text{Me}]\text{Cl}$, forming $[\text{NET}_3\text{Me}][\text{Cl}(\text{Cl}_2)_n]$, and can be completely released by the

addition of water. Alternatively, heat can be used to achieve partial release of chlorine. Based on the investigation of chlorine vapor pressure of $[\text{NET}_3\text{Me}][\text{Cl}(\text{Cl}_2)_n]$, controlled chlorine release from $[\text{NET}_3\text{Me}][\text{Cl}(\text{Cl}_2)_{1.7}]$ to $[\text{NET}_3\text{Me}][\text{Cl}(\text{Cl}_2)_{1.2}]$ can be achieved by increasing the temperature to $80 \text{ }^\circ\text{C}$. As this temperature can be easily realized by an abundant process and $[\text{NET}_3\text{Me}][\text{Cl}(\text{Cl}_2)_{1.2}]$ is still an ionic liquid, which can be pumped within a plant, the utilization of chlorine storage in this range is industrially advantageous. To investigate the potential of upscaling for flexibilization of chlorine production, we investigated the reaction enthalpy of chlorine storage and release showing that the formation of $[\text{NET}_3\text{Me}][\text{Cl}(\text{Cl}_2)_{1.7}]$ from $[\text{NET}_3\text{Me}][\text{Cl}(\text{Cl}_2)_{1.2}]$ is only moderately exothermic with 16.4 kJ mol^{-1} . The collection of further process parameters is envisioned to allow an economic analysis as well as a life cycle assessment and will be published elsewhere. As $[\text{NET}_3\text{Me}][\text{Cl}(\text{Cl}_2)_n]$ can directly react with CO to industrially crucial phosgene, a process can be envisioned, combining $[\text{NET}_3\text{Me}]\text{Cl}$ as a storage medium and $[\text{NET}_3\text{Me}][\text{Cl}(\text{Cl}_2)_n]$ as a reagent for industrially important chlorination reactions.

EXPERIMENTAL SECTION

Apparatus and Materials. All substances sensitive to water and oxygen were handled under an argon atmosphere using standard Schlenk techniques and oil pump vacuum up to 10^{-3} mbar. Commercially available alkyl ammonium chloride salts, amines, and methyl chloroformate were used without further purification. $[\text{NR}_n^{18}\text{R}_m^{20}\text{R}_3^{21}]\text{Cl}$, $[\text{PR}_3\text{Me}]\text{Cl}$, and $[\text{SMe}_3]\text{Cl}$ were prepared according to literature procedures.²⁵ All salts were dried in vacuo at $100 \text{ }^\circ\text{C}$ for 1 h to 1 day prior to use. Raman spectra were recorded at room temperature on a Bruker (Karlsruhe, Germany) MultiRAM II equipped with a low-temperature Ge detector (1064 nm , $100\text{--}180 \text{ mW}$, resolution of 4 cm^{-1}). Electrospray ionization mass spectrometry was performed on an Advion expression LCMS spectrometer with low fragmentation and acetonitrile as the solvent. NMR spectra were recorded on a 400 MHz ECS or ECZ spectrometer by JEOL. Melting points are determined by placing the sample in a beaker with cold ethanol that is slowly heated until the sample melts. Viscosities are measured using an Ubbelohde viscometer. Densities are determined using a pressure-stable Schlenk tube with a volume scale in which a defined volume of the substance is weighed, or by transferring a sample into a measuring cylinder followed by weighing the sample. Vapor pressure determinations above one bar were performed in a glass autoclave (tinyclave by BüchiGlasUster). Calorimetric measurements were performed with an EasyMax 102 Thermostat System by Mettler Toledo (100 mL glass reactor, temperature sensor: Pt100 FEP-coated) using the HFCal upgrade kit. Deviating from the standard system, all experiments involving $[\text{NET}_3\text{Me}][\text{Cl}_3]$ were performed with a glass-mantled calibration heater and a glass-mantled Pt100 thermometer.

General Procedure for the Preparation of $[\text{Cat}][\text{Cl}(\text{Cl}_2)_n]$. The preparation of polychlorides was performed following two different procedures: (A) In a pressure vessel, an excess of chlorine is condensed onto a chloride salt. Warming to room temperature yields 1–2 liquid phases. Surplus chlorine is evaporated until the system reaches 1.0 bar chlorine pressure. (B) The chloride salt is placed in a flask, dried, and chlorine is added until the system retains a pressure of 1 bar. While for smaller sample sizes, the amount of stored chlorine is higher when method A is used compared to method B, at larger sample sizes, the same results are observed. This indicates that absorption via the gas phase is kinetically hindered to some extent. Therefore, for the determination of the storage capacities and physical properties, the polychlorides were prepared according to method A.

Determination of Storage Capacities. A defined amount of chloride salt was loaded into a pressure-stable flask. Polychloride was

prepared according to method A described above. The amount of chlorine stored on the chloride salt was determined by weighing.

Long-Term Stability Tests for [NEt₃Me][Cl(Cl₂)_n] and [NBu₄][Cl(Cl₂)_n]. Samples of [NEt₃Me][Cl(Cl₂)_n] (*n* = 1 and 1.45) and [NBu₄][Cl(Cl₂)_n] (*n* = 2.18) were prepared and stored in sealed glass ampules. The sample of [NBu₄][Cl(Cl₂)_n] was stored at room temperature in the presence of light for half a year. For [NEt₃Me][Cl(Cl₂)_n] (*n* = 1 and 1.45), four samples were prepared that were stored under the following conditions for 75 days: r.t. in the presence of light, r.t. in the absence of light, 0 °C in the absence of light, and 50 °C in the absence of light. After 75 days, all samples were stored at room temperature in the presence of light. The samples were monitored by Raman spectroscopy and the decomposition products of [NBu₄][Cl(Cl₂)_n] were analyzed by ESI-mass spectrometry.

Chlorine Release Experiments. To determine how much chlorine can be released from the polychloride system, a setup was designed in which a sample of polychloride is stirred in a Schlenk flask and an argon stream was passed over the sample (Figure S20). The released chlorine was condensed in a cooling trap at -145 °C and weighted afterward. The experiment was repeated while the sample was heated to 80 °C. For chlorine release by the addition of water, 10 equiv of water was added to a stirred sample of [NEt₃Me][Cl(Cl₂)₁]. An additional cooling trap at -30 °C was used to hold back water vapor. To determine the minimal amount of water needed to complete chlorine release, water was added in portions of 0.1 equiv.

Vapor Pressure Determination for [NEt₃MeCl][Cl(Cl₂)_n]. The vapor pressure of [NEt₃MeCl][Cl(Cl₂)_n] for different values of *n* was determined by two different methods: (A) [NEt₃MeCl] (13.8 g) was placed in a 100 mL flask, dried, and chlorine was added until the system retained a pressure of 840 mbar (the pressure was determined using a Solid Sense II pressure sensor from Brooks Instruments). The amount of chlorine was determined by weighing the flask. Vacuum was applied to the sample for a short time to remove some chlorine. After equilibration of the system, the amount of remaining chlorine was determined by again weighing the flask. (B) Predried [NEt₃MeCl] (6.4 g) was placed in a glass autoclave. Defined amount of chlorine was added using a mass flow controller (SLA5850 from Brooks Instrument). The temperature in the system was controlled by immersing the autoclave into an oil bath. Vapor pressures for different values of *n* were determined using a Solid Sense II pressure sensor from Brooks Instruments.

Determination of the Hydration Enthalpy of [NEt₃Me]Cl. A 100 mL reactor vessel was charged with 50 mL of water and equipped with a calibration heater and a thermal sensor of the EasyMax 102 system. Then, a pre-designed program (for details, see Supporting Information e2) was run, including the portionwise addition of [NEt₃Me]Cl (10 g, 66 mmol) that was preheated to 25 °C. Using the EasyMax 102 software, the solvation enthalpy for the solvation of 0.066 mol [NEt₃Me]Cl in water was determined. This can be used for the calculation of the molar solvation enthalpy at *p* = 1 atm and *T* = 25 °C according to eq 4: All measurements were performed in triplicate and the reported solvation enthalpy ($\Delta H_{\text{solv}}^{\text{mol}} = 18.95 \text{ kJ/mol}$) is the arithmetic average of all three values (18.73, 18.14, and 19.98 kJ mol⁻¹)

$$\Delta H_{\text{solv}}^{\text{mol}} = \frac{1}{0.066} \times \Delta H_{\text{solv}} \quad (4)$$

Determination of the Reaction Enthalpy of [NEt₃Me][Cl(Cl₂)_n] (*n* = 1.16, 1.68) with 5 equiv of Water. A 100 mL reactor vessel was charged with [NEt₃Me][Cl(Cl₂)_n] (see Supporting Information e3 and e4) and equipped with a calibration heater and a thermal sensor of the EasyMax 102 system. Then, a pre-designed program was run including the continuous addition of 19 mL of water over 20 min using a syringe pump (Fisherbrand KDS100). Using the EasyMax 102 software, the reaction enthalpy for the reaction of [NEt₃Me][Cl(Cl₂)_n] with water was determined. This can be used for the calculation of molar reaction enthalpy. All measurements were performed in triplicate and the reported reaction enthalpies ($\Delta H_{\text{reaction}}^{\text{mol}} = 18.99 \text{ kJ/mol}$ for *n* = 1.16 and $\Delta H_{\text{reaction}}^{\text{mol}} = 35.36 \text{ kJ/mol}$ for *n* = 1.68

and) are the arithmetic averages of all three values (18.73, 18.14, and 19.98 kJ mol⁻¹ and 34.01, 37.02, and 35.05 kJ mol⁻¹).

■ ASSOCIATED CONTENT

SI Supporting Information

The Supporting Information is available free of charge at <https://pubs.acs.org/doi/10.1021/acssuschemeng.2c02186>.

Raman spectra of polychloride salts and for long-term stability tests, mass spectra of the decomposed [NBu₄][Cl(Cl₂)_n], a picture of the setup for chlorine release, vapor pressure curves of [NEt₃Me][Cl(Cl₂)_n], curves for the kinetics of chlorine release, ¹H NMR spectrum of recycled [NEt₃Me]Cl, optimization of the amount of H₂O needed for chlorine release, results for chlorine release by polar solvents, complete table with storage capacities, picture of a setup for calorimetric measurements, and summary of calorimetric measurements (PDF)

Large-scale preparations and is applied for the synthesis of 1 kg of [NEt₃Me][Cl(Cl₂)_{1.68}] (MP4)

Industrial methods applying heat, vacuum or by addition of water, allowing a substantial liberation of chlorine within minutes (MP4)

■ AUTHOR INFORMATION

Corresponding Author

Sebastian Riedel – Institut für Chemie und Biochemie, Freie Universität Berlin, Berlin D-14195, Germany; orcid.org/0000-0003-4552-5719; Email: s.riedel@fu-berlin.de

Authors

Patrick Voßnacker – Institut für Chemie und Biochemie, Freie Universität Berlin, Berlin D-14195, Germany

Nico Schwarze – Institut für Chemie und Biochemie, Freie Universität Berlin, Berlin D-14195, Germany

Thomas Keilhack – Institut für Chemie und Biochemie, Freie Universität Berlin, Berlin D-14195, Germany

Merlin Kleoff – Institut für Chemie und Biochemie, Freie Universität Berlin, Berlin D-14195, Germany

Simon Steinhauer – Institut für Chemie und Biochemie, Freie Universität Berlin, Berlin D-14195, Germany

Yuliya Schiesser – Covestro Deutschland AG, Leverkusen D-51365, Germany

Maxime Paven – Covestro Deutschland AG, Leverkusen D-51365, Germany

Sivathmehhan Yogendra – Covestro Deutschland AG, Leverkusen D-51365, Germany

Rainer Weber – Covestro Deutschland AG, Leverkusen D-51365, Germany

Complete contact information is available at:

<https://pubs.acs.org/doi/10.1021/acssuschemeng.2c02186>

Notes

The authors declare the following competing financial interest(s): N.S., S.S., Y.S., M.P., R.W., S.R. are inventors on a pending patent related to this work filed by Covestro Intellectual Property GmbH & Co. KG (no. WO 2019215037 A1, filed 2018). T.K., S.S., Y.S., M.P., S.Y., R.W., S.R. are inventors on a pending patent related to this work filed by Covestro Intellectual Property GmbH & Co. KG (no. WO 2021069757 A1, filed 2021). The authors declare that they have no other competing interests.

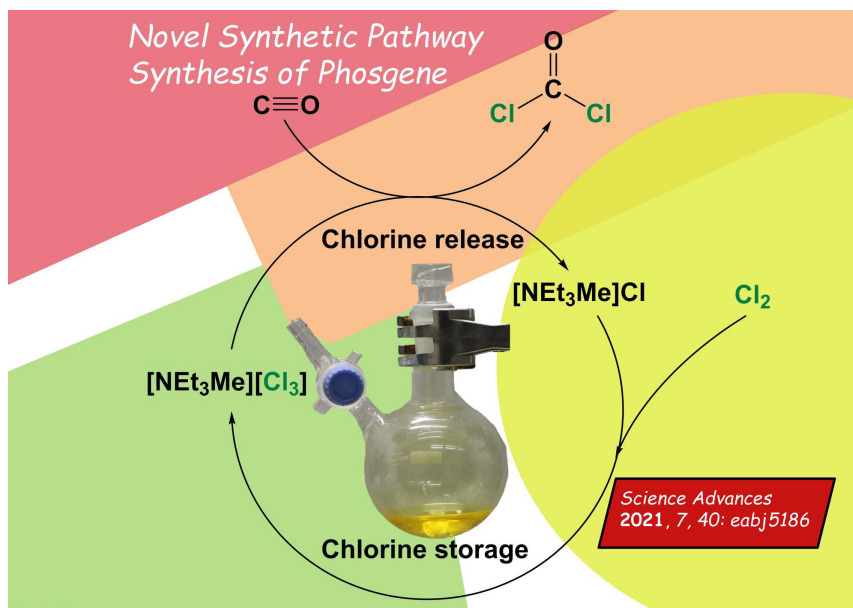
ACKNOWLEDGMENTS

The authors are grateful to Stefan Leisering and Dr. Anja Wiesner (both FU Berlin) for helpful discussions. The authors also acknowledge the assistance of the Core Facility BioSupraMol supported by the DFG.

REFERENCES

- (1) Lin, R.; Amrute, A. P.; Pérez-Ramírez, J. Halogen-Mediated Conversion of Hydrocarbons to Commodities. *Chem. Rev.* **2017**, *117*, 4182–4247.
- (2) Schmittinger, P.; Florkiewicz, T.; Curlin, L. C.; Lüke, B.; Scannell, R.; Navin, T.; Zelfel, E.; Bartsch, R. Chlorine. In *Ullmann's Encyclopedia of Industrial Chemistry*; Wiley-VCH: Weinheim, 2011, 531–621.
- (3) *Flexibilitäts Optionen in der Grundstoffindustrie. Report commissioned by Federal Ministry of Education and Research*, 1st ed.; Ausfelder, F.; Seitz, A.; von Roon, S. Eds.; Frankfurt am Main, 2019. ISBN 978-3-89746-219-9.
- (4) Gils, H. C. Assessment of the theoretical demand response potential in Europe. *Energy* **2014**, *67*, 1–18.
- (5) Klauke, F.; Hoffmann, C.; Hofmann, M.; Tsatsaronis, G. Impact of the chlorine value chain on the demand response potential of the chloralkali process. *Appl. Energy* **2020**, *276*, No. 115366.
- (6) Otashu, J. I.; Baldea, M. Demand response-oriented dynamic modeling and operational optimization of membrane-based chlor-alkali plants. *Comput. Chem. Eng.* **2019**, *121*, 396–408.
- (7) Hearn, J. D.; Weber, R.; Nichols, R.; Henley, M. V.; Fox, S. Deposition of Cl₂ on soils during outdoor releases. *J. Hazard. Mater.* **2013**, *252–253*, 107–114.
- (8) Barrett, A. M. Cost Effectiveness of On-Site Chlorine Generation for Chlorine Truck Attack Prevention. *Decis. Anal.* **2010**, *7*, 366–377.
- (9) Trieu, V.; Langstein, G.; Heinz, P.; Weber, R.; Schiesser, Y.; Werner, K.; Haverkamp, V.; Polarz, S.; Schachtschneider, A. Storage Material and Method for Chlorine Storage. WO2017220476 A1, 2017.
- (10) Sonnenberg, K.; Mann, L.; Redeker, F. A.; Schmidt, B.; Riedel, S. Polyhalogen and Polyinterhalogen Anions from Fluorine to Iodine. *Angew. Chem., Int. Ed.* **2020**, *59*, 5464–5493; *Angew. Chem.* **2020**, *132*, 5506–5535.
- (11) Keil, H.; Sonnenberg, K.; Müller, C.; Herbst-Irmer, R.; Beckers, H.; Riedel, S.; Stalke, D. Insights into the Topology and the Formation of a Genuine $\text{pp}\sigma$ Bond: Experimental and Computed Electron Densities in Monoanionic Trichlorine [Cl₃][−]. *Angew. Chem., Int. Ed.* **2021**, *60*, 2569–2573; *Angew. Chem.* **2021**, *133*, 2600–2604.
- (12) Sonnenberg, K.; Pröhm, P.; Schwarze, N.; Müller, C.; Beckers, H.; Riedel, S. Investigation of Large Polychloride Anions: [Cl₁₁][−], [Cl₁₂][−], and [Cl₁₃][−]. *Angew. Chem., Int. Ed.* **2018**, *57*, 9136–9140; *Angew. Chem.* **2018**, *130*, 9274–9278.
- (13) Taraba, J.; Zak, Z. Diphenyldichlorophosphonium Trichloride–Chlorine Solvate 1:1, [PPh₂Cl₂]⁺Cl₃[−]Cl₂: An Ionic Form of Diphenyltrichlorophosphorane. Crystal Structures of [PPh₂Cl₂]⁺Cl₃[−]Cl₂ and [(PPh₂Cl₂)₂]⁺[InCl₅]^{2−}. *Inorg. Chem.* **2003**, *42*, 3591–3594.
- (14) Pröhm, P.; Schwarze, N.; Müller, C.; Steinhauer, S.; Beckers, H.; Rupp, S. M.; Riedel, S. Non-classical polyinterhalides of chlorine monofluoride: experimental and theoretical characterization of [F(ClF)₃][−]. *Chem. Commun.* **2021**, *57*, 4843–4846.
- (15) Voßnacker, P.; Keilhack, T.; Schwarze, N.; Sonnenberg, K.; Seppelt, K.; Malischewski, M.; Riedel, S. From Missing Links to New Records: A Series of Novel Polychlorine Anions. *Eur. J. Inorg. Chem.* **2021**, 1034–1040.
- (16) Schlama, T.; Gabriel, K.; Gouverneur, V.; Mioskowski, C. Tetraethylammonium Trichloride: A Versatile Reagent for Chlorinations and Oxidations. *Angew. Chem., Int. Ed.* **1997**, *36*, 2342–2344; *Angew. Chem.* **1997**, *109*, 2440–2442.
- (17) Voßnacker, P.; Wüst, A.; Keilhack, T.; Müller, C.; Steinhauer, S.; Beckers, H.; Yogendra, S.; Schiesser, Y.; Weber, R.; Reimann, M.; Müller, R.; Kaupp, M.; Riedel, S. Novel synthetic pathways for the production of phosgene. *Sci. Adv.* **2021**, *7*, No. eabj5186.
- (18) Li, X.; van den Bossche, A.; Vander Hoogerstraete, T.; Binnemans, K. Ionic liquids with trichloride anions for oxidative dissolution of metals and alloys. *Chem. Commun.* **2018**, *54*, 475–478.
- (19) Li, X.; Li, Z.; Orefice, M.; Binnemans, K. Metal Recovery from Spent Samarium–Cobalt Magnets Using a Trichloride Ionic Liquid. *ACS Sustainable Chem. Eng.* **2019**, *7*, 2578–2584.
- (20) Yao, A.; Qu, F.; Liu, Y.; Qu, G.; Lin, H.; Hu, S.; Wang, X.; Chu, T. Ionic liquids with polychloride anions as effective oxidants for the dissolution of UO₂. *Dalton Trans.* **2019**, *48*, 16249–16257.
- (21) Paven, M.; Schiesser, Y.; Weber, R.; Langstein, G.; Trieu, V.; Hasenstab-Riedel, S.; Schwarze, N.; Steinhauer, S. Storage Medium and a Method of Separating, Storage and Transportation of Chlorine Derived from Chlorine-Containing Gases. WO2019215037 A1, 2018.
- (22) Nizzi, K. E.; Pommerening, C. A.; Sunderlin, L. S. Gas-Phase Thermochemistry of Polyhalide Anions. *J. Phys. Chem. A* **1998**, *102*, 7674–7679.
- (23) Sherrill, M. S.; IZard, E. F. The solubility of chlorine in aqueous solutions of chlorides and the free energy of trichloride ion. *J. Am. Chem. Soc.* **1931**, *53*, 1667–1674.
- (24) Paven, M.; Schiesser, Y.; Weber, R.; Bramer-Weger, E.; Yogendra, S.; Hasenstab-Riedel, S.; Steinhauer, S.; Keilhack, T. Method for Releasing Chlorine Gas from Polychloride-Based Storage Media by Means of Chlorine-Releasing Agents and Use in Chemical Reactions. WO2021069757, 2021.
- (25) Kobler, H.; Munz, R.; Gasser, G. A.; Simchen, G. Eine einfache Synthese von Tetraalkylammoniumsalzen mit funktionellen Anionen. *Justus Liebigs Ann. Chem.* **1978**, *1978*, 1937–1945.

3.4 Novel Synthetic Pathway for the Production of Phosgene



Patrick Voßnacker, Alisa Wüst, Thomas Keilhack, Carsten Müller, Simon Steinhauer, Helmut Beckers, Sivathmeehan Yogendra, Yuliya Schiesser, Rainer Weber, Marc Reimann, Robert Müller, Martin Kaupp, Sebastian Riedel*

Sci. Adv. **2021**, 7, eabj5186.

<https://doi.org/10.1126/sciadv.abj5186>

© 2021 The Authors, some rights reserved; exclusive licensee American Association for the Advancement of Science. No claim to original U.S. Government Works. Distributed under a [Creative Commons Attribution License 4.0 \(CC BY\)](#).

Author contributions

Patrick Voßnacker designed the project, performed most of the experiments and wrote the manuscript. Thomas Keilhack and Alisa Wüst performed some of the experiments. Marc Reimann and Robert Müller performed quantum-chemical calculations. Carsten Müller performed quantum chemical calculations and wrote part of the manuscript. Simon Steinhauer and Helmut Beckers revised the manuscript and provided scientific guidance. Yuliya Schiesser, Sivathmeehan Yogendra and Rainer Weber provided scientific guidance. Sebastian Riedel and Martin Kaupp managed the project and revised the manuscript.

CHEMISTRY

Novel synthetic pathway for the production of phosgene

Patrick Voßnacker¹, Alisa Wüst¹, Thomas Keilhack¹, Carsten Müller¹, Simon Steinhauer¹, Helmut Beckers¹, Sivathmeehan Yogendra², Yuliya Schiesser², Rainer Weber², Marc Reimann³, Robert Müller³, Martin Kaupp³, Sebastian Riedel^{1*}

Chloride ions are efficient catalysts for the synthesis of phosgene from carbon monoxide and elemental chlorine at room temperature and atmospheric pressure. Control experiments rule out a radical mechanism and highlight the role of triethylmethylammonium trichloride, [NET₃Me][Cl₃], as active species. In the catalytic reaction, commercially available [NET₃Me]Cl reacts with Cl₂ to form [NET₃Me][Cl₃], enabling the insertion of CO into an activated Cl–Cl bond with a calculated energy barrier of 56.9 to 77.6 kJ mol⁻¹. As [NET₃Me]Cl is also a useful chlorine storage medium, it could serve as a catalyst for phosgene production and as chlorine storage in a combined industrial process.

INTRODUCTION

Since its discovery in 1812 by Davy (1), phosgene [C(O)Cl₂] has evolved as one of the most important industrial chemicals along with, sulfuric acid, ammonia, ethylene, and chlorine. As an “intermediate” chemical, it serves as starting material for polymers, agrochemicals, and pharmaceuticals to mention only a few (2). Currently, 12 million metric tons are produced per year mainly for the synthesis of polyurethanes and polycarbonates, and it is estimated that the production of phosgene will rise to 18.6 million metric tons/year until 2030 (2). Because of its high toxicity, phosgene is only manufactured by a few specialized companies, typically on multi-ton scale requiring a multilevel safety concept. It is obtained by gas phase reaction of carbon monoxide and chlorine at elevated temperature using activated carbon as a catalyst (Eq. 1) (2)



Although the exact mechanism of the phosgene formation is still under debate, it is widely accepted that the reaction is initiated by activation of the Cl–Cl bond. As proposed by Lennon and co-workers (3), the first step is a dissociative chemisorption of Cl₂ on the carbon surface. The adsorbed chlorine atoms react with gaseous CO (Eley-Rideal mechanism) to form a surface-bound acyl chloride entity [C(O)Cl_(ad)], which further reacts with a surface-bound chlorine atom, leading to phosgene (Langmuir-Hinshelwood mechanism). In contrast, Lercher and co-workers (4) assume a two-step Eley-Rideal mechanism, when C₆₀ fullerene is used as model system, while the catalytically active species is the surface-bound triplet diradical [C₆₀···Cl₂]^{••}. Further studies on nitrogen-modified carbon materials propose a polarization of the Cl–Cl bond by interaction with electropositive carbon sites of the material (Lewis acid catalysis). Reaction with CO leads to an acyl chloride cation [C(O)Cl⁺] and a weakly bound Cl^{-δ}, which react with each other to form phosgene (5).

The carbon-based catalysts lower the activation energy for phosgene formation to relatively low values of 32 to 56 kJ mol⁻¹ (4, 6–8).

However, the high exothermicity of the reaction ($\Delta H = -107.6$ kJ mol⁻¹) and subsequent dissipation of process heat is more problematic as the temperature in the iron tube reactors can rise up to 550°C at hotspot reaction sites (2). Because of the high temperatures, the catalysts also slowly degrade by attack of Cl₂ and Cl[•] atoms on carbon defects, leading to the corrosive formation of HCl and CCl₄, which leads to shorter maintenance cycles of the reactor (7, 9).

At the outset of this work, we anticipated that the reaction of CO and Cl₂ to C(O)Cl₂ could be catalyzed by activation of Cl₂ using a weakly coordinated chloride anion. In the reaction of Cl⁻ and Cl₂, polychlorides are formed, which show a broad structural diversity and promising applications (10).

The bonding properties of various trichlorides, the simplest polychlorides, were recently analyzed by experimental and computed electron density studies. Accordingly, there seems to be a smooth transition from an asymmetric [Cl···Cl–Cl]⁻ unit to a symmetric [Cl–Cl–Cl]⁻ anion with two equal Cl–Cl bonds in a crystalline environment. These different bonding types of the [Cl₃]⁻ anion are crucial for its chemical reactivity (11).

Depending on the cation, the trichloride [Cl₃]⁻ is a yellowish salt or a room temperature ionic liquid (RT-IL). Alkylammonium salts

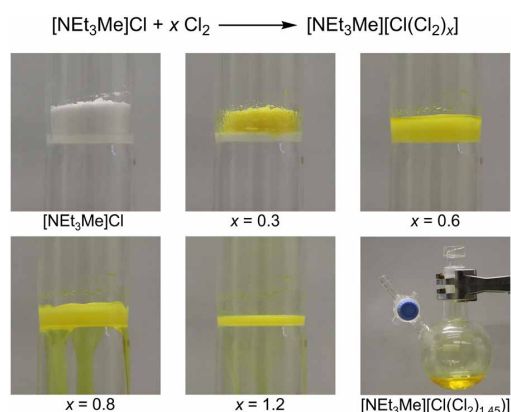


Fig. 1. Treatment of solid [NET₃Me]Cl with elemental chlorine afforded a stable yellowish RT-IL. Photo credit: Patrick Voßnacker, FU Berlin.

¹Freie Universität Berlin, Institut für Chemie und Biochemie–Anorganische Chemie, Fabockstr. 34-36, D-14195 Berlin, Germany. ²Covestro Deutschland AG, 51365 Leverkusen, Germany. ³Technische Universität Berlin, Institut für Chemie Theoretische–Chemie, Straße des 17. Juni 135, D-10623 Berlin, Germany.

*Corresponding author. Email: s.riedel@fu-berlin.de

SCIENCE ADVANCES | RESEARCH ARTICLE

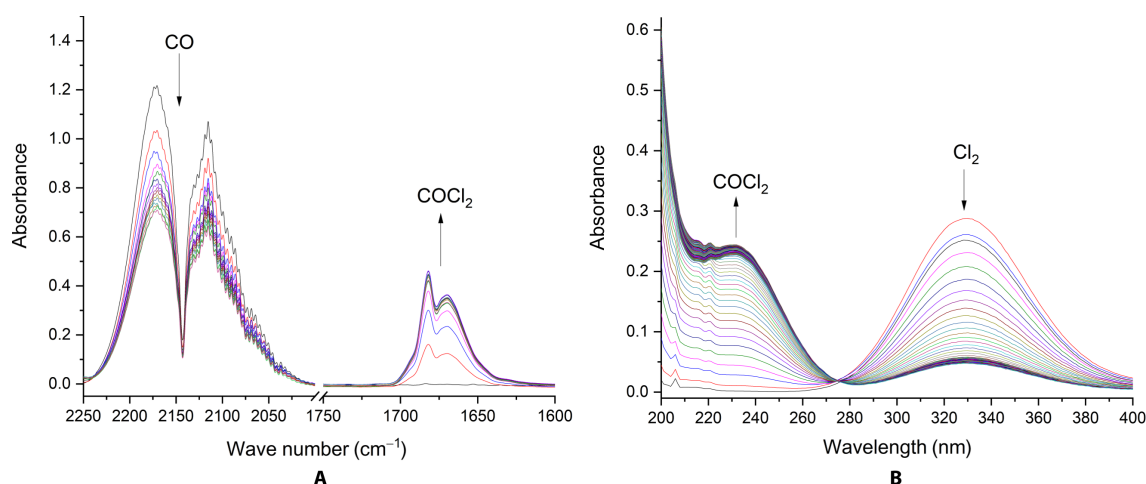


Fig. 2. Monitoring the reaction of CO with $[\text{NEt}_3\text{Me}][\text{Cl}(\text{Cl}_2)_x]$ ($x = 1.45$). IR (A) and UV spectra (B) were recorded for 420 min and are shown with 30-min (IR) and 5-min intervals (UV).

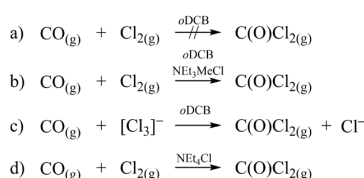


Fig. 3. Control reactions of CO with Cl_2 and $[\text{NEt}_3\text{Me}][\text{Cl}_3]$ or catalyzed by chloride salts.

such as triethylmethylammonium chloride, $[\text{NEt}_3\text{Me}]\text{Cl}$, are considered to be potential materials for the efficient and convenient storage of elemental chlorine as an RT-IL at atmospheric pressure (12). This could enable a more flexible chlorine production that can be adapted to the availability of (renewable) electrical energy and thus represents a secondary energy storage system. Here, we report a preparation of phosgene from carbon monoxide and elemental chlorine that proceeds in a homogeneous reaction at room temperature and atmospheric pressure using a $[\text{NEt}_3\text{Me}]\text{Cl}/[\text{NEt}_3\text{Me}][\text{Cl}_3]$ catalyst system.

RESULTS AND DISCUSSION

First, $[\text{NEt}_3\text{Me}]\text{Cl}$ was reacted with elemental chlorine gas, forming $[\text{NEt}_3\text{Me}][\text{Cl}_3]$ and higher polychlorides. The amount of absorbed chlorine can be expressed by the general sum formula $[\text{NEt}_3\text{Me}][\text{Cl}(\text{Cl}_2)_x]$ where x depends on the partial pressure of chlorine and the size of x has a great influence on the properties of the system (see the Supplementary Materials). When $x < 0.8$, the system exists as a yellow solid, while an increase of the chlorine concentration ($x > 0.8$) results in the formation of an RT-IL (see Fig. 1 and movie S1).

Initially, the stoichiometric reaction of CO with liquid $[\text{NEt}_3\text{Me}][\text{Cl}(\text{Cl}_2)_x]$ ($x = 1.1$) to $\text{C}(\text{O})\text{Cl}_2$ at room temperature was investigated by gas-phase infrared (IR) spectroscopy, indicating rapid formation of phosgene. If by consumption of Cl_2 x becomes smaller than 0.8, $[\text{NEt}_3\text{Me}][\text{Cl}(\text{Cl}_2)_x]$ starts to solidify, which results in a decreased

reaction rate. Thus, $[\text{NEt}_3\text{Me}][\text{Cl}(\text{Cl}_2)_x]$ was dispersed in *ortho*-dichlorobenzene (*o*DCB), a standard solvent in phosgene manufacturing. Using an excess of CO (2.3 equiv.), a quantitative conversion of $[\text{NEt}_3\text{Me}][\text{Cl}(\text{Cl}_2)_x]$ to $\text{C}(\text{O})\text{Cl}_2$ and $[\text{NEt}_3\text{Me}]\text{Cl}$ was observed. An excess of CO avoids chlorine contamination of the phosgene product, which is difficult to remove, whereas separation of CO and $\text{C}(\text{O})\text{Cl}_2$ is industrial praxis. CO consumption proceeds with a half-life time of 287 ± 14 min (see the Supplementary Materials).

Because the reaction of $[\text{NEt}_3\text{Me}]\text{Cl}$ and Cl_2 is very fast, we envisaged a catalytic process by in situ regeneration of $[\text{NEt}_3\text{Me}][\text{Cl}(\text{Cl}_2)_x]$. Even with a relatively low catalyst loading of 3.5 mole percent (mol %) $[\text{NEt}_3\text{Me}]\text{Cl}$, full conversion of Cl_2 to phosgene was achieved.

To improve the contact time between liquid and gaseous reactants, we designed a flow setup, which consists of a gas-washing bottle, filled with a dispersion of $[\text{NEt}_3\text{Me}][\text{Cl}(\text{Cl}_2)_x]$ in *o*DCB, and a peristaltic pump for continuously circulating gaseous CO and already formed $\text{C}(\text{O})\text{Cl}_2$ in the system (see figs. S1 and S2). This setup allows a spectroscopic in situ monitoring of the reaction progress by passing the gas mixture through IR and ultraviolet/visible (UV/Vis) cells. The consumption of CO (IR spectrum; Fig. 2A) and Cl_2 (UV/Vis spectrum; Fig. 2B) as well as a simultaneous formation of $\text{C}(\text{O})\text{Cl}_2$ were recorded, indicating an immediate start of the reaction.

Control experiments with Cl_2 and CO in our setup have shown that both the beam of the UV/Vis spectrometer and visible light slightly contribute to the formation of $\text{C}(\text{O})\text{Cl}_2$ by photolytic activation of Cl_2 . Therefore, all experiments were conducted in the dark to avoid light-induced radical formation and to emulate industrial processing of phosgene in stainless steel tubes. To demonstrate that the phosgene formation requires no photoactivation, we conducted a series of control experiments. CO was treated with Cl_2 without a chloride salt (a), in the presence of catalytic amounts of solid $[\text{NEt}_3\text{Me}]\text{Cl}$ (b), and with liquid $[\text{NEt}_3\text{Me}][\text{Cl}(\text{Cl}_2)_x]$ ($x = 1.45$), to mimic the use of a chlorine storage medium, instead of Cl_2 (c; see Fig. 3 and the Supplementary Materials). In experiment a, no formation of phosgene

SCIENCE ADVANCES | RESEARCH ARTICLE

was observed in the dark, but in experiments **b** and **c**, $\text{C}(\text{O})\text{Cl}_2$ was formed (see fig. S22), highlighting the involvement of $[\text{NET}_3\text{Me}][\text{Cl}_3]$ as reactive species. In addition, $[\text{NET}_4]\text{Cl}$, which forms at room temperature the solid trichloride salt $[\text{NET}_4][\text{Cl}_3]$, was applied as another catalyst to investigate whether a solid/gas reaction could be used for the production of phosgene (**d**). Using this catalyst, formation of $\text{C}(\text{O})\text{Cl}_2$ was substantially slower compared to reaction **b** (see the Supplementary Materials). Notably, no attack of the cation $[\text{NET}_3\text{Me}]^+$ in $[\text{NET}_3\text{Me}][\text{Cl}(\text{Cl}_2)_x]$ ($x = 1.6$) was observed, when stored under an atmosphere of chlorine gas at 1 bar at room temperature for years, as shown by Raman spectroscopy.

To rule out a radical mechanism, we treated the ionic liquid $[\text{NET}_3\text{Me}][\text{Cl}_3]$ with methane in the dark. As neither chlorinated methane nor HCl was observed IR spectroscopically (for details, see the Supplementary Materials), a radical-based mechanism for the formation of phosgene under these conditions was rejected.

To achieve further mechanistic understanding, we carried out quantum-chemical CCSD(T)-F12 single-point energy calculations based on spin-component-scaled (SCS) second-order Møller–Plesset perturbation theory (MP2) structure optimizations using the conductor-like screening model for realistic solvents (COSMO-RS) solvent model for *o*DCB and with or without inclusion of one $[\text{NET}_3\text{Me}]^+$ cation (see computational details). Gibbs free reaction energies were computed from the electronic energies at these levels and thermal contributions obtained from normal mode analyses at SCS-MP2 level. On the basis of these calculations, the reaction is initiated by the formation of a very weakly bound encounter complex of CO and $[\text{Cl}_3]^-$ ($[\text{EC}]^-$ in Fig. 4; with closest C–Cl distances of about 3.4 Å). Shortening of C–Cl distances leads to a transition state ($[\text{TSS}]^-$) with a relative Gibbs free energy of 78 kJ mol^{-1} (including one $[\text{NET}_3\text{Me}]^+$ cation) or 57 kJ mol^{-1} (neglecting cations), which can be described as a chloride ion loosely bound to an almost linear O–C–Cl–Cl moiety $[\text{Cl}^- \cdots \text{C}(\text{O})-\text{Cl}-\text{Cl}]$. Charge transfer from the chloride to the O–C–Cl–Cl moiety leads to a $[\text{ClC}(\text{O})\text{Cl}]^-$ intermediate complex, ($[\text{IC}]^-$ in Fig. 4), which spontaneously dissociates into $\text{C}(\text{O})\text{Cl}_2$ and Cl^- . In summary, the reaction of CO and $[\text{Cl}_3]^-$ can be regarded as the insertion of CO into an activated Cl–Cl bond, leading to $\text{C}(\text{O})\text{Cl}_2$ and Cl^- by releasing about 60 kJ mol^{-1} .

However, the computational estimation of the reaction barrier depends on cation-anion interactions. When the influence of only one cation is taken into account, the free energy of the transition state is relatively high (77.6 kJ mol^{-1}). In contrast, when no cation effects but only solvent effects are considered, the transition state is calculated to have a substantially lower energy (56.9 kJ mol^{-1}). As the real system involves the interaction of multiple cations and solvent molecules, the real free energy of the transition state can be expected to be in the same range between 56.9 and 77.6 kJ mol^{-1} . For the uncatalyzed reaction of CO and Cl_2 to phosgene, a free energy activation barrier of about 230 kJ mol^{-1} was calculated. This indicates that the activation barrier is tremendously reduced by our chloride catalyst comparable to the activated carbon-catalyzed process.

On the basis of these results, a catalytic reaction scheme can be proposed in which phosgene is prepared at room temperature by chloride catalysis. The prepared phosgene can be used for further processes, most importantly the synthesis of isocyanates to produce polyurethanes. This was demonstrated for the synthesis of phenyl isocyanate by adding aniline to the generated phosgene solution (see the Supplementary Materials). In the reaction of amines with phosgene to isocyanates, HCl is released, which, in an industrial process, is to some extent typically electrolyzed to regenerate elemental chlorine (Fig. 5).

Concluding, a new synthesis of phosgene was developed, enabled by the main-group catalyst $[\text{NET}_3\text{Me}]\text{Cl}$. As an active intermediate, the ionic liquid $[\text{NET}_3\text{Me}][\text{Cl}_3]$ reacts with carbon monoxide at room temperature and atmospheric pressure to $\text{C}(\text{O})\text{Cl}_2$ in an ionic process. Quantum-chemical calculations suggest an insertion of CO into an activated Cl_2 moiety with a relatively low barrier between 56.9 and 77.6 kJ mol^{-1} . The unique property of $[\text{NET}_3\text{Me}]\text{Cl}$ to serve

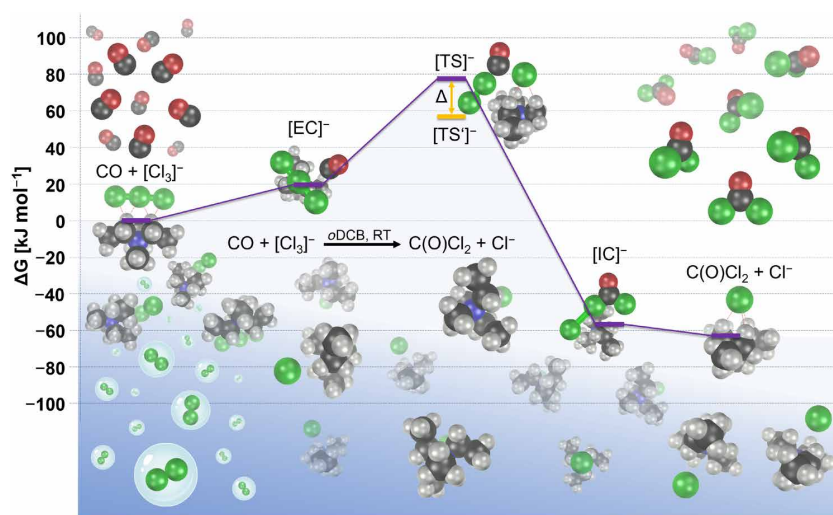


Fig. 4. Calculated pathway for the reaction of CO and $[\text{Cl}_3]^-$ to $\text{C}(\text{O})\text{Cl}_2$ and Cl^- . The calculated energies include zero-point energy correction, temperature effects at 298.15 K, solvent effects for *o*DCB, and one $[\text{NET}_3\text{Me}]^+$ cation. $[\text{EC}]^-$, encounter complex; $[\text{TSS}]^-$, transition state including one $[\text{NET}_3\text{Me}]^+$ cation; $[\text{TS}]^-$, transition state without any cation; $[\text{IC}]^-$, intermediate complex; RT, room temperature.

SCIENCE ADVANCES | RESEARCH ARTICLE

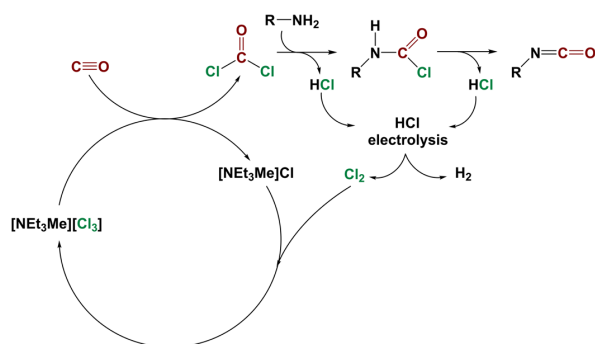


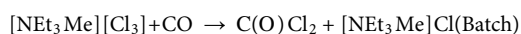
Fig. 5. Proposed scheme for a phosgene synthesis using [NEt₃Me]Cl as a catalyst coupled with a subsequent phosgenation of amines and chlorine regeneration.

both as a convenient chlorine storage medium and as an efficient catalyst for the production of phosgene opens up new industrial options.

MATERIALS AND METHODS

Apparatus and materials

All substances sensitive to water and oxygen were handled under an argon atmosphere using standard Schlenk techniques and oil pump vacuum up to 10^{-3} mbar. Dry *o*DCB was obtained after storage over activated 3-Å molecular sieves. Commercially available triethylmethylammonium chloride (TCI) and tetraethylammonium chloride (TEA) were dried in vacuo at 150°C for 1 hour before use. Aniline (Acros), chlorine (5.0, Linde), and carbon monoxide (2.0, Linde) were used without further purification. Raman spectra were recorded on a Bruker (Karlsruhe, Germany) MultiRAM II equipped with a low-temperature Ge detector (1064 nm, 100 to 180 mW, resolution of 4 cm^{-1}). IR spectra were recorded on a Nicolet iS5 Fourier transform IR (FTIR) spectrometer (gas IR cell: 10 cm, KBr windows) or a Bruker Vector 22 FTIR spectrometer (gas IR cell: 10 or 20 cm, silicon windows). UV/Vis spectra were recorded on a PerkinElmer Lambda 465



[NEt₃Me]Cl (0.371 g, 2.446 mmol, 0.35 equiv.) was loaded into a 500-ml Schlenk flask, dried in vacuo at 150°C for 1 hour, and suspended in 1.5 ml of *o*DCB. The solution was degassed, and chlorine was added until the system retained a pressure of 200 mbar (0.493 g, 6.953 mmol, 1 equiv.). CO (800 mbar) (ca. 16 mmol, 2.3 equiv.) was added to the flask, and the reaction mixture was stirred for 2 days in the dark. To isolate the C(O)Cl₂, the flask was cooled to -15°C, and volatile constituents were distilled in vacuo in two cooled traps held at -60°C (*o*DCB) and -196°C [C(O)Cl₂, Cl₂]. Phosgene was transferred into a pressure-stable Schlenk tube, weighted (0.710 g, 7.178 mmol, 103%), and identified by its known Raman (Raman spectrum shows no bands of Cl₂; fig. S5) and IR spectra (fig. S6).

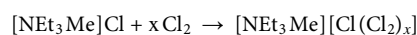
IR (gas phase): $\tilde{\nu} = 2349$ (CO₂), 1827 (s), 1675 (w), 1409 (vw), 1007 (w), 849 (vs), 580 cm^{-1} (w).

Raman (liquid): $\tilde{\nu} = 1809$ (m), 832 (vw), 571 (vs), 444 (m), 301 cm^{-1} (m)



[NEt₃Me]Cl (0.053 g, 0.351 mmol, 0.035 equiv.) was loaded into a 500-ml Schlenk flask, dried in vacuo at 150°C for 1 hour, and suspended in 20 ml of *o*DCB. The solution was degassed, and chlorine was added until the system retained a pressure of 200 mbar (0.700 g, 10.009 mmol, 1 equiv.). CO (800 mbar) (ca. 16 mmol, 1.6 equiv.) was added to the flask, and the reaction mixture was stirred for 7 days in the dark. To isolate the C(O)Cl₂, the flask was cooled to -15°C, and all volatile constituents were distilled in vacuo in two cooled traps held at -60°C (*o*DCB) and -196°C [C(O)Cl₂, Cl₂]. Phosgene was transferred into a pressure-stable Schlenk tube, weighted (1.006 g, 10.272 mmol, 103%), and identified by its IR spectrum (fig. S7).

IR (gas phase): $\tilde{\nu} = 2349$ (CO₂), 1827 (s), 1675 (w), 1409 (vw), 1007 (w), 849 (vs), 580 cm^{-1} (w)

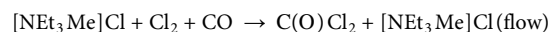


[NEt₃Me]Cl (10.1 g, 66.5 mmol) was dried in vacuo at 150°C for 1 hour. Chlorine was added until the system retained a pressure of 800 mbar (6.9 g, 97.3 mmol, 1.45 equiv.). A yellow liquid was obtained, which was identified by its Raman spectrum (fig. S8).

Raman (liquid): $\tilde{\nu} = 3022$ (w), 2988 (s), 2947 (s), 1456 (w), 1071 (vw), 681 (w), 454 (s), 276 cm^{-1} (vs).

General description of the flow setup

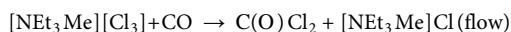
To investigate the kinetics of the reaction between [NEt₃Me][Cl₃] and CO, a glass vacuum line was connected to a gas-washing bottle (reactor) via a peristaltic pump, which successively circulates gaseous reactants through the reactor, a UV/Vis, and an IR flow cell, to monitor the formation of C(O)Cl₂ and the consumption of Cl₂ and CO as well (see figs. S1 and S2). To ensure proper mixing of all reactants, the liquid and solid reactants were filled into the gas-washing bottle, and all gaseous reactants are pumped through the system. All connections were made using either perfluoroalkoxy alkane or C-Flex Ultra (Cole-Parmer) tubing. This setup was used for experiments using stoichiometric and varying catalytic amounts of [NEt₃Me]Cl for the reaction of CO + Cl₂. In addition, blind experiments for the noncatalyzed reaction between Cl₂ and CO were performed, which showed that the beam of the UV/Vis spectrometer and visible light can induce the formation of phosgene from Cl₂ and CO. Therefore, all following experiments have been performed in the dark (see fig. S3). Also, the reaction between [NEt₃Me]Cl, Cl₂, and CH₄ was studied to verify a nonradical mechanism. The progress of the reaction was monitored by integrated absorbances of the IR bands in the spectral regions between 1995 and 2250 cm^{-1} (CO) and 1760 and 1885 cm^{-1} [C(O)Cl₂]



[NEt₃Me]Cl (0.460 g, 3.033 mmol) and 20 ml of *o*DCB were filled into a gas-washing bottle, which was connected to a glass vacuum line and an IR flow cell. The reaction mixture was degassed, and the system was filled with a mixture of CO and Cl₂ (CO: 1000 mbar, 22.32 mmol, 553 ml; Cl₂: 208 mbar, 4.65 mmol, 553 ml). The gaseous reactants were pumped through the system using a peristaltic pump for 226 min. IR spectra were recorded after 0, 6, 11, 16, 21, 26,

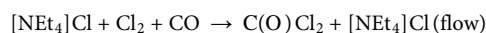
SCIENCE ADVANCES | RESEARCH ARTICLE

31, 36, 41, 46, 51, 56, 61, 66, 71, 76, 81, 86, 91, 96, 101, 106, 111, 116, 121, 126, 131, 136, 141, 184, 191, 196, 201, 206, 211, 216, 221, and 226 min (figs. S9 to S11)

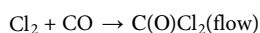


$[\text{NEt}_3\text{Me}][\text{Cl}(\text{Cl}_2)_{1.50}]$ (0.783 g, 3.033 mmol $[\text{NEt}_3\text{Me}]\text{Cl}$ + 4.555 mmol Cl_2) and 20 ml of *o*DCB were filled into a gas-washing bottle, which was connected to a glass vacuum line and an IR flow cell. The reaction mixture was degassed, and the system was filled with CO (1000 mbar, 553 ml, 22.32 mmol). The gaseous reactants were pumped through the system using a peristaltic pump for 153 min. IR spectra were recorded after 0, 5, 10, 15, 20, 25, 30, 35, 40, 45, 50, 55, 60, 65, 70, 75, 80, 85, 98, 103, 108, 113, 123, 128, 133, 138, 144, 154, 164, 174, 184, 194, 204, 214, and 224 min (figs. S12 to S14).

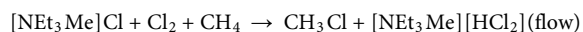
$[\text{NEt}_3\text{Me}][\text{Cl}(\text{Cl}_2)_{1.47}]$ [3.904 g, 15.30 mmol (22.49 mmol Cl_2)] and 20 ml of *o*DCB were filled into a gas-washing bottle, which was connected to a glass vacuum line, an IR flow cell, and a UV/Vis flow cell. The reaction mixture was degassed, and the system was filled with CO (1000 mbar, 800 ml, ca. 32 mmol). The gaseous reactants were pumped through the system using a peristaltic pump for 420 min. IR and UV spectra were recorded every 5 min



$[\text{NEt}_4]\text{Cl}$ (0.230 g, 1.393 mmol) was filled into a gas-washing bottle, which was connected to a glass vacuum line and an IR flow cell. The system was evacuated and filled with a mixture of CO and Cl_2 (CO: 850 mbar, 20.20 mmol, 588 ml; Cl_2 : 150 mbar, 3.530 mmol, 588 ml). The gaseous reactants were pumped through the system using a peristaltic pump for 628 min. IR spectra were recorded after 0, 1, 6, 11, 21, 27, 32, 37, 42, 47, 52, 65, 77, 137, 197, 257, 317, 377, 437, 497, 558, and 628 min (figs. S15 to S17)



*o*DCB (20 ml) was filled into a gas-washing bottle, which was connected to a glass vacuum line and an IR flow cell. The *o*DCB was degassed, and the system was filled with a mixture of CO and Cl_2 (CO: 850 mbar, 20.20 mmol, 588 ml; Cl_2 : 150 mbar, 3.53 mmol, 588 ml). The gaseous reactants were pumped through the system using a peristaltic pump for 811 min. IR spectra were recorded after 0, 4, 9, 14, 18, 19, 34, 49, 64, 79, 94, 109, 124, 139, 154, 261, 262, 323, 384, 445, 506, 567, 628, 689, 750, and 811 min (figs. S18 to S20). Repetition of the experiment without exclusion of light yields the formation of phosgene, which was shown by gas-phase IR spectroscopy (fig. S21)



$[\text{NEt}_3\text{Me}]\text{Cl}$ (0.499 g, 3.290 mmol) and 20 ml of *o*DCB were filled into a gas-washing bottle, which was connected to a glass vacuum line and an IR flow cell. The reaction mixture was degassed, and the system was filled with a mixture of argon, CH_4 , and Cl_2 (argon: 705 mbar, 588 ml; CH_4 : 95 mbar, 588 ml, 2.25 mmol; Cl_2 : 200 mbar, 4.74 mmol, 588 ml). The gaseous reactants were pumped through the system using a peristaltic pump for 242 min. IR spectra were recorded 0, 3, 6, 9, 12, 15, 19, 22, 25, 28, 39, 40, 100, 161, 221, 282, 342, 403, 363, and 524 min (fig. S23).

Proof for the formation of phenyl isocyanate

$[\text{NEt}_3\text{Me}]\text{Cl}$ (0.367 g, 2.420 mmol, 0.31 equiv.) was loaded into a 500-ml two-neck Schlenk flask, dried in vacuo at 150°C for 1 hour, and suspended in 20 ml of *o*DCB. The solution was degassed, and chlorine was added until the system retained a pressure of 200 mbar (0.560 g, 7.898 mmol, 1 equiv.). CO (800 mbar) (ca. 16 mmol, 2.3 equiv.) was added to the flask, and the reaction mixture was stirred for 3 days in the dark. The reaction mixture was cooled to -196°C and degassed. Then, the system was filled with dry argon gas and connected to a dropping funnel and a condenser that was cooled by using -15°C cold ethanol. The condenser was opened to the fume hood via a gas bubbler and a series of four gas-washing bottles, two of which are filled with a KOH solution and an NH_4OH solution, respectively, each followed by an empty bottle. A solution of 0.5 ml of aniline (0.51 g, 5.476 mmol, 0.69 equiv.) in 5 ml of *o*DCB was added slowly via the dropping funnel to the reaction mixture held at -15°C, and the reaction mixture was then heated to 100°C for 8 hours. After that, excess of phosgene was removed in vacuo, and the analysis of the reaction products using gas-phase IR spectroscopy revealed the characteristic NCO stretching band at 2273 cm^{-1} of the reaction product (fig. S24).

Computational details

Structure optimizations at density functional theory (DFT) and SCS-MP2 (13) levels, as well as with the ONIOM (14) procedure to mix quantum-chemical levels, were performed with the Gaussian 16 program, Revision A.03 (15). Structure optimizations at the SCS-MP2 level were enabled by specifying IOP(3/125=0333312000) in the root section of the input file during MP2 optimizations. Additional single-point SCS-MP2 and CCSD(T)-F12 calculations were performed with the Molpro program, version 2019.1 (16, 17). For all atoms of the CO + $[\text{Cl}_3]^-$ system, aug-cc-pVTZ basis sets (18–20) were used. For all atoms in the $[\text{NEt}_3\text{Me}]^+$ cation, smaller cc-pVTZ basis sets were applied in the second layer of the ONIOM calculations (see below), while full aug-cc-pVTZ basis sets were used for the entire system in subsequent SCS-MP2 single-point energy calculations. For the CCSD(T)-F12 calculations, the associated default auxiliary basis sets (cc-pVTZ-JKFIT, aug-cc-pVTZ-JKFIT, and aug-cc-pVTZ-MP2FIT) (21) were used. Solvent effects were included during the structure optimizations in Gaussian via an integral equation formalism polarizable continuum model (22–39) with $\epsilon = 9.9949$, specifying SCRF=(Solvent=*o*-DiChloroBenzene), or a posteriori for energies via the COSMO-RS scheme. For the calculation with one $[\text{NEt}_3\text{Me}]^+$ cation, ONIOM calculations with two layers were performed. The first layer included the anionic species Cl^- , $[\text{Cl}_3]^-$, the CO $[\text{Cl}_3]^-$ encounter complex, or the $[\text{C(O)Cl}_2][\text{Cl}]^-$ intermediate complex and was treated at the SCS-MP2/aug-cc-pVTZ level. The second layer included the cation and was treated at the M06-2X/cc-pVTZ level. The relative energies, characteristic for the reaction profile, were calculated in several steps. From the total electronic energies for all systems optimized in vacuum at the SCS-MP2 level or mixed ONIOM SCS-MP2:M06-2X level, $\Delta E_{\text{SCS-MP2}}^{\text{OK}}$ was calculated with respect to the energies of free CO and $[\text{Cl}_3]^-$. Zero-point energy corrections (ΔE_{ZPE}) as well as thermal correction ($\Delta E_{\text{therm.}}^{298.15\text{K}}$) and entropic contributions ($-T\Delta S$) were obtained from harmonic normal mode analyses. To incorporate higher-order electron correlation effects, a correction term $\Delta E_{\text{CCSD(T)-F12}}$ was calculated from the difference of the SCS-MP2 and CCSD(T)-F12 energies of the anionic systems in vacuum

and without any counterion. Correction terms to the Gibbs free energies of reactions in solution under standard conditions ($\Delta G_{\text{COSMO-RS}}^{298.15\text{ K}, 0.1\text{ MPa}}$) were obtained using the COSMO-RS solvation model (40–43). To this end, additional single-point calculations at the vacuum and polarizable continuum model (PCM) optimized structures were carried out using the TURBOMOLE program version 7.5.0 (44–46). These calculations were performed at the DFT-BP86 (47, 48) level of theory in conjunction with def2-TZVPD (49) basis sets for all atoms, the multipole-accelerated resolution-of-identity approximation, and the refined COSMO cavity construction algorithm (keyword `$cosmo_isorad`) (50–54). Subsequent COSMO-RS computations used the COSMOTHERM program version C30_1201 and a BP-TZVPD-FINE level parameterization (BP_TZVPD_FINE_HB2012_C30_1201). For an in-depth analysis of the reaction profile in terms of its thermochemistry, different thermochemical quantities were evaluated: the pure electronic energy ΔE^{OK} , the enthalpy at 298.15 K with zero-point energy corrections added, $\Delta H^{298.15\text{ K}}$, the Gibbs free energy in vacuum, $\Delta G^{298.15\text{ K}}$, and the Gibbs free energy in oDCB solvent, $\Delta G^{298.15\text{ K}, \text{oDCB}}$. All consecutive steps of the reaction of $[\text{Cl}_3]^-$ with CO were modeled with and without inclusion of the counter-cation $[\text{NEt}_3\text{Me}]^+$.

SUPPLEMENTARY MATERIALS

Supplementary material for this article is available at <https://science.org/doi/10.1126/sciadv.abj5186>

REFERENCES AND NOTES

- J. Davy, VI. On a gaseous compound of carbonic oxide and chlorine. *Phil. Trans. R. Soc.* **102**, 144–151 (1812).
- L. Cotarca, C. Lange, K. Meurer, J. Pauluhn, *Ullmann's Encyclopedia of Industrial Chemistry* (Phosgene, 2019), pp. 1–30.
- G. E. Rossi, J. M. Winfield, N. Meyer, D. H. Jones, R. H. Carr, D. Lennon, Phosgene formation via carbon monoxide and dichlorine reaction over an activated carbon catalyst: Towards a reaction model. *Appl. Catal. Gen.* **609**, 117900 (2021).
- N. K. Gupta, A. Pashigreva, E. A. Pidko, E. J. M. Hensen, L. Mleczko, S. Roggan, E. E. Ember, J. A. Lercher, Bent carbon surface moieties as active sites on carbon catalysts for phosgene synthesis. *Angew. Chem. Int. Ed.* **55**, 1728–1732 (2016).
- N. K. Gupta, B. Peng, G. L. Haller, E. E. Ember, J. A. Lercher, Nitrogen modified carbon nano-materials as stable catalysts for phosgene synthesis. *ACS Catal.* **6**, 5843–5855 (2016).
- G. E. Rossi, J. M. Winfield, C. J. Mitchell, N. Meyer, D. H. Jones, R. H. Carr, D. Lennon, Phosgene formation via carbon monoxide and dichlorine reaction over an activated carbon catalyst: Reaction kinetics and mass balance relationships. *Appl. Catal. Gen.* **602**, 117688 (2020).
- C. J. Mitchell, W. van der Borden, K. van der Velde, M. Smit, R. Scheringa, K. Ahrika, D. H. Jones, Selection of carbon catalysts for the industrial manufacture of phosgene. *Cat. Sci. Technol.* **2**, 2109 (2012).
- S. K. Ajmera, M. W. Losey, K. F. Jensen, M. A. Schmidt, Microfabricated packed-bed reactor for phosgene synthesis. *AIChE J.* **47**, 1639–1647 (2001).
- L. Khachatryan, B. Dellinger, Formation of chlorinated hydrocarbons from the reaction of chlorine atoms and activated carbon. *Chemosphere* **52**, 709–716 (2003).
- K. Sonnenberg, L. Mann, F. A. Redeker, B. Schmidt, S. Riedel, Polyhalogen and polyinterhalogen anions from fluorine to iodine. *Angew. Chem. Int. Ed.* **59**, 5464–5493 (2020).
- H. Keil, D. Sonnenberg, C. Müller, R. Herbst-Irmer, H. Beckers, S. Riedel, D. Stalke, Insights in the topology and the formation of a genuine ppg bond: Experimental and computed electron densities in mono anionic trichlorine $[\text{Cl}_3]^-$. *Angew. Chem.* **60**, 2569–2573 (2020).
- M. Paven, Y. Schiesser, R. Weber, G. Langstein, V. Trieu, S. Hasenstab-Riedel, N. Schwarze, S. Steinhauer, Storage medium and a method of separating, storage and transportation of chlorine derived from chlorine-containing gases, WO2019215037A1 (2018).
- S. Grimme, Improved second-order Møller–Plesset perturbation theory by separate scaling of parallel- and antiparallel-spin pair correlation energies. *J. Chem. Phys.* **118**, 9095–9102 (2003).
- S. Dapprich, I. Komáromi, K. S. Byun, K. Morokuma, M. J. Frisch, A new ONIOM implementation in Gaussian98. Part I. The calculation of energies, gradients, vibrational frequencies and electric field derivatives. *J. Mol. Struct.* **461–462**, 1–21 (1999).
- M. J. Frisch, G. W. Trucks, H. B. Schlegel, G. E. Scuseria, M. A. Robb, J. R. Cheeseman, G. Scalmani, V. Barone, G. A. Petersson, H. Nakatsuji, X. Li, M. Caricato, A. V. Marenich, J. Bloino, B. G. Janesko, R. Gomperts, B. Mennucci, H. P. Hratchian, J. V. Ortiz, A. F. Izmaylov, J. L. Sonnenberg, D. Williams-Young, F. Ding, F. Lipparini, F. Egidi, J. Goings, B. Peng, A. Petrone, T. Henderson, D. Ranasinghe, V. G. Zakrzewski, J. Gao, N. Rega, G. Zheng, W. Liang, M. Hada, M. Ehara, K. Toyota, R. Fukuda, J. Hasegawa, M. Ishida, T. Nakajima, Y. Honda, O. Kitao, H. Nakai, T. Vreven, K. Throssell, J. A. Montgomery, Jr., J. E. Peralta, F. Ogliaro, M. J. Bearpark, J. J. Heyd, E. N. Brothers, K. N. Kudin, V. N. Staroverov, T. A. Keith, R. Kobayashi, J. Normand, K. Raghavachari, A. P. Rendell, J. C. Burant, S. S. Iyengar, J. Tomasi, M. Cossi, J. M. Millam, M. Klene, C. Adamo, R. Cammi, J. W. Ochterski, R. L. Martin, K. Morokuma, O. Farkas, J. B. Foresman, and D. J. Fox, *Gaussian 16* (Gaussian Inc., 2016).
- H.-J. Werner, P. J. Knowles, G. Knizia, F. R. Manby, M. Schütz, Molpro: A general-purpose quantum chemistry program package. *WIREs Comput. Mol. Sci.* **2**, 242–253 (2012).
- H.-J. Werner, P. J. Knowles, G. Knizia, F. R. Manby, M. Schütz, P. Celani, W. G. J. Orloff, D. Kats, T. Korona, R. Lindh, A. Mitrushenkov, G. Rauhut, K. R. Shamasundar, T. B. Adler, R. D. Amos, S. J. Bennie, A. Bernhardsson, A. Berning, D. L. Cooper, M. J. O. Deegan, A. J. Dobbyn, F. Eckert, E. Goll, C. Hampel, A. Hesselmann, G. Hetzer, T. Hrenar, G. Jansen, C. Köppl, S. J. R. Lee, Y. Liu, A. W. Lloyd, Q. Ma, R. A. Mata, A. J. May, S. J. McNicholas, W. Meyer, T. F. Müller III, M. E. Mura, A. Nicklass, D. P. O'Neill, P. Palmieri, D. Peng, K. Pflüger, R. Pitzer, M. Reiher, T. Shiozaki, H. Stoll, A. J. Stone, R. Tarroni, T. Thorsteinsson, M. Wang, M. Welborn, *MOLPRO, version 2019.2, a package of ab initio programs*.
- T. H. Dunning Jr., Gaussian basis sets for use in correlated molecular calculations. I. The atoms boron through neon and hydrogen. *J. Chem. Phys.* **90**, 1007–1023 (1989).
- R. A. Kendall, T. H. Dunning, R. J. Harrison, Electron affinities of the first-row atoms revisited. Systematic basis sets and wave functions. *J. Chem. Phys.* **96**, 6796–6806 (1992).
- D. E. Woon, T. H. Dunning Jr., Gaussian basis sets for use in correlated molecular calculations. III. The atoms aluminum through argon. *J. Chem. Phys.* **98**, 1358–1371 (1993).
- F. Weigend, A fully direct RI-HF algorithm: Implementation, optimised auxiliary basis sets, demonstration of accuracy and efficiency. *Phys. Chem. Chem. Phys.* **4**, 4285–4291 (2002).
- S. Miertuš, E. Scrocco, J. Tomasi, Electrostatic interaction of a solute with a continuum. A direct utilization of AB initio molecular potentials for the prevision of solvent effects. *Chem. Phys.* **55**, 117–129 (1981).
- S. Miertuš, J. Tomasi, Approximate evaluations of the electrostatic free energy and internal energy changes in solution processes. *Chem. Phys.* **65**, 239–245 (1982).
- J. L. Pascual-Ahuir, E. Silla, I. Tuñón, GEPOL: An improved description of molecular surfaces. III. A new algorithm for the computation of a solvent-excluding surface. *J. Comput. Chem.* **15**, 1127–1138 (1994).
- M. Cossi, V. Barone, R. Cammi, J. Tomasi, Ab initio study of solvated molecules: A new implementation of the polarizable continuum model. *Chem. Phys. Lett.* **255**, 327–335 (1996).
- E. Cancès, B. Mennucci, J. Tomasi, A new integral equation formalism for the polarizable continuum model: Theoretical background and applications to isotropic and anisotropic dielectrics. *J. Chem. Phys.* **107**, 3032–3041 (1997).
- V. Barone, M. Cossi, J. Tomasi, A new definition of cavities for the computation of solvation free energies by the polarizable continuum model. *J. Chem. Phys.* **107**, 3210–3221 (1997).
- B. Mennucci, J. Tomasi, Continuum solvation models: A new approach to the problem of solute's charge distribution and cavity boundaries. *J. Chem. Phys.* **106**, 5151–5158 (1997).
- B. Mennucci, E. Cancès, J. Tomasi, Evaluation of solvent effects in isotropic and anisotropic dielectrics and in ionic solutions with a unified integral equation method: Theoretical bases, computational implementation, and numerical applications. *J. Phys. Chem. B* **101**, 10506–10517 (1997).
- V. Barone, M. Cossi, Quantum calculation of molecular energies and energy gradients in solution by a conductor solvent model. *J. Phys. Chem. A* **102**, 1995–2001 (1998).
- M. Cossi, V. Barone, B. Mennucci, J. Tomasi, Ab initio study of ionic solutions by a polarizable continuum dielectric model. *Chem. Phys. Lett.* **286**, 253–260 (1998).
- V. Barone, M. Cossi, J. Tomasi, Geometry optimization of molecular structures in solution by the polarizable continuum model. *J. Comput. Chem.* **19**, 404–417 (1998).
- R. Cammi, B. Mennucci, J. Tomasi, Second-order Møller–Plesset analytical derivatives for the polarizable continuum model using the relaxed density approach. *J. Phys. Chem. A* **103**, 9100–9108 (1999).
- J. Tomasi, B. Mennucci, E. Cancès, The IEF version of the PCM solvation method: An overview of a new method addressed to study molecular solutes at the QM ab initio level. *J. Mol. Struct. (THEOCHEM)* **464**, 211–226 (1999).
- M. Cossi, N. Rega, G. Scalmani, V. Barone, Polarizable dielectric model of solvation with inclusion of charge penetration effects. *J. Chem. Phys.* **114**, 5691–5701 (2001).
- M. Cossi, G. Scalmani, N. Rega, V. Barone, New developments in the polarizable continuum model for quantum mechanical and classical calculations on molecules in solution. *J. Chem. Phys.* **117**, 43–54 (2002).

SCIENCE ADVANCES | RESEARCH ARTICLE

37. M. Cossi, N. Rega, G. Scalmani, V. Barone, Energies, structures, and electronic properties of molecules in solution with the C-PCM solvation model. *J. Comput. Chem.* **24**, 669–681 (2003).
38. G. Scalmani, M. J. Frisch, Continuous surface charge polarizable continuum models of solvation. I. General formalism. *J. Chem. Phys.* **132**, 114110 (2010).
39. F. Lipparini, G. Scalmani, B. Mennucci, E. Cancès, M. Caricato, M. J. Frisch, A variational formulation of the polarizable continuum model. *J. Chem. Phys.* **133**, 014106 (2010).
40. F. Eckert, A. Klamt, Fast solvent screening via quantum chemistry: COSMO-RS approach. *AIChE J.* **48**, 369–385 (2002).
41. A. Klamt, The COSMO and COSMO-RS solvation models. *Wiley Interdiscip. Rev. Comput. Mol. Sci.* **1**, 699–709 (2011).
42. A. Klamt, M. Diedenhofen, Calculation of solvation free energies with DCOSMO-RS. *J. Phys. Chem. A* **119**, 5439–5445 (2015).
43. A. Hellweg, F. Eckert, Brick by brick computation of the gibbs free energy of reaction in solution using quantum chemistry and COSMO-RS. *AIChE J.* **63**, 3944–3954 (2017).
44. R. Ahlrichs, M. Bär, M. Häser, H. Horn, C. Kölmel, Electronic structure calculations on workstation computers: The program system turbomole. *Chem. Phys. Lett.* **162**, 165–169 (1989).
45. O. Treutler, R. Ahlrichs, Efficient molecular numerical integration schemes. *J. Chem. Phys.* **102**, 346–354 (1995).
46. M. V. Arnim, R. Ahlrichs, Performance of parallel TURBOMOLE for density functional calculations. *J. Comput. Chem.* **19**, 1746–1757 (1998).
47. A. D. Becke, Density-functional exchange-energy approximation with correct asymptotic behavior. *Phys. Rev. A* **38**, 3098–3100 (1988).
48. J. P. Perdew, Density-functional approximation for the correlation energy of the inhomogeneous electron gas. *Phys. Rev. B* **33**, 8822–8824 (1986).
49. F. Weigend, R. Ahlrichs, Balanced basis sets of split valence, triple zeta valence and quadruple zeta valence quality for H to Rn: Design and assessment of accuracy. *Phys. Chem. Chem. Phys.* **7**, 3297–3305 (2005).
50. K. Eichkorn, O. Treutler, H. Öhm, M. Häser, R. Ahlrichs, Auxiliary basis sets to approximate Coulomb potentials. *Chem. Phys. Lett.* **242**, 652–660 (1995).
51. K. Eichkorn, F. Weigend, O. Treutler, R. Ahlrichs, Auxiliary basis sets for main row atoms and transition metals and their use to approximate Coulomb potentials. *Theor. Chem. Acc.* **97**, 119–124 (1997).
52. F. Weigend, Accurate Coulomb-fitting basis sets for H to Rn. *Phys. Chem. Chem. Phys.* **8**, 1057–1065 (2006).
53. M. Sierka, A. Hogekamp, R. Ahlrichs, Fast evaluation of the Coulomb potential for electron densities using multipole accelerated resolution of identity approximation. *J. Chem. Phys.* **118**, 9136–9148 (2003).
54. A. Klamt, M. Diedenhofen, A refined cavity construction algorithm for the conductor-like screening model. *J. Comput. Chem.* **39**, 1648–1655 (2018).
55. S. Grimme, J. Antony, S. Ehrlich, H. Krieg, A consistent and accurate ab initio parametrization of density functional dispersion correction (DFT-D) for the 94 elements H-Pu. *J. Chem. Phys.* **132**, 154104 (2010).
56. NIST Chemistry WebBook, Sadtler Research Labs Under US-EPA Contract (10 February 2021); <https://webbook.nist.gov/cgi/cbook.cgi?ID=C103719&Type=IR-SPEC&Index=0#IR-SPEC>.

Acknowledgments: We acknowledge the Zentraleinrichtung für Datenverarbeitung (ZEDAT) of the Freie Universität Berlin for the allocation of computing resources. P.V. thanks M. Kleoff for helpful discussions. **Funding:** We also thank the COVESTRO company for continuous financial and technical support of our research. **Author contributions:** Conceptualization: S.R., R.W., S.S., S.Y., and Y.S. Methodology: P.V., C.M., M.R., and R.M. Investigation: P.V., A.W., T.K., C.M., M.R., and R.M. Visualization: P.V. and C.M. Project administration: S.R. Supervision: S.R. and M.K. Writing—original draft: P.V., S.R., and C.M. Writing—review and editing: P.V., S.R., M.K., H.B., R.W., S.Y., and C.M. **Competing interests:** Y.S., R.W., S.R., and S.S. are inventors on a pending patent related to this work filed by Covestro Intellectual Property GmbH & Co. KG (no. WO 2019215037 A1, filed 2018). S.Y., S.R., P.V., R.W., Y.S., T.K., and S.S. are inventors on two pending patents related to this work filed by Covestro Deutschland AG (no. EP20213933.3, filed 2020 and no. EP20213938, filed 2020). The authors declare that they have no other competing interests. **Data and materials availability:** All data needed to evaluate the conclusions in the paper are present in the paper and/or the Supplementary Materials.

Submitted 18 May 2021
Accepted 6 August 2021
Published 29 September 2021
10.1126/sciadv.abj5186

Citation: P. Voßnacker, A. Wüst, T. Keilhack, C. Müller, S. Steinhauer, H. Beckers, S. Yogendra, Y. Schiesser, R. Weber, M. Reimann, R. Müller, M. Kaupp, S. Riedel, Novel synthetic pathway for the production of phosgene. *Sci. Adv.* **7**, eabj5186 (2021).

3.5 Synthesis of a Hexachloro Sulfate(IV) Dianion Enabled by Polychloride Chemistry



Patrick Voßnacker, Alisa Wüst, Carsten Müller, Merlin Kleoff, Sebastian Riedel*

Angew. Chem. Int. Ed. **2022**, 61, e202209684.

Angew. Chem. **2022**, 134, e202209684.

<https://doi.org/10.1002/anie.202209684>

<https://doi.org/10.1002/ange.202209684>

© 2022 *Angewandte Chemie International Edition* published by Wiley-VCH GmbH. This is an open-access article distributed under the terms of the [Creative Commons Attribute 4.0 International license](https://creativecommons.org/licenses/by/4.0/).

Author contributions

Patrick Voßnacker designed the project, performed most of the experiments and wrote the manuscript. Alisa Wüst performed some of the experiments. Carsten Müller performed quantum chemical calculations and wrote parts of the manuscript. Merlin Kleoff wrote parts of the manuscript and provided scientific guidance. Sebastian Riedel managed the project and revised the manuscript.

VIP **Sulfur Compounds** Very Important Paper
How to cite: *Angew. Chem. Int. Ed.* **2022**, *61*, e202209684

International Edition: doi.org/10.1002/anie.202209684

German Edition: doi.org/10.1002/ange.202209684

Synthesis of a Hexachloro Sulfate(IV) Dianion Enabled by Polychloride Chemistry

Patrick Voßnacker, Alisa Wüst, Carsten Müller, Merlin Kleoff, and Sebastian Riedel*

In memory of Professor Ralf Stuedel

Abstract: The preparation and structural characterization of $[\text{NEt}_3\text{Me}]_2[\text{SCl}_6]$ is described, which is the first example of a $[\text{SCl}_6]^{2-}$ dianion and of a halosulfate anion of the type $[\text{S}_x\text{X}_y]^{z-}$ in general. This dianion belongs to the group of 14-valence electron AB_6E systems and forms an octahedral structure in the solid-state. Interestingly, co-crystallization with CH_2Cl_2 affords $[\text{NEt}_3\text{Me}]_2[\text{SCl}_6] \cdot 4\text{CH}_2\text{Cl}_2$ containing $[\text{SCl}_6]^{2-}$ dianions with C_{4v} symmetry. As suggested by quantum-chemical calculations, the distortion of the structure is not caused by a stereochemically active lone pair but by enhanced hydrogen bonding interactions with CH_2Cl_2 . At elevated temperatures, $[\text{NEt}_3\text{Me}]_2[\text{SCl}_6]$ decomposes to various sulfur chlorine compounds as shown by Raman spectroscopy. Cooling back to room temperature results in the selective formation of $[\text{NEt}_3\text{Me}]_2[\text{SCl}_6]$ which is comparable to the well-studied SCl_4 .

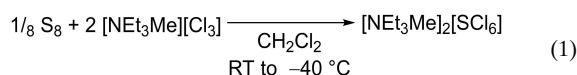
The chlorination of small molecules is a topic of major relevance both for industrial and academic research.^[1] Very recently, our group in cooperation with Covestro investigated $[\text{NEt}_3\text{Me}]\text{Cl}$ as a practical chlorine storage medium which forms the corresponding trichloride $[\text{NEt}_3\text{Me}][\text{Cl}_3]$ by addition of chlorine.^[2] More importantly, we found that $[\text{NEt}_3\text{Me}][\text{Cl}_3]$ is also a useful chlorinating agent reacting with carbon monoxide to the base chemical phosgene (COCl_2). Interestingly, our studies indicate that the trichloride anion in $[\text{NEt}_3\text{Me}][\text{Cl}_3]$ has a Cl–Cl bond which is much weaker than in elemental chlorine facilitating the insertion of carbon monoxide into the Cl–Cl bond of the trichloride.^[3]

In contrast to elemental chlorine, $[\text{NEt}_3\text{Me}][\text{Cl}_3]$ contains the chemically inert cation $[\text{NEt}_3\text{Me}]^+$ which has proven to be very useful to stabilize various reactive anions.^[4] Therefore, we speculated that the exceptional ability of

$[\text{NEt}_3\text{Me}][\text{Cl}_3]$ to serve both as a strong chlorination reagent and to form stable salts with unique anions would enable the preparation of unknown chlorine-containing compounds. While focusing on sulfur compounds, we noted that most sulfur chlorides are relatively unstable species. Reaction of elemental sulfur with chlorine leads primarily to S_2Cl_2 , which can be further reacted with an excess of chlorine in the presence of FeCl_3 as catalyst to SCl_2 .^[5] While S_2Cl_2 is comparably stable, SCl_2 decomposes at room temperature slowly to S_2Cl_2 and Cl_2 . At -78 °C , SCl_2 reacts with liquid Cl_2 to SCl_4 but decomposes to SCl_2 and Cl_2 when warmed above its melting point of -30 °C . Below that temperature, SCl_4 exists in the ionic structure $[\text{SCl}_3]^+[\text{Cl}]^-$, as suggested by IR and Raman spectroscopy and powder XRD analysis.^[6] Beside SCl_4 , various salts of the type $[\text{SCl}_3]^+[\text{X}]^-$ with, e.g., $\text{X} = [\text{ICl}_4]^-$,^[7] $[\text{SbF}_6]^-$,^[8] $[\text{F}(\text{Al}(\text{OC}_4\text{F}_9)_3)_2]^-$ ^[9] have been prepared. The highest possible binary sulfur chlorine species, SCl_6 , is not known, while the lighter homologue SF_6 is a stable compound that found various industrial applications.^[10] Surprisingly, chlorosulfates, $[\text{S}_x\text{Cl}_y]^{z-}$, have not been prepared thus far, although afterglow-tandem mass spectrometric experiments gave a $D_0(\text{SCl}_2-\text{Cl}^-)$ bond energy of $85 \pm 8\text{ kJ mol}^{-1}$ for the $[\text{SCl}_3]^-$ which is in the same range as the bond energy within the $[\text{Cl}_3]^-$ anion ($99 \pm 5\text{ kJ mol}^{-1}$).^[11] In contrast, for the heavier elements Se and Te a plethora of chloroselenates and chlorotellurates in the oxidation states II and IV are known for decades (e.g., $[\text{Se}_2\text{Cl}_4]^{2-}$,^[12] $[\text{Se}_4\text{Cl}_{12}]^{2-}$,^[13] $[\text{ChCl}_6]^{2-}$,^[14] $[\text{Ch}_2\text{Cl}_{10}]^{2-}$,^[13,15] $[\text{Ch}_3\text{Cl}_{13}]^-$ ^[16] ($\text{Ch} = \text{Se}, \text{Te}$)).

At the outset, we prepared the ionic liquid $[\text{NEt}_3\text{Me}][\text{Cl}_3]$ by the reaction of commercially available $[\text{NEt}_3\text{Me}]\text{Cl}$ with elemental chlorine as previously described.^[3]

A solution of $[\text{NEt}_3\text{Me}][\text{Cl}_3]$ in CH_2Cl_2 was reacted with elemental sulfur at room temperature for 16 h [Eq. (1)]. Slowly cooling to -40 °C yielded yellow crystals that could be analyzed by X-ray diffraction revealing the formation of $[\text{NEt}_3\text{Me}]_2[\text{SCl}_6]$ (Figure 1, left).



In this structure, the $[\text{SCl}_6]^{2-}$ dianion has an almost octahedral geometry with S–Cl bond lengths of 231.2(1), 231.5(1) and 232.3(1) pm and bond angles between 88.9(1) and 91.1(1)°. The $[\text{SCl}_6]^{2-}$ dianion is stabilized by weak

[*] P. Voßnacker, A. Wüst, Dr. C. Müller, Dr. M. Kleoff, Prof. Dr. S. Riedel
 Institut für Chemie und Biochemie—Anorganische Chemie, Freie Universität Berlin
 Fabeckstraße 34/36, 14195 Berlin (Germany)
 E-mail: s.riedel@fu-berlin.de

© 2022 The Authors. Angewandte Chemie International Edition published by Wiley-VCH GmbH. This is an open access article under the terms of the Creative Commons Attribution License, which permits use, distribution and reproduction in any medium, provided the original work is properly cited.

a stabilization of the system, also known as a second-order Jahn–Teller effect. For an octahedral structure the lone pair is located in the *s* orbital of the central atom and therefore stereochemically inactive. Lowering the symmetry increases the *p* character of the lone pair. It becomes stereochemically active and can be located at the plane (C_{3v}), edge (C_{2v}), or corner (C_{4v}) of the octahedron (see Figure S8), with the former being the generally favored and the latter the least probable possibility. The second, contrary, effect is the electronic repulsion between the ligands making an octahedral structure more favorable. For many systems, there is a delicate balance between the symmetrical octahedral and the distorted structure. Therefore, already weak interactions of the anion with its molecular environment, e.g., by hydrogen bonding to the cation can determine the structure.^[17,18]

As mentioned above, the distortion from an O_h symmetry to a C_{4v} geometry, as found for $[\text{NEt}_3\text{Me}]_2[\text{SCl}_6] \cdot 4\text{CH}_2\text{Cl}_2$, is quite unusual. Therefore, an NBO analysis of the distorted $[\text{SCl}_6]^{2-}$ was performed and revealed that the lone pair of the sulfur is located in the 3*s* orbital and is stereochemically inactive (see Figure S9).

To further investigate the energetical influence of a distortion of $[\text{SCl}_6]^{2-}$, a relaxed surface scan was performed by starting from an octahedral structure and subsequently increasing one S–Cl bond (see Figure S10 to S12). An elongation of the S–Cl2 bond by 10 pm translates to an energetical increase of only 0.6 kJ mol⁻¹. On the other hand, this distortion leads to an increased negative charge on Cl2 (Natural Charge –0.43 vs. –0.49) which enables stronger hydrogen bonding interactions.

Indeed, these interactions are found by Hirshfeld analysis of the solid state structure of $[\text{NEt}_3\text{Me}]_2[\text{SCl}_6] \cdot 4\text{CH}_2\text{Cl}_2$ (Figure 2). Overall, the Cl2 has five H...Cl interactions below the sum of the van der Waals radii ($\Sigma_{\text{vdW}}(\text{H} \cdots \text{Cl}) = 285$ pm).

As one of the S–Cl bonds is significantly elongated, the $[\text{SCl}_6]^{2-}$ species could be described as a $[\text{SCl}_5]^-$ fragment and a Cl^- anion. In this description, the $[\text{SCl}_5]^-$ species consists of four equatorial S–Cl bonds formed by 3-center-4-electron bonds and one axial S–Cl bond which is a classical 2-center-2-electron bond (Figure 3A). Therefore, we calculated the electrostatic potential of $[\text{SCl}_5]^-$ and mapped it onto the

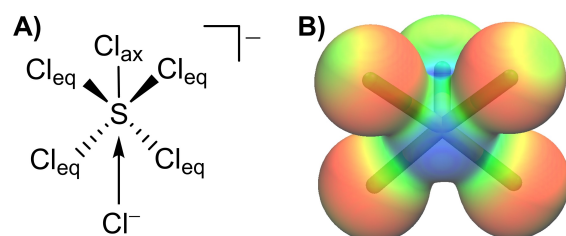


Figure 3. A) Interaction of Cl^- with the σ -hole of $[\text{SCl}_5]^-$ formally forming $[\text{SCl}_6]^{2-}$. B) Electrostatic potential of $[\text{SCl}_5]^-$ in a range of: –0.15 (red) to 0.05 a.u. (blue) mapped onto the electron density (isosurface value 0.025 a.u.) calculated on B3LYP-D4/def2-TZVPP level of theory.

electron density (Figure 3B). According to these calculations, there is a high negative charge located on the equatorial Cl atoms while a more positive electrostatic potential can be found on the central sulfur atom along the S–Cl_{ax} bond, the so called σ -hole. Thus, the Cl^- can interact with this positively charged region of the $[\text{SCl}_5]^-$ fragment. Additionally, the Cl^- can donate electron density into the σ^* orbital (S–Cl_{ax}, LUMO) resulting in a weakening and elongation of the S–Cl_{ax} bond. This bonding situation is similar to that found in polyhalides.^[27]

An atoms in molecules (AIM) analysis based on periodic DFT calculations shows an ionic character of the S–Cl interaction in the dianion. At all corresponding bond critical points, the Laplacian is small and positive (ca. 1.7–1.8 e Å⁻⁵), the ratio of the absolute potential ($|V|$) and kinetic energy density (*G*) is below 2.0 (1.6), and the value of the electron localization function (ELF) is only about 0.6—all indicative for a non-shared interaction (see Table S5).

At last, we investigated the influence of the temperature on the formation of $[\text{NEt}_3\text{Me}]_2[\text{SCl}_6]$ from a stoichiometric mixture of S_8 and $[\text{NEt}_3\text{Me}][\text{Cl}_3]$ by Raman spectroscopy (Figure 4). Interestingly, at 40 °C the mixture exists as a liquid consisting of various species including $[\text{Cl}_3]^-$ and S_2Cl_2 as indicated by comparison with reference substances (see Figure S6). In addition, the presence of $[\text{SCl}_5]^-$ could be

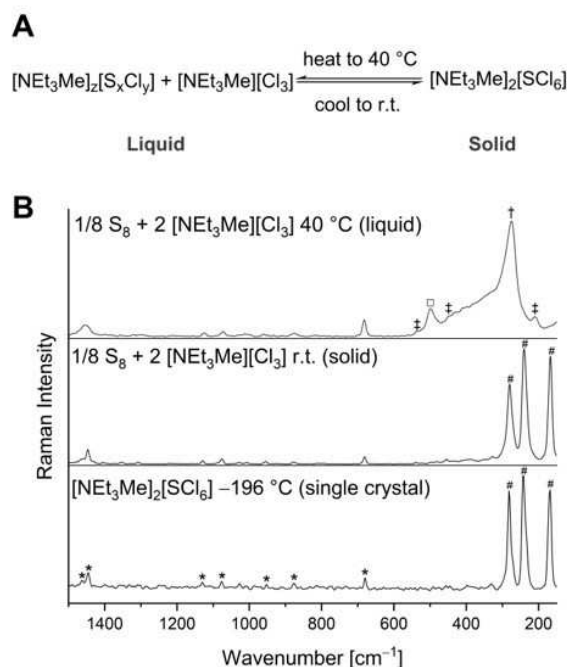


Figure 4. A) The thermal equilibrium of $[\text{NEt}_3\text{Me}]_2[\text{SCl}_6]$ with various sulfur chlorine compounds. B) Raman spectrum of the reaction mixture of sulfur and $[\text{NEt}_3\text{Me}][\text{Cl}_3]$ at 40 °C (above) and room temperature (middle) and comparison to the Raman spectrum of the single crystal of $[\text{NEt}_3\text{Me}]_2[\text{SCl}_6]$ (below). Bands are assigned as follows (* = cation, # = $[\text{SCl}_6]^{2-}$, † = $[\text{Cl}_3]^-$, ‡ = S_2Cl_2 , □ = presumably $[\text{SCl}_5]^-$). See Figure S6 for reference spectra.

assumed as the calculated spectrum at SCS-MP2/def2-TZVPP level of theory is in good agreement with the measured spectrum (see Figure S6). When cooled to room temperature, the mixture solidified and the measured Raman spectrum thereof was consistent with those obtained for the single crystals of $[\text{NEt}_3\text{Me}]_2[\text{SCl}_6]$ suggesting its selective formation. This highlights that the crystallization of $[\text{NEt}_3\text{Me}]_2[\text{SCl}_6]$ is energetically highly favored due to its comparably large lattice energy. A rough estimation of the stabilization energy the dianion meets due to the periodic cation-lattice yields about 240 kJ mol^{-1} (see Supporting Information, chapter h). When the solidified $[\text{NEt}_3\text{Me}]_2[\text{SCl}_6]$ is heated to 40 C again, a similar spectrum is observed as for the reaction mixture. Thus, it can be assumed that there is an equilibrium between various sulfur chlorides in the liquid mixture and $[\text{SCl}_6]^{2-}$ in the solid (Figure 4A). Given these results, the thermal behavior of $[\text{NEt}_3\text{Me}]_2[\text{SCl}_6]$ is comparable to SCl_4 , which is only stable below -30 C and decomposes above this temperature to SCl_2 and Cl_2 .

In conclusion, we synthesized $[\text{NEt}_3\text{Me}]_2[\text{SCl}_6]$, which is the first example of a halosulfate anion of the type $[\text{S}_x\text{X}_y]^{z-}$. Additionally, this unprecedented molecule is one of the few examples for a 14-valence electron AB_6E system with a central atom of the third period. In general, AB_6E systems can either adopt an octahedral symmetry or a distorted structure with a stereochemically active lone pair. In $[\text{NEt}_3\text{Me}]_2[\text{SCl}_6]$, we found an octahedral symmetry for the $[\text{SCl}_6]^{2-}$ dianion in the solid-state structure. However, when CH_2Cl_2 co-crystallized, $[\text{NEt}_3\text{Me}]_2[\text{SCl}_6] \cdot 4 \text{CH}_2\text{Cl}_2$ was formed with an unusual C_{4v} structure, with one elongated and one shortened axial S–Cl bond. Quantum-chemical calculations revealed that this distortion cannot be attributed to a stereochemically active lone pair but is a result of enhanced hydrogen bonding interactions with CH_2Cl_2 .

Notably, $[\text{NEt}_3\text{Me}]_2[\text{SCl}_6]$ decomposes to various sulfur chlorine compounds at 40 C while cooling back to room temperature results in the selective formation of $[\text{NEt}_3\text{Me}]_2[\text{SCl}_6]$ highlighting the similarity to the well-studied SCl_4 . This work demonstrates the unique ability of $[\text{NEt}_3\text{Me}][\text{Cl}_3]$ to serve as a versatile chlorination agent while stabilizing unprecedented anions.

Acknowledgements

We thank Dr. Daniel Franz (FU Berlin) for recording the SCXRD data of $[\text{NEt}_3\text{Me}]_2[\text{SCl}_6]$ and Prof. Martin Kaupp for fruitful discussions. We would like to acknowledge the assistance of the Core Facility BioSupraMol supported by the DFG, the HPC Service of ZEDAT, Freie Universität Berlin, for computing time and the ERC Project HighPotOx (Grant agreement ID: 818862) for funding. Open Access funding enabled and organized by Projekt DEAL.

Conflict of Interest

The authors declare no conflict of interest.

Data Availability Statement

The data that support the findings of this study are available from the corresponding author upon reasonable request.

Keywords: Ionic Liquids · Polychlorides · Quantum Chemistry · Sulfur · VSEPR Model

- [1] a) R. Lin, A. P. Amrute, J. Pérez-Ramírez, *Chem. Rev.* **2017**, *117*, 4182; b) P. Schmittinger, T. Florkiewicz, L. C. Curlin, B. Lüke, R. Scannell, T. Navin, E. Zelfel, R. Bartsch, in *Ullmann's Encyclopedia of Industrial Chemistry (Chlorine)*, Wiley-VCH, Weinheim, **2011**.
- [2] P. Voßnacker, N. Schwarze, T. Keilhack, M. Kleoff, S. Steinhauer, Y. Schiesser, M. Paven, S. Yogendra, R. Weber, S. Riedel, *ACS Sustainable Chem. Eng.* **2022**, *10*, 9525.
- [3] P. Voßnacker, A. Wüst, T. Keilhack, C. Müller, S. Steinhauer, H. Beckers, S. Yogendra, Y. Schiesser, R. Weber, M. Reimann, et al., *Sci. Adv.* **2021**, *7*, eabj5186.
- [4] a) P. Pröhm, J. R. Schmid, K. Sonnenberg, S. Steinhauer, C. J. Schattenberg, R. Müller, M. Kaupp, P. Voßnacker, S. Riedel, *Angew. Chem. Int. Ed.* **2020**, *59*, 16002; *Angew. Chem.* **2020**, *132*, 16136; b) J. R. Schmid, P. Pröhm, P. Voßnacker, G. Thiele, M. Ellwanger, S. Steinhauer, S. Riedel, *Eur. J. Inorg. Chem.* **2020**, 4497; c) T. A. Gully, P. Voßnacker, J. R. Schmid, H. Beckers, S. Riedel, *ChemistryOpen* **2021**, *10*, 255; d) S. Kotsyuda, A. Wiesner, S. Steinhauer, S. Riedel, *Z. Anorg. Allg. Chem.* **2020**, *57*, 13982.
- [5] M. Baudler, G. Brauer, *Handbuch der präparativen anorganischen Chemie in drei Bänden, Vol. 1*, 3rd ed., Ferdinand Enke, Stuttgart, **1975**.
- [6] a) R. Steudel, D. Jensen, B. Plinke, *Z. Naturforsch. B* **1987**, *42*, 163; b) R. Kniep, L. Körte, D. Mootz, *Z. Naturforsch. B* **1984**, *39*, 305.
- [7] a) A. J. Edwards, *J. Chem. Soc. Dalton Trans.* **1978**, 1723; b) A. Finch, P. N. Gates, T. H. Page, *Inorg. Chim. Acta* **1977**, *25*, L49–L50.
- [8] J. Passmore, P. D. Boyle, G. Schatte, T. Way, T. S. Cameron, *Can. J. Chem.* **1996**, *74*, 1671.
- [9] P. Weis, D. C. Röhner, R. Prediger, B. Butschke, H. Scherer, S. Weber, I. Krossing, *Chem. Sci.* **2019**, *10*, 10779.
- [10] D. Dirican, N. Pfister, M. Wozniak, T. Braun, *Chem. Eur. J.* **2020**, *26*, 6945.
- [11] a) B. D. Gailbreath, C. A. Pommerening, S. M. Bachrach, L. S. Sunderlin, *J. Phys. Chem. A* **2000**, *104*, 2958; b) K. E. Nizzi, C. A. Pommerening, L. S. Sunderlin, *J. Phys. Chem. A* **1998**, *102*, 7674.
- [12] B. Krebs, E. Lühns, R. Willmer, F.-P. Ahlers, *Z. Anorg. Allg. Chem.* **1991**, *592*, 17.
- [13] W. Czado, M. Maurer, U. Müller, *Z. Anorg. Allg. Chem.* **1998**, *624*, 1871.
- [14] P. J. Hendra, Z. Jovi, *J. Chem. Soc. A* **1968**, 600.
- [15] M. A. James, O. Knop, T. S. Cameron, *Can. J. Chem.* **1992**, *70*, 1795.
- [16] F.-P. Ahlers, E. Lühns, B. Krebs, *Z. Anorg. Allg. Chem.* **1991**, *594*, 7.
- [17] R. A. Wheeler, P. N. V. P. Kumar, *J. Am. Chem. Soc.* **1992**, *114*, 4776.
- [18] M. Kaupp, C. van Wuellen, R. Franke, F. Schmitz, W. Kutzelnigg, *J. Am. Chem. Soc.* **1996**, *118*, 11939.
- [19] M. Gawrilow, H. Beckers, S. Riedel, L. Cheng, *J. Phys. Chem. A* **2018**, *122*, 119.
- [20] J. N. Cutler, G. M. Bancroft, J. D. Bozek, K. H. Tan, G. J. Schrobilgen, *J. Am. Chem. Soc.* **1991**, *113*, 9125.
- [21] A. R. Mahjoub, K. Seppelt, *Angew. Chem.* **1991**, *103*, 309.



- [22] A. R. Mahjoub, X. Zhang, K. Seppelt, *Chem. Eur. J.* **1995**, *1*, 261.
- [23] K. O. Christe, W. W. Wilson, R. V. Chirakal, J. C. P. Sanders, G. J. Schrobilgen, *Inorg. Chem.* **1990**, *29*, 3506.
- [24] A. R. Mahjoub, A. Hoser, J. Fuchs, K. Seppelt, *Angew. Chem. Int. Ed. Engl.* **1989**, *28*, 1526; *Angew. Chem.* **1989**, *101*, 1528.
- [25] a) W. Abriel, *Acta Crystallogr. Sect. C* **1986**, *42*, 1113; b) U. Müller, B. Eckhoff, *Z. Kristallogr. New Cryst. Struct.* **1999**, *214*, 505.
- [26] W. Abriel, *Z. Naturforsch. B* **1986**, *41*, 592.
- [27] K. Sonnenberg, L. Mann, F. A. Redeker, B. Schmidt, S. Riedel, *Angew. Chem. Int. Ed.* **2020**, *59*, 5464–5493; *Angew. Chem.* **2020**, *132*, 5506–5535.

Manuscript received: July 2, 2022

Accepted manuscript online: August 4, 2022

Version of record online: August 30, 2022

3.6 The Rise of Trichlorides Enabling an Improved Chlorine Technology



Merlin Kleoff, Patrick Voßnacker, Sebastian Riedel*

Angew. Chem. Int. Ed. **2023**, 62, e202216586

Angew. Chem. **2023**, 135, e202216586.

<https://doi.org/10.1002/anie.202216586>

<https://doi.org/10.1002/ange.202216586>

© 2023 *Angewandte Chemie International Edition* published by Wiley-VCH GmbH. This is an open-access article distributed under the terms of the [Creative Commons Attribute 4.0 International license](https://creativecommons.org/licenses/by/4.0/).

Author contributions

Merlin Kleoff designed the project and wrote most of the manuscript. Patrick Voßnacker wrote part of the manuscript and provided scientific guidance. Sebastian Riedel managed the project and revised the manuscript.

Chlorine Chemistry

How to cite: *Angew. Chem. Int. Ed.* **2023**, *62*, e202216586

International Edition: doi.org/10.1002/anie.202216586

German Edition: doi.org/10.1002/ange.202216586

The Rise of Trichlorides Enabling an Improved Chlorine Technology

Merlin Kleoff, Patrick Voßnacker, and Sebastian Riedel*



Abstract: Chlorine plays a central role for the industrial production of numerous materials with global relevance. More recently, polychlorides have been evolved from an area of academic interest to a research topic with enormous industrial potential. In this minireview, the value of trichlorides for chlorine storage and chlorination reactions are outlined. Particularly, the inexpensive ionic liquid $[\text{NET}_3\text{Me}][\text{Cl}_3]$ shows a similar and sometimes even advantageous reactivity compared to chlorine gas, while offering a superior safety profile. Used as a chlorine storage, $[\text{NET}_3\text{Me}][\text{Cl}_3]$ could help to overcome the current limitations of storing and transporting chlorine in larger quantities. Thus, trichlorides could become a key technique for the flexibilization of the chlorine production enabling an exploitation of renewable, yet fluctuating, electrical energy. As the loaded storage, $[\text{NET}_3\text{Me}][\text{Cl}_3]$, is a proven chlorination reagent, it could directly be employed for downstream processes, paving the path to a more practical and safer chlorine industry.

1. The Importance of Chlorine for the Modern World

The importance of chlorine for our daily live can hardly be overestimated. It is estimated that chlorine is involved in the synthesis of 50 % of all industrial compounds, 30 % of all agrochemicals, and 20 % of all pharmaceuticals rendering chlorine one of the most important base chemicals.^[1,2]

The industrial utilization of chlorine can be illustrated by the “chlorine tree” (Figure 1), highlighting important intermediate chemicals (the branches) obtained from elemental chlorine that are used in the production of indispensable materials (the leaves).^[3]

Chlorine itself is widely used for water treatment, may it be for the degermination of water in public swimming pools or of tap water.^[4] Although hydrogen chloride is a side product in many processes, highly pure hydrogen chloride is industrially formed by direct synthesis from hydrogen and chlorine gas in a combustion chamber.^[5]

However, in most cases, chlorine is further processed to intermediate chemicals. One of the most important examples is phosgene (COCl_2 , **17**), which is produced by the reaction of chlorine and carbon monoxide in a volume of 12 million metric tons per year. Phosgene (**17**) is a versatile chemical that found numerous applications both in academia and industry, but primarily it is used for the manufacturing of polyurethanes and polycarbonates.^[6]

Another crucial bulk chemical that relies on the use of chlorine is 1,2-dichloroethane which global production reached 34.5 million tons per year in 2013^[7] and is estimated to reach 58 million tons per year by the end of 2027.^[8] Approximately 98 % of it are used to produce vinyl chloride by thermal decomposition of 1,2-dichloroethane. Polymerization of vinyl chloride affords poly vinyl chloride (PVC) which is ranked as the third most produced polymer in the United States of America (approximately 5.8 million tons per year in 2008).^[9]

Industrially, glacial acetic acid is chlorinated in the presence of acetic anhydride providing predominantly chloroacetic acid and smaller quantities of di- and trichloroacetic acid. Most of chloroacetic acid is used to produce carboxymethyl cellulose in a volume of several hundred thousand tons per year. Further chlorination of chloroacetic acid with, e.g., phosgene (**17**), affords chloroacetyl chloride that is a valuable building block for the synthesis of pharmaceuticals such as adrenalin (epinephrine).^[10]

An industrially important C_3 -building block is allyl chloride, which is produced by radical chlorination of propene at temperatures of ≈ 500 C. It is a versatile intermediate for the synthesis of various allyl compounds (e.g., allyl alcohol and allyl isothiocyanate) but the majority of allyl chloride is processed to epichlorohydrin, which is used for the manufacturing of glycerol and epoxy resins.^[11]

In addition to these organic compounds, numerous inorganic chlorides are produced from chlorine. For instance, the combustion of white phosphorus with elemental chlorine affords phosphorus trichloride which is extensively used for the synthesis of medicines, pesticides, and flame retardants.^[12]

Interestingly, chlorine also plays a crucial role for the purification of titanium dioxide, which is the most important pigments in the color industry. As raw titanium dioxide (obtained from, e.g., Rutile) is contaminated with other pigments, it is chlorinated to titanium tetrachloride. The pure titanium tetrachloride is distilled and subsequently burned with oxygen to provide pure titanium dioxide suitable for colors at a rate of over 4 million tons per year.^[13]

2. The Energy-Demanding Production of Chlorine

Considering the countless industrial processes involving chlorine, it can be stated, that our modern life could hardly be realized without chlorine. To meet the global need of chlorine, it is produced primarily by chloralkali electrolysis in an enormous volume of approximately 88 million tons per year, and is predicted to grow to approximately 92 million tons in 2024.^[14] However, this is a highly energy demanding process that consumes approximately 205 million MWh per year worldwide.^[15] In Germany, the country with the biggest chlorine production in Europe, chloralkali electrolysis has an energy demand of 12 million MWh which corresponds to ≈ 2 % of the electrical energy in Germany.^[15-17] In fact, the electrochemical chlorine production ranks among the most

[*] Dr. M. Kleoff, P. Voßnacker, Prof. Dr. S. Riedel
Fachbereich Biologie, Chemie, Pharmazie, Institut für Chemie und Biochemie—Anorganische Chemie
Fabeckstr. 34/36, 14195 Berlin (Germany)
E-mail: s.riedel@fu-berlin.de

© 2023 The Authors. Angewandte Chemie International Edition published by Wiley-VCH GmbH. This is an open access article under the terms of the Creative Commons Attribution Non-Commercial License, which permits use, distribution and reproduction in any medium, provided the original work is properly cited and is not used for commercial purposes.

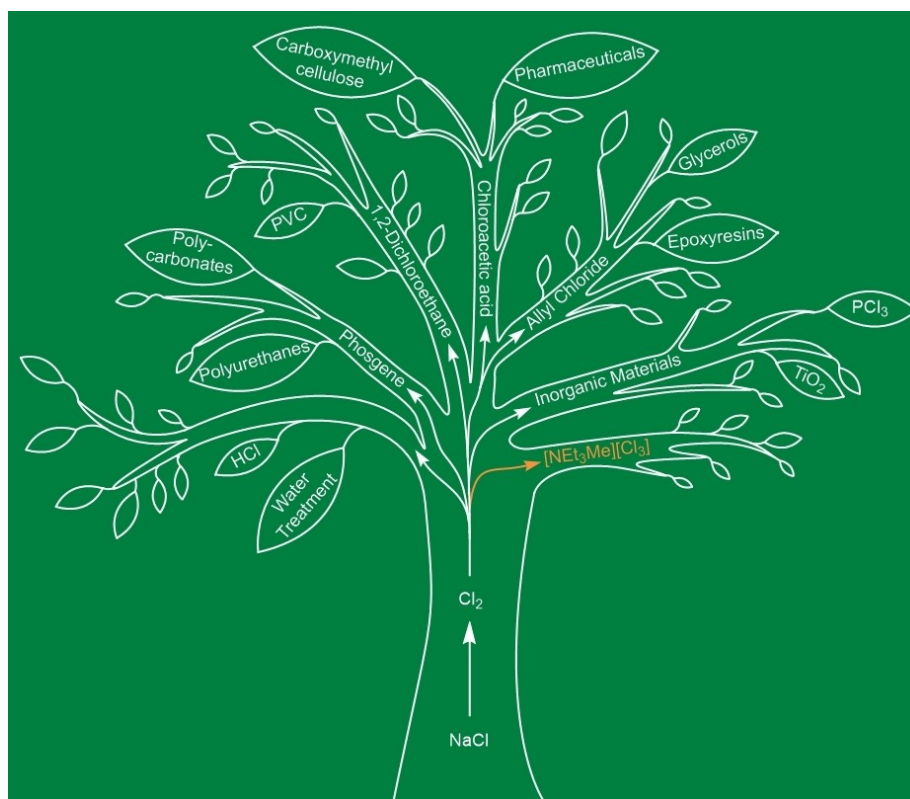
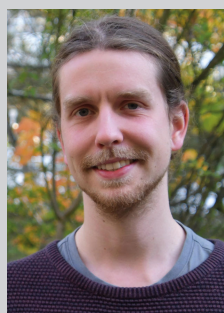


Figure 1. The “chlorine tree” highlighting important applications of chlorine as chemicals (branches) that are used for the production of important materials (leaves). Drawn by the authors, inspired by “the chlorine tree” of Eurochlor (eurochlor.org, 2016).



Merlin Kleoff, born in Berlin, Germany, in 1994, studied chemistry at Freie Universität Berlin where he received his M.Sc. in 2018. He obtained his Ph.D. in the group of Prof. Dr. Philipp Heretsch at Freie Universität Berlin. Then, he joined the group of Prof. Dr. Sebastian Riedel (Freie Universität Berlin) where he is researching on polychlorides and their applications in chemical industry.



Patrick Voßnacker, born in Munich, Germany, in 1994, studied chemistry at Freie Universität Berlin and Uppsala University. He received his M.Sc. in 2018 and is now pursuing his Ph.D. in the group of Prof. Dr. Sebastian Riedel (Freie Universität Berlin) with a focus on polychlorides and their reactivity.



Sebastian Riedel was born in Groß-Gerau (Germany) in 1975 and was trained as a chemistry laboratory technician at Siemens and Degussa in Hanau-Wolfgang. He then studied chemistry at the Universities of Siegen and Würzburg and obtained his Ph.D. in theoretical chemistry at the institute of inorganic chemistry in 2006. As a Humboldt postdoctoral fellow, he joined the groups of Räsänen and Pyykkö and afterwards carried out a second postdoctoral stay in the group of Schrobilgen. Having finished his habilitation at Universität Freiburg in 2013, he became a full professor of inorganic chemistry at the Freie Universität Berlin where he was appointed in 2021 as Einstein-Professor.

expensive and energy-intensive processes in chemical industry with an energy demand translating to approximately 50 % of the production costs.^[18] This becomes even more striking in view of the climate change pointing out the necessity to reduce the anthropogenic carbon dioxide emission. Renewable energies could help to address this problem, which already provide 41 % of the electrical energy in Germany.^[19]

However, they provide an inconsistent power supply depending on current weather circumstances (e.g., sun light, wind). When the chloralkali electrolysis is driven by renewable energies, this would result in a fluctuation of chlorine supply. While the chloralkali electrolysis is relatively adoptable to electricity fluctuations, most of the downstream processes of chlorine are not. Therefore, the chlorine production is currently highly dependent on baseload electricity provided by fossil fuels. This issue could be partially solved by an efficient chlorine storage medium allowing to exploit temporary energy excesses to produce chlorine.^[20] Then, periods of an energy deficit (“dark doldrums”) could be bypassed by releasing chlorine from the storage. However, at the moment, “chlorine cannot be easily stored in large amounts”, as “the safety requirements for its storage are particularly high” and consequently, chlorine is typically stored for several hours when it “is unavoidable”.^[20a] Thus, the development of a useful chlorine storage is closely associated to the challenge to tame the dangers of elemental chlorine.^[20,21]

3. The Properties and Dangers of Elemental Chlorine

Elemental chlorine is a greenish-yellow gas having a boiling point of -34 C and a melting point of -101 C. Due to the relatively high density of chlorine gas compared to air (density relative to air of 2.48), chlorine gas tends to persist on the ground.^[22] Therefore, it had found questionable use as war gas in the first world war offering the military advantage to “crawl” in the trenches on the front lines.^[23] Due to the high reactivity and toxicity of chlorine, it is oxidizing most materials and causes severe burns on the skin, eyes, and the respiratory system and, at higher doses, damaging the lungs eventually leading to death. In addition, many chlorinated compounds are toxic for plants, animals, and humans and have been found to be carcinogenic. Besides, many chlorinated compounds are highly persistent organic pollutants and show a high bioaccumulation potential. Therefore, the use of e.g., chlorinated pesticides and the incorrect waste disposal of chlorinated materials have resulted in a contamination of the environment with global dimensions.^[24]

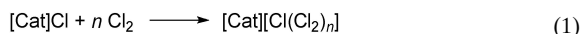
Already the transportation and use of chlorine is of inherent danger not only for the people working with it but also for the environment as it has been witnessed from numerous accidents (one of them was very recently on June 27, 2022 at the Jordan’s red sea port of Aqaba where 25 t of chlorine killed 13 people and injured more than 250

others).^[25] Studies of Hearn and co-workers simulated the rupture of transporting vessels releasing 1814 kg of liquefied chlorine demonstrating a significant chlorine deposition in the area.^[26]

Thus, it is understandable that chlorine has a somewhat bad public reputation. In fact, taming the dangers of gaseous chlorine has been the major motivation for the development of numerous chlorinating reagents such as thionyl chloride (SOCl_2), *N*-chlorosuccinimide (NCS), and trichloroisocyanuric acid (TCCA) that are industrially produced on large scale. What most of these reagents have in common is that they are solids or liquids which can be more easily handled compared to chlorine gas and offer an improved safety profile. However, most of these reagents show a reactivity profile that is in many aspects different from that of elemental chlorine making them only suitable for the replacement of chlorine in some reaction types. More importantly, all chlorination reagents are more expensive than elemental chlorine itself, which is certainly not limiting their exploitation in academic research but is a huge drawback for large industrial processes.^[27]

4. Trichlorides as Alternative to Elemental Chlorine

Among the established chlorination reagents, trichlorides ($[\text{Cl}_3]^-$, also known as trichlorine monoanions) with organic cations are of particular interest. The bonding situation of the symmetric trichloride with Cl–Cl bonds of equal length can be best described as a 3c–4e bond. However, in most compounds the trichloride is asymmetric due to interactions with the cations or crystallographic effects.^[25,26] The asymmetric trichlorides $[\text{Cl}\cdots\text{Cl}\cdots\text{Cl}]^-$ can be described to consist of a dichlorine molecule (Cl_2) and a chloride (Cl^-). The dichlorine having an area of low electron density (so-called σ -hole) along the Cl–Cl bond can act as a Lewis-acid, while the Lewis-basic chloride can donate electron density into this σ -hole forming the trichloride $[\text{Cl}_3]^-$. As the chloride is donating electron-density into the antibonding orbitals of the dichlorine molecule, the Cl–Cl bond in trichlorides is weaker and longer compared to that of elemental chlorine, resulting in a higher reactivity.^[28,29]



Typically, trichlorides are prepared by the reaction of a chloride salt (Cat = cation) with elemental chlorine [Eq. (1)]. Depending on the equivalents of chlorine, various polychlorides can be prepared in this way, reaching from trichlorides ($[\text{Cl}_3]^-$, $n=1$) up to tridecachloride ($[\text{Cl}_{13}]^-$, $n=6$).^[30] Notably, also mixed systems can be prepared having non-integer values of n . As the bond strength of chlorine in polychlorides decreases with the coordination number, polychlorides have a chlorine vapor pressure that increases the larger the value of n is. Therefore, most trichlorides have a relatively low vapor pressure making them the most practical polychlorides being stable for an essentially unlimited time.^[21,28,32]

It has to be outlined that the cation has a strong influence on the properties of a polychloride, particularly on its melting point. For instance, $[\text{NET}_4][\text{Cl}_3]$ is a solid at room temperature, while $[\text{NET}_3\text{Me}][\text{Cl}_3]$ is an ionic liquid having a melting point of $-10\text{ }^\circ\text{C}$ due to the asymmetry of the cation. Thus, the modification of the cation allows to tailor made the properties of a trichloride for its envisioned application. However, it has been observed that cations with longer alkyl chains (e.g., butyl) or electron-rich arenes undergo chlorination limiting the flexibility for the choice of substituents.^[21]

In general, trichlorides are much easier and safer to handle compared to elemental chlorine, as they are liquids or solids and have a relatively low chlorine vapor pressure (e.g., 0.9 bar for $[\text{NET}_3\text{Me}][\text{Cl}_3]$ at $20\text{ }^\circ\text{C}$). In addition, $[\text{NET}_4][\text{Cl}_3]$ and $[\text{NET}_3\text{Me}][\text{Cl}_3]$ can easily be prepared by the reaction of abundant $[\text{NET}_4]\text{Cl}$ or $[\text{NET}_3\text{Me}]\text{Cl}$, respectively, with Cl_2 and are even commercially available.^[21,32]

5. The Reactivity of Trichlorides

Although the first trichloride was already discovered in 1923, it was not until 1996 that the potential of trichlorides as reagents for organic synthesis were explored by Mioskowski and co-workers.^[28,31] Based on this seminal work, various

reactions have been performed using trichlorides with organic cations (Figure 2).

Cl_2	$[\text{NET}_3\text{Me}][\text{Cl}_3]$
- greenish-yellow gas	- yellow ionic liquid at $20\text{ }^\circ\text{C}$
- m.p. $-101\text{ }^\circ\text{C}$, b.p. $-34\text{ }^\circ\text{C}$	- m.p. $-10\text{ }^\circ\text{C}$
- $\rho = 1.38\text{ g/cm}^3$ (7.7 bar, $25\text{ }^\circ\text{C}$)	- $\rho = 1.21\text{ g/cm}^3$ (1 atm, $25\text{ }^\circ\text{C}$)
- $\rho = 6.7\text{ bar}$ ($20\text{ }^\circ\text{C}$)	- $\rho = 0.9\text{ bar}$ ($20\text{ }^\circ\text{C}$)
- toxic	- easier to handle
- very reactive and corrosive	- similar reactivity as Cl_2

Figure 2. Top left: Physical properties of elemental chlorine.^[22,33] Top right: Physical properties of $[\text{NET}_3\text{Me}][\text{Cl}(\text{Cl}_2)_{1.68}]$ simplified as $[\text{NET}_3\text{Me}][\text{Cl}_3]$ for clarity.^[21] Bottom left: Picture of a controlled rupture of a chlorine vessel during the Jack Rabbit Program (Copyright: Utah Valley University).^[34] Bottom right: Picture of transferring $[\text{NET}_3\text{Me}][\text{Cl}_3]$ without gas evolution.

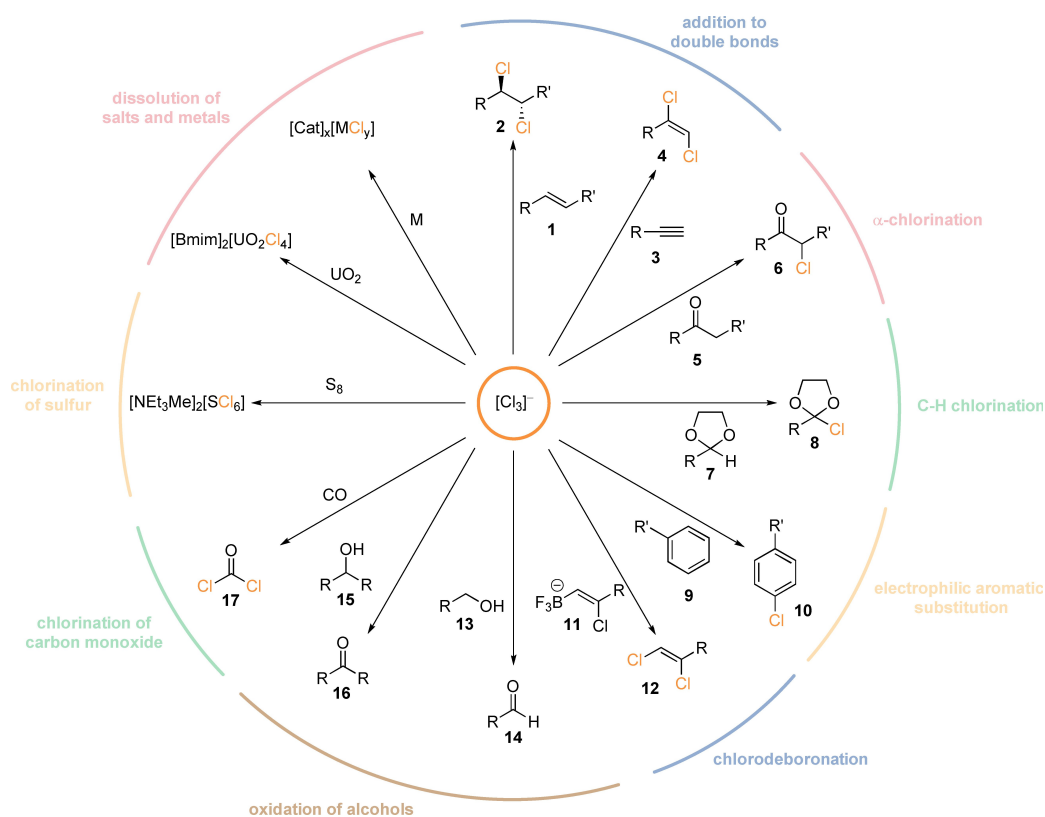


Figure 3. Overview of the reactivity of trichlorides with various substrates. M = metals, R = alkyl or aryl, R' = OR or NR₂, Cat = $[\text{P}(\text{C}_4\text{H}_9)_3(\text{C}_{14}\text{H}_{29})][\text{Cl}_3]$, Bmim = 1-butyl-3-methylimidazolium trichloride.

As elemental chlorine, trichlorides react with alkenes **1** and alkynes **3** in an anti-addition to the corresponding vicinal dichlorinated alkanes **2** or alkenes **4**, respectively. In the case of α,β -unsaturated ketones, α,β -unsaturated α -chloroketones are formed supposedly by dichlorination of the terminal double bond and subsequent elimination.^[31]

Ketones **5** are chlorinated in α -position to α -chloroketones **6**; however, when aldehydes are reacted, the α -dichlorinated products are isolated. Notably, even less activated C–H bonds, e.g., the tertiary C–H bond of acetals **7**, undergo chlorination affording the corresponding chlorinated species **8**.^[31]

Beside these functionalizations of aliphatic compounds, also electron-rich aromatic compounds **9** bearing ether^[31] or amine^[55] functionalities are chlorinated with trichlorides primarily in *para*-position giving chloroarenes **10**. Remarkably, aromatic compounds bearing an alkyne functionality are selectively chlorinated in *para*-position while the alkyne moiety remains untouched.^[31] As discovered by Yan and co-workers, tetrabutylammonium trichloride can also be employed in substitution reactions for the chlorodeboronation of chlorovinyl trifluoroborates **11** to the corresponding (*Z*)-1,2-dichloroalkenes **12**.^[36]

In addition, trichlorides can be used for the oxidation of the primary alcohols **13** and secondary alcohols **15** to the corresponding aldehydes **14** or ketones **16**, respectively. In difference to many commonly used oxidizing reagents,^[38] trichlorides allow the selective oxidation of secondary alcohols in presence of primary alcohols.^[31] However, in the case of allyl alcohols, the chlorination of the double bond is observed.^[31]

Carbon monoxide is oxidized with $[\text{NEt}_3\text{Me}][\text{Cl}_3]$ to the industrially important C1 building block phosgene (**17**), as recently discovered by our group in cooperation with Covestro company. According to quantum-chemical calculations, the phosgene formation proceeds by insertion of carbon monoxide into the weakened Cl–Cl bond of the trichloride anion in an exergonic reaction with a low energy barrier. As this reaction can also be performed with only catalytically amounts of $[\text{NEt}_3\text{Me}]\text{Cl}$ under an chlorine atmosphere, this highlights the function of the ammonium chloride as Lewis base catalyst activating molecular chlorine.^[38]

Very recently, the first synthesis of a hexachlorosulfate ($[\text{SCl}_6]^{2-}$) was achieved by treating elemental sulfur with $[\text{NEt}_3\text{Me}][\text{Cl}_3]$. For comparison, oxidation of elemental sulfur with chlorine gas affords instable SCl_4 which decomposes at temperatures above -30 °C to SCl_2 and Cl_2 . When $[\text{NEt}_3\text{Me}][\text{Cl}_3]$ is used instead, it could be speculated that SCl_4 is formed as intermediate that further reacts with $[\text{NEt}_3\text{Me}]\text{Cl}$ to $[\text{NEt}_3\text{Me}]_2[\text{SCl}_6]$. This highlights the unique ability of $[\text{NEt}_3\text{Me}][\text{Cl}_3]$ to serve as a chlorination agent while stabilizing unprecedented anions.^[39]

Accordingly, trichlorides have been utilized for the dissolution of salts and metals. Chu and co-workers employed 1-butyl-3-methylimidazolium trichloride ($[\text{Bmim}][\text{Cl}_3]$) to dissolve uranium dioxide (UO_2), an important component of nuclear fuels, forming $[\text{Bmim}]_2[\text{UO}_2\text{Cl}_4]$ in the ionic liquid. When mixtures of uranium dioxide and

lanthanide oxides are dissolved in $[\text{Bmim}][\text{Cl}_3]$, selective crystallization of $[\text{Bmim}]_2[\text{UO}_2\text{Cl}_4]$ is observed allowing the separation of uranium from lanthanides.^[40]

In a related study, Binnemans and co-workers investigated the oxidative dissolution of in total twelve metals and two alloys using the ionic liquid $[\text{P}(\text{C}_4\text{H}_9)_3(\text{C}_{14}\text{H}_{29})][\text{Cl}_3]$. While copper and iron powder were dissolved within one hour, platinum or tantalum could not be dissolved at all according to total reflection X-ray fluorescence (TXRF) of the liquids.^[41]

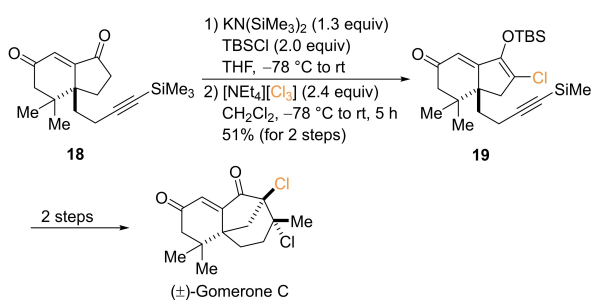
6. The Selectivity of Trichlorides in Organic Synthesis

As reactions with trichlorides are usually conducted in solution at temperatures between -78 °C and room temperature, good selectivities can be achieved while many functional groups are tolerated. For these reasons, trichlorides have found numerous applications for the synthesis of complex molecules in natural product synthesis.^[42]

In the total synthesis of the chlorinated sesquiterpene (\pm)-Gomerone C it was necessary to introduce a chlorine substituent to the relatively complex intermediate **18** (Scheme 1).

By conversion of ketone **18** to the corresponding silyl enol ether and subsequent treatment with $[\text{NEt}_4][\text{Cl}_3]$ the desired α -chlorinated silyl enol ether **19** was obtained in 51 % yield, while many other chlorination reagents failed. Remarkably, the silyl groups, the alkyne, and the olefine moiety were tolerated in this reaction.^[42d]

Very recently, Gooßen and co-workers developed a protocol for a photochemical Sandmeyer-type chlorination of aryl diazonium tetrafluoroborates **20**. However, photo-oxidation of aryl diazonium salts at ≈ 370 nm leads to the formation of diazo radicals that undergo undesired side reactions. Therefore, the reaction had to be initiated with light of lower energy, excluding *N*-chlorosuccinimide absorbing light below 270 nm. In contrast, $[\text{NEt}_4][\text{Cl}_3]$ offers the advantage to absorb visible light beyond 400 nm. Employing blue LED light ($\lambda=447$ nm) and three equiv-



Scheme 1. Synthesis of the chlorinated intermediate **19** in the total synthesis of (\pm)-Gomerone C utilizing $[\text{NEt}_4][\text{Cl}_3]$. TBS = *tert*-butyldimethylsilyl.

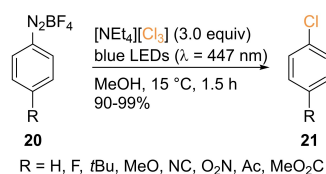
alents of $[\text{NEt}_4][\text{Cl}_3]$, various functionalized aryl diazonium tetrafluoroborates **20** could be converted to the corresponding aryl chlorides **21** in excellent yields and selectivities (Scheme 2).^[43]

7. Trichlorides as a Unique Chlorine Storage

Beside these numerous applications of trichlorides as reagents for both organic and inorganic substrates, Riedel and co-workers investigated in cooperation with Covestro company the utilization of trichlorides as a chlorine storage medium. After determination of the physical properties of various trichlorides, the research was focused on $[\text{NEt}_3\text{Me}][\text{Cl}_3]$. This trichloride is readily prepared by the reaction of $[\text{NEt}_3\text{Me}]\text{Cl}$ and Cl_2 and is an ionic liquid at room temperature which is advantageous for the transport by pumping within an industrial plant. It is stable over years at room temperature and shows also no decomposition when stored in the sunlight at 50 °C.^[21] $[\text{NEt}_3\text{Me}][\text{Cl}_3]$ stores up to 0.79 kg chlorine per kilogram of $[\text{NEt}_3\text{Me}]\text{Cl}$, and is comparably cheap as $[\text{NEt}_3\text{Me}]\text{Cl}$ is industrially prepared from two base chemicals, NEt_3 and MeCl .^[21]

Notably, $[\text{NEt}_3\text{Me}][\text{Cl}_3]$ has a much lower vapor pressure than elemental chlorine at room temperature. Therefore, it can easily be handled, e.g., on air and offers an improved safety profile compared to gaseous chlorine which shows a pressure of 6.7 bar at 20 °C, see Figure 2. More importantly, the use of trichlorides would tame the danger of a rupture of a chlorine vessel containing pressure-liquefied chlorine. Given the safety advantages of trichlorides as chlorine storage, it could allow to transport and store chlorine in much larger quantities as it is currently possible. Therefore, the current limitations and regulations of elemental chlorine transport in highly populated areas like in the Valais, Switzerland, could perhaps be overcome.^[44] By applying heat, the chlorine vapor pressure of the trichloride is increased. In this way, chlorine can easily be released from $[\text{NEt}_3\text{Me}][\text{Cl}_3]$ leading back to the unloaded chlorine storage $[\text{NEt}_3\text{Me}]\text{Cl}$ which can be reused. Another possibility to release chlorine from the storage is to apply vacuum. It was found that also the addition of water allows the complete release of chlorine from $[\text{NEt}_3\text{Me}][\text{Cl}_3]$, offering a valuable alternative to the use of heat or vacuum, when technical possibilities are limited.^[21]

However, the full potential of the ionic liquid $[\text{NEt}_3\text{Me}][\text{Cl}_3]$ would be released when it is used as a chlorine storage and as chlorination reagent in a combined process. As



Scheme 2. Photochemical Sandmeyer-type chlorination of aryl diazonium tetrafluoroborates **20** with $[\text{NEt}_4][\text{Cl}_3]$.

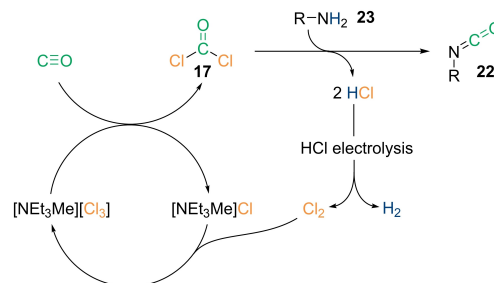
described above, $[\text{NEt}_3\text{Me}][\text{Cl}_3]$ can be used for the production of phosgene (**17**) from carbon monoxide which is industrially further processed to, e.g., isocyanates **22**, by reaction with amines **23**.^[6] In this reaction, HCl is formed that is industrially electrolyzed affording H_2 and Cl_2 .^[18] The obtained Cl_2 could then be used to load the chlorine storage $[\text{NEt}_3\text{Me}]\text{Cl}$ providing $[\text{NEt}_3\text{Me}][\text{Cl}_3]$, again (Scheme 3).

More importantly, this combined process could go hand in hand with renewable energy sources to exploit temporary energy excesses. For example, on sunny days, when solar energy is abundant, it could be used to produce large quantities of chlorine by chloralkali electrolysis which is stored safely and efficiently as $[\text{NEt}_3\text{Me}][\text{Cl}_3]$. In turn, temporary energy shortages could be faced by drawing on reserves of previously produced $[\text{NEt}_3\text{Me}][\text{Cl}_3]$. This would provide a continuous supply of $[\text{NEt}_3\text{Me}][\text{Cl}_3]$ which is independent of weather circumstances.

From an industrial perspective, the realization of this concept would be more attractive, if the stored chlorine in $[\text{NEt}_3\text{Me}][\text{Cl}_3]$ is further processed to important chemicals. In this way, for instance, the base chemical phosgene (**17**) can be produced as it has been shown by our group in cooperation with Covestro company.^[38] However, many more industrial processes that currently rely on elemental chlorine could possibly be performed with $[\text{NEt}_3\text{Me}][\text{Cl}_3]$ in the future opening up new avenues in chlorine industry.

8. Conclusion

In conclusion, chlorinated materials have a fundamental importance in many areas of both industry and academic research. Generally, for chlorinating agents, there is a delicate balance between a) the utility, b) the safety and transportation, and c) the cost of a chlorination agent. Improving one of these aspects usually goes hand in hand with disadvantages regarding the other aspects. In contrast, trichlorides such as $[\text{NEt}_3\text{Me}][\text{Cl}_3]$ show a) a similar reactivity as elemental chlorine, b) are easy-to-handle, and c) are relatively inexpensive to prepare. In many transformations, trichlorides react as elemental chlorine, but sometimes they show an enhanced reactivity as in the synthesis of phosgene



Scheme 3. Envisioned process combining the use of $[\text{NEt}_3\text{Me}]\text{Cl}$ as chlorine storage and $[\text{NEt}_3\text{Me}][\text{Cl}_3]$ as chlorination reagent for the production of phosgene (**17**) which is further used for the synthesis of isocyanates **22**.

(17), offer an improved selectivity in natural product synthesis, or enable the preparation of unprecedented molecules such as $[\text{NEt}_3\text{Me}]_2[\text{SCl}_6]$ (Figure 3). Compared to chlorine gas, $[\text{NEt}_3\text{Me}][\text{Cl}_3]$ is an ionic liquid at room temperature with a chlorine vapor pressure below 1 bar making it safe to handle and to transport. In addition, $[\text{NEt}_3\text{Me}][\text{Cl}_3]$ can be easily prepared from abundant materials (NEt_3 , MeCl , and Cl_2).

More importantly, $[\text{NEt}_3\text{Me}][\text{Cl}_3]$ is a safe chlorine storage at ambient pressure and temperature. As the storage of large quantities of chlorine by pressure-liquefaction is potentially dangerous it is only performed when it is unavoidable. Therefore, the use of $[\text{NEt}_3\text{Me}][\text{Cl}_3]$ as a safer storage technique could help to overcome this limitation and enable the exploitation of renewable, yet fluctuating, energy sources to allow the production of chlorine. Finally, the loaded chlorine-storage could directly be employed as a versatile chlorination reagent. In this context, $[\text{NEt}_3\text{Me}][\text{Cl}_3]$ could make a contribution along with other technologies such as the oxygen consumption electrode or the flexibilization of downstream processes to reach a modern chlorine technology that is more adoptable to renewable energies.

Acknowledgements

We want to thank Dr. Anja Wiesner, Stefan Leisering, Gene Senges (FU Berlin), Dr. Rainer Weber, Dr. Yuliya Schiesser, Dr. Maxime Paven, Dr. Sivathmehhan Yogendra (Covestro AG), as well as Dr. Franziska Klauke (TU Berlin) for helpful discussions. Open Access funding enabled and organized by Projekt DEAL.

Conflict of Interest

The authors declare the following competing financial interests: S.R. is inventor on two pending patents related to this work filed by Covestro Intellectual Property GmbH & Co. KG (no. WO 2019215037 A1, filed 2018 and no. WO2021069757 A1, filed 2021). P.V. and S.R. are inventors on two pending patents related to this work filed by Covestro Deutschland AG (no. EP20213933.3, filed 2020 and no. EP20213938, filed 2020). The authors declare that they have no other competing interests.

Keywords: Chlorine · Industrial Chemistry · Ionic Liquids · Polychlorides · Synthetic Methods

- [1] R. Lin, A. P. Amrute, J. Pérez-Ramírez, *Chem. Rev.* **2017**, *117*, 4182–4247.
- [2] P. Schmittinger, T. Florkiewicz, L. C. Curlin, B. Lüke, R. Scannell, T. Navin, E. Zelfel, R. Bartsch, Chlorine in *Ullmann's Encyclopedia of Industrial Chemistry*, Wiley-VCH, Weinheim, **2012**.
- [3] <https://www.eurochlor.org/wp-content/uploads/2021/04/02-The-Chlorine-Tree-Infosheet.pdf> (26.06.2022).
- [4] P. Schmittinger, *Chlorine*, Wiley-VCH, Weinheim, **2000**, p. 160.
- [5] P. Schmittinger, *Chlorine*, Wiley-VCH, Weinheim, **2000**, p. 169.
- [6] L. Cotarca, C. Lange, K. Meurer, J. Pauluhn, Phosgene in *Ullmann's Encyclopedia of Industrial Chemistry*, Wiley-VCH, Weinheim, **2019**.
- [7] <https://mcgroup.co.uk/news/20141121/north-america-ranks-worldwide-ethylene-dichloride-edc-market.html> (26.06.2022).
- [8] <https://www.researchnester.com/reports/ethylene-dichloride-market/1002> (26.06.2022).
- [9] H. A. Wittcoff, B. G. Reuben, J. S. Plotkin, *Industrial Organic Chemicals*, Wiley-VCH, Weinheim, **2013**, p. 565.
- [10] a) G. Koenig, E. Lohmar, N. Rupprich, M. Lison, A. Gnass, Chloroacetic Acids in *Ullmann's Encyclopedia of Industrial Chemistry*, Wiley-VCH, Weinheim, **2014**; b) P. Schmittinger, *Chlorine*, Wiley-VCH, Weinheim, **2000**, p. 197.
- [11] a) P. Schmittinger, *Chlorine*, Wiley-VCH, Weinheim, **2000**, pp. 199–200; b) H. A. Wittcoff, B. G. Reuben, J. S. Plotkin, *Industrial Organic Chemicals*, Wiley-VCH, Weinheim, **2013**, pp. 263–264; c) L. Krähling, J. Krey, G. Jakobson, J. Grolig, L. Miksche, Allyl Compounds in *Ullmann's Encyclopedia of Industrial Chemistry*, Wiley-VCH, Weinheim, **2012**.
- [12] a) P. Schmittinger, *Chlorine*, Wiley-VCH, Weinheim, **2000**, p. 166; b) J.-L. Montchamp, *Phosphorus Sulfur Silicon Relat. Elem.* **2013**, *188*, 66–75.
- [13] a) R. H. West, G. J. O. Beran, W. H. Green, M. Kraft, *J. Phys. Chem. A* **2007**, *111*, 3560–3565; b) P. Schmittinger, *Chlorine*, Wiley-VCH, Weinheim, **2000**, pp. 174–175.
- [14] <https://www.offshore-technology.com/comment/chlorine-growth-2024/> (27.09.2022).
- [15] N. Wagner, Energiespeichersymposium **2017**, Stuttgart, <https://elib.dlr.de/116102/1/Chlor-Alkali-Elektrolyse%20Wagner%20Vortrag%20freigegeben.pdf> (29.09.2022).
- [16] <https://www.statista.com/statistics/1186170/production-capacity-chlorine-europe-by-country/> (27.09.2022).
- [17] <https://www.destatis.de/DE/Themen/Branchen-Unternehmen/Energie/Erzeugung/inhalt.html> (29.09.2022).
- [18] J. Pérez-Ramírez, C. Mondelli, T. Schmidt, O. F.-K. Schlüter, A. Wolf, L. Mleczko, T. Dreier, *Energy Environ. Sci.* **2011**, *4*, 4786–4799.
- [19] <https://www.umweltbundesamt.de/themen/klima-energie/erneuerbare-energien/erneuerbare-energien-in-zahlen#uberblick> (30.06.2022).
- [20] a) F. Klauke, C. Hoffmann, M. Hoffmann, G. Tsatsaronis, *Appl. Energy* **2020**, *276*, 115366; b) H. G. Gils, *Energy* **2014**, *67*, 1–18; c) M. Hofmann, R. Müller, A. Christidis, P. Fischer, F. Klauke, S. Vomberg, G. Tsatsaronis, *AIChE J.* **2022**, *68*, e17480; d) *Flexibilitäts Optionen in der Grundstoffindustrie. Report commissioned by Federal Ministry of Education and Research*, 1st ed. (Eds.: F. Ausfelder, A. Seitz, S. von Roon), Frankfurt am Main, **2019**; e) See also the Kopernikus Project “SynErgie” focusing on possibilities for the flexibilization of industrial processes. <https://www.kopernikus-projekte.de/projekte/synergie> (01.07.2022).
- [21] a) P. Voßnacker, N. Schwarze, T. Keilhack, M. Kleoff, S. Steinhauer, Y. Schiesser, M. Paven, S. Yogendra, R. Weber, S. Riedel, *ACS Sustainable Chem. Eng.* **2022**, *10*, 9525–9531; b) M. Paven, Y. Schiesser, R. Weber, G. Langstein, V. Trieu, S. Riedel, N. Schwarze, S. Steinhauer, Patent WO 2019215037 A1, **2018**.
- [22] P. Schmittinger, *Chlorine*, Wiley-VCH, Weinheim, **2000**, p. 3.
- [23] H. R. Slotten, *J. Am. Hist.* **1990**, *77*, 476–498.
- [24] a) A. P. Annachhatre, S. H. Gheewala, *Biotechnol. Adv.* **1996**, *14*, 35–56; b) C. M. Villanueva, K. P. Cantor, J. O. Grimalt, N. Malats, D. Silverman, A. Tardon, R. Garcia-Closas, C. Serra, A. Carrato, G. Castaño-Vinyals, R. Marcos, N. Rothman, F. X. Real, M. Dosemeci, M. Kogevinas, *Am. J. Epidemiol.* **2007**, *165*, 148–156; c) K. Kobetičová, R. Černý, *Sci. Total Environ.* **2018**, *640–641*, 523–528; d) V. Nevondo, O. J. Okonkwo, *Environ. Sci. Pollut. Res. Int.* **2021**, *28*, 52844–52861; e) J.

- Vijgen, B. de Brost, R. Weber, T. Stobiecki, M. Forter, *Environ. Pollut.* **2019**, *248*, 696–705; f) J. Glüge, Z. Wang, C. Bogdal, M. Scheringer, K. Hungerbühler, *Sci. Total Environ.* **2016**, *573*, 1132–1146.
- [25] a) <https://www.scientificamerican.com/article/chlorine-accidents-take-big-human-toll/> (26.06.2022); b) <https://taz.de/Chlorgas-Unglueck-in-Jordanien/15863701/> (07.11.2022).
- [26] J. D. Hearn, R. Weber, R. Nichols, M. V. Henley, S. Fox, *J. Hazard. Mater.* **2013**, *252–253*, 107–114.
- [27] a) Z. Lu, Q. Li, M. Tang, P. Jiang, H. Zheng, X. Yang, *Chem. Commun.* **2015**, *51*, 14852–14855; b) C. Jimeno, L. Cao, P. Renaud, *J. Org. Chem.* **2016**, *81*, 1251–1255; c) R. A. Rodriguez, C.-M. Pan, Y. Yabe, Y. Kawamata, M. D. Eastgate, P. S. Baran, *J. Am. Chem. Soc.* **2014**, *136*, 6908–6911; d) M. Wang, Y. Zhang, T. Wang, C. Wang, D. Xue, J. Xiao, *Org. Lett.* **2016**, *18*, 1976–1979; e) G. F. Mendonça, M. C. S. de Mattos, *Curr. Org. Synth.* **2013**, *10*, 820–836; f) S. Gaspa, M. Carraro, L. Pisano, A. Porcheddu, L. De Luca, *Eur. J. Org. Chem.* **2019**, 3544–3552; g) L. Mohammadkhani, M. M. Heravi, *Chemistry-Select* **2019**, *4*, 6309–6337; h) S. Ponath, M. Menger, L. Grothues, M. Weber, D. Lentz, C. Strohmman, M. Christmann, *Angew. Chem. Int. Ed.* **2018**, *57*, 11683–11687; *Angew. Chem.* **2018**, *130*, 11857–11861.
- [28] K. Sonnenberg, L. Mann, F. A. Redeker, B. Schmidt, S. Riedel, *Angew. Chem. Int. Ed.* **2020**, *59*, 5464–5493; *Angew. Chem.* **2020**, *132*, 5506–5535.
- [29] H. Keil, K. Sonnenberg, C. Müller, R. Herbst-Irmer, H. Beckers, S. Riedel, D. Stalke, *Angew. Chem. Int. Ed.* **2021**, *60*, 2569–2573; *Angew. Chem.* **2021**, *133*, 2600–2604.
- [30] K. Sonnenberg, P. Pröhm, N. Schwarze, C. Müller, H. Beckers, S. Riedel, *Angew. Chem. Int. Ed.* **2018**, *57*, 9136–9140; *Angew. Chem.* **2018**, *130*, 9274–9278.
- [31] T. Schlama, K. Gabriel, V. Gouverneur, C. Mioskowski, *Angew. Chem. Int. Ed. Engl.* **1997**, *36*, 2342–2344; *Angew. Chem.* **1997**, *109*, 2440–2442.
- [32] Both compounds are available from abcr ([NET₃][Cl₃] article ID: AB568860; [NET₃Me][Cl₃] article ID: AB568861).
- [33] D. R. Stull, *Ind. Eng. Chem.* **1947**, *39*, 517–540.
- [34] The picture was taken during the Jack Rabbit II project in 2016. <https://www.uvu.edu/es/jack-rabbit/> (30.06.2022). Copyright: Utah Valley University.
- [35] X. Xiong, Y. Y. Yeung, *Angew. Chem. Int. Ed.* **2016**, *55*, 16101–16105; *Angew. Chem.* **2016**, *128*, 16335–16339.
- [36] N. Thou, Q. Wang, A. J. Lough, H. Yan, *Can. J. Chem.* **2012**, *90*, 625–630.
- [37] J. B. Arterburn, *Tetrahedron* **2001**, *57*, 9765–9788.
- [38] a) P. Voßnacker, A. Wüst, T. Keilhack, C. Müller, S. Steinhauer, H. Beckers, S. Yogendra, Y. Schiesser, R. Weber, M. Reimann, R. Müller, M. Kaupp, S. Riedel, *Sci. Adv.* **2021**, *7*, eabj5186; b) M. Paven, Y. Schiesser, R. Weber, E. Bramer-Weger, S. Yogendra, S. Riedel, S. Steinhauer, T. Keilhack, Patent WO 2021069757 A1, **2021**; c) S. Yogendra, S. Riedel, P. Voßnacker, R. Weber, Y. Schiesser, T. Keilhack, S. Steinhauer, Patent EP20213933.3, **2020**; d) S. Yogendra, S. Riedel, P. Voßnacker, R. Weber, Y. Schiesser, T. Keilhack, S. Steinhauer, Patent EP20213938, **2020**.
- [39] P. Voßnacker, A. Wüst, C. Müller, M. Kleoff, S. Riedel, *Angew. Chem. Int. Ed.* **2022**, *61*, e202209684; *Angew. Chem.* **2022**, *134*, e202209684.
- [40] A. Yao, F. Qu, Y. Liu, G. Qu, H. Lin, S. Hu, X. Wang, T. Chu, *Dalton Trans.* **2019**, *48*, 16249–16257.
- [41] X. Li, A. van den Bossche, T. Vander Hoogerstraete, K. Binne-mans, *Chem. Commun.* **2018**, *54*, 475–478.
- [42] a) Z. A. Könst, A. R. Szklarski, S. Pellegrino, S. E. Michalak, M. Meyer, C. Zanetta, R. Cencic, S. Nam, V. K. Voora, D. A. Horne, J. Pelletier, D. L. Mobley, G. Yusupova, C. D. Vanderwal, *Nat. Chem.* **2017**, *9*, 1140–1149; b) Y. Dai, F. Ma, Y. Shen, T. Xie, S. Gao, *Org. Lett.* **2018**, *20*, 2872–2875; c) C. Nilewski, N. R. Deprez, T. C. Fessard, D. B. Li, R. W. Geisser, E. M. Carreira, *Angew. Chem. Int. Ed.* **2011**, *50*, 7940–7943; *Angew. Chem.* **2011**, *123*, 8087–8091; d) N. Huwyler, E. M. Carreira, *Angew. Chem. Int. Ed.* **2012**, *60*, 13066–13069; *Angew. Chem.* **2012**, *124*, 13243–13246; e) W. J. Chung, J. S. Carlson, D. K. Bedke, C. D. Vanderwal, *Angew. Chem. Int. Ed.* **2013**, *52*, 10052–10055; *Angew. Chem.* **2013**, *125*, 10236–10239; f) C. V. Vogel, H. Pietraszkiewicz, O. M. Sabry, W. H. Gerwick, F. A. Valeriote, C. D. Vanderwal, *Angew. Chem. Int. Ed.* **2014**, *53*, 12205–12209; *Angew. Chem.* **2014**, *126*, 12401–12405; g) W. Ju, X. Wang, H. Tian, J. Gui, *J. Am. Chem. Soc.* **2021**, *143*, 13016–13021; h) D. K. Bedke, G. M. Shibuya, A. Pereira, W. H. Gerwick, T. H. Haines, C. D. Vanderwal, *J. Am. Chem. Soc.* **2009**, *131*, 7570–7572; i) D. K. Bedke, G. M. Shibuya, A. R. Pereira, W. H. Gerwick, C. D. Vanderwal, *J. Am. Chem. Soc.* **2010**, *132*, 2542–2543; j) J. S. Kanady, J. D. Nguyen, J. W. Ziller, C. D. Vanderwal, *J. Org. Chem.* **2009**, *74*, 2175–2178; k) W. J. Chung, J. S. Carlson, C. D. Vanderwal, *J. Org. Chem.* **2014**, *79*, 2226–2241; l) C. Nilewski, R. W. Geisser, E. M. Carreira, *Nature* **2009**, *457*, 573–576.
- [43] N. Sivendran, F. Belitz, D. S. Prendes, Á. M. Martínez, R. Schmid, L. J. Gooßen, *Chem. Eur. J.* **2022**, *28*, e202103669.
- [44] a) <https://www.srf.ch/news/schweiz/rollende-zeitbomben-chlor-transporte-mit-der-bahn> (07.11.2022); b) <https://www.1815.ch/news/newsletter/wb/chlortransporte/> (07.11.2022).

Manuscript received: November 10, 2022

Accepted manuscript online: January 9, 2023

Version of record online: February 16, 2023

4. Conclusion and Outlook

4.1 Conclusion

In the first part of this work, hydrogen halides and chlorine were used to synthesize novel poly(hydrogen halide) halogenates ($-I$) and polychlorides. A series of salts of the type $[\text{Cat}][\text{X}(\text{HCl})_n]$ ($\text{Cat} = [\text{PPh}_4]^+$, $[\text{PNP}]^+$, $\text{X} = \text{Cl}, \text{Br}, \text{I}$, $n = 3$ or 4 , Figure 18 left) were synthesized by treating $[\text{Cat}]\text{X}$ with HCl . By combining single-crystal X-ray diffraction, Raman spectroscopy and quantum-chemical calculations, some trends about the hydrogen bond strength within these molecules were concluded. When a series of poly(hydrogen chloride) halogenates with the same coordination number ($[\text{X}(\text{HCl})_4]^-$) is considered, the hydrogen bond energy was shown to decrease from $\text{X} = \text{I}$ to Cl which is consistent with the basicity of the halide ions. On the other hand, the hydrogen bond energy significantly increases with a decreasing coordination number. This was rationalized by the reduced charge on the central halide ion with increasing coordination number allowing less charge transfer to the next added hydrogen halide resulting in weaker hydrogen bonds.

Additionally, the behavior of halide ions in anhydrous HF (aHF) was studied. Interestingly, when $[\text{PPh}_4]\text{X}$ was treated with HF and cooled to $-80\text{ }^\circ\text{C}$, single crystals of $[\text{PPh}_4][\text{X}(\text{HF})_2(\text{HX})]$ ($\text{X} = \text{Br}, \text{I}$) were obtained. The presence of both X^- and HX in the solid state structure indicates that both species must be present in solution to some extent. This is surprising as HF is a significantly weaker acid than the other hydrogen halides in the gas phase and therefore should not be able to protonate halide ions. Nevertheless, the acidity of a compound is heavily influenced by the stabilization of the formed anion. In aHF the fluoride anion, which is formed during the protonation reaction, is strongly stabilized by hydrogen bonding interactions to the solvent, making aHF a strong acid. Quantum-chemical calculations taking solvation into account, consequently showed that all hydrogen halides have very similar acidities in aHF which explains the presence of X^- and HX in solution.

Furthermore, in this work the $[\text{Cl}(\text{Cl}_2)_4]^-$ anion (Figure 18 right) could be obtained for the first time by the reaction of $[\text{NPr}_4]\text{Cl}$ with chlorine in acetonitrile. It has a distorted tetrahedral structure with short $\text{Cl}-\text{Cl}$ contacts to the next $[\text{Cl}(\text{Cl}_2)_4]^-$ yielding a three-dimensional network. Additionally, the reaction of dexamethylferrocene (Cp^*Fe) with a large excess of chlorine yielded in the formation of $[\text{Cp}^*\text{Fe}]_2[\text{Cl}_{20}]$. The $[\text{Cl}_{20}]^{2-}$ dianion can be described as two

pyramidal $[\text{Cl}(\text{Cl}_2)_4]^-$ units which are connected by a Cl_2 molecule and is the largest known polychloride to date. Interestingly, when small amounts of HF are present in the reaction mixture of Cp^*Fe and chlorine, $[\text{Cp}^*\text{Fe}][\text{Cl}(\text{Cl}_2)_4(\text{HF})]$ is obtained stabilized by strong hydrogen and halogen bonding interactions (Figure 18 middle). Due to the large polarization of the HF bond, the fluorine atom has a partial negative charge and can act as a good halogen bond acceptor. This results in the formation of a three-dimensional network in the solid state of $[\text{Cp}^*\text{Fe}][\text{Cl}(\text{Cl}_2)_4(\text{HF})]$. Both, the chloride ion and the fluorine atom of the HF molecules have five binding partners which results in a hexagonal prismatic arrangement of the anions with the cations in the center of the prism.

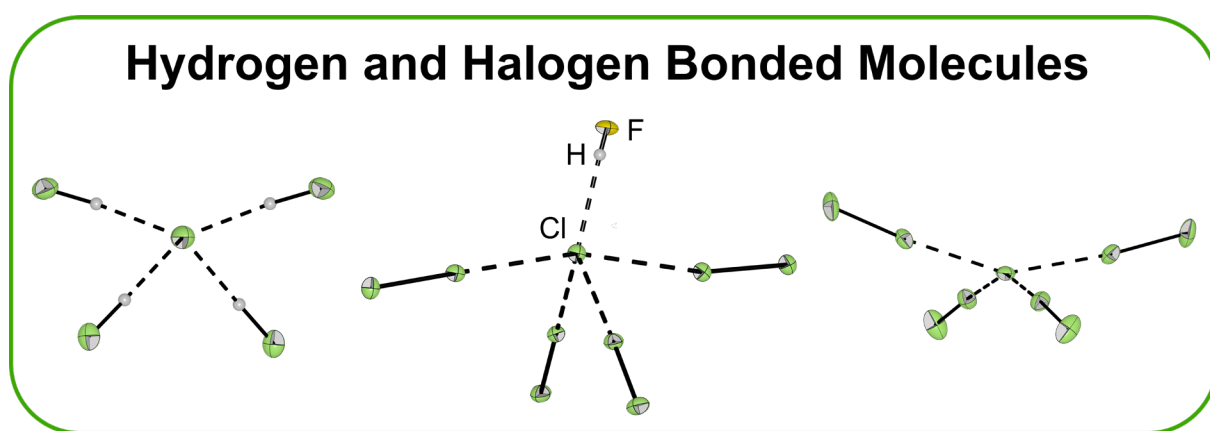


Figure 18. Molecular structure in the solid state of $[\text{PNP}][\text{Cl}(\text{HCl})_4]$ (left), $[\text{Cp}^*\text{Fe}][\text{Cl}(\text{Cl}_2)_4(\text{HF})]$ (middle) and $[\text{NPr}_4][\text{Cl}(\text{Cl}_2)_4]$ (right).

In the second part of this work, polychlorides were tested towards their capability to act as an efficient chlorine storage media. When chloride salts with organic cations are treated with chlorine gas, relatively high amount of chlorine ($0.5\text{--}0.7 \text{ kg L}^{-1}$, compared to 1.38 kg L^{-1} for liquid chlorine) are absorbed and either liquid or solid polychlorides salts are formed. Therefore, polychlorides are significantly easier to handle and safer to store in contrast to gaseous elemental chlorine (Figure 19). Several ammonium chloride salts have been tested as storage materials and $[\text{NEt}_3\text{Me}]\text{Cl}$ was chosen to be the most promising one based on several characteristics. It has a high storage capacity of $0.79 \text{ kg chlorine per kg storage material}$ and can readily be prepared from the abundant starting materials NEt_3 and MeCl . Moreover, the loaded storage $[\text{NEt}_3\text{Me}][\text{Cl}(\text{Cl}_2)_n]$ is a liquid at room temperature, which is advantages for industrial processing, and is stable for extended times. A release of chlorine from the polychlorides can be realized by using some physical methods, e.g., by heating the storage or by applying vacuum. Furthermore, the addition of water also yields in a release of chlorine since the solvation energy of Cl^- is higher compared to the $[\text{Cl}_3]^-$ anion. The formation of strong

hydrogen bonds between the chloride ions and water compensates the breaking of the halogen bond within the $[\text{Cl}_3]^-$ which results in the release of chlorine. To evaluate the upscaling possibility of the chlorine storage process, calorimetric measurements were performed to determine the energy released when loading the storage medium and required to liberate chlorine again. While fully loading the system with 1.7 equivalents of chlorine is 54.4 kJ mol^{-1} exothermic, the release of 0.5 equivalents from the fully loaded system, achievable by heating to $80 \text{ }^\circ\text{C}$, requires only 16.4 kJ mol^{-1} . This is in agreement with quantum-chemical calculations which shows that the formation of the $[\text{Cl}_3]^-$ creates the strongest halogen bond while the addition of more chlorine molecules is less favorable.

Safe and Efficient Chlorine Storage


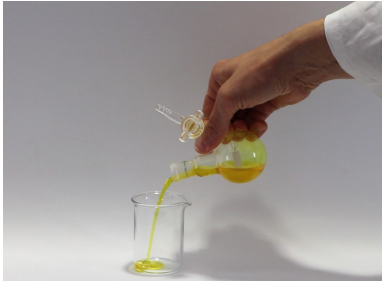
Cl_2	$[\text{NEt}_3\text{Me}][\text{Cl}_3]$
<ul style="list-style-type: none"> - greenish-yellow gas - m.p. $-101 \text{ }^\circ\text{C}$, b.p. $-34 \text{ }^\circ\text{C}$ - $\rho = 1.38 \text{ g/cm}^3$ (7.7 bar, $25 \text{ }^\circ\text{C}$) - $p = 6.7 \text{ bar}$ ($20 \text{ }^\circ\text{C}$) - toxic - very reactive and corrosive 	<ul style="list-style-type: none"> - yellow ionic liquid at $20 \text{ }^\circ\text{C}$ - m.p. $-10 \text{ }^\circ\text{C}$ - $\rho = 1.21 \text{ g/cm}^3$ (1 atm, $25 \text{ }^\circ\text{C}$) - $p = 0.9 \text{ bar}$ ($20 \text{ }^\circ\text{C}$) - easier to handle - similar reactivity as Cl_2
	

Figure 19. Comparison of elemental chlorine and the chlorine storage material $[\text{NEt}_3\text{Me}][\text{Cl}_3]$. Reproduced from Ref. [214] with permission from Wiley-VCH Verlag GmbH & Co. KGaA.

As illustrate in the previous section, releasing chlorine from the storage medium $[\text{NEt}_3\text{Me}][\text{Cl}(\text{Cl}_2)_n]$ requires significant amounts of energy. To further improve the efficiency of the storage system, it is desirable to use the loaded storage directly as a chlorination reagent which is a valid option as $[\text{Cl}_3]^-$ has already been used in several organic transformations (see chapter 1.2.5). To further develop this approach, in the third part of this work the reactivity of the $[\text{Cl}_3]^-$ was investigated. It was shown that phosgene, which is a major intermediate chemical, can directly be prepared by the reaction of $[\text{NEt}_3\text{Me}][\text{Cl}_3]$ with CO at room temperature without further activation. Additionally, also catalytic amounts of $[\text{NEt}_3\text{Me}]\text{Cl}$ results in the full conversion of CO and Cl_2 to COCl_2 . To rationalize this, quantum-chemical

calculations on the reaction pathway were performed which indicates that the reaction can be described as an insertion of the CO molecule into the Cl-Cl bond (Figure 20 left). In comparison to elemental chlorine, the Cl-Cl bond within the $[\text{Cl}_3]^-$ is significantly weakened due its 3c-4e bonding character. This results in a drastically reduced energy barrier of 57 to 78 kJ mol^{-1} for the insertion of CO into the Cl-Cl bond compared to 230 kJ mol^{-1} for the uncatalyzed reaction between chlorine and carbon monoxide.

Besides its use for the production of industrial important chlorinated chemicals, $[\text{Cl}_3]^-$ was also used for the synthesis of unprecedented molecules. Reacting $[\text{NEt}_3\text{Me}][\text{Cl}_3]$ with elemental sulfur yields in the formation of $[\text{NEt}_3\text{Me}]_2[\text{SCl}_6]$ (Figure 20, right) which is the first example of a compound containing the $[\text{SCl}_6]^{2-}$ dianion. The $[\text{SCl}_6]^{2-}$ dianion belongs to the group of 14-valence electron AB_6E systems which can either have an octahedral or distorted octahedral structure depending on the lone-pair being stereochemically active or not. Within $[\text{NEt}_3\text{Me}]_2[\text{SCl}_6]$, the $[\text{SCl}_6]^{2-}$ dianion has an octahedral structure while NBO calculations confirmed that the lone-pair of the molecule is located in the s-orbital of the sulfur atom and is therefore stereochemically inactive. Interestingly, when a diluted solution of sulfur and $[\text{NEt}_3\text{Me}][\text{Cl}_3]$ in CH_2Cl_2 was cooled to $-80\text{ }^\circ\text{C}$, co-crystallization of CH_2Cl_2 was observed resulting in the formation of $[\text{NEt}_3\text{Me}]_2[\text{SCl}_6]\cdot 4\text{CH}_2\text{Cl}_2$. In this salt, the $[\text{SCl}_6]^{2-}$ has a C_{4v} symmetric structure with one shorter and one longer S-Cl bond. Further quantum-chemical studies showed that this distortion is not a result of a stereochemically active lone pair but a result of a strong hydrogen bonding interaction to the co-crystallized solvent molecules. In comparison to the neutral SCl_4 , which decomposes into SCl_2 and chlorine already at $-30\text{ }^\circ\text{C}$, $[\text{NEt}_3\text{Me}]_2[\text{SCl}_6]$ is surprisingly stable. Raman spectroscopic investigations show its decomposition into $[\text{NEt}_3\text{Me}][\text{Cl}_3]$ and various sulfur chlorides only at temperatures above $40\text{ }^\circ\text{C}$.

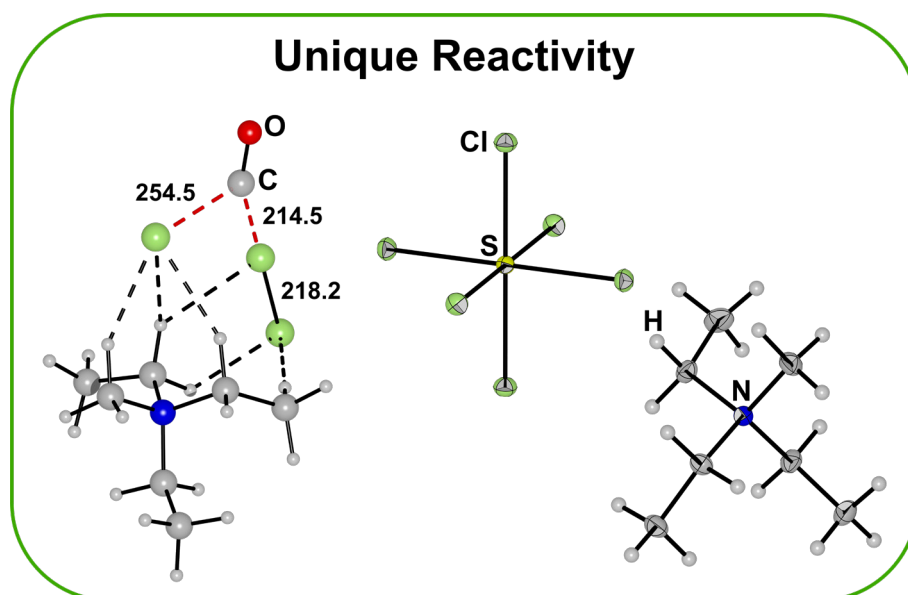


Figure 20. Transition state for the reaction of [NEt₃Me][Cl₃] with CO (left) and molecular structure in the solid state of [NEt₃Me]₂[SCl₆] (right). Bond length are given in pm.

Overall, this work highlights the importance of intermolecular interactions like hydrogen and halogen bonding for the stabilization of unprecedented molecules (see chapter 3.1 and 3.2), for useful applications, e.g., storage of chlorine (see chapter 3.3 and 3.6) and as a tool to tune the reactivity of molecules (see chapter 3.4, 3.5 and 3.6). The strength of this interaction within the presented compounds covers a wide energy range. Poly(hydrogen halides) halogenates [X(HX)_n]⁻ and polyhalides [X(X₂)_n]⁻ (*n* = 1-2) are examples for systems stabilized by very strong hydrogen or halogen bonds with bonding energies up to 180 kJ mol⁻¹.^[215] The strong halogen bonds stabilizing the [NEt₃Me][Cl(Cl₂)_{1.7}] system were shown to be in an optimal energy regime to allow its use as an efficient chlorine storage medium. While lower binding energies would lead to significantly lower storage capacities, for a more strongly bounded system a release of chlorine could only be achieved under much harsher conditions and would require more energy. Additionally, the reactivity of [NEt₃Me][Cl(Cl₂)_{1.7}] is often very similar or even enhanced in comparison to elemental chlorine. This enhanced reactivity is rationalized by a charge transfer from the chloride into the σ* orbital of the Cl₂ molecule during halogen bonding resulting in a weakened Cl-Cl bond and an increased reactivity as demonstrated for the reaction of [Cl₃]⁻ with CO. Overall this makes [NEt₃Me][Cl(Cl₂)_{1.7}] a suitable replacement for elemental chlorine, in contrast to many other chlorination reagents, e.g., SOCl₂, NCS or POCl₃, which contain covalent element chlorine bonds resulting in a significantly different reactivity profile.

The bonding energy in larger poly(hydrogen halides) halogenates $[X(HX)_n]^-$ and polyhalides $[X(X_2)_n]^-$ ($n > 2$) is significantly lower and the elimination of HX or X_2 is often endergonic by only 10 kJ mol^{-1} . Therefore, in the solid state, larger polyhalides are often stabilized by additional intermolecular halogen bonding. This is possible since dihalogens have an anisotropic electron density with an area of low electron density on the bonding axis, the so-called σ -hole, and a belt of higher electron density perpendicular to the bond axis (see chapter 1.2.1). The different sides of the dihalogen molecule can act as a Lewis acid or a Lewis base, respectively, which allows the formation of three-dimensional networks in the solid state as observed for $[Cl(Cl_2)_4]^-$ and $[Cl_{20}]^{2-}$. In contrast, hydrogen halides have a strongly polarized bond with a positive, Lewis acidic hydrogen atom and a negative, Lewis basic halogen atom. Thus, the $[X(HX)_n]^-$ anion often exists as isolated ions in the solid state. The use of weakly coordinating cations is essential to stabilize large poly(hydrogen halide) halogenates ($-I$) in the solid state since strong interactions to the cation results in a reduced basicity of the central halide yielding in weaker hydrogen bonds and therefore a destabilization of larger poly(hydrogen halide) halogenates.

4.2 Outlook

Chlorine is one of the most important industrial chemicals and our daily life is hardly possible without it. Nevertheless, a constant evaluation of the chlorine industry is necessary as chlorine and its products are potentially hazardous. Many problems of the chlorine industry could already be at least partially solved. However, there are still two major problems related to chlorine industry, namely the storage and transportation of chlorine as well as its energy intensive production. In this work, the foundation for solving these problems was established by fundamental research on the polychloride system. The next step should be the evaluation of polychloride-based storage systems for industrial processes.

The following scheme can be proposed for a more sustainable chlorine technology based on the analyzed use of polychlorides as a chlorine storage (Figure 21): Chlorine is produced by electrolysis and is then safely stored within a polychloride salt enabling a flexible production of chlorine when renewable energies are available. In a first step, chlorine can be released from the storage by heating it to 80 °C. Even though the release of chlorine requires energy, this is not problematic as many downstream processes of the chlorine industry are exothermic and therefore generate heat which can be used to release chlorine from the storage. Additionally, when the polychloride is used as a classical storage medium and gaseous chlorine is released, the storage can be easily integrated into existing infrastructure without changing the setup for downstream processes. In a second step, the process can be even more improved if the chlorine release is achieved by using the loaded storage as a chlorination reagent, for example, for the production of phosgene. Many processes involving chlorine generate hydrogen chloride as a byproduct. For instance, if phosgene is reacted with amines to generate isocyanides, two equivalents of HCl are generated. As illustrated in the first part of this work, HCl also has a high affinity to chloride ions and can be bound by them forming a poly(hydrogen chloride) chlorate (-I) which is also a low viscous ionic liquid. This ionic liquid can directly be electrolyzed to regenerate $[\text{Cl}_3]^-$. Overall, this scheme allows for the use of larger amounts of renewable energy for the generation of chlorine. Additionally, it would allow a chlorine technology without the need of neither gaseous chlorine or hydrogen chloride. Both are efficiently stored by the ammonium chloride salt significantly increasing the safety profile of the process. The icing on the cake would be the generation of hydrogen, a valuable resource for a sustainable energy system, through the use of renewable energies.

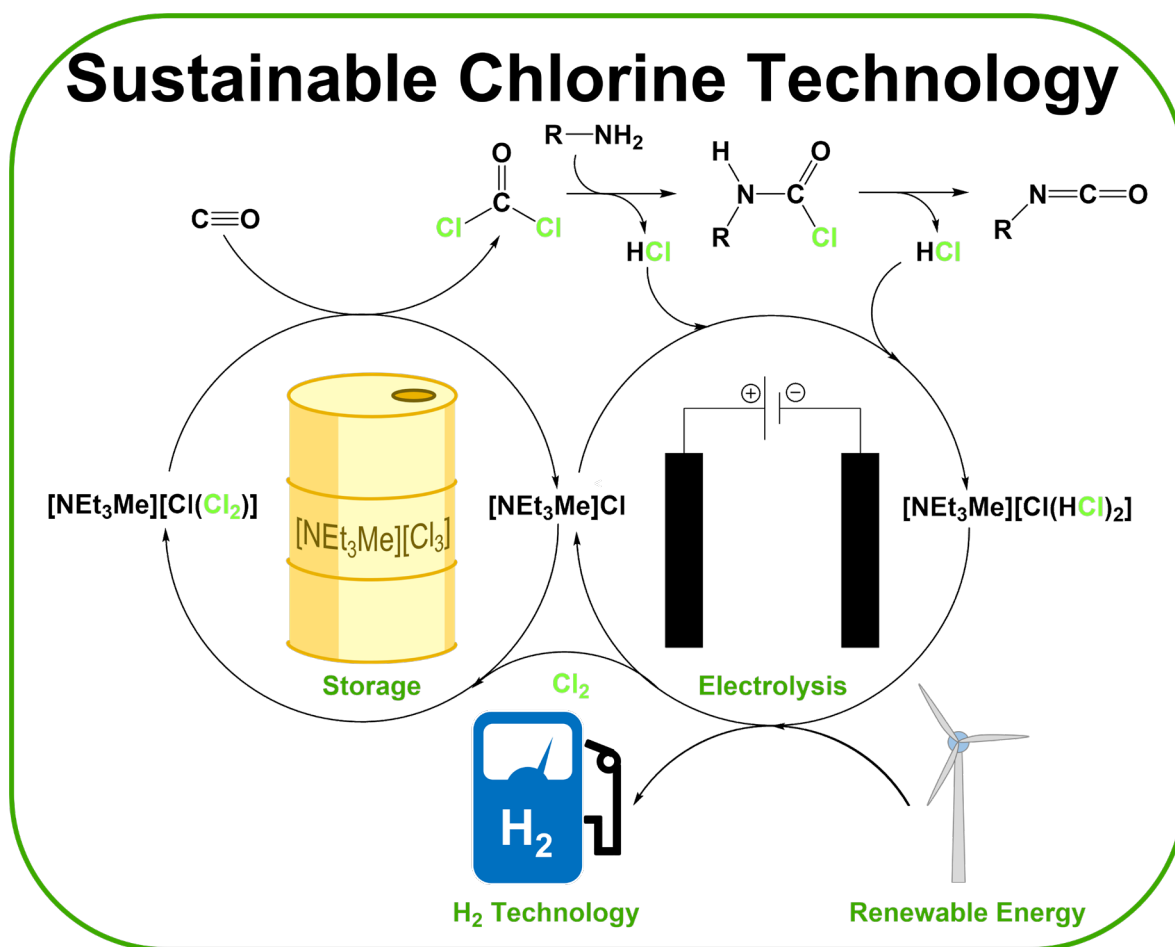


Figure 21. Proposed scheme for a safe and sustainable chlorine technology.

Overall, the introduction of polychlorides enables a potential chemical system for the conversion of resources and thus the sustainable and safe redesign of the chlorine industry. The further development might be an adventure of the next century.

5. References

- [1] <https://www.statista.com/statistics/1310477/chlorine-market-volume-worldwide/>, accessed 21.11.2022.
- [2] P. Schmittinger, T. Florkiewicz, L. C. Curlin, B. Lüke, R. Scannell, T. Navin, E. Zelfel, R. Bartsch *Ullmann's Encyclopedia of Industrial Chemistry (Chlorine)*, Wiley-VCH Verlag GmbH & Co. KGaA, Weinheim, **2012**.
- [3] <https://www.destatis.de/DE/Themen/Branchen-Unternehmen/Energie/Erzeugung/Tabellen/bruttostromerzeugung/>, accessed 21.11.2022.
- [4] <https://www.chlorineindustryreview.com/>, accessed 22.11.2022.
- [5] <https://www.statista.com/statistics/1186170/production-capacity-chlorine-europe-by-country/>, accessed 21.11.2022.
- [6] Y.-R. Luo, *Comprehensive Handbook of Chemical Bond Energies*, CRC Press, Boca Raton, Florida, **2007**.
- [7] <https://gestis.dguv.de/data?name=007170>, accessed 23.11.2022.
- [8] A. P. Annachatre, S. H. Gheewala, *Biotechnol. Adv.* **1996**, *14*, 35.
- [9] C. M. Villanueva, K. P. Cantor, J. O. Grimalt, N. Malats, D. Silverman, A. Tardon, R. Garcia-Closas, C. Serra, A. Carrato, G. Castaño-Vinyals, R. Marcos, N. Rothman, F. X. Real, M. Dosemeci, M. Kogevinas, *Am. J. Epidemiol.* **2007**, *165*, 148.
- [10] R. Lin, A. P. Amrute, J. Pérez-Ramírez, *Chem. Rev.* **2017**, *117*, 4182.
- [11] J. Pérez-Ramírez, C. Mondelli, T. Schmidt, O. F.-K. Schlüter, A. Wolf, L. Mleczko, T. Dreier, *Energy Environ. Sci.* **2011**, *4*, 4786.
- [12] P. Schmittinger, *Chlorine*, Wiley-VCH, Weinheim, **2000**.
- [13] W. Roeske, Ch. Müller, *Brauwelt* **2003**, *11*, 287.
- [14] C. R. Darnall, *J. Am. Public Health Assoc* **1911**, *1*, 783.
- [15] J. C. Crittenden, D. W. Hand, G. Tchobanoglous, R. R. Trussell, K. J. Howe, *Principles of water treatment*, Wiley, Hoboken, **2012**.
- [16] L. Cotarca, C. Lange, K. Meurer, J. Pauluhn *Ullmann's Encyclopedia of Industrial Chemistry (Phosgene)*, Wiley-VCH Verlag GmbH & Co. KGaA, Weinheim, **2019**.
- [17] G. Brereton, R. M. Emanuel, R. Lomax, K. Pennington, T. Ryan, H. Tebbe, M. Timm, P. Ware, K. Winkler, T. Yuan, Z. Zhu, N. Adam, G. Avar, H. Blankenheim, W. Friederichs,

- M. Giersig, E. Weigand, M. Halfmann, F.-W. Wittbecker, D.-R. Larimer, U. Maier, S. Meyer-Ahrens, K.-L. Noble, H.-G. Wussow *Ullmann's Encyclopedia of Industrial Chemistry (Polyurethanes)*, Wiley-VCH Verlag GmbH & Co. KGaA, Weinheim, **2019**.
- [18] G. Abts, T. Eckel, R. Wehrmann *Ullmann's Encyclopedia of Industrial Chemistry (Polycarbonates)*, Wiley-VCH Verlag GmbH & Co. KGaA, Weinheim, Germany, **2014**.
- [19] I. Fischer, W. F. Schmitt, H.-C. Porth, M. W. Allsopp, G. Vianello *Ullmann's Encyclopedia of Industrial Chemistry (Poly(Vinyl Chloride))*, Wiley-VCH Verlag GmbH & Co. KGaA, Weinheim, **2014**.
- [20] <https://plasticseurope.org/de/knowledge-hub/plastics-the-facts-2020/>, accessed 08.03.2023.
- [21] <https://www.researchnester.com/reports/ethylene-dichloride-market/1002>, accessed 08.03.2023.
- [22] A. Ohligschläger, K. Menzel, A. T. Kate, J. R. Martinez, C. Frömbgen, J. Arts, A. McCulloch, M. Rossberg, W. Lendle, G. Pfeiderer, A. Tögel, T. R. Torkelson, K. K. Beutel *Ullmann's Encyclopedia of Industrial Chemistry (Chloromethanes)*, Wiley-VCH Verlag GmbH & Co. KGaA, Weinheim, **2019**.
- [23] A. Ohligschläger, K. Menzel, A. T. Kate, J. R. Martinez, C. Frömbgen, J. Arts, A. McCulloch, M. Rossberg, W. Lendle, G. Pfeiderer, A. Tögel, T. R. Torkelson, K. K. Beutel *Ullmann's Encyclopedia of Industrial Chemistry (Chloromethanes)*, Wiley-VCH Verlag GmbH & Co. KGaA, Weinheim, **2019**.
- [24] G. J. Puts, P. Crouse, B. M. Ameduri, *Chem. Rev.* **2019**, *119*, 1763.
- [25] E.-L. Dreher, K. K. Beutel, J. D. Myers, T. Lübbe, S. Krieger, L. H. Pottenger *Ullmann's Encyclopedia of Industrial Chemistry (Chloroethanes and Chloroethylenes)*, Wiley-VCH Verlag GmbH & Co. KGaA, Weinheim, **2014**.
- [26] E. Langer, H. Rassaerts, P. Kleinschmidt, T. R. Torkelson, K. K. Beutel *Ullmann's Encyclopedia of Industrial Chemistry (Chloropropanes, Chlorobutanes, and Chlorobutenes)*, Wiley-VCH Verlag GmbH & Co. KGaA, Weinheim, **2012**.
- [27] G. Y. T. Liu, W. F. Richey, J. E. Betso, B. Hughes, J. Klapacz, J. Lindner *Ullmann's Encyclopedia of Industrial Chemistry (Chlorohydrins)*, Wiley-VCH Verlag GmbH & Co. KGaA, Weinheim, **2014**.

- [28] K.-A. Lipper, E. Löser, O. Brücher *Ullmann's Encyclopedia of Industrial Chemistry (Benzyl Chloride and Other Side-Chain-Chlorinated Aromatic Hydrocarbons)*, Wiley-VCH Verlag GmbH & Co. KGaA, Weinheim, **2017**.
- [29] J.-L. Montchamp, *Phosphorus, Sulfur, and Silicon Relat. Elem.* **2013**, 188, 66.
- [30] G. Bettermann, W. Krause, G. Riess, T. Hofmann *Ullmann's Encyclopedia of Industrial Chemistry (Phosphorus Compounds, Inorganic)*, Wiley-VCH Verlag GmbH & Co. KGaA, Weinheim, **2012**.
- [31] H. G. Völz *Ullmann's Encyclopedia of Industrial Chemistry (Pigments, Inorganic, 1. General)*, Wiley-VCH Verlag GmbH & Co. KGaA, Weinheim, **2012**.
- [32] H. Sibus, V. Güther, O. Roidl, F. Habashi, H. Uwe Wolf, C. Siemers *Ullmann's Encyclopedia of Industrial Chemistry (Titanium, Titanium Alloys, and Titanium Compounds)*, Wiley-VCH Verlag GmbH & Co. KGaA, Weinheim, **2017**.
- [33] H. G. Völz, J. Kischkewitz, P. Woditsch, A. Westerhaus, W.-D. Griebler, M. de Liedekerke, G. Buxbaum, H. Printzen, M. Mansmann, D. Råde, G. Trenczek, V. Wilhelm, S. Schwarz, H. Wienand, J. Adel, G. Adrian, K. Brandt, W. B. Cork, H. Winkeler, W. Mayer, K. Schneider, L. Leitner, H. Kathrein, E. Schwab, H. Jakusch, M. Ohlinger, R. Veitch, G. Etzrodt, G. Pfaff, K.-D. Franz, R. Emmert, K. Nitta, R. Besold, H. Gaedcke *Ullmann's Encyclopedia of Industrial Chemistry (Pigments, Inorganic)*, Wiley-VCH Verlag GmbH & Co. KGaA, Weinheim, **2005**.
- [34] C. W. Scheele, *Sv. Akad. Handl.* **1774**, 35, 89.
- [35] R. T. Baldwin, *J. Chem. Educ.* **1927**, 4, 313.
- [36] <https://de.wikipedia.org/wiki/Chloralkali-Elektrolyse#/media/Datei:Chloralkali.svg>, accessed 26.04.2023.
- [37] [https://de.wikipedia.org/wiki/Chloralkali-Elektrolyse#/media/Datei:Diaphragmaverfahren_\(german\).svg](https://de.wikipedia.org/wiki/Chloralkali-Elektrolyse#/media/Datei:Diaphragmaverfahren_(german).svg), accessed 02.03.2023.
- [38] [https://de.wikipedia.org/wiki/Chloralkali-Elektrolyse#/media/Datei:Membranverfahren_\(german\).svg](https://de.wikipedia.org/wiki/Chloralkali-Elektrolyse#/media/Datei:Membranverfahren_(german).svg), accessed 02.03.2023.
- [39] J. Jörissen, T. Turek, R. Weber, *Chem. Unserer Zeit* **2011**, 45, 172.
- [40] I. Moussallem, S. Pinnow, T. Turek, *Chem. Ing. Tech.* **2009**, 81, 489.
- [41] <https://www.covestro.com/de/sustainability/flagship-solutions/oxygen-depolarized-cathode>, accessed 03.03.2023.
- [42] F. Klaucke, C. Hoffmann, M. Hofmann, G. Tsatsaronis, *Appl. Energy* **2020**, 276, 115366.

- [43] E. Homberger, G. Reggiani, J. Sambeth, H. K. Wipf, *Ann. occup. Hyg.* **1979**, *22*, 327.
- [44] Hend Galal-Gorchev, *Pure Appl. Chem.* **1996**, *68*, 1731.
- [45] <https://waterandhealth.org/safe-drinking-water/wp/>, accessed 14.03.2023.
- [46] <https://unric.org/en/sdg-6/>, accessed 14.03.2023.
- [47] M. J. McGuire, *J. Am. WATER Work. Assoc.* **2006**, *98*, 123.
- [48] <https://www.mattchlor.com/how-chlorination-is-improving-health/>, accessed 26.04.2023.
- [49] *Guidelines for drinking-water quality*, World Health Organization, Geneva, **2022**.
- [50] H. K. Knutsen, J. Alexander, L. Barregård, M. Bignami, B. Brüschweiler, S. Ceccatelli, B. Cottrill, M. Dinovi, L. Edler, B. Grasl-Kraupp, C. Hogstrand, C. S. Nebbia, I. P. Oswald, A. Petersen, M. Rose, A.-C. Roudot, T. Schwerdtle, C. Vleminckx, G. Vollmer, H. Wallace, P. Fürst, H. Håkansson, T. Halldorsson, A.-K. Lundebye, R. Pohjanvirta, L. Rylander, A. Smith, H. van Loveren, I. Waalkens-Berendsen, M. Zeilmaker, M. Binaglia, J. Á. Gómez Ruiz, Z. Horváth, E. Christoph, L. Ciccolallo, L. Ramos Bordajandi, H. Steinkellner, L. R. Hoogenboom, *EFSA Journal* **2018**, *16*, e05333.
- [51] <https://cfpub.epa.gov/ncea/risk/recordisplay.cfm?deid=159286>, accessed 16.03.2023.
- [52] U. Quass, M. Fermann, G. Bröker, *Chemosphere* **2004**, *54*, 1319.
- [53] O. Zeidler, *Chem. Ber.* **1874**, *7*, 1180.
- [54] R. L. Metcalf, *J. Agric. Food Chem.* **1973**, *21*, 511.
- [55] <https://www.nobelprize.org/prizes/medicine/1948/summary/>, accessed 16.03.2023.
- [56] W. J. Rogan, A. Chen, *Lancet* **2005**, *366*, 763.
- [57] E. F. Knipling, *J. Econ. Entomol.* **1953**, *46*, 1.
- [58] C. D. Lundholm, *Comp. Biol. Physiol.* **1997**, *118C*, 113.
- [59] <http://chm.pops.int/TheConvention/ThePOPs/The12InitialPOPs/tabid/296/>, accessed 23.03.2023.
- [60] http://whqlibdoc.who.int/hq/2006/WHO_HTM_MAL_2006.1112_eng.pdf, accessed 16.03.2023.
- [61] <https://bit.ly/3VgvIKD>, accessed 23.03.2023.
- [62] B. Eskenazi, J. Chevrier, L. G. Rosas, H. A. Anderson, M. S. Bornman, H. Bouwman, A. Chen, B. A. Cohn, C. de Jager, D. S. Henshel, F. Leipzig, J. S. Leipzig, E. C. Lorenz, S. M. Snedeker, D. Stapleton, *Environ. Health Perspect.* **2009**, *117*, 1359.
- [63] <https://www.eurekalert.org/news-releases/744976>, accessed 16.03.2023.

- [64] J. Pelletier, J. B. Caventou, *Ann. Chim. Phys.* **1819**, 142.
- [65] H. Haller, S. Riedel, *Z. Anorg. Allg. Chem.* **2014**, 640, 1281.
- [66] K. Sonnenberg, L. Mann, F. A. Redeker, B. Schmidt, S. Riedel, *Angew. Chem. Int. Ed.* **2020**, 59, 5464; *Angew. Chem.* **2020**, 132, 5506.
- [67] P. H. Svensson, L. Kloo, *Chem. Rev.* **2003**, 103, 1649.
- [68] L. C. Pauling, *The Nature of the Chemical Bond*, 2. Ed., Cornell University Press, Ithaca, New York, **1940**.
- [69] G. E. Kimball, *J. Chem. Phys.* **1940**, 8, 188.
- [70] R. J. Hach, R. E. Rundle, *J. Am. Chem. Soc.* **1951**, 73, 4321.
- [71] G. C. Pimentel, *J. Chem. Phys.* **1951**, 19, 446.
- [72] M. L. Munzarová, R. Hoffmann, *J. Am. Chem. Soc.* **2002**, 124, 4787.
- [73] K. S. Thanthiriwatte, J. M. Spruell, D. A. Dixon, K. O. Christe, H. D. B. Jenkins, *Inorg. Chem.* **2014**, 53, 8136.
- [74] C. Wang, D. Danovich, S. Shaik, Y. Mo, *Chem. Eur. J.* **2017**, 23, 8719.
- [75] B. Braïda, P. C. Hiberty, *Nat. Chem.* **2013**, 5, 417.
- [76] B. Braïda, P. C. Hiberty, *J. Phys. Chem. A* **2008**, 112, 13045.
- [77] B. Braïda, T. Ribeyre, P. C. Hiberty, *Chem. Eur. J.* **2014**, 20, 9643.
- [78] C. A. Coulson, *J. Chem. Soc.* **1964**, 19, 1442.
- [79] S. Shaik, D. Danovich, J. M. Galbraith, B. Braïda, W. Wu, P. C. Hiberty, *Angew. Chem. Int. Ed.* **2020**, 59, 984; *Angew. Chem.* **2020**, 132, 996.
- [80] S. Shaik, D. Danovich, W. Wu, P. C. Hiberty, *Nat. Chem.* **2009**, 1, 443.
- [81] S. S. Shaik, P. C. Hiberty, *A Chemist's Guide to Valence Bond Theory*, Wiley-Interscience, Hoboken, New Jersey, **2008**.
- [82] H. Keil, K. Sonnenberg, C. Müller, R. Herbst-Irmer, H. Beckers, S. Riedel, D. Stalke, *Angew. Chem. Int. Ed.* **2021**, 60, 2569; *Angew. Chem.* **2021**, 133, 2600.
- [83] G. A. Landrum, N. Goldberg, R. Hoffmann, *J. Chem. Soc., Dalton Trans.* **1997**, 3605.
- [84] R. Brückner, H. Haller, M. Ellwanger, S. Riedel, *Chem. Eur. J.* **2012**, 18, 5741.
- [85] T. Clark, *WIREs Comput. Mol. Sci.* **2013**, 3, 13.
- [86] P. Metrangolo, G. Resnati, *Halogen Bonding*, Springer, Berlin, Heidelberg, New York, **2008**.
- [87] B. S. Ault, L. Andrews, *J. Am. Chem. Soc.* **1976**, 98, 1591.
- [88] B. S. Ault, L. Andrews, *Inorg. Chem.* **1977**, 16, 2024.

- [89] T. Vent-Schmidt, F. Brosi, J. Metzger, T. Schlöder, X. Wang, L. Andrews, C. Müller, H. Beckers, S. Riedel, *Angew. Chem. Int. Ed.* **2015**, *54*, 8279; *Angew. Chem.* **2015**, *127*, 8397.
- [90] F. A. Redeker, H. Beckers, S. Riedel, *RSC Adv.* **2015**, *5*, 106568.
- [91] A. A. Tuinman, A. A. Gakh, R. J. Hinde, R. N. Compton, *J. Am. Chem. Soc.* **1999**, *121*, 8397.
- [92] A. Artau, K. E. Nizzi, B. T. Hill, L. S. Sunderlin, P. G. Wenthold, *J. Am. Chem. Soc.* **2000**, *122*, 10667.
- [93] S. Riedel, T. Köchner, X. Wang, L. Andrews, *Inorg. Chem.* **2010**, *49*, 7156.
- [94] F. D. Chattaway, G. Hoyle, *J. Chem. Soc. Trans.* **1923**, *123*, 654.
- [95] J. C. Evans, G. Y. S. Lo, *J. Chem. Phys.* **1966**, *44*, 3638.
- [96] B. S. Ault, L. Andrews, *J. Chem. Phys.* **1976**, *64*, 4853.
- [97] F. A. Redeker, H. Beckers, S. Riedel, *Chem. Commun.* **2017**, *53*, 12958.
- [98] M. P. Bogaard, J. Peterson, A. D. Rae, *Acta Cryst. B* **1981**, *37*, 1357.
- [99] T. Chivers, J. F. Richardson, N. R. M. Smith, *Inorg. Chem.* **1985**, *24*, 2453.
- [100] M. Jansen, S. Strojek, *Z. Naturforsch.* **1995**, *50b*, 1171.
- [101] R. T. Boéré, A. W. Cordes, S. L. Craig, R. T. Oakley, R. W. Reed, *J. Am. Chem. Soc.* **1987**, *109*, 868.
- [102] J. Broekema, E. E. Havinga, E. H. Wiebenga, *Acta Cryst.* **1957**, *10*, 596.
- [103] J. Taraba, Z. Zak, *Inorg. Chem.* **2003**, *42*, 3591.
- [104] A. Bondi, *J. Phys. Chem.* **1964**, *68*, 441.
- [105] K. Sonnenberg, P. Pröhm, N. Schwarze, C. Müller, H. Beckers, S. Riedel, *Angew. Chem. Int. Ed.* **2018**, *57*, 9136; *Angew. Chem.* **2018**, *130*, 9274.
- [106] P. Pröhm, N. Schwarze, C. Müller, S. Steinhauer, H. Beckers, S. M. Rupf, S. Riedel, *Chem. Commun.* **2021**, *57*, 4834.
- [107] R. Brückner, P. Pröhm, A. Wiesner, S. Steinhauer, C. Müller, S. Riedel, *Angew. Chem. Int. Ed.* **2016**, *55*, 10904; *Angew. Chem.* **2016**, *128*, 11064.
- [108] B. M. Powell, K. M. Heal, B. H. Torrie, *Mol. Phys.* **1984**, *53*, 929.
- [109] A. Gräfe-Kavoosian, S. Nafepour, K. Nagel, K.-F. Tebbe, *Z. Naturforsch. B* **1998**, *53*, 641.
- [110] E. E. Havinga, K. H. Boswijk, E. H. Wiebenga, *Acta Cryst. A* **1954**, *7*, 487.
- [111] K. N. Robertson, P. K. Bakshi, T. S. Cameron, O. Knop, *Z. Anorg. Allg. Chem.* **1997**, *623*, 104.
- [112] K. Sonnenberg, P. Pröhm, S. Steinhauer, A. Wiesner, C. Müller, S. Riedel, *Z. Anorg. Allg. Chem.* **2017**, *643*, 101.

- [113] R. Brückner, H. Haller, S. Steinhauer, C. Müller, S. Riedel, *Angew. Chem. Int. Ed.* **2015**, *54*, 15579; *Angew. Chem.* **2015**, *127*, 15800.
- [114] F. Pichierri, *Chem. Phys. Lett.* **2011**, *515*, 116.
- [115] M. Bakavoli, A. M. Kakhky, A. Shiri, M. Ghabdian, A. Davoodnia, H. Eshghi, M. Khatami, *Chin. Chem. Lett.* **2010**, *21*, 651.
- [116] P. D. Boyle, W. I. Cross, S. M. Godfrey, C. A. McAuliffe, R. G. Pritchard, S. J. Teat, *J. Chem. Soc., Dalton Trans.* **1999**, 2845.
- [117] V. Vitske, H. Herrmann, M. Enders, E. Kaifer, H.-J. Himmel, *Chem. Eur. J.* **2012**, *18*, 14108.
- [118] J. C. Evans, G. Y.-S. Lo, *Inorg. Chem.* **1967**, *6*, 1483.
- [119] X. Chen, M. A. Rickard, J. W. Hull, C. Zheng, A. Leugers, P. Simoncic, *Inorg. Chem.* **2010**, *49*, 8684.
- [120] M. Wolff, A. Okrut, C. Feldmann, *Inorg. Chem.* **2011**, *50*, 11683.
- [121] H. Haller, M. Ellwanger, A. Higelin, S. Riedel, *Angew. Chem. Int. Ed.* **2011**, *50*, 11528; *Angew. Chem.* **2011**, *123*, 11732.
- [122] H. Haller, M. Ellwanger, A. Higelin, S. Riedel, *Z. Anorg. Allg. Chem.* **2012**, *638*, 553.
- [123] H. Haller, J. Schröder, S. Riedel, *Angew. Chem. Int. Ed.* **2013**, *52*, 4937; *Angew. Chem.* **2013**, *125*, 5037.
- [124] K. O. Strømme, *Acta Chem. Scand.* **1959**, *13*, 2089.
- [125] K. Sonnenberg, P. Pröhm, C. Müller, H. Beckers, S. Steinhauer, D. Lentz, S. Riedel, *Chem. Eur. J.* **2018**, *24*, 1072.
- [126] M. Wolff, J. Meyer, C. Feldmann, *Angew. Chem. Int. Ed.* **2011**, *50*, 4970; *Angew. Chem.* **2011**, *123*, 5073.
- [127] L. Mann, G. Senges, K. Sonnenberg, H. Haller, S. Riedel, *Eur. J. Inorg. Chem.* **2018**, *2018*, 3330.
- [128] M. E. Easton, A. J. Ward, T. Hudson, P. Turner, A. F. Masters, T. Maschmeyer, *Chem. Eur. J.* **2015**, *21*, 2961.
- [129] C. W. Cunningham, G. R. Burns, V. McKee, *Inorg. Chim. Acta* **1990**, *167*, 135.
- [130] K. M. Fromm, R. D. Bergougnant, A. Y. Robin, *Z. Anorg. Allg. Chem.* **2006**, *632*, 828.
- [131] T. Schlama, K. Gabriel, V. Gouverneur, C. Mioskowski, *Angew. Chem. Int. Ed.* **1997**, *36*, 2342; *Angew. Chem.* **1997**, *109*, 2440.
- [132] N. Huwyler, E. M. Carreira, *Angew. Chem. Int. Ed.* **2012**, *51*, 13066; *Angew. Chem.* **2012**, *124*, 3531.

- [133] Z. A. Könst, A. R. Szklarski, S. Pellegrino, S. E. Michalak, M. Meyer, C. Zanette, R. Cencic, S. Nam, V. K. Voora, D. A. Horne, J. Pelletier, D. L. Mobley, G. Yusupova, M. Yusupov, C. D. Vanderwal, *Nat. Chem.* **2017**, *9*, 1140.
- [134] C. Nilewski, R. W. Geisser, E. M. Carreira, *Nature* **2009**, *457*, 573.
- [135] W. Ju, X. Wang, H. Tian, J. Gui, *J. Am. Chem. Soc.* **2021**, *143*, 13016.
- [136] N. Zhou, Q. Wang, A. J. Lough, H. Yan, *Can. J. Chem.* **2012**, *90*, 625.
- [137] X. Xiong, Y.-Y. Yeung, *Angew. Chem. Int. Ed.* **2016**, *55*, 16101; *Angew. Chem.* **2016**, *128*, 16335.
- [138] N. Sivendran, F. Belitz, D. Sowa Prendes, Á. Manu Martínez, R. Schmid, L. J. Gooßen, *Chem. Eur. J.* **2022**, *28*, e202103669.
- [139] T. M. Beck, H. Haller, J. Streuff, S. Riedel, *Synthesis* **2014**, *46*, 740.
- [140] J. Berthelot, Y. Benammar, C. Lange, *Tetrahedron Lett.* **1991**, *32*, 4135.
- [141] I. Saikia, A. J. Borah, P. Phukan, *Chem. Rev.* **2016**, *116*, 6837.
- [142] U. Bora, M. K. Chaudhuri, D. Dey, S. S. Dhar, *Pure Appl. Chem.* **2001**, *73*, 93.
- [143] J. Jacques, A. Marquet, *Org. Synth.* **1973**, *53*, 111.
- [144] M. Sawa, K. Mizuno, H. Harada, H. Tateishi, Y. Arai, S. Suzuki, M. Oue, H. Tsujiuchi, Y. Furutani, S. Kato, *Bioorg. Med. Chem. Lett.* **2005**, *15*, 1061.
- [145] M. Avramoff, J. Weiss, O. Schächter, *J. Org. Chem.* **1963**, *28*, 3256.
- [146] M. K. Chaudhuri, A. T. Khan, B. K. Patel, D. Dey, W. Kharmawopflang, T. R. Lakshmi Prabha, G. C. Mandal, *Tetrahedron Lett.* **1998**, *39*, 8163.
- [147] C. Dai, J. Zhang, C. Huang, Z. Lei, *Chem. Rev.* **2017**, *117*, 6929.
- [148] P. Wasserscheid, T. Welton *Ionic Liquids in Synthesis*, Wiley-VCH Verlag GmbH & Co. KGaA, Weinheim, **2008**.
- [149] N. V. Plechkova, K. R. Seddon, *Chem. Soc. Rev.* **2008**, *37*, 123.
- [150] M. Watanabe, M. L. Thomas, S. Zhang, K. Ueno, T. Yasuda, K. Dokko, *Chem. Rev.* **2017**, *117*, 7190.
- [151] Z. Zhang, J. Song, B. Han, *Chem. Rev.* **2017**, *117*, 6834.
- [152] Z. Lei, B. Chen, Y.-M. Koo, D. R. MacFarlane, *Chem. Rev.* **2017**, *117*, 6633.
- [153] G. W. Meindersma, M. Maase, A. B. de Haan *Ullmann's Encyclopedia of Industrial Chemistry (Ionic Liquids)*, Wiley-VCH Verlag GmbH & Co. KGaA, Weinheim, **2012**.
- [154] M. Freemantle, *Chem. Eng. News* **2003**, *81*, 9.

- [155] V. Stegmann, K. Masonne, BASF AG, *Verfahren zur Herstellung von Halogenalkanen aus Alkoholen*. WO 2005026089 A2, **2005**.
- [156] M. Armand, F. Endres, D. R. MacFarlane, H. Ohno, B. Scrosati, *Nat. Mater.* **2009**, *8*, 621.
- [157] A. P. Abbott, G. Capper, D. L. Davies, R. K. Rasheed, V. Tambyrajah, *Trans. Inst. Met. Fin.* **2001**, *79*, 204.
- [158] A. P. Abbott, G. Capper, D. L. Davies, R. K. Rasheed, J. Archer, C. John, *Trans. Inst. Met. Fin.* **2004**, *82*, 14.
- [159] A. P. Abbott, G. Capper, D. L. Davies, R. K. Rasheed, *Chem. Eur. J.* **2004**, *10*, 3769.
- [160] D. J. Tempel, P. B. Henderson, J. R. Brzozowski, R. M. Pearlstein, H. Cheng, *J. Am. Chem. Soc.* **2008**, *130*, 400.
- [161] X. Li, A. van den Bossche, T. Vander Hoogerstraete, K. Binnemans, *Chem. Commun.* **2018**, *54*, 475.
- [162] X. Li, Z. Li, M. Orefice, K. Binnemans, *ACS Sustainable Chem. Eng.* **2019**, *7*, 2578.
- [163] A. van den Bossche, N. Rodriguez Rodriguez, S. Riaño, W. Dehaen, K. Binnemans, *RSC Adv.* **2021**, *11*, 10110.
- [164] A. van den Bossche, W. Vereycken, T. Vander Hoogerstraete, W. Dehaen, K. Binnemans, *ACS Sustainable Chem. Eng.* **2019**, *7*, 14451.
- [165] A. van den Bossche, E. de Witte, W. Dehaen, K. Binnemans, *Green Chem.* **2018**, *20*, 3327.
- [166] A. Yao, F. Qu, Y. Liu, G. Qu, H. Lin, S. Hu, X. Wang, T. Chu, *Dalton Trans.* **2019**, *48*, 16249.
- [167] X. Li, Z. Li, K. Binnemans, *Sep. Purif. Technol.* **2021**, *275*, 119158.
- [168] T. A. Gully, P. Voßnacker, J. R. Schmid, H. Beckers, S. Riedel, *ChemistryOpen* **2021**, 255.
- [169] K. Binnemans, P. T. Jones, B. Blanpain, T. van Gerven, Y. Yang, A. Walton, M. Buchert, *J. Clean. Prod.* **2013**, *51*, 1.
- [170] H. Haller, M. Hog, F. Scholz, H. Scherer, I. Krossing, S. Riedel, *Z. Naturforsch.* **2013**, *68b*, 1103.
- [171] I. Rubinstein, M. Bixon, E. Gileadi, *J. Phys. Chem.* **1980**, *84*, 715.
- [172] E. Lancry, B.-Z. Magnes, I. Ben-David, M. Freiberg, *ECS Trans.* **2013**, *53*, 107.
- [173] S. Park, H. Kim, J. Chae, J. Chang, *J. Phys. Chem. C* **2016**, *120*, 3922.
- [174] G. Boschloo, A. Hagfeldt, *Acc. Chem. Res.* **2009**, *42*, 1819.
- [175] K. Kakiage, T. Tokutome, S. Iwamoto, T. Kyomen, M. Hanaya, *Chem. Commun.* **2013**, *49*, 179.

- [176] C. Teng, X. Yang, C. Yuan, C. Li, R. Chen, H. Tian, S. Li, A. Hagfeldt, L. Sun, *Org. Lett.* **2009**, *11*, 5542.
- [177] Z.-S. Wang, K. Sayama, H. Sugihara, *J. Phys. Chem. B* **2005**, *109*, 22449.
- [178] G. Caldwell, P. Kebarle, *Can. J. Chem.* **1985**, *63*, 1399.
- [179] B. Gao, L. Zhang, Q. Zheng, F. Zhou, L. M. Klivansky, J. Lu, Y. Liu, J. Dong, P. Wu, K. B. Sharpless, *Nat. Chem.* **2017**, *9*, 1083.
- [180] R. Franz, *J. Fluorine Chem.* **1980**, *15*, 423.
- [181] G. Alvernhe, A. Laurent, G. Haufe, *Synthesis* **1987**, *6*, 562.
- [182] G. A. Olah, M. Nojima, I. Kerekes, *Synthesis* **1973**, *12*, 779.
- [183] G. A. Olah, M. Nojima, I. Kerekes, *Synthesis* **1973**, *12*, 780.
- [184] G. A. Olah, J. T. Welch, Y. D. Vankar, M. Nojima, I. Kerekes, J. A. Olah, *J. Org. Chem.* **1979**, *44*, 3872.
- [185] D. Mootz, D. Boenigk, *Z. Anorg. Allg. Chem.* **1987**, *544*, 159.
- [186] D. Mootz, J. Hocken, *Angew. Chem. Int. Ed.* **1989**, *28*, 1697; *Angew. Chem.* **1989**, *101*, 1713.
- [187] D. Mootz, A. Deeg, *Z. Anorg. Allg. Chem.* **1992**, *615*, 109.
- [188] D. Mootz, J. Hocken, *Z. Naturforsch.* **1989**, *44b*, 1239.
- [189] D. Mootz, W. Poll, *Z. Naturforsch.* **1984**, *39b*, 1300.
- [190] D. Wiechert, D. Mootz, R. Franz, G. Siegemund, *Chem. Eur. J.* **1998**, *4*, 1043.
- [191] R. Hagiwara, T. Hirashige, T. Tsuda, Y. Ito, *J. Electrochem. Soc.* **2002**, *149*, D1-D6.
- [192] H. Yoshino, K. Matsumoto, R. Hagiwara, Y. Ito, K. Oshima, S. Matsubara, *J. Fluorine Chem.* **2006**, *127*, 29.
- [193] A. R. Mahjoub, X. Zhang, K. Seppelt, *Chem. Eur. J.* **1995**, *1*, 261.
- [194] W. W. Wilson, K. O. Christe, J. Feng, R. Bau, *Can. J. Chem.* **1989**, *67*, 1898.
- [195] B. Alič, G. Tavčar, *J. Fluorine Chem.* **2016**, *192*, 141.
- [196] J. T. Goettel, N. Kostiuik, M. Gerken, *Inorg. Chem.* **2016**, *55*, 7126.
- [197] I. M. Shlyapnikov, E. A. Goresnik, Z. Mazej, *Eur. J. Inorg. Chem.* **2018**, *2018*, 5246.
- [198] J. Wessel, U. Behrens, E. Lork, T. Borrmann, W.-D. Stohrer, R. Mews, *Inorg. Chem.* **2002**, *41*, 4715.
- [199] R. Rathore, S. V. Lindeman, C.-J. Zhu, T. Mori, P. v. R. Schleyer, J. K. Kochi, *J. Org. Chem.* **2002**, *67*, 5106.
- [200] J. L. Atwood, S. G. Bott, C. M. Means, A. W. Coleman, H. Zhang, M. T. May, *Inorg. Chem.* **1990**, *29*, 467.

- [201] G. W. Driver, I. Mutikainen, *Dalton Trans.* **2011**, 40, 10801.
- [202] J. L. E. Campbell, K. E. Johnson, *Inorg. Chem.* **1993**, 32, 3809.
- [203] I. G. Shenderovich, S. N. Smirnov, G. S. Denisov, V. A. Gindin, N. S. Golubev, A. Dunger, R. Reibke, S. Kirpekar, O. L. Malkina, H.-H. Limbach, *Ber. Bunsenges. Phys. Chem.* **1998**, 102, 422.
- [204] M. Jaccaud, R. Faron, D. Devilliers, R. Romano, S. Riedel, H. Pernice *Ullmann's Encyclopedia of Industrial Chemistry (Fluorine)*, Wiley-VCH Verlag GmbH & Co. KGaA, Weinheim, **2020**.
- [205] P. Kirsch, *Modern Fluoroorganic Chemistry. Synthesis, Reactivity, Applications*, 2. Ed., Wiley-VCH, Weinheim, **2013**.
- [206] Martin A. McClinton, *Aldrichimica Acta* **1995**, 28, 31.
- [207] M. B. Giudicelli, D. Picq, B. Veyron, *Tetrahedron Lett.* **1990**, 31, 6527.
- [208] E. Vedejs, R. W. Chapman, S. C. Fields, S. Lin, M. R. Schrimpf, *J. Org. Chem.* **1995**, 60, 3020.
- [209] G. A. Molander, B. Canturk, *Angew. Chem. Int. Ed.* **2009**, 48, 9240; *Angew. Chem.* **2009**, 121, 9404.
- [210] E. L. Thierry Brigaud, *Tetrahedron Lett.* **1990**, 31, 2287.
- [211] J. Dong, L. Krasnova, M. G. Finn, K. B. Sharpless, *Angew. Chem. Int. Ed.* **2014**, 53, 9430; *Angew. Chem.* **2014**, 126, 9584.
- [212] C. J. Smedley, Q. Zheng, B. Gao, S. Li, A. Molino, H. M. Duivenvoorden, B. S. Parker, Wilson, David J. D., K. B. Sharpless, J. E. Moses, *Angew. Chem. Int. Ed.* **2019**, 58, 4552; *Angew. Chem.* **2019**, 131, 4600.
- [213] G. Driver, K. E. Johnson, *Green Chem.* **2003**, 5, 163.
- [214] M. Kleoff, P. Voßnacker, S. Riedel, *Angew. Chem. Int. Ed. Engl.* **2023**, 62, e202216586.
- [215] P. Metrangolo, H. Neukirch, T. Pilati, G. Resnati, *Acc. Chem. Res.* **2005**, 38, 386.

6. Publications, Patents and Conference Contributions

6.1. Publications

- (1) **The Rise of Trichlorides Enabling an Improved Chlorine Technology**
Merlin Kleoff, Patrick Voßnacker, Sebastian Riedel, *Angew. Chem. Int. Ed.* **2023**, *62*, e202216586, <https://doi.org/10.1002/anie.202216586>.
- (2) **Synthesis of a Hexachloro Sulfate(IV) Dianion Enabled by Polychloride Chemistry**
Patrick Voßnacker, Alisa Wüst, Carsten Müller, Merlin Kleoff, Sebastian Riedel *Angew. Chem. Int. Ed.* **2022**, *61*, e202209684, <https://doi.org/10.1002/anie.202209684>.
- (3) **Alkyl Ammonium Chloride Salts for Efficient Chlorine Storage at Ambient Conditions**
Patrick Voßnacker, Nico Schwarze, Thomas Keilhack, Merlin Kleoff, Simon Steinhauer, Yuliya Schiesser, Maxime Paven, Sivathmeehan Yogendra, Rainer Weber, Sebastian Riedel, *ACS Sustainable Chem. Eng.* **2022**, *10*, 9525, <https://doi.org/10.1021/acssuschemeng.2c02186>
- (4) **Novel Synthetic Pathway for the Production of Phosgene**
Patrick Voßnacker, Alisa Wüst, Thomas Keilhack, Carsten Müller, Simon Steinhauer, Helmut Beckers, Sivathmeehan Yogendra, Yuliya Schiesser, Rainer Weber, Marc Reimann, Robert Müller, Martin Kaupp, Sebastian Riedel, *Sci. Adv.* **2021**, *7*, eabj5186, <https://doi.org/10.1126/sciadv.abj5186>.
- (5) **From Missing Links to New Records: A Series of Novel Polychlorine Anions**
Patrick Voßnacker, Thomas Keilhack, Nico Schwarze, Karsten Sonnenberg, Konrad Seppelt, Moritz Malischewski, Sebastian Riedel, *Eur. J. Inorg. Chem.* **2021**, *2021*, 1034, <https://doi.org/10.1002/ejic.202001072>.
- (6) **Synthesis and Characterization of Poly(hydrogen halide) Halogenates (-I)**
Patrick Voßnacker, Simon Steinhauer, Julia Bader, Sebastian Riede, *Chem. Eur. J.* **2020**, *26*, 13256, <https://doi.org/10.1002/chem.202001864>.
- (7) **Reactivity of [AuF₃(SIMes)] – Pathway to Unprecedented Structural Motifs**
Marlon Winter, Mathias A. Ellwanger, Niklas Limberg, Alberto Pérez-Bitrián, Patrick Voßnacker, Simon Steinhauer, Sebastian Riedel, *Chem. Eur. J.* **2023**, e202301684, <https://doi.org/10.1002/chem.202301684>.
- (8) **Gold Teflates Revisited: From the Lewis Superacid [Au(OTeF₅)₃] to the Anion [Au(OTeF₅)₄]⁻**
Marlon Winter, Natallia Peshkur, Mathias A. Ellwanger, Alberto Pérez-Bitrián, Patrick Voßnacker, Simon Steinhauer, Sebastian Riedel, *Chem. Eur. J.* **2023**, e202203634, <https://doi.org/10.1002/chem.202203634>.
- (9) **Noncovalent Interactions in Halogenated Pyridinium Salts of the Weakly Coordinating Anion [Al(OTeF₅)₄]⁻**
Sofiya Kotsyuda, Ahmed N. Toraman, Patrick Voßnacker, Mathias A. Ellwanger, Simon Steinhauer, Carsten Müller, Sebastian Riedel, *Chem. Eur. J.* **2023**, *29*, e202202749, <https://doi.org/10.1002/chem.202202749>.

- (10) **[NEt₃Me][O₃], Synthesis, Crystal Growth and Crystal Structure Analysis**
Jonas R. Schmid, Patrick Voßnacker, Martin Jansen, Sebastian Riedel, *Z. Anorg. Allg. Chem.* **2022**, 648, e202200225, <https://doi.org/10.1002/zaac.202200225>.
- (11) **Synthesis of 3-*epi*-Hypatulin B Featuring a Late-Stage Photo-Oxidation in Flow**
Stefan Leisering, Sebastian Ponath, Kamar Shakeri, Alexandros Mavroskoufis, Merlin Kleoff, Patrick Voßnacker, Simon Steinhauer, Manuela Weber, and Mathias Christmann, *Org. Lett.* **2022**, 24, 4305, <https://doi.org/10.1021/acs.orglett.2c00689>.
- (12) **(Noble gas)_n-NC⁺ Molecular Ions in Noble Gas Matrices: Matrix Infrared Spectra and Electronic Structure Calculations**
Yetsedaw Tsegaw, Hongmin Li, Lester Andrews, Han-Gook Cho, Patrick Voßnacker, Helmut Beckers, Sebastian Riedel, *Chem. Eur J.* **2022**, 28, e202103142, <https://doi.org/10.1002/chem.202103142>.
- (13) **Investigation of bis(perfluoro-*tert*-butoxy) Halogenates(I/III)**
Patrick Pröhm, Willi R. Berg, Susanne M. Rupf, Patrick Voßnacker, Sebastian Riedel, *Chem. Eur. J.* **2021**, 27, 17676, <https://doi.org/10.1002/chem.202103325>.
- (14) **Activation of Tetrahydrofuran with 2-((Fluoroalkyl)thio)Benzothiazolium Reagents**
Lilian M. Maas, Jonas R. Schmid, Carlo Fasting, Patrick Voßnacker, Andreas Mavroskoufis, Matthew N. Hopkinson, *Tetrahedron* **2021**, 101, 132512, <https://doi.org/10.1016/j.tet.2021.132512>.
- (15) **Synthesis of Plakortolides E and I Enabled by Base Metal Catalysis**
Stefan Leisering, Alexandros Mavroskoufis, Patrick Voßnacker, Reinhold Zimmer, Mathias Christmann, *Org. Lett.* **2021**, 23, 4731, <https://doi.org/10.1021/acs.orglett.1c01457>.
- (16) **Conductivity and Standard Potentials of the Ionic Liquid Trihalogen Monoanions, [X₃]⁻ and [XY₂]⁻, [BrF₄]⁻, X = Cl, Br, I and Y = Cl, Br**
Tyler A. Gully, Patrick Voßnacker, Jonas R. Schmid, Sebastian Riedel, *ChemistryOpen* **2021**, 10, 255, <https://doi.org/10.1002/open.202000263>.
- (17) **Soluble Fluoridobromates as Well-Behaved Strong Fluorination Reagents**
Jonas R. Schmid, Patrick Pröhm, Patrick Voßnacker, Günther Thiele, Mathias A. Ellwanger, Simon Steinhauer, Sebastian Riedel, *Eur. J. Inorg. Chem.* **2020**, 2020, 4497, <https://doi.org/10.1002/ejic.202000847>.
- (18) **In Situ Synthesis and Applications for Polyinterhalides Based on BrCl**
Benjamin Schmidt, Sebastian Ponath, Johannes Hannemann, Patrick Voßnacker, Karsten Sonnenberg, Mathias Christmann, Sebastian Riedel, *Chem. Eur. J.* **2020**, 26, 15183, <https://doi.org/10.1002/chem.202001267>.
- (19) **Friedel-Crafts type methylation with dimethylhalonium salts**
Sebastian Hämmerling, Patrick Voßnacker, Simon Steinhauer, Helmut Beckers, Sebastian Riedel, *Chem. Eur. J.* **2020**, 26, 14377, <https://doi.org/10.1002/chem.202001457>.
- (20) **Improved Access to Organo-Soluble Di- and Tetrafluoridochlorate(I)/(III) Salts**
Patrick Pröhm, Jonas R. Schmid, Karsten Sonnenberg, Patrick Voßnacker, Simon Steinhauer, Caspar. J. Schattenberg, Robert Müller, Martin Kaupp, Sebastian Riedel, *Angew. Chem. Int. Ed.* **2020**, 59, 16002, <https://doi.org/10.1002/anie.202006268>.

- (21) **Friedel-Crafts type methylation with dimethylhalonium salts**
Lisa Mann, Patrick Voßnacker, Carsten Müller, Sebastian Riedel, *Chem. Eur. J.* **2017**, 23, 244, <https://doi.org/10.1002/chem.201605421>.

6.2. Patents

- (1) **Process for Producing Phosgene by Reaction of Polychlorine Anions and Carbon Monoxide**
Sivathmeehan Yogendra, Sebastian Riedel, Rainer Weber, Patrick Voßnacker, Yuliya Schiesser, Simon Steinhauer, Thomas Keilhack, WO2022128951 A1, **2022**
- (2) **Phosgene Synthesis by Conversion of a Gas Mixture Containing Chlorine and Carbon Monoxide on an Organic Catalyst Containing Chloride Anions**
Sivathmeehan Yogendra, Sebastian Riedel, Patrick Voßnacker, Rainer Weber, Yuliya Schiesser, Simon Steinhauer, Thomas Keilhack, WO2022128950 A1, **2022**
- (3) **Storage Medium for Storing Hydrogen Chloride and Method for Separating and Storing Hydrogen Chloride HCl from HCl containing gas**
Sebastian Riedel, Patrick Voßnacker, WO2023020942 A1, **2023**.

6.3. Conference Contributions – Oral and Poster Presentations

- (1) **Synthesis of Novel Polyhydrogenhalide Halogenates (–I)**
Patrick Voßnacker, Simon Steinhauer, Sebastian Riedel, *7. Tag der Anorganischen Chemie*, Berlin, **2019**.
- (2) **Using Hydrogen Bonding in the Synthesis of Polyhydrogenhalide Halogenates (–I)**
Patrick Voßnacker, Simon Steinhauer, Sebastian Riedel, *Halchem IX the 9th International Meeting on Halogen Chemistry*, Perugia, **2019**.
- (3) **Trichloride Salts as Chlorine Storage Media and Reagents for Phosgene Synthesis**
Patrick Voßnacker, Alisa Wüst, Thomas Keilhack, Nico Schwarze, Sebastian Riedel *GDCh-Wissenschaftsforum (WiFo) Chemie*, online, **2021**.
- (4) **Trichloride Salts as Efficient Chlorine Storage Media and Useful Chlorination Reagents**
Patrick Voßnacker, Alisa Wüst, Thomas Keilhack, Nico Schwarze, Sebastian Riedel, *21th Conference on Inorganic Chemistry (Wöhler-Vereinigung)*, Marburg, **2022**.
- (5) **Trichloride Salts as Efficient Chlorine Storage Media and Useful Chlorination Reagents**
Patrick Voßnacker, Sebastian Riedel, *8. Tag der Anorganischen Chemie*, Berlin, **2022**.

7. Curriculum Vitae

The curriculum vitae is not included for reasons of data protection

8. Appendix

8.1 SI of Synthesis and Characterization of Poly(hydrogen halide) Halogenates (–I)

Patrick Voßnacker, Simon Steinhauer, Julia Bader, Sebastian Riedel*

Chem. Eur. J. **2020**, *26*, 13256.

<https://doi.org/10.1002/chem.202001864>

© 2020 The Authors. Published by Wiley-VCH Verlag GmbH.

Chemistry–A European Journal

Supporting Information

Synthesis and Characterization of Poly(hydrogen halide) Halogenates (-I)

Patrick Voßnacker, Simon Steinhauer, Julia Bader, and Sebastian Riedel*^[a]

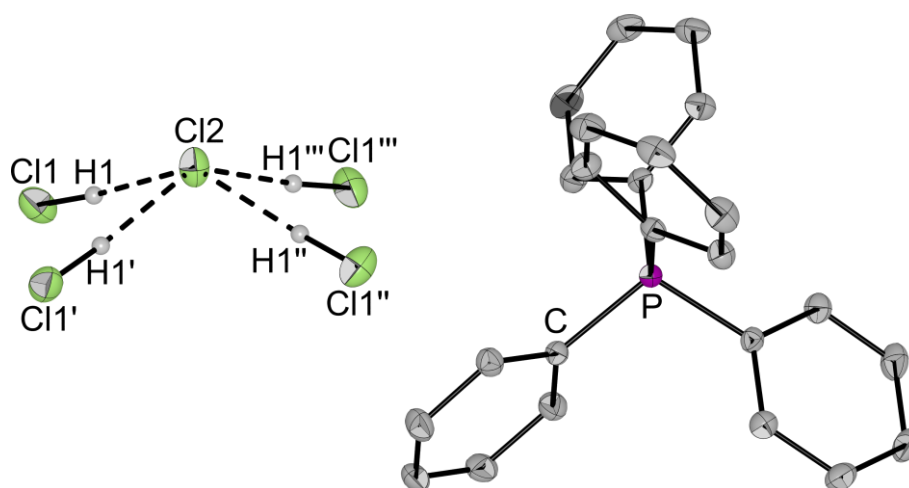
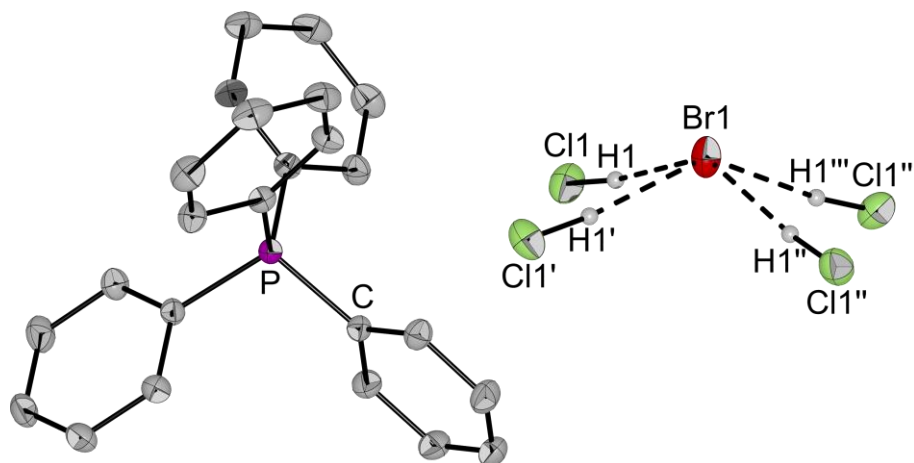
Table of Contents

a) Molecular Structures Including Cations and Disorders	2
a1. [PPh ₄][X(HCl) _n] and [AsPh ₄][Cl(HCl) ₄]	2
a2. [PPN][X(HCl) ₄]	4
a3. [PPh ₄][X(HF) ₂ (HX)]	7
a4. Further Hydrogen Bonded Structures	8
b) Experimental and Calculated Raman Spectra	10
c) Quantum Chemically Optimized Structures	14
d) Calculated Energies and Free Reaction Energies	16
d1) B3LYP(D3BJ)/def2-TZVPP Energies	16
d2) SCS-MP2/def2-TZVPP Energies	18
d3) SCS-MP2(COSMO)/def2-TZVPP Energies	20
d4) Free Reaction Energy Calculation	20
d5) Comparison of Different Geometries for the [X(HCl) ₄] ⁻ Anion	24
e) Coordinates of Optimized Structures	25
f) Calculated Vibrational Spectra	55
g) Raman Spectra of Samples Cooled to -196 °C	74

a) Molecular Structures Including Cations and Disorders

a1. $[\text{PPh}_4][\text{X}(\text{HCl})_n]$ and $[\text{AsPh}_4][\text{Cl}(\text{HCl})_4]$ **Table S 1.** Comparison of interatomic distances and angles for $[\text{PPh}_4][\text{X}(\text{HCl})_4]$ (X = Cl, Br).

Property	Cl	Br
Cl-X distance [pm]	340.1(1)	353.4(1)
Cl-X-Cl'' angle [°]	144.3 (1)	145.1(1)

**Figure S 1.** Molecular structure of $[\text{PPh}_4][\text{Cl}(\text{HCl})_4]$ in the solid state with thermal ellipsoids shown at 50 % probability.**Figure S 2.** Molecular structure of $[\text{PPh}_4][\text{Br}(\text{HCl})_4]$ in the solid state with thermal ellipsoids shown at 50 % probability. A chloride ion occupies the position of Br1 with a probability of 13.7(3) %, which might be explained by a protonation of bromide ions and the formation of Cl^- and HBr .

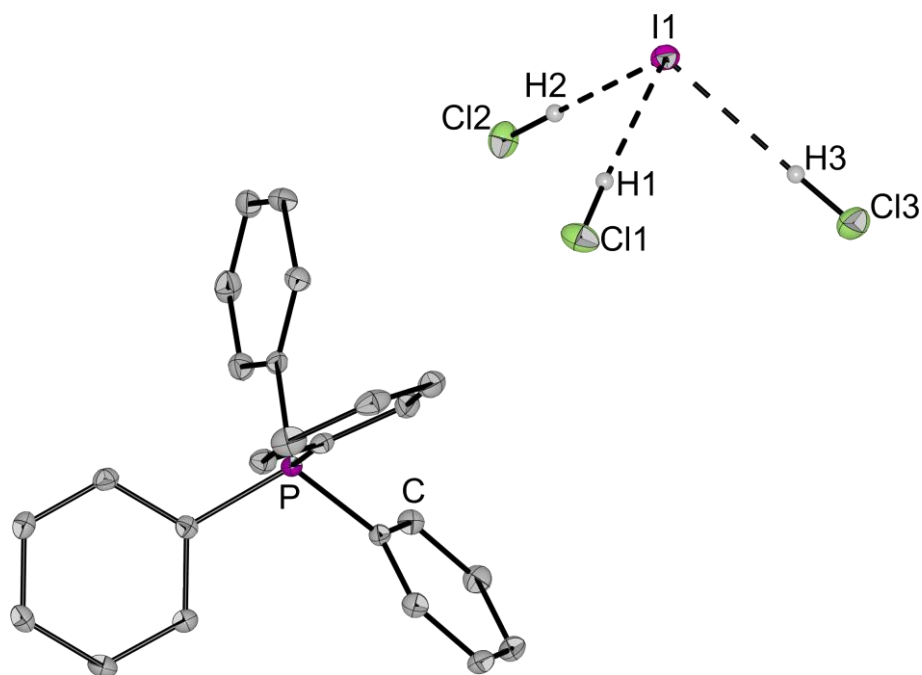


Figure S 3. Molecular structure of $[PPh_4][I(HCl)_3]$ in the solid state with thermal ellipsoids shown at 50 % probability.

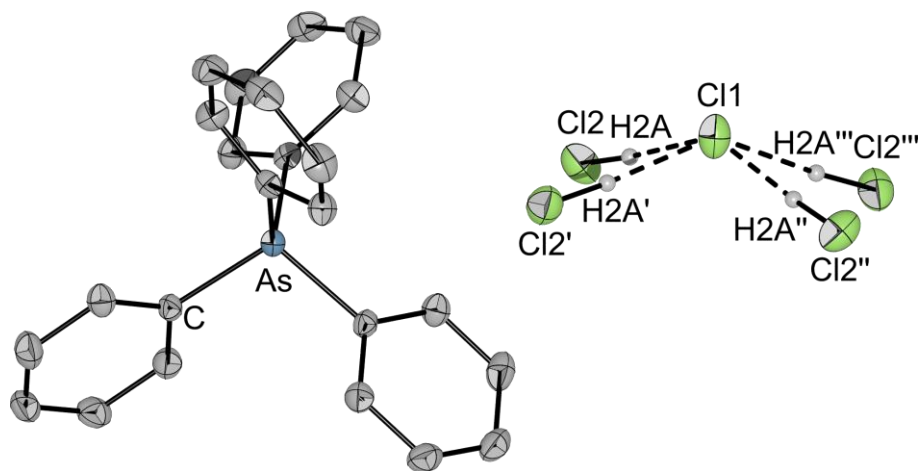
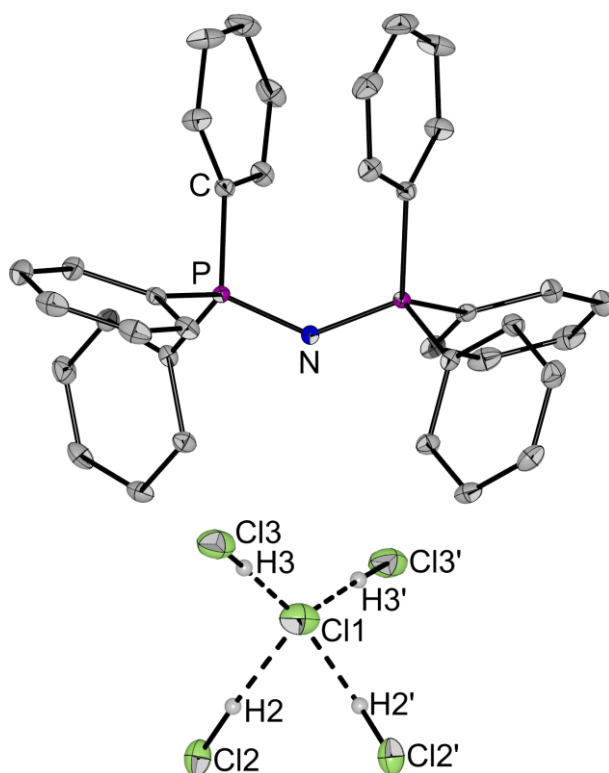


Figure S 4. Molecular structure of $[AsPh_4][Cl(HCl)_4]$ in the solid state with thermal ellipsoids shown at 50 % probability. A bromide ion occupies the position of Cl1 with a probability of 13.5(3) %, which might be explained by a contamination of the starting material.

a2. [PPN][X(HCl)₄]**Table S 2.** Comparison of interatomic distances and angles for [PPN][X(HCl)₄] (X = Cl, Br, I).

Property	Cl	Br	I
Cl-X distance (1) [pm]	334.8(1)	347.6(1)	370.4(2)
Cl-X distance (2) [pm]	341.6(1)	354.0(2)	374.8(2)
Cl-X angle (1) [°]	97.7(1)	97.7(1)	91.6(1)
Cl-X angle (2) [°]	144.1(1)	141.6(1)	138.0(1)
Cl-X angle (3) [°]	84.3(1)	84.3	89.2(1)
Cl-X angle (4) [°]	122.1(1)	122.1(1)	120.9(1)

**Figure S 5.** Molecular structure of [PPN][Cl(HCl)₄] in the solid state with thermal ellipsoids shown at 50 % probability.

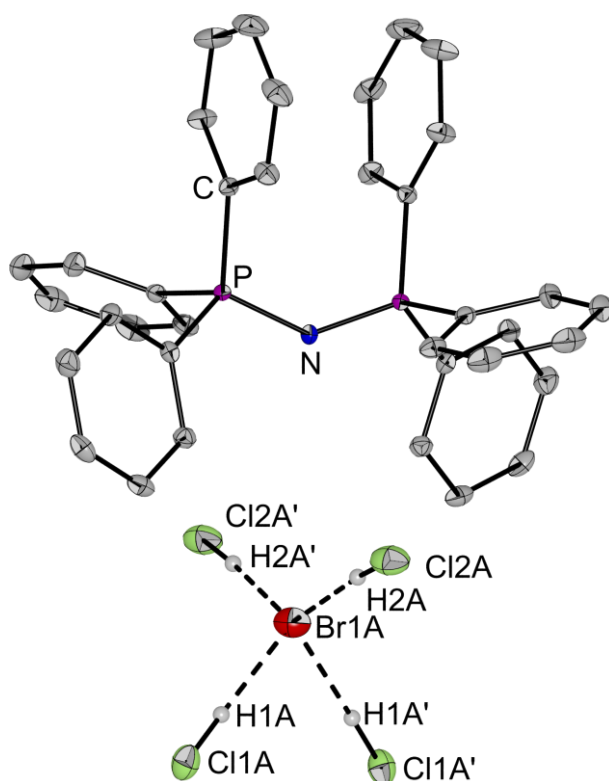


Figure S 6. Molecular structure of $[\text{PPN}][\text{Br}(\text{HCl})_4]$ in the solid state with thermal ellipsoids shown at 50 % probability.

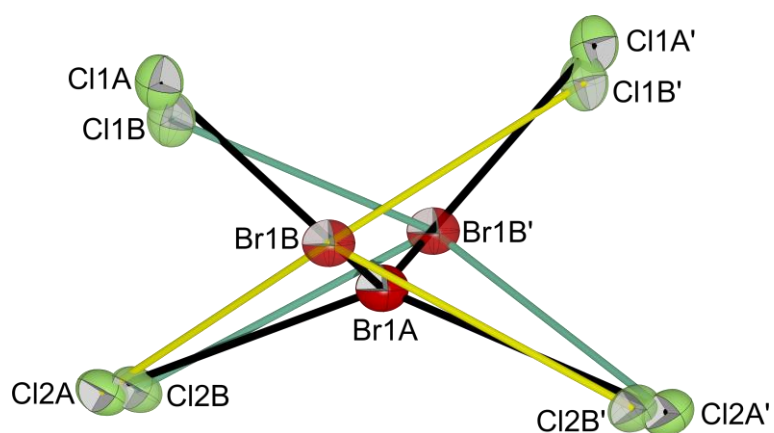


Figure S 7. Representation of the disorder of the anion in the solid state structure of $[\text{PPN}][\text{Br}(\text{HCl})_4]$. Thermal ellipsoids are shown at 50 % probability. The occupation numbers for the halide atoms were determined to be 0.928(1) for Br1A and Cl1A, 0.964(1) for Cl2A and 0.036(1) for Br1B, Cl1B and Cl2B. Therefore the anion position within the crystal is occupied by a $[\text{Br}(\text{HCl})_4]^-$ anion (black lines) with a probability of 92.8(1) % and occupied by a $[\text{Br}(\text{HCl})_3]^-$ anion (yellow and green lines) with 7.2(1) % probability.

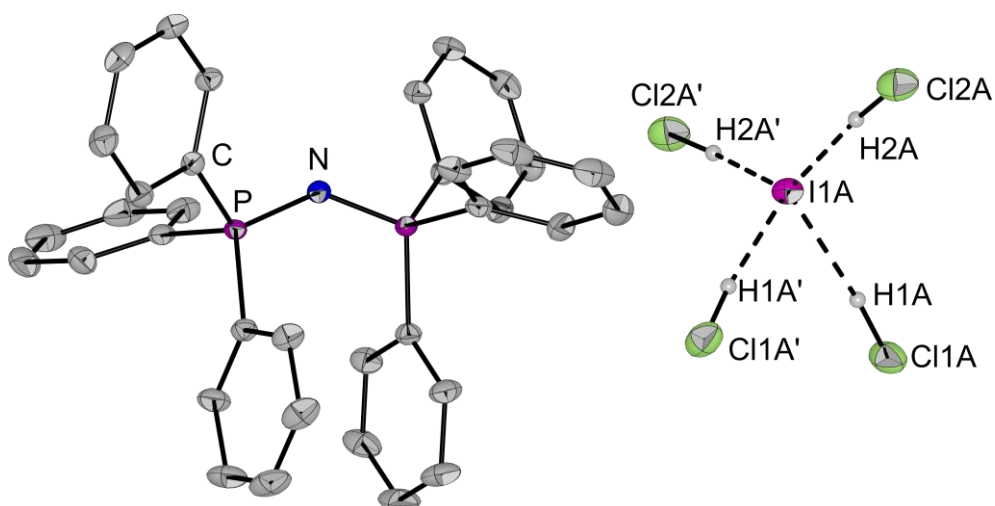


Figure S 8. Molecular structure of [PPN][I(HCl)₄] in the solid state with thermal ellipsoids shown at 50 % probability.

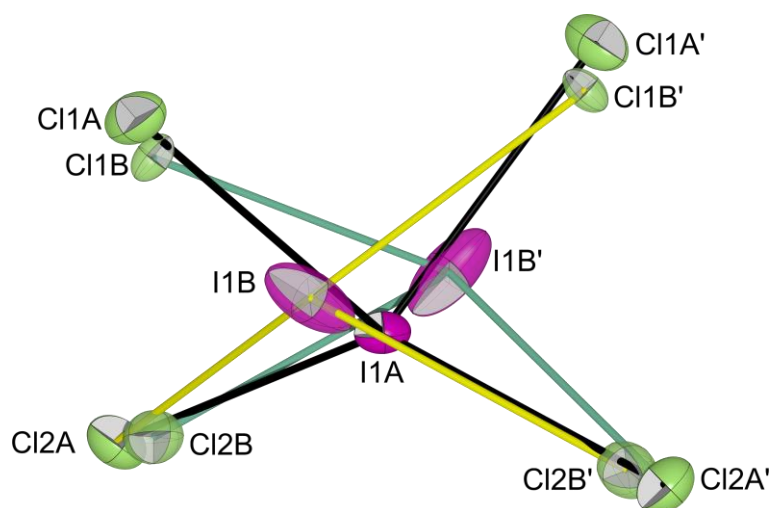


Figure S 9. Representation of the disorder of the anion in the molecular structure of [PPN][Br(HCl)₄] in the solid state. Thermal ellipsoids are shown at 50 % probability. The occupation numbers for the halogen atoms were determined to be 0.777(2) for I1A and Cl1A, 0.889(1) for Cl2A and 0.111(1) for I1B, Cl1B and Cl2B. Therefore the anion position within the crystal is occupied by a [I(HCl)₄]⁻ anion (black lines) with a probability of 77.7(2) % and occupied by a [I(HCl)₃]⁻ anion (yellow and green lines) with 22.2(1) % probability.

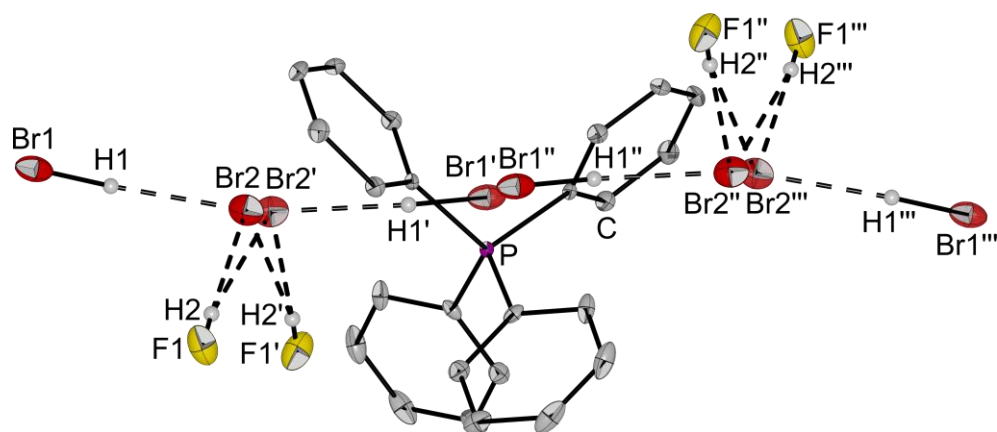
a3. $[\text{PPh}_4][\text{X}(\text{HF})_2(\text{HX})]$ 

Figure S 10. Molecular structure of $[\text{PPh}_4][\text{Br}(\text{HF})_2(\text{HBr})]$ in the solid state with thermal ellipsoids shown at 50 % probability.

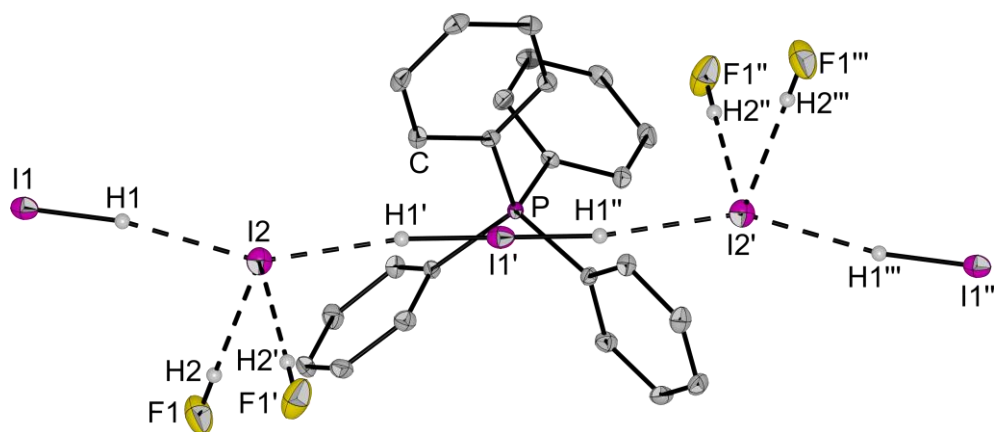


Figure S 11. Molecular structure of $[\text{PPh}_4][\text{I}(\text{HF})_2(\text{HI})]$ in the solid state with thermal ellipsoids shown at 50 % probability.

a4. Further Hydrogen Bonded Structures

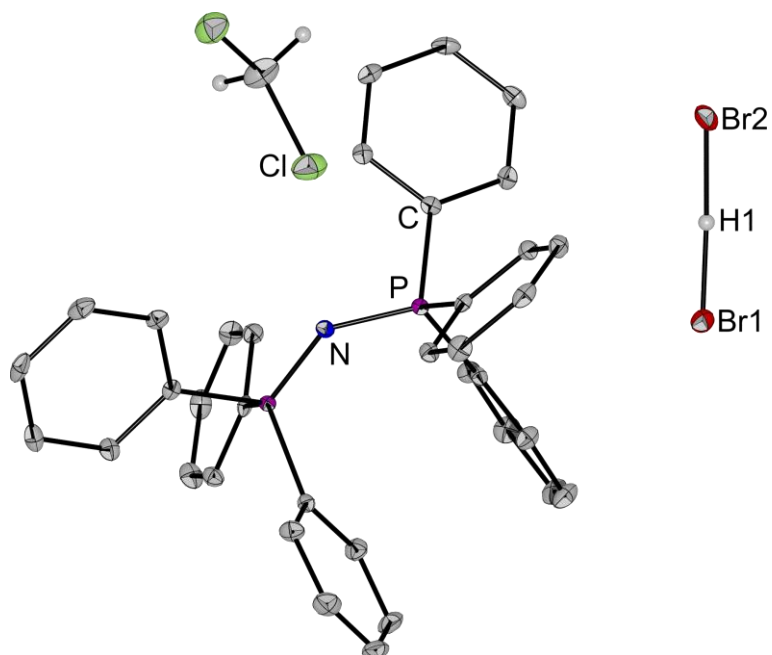


Figure S 12. Molecular structure of $[\text{PPN}][\text{BrHBr}] \cdot \text{CH}_2\text{Cl}_2$ in the solid state with $R(\text{Br1}-\text{Br2}) = 341.6(1)$ pm. Thermal ellipsoids are shown at 50 % probability.

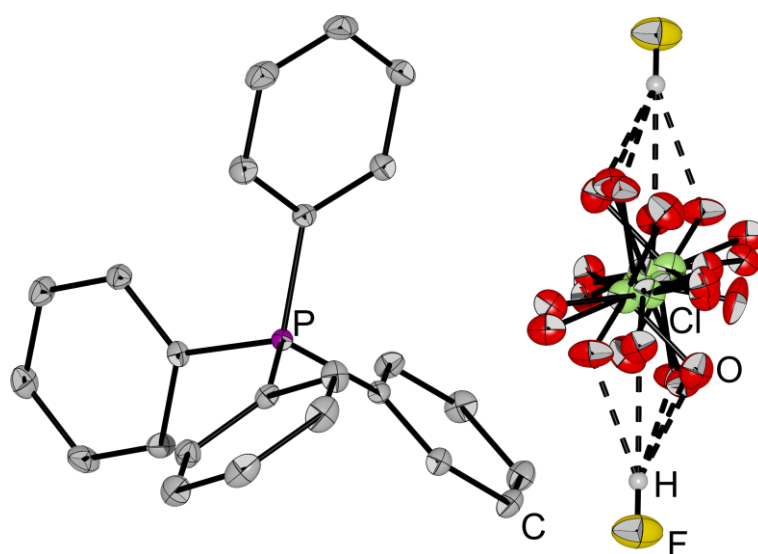


Figure S 13. Molecular structure of $[\text{PPh}_4][\text{ClO}_4(\text{HF})_2]$ in the solid state including the disorder of the perchlorate anion. Thermal ellipsoids are shown at 50 % probability.

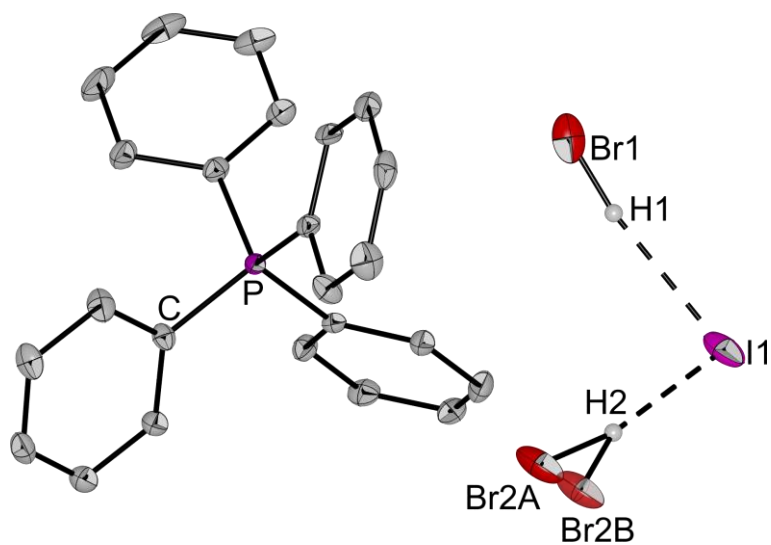


Figure S 14. Molecular structure of $[PPh_4][I(HBr)_2]$ in the solid state including the disorder of the anion. The occupation number of Br2A equals 0.741(3). Thermal ellipsoids are shown at 50 % probability.

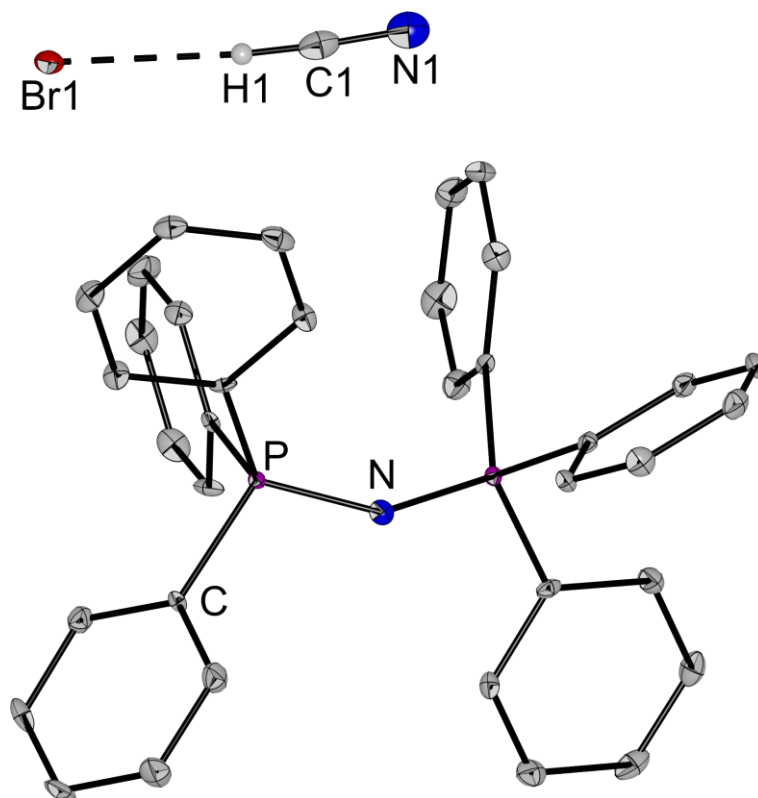


Figure S 15. Molecular structure of $[PPN][Br(HCN)]$ in the solid state. Thermal ellipsoids are shown at 50 % probability.

b) Experimental and Calculated Raman Spectra

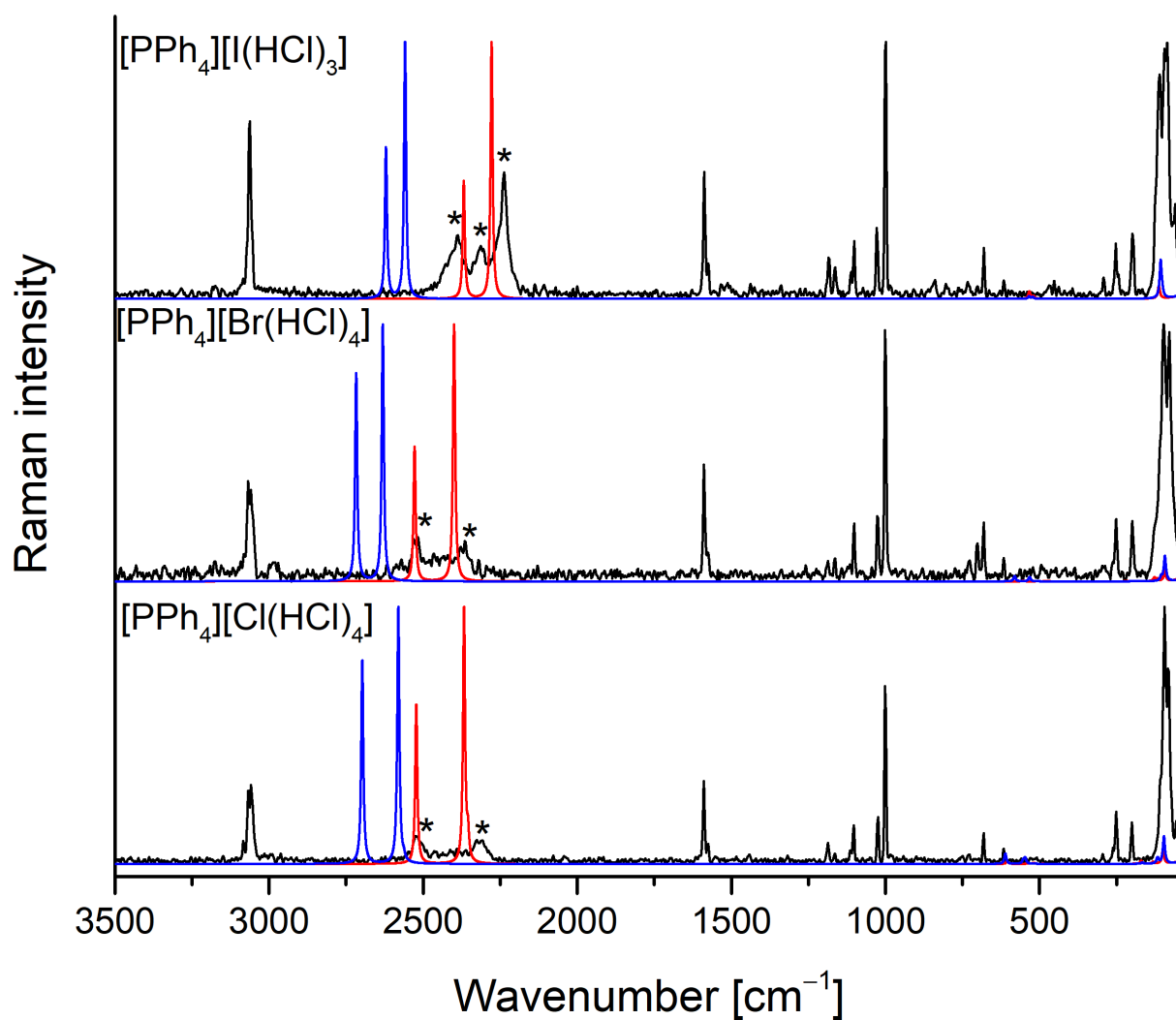


Figure S 16. Experimental (black) Raman spectrum of $[\text{PPh}_4][\text{X}(\text{HCl})_n]$ ($\text{X} = \text{Cl}, \text{Br}, \text{I}$) and calculated (B3LYP/def2-TZVPP (red) and MP2/def2-TZVPP (blue)) spectra. Bands highlighted with asterisk are associated to $[\text{X}(\text{HCl})_n]^-$.

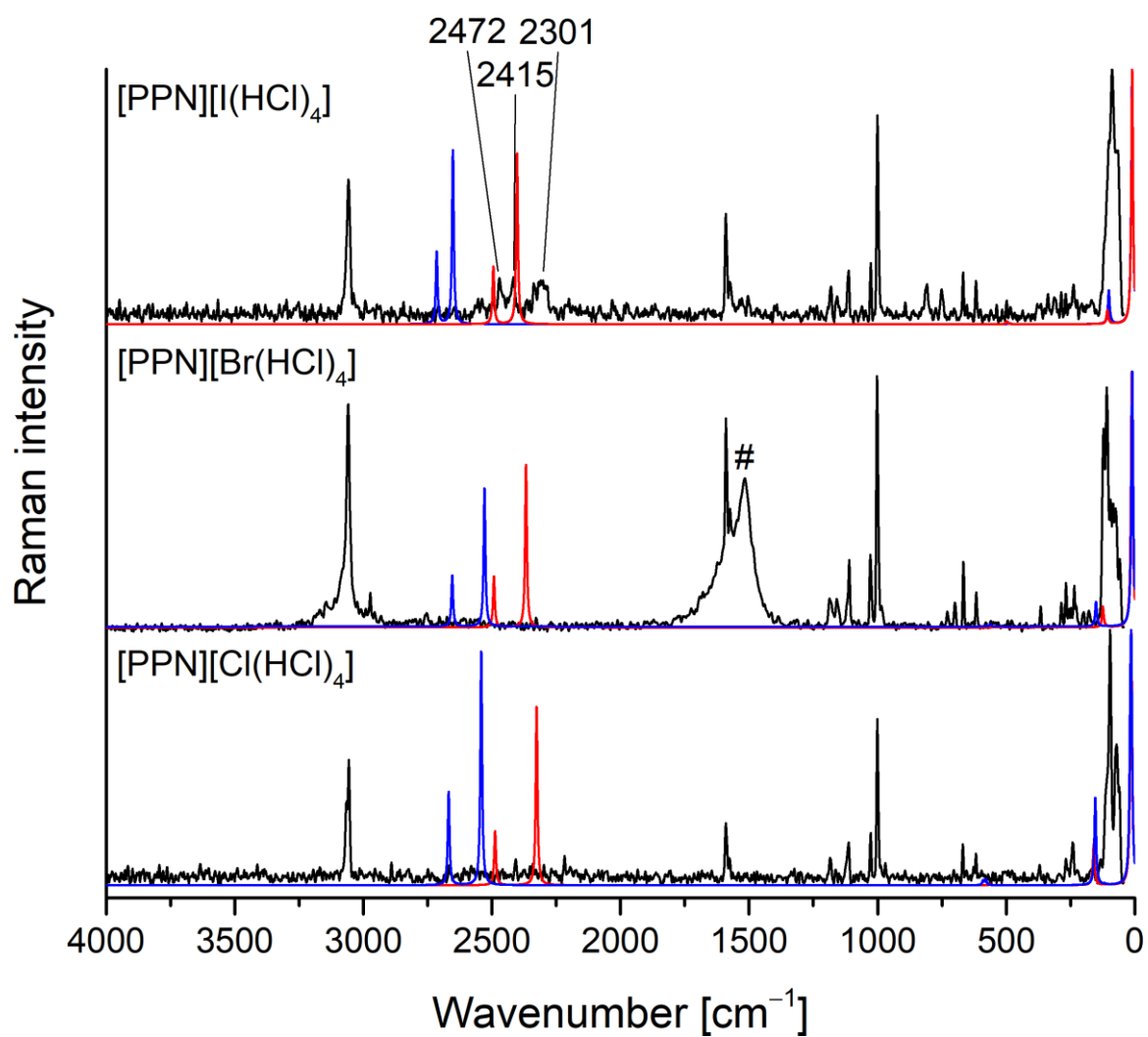


Figure S 17. Experimental (black) Raman spectrum of [PPN][X(HCl)₄] (X = Cl, Br, I) and calculated (B3LYP/def2-TZVPP (red) and MP2/def2-TZVPP (blue)) spectra. The band marked with a dagger is due to liquid oxygen resulting from the measurement at -196 °C.

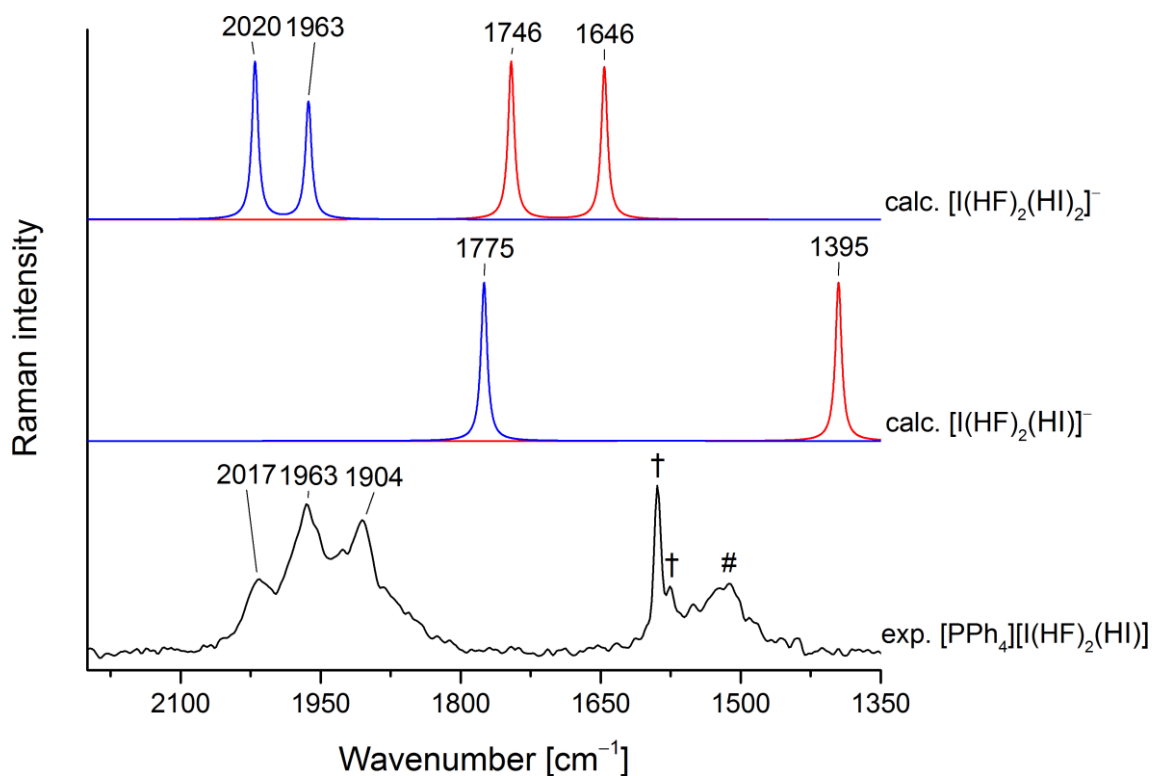


Figure S 18. Experimental (black) Raman spectrum of $[\text{PPh}_4][\text{I}(\text{HF})_2(\text{HI})]$ and calculated (B3LYP/def2-TZVPP (red) and MP2/def2-TZVPP (blue)) spectra of $[\text{I}(\text{HF})_2(\text{HI})]^-$, $[\text{I}(\text{HF})_2(\text{HI})_2]^-$. Bands highlighted with a hash belong to the cation, while bands highlighted with a dagger are due to liquid oxygen resulting from the measurement at -196°C .

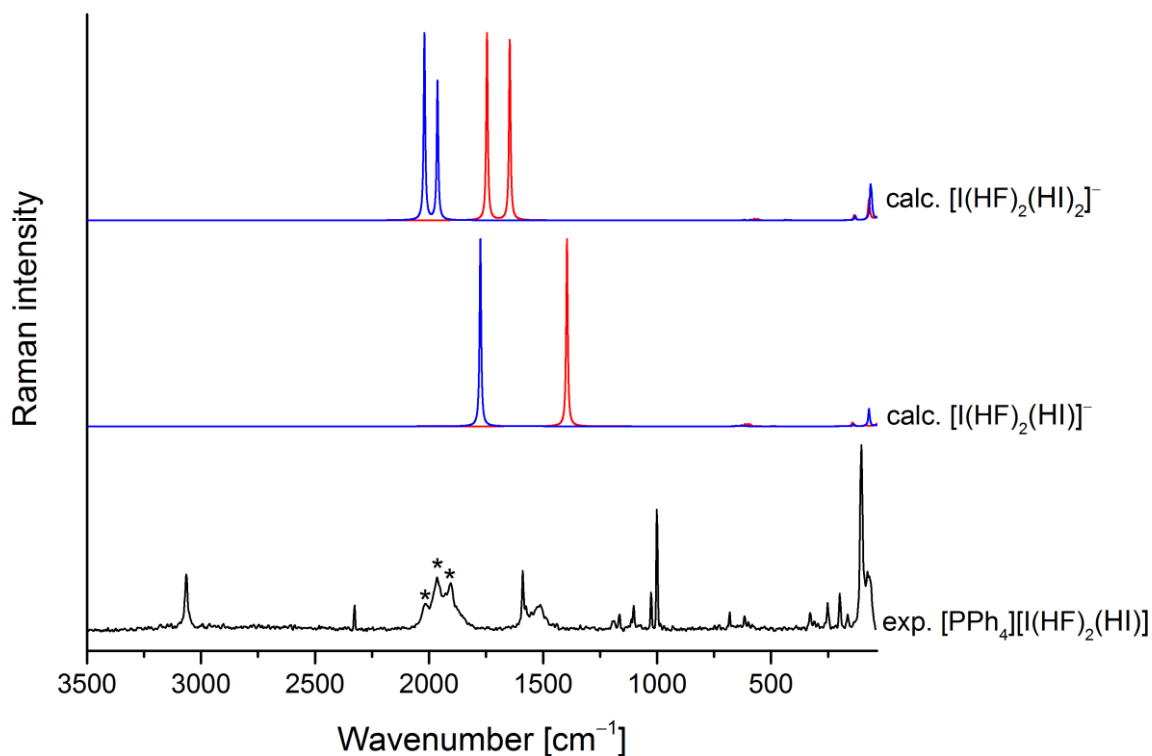


Figure S 19. Experimental (black) Raman spectrum of $[\text{PPh}_4][\text{I}(\text{HF})_2(\text{HI})]$ and calculated (B3LYP/def2-TZVPP (red) and MP2/def2-TZVPP (blue)) spectra of $[\text{I}(\text{HF})_2(\text{HI})]^-$, $[\text{I}(\text{HF})_2(\text{HI})_2]^-$. Bands highlighted with an asterisk are associated to $[\text{I}(\text{HF})_2(\text{HI})]^-$.

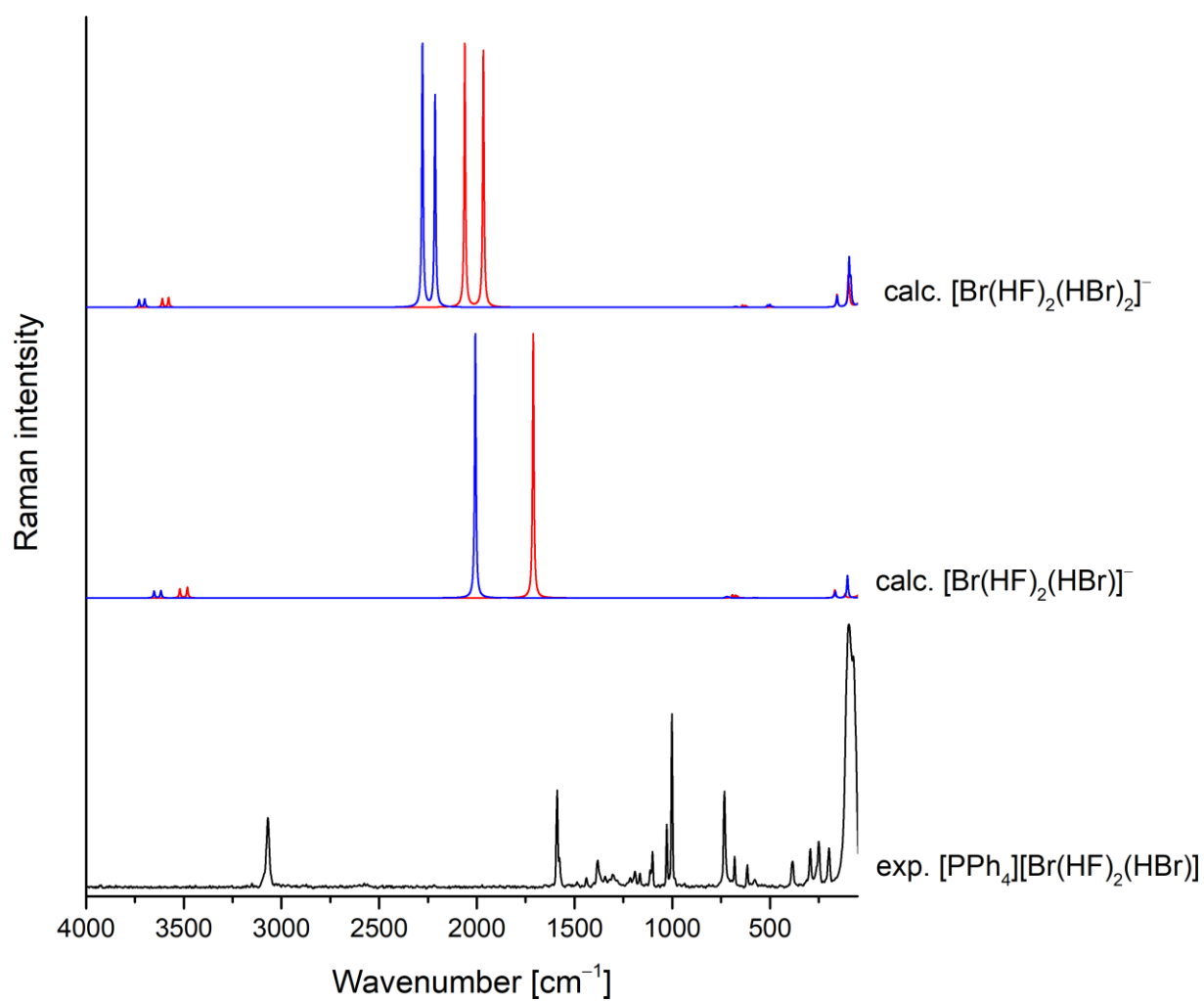


Figure S 20. Experimental (black) Raman spectrum of $[\text{PPh}_4][\text{Br}(\text{HF})_2(\text{HBr})]$ and calculated (B3LYP/def2-TZVPP (red) and MP2/def2-TZVPP (blue)) spectra of $[\text{Br}(\text{HF})_2(\text{HBr})]^-$.

c) Quantum Chemically Optimized Structures

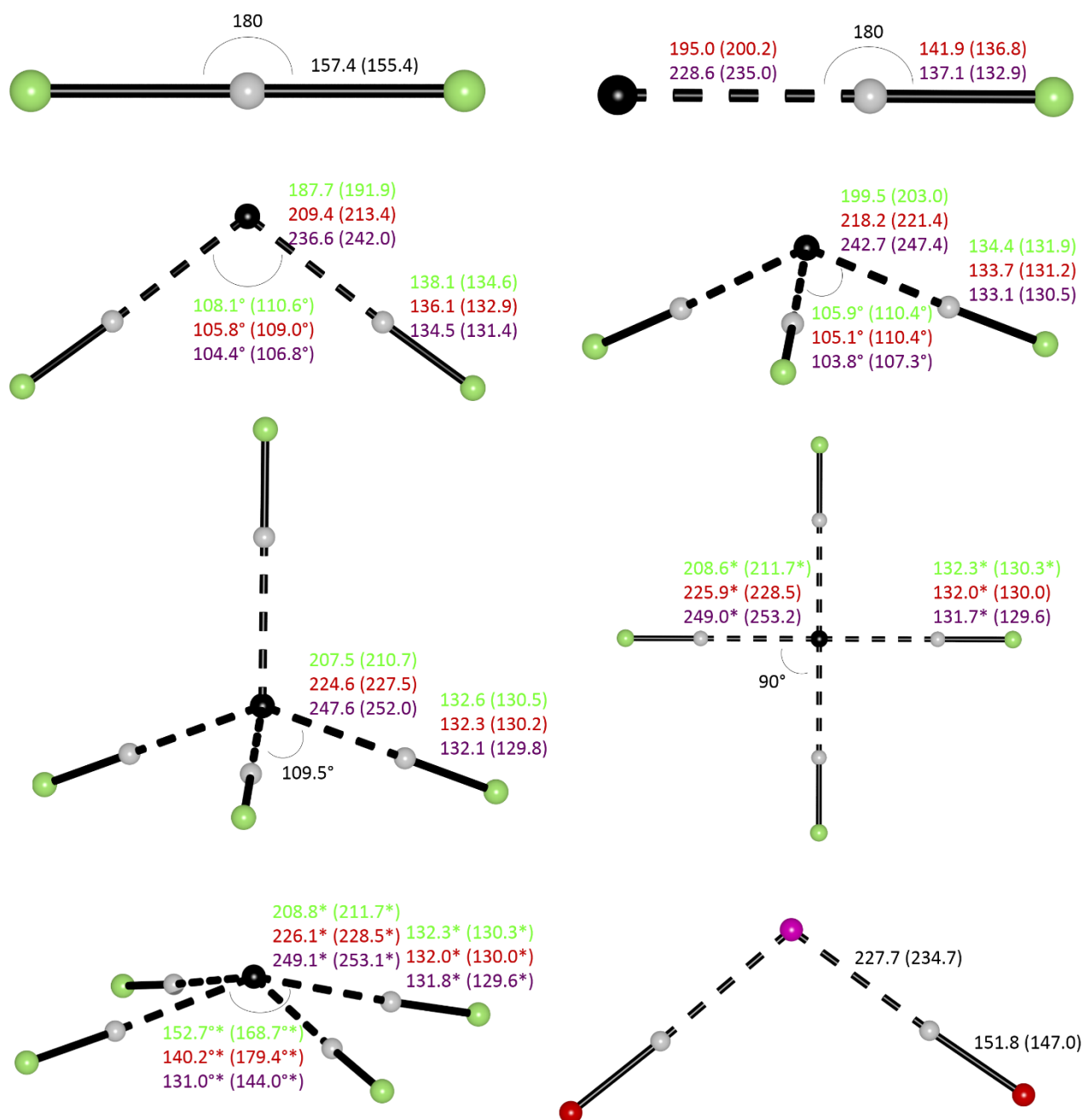


Figure S 21. Optimized structures of $[X(HY)_n]^-$ ($n = 1, 3, 4$ ($X = \text{Cl, Br, I}; Y = \text{Cl}$), $n = 2$ ($X = \text{Cl, Br, I}; Y = \text{Cl, Br}$ (only for $X = \text{I}$))) calculated on the B3LYP(D3BJ)/def2-TZVPP (MP2/def2-TZVPP) level of theory. Bond distances are given in pm. For structures with colored annotations, the central atom of the structure is a chloride (green), bromide (red) or iodide (violet). Bond length marked with an asterisk belong to non-minimum structures.

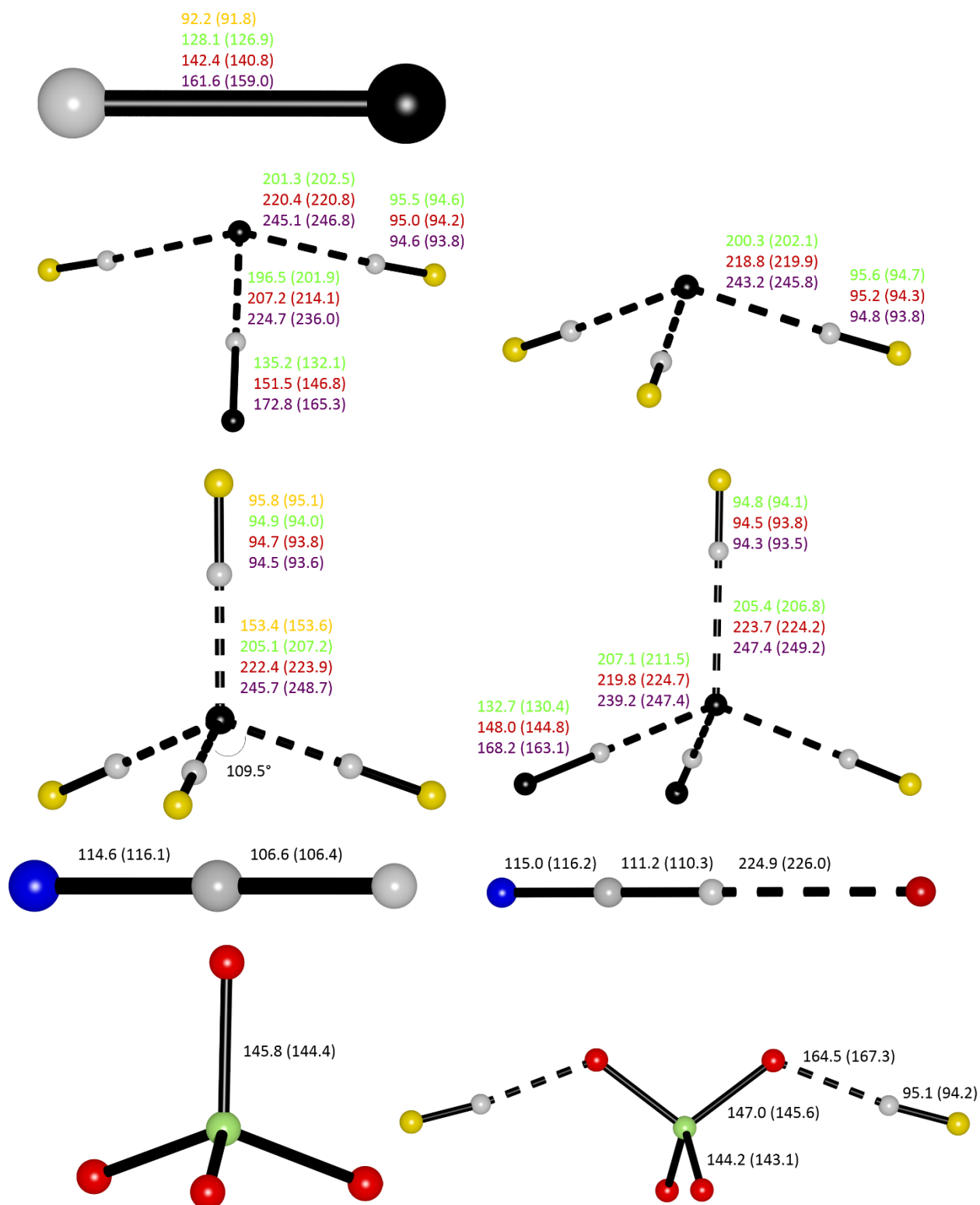


Figure S 22. Optimized structures of HX ($X = \text{F}, \text{Cl}, \text{Br}, \text{I}, \text{CN}$), $[\text{X}(\text{HY})_n]^-$ ($n = 1$ ($X = \text{Br}; Y = \text{CN}$), $n = 2$ ($X = \text{ClO}_4; Y = \text{F}$)) and $[\text{X}(\text{HF})_2(\text{HX})_n]^-$ ($n = 1, 2; X = \text{Cl}, \text{Br}, \text{I}$) calculated on the B3LYP(D3BJ)/def2-TZVPP (MP2/def2-TZVPP) level of theory. Bond distances are given in pm. For structures with colored annotations, the black atoms are equal to chlorine (green), bromine (red) or iodine (violet).

d) Calculated Energies and Free Reaction Energies

d1) B3LYP(D3BJ)/def2-TZVPP Energies

All Free Enthalpy calculations were carried out for T = 298.15 K and p = 1.0 bar if not stated otherwise.

Table S 3. Calculated energies on the B3LYP(D3BJ)/def2-TZVPP level of theory.

Verbindung	$E_{\text{tot}} [E_{\text{H}}]$	$E_{\text{tot}} [\text{kJ/mol}^{-1}]$	G (kJ mol ⁻¹)
F ⁻	-99.83878290	-262126.72	-262163.89
Cl ⁻	-460.22009153	-1208307.85	-1208347.34
Br ⁻	-2574.12130509	-6758355.49	-6758398.00
I ⁻	-297.79901555	-781871.32	-781915.54
[ClHCl] ⁻	-921.03498878	-2418177.36	-2418221.40
[Br(HCl)] ⁻	-3034.92480079	-7968195.06	-7968242.33
[I(HCl)] ⁻	-758.59431186	-1991689.37	-1991738.45
[Cl(HCl) ₂] ⁻	-1381.83086281	-3627996.93	-3628038.71
[Br(HCl) ₂] ⁻	-3495.71844848	-9178008.79	-9178054.78
[I(HCl) ₂] ⁻	-1219.38440676	-3201493.76	-3201543.55
[Cl(HCl) ₃] ⁻	-1842.62129282	-4837802.20	-4837839.27
[Br(HCl) ₃] ⁻	-3956.50712263	-10387809.45	-10387852.55
[I(HCl) ₃] ⁻	-1680.17097613	-4411288.90	-4411337.29
[Cl(HCl) ₄] ⁻ (<i>T_d</i>)	-2303.40766790	-6047596.83	-6047628.85
[Br(HCl) ₄] ⁻ (<i>T_d</i>)	-4417.29227743	-11597600.87	-11597640.15
[I(HCl) ₄] ⁻ (<i>T_d</i>)	-2140.95474183	-5621076.67	-5621122.09
[Cl(HCl) ₄] ⁻ (<i>C_{4v}</i>)	-2303.40537183	-6047590.80	-
[Br(HCl) ₄] ⁻ (<i>C_{4v}</i>)	-4417.29053744	-11597596.31	-
[I(HCl) ₄] ⁻ (<i>C_{4v}</i>)	-2140.95342236	-5621073.21	-
[Cl(HCl) ₄] ⁻ (<i>D_{4h}</i>)	-2303.40521150	-6047590.38	-
[Br(HCl) ₄] ⁻ (<i>D_{4h}</i>)	-4417.29018688	-11597595.39	-
[I(HCl) ₄] ⁻ (<i>D_{4h}</i>)	-2140.95285991	-5621071.73	-

8.1 *SI of Synthesis and Characterization of Poly(hydrogen halide) Halogenates (-I)*

Verbindung	$E_{\text{tot}} [E_{\text{H}}]$	$E_{\text{tot}} [\text{kJ/mol}^{-1}]$	$G (\text{kJ mol}^{-1})$
HF	-100.45529924	-263745.39	-263764.34
HCl	-460.76800069	-1209746.39	-1209775.98
HBr	-2574.64739822	-6759736.74	-6759771.82
HI	-298.30894626	-783210.14	-783249.49
$[\text{Cl}(\text{HF})_3]^-$	-761.69417796	-1999828.06	-1999828.94
$[\text{Br}(\text{HF})_3]^-$	-2875.57908480	-7549832.89	-7549840.04
$[\text{I}(\text{HF})_3]^-$	-599.24170540	-1573309.10	-1573321.72
$[\text{F}(\text{HF})_4]^-$	-501.86273987	-1317640.62	-1317602.35
$[\text{Cl}(\text{HF})_4]^-$	-862.17285192	-2263634.82	-2263617.09
$[\text{Br}(\text{HF})_4]^-$	-2976.05574034	-7813634.35	-7813623.94
$[\text{I}(\text{HF})_4]^-$	-699.71613583	-1837104.71	-1837101.53
$[\text{Cl}(\text{HF})_2(\text{HCl})]^-$	-1122.00327912	-2945819.61	-2945835.14
$[\text{Br}(\text{HF})_2(\text{HBr})]^-$	-5349.76873758	-14045817.82	-14045844.97
$[\text{I}(\text{HF})_2(\text{HI})]^-$	-797.09272783	-2092766.96	-2092803.93
$[\text{Cl}(\text{HF})_2(\text{HCl})_2]^-$	-1582.79017767	-4155615.61	-4155626.89
$[\text{Br}(\text{HF})_2(\text{HBr})_2]^-$	-7924.43294153	-20805598.69	-20805628.50
$[\text{I}(\text{HF})_2(\text{HI})_2]^-$	-1095.41551949	-2876013.45	-2876059.60
HCN	-93.41448394	-245259.73	-245268.06
$[\text{Br}(\text{HCN})]^-$	-2667.57045814	-7003706.24	-7003731.25
$[\text{ClO}_4]^-$	-760.88102990	-1997693.14	-1997717.60
$[\text{ClO}_4(\text{HF})_2]^-$	-961.84615092	-2525327.07	-2525321.74
$[\text{I}(\text{HBr})_2]^-$	-5447.14613091	-14301482.17	-14301543.31

d2) SCS-MP2/def2-TZVPP Energies

Table S 4. Calculated energies on the SCS-MP2/def2-TZVPP level of theory.

Verbindung	E_{tot} [E _H]	E_{MP2} [E _H]	$E_{\text{tot+MP2}}$ [kJ/mol ⁻¹]	G (kJ mol ⁻¹)
F ⁻	-99.44317906	-0.28553667	-261837.74	-261874.91
Cl ⁻	-459.55562243	-0.34621209	-1207472.27	-1207511.75
Br ⁻	-2572.48103042	-0.3269252	-6754907.29	-6754949.80
I ⁻	-296.74067393	-0.52332097	-780466.62	-780510.85
[ClHCl] ⁻	-919.68258054	-0.71488027	-2416503.53	-2416548.15
[Br(HCl)] ⁻	-3032.60126224	-0.69261723	-7963913.08	-7963958.39
[I(HCl)] ⁻	-756.85498183	-0.88706869	-1989451.75	-1989498.66
[Cl(HCl) ₂] ⁻	-1379.80304795	-1.07440499	-3625493.75	-3625532.33
[Br(HCl) ₂] ⁻	-3492.71796406	-1.05412848	-9172898.63	-9172941.03
[I(HCl) ₂] ⁻	-1216.96744012	-1.24878262	-3198426.69	-3198472.71
[Cl(HCl) ₃] ⁻	-1839.91936951	-1.43369196	-4834472.46	-4834505.44
[Br(HCl) ₃] ⁻	-3952.83175140	-1.41445618	-10381873.42	-10381911.75
[I(HCl) ₃] ⁻	-1677.07819556	-1.60943753	-4407394.38	-4407437.56
[Cl(HCl) ₄] ⁻ (<i>T_d</i>)	-2300.03278462	-1.79243470	-6043442.11	-6043466.68
[Br(HCl) ₄] ⁻ (<i>T_d</i>)	-4412.94331240	-1.77412492	-11590840.63	-11590872.65
[I(HCl) ₄] ⁻ (<i>T_d</i>)	-2137.18750295	-1.96940329	-5616356.46	-5616394.51
[Cl(HCl) ₄] ⁻ (<i>C_{4v}</i>)	-2300.03034246	-1.79274818	-6043436.52	-
[Br(HCl) ₄] ⁻ (<i>C_{4v}</i>)	-4412.94147674	-1.77454505	-11590836.92	-
[I(HCl) ₄] ⁻ (<i>C_{4v}</i>)	-2137.18601756	-1.96956624	-5616352.99	-
[Cl(HCl) ₄] ⁻ (<i>D_{4h}</i>)	-2300.03039555	-1.79269401	-6043436.52	-
[Br(HCl) ₄] ⁻ (<i>D_{4h}</i>)	-4412.94147688	-1.77454523	-11590836.92	-11590864.57
[I(HCl) ₄] ⁻ (<i>D_{4h}</i>)	-2137.18623150	-1.96929017	-5616352.82	-5616396.26
HF	-100.06531033	-0.28555788	-263471.20	-263489.53
HCl	-460.09919729	-0.35546237	-1208923.71	-1208952.42
HBr	-2573.00161502	-0.33803472	-6756303.25	-6756337.53
HI	-297.24261157	-0.53552182	-781816.49	-781854.83

8.1 SI of Synthesis and Characterization of Poly(hydrogen halide) Halogenates (-I)

Verbindung	E_{tot} [E _H]	E_{MP2} [E _H]	$E_{\text{tot+MP2}}$ [kJ/mol ⁻¹]	G (kJ mol ⁻¹)
[Cl(HF) ₃] ⁻	-759.83733362	-1.21746339	-1998149.37	-1998145.70
[Br(HF) ₃] ⁻	-2872.74826668	-1.19844224	-7545547.08	-7545550.13
[I(HF) ₃] ⁻	-596.99304707	-1.39365936	-1571064.30	-1571071.78
[F(HF) ₄] ⁻	-499.88269487	-1.44276685	-1316230.00	-1316187.06
[Cl(HF) ₄] ⁻	-859.92224572	-1.50526207	-2261677.92	-2261655.64
[Br(HF) ₄] ⁻	-2972.83074047	-1.48706458	-7809071.40	-7809055.51
[I(HF) ₄] ⁻	-697.07269585	-1.68251934	-1834581.82	-1834577.63
[Cl(HF) ₂ (HCl)] ⁻	-1119.86466933	-1.28949297	-2943590.25	-2943603.66
[Br(HF) ₂ (HBr)] ⁻	-5345.67730279	-1.25411993	-14038368.45	-
[I(HF) ₂ (HI)] ⁻	-794.16045856	-1.64842598	-2089396.23	-2089430.07
[Cl(HF) ₂ (HCl) ₂] ⁻	-1579.97762209	-1.64863075	-4152559.73	-4152564.22
[Br(HF) ₂ (HBr) ₂] ⁻	-7918.68950195	-1.59711763	-20794712.52	-20794735.56
[I(HF) ₂ (HI) ₂] ⁻	-1091.40906448	-2.18995181	-2871244.22	-2871284.31
HCN	-92.91031160	-0.38185792	-244938.59	-244947.72
[Br(HCN)] ⁻	-2665.42020359	-0.71296727	-6999932.64	-6999955.88
[ClO ₄] ⁻	-758.83986267	-1.36504250	-1995917.98	-1995939.28
[ClO ₄ (HF) ₂] ⁻	-959.01336844	-1.94300522	-2522990.96	-2522979.41
[I(HBr) ₂] ⁻	-5442.77003718	-1.21681424	-14293187.48	-14293245.47

d3) SCS-MP2(COSMO)/def2-TZVPP Energies

Table S 5. Calculated energies on the SCS-MP2/def2-TZVPP level of theory including a COSMO solvent model ($\epsilon_r = 83.6$).

Verbindung	$E_{\text{tot+MP2+Cosmo}} [E_H]$	G [kJ mol ⁻¹]	G ^{220 K} [kJ mol ⁻¹]
HF	-100.35975152	-263463.48	-263500.3976
HCl	-460.45952135	-1208735.39	-1208951.353
HBr	-2573.34382115	-6755062.13	-6756333.602
HI	-297.78122862	-781714.29	-781847.3757
[F(HF) ₄] ⁻	-501.40579715	-1316154.36	-1316374.78
[Cl(HF) ₄] ⁻	-861.50159252	-2261429.29	-2261825.281
[Br(HF) ₄] ⁻	-2974.39012800	-7807767.83	-7809219.091
[I(HF) ₄] ⁻	-698.82498418	-1834412.56	-1834723.916
F ⁻	-99.87812886	-262217.26	-262216.13
Cl ⁻	-460.02518246	-1207605.59	-1207604.46
Br ⁻	-2572.92321899	-6753965.96	-6753964.83
I ⁻	-297.36910044	-780638.12	-780636.99

d4) Free Reaction Energy Calculation

Table S 6. ΔE and ΔG for the reaction of $[X(\text{HCl})_n]^- + \text{HCl} \rightarrow [X(\text{HCl})_{n+1}]^-$ calculated on the B3LYP(D3BJ)/def2-TZVPP and SCS-MP2/def2-TZVPP level of theory.

X	n	$\Delta E_{B3LYP} [\text{kJ mol}^{-1}]$	$\Delta G_{B3LYP} [\text{kJ mol}^{-1}]$	$\Delta E_{MP2} [\text{kJ mol}^{-1}]$	$\Delta G_{MP2} [\text{kJ mol}^{-1}]$
Cl	1	-73.18	-41.33	-66.51	-31.76
Cl	2	-58.89	-24.59	-55.00	-20.69
Cl	3	-48.24	-13.60	-45.94	-8.82
Br	1	-67.34	-36.47	-61.84	-30.22
Br	2	-54.28	-21.80	-51.08	-18.30
Br	3	-45.04	-11.63	-43.50	-8.48
I	1	-58.01	-29.13	-51.23	-21.63
I	2	-48.75	-17.76	-43.98	-12.43
I	3	-41.39	-8.83	-38.37	-4.53

Table S 7. ΔE and ΔG for the reaction of $[X(\text{HF})_4]^- + \text{HF} \rightarrow [\text{F}(\text{HF})_4]^- + \text{HX}$ calculated on the B3LYP(D3BJ)/def2-TZVPP and SCS-MP2/def2-TZVPP level of theory.

X	ΔE_{B3LYP} [kJ mol ⁻¹]	ΔG_{B3LYP} [kJ mol ⁻¹]	ΔE_{MP2} [kJ mol ⁻¹]	ΔG_{MP2} [kJ mol ⁻¹]
Cl	-6.80	3.10	-4.58	5.70
Br	2.37	14.10	9.35	20.45
I	-0.66	14.03	6.53	25.27

Table S 8. ΔE , ΔG (298 K and 220 K) and K_{eq} (298 K and 220 K) for the reaction of $[X(\text{HF})_4]^- + \text{HF} \rightarrow [\text{F}(\text{HF})_4]^- + \text{HX}$ calculated on the SCS-MP2(COSMO)/def2-TZVPP level of theory.

X	$\Delta E_{\text{COSMO,MP2}}$ [kJ mol ⁻¹]	$\Delta G^{298\text{K}}_{\text{COSMO,MP2}}$ [kJ mol ⁻¹]	K_{eq} (298 K)	$\Delta G^{220\text{K}}_{\text{COSMO,MP2}}$ [kJ mol ⁻¹]	K_{eq} (220 K)
Cl	-10.43	3.02	0.2959	-0.45	1.2824
Br	0.69	14.82	0.0025	11.11	0.0023
I	-6.01	7.40	0.0505	2.16	0.3074

Table S 9. ΔE and ΔG for the reaction of $X^- + \text{HF} \rightarrow \text{F}^- + \text{HX}$ calculated on the B3LYP(D3BJ)/def2-TZVPP and SCS-MP2/def-TZVPP level of theory.

X	ΔE_{B3LYP} [kJ mol ⁻¹]	ΔG_{B3LYP} [kJ mol ⁻¹]	ΔE_{MP2} [kJ mol ⁻¹]	ΔG_{MP2} [kJ mol ⁻¹]
Cl	180.13	171.81	182.02	173.96
Br	237.41	226.62	237.50	226.89
I	279.84	266.50	283.59	270.64

Table S 10. ΔE , ΔG (298 K and 220 K) and K_{eq} (298 K and 220 K) for the reaction of $X^- + \text{HF} \rightarrow \text{F}^- + \text{HX}$ calculated on the SCS-MP2(COSMO)/def2-TZVPP level of theory.

X	$\Delta E_{\text{COSMO,MP2}}$ [kJ mol ⁻¹]	$\Delta G^{298\text{K}}_{\text{COSMO,MP2}}$ [kJ mol ⁻¹]	K_{eq} (298 K)	$\Delta G^{220\text{K}}_{\text{COSMO,MP2}}$ [kJ mol ⁻¹]	K_{eq} (220 K)
Cl	124,14	116,44	3,88E-21	117,45	1,295E-28
Br	160,21	150,08	4,92E-27	152,02	8,026E-37
I	182,46	170,09	1,53E-30	172,63	1,026E-41

Table S 11. ΔE and ΔG for the reaction of $X^- + 4 HF \rightarrow [X(HF)_4]^-$ calculated on the B3LYP(D3BJ)/def2-TZVPP and SCS-MP2/def-TZVPP level of theory.

X	ΔE_{B3LYP} [kJ mol ⁻¹]	ΔG_{B3LYP} [kJ mol ⁻¹]	ΔE_{MP2} [kJ mol ⁻¹]	ΔG_{MP2} [kJ mol ⁻¹]
F	-532.35	-381.11	-507.44	-354.01
Cl	-345.42	-212.40	-320.84	-185.75
Br	-297.31	-168.59	-279.29	-147.57
I	-251.85	-128.64	-230.38	-108.64

Table S 12. ΔE and ΔG for the reaction of $[X(HF)_4]^- + 2 HX \rightarrow [X(HF)_2(HX)_2]^- + 2 HF$ calculated on the B3LYP(D3BJ)/def2-TZVPP and SCS-MP2/def-TZVPP level of theory.

X	ΔE_{B3LYP} [kJ mol ⁻¹]	ΔG_{B3LYP} [kJ mol ⁻¹]	ΔE_{MP2} [kJ mol ⁻¹]	ΔG_{MP2} [kJ mol ⁻¹]
Cl	-21.21	-13.48	-23.20	-17.19
Br	-18.37	-10.41	-22.97	-15.94
I	-20.77	-12.24	-28.17	-23.91

Table S 13. ΔE and ΔG for the reaction of $[X(HF)_3]^- + HX \rightarrow [X(HF)_2(HX)]^- + HF$ calculated on the B3LYP(D3BJ)/def2-TZVPP and SCS-MP2/def-TZVPP level of theory.

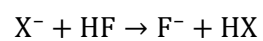
X	ΔE_{B3LYP} [kJ mol ⁻¹]	ΔG_{B3LYP} [kJ mol ⁻¹]	ΔE_{MP2} [kJ mol ⁻¹]	ΔG_{MP2} [kJ mol ⁻¹]
Cl	-9.45	-5.44	-11.62	-4.92
Br	-6.42	-2.55	-10.68	-
I	-6.89	-2.94	-13.36	-7.01

Table S 14. ΔE and ΔG for the reaction of $[Br(HCl)]^- + HCN \rightarrow [Br(HCN)]^- + 2 HCl$ calculated on B3LYP(D3BJ)/def2-TZVPP and SCS-MP2/def-TZVPP level of theory.

ΔE_{B3LYP} [kJ mol ⁻¹]	ΔG_{B3LYP} [kJ mol ⁻¹]	ΔE_{MP2} [kJ mol ⁻¹]	ΔG_{MP2} [kJ mol ⁻¹]
2.17	3.17	-4.68	-2.19

Table S 15. ΔE and ΔG for the reaction of $[ClO_4]^- + 2 HF \rightarrow [ClO_4(HF)_2]^-$ calculated on B3LYP(D3BJ)/def2-TZVPP and SCS-MP2/def-TZVPP level of theory.

ΔE_{B3LYP} [kJ mol ⁻¹]	ΔG_{B3LYP} [kJ mol ⁻¹]	ΔE_{MP2} [kJ mol ⁻¹]	ΔG_{MP2} [kJ mol ⁻¹]
-143.15	-75.46	-130.57	-61.06



$$K_{eq} = \frac{c(F^-) * c(HX)}{c(X^-) * c(HF)}$$

$$c_0(X^-) = c_0(HF); c_0(F^-) = c_0(HX) = 0$$

$$K_{eq} = \frac{c^2(HX)}{c^2(X^-)}$$

$$\sqrt{K_{eq}} = \frac{c(HX)}{c(X^-)}$$

Scheme S 1. Calculation of the ratio of $c(HX)/c(X^-)$ from the K_{eq} .

d5) Comparison of Different Geometries for the $[X(\text{HCl})_4]^-$ Anion**Table S 16.** Comparison of different geometries for the $[X(\text{HCl})_4]^-$ anion calculated on the B3LYP(D3BJ)/def2-TZVPP and SCS-MP2/def-TZVPP level of theory.

X	Structure	ΔE_{B3LYP}	ΔG_{B3LYP}	ΔE_{MP2}	ΔG_{B3LYP}
Cl	T_d	0.00	0.00	0.00	0.00
Cl	C_{4v}	6.03	-	5.59	-
Cl	D_{4h}	6.45	-	5.59	-
Br	T_d	0.00	0.00	0.00	0.00
Br	C_{4v}	4.57	-	3.72	-
Br	D_{4h}	5.49	-	3.72	8.09
I	T_d	0.00	0.00	0.00	0.00
I	C_{4v}	3.46	-	3.47	-
I	D_{4h}	4.94	-	3.64	-1.75

e) Coordinates of Optimized Structures

HF

B3LYP(D3BJ)/def2-TZVPP

H 0.000000 0.000000 -0.461179

F 0.000000 0.000000 0.461179

SCS-MP2/def2-TZVPP

H 0.000000 0.000000 -0.458911

F 0.000000 0.000000 0.458911

SCS-MP2(Cosmo)/def2-TZVPP

H 0.000000 0.000000 -0.461744

F 0.000000 0.000000 0.461744

HCl

B3LYP(D3BJ)/def2-TZVPP

Cl 0.000000 0.000000 -0.640328

H 0.000000 0.000000 0.640328

SCS-MP2/def2-TZVPP

Cl 0.000000 0.000000 -0.634481

H 0.000000 0.000000 0.634481

SCS-MP2(Cosmo)/def2-TZVPP

Cl 0.000000 0.000000 -0.636892

H 0.000000 0.000000 0.636892

HBr

B3LYP(D3BJ)/def2-TZVPP

Br 0.000000 0.000000 -0.712233

H 0.000000 0.000000 0.712233

SCS-MP2/def2-TZVPP

Br 0.000000 0.000000 -0.704014

H 0.000000 0.000000 0.704014

SCS-MP2(Cosmo)/def2-TZVPP

Br 0.000000 0.000000 -0.705872

H 0.000000 0.000000 0.705872

HI

B3LYP(D3BJ)/def2-TZVPP

I 0.000000 0.000000 -0.808006

H 0.000000 0.000000 0.808006

SCS-MP2/def2-TZVPP

I 0.000000 0.000000 -0.795165

H 0.000000 0.000000 0.795165

SCS-MP2(Cosmo)/def2-TZVPP

I 0.000000 0.000000 -0.796356

H 0.000000 0.000000 0.796356

[ClHCl]⁻

B3LYP(D3BJ)/def2-TZVPP

H	0.000000	0.000000	0.000000
Cl	0.000000	0.000000	1.573967
Cl	0.000000	0.000000	-1.573967

SCS-MP2/def2-TZVPP

H	0.000000	0.000000	0.000000
Cl	0.000000	0.000000	1.553706
Cl	0.000000	0.000000	-1.553706

[Br(HCl)]⁻

B3LYP(D3BJ)/def2-TZVPP

Br	0.000000	0.000000	-1.772801
H	0.000000	0.000000	0.177039
Cl	0.000000	0.000000	1.595761

SCS-MP2/def2-TZVPP

Br	0.000000	0.000000	-1.790977
H	0.000000	0.000000	0.211286
Cl	0.000000	0.000000	1.579691

[I(HCl)]⁻

B3LYP(D3BJ)/def2-TZVPP

I	0.000000	0.000000	-1.981020
H	0.000000	0.000000	0.305121
Cl	0.000000	0.000000	1.675899

SCS-MP2/def2-TZVPP

I	0.000000	0.000000	-2.009612
H	0.000000	0.000000	0.340109
Cl	0.000000	0.000000	1.669504

[Cl(HCl)₂]⁻

B3LYP(D3BJ)/def2-TZVPP

Cl	0.000000	0.000000	-1.189832
H	1.519875	0.000000	-0.087011
Cl	2.666892	0.000000	0.681932
H	-1.519875	0.000000	-0.087011
Cl	-2.666892	0.000000	0.681932

SCS-MP2/def2-TZVPP

Cl	0.000000	0.000000	-1.167151
H	1.577917	0.000000	-0.075525
Cl	2.705578	0.000000	0.659105
H	-1.577917	0.000000	-0.075525
Cl	-2.705578	0.000000	0.659105

[Br(HCl)₂]⁻

B3LYP(D3BJ)/def2-TZVPP

Br	0.000000	0.000000	-1.325421
H	1.670105	0.000000	-0.061451
Cl	2.781437	0.000000	0.724181
H	-1.670105	0.000000	-0.061451
Cl	-2.781437	0.000000	0.724181

SCS-MP2/def2-TZVPP

Br	0.000000	0.000000	-1.291113
H	1.736878	0.000000	-0.051867
Cl	2.834406	0.000000	0.697444
H	-1.736878	0.000000	-0.051867
Cl	-2.834406	0.000000	0.697444

[I(HCl)₂]⁻

B3LYP(D3BJ)/def2-TZVPP

I	0.000000	0.000000	-1.477137
H	1.869464	0.000000	-0.026730
Cl	2.957217	0.000000	0.765467
H	-1.869464	0.000000	-0.026730
Cl	-2.957217	0.000000	0.765467

SCS-MP2/def2-TZVPP

I	0.000000	0.000000	-1.459194
H	1.943319	0.000000	-0.017041
Cl	3.012660	0.000000	0.746805
H	-1.943319	0.000000	-0.017041
Cl	-3.012660	0.000000	0.746805

[Cl(HCl)₃]⁻

B3LYP(D3BJ)/def2-TZVPP

Cl	0.000000	0.000000	-0.879072
H	-0.919089	1.591909	-0.103460
H	-0.919089	-1.591909	-0.103460
H	1.838178	0.000000	-0.103460
Cl	-1.545523	2.676924	0.384014
Cl	-1.545523	-2.676924	0.384014
Cl	3.091046	0.000000	0.384014

SCS-MP2/def2-TZVPP

Cl	0.000000	0.000000	-0.725716
H	-0.962451	1.667013	-0.082150
H	-0.962451	-1.667013	-0.082150
H	1.924901	0.000000	-0.082150
Cl	-1.591766	2.757019	0.311586
Cl	-1.591766	-2.757019	0.311586
Cl	3.183531	0.000000	0.311586

[Br(HCl)₃]⁻

B3LYP(D3BJ)/def2-TZVPP

Br	0.000000	0.000000	-0.947131
H	-0.999944	1.731953	-0.075508
H	-0.999944	-1.731953	-0.075508
H	1.999887	0.000000	-0.075508
Cl	-1.621384	2.808319	0.417815
Cl	-1.621384	-2.808319	0.417815
Cl	3.242768	0.000000	0.417815

SCS-MP2/def2-TZVPP

Br	0.000000	0.000000	-0.759237
H	-1.049633	1.818017	-0.056990
H	-1.049633	-1.818017	-0.056990
H	2.099265	0.000000	-0.056990
Cl	-1.675478	2.902013	0.336665
Cl	-1.675478	-2.902013	0.336665
Cl	3.350956	0.000000	0.336665

[I(HCl)₃]⁻

B3LYP(D3BJ)/def2-TZVPP

I	0.000000	0.000000	-1.094932
H	-1.102429	1.909463	-0.079987
H	-1.102429	-1.909463	-0.079987
H	2.204858	0.000000	-0.079987
Cl	-1.716120	2.972407	0.434200
Cl	-1.716120	-2.972407	0.434200
Cl	3.432240	0.000000	0.434200

SCS-MP2/def2-TZVPP

I	0.000000	0.000000	-1.954157
H	-0.747144	1.294092	-0.182502
H	-0.747144	-1.294092	-0.182502
H	1.494289	0.000000	-0.182502
Cl	-1.165476	2.018664	0.823123
Cl	-1.165476	-2.018664	0.823123
Cl	2.330953	0.000000	0.823123

[Cl(HCl)₄]⁻ (T_d)

B3LYP(D3BJ)/def2-TZVPP

Cl	0.000000	0.000000	0.000000
H	-1.197810	1.197810	1.197810
H	1.197810	-1.197810	1.197810
H	1.197810	1.197810	-1.197810
H	-1.197810	-1.197810	-1.197810
Cl	-1.963477	1.963477	1.963477
Cl	1.963477	-1.963477	1.963477
Cl	-1.963477	-1.963477	-1.963477
Cl	1.963477	1.963477	-1.963477

SCS-MP2/def2-TZVPP

Cl	0.000000	0.000000	0.000000
H	-1.216419	1.216419	1.216419
H	1.216419	-1.216419	1.216419
H	1.216419	1.216419	-1.216419
H	-1.216419	-1.216419	-1.216419
Cl	-1.970050	1.970050	1.970050
Cl	1.970050	-1.970050	1.970050
Cl	-1.970050	-1.970050	-1.970050
Cl	1.970050	1.970050	-1.970050

[Br(HCl)₄]⁻ (T_d)

B3LYP(D3BJ)/def2-TZVPP

Br	0.000000	0.000000	0.000000
H	-1.296774	1.296774	1.296774
H	1.296774	-1.296774	1.296774
H	1.296774	1.296774	-1.296774
H	-1.296774	-1.296774	-1.296774
Cl	-2.060803	2.060803	2.060803
Cl	2.060803	-2.060803	2.060803
Cl	-2.060803	-2.060803	-2.060803
Cl	2.060803	2.060803	-2.060803

SCS-MP2/def2-TZVPP

Br	0.000000	0.000000	0.000000
H	-1.313284	1.313284	1.313284
H	1.313284	-1.313284	1.313284
H	1.313284	1.313284	-1.313284
H	-1.313284	-1.313284	-1.313284
Cl	-2.065142	2.065142	2.065142
Cl	2.065142	-2.065142	2.065142
Cl	-2.065142	-2.065142	-2.065142
Cl	2.065142	2.065142	-2.065142

[I(HCl)₄]⁻ (T₀)

B3LYP(D3BJ)/def2-TZVPP

I	0.000000	0.000000	0.000000
H	-1.429803	1.429803	1.429803
H	1.429803	-1.429803	1.429803
H	1.429803	1.429803	-1.429803
H	-1.429803	-1.429803	-1.429803
Cl	-2.192207	2.192207	2.192207
Cl	2.192207	-2.192207	2.192207
Cl	-2.192207	-2.192207	-2.192207
Cl	2.192207	2.192207	-2.192207

SCS-MP2/def2-TZVPP

I	0.000000	0.000000	0.000000
H	-1.454771	1.454771	1.454771
H	1.454771	-1.454771	1.454771
H	1.454771	1.454771	-1.454771
H	-1.454771	-1.454771	-1.454771
Cl	-2.204221	2.204221	2.204221
Cl	2.204221	-2.204221	2.204221
Cl	-2.204221	-2.204221	-2.204221
Cl	2.204221	2.204221	-2.204221

[Cl(HCl)₄]⁻ (C_{4v})

B3LYP(D3BJ)/def2-TZVPP

Cl	2.343520	-2.343520	0.209007
Cl	2.343520	2.343520	0.209007
Cl	-2.343520	2.343520	0.209007
Cl	-2.343520	-2.343520	0.209007
H	1.430237	-1.430237	-0.078022
H	1.430237	1.430237	-0.078022
H	-1.430237	1.430237	-0.078022
H	-1.430237	-1.430237	-0.078022
Cl	0.000000	0.000000	-0.596460

SCS-MP2/def2-TZVPP

I	0.000000	0.000000	-0.858598
Cl	-2.580905	2.580905	0.291250
Cl	-2.580905	-2.580905	0.291250
Cl	2.580905	-2.580905	0.291250
H	-1.701759	1.701759	-0.076619
H	-1.701759	-1.701759	-0.076619
H	1.701759	-1.701759	-0.076619
H	1.701759	1.701759	-0.076619
Cl	2.580905	2.580905	0.291250

[Br(HCl)₄]⁻ (C_{4v})

B3LYP(D3BJ)/def2-TZVPP

Br	0.000000	0.000000	-0.895160
Cl	-2.381303	2.381303	0.322298
Cl	-2.381303	-2.381303	0.322298
Cl	2.381303	-2.381303	0.322298
H	-1.496408	1.496408	-0.098527
H	-1.496408	-1.496408	-0.098527
H	1.496408	-1.496408	-0.098527
H	1.496408	1.496408	-0.098527
Cl	2.381303	2.381303	0.322298

SCS-MP2/def2-TZVPP

Br	0.000000	0.000000	-0.014293
Cl	-2.535096	2.535096	0.005359
Cl	-2.535096	-2.535096	0.005359
Cl	2.535096	-2.535096	0.005359
H	-1.615808	1.615808	-0.001804
H	-1.615808	-1.615808	-0.001804
H	1.615808	-1.615808	-0.001804
H	1.615808	1.615808	-0.001804
Cl	2.535096	2.535096	0.005359

[I(HCl)₄]⁻ (C_{4v})

B3LYP(D3BJ)/def2-TZVPP

I	0.000000	0.000000	-1.175025
Cl	-2.450390	2.450390	0.404631
Cl	-2.450390	-2.450390	0.404631
Cl	2.450390	-2.450390	0.404631
H	-1.592900	1.592900	-0.110894
H	-1.592900	-1.592900	-0.110894
H	1.592900	-1.592900	-0.110894
H	1.592900	1.592900	-0.110894
Cl	2.450390	2.450390	0.404631

SCS-MP2/def2-TZVPP

I	0.000000	0.000000	-1.696015
Cl	-1.995239	1.995239	0.621679
Cl	-1.995239	-1.995239	0.621679
Cl	1.995239	-1.995239	0.621679
H	-1.280962	1.280962	-0.197694
H	-1.280962	-1.280962	-0.197694
H	1.280962	-1.280962	-0.197694
H	1.280962	1.280962	-0.197694
Cl	1.995239	1.995239	0.621679

[Cl(HCl)₄]⁻ (D_{4h})

B3LYP(D3BJ)/def2-TZVPP

Cl	0.000000	0.000000	0.000000
H	-1.475152	-1.475152	0.000000
H	-1.475152	1.475152	0.000000
H	1.475152	1.475152	0.000000
H	1.475152	-1.475152	0.000000
Cl	2.410450	-2.410450	0.000000
Cl	2.410450	2.410450	0.000000
Cl	-2.410450	2.410450	0.000000
Cl	-2.410450	-2.410450	0.000000

SCS-MP2/def2-TZVPP

Cl	0.000000	0.000000	0.000000
H	-1.497088	-1.497088	0.000000
H	-1.497088	1.497088	0.000000
H	1.497088	1.497088	0.000000
H	1.497088	-1.497088	0.000000
Cl	2.418555	-2.418555	0.000000
Cl	2.418555	2.418555	0.000000
Cl	-2.418555	2.418555	0.000000
Cl	-2.418555	-2.418555	0.000000

[Br(HCl)₄]⁻ (D_{4h})

B3LYP(D3BJ)/def2-TZVPP

Br	0.000000	0.000000	0.000000
H	-1.597153	-1.597153	0.000000
H	-1.597153	1.597153	0.000000
H	1.597153	1.597153	0.000000
H	1.597153	-1.597153	0.000000
Cl	2.530408	-2.530408	0.000000
Cl	2.530408	2.530408	0.000000
Cl	-2.530408	2.530408	0.000000
Cl	-2.530408	-2.530408	0.000000

SCS-MP2/def2-TZVPP

Br	0.000000	0.000000	0.000000
H	-1.615832	-1.615832	0.000000
H	-1.615832	1.615832	0.000000
H	1.615832	1.615832	0.000000
H	1.615832	-1.615832	0.000000
Cl	2.535133	-2.535133	0.000000
Cl	2.535133	2.535133	0.000000
Cl	-2.535133	2.535133	0.000000
Cl	-2.535133	-2.535133	0.000000

[I(HCl)₄]⁻ (D_{4h})

B3LYP(D3BJ)/def2-TZVPP

I	0.000000	0.000000	0.000000
H	-1.760388	-1.760388	0.000000
H	-1.760388	1.760388	0.000000
H	1.760388	1.760388	0.000000
H	1.760388	-1.760388	0.000000
Cl	2.691606	-2.691606	0.000000
Cl	2.691606	2.691606	0.000000
Cl	-2.691606	2.691606	0.000000
Cl	-2.691606	-2.691606	0.000000

SCS-MP2/def2-TZVPP

I	0.000000	0.000000	0.000000
H	-1.790623	-1.790623	0.000000
H	-1.790623	1.790623	0.000000
H	1.790623	1.790623	0.000000
H	1.790623	-1.790623	0.000000
Cl	2.707147	-2.707147	0.000000
Cl	2.707147	2.707147	0.000000
Cl	-2.707147	2.707147	0.000000
Cl	-2.707147	-2.707147	0.000000

[Cl(HF)₃]⁻

B3LYP(D3BJ)/def2-TZVPP

Cl	0.000000	0.000000	-0.720767
H	-0.940389	1.628802	-0.030464
H	-0.940389	-1.628802	-0.030464
H	1.880779	0.000000	-0.030464
F	-1.394358	2.415099	0.270722
F	-1.394358	-2.415099	0.270722
F	2.788716	0.000000	0.270722

SCS-MP2/def2-TZVPP

Cl	0.000000	0.000000	-0.659658
H	-0.959930	1.662647	-0.027505
H	-0.959930	-1.662647	-0.027505
H	1.919860	0.000000	-0.027505
F	-1.413022	2.447426	0.247393
F	-1.413022	-2.447426	0.247393
F	2.826044	0.000000	0.247393

[Br(HF)₃]⁻

B3LYP(D3BJ)/def2-TZVPP

Br	0.000000	0.000000	-0.799669
H	-1.022128	1.770378	-0.019595
H	-1.022128	-1.770378	-0.019595
H	2.044256	0.000000	-0.019595
F	-1.473093	2.551472	0.286154
F	-1.473093	-2.551472	0.286154
F	2.946186	0.000000	0.286154

SCS-MP2/def2-TZVPP

Br	0.000000	0.000000	-0.717639
H	-1.042639	1.805904	-0.018553
H	-1.042639	-1.805904	-0.018553
H	2.085279	0.000000	-0.018553
F	-1.493501	2.586820	0.257769
F	-1.493501	-2.586820	0.257769
F	2.987003	0.000000	0.257769

[I(HF)₃]⁻

B3LYP(D3BJ)/def2-TZVPP

I	0.000000	0.000000	-0.957356
H	-1.119553	1.939122	-0.007921
H	-1.119553	-1.939122	-0.007921
H	2.239106	0.000000	-0.007921
F	-1.563212	2.707563	0.327042
F	-1.563212	-2.707563	0.327042
F	3.126425	0.000000	0.327042

SCS-MP2/def2-TZVPP

I	0.000000	0.000000	-0.927171
H	-1.140239	1.974952	-0.008867
H	-1.140239	-1.974952	-0.008867
H	2.280479	0.000000	-0.008867
F	-1.580235	2.737048	0.317926
F	-1.580235	-2.737048	0.317926
F	3.160471	0.000000	0.317926

[F(HF)₄]⁻

B3LYP(D3BJ)/def2-TZVPP

F	0.000000	0.000000	0.000000
H	-0.885406	0.885406	0.885406
H	0.885406	-0.885406	0.885406
H	0.885406	0.885406	-0.885406
H	-0.885406	-0.885406	-0.885406
F	-1.438722	1.438722	1.438722
F	1.438722	-1.438722	1.438722
F	-1.438722	-1.438722	-1.438722
F	1.438722	1.438722	-1.438722

SCS-MP2/def2-TZVPP

F	0.000000	0.000000	0.000000
H	-0.886007	0.886007	0.886007
H	0.886007	-0.886007	0.886007
H	0.886007	0.886007	-0.886007
H	-0.886007	-0.886007	-0.886007
F	-1.435248	1.435248	1.435248
F	1.435248	-1.435248	1.435248
F	-1.435248	-1.435248	-1.435248
F	1.435248	1.435248	-1.435248

SCS-MP2(Cosmo)/def2-TZVPP

F	0.000000	0.000000	0.000000
H	-0.871966	0.871966	0.871966
H	0.871966	-0.871966	0.871966
H	0.871966	0.871966	-0.871966
H	-0.871966	-0.871966	-0.871966
F	-1.421939	1.421939	1.421939
F	1.421939	-1.421939	1.421939
F	-1.421939	-1.421939	-1.421939
F	1.421939	1.421939	-1.421939

[Cl(HF)₄]⁻

B3LYP(D3BJ)/def2-TZVPP

Cl	0.000000	0.000000	0.000000
H	-1.183878	1.183878	1.183878
H	1.183878	-1.183878	1.183878
H	1.183878	1.183878	-1.183878
H	-1.183878	-1.183878	-1.183878
F	-1.731777	1.731777	1.731777
F	1.731777	-1.731777	1.731777
F	-1.731777	-1.731777	-1.731777
F	1.731777	1.731777	-1.731777

SCS-MP2/def2-TZVPP

Cl	0.000000	0.000000	0.000000
H	-1.196327	1.196327	1.196327
H	1.196327	-1.196327	1.196327
H	1.196327	1.196327	-1.196327
H	-1.196327	-1.196327	-1.196327
F	-1.739316	1.739316	1.739316
F	1.739316	-1.739316	1.739316
F	-1.739316	-1.739316	-1.739316
F	1.739316	1.739316	-1.739316

SCS-MP2(Cosmo)/def2-TZVPP

Cl	0.000000	0.000000	0.000000
H	-1.177918	1.177918	1.177918
H	1.177918	-1.177918	1.177918
H	1.177918	1.177918	-1.177918
H	-1.177918	-1.177918	-1.177918
F	-1.721341	1.721341	1.721341
F	1.721341	-1.721341	1.721341
F	-1.721341	-1.721341	-1.721341
F	1.721341	1.721341	-1.721341

[Br(HF)₄]⁻

B3LYP(D3BJ)/def2-TZVPP

Br	0.000000	0.000000	0.000000
H	-1.284047	1.284047	1.284047
H	1.284047	-1.284047	1.284047
H	1.284047	1.284047	-1.284047
H	-1.284047	-1.284047	-1.284047
F	-1.830661	1.830661	1.830661
F	1.830661	-1.830661	1.830661
F	-1.830661	-1.830661	-1.830661
F	1.830661	1.830661	-1.830661

SCS-MP2/def2-TZVPP

Br	0.000000	0.000000	0.000000
H	-1.292553	1.292553	1.292553
H	1.292553	-1.292553	1.292553
H	1.292553	1.292553	-1.292553
H	-1.292553	-1.292553	-1.292553
F	-1.834306	1.834306	1.834306
F	1.834306	-1.834306	1.834306
F	-1.834306	-1.834306	-1.834306
F	1.834306	1.834306	-1.834306

SCS-MP2(Cosmo)/def2-TZVPP

Br	0.000000	0.000000	0.000000
H	-1.273450	1.273450	1.273450
H	1.273450	-1.273450	1.273450
H	1.273450	1.273450	-1.273450
H	-1.273450	-1.273450	-1.273450
F	-1.815565	1.815565	1.815565
F	1.815565	-1.815565	1.815565
F	-1.815565	-1.815565	-1.815565
F	1.815565	1.815565	-1.815565

[I(HF)₄]⁻

B3LYP(D3BJ)/def2-TZVPP

I	0.000000	0.000000	0.000000
H	-1.418277	1.418277	1.418277
H	1.418277	-1.418277	1.418277
H	1.418277	1.418277	-1.418277
H	-1.418277	-1.418277	-1.418277
F	-1.963592	1.963592	1.963592
F	1.963592	-1.963592	1.963592
F	-1.963592	-1.963592	-1.963592
F	1.963592	1.963592	-1.963592

SCS-MP2/def2-TZVPP

I	0.000000	0.000000	0.000000
H	-1.435630	1.435630	1.435630
H	1.435630	-1.435630	1.435630
H	1.435630	1.435630	-1.435630
H	-1.435630	-1.435630	-1.435630
F	-1.975744	1.975744	1.975744
F	1.975744	-1.975744	1.975744
F	-1.975744	-1.975744	-1.975744
F	1.975744	1.975744	-1.975744

SCS-MP2(Cosmo)/def2-TZVPP

I	0.000000	0.000000	0.000000
H	-1.413038	1.413038	1.413038
H	1.413038	-1.413038	1.413038
H	1.413038	1.413038	-1.413038
H	-1.413038	-1.413038	-1.413038
F	-1.953566	1.953566	1.953566
F	1.953566	-1.953566	1.953566
F	-1.953566	-1.953566	-1.953566
F	1.953566	1.953566	-1.953566

[Cl(HF)₂(HCl)]⁻

B3LYP(D3BJ)/def2-TZVPP

Cl	-0.603826	-0.476276	0.000000
H	1.142484	-1.377394	0.000000
H	-0.684001	0.698976	1.631766
H	-0.684001	0.698976	-1.631766
Cl	2.327111	-2.029983	0.000000
F	-0.748873	1.242994	-2.414068
F	-0.748873	1.242994	2.414068

SCS-MP2/def2-TZVPP

Cl	-0.526306	-0.402665	0.000000
H	1.215126	-1.424323	0.000000
H	-0.706374	0.728021	1.670581
H	-0.706374	0.728021	-1.670581
Cl	2.340112	-2.116489	0.000000
F	-0.808081	1.243861	-2.457551
F	-0.808081	1.243861	2.457551

[Br(HF)₂(HBr)]⁻

B3LYP(D3BJ)/def2-TZVPP

Br	-0.686766	-0.551129	0.000000
H	1.177838	-1.455566	0.000000
H	-0.726065	0.764258	1.768316
H	-0.726065	0.764258	-1.768316
Br	2.521607	-2.155385	0.000000
F	-0.780265	1.316925	-2.539056
F	-0.780265	1.316925	2.539056

SCS-MP2/def2-TZVPP

Br	-0.567480	-0.435697	0.000000
H	1.281867	-1.513991	0.000000
H	-0.759827	0.800865	1.819516
H	-0.759827	0.800865	-1.819516
Br	2.533362	-2.282132	0.000000
F	-0.864036	1.315188	-2.601834
F	-0.864036	1.315188	2.601834

[I(HF)₂(HI)]⁻

B3LYP(D3BJ)/def2-TZVPP

I	-0.794966	-0.631007	0.000000
H	1.245197	-1.573076	0.000000
H	-0.788879	0.857573	1.947342
H	-0.788879	0.857573	-1.947342
I	2.790506	-2.346627	0.000000
F	-0.831479	1.417925	-2.708239
F	-0.831479	1.417925	2.708239

SCS-MP2/def2-TZVPP

I	-0.733837	-0.564453	0.000000
H	1.361298	-1.650223	0.000000
H	-0.828860	0.894000	1.988542
H	-0.828860	0.894000	-1.988542
I	2.811635	-2.443970	0.000000
F	-0.890678	1.435466	-2.751708
F	-0.890678	1.435466	2.751708

[Cl(HF)₂(HCl)₂]⁻

B3LYP(D3BJ)/def2-TZVPP

Cl	0.000000	0.000000	0.069724
H	0.000000	-1.684662	1.244022
H	0.000000	1.684662	1.244022
H	-1.679324	0.000000	-1.142979
H	1.679324	0.000000	-1.142979
F	0.000000	-2.463116	1.786024
F	0.000000	2.463116	1.786024
Cl	2.754443	0.000000	-1.921247
Cl	-2.754443	0.000000	-1.921247

SCS-MP2/def2-TZVPP

Cl	0.000000	0.000000	0.058175
H	0.000000	-1.685960	1.256328
H	0.000000	1.685960	1.256328
H	-1.726910	0.000000	-1.162551
H	1.726910	0.000000	-1.162551
F	0.000000	-2.455018	1.798515
F	0.000000	2.455018	1.798515
Cl	2.788182	0.000000	-1.920697
Cl	-2.788182	0.000000	-1.920697

[Br(HF)₂(HBr)₂]⁻

B3LYP(D3BJ)/def2-TZVPP

Br	0.000000	0.000000	0.092030
H	0.000000	-1.842430	1.360038
H	0.000000	1.842430	1.360038
H	-1.767674	0.000000	-1.214027
H	1.767674	0.000000	-1.214027
F	0.000000	-2.617982	1.900232
F	0.000000	2.617982	1.900232
Br	2.959508	0.000000	-2.091576
Br	-2.959508	0.000000	-2.091576

SCS-MP2/def2-TZVPP

Br	0.000000	0.000000	0.070083
H	0.000000	-1.827120	1.369936
H	0.000000	1.827120	1.369936
H	-1.830186	0.000000	-1.234317
H	1.830186	0.000000	-1.234317
F	0.000000	-2.593499	1.910884
F	0.000000	2.593499	1.910884
Br	3.003923	0.000000	-2.080862
Br	-3.003923	0.000000	-2.080862

[I(HF)₂(HI)₂]⁻

B3LYP(D3BJ)/def2-TZVPP

I	0.000000	0.000000	0.106405
H	0.000000	-2.034170	1.515033
H	0.000000	2.034170	1.515033
H	-1.927296	0.000000	-1.310731
H	1.927296	0.000000	-1.310731
F	0.000000	-2.807844	2.053495
F	0.000000	2.807844	2.053495
I	3.280115	0.000000	-2.310317
I	-3.280115	0.000000	-2.310317

SCS-MP2/def2-TZVPP

I	0.000000	0.000000	0.096166
H	0.000000	-2.037437	1.530367
H	0.000000	2.037437	1.530367
H	-2.012879	0.000000	-1.342672
H	2.012879	0.000000	-1.342672
F	0.000000	-2.804479	2.065453
F	0.000000	2.804479	2.065453
I	3.332435	0.000000	-2.300549
I	-3.332435	0.000000	-2.300549

HCN

B3LYP(D3BJ)/def2-TZVPP

N	0.000000	0.000000	-1.119691
C	0.000000	0.000000	0.026672
H	0.000000	0.000000	1.093019

SCS-MP2/def2-TZVPP

N	0.000000	0.000000	-1.128806
C	0.000000	0.000000	0.032387
H	0.000000	0.000000	1.096419

[Br(HCN)]⁻

B3LYP(D3BJ)/def2-TZVPP

N	0.000000	0.000000	-1.981358
C	0.000000	0.000000	-0.830885
H	0.000000	0.000000	0.281576
Br	0.000000	0.000000	2.530666

SCS-MP2/def2-TZVPP

N	0.000000	0.000000	-1.989153
C	0.000000	0.000000	-0.825273
H	0.000000	0.000000	0.277276
Br	0.000000	0.000000	2.537150

[ClO₄]⁻

B3LYP(D3BJ)/def2-TZVPP

Cl	0.000000	0.000000	0.000000
O	-0.841533	-0.841533	-0.841533
O	0.841533	0.841533	-0.841533
O	0.841533	-0.841533	0.841533
O	-0.841533	0.841533	0.841533

SCS-MP2/def2-TZVPP

Cl	0.000000	0.000000	0.000000
O	-0.833959	-0.833959	-0.833959
O	0.833959	0.833959	-0.833959
O	0.833959	-0.833959	0.833959
O	-0.833959	0.833959	0.833959

[ClO₄(HF)₂]⁻

B3LYP(D3BJ)/def2-TZVPP

Cl	0.000000	0.000000	-0.152634
O	-1.188516	0.000000	-0.968721
O	0.000000	1.176691	0.729168
H	0.000000	2.714659	0.146034
F	0.000000	3.636671	-0.088983
O	1.188516	0.000000	-0.968721
O	0.000000	-1.176691	0.729168
H	0.000000	-2.714659	0.146034
F	0.000000	-3.636671	-0.088983

SCS-MP2/def2-TZVPP

Cl	0.000000	0.000000	-0.149360
O	-1.178670	0.000000	-0.960470
O	0.000000	1.167777	0.719627
H	0.000000	2.736501	0.138995
F	0.000000	3.652335	-0.082289
O	1.178670	0.000000	-0.960470
O	0.000000	-1.167777	0.719627
H	0.000000	-2.736501	0.138995
F	0.000000	-3.652335	-0.082289

[I(HBr)₂]⁻

B3LYP(D3BJ)/def2-TZVPP

I	0.000000	0.000000	1.486489
H	-1.790372	0.000000	0.078445
Br	-3.013908	0.000000	-0.820384
H	1.790372	0.000000	0.078445
Br	3.013908	0.000000	-0.820384

SCS-MP2/def2-TZVPP

I	0.000000	0.000000	1.450730
H	-1.890524	0.000000	0.059807
Br	-3.094313	0.000000	-0.783867
H	1.890524	0.000000	0.059807
Br	3.094313	0.000000	-0.783867

f) Calculated Vibrational Spectra

Table S 17. HF.

B3LYP(D3BJ)/def2-TZVPP				SCS-MP2/def2-TZVPP			
Nr.	Symmetry	Wavenumber [cm ⁻¹]	IR intensity [km mol ⁻¹]	Nr.	Symmetry	Wavenumber [cm ⁻¹]	IR intensity [km mol ⁻¹]
1	Σ^+	4081.2	106	1	Σ^+	4146.9	111

Table S 18. HCl.

B3LYP(D3BJ)/def2-TZVPP				SCS-MP2/def2-TZVPP			
Nr.	Symmetry	Wavenumber [cm ⁻¹]	IR intensity [km mol ⁻¹]	Nr.	Symmetry	Wavenumber [cm ⁻¹]	IR intensity [km mol ⁻¹]
1	Σ^+	2949.0	35	1	Σ^+	3062.9	40

Table S 19. HBr.

B3LYP(D3BJ)/def2-TZVPP				SCS-MP2/def2-TZVPP			
Nr.	Symmetry	Wavenumber [cm ⁻¹]	IR intensity [km mol ⁻¹]	Nr.	Symmetry	Wavenumber [cm ⁻¹]	IR intensity [km mol ⁻¹]
1	Σ^+	2618.4	9	1	Σ^+	2719.9	10

Table S 20. HI.

B3LYP(D3BJ)/def2-TZVPP				SCS-MP2/def2-TZVPP			
Nr.	Symmetry	Wavenumber [cm ⁻¹]	IR intensity [km mol ⁻¹]	Nr.	Symmetry	Wavenumber [cm ⁻¹]	IR intensity [km mol ⁻¹]
1	Σ^+	2291.9	1	1	Σ^+	2427.4	1

Table S 21. Computed vibrational frequencies calculated on SCS-MP2(Cosmo)/def2-TZVPP ($\epsilon_r=83.6$).

HF				HCl			
Nr.	Symmetry	Wavenumber [cm ⁻¹]	IR intensity [km mol ⁻¹]	Nr.	Symmetry	Wavenumber [cm ⁻¹]	IR intensity [km mol ⁻¹]
1	Σ^+	4053.3	223	1	Σ^+	3017.3	116
HBr				HI			
Nr.	Symmetry	Wavenumber [cm ⁻¹]	IR intensity [km mol ⁻¹]	Nr.	Symmetry	Wavenumber [cm ⁻¹]	IR intensity [km mol ⁻¹]
1	Σ^+	2691.0	47	1	Σ^+	2412.6	4

Table S 22. [ClHCl]⁻.

B3LYP(D3BJ)/def2-TZVPP				SCS-MP2/def2-TZVPP			
Nr.	Symmetry	Wavenumber [cm ⁻¹]	IR intensity [km mol ⁻¹]	Nr.	Symmetry	Wavenumber [cm ⁻¹]	IR intensity [km mol ⁻¹]
1	Σ_g^+	324.5	0	1	Σ_g^+	342.5	0
2	Σ_u^-	744.0	5192	2	Σ_u^-	492.9	6365
3	Π_u	834.3	13	3	Π_u	892.0	16
4	Π_u	834.3	13	4	Π_u	892.0	16

Table S 23. [Br(HCl)]⁻.

B3LYP(D3BJ)/def2-TZVPP				SCS-MP2/def2-TZVPP			
Nr.	Symmetry	Wavenumber [cm ⁻¹]	IR intensity [km mol ⁻¹]	Nr.	Symmetry	Wavenumber [cm ⁻¹]	IR intensity [km mol ⁻¹]
1	Σ^+	183.6	53	1	Σ^+	165.6	55
2	Π	717.5	8	2	Π	725.8	12
3	Π	717.5	8	3	Π	725.8	12
4	Σ^+	1484.3	4504	4	Σ^+	1810.2	4392

Table S 24. [I(HCl)]⁻.

B3LYP(D3BJ)/def2-TZVPP				SCS-MP2/def2-TZVPP			
Nr.	Symmetry	Wavenumber [cm ⁻¹]	IR intensity [km mol ⁻¹]	Nr.	Symmetry	Wavenumber [cm ⁻¹]	IR intensity [km mol ⁻¹]
1	Σ^+	135.1	20	1	Σ^+	123.5	18
2	Π	604.4	7	2	Π	607.0	10
3	Π	604.4	7	3	Π	607.0	10
4	Σ^+	1893.0	4061	4	Σ^+	2262.3	3282

Table S 25. [Cl(HCl)₂]⁻.

B3LYP(D3BJ)/def2-TZVPP				SCS-MP2/def2-TZVPP			
Nr.	Symmetry	Wavenumber [cm ⁻¹]	IR intensity [km mol ⁻¹]	Nr.	Symmetry	Wavenumber [cm ⁻¹]	IR intensity [km mol ⁻¹]
1	A_1	23.3	0	1	A_1	21.3	0
2	A_1	194.8	23	2	A_1	181.4	25
3	B_1	198.4	168	3	B_1	182.5	156
4	B_1	677.2	0	4	B_1	693.6	2
5	B_2	689.4	30	5	B_2	706.0	38
6	A_2	697.1	0	6	A_2	710.7	0
7	A_1	752.1	16	7	A_1	747.1	21
8	B_1	1683.0	5745	8	B_1	1965.9	5412
9	A_1	1912.2	1683	9	A_1	2156.4	1545

Table S 26. [Br(HCl)₂]⁻.

B3LYP(D3BJ)/def2-TZVPP				SCS-MP2/def2-TZVPP			
Nr.	Symmetry	Wavenumber [cm ⁻¹]	IR intensity [km mol ⁻¹]	Nr.	Symmetry	Wavenumber [cm ⁻¹]	IR intensity [km mol ⁻¹]
1	A ₁	17.0	0	1	A ₁	16.4	0
2	B ₁	149.4	51	2	A ₁	139.6	11
3	A ₁	149.5	11	3	B ₁	141.5	47
4	B ₁	608.5	0	4	B ₁	621.8	3
5	B ₂	618.3	22	5	B ₂	636.3	28
6	A ₂	626.0	0	6	A ₂	640.6	0
7	A ₁	665.0	12	7	A ₁	661.5	15
8	B ₁	1923.9	5030	8	B ₁	2214.9	4462
9	A ₁	2064.6	1801	9	A ₁	2324.2	1520

Table S 27. [(HCl)₂]⁻.

B3LYP(D3BJ)/def2-TZVPP				SCS-MP2/def2-TZVPP			
Nr.	Symmetry	Wavenumber [cm ⁻¹]	IR intensity [km mol ⁻¹]	Nr.	Symmetry	Wavenumber [cm ⁻¹]	IR intensity [km mol ⁻¹]
1	A ₁	12.9	0.1	1	A ₁	12.3	0
2	A ₁	121.5	7	2	A ₁	111.8	6
3	B ₁	122.7	22	3	B ₁	114.2	19
4	B ₁	537.0	0.3	4	B ₁	546.9	3
5	B ₂	544.9	16	5	B ₂	557.8	23
6	A ₂	551.6	0	6	A ₂	561.6	0
7	A ₁	580.9	10	7	A ₁	576.0	13
8	B ₁	2104.2	4588	8	B ₁	2426.6	3550
9	A ₁	2186.6	1942	9	A ₁	2484.1	1462

Table S 28. $[\text{Cl}(\text{HCl})_3]^-$.

B3LYP(D3BJ)/def2-TZVPP				SCS-MP2/def2-TZVPP			
Nr.	Symmetry	Wavenumber [cm ⁻¹]	IR intensity [km mol ⁻¹]	Nr.	Symmetry	Wavenumber [cm ⁻¹]	IR intensity [km mol ⁻¹]
1	<i>E</i>	17.5	0	1	<i>A</i> ₁	16.1	0
2	<i>E</i>	17.5	0	2	<i>E</i>	17.0	0
3	<i>A</i> ₁	18.9	0	3	<i>E</i>	17.0	0
4	<i>A</i> ₁	160.1	6	4	<i>A</i> ₁	144.5	4
5	<i>E</i>	173.9	69	5	<i>E</i>	166.7	68
6	<i>E</i>	173.9	69	6	<i>E</i>	166.7	68
7	<i>A</i> ₂	585.8	0	7	<i>A</i> ₂	603.0	0
8	<i>E</i>	594.3	7	8	<i>E</i>	612.8	8
9	<i>E</i>	594.3	7	9	<i>E</i>	612.8	8
10	<i>A</i> ₁	630.5	39	10	<i>A</i> ₁	632.5	51
11	<i>E</i>	649.9	11	11	<i>E</i>	652.1	15
12	<i>E</i>	649.9	11	12	<i>E</i>	652.1	15
13	<i>E</i>	2102.3	3774	13	<i>E</i>	2346.8	3406
14	<i>E</i>	2102.3	3774	14	<i>E</i>	2346.8	3406
15	<i>A</i> ₁	2289.9	632	15	<i>A</i> ₁	2496.0	393

Table S 29. $[\text{Br}(\text{HCl})_3]^-$.

B3LYP(D3BJ)/def2-TZVPP				SCS-MP2/def2-TZVPP			
Nr.	Symmetry	Wavenumber [cm ⁻¹]	IR intensity [km mol ⁻¹]	Nr.	Symmetry	Wavenumber [cm ⁻¹]	IR intensity [km mol ⁻¹]
1	<i>A</i> ₁	13.5	0	1	<i>A</i> ₁	11.1	0
2	<i>E</i>	13.9	0	2	<i>E</i>	13.9	0
3	<i>E</i>	13.9	0	3	<i>E</i>	13.9	0
4	<i>A</i> ₁	130.0	3	4	<i>A</i> ₁	120.5	2
5	<i>E</i>	133.9	28	5	<i>E</i>	130.4	27
6	<i>E</i>	133.9	28	6	<i>E</i>	130.4	27
7	<i>A</i> ₂	541.5	0	7	<i>A</i> ₂	563.1	0
8	<i>E</i>	546.8	4	8	<i>E</i>	571.3	6
9	<i>E</i>	546.8	4	9	<i>E</i>	571.3	6
10	<i>A</i> ₁	576.2	30	10	<i>A</i> ₁	585.0	39
11	<i>E</i>	593.0	7	11	<i>E</i>	601.3	9
12	<i>E</i>	593.0	7	12	<i>E</i>	601.3	9
13	<i>E</i>	2197.5	3609	13	<i>E</i>	2450.5	3133
14	<i>E</i>	2197.5	3609	14	<i>E</i>	2450.5	3133
15	<i>A</i> ₁	2331.0	724	15	<i>A</i> ₁	2552.4	407

Table S 30. $[(\text{HCl})_3]^-$.

B3LYP(D3BJ)/def2-TZVPP				SCS-MP2/def2-TZVPP			
Nr.	Symmetry	Wavenumber [cm ⁻¹]	IR intensity [km mol ⁻¹]	Nr.	Symmetry	Wavenumber [cm ⁻¹]	IR intensity [km mol ⁻¹]
1	A ₁	10.9	0	1	A ₁	10.2	0
2	E	11.4	0	2	E	11.6	0
3	E	11.4	0	3	E	11.6	0
4	A ₁	111.2	2	4	A ₁	101.7	2
5	E	113.1	14	5	E	107.1	13
6	E	113.1	14	6	E	107.1	13
7	A ₂	491.0	0	7	A ₂	503.5	0
8	E	493.9	2	8	E	507.9	6
9	E	493.9	2	9	E	507.9	6
10	A ₁	519.9	23	10	A ₁	522.1	31
11	E	533.3	5	11	E	534.0	7
12	E	533.3	5	12	E	534.0	7
13	E	2278.0	3524	13	E	2558.6	2704
14	E	2278.0	3524	14	E	2558.6	2704
15	A ₁	2368.3	906	15	A ₁	2620.7	557

Table S 31. $[\text{Cl}(\text{HCl})_4]^-$ (*T_d*).

B3LYP(D3BJ)/def2-TZVPP				SCS-MP2/def2-TZVPP			
Nr.	Symmetry	Wavenumber [cm ⁻¹]	IR intensity [km mol ⁻¹]	Nr.	Symmetry	Wavenumber [cm ⁻¹]	IR intensity [km mol ⁻¹]
1	E	12.7	0	1	E	13.2	0
2	E	12.7	0	2	E	13.2	0
3	T ₂	15.1	0	3	T ₂	17.0	0
4	T ₂	15.1	0	4	T ₂	17.0	0
5	T ₂	15.1	0	5	T ₂	17.0	0
6	A ₁	122.4	0	6	A ₁	116.7	0
7	T ₂	159.7	41	7	T ₂	153.6	36
8	T ₂	159.7	41	8	T ₂	153.6	36
9	T ₂	159.7	41	9	T ₂	153.6	36
10	T ₁	521.8	0	10	T ₁	543.1	0
11	T ₁	521.8	0	11	T ₁	543.1	0
12	T ₁	521.8	0	12	T ₁	543.1	0
13	T ₂	562.5	34	13	T ₂	579.3	45
14	T ₂	562.5	34	14	T ₂	579.3	45
15	T ₂	562.5	34	15	T ₂	579.3	45
16	E	580.4	0	16	E	589.8	0
17	E	580.4	0	17	E	589.8	0
18	T ₂	2326.2	2846	18	T ₂	2541.6	2356
19	T ₂	2326.2	2846	19	T ₂	2541.6	2356
20	T ₂	2326.2	2846	20	T ₂	2541.6	2356
21	A ₁	2487.8	0	21	A ₁	2668.3	0

Table S 32. $[\text{Br}(\text{HCl})_4]^- (T_d)$.

B3LYP(D3BJ)/def2-TZVPP				SCS-MP2/def2-TZVPP			
Nr.	Symmetry	Wavenumber [cm ⁻¹]	IR intensity [km mol ⁻¹]	Nr.	Symmetry	Wavenumber [cm ⁻¹]	IR intensity [km mol ⁻¹]
1	<i>E</i>	11.1	0	1	<i>E</i>	11.4	0
2	<i>E</i>	11.1	0	2	<i>E</i>	11.4	0
3	<i>T</i> ₂	11.7	0	3	<i>T</i> ₂	11.7	0
4	<i>T</i> ₂	11.7	0	4	<i>T</i> ₂	11.7	0
5	<i>T</i> ₂	11.7	0	5	<i>T</i> ₂	11.7	0
6	<i>A</i> ₁	110.0	0	6	<i>A</i> ₁	105.4	0
7	<i>T</i> ₂	124.2	19	7	<i>T</i> ₂	120.9	16
8	<i>T</i> ₂	124.2	19	8	<i>T</i> ₂	120.9	16
9	<i>T</i> ₂	124.2	19	9	<i>T</i> ₂	120.9	16
10	<i>T</i> ₁	490.6	0	10	<i>T</i> ₁	519.2	0
11	<i>T</i> ₁	490.6	0	11	<i>T</i> ₁	519.2	0
12	<i>T</i> ₁	490.6	0	12	<i>T</i> ₁	519.2	0
13	<i>T</i> ₂	519.9	21	13	<i>T</i> ₂	544.9	31
14	<i>T</i> ₂	519.9	21	14	<i>T</i> ₂	544.9	31
15	<i>T</i> ₂	519.9	21	15	<i>T</i> ₂	544.9	31
16	<i>E</i>	540.9	0	16	<i>E</i>	556.0	0
17	<i>E</i>	540.9	0	17	<i>E</i>	556.0	0
18	<i>T</i> ₂	2367.5	2867	18	<i>T</i> ₂	2591.5	2286
19	<i>T</i> ₂	2367.5	2867	19	<i>T</i> ₂	2591.5	2286
20	<i>T</i> ₂	2367.5	2867	20	<i>T</i> ₂	2591.5	2286
21	<i>A</i> ₁	2492.2	0	21	<i>A</i> ₁	2685.5	0

Table S 33. $[(\text{HCl})_4]^- (T_d)$.

B3LYP(D3BJ)/def2-TZVPP				SCS-MP2/def2-TZVPP			
Nr.	Symmetry	Wavenumber [cm ⁻¹]	IR intensity [km mol ⁻¹]	Nr.	Symmetry	Wavenumber [cm ⁻¹]	IR intensity [km mol ⁻¹]
1	<i>T</i> ₂	10.0	0	1	<i>E</i>	10.0	0
2	<i>T</i> ₂	10.0	0	2	<i>E</i>	10.0	0
3	<i>T</i> ₂	10.0	0	3	<i>T</i> ₂	10.8	0
4	<i>E</i>	10.0	0	4	<i>T</i> ₂	10.8	0
5	<i>E</i>	10.0	0	5	<i>T</i> ₂	10.8	0
6	<i>A</i> ₁	98.5	0	6	<i>A</i> ₁	91.3	0
7	<i>T</i> ₂	106.6	11	7	<i>T</i> ₂	100.9	9
8	<i>T</i> ₂	106.6	11	8	<i>T</i> ₂	100.9	9
9	<i>T</i> ₂	106.6	11	9	<i>T</i> ₂	100.9	9
10	<i>T</i> ₁	452.2	0	10	<i>T</i> ₁	469.5	0
11	<i>T</i> ₁	452.2	0	11	<i>T</i> ₁	469.5	0
12	<i>T</i> ₁	452.2	0	12	<i>T</i> ₁	469.5	0
13	<i>T</i> ₂	474.9	14	13	<i>T</i> ₂	487.8	25
14	<i>T</i> ₂	474.9	14	14	<i>T</i> ₂	487.8	25
15	<i>T</i> ₂	474.9	14	15	<i>T</i> ₂	487.8	25
16	<i>E</i>	496.3	0	16	<i>E</i>	500.0	0
17	<i>E</i>	496.3	0	17	<i>E</i>	500.0	0
18	<i>T</i> ₂	2402.4	2985	18	<i>T</i> ₂	2651.8	2167
19	<i>T</i> ₂	2402.4	2985	19	<i>T</i> ₂	2651.8	2167
20	<i>T</i> ₂	2402.4	2985	20	<i>T</i> ₂	2651.8	2167
21	<i>A</i> ₁	2494.4	0	21	<i>A</i> ₁	2714.8	0

Table S 34. $[\text{Cl}(\text{HCl})_4]^-$ (C_{4v}).

B3LYP(D3BJ)/def2-TZVPP				SCS-MP2/def2-TZVPP			
Nr.	Symmetry	Wavenumber [cm ⁻¹]	IR intensity [km mol ⁻¹]	Nr.	Symmetry	Wavenumber [cm ⁻¹]	IR intensity [km mol ⁻¹]
1	B_2	-10.6	0	1	B_2	-10.3	0
2	A_1	15.7	0	2	A_1	10.5	0
3	E	18.9	0	3	E	19.1	0
4	E	18.9	0	4	E	19.1	0
5	B_1	22.1	0	5	B_1	21.9	0
6	B_2	99.7	0	6	B_2	96.5	0
7	A_1	131.9	1	7	A_1	117.2	0
8	E	170.4	72	8	E	166.5	71
9	E	170.4	72	9	E	166.5	71
10	B_2	489.8	0	10	B_2	512.2	0
11	A_2	492.6	0	11	A_2	516.6	0
12	E	518.7	14	12	E	546.7	18
13	E	518.7	14	13	E	546.7	18
14	E	539.6	35	14	A_1	550.4	75
15	E	539.6	35	15	E	553.1	34
16	A_1	539.6	58	16	E	553.1	34
17	B_1	604.7	0	17	B_1	611.1	0
18	E	2354.5	3929	18	E	2562.4	3451
19	E	2354.5	3929	19	E	2562.4	3451
20	B_2	2367.4	0	20	B_2	2580.6	0
21	A_1	2522.4	177	21	A_1	2697.6	26

Table S 35. $[\text{Br}(\text{HCl})_4]^-$ (C_{4v}).

B3LYP(D3BJ)/def2-TZVPP				SCS-MP2/def2-TZVPP			
Nr.	Symmetry	Wavenumber [cm ⁻¹]	IR intensity [km mol ⁻¹]	Nr.	Symmetry	Wavenumber [cm ⁻¹]	IR intensity [km mol ⁻¹]
1	B_2	-7.1	0	1	B_2	-6.1	0
2	E	14.6	0	2	A_1	13.9	0
3	E	14.6	0	3	E	16.1	0
4	A_1	14.7	0	4	E	16.1	0
5	B_1	18.7	0	5	B_1	18.5	0
6	B_2	93.8	0	6	B_2	93.4	0
7	A_1	117.9	2	7	A_1	105.1	0
8	E	127.1	27	8	E	128.5	30
9	E	127.1	27	9	E	128.5	30
10	A_2	462.1	0	10	B_2	505.6	0
11	B_2	471.8	0	11	A_2	505.9	0
12	E	479.7	14	12	A_1	530.2	62
13	E	479.7	14	13	E	531.2	33
14	E	502.4	18	14	E	531.2	33
15	E	502.4	18	15	E	532.4	0
16	A_1	512.6	40	16	E	532.4	0
17	B_1	554.0	0	17	B_1	580.7	0
18	E	2397.9	3639	18	E	2612.9	3381
19	E	2397.9	3639	19	E	2612.9	3381
20	B_2	2400.2	0	20	B_2	2631.0	0
21	A_1	2527.9	433	21	A_1	2717.4	0

Table S 36. $[(\text{HCl})_4]^-$ (C_{4v}).

B3LYP(D3BJ)/def2-TZVPP				SCS-MP2/def2-TZVPP			
Nr.	Symmetry	Wavenumber [cm ⁻¹]	IR intensity [km mol ⁻¹]	Nr.	Symmetry	Wavenumber [cm ⁻¹]	IR intensity [km mol ⁻¹]
1	B_2	-3.0	0	1	B_2	-5.2	0
2	E	10.6	0	2	A_1	9.0	0
3	E	10.6	0	3	E	11.3	0
4	A_1	12.9	0	4	E	11.3	0
5	B_1	14.7	0	5	B_1	13.8	0
6	B_2	87.3	0	6	B_2	83.2	0
7	A_1	105.5	2	7	A_1	94.5	1
8	E	107.2	14	8	E	104.0	13
9	E	107.2	14	9	E	104.0	13
10	A_2	426.6	0	10	A_2	450.0	0
11	E	437.4	11	11	B_2	454.0	0
12	E	437.4	11	12	E	461.3	16
13	B_2	443.2	0	13	E	461.3	16
14	E	457.5	11	14	E	474.6	9
15	E	457.5	11	15	E	474.6	9
16	A_1	476.5	28	16	A_1	477.3	43
17	B_1	496.3	0	17	B_1	508.0	0
18	B_2	2428.3	0	18	E	2668.7	2859
19	E	2433.5	3487	19	E	2668.7	2859
20	E	2433.5	3487	20	B_2	2673.7	0
21	A_1	2530.6	778	21	A_1	2737.2	327

Table S 37. $[\text{Cl}(\text{HCl})_4]^-$ (D_{4h}).

B3LYP(D3BJ)/def2-TZVPP				SCS-MP2/def2-TZVPP			
Nr.	Symmetry	Wavenumber [cm ⁻¹]	IR intensity [km mol ⁻¹]	Nr.	Symmetry	Wavenumber [cm ⁻¹]	IR intensity [km mol ⁻¹]
1	A_{2u}	-13.3	0	1	B_{1u}	-19,5	0
2	B_{1u}	-11.9	0	2	A_{2u}	17,8	0
3	E_u	16.4	0	3	E_u	19,5	0
4	E_u	16.4	0	4	E_u	19,5	0
5	B_{1g}	20.2	0	5	B_{1g}	21,9	0
6	B_{2g}	101.0	0	6	B_{2g}	96,6	0
7	A_{1g}	119.4	0	7	A_{1g}	114,7	0
8	E_u	173.9	80	8	E_u	167,2	72
9	E_u	173.9	80	9	E_u	167,2	72
10	B_{1u}	478.4	0	10	A_{2g}	516,7	0
11	A_{2g}	493.6	0	11	B_{1u}	527,6	0
12	A_{2u}	517.2	65	12	E_u	550,5	52
13	E_u	527.0	46	13	E_u	550,5	52
14	E_u	527.0	46	14	A_{2u}	563,6	78
15	E_g	528.6	0	15	E_g	564,4	0
16	E_g	528.6	0	16	E_g	564,4	0
17	B_{1g}	601.5	0	17	B_{1g}	609,5	0
18	E_u	2354.2	4242	18	E_u	2562,4	3491
19	E_u	2354.2	4242	19	E_u	2562,4	3491
20	B_{2g}	2381.1	0	20	B_{2g}	2582,2	0
21	A_{1g}	2525.6	0	21	A_{1g}	2698,0	0

Table S 38. $[\text{Br}(\text{HCl})_4]^-$ (D_{4h}).

B3LYP(D3BJ)/def2-TZVPP				SCS-MP2/def2-TZVPP			
Nr.	Symmetry	Wavenumber [cm ⁻¹]	IR intensity [km mol ⁻¹]	Nr.	Symmetry	Wavenumber [cm ⁻¹]	IR intensity [km mol ⁻¹]
1	A_{2u}	-11.1	0	1	E_u	16.3	0
2	B_{1u}	-10.2	0	2	E_u	16.3	0
3	E_u	10.5	0	3	B_{1u}	18.5	0
4	E_u	10.5	0	4	B_{1g}	18.6	0
5	B_{1g}	15.9	0	5	A_{2u}	18.8	0
6	B_{2g}	95.2	0	6	B_{2g}	93.3	0
7	A_{1g}	107.0	0	7	A_{1g}	105.0	0
8	E_u	130.6	34	8	E_u	128.6	30
9	E_u	130.6	34	9	E_u	128.6	30
10	B_{1u}	452.5	0	10	A_{2g}	505.8	0
11	A_{2g}	465.1	0	11	B_{1u}	506.9	0
12	A_{2u}	476.2	52	12	E_u	531.1	33
13	E_u	483.2	28	13	E_u	531.1	33
14	E_u	483.2	28	14	A_{2u}	531.5	62
15	E_g	496.4	0	15	E_g	533.8	0
16	E_g	496.4	0	16	E_g	533.8	0
17	B_{1g}	551.1	0	17	B_{1g}	580.7	0
18	E_u	2397.6	4264	18	E_u	2612.9	3381
19	E_u	2354.2	4242	19	E_u	2612.9	3381
20	B_{2g}	2381.1	0	20	B_{2g}	2631.0	0
21	A_{1g}	2525.6	0	21	A_{1g}	2717.4	0

Table S 39. $[(\text{HCl})_4]^-$ (D_{4h}).

B3LYP(D3BJ)/def2-TZVPP				SCS-MP2/def2-TZVPP			
Nr.	Symmetry	Wavenumber [cm ⁻¹]	IR intensity [km mol ⁻¹]	Nr.	Symmetry	Wavenumber [cm ⁻¹]	IR intensity [km mol ⁻¹]
1	A_{2u}	-10.2	0	1	B_{1u}	1.0	0
2	B_{1u}	-9.5	0	2	A_{2u}	10.7	0
3	E_u	5.0	0	3	E_u	11.7	0
4	E_u	5.0	0	4	E_u	11.7	0
5	B_{1g}	12.4	0	5	B_{1g}	14.5	0
6	B_{2g}	88.2	0	6	B_{2g}	84.5	0
7	A_{1g}	95.9	0	7	A_{1g}	90.6	0
8	E_u	110.1	19	8	E_u	106.0	15
9	E_u	110.1	19	9	E_u	106.0	15
10	B_{1u}	413.9	0	10	A_{2g}	449.5	0
11	A_{2g}	428.7	0	11	B_{1u}	461.1	0
12	A_{2u}	428.9	42	12	E_u	461.6	24
13	E_u	434.5	18	13	E_u	461.6	24
14	E_u	434.5	18	14	A_{2u}	475.7	54
15	E_g	454.7	0	15	E_g	487.2	0
16	E_g	454.7	0	16	E_g	487.2	0
17	B_{1g}	494.6	0	17	B_{1g}	504.0	0
18	E_u	2434.2	4409	18	E_u	2672.8	3163
19	E_u	2434.2	4409	19	E_u	2672.8	3163
20	B_{2g}	2458.4	0	20	B_{2g}	2686.6	0
21	A_{1g}	2540.1	0	21	A_{1g}	2744.3	0

Table S 40. [Cl(HF)₃]⁻.

B3LYP(D3BJ)/def2-TZVPP				SCS-MP2/def2-TZVPP			
Nr.	Symmetry	Wavenumber [cm ⁻¹]	IR intensity [km mol ⁻¹]	Nr.	Symmetry	Wavenumber [cm ⁻¹]	IR intensity [km mol ⁻¹]
1	A ₁	23.7	0	1	A ₁	24.2	0
2	E	27.1	0	2	E	27.7	0
3	E	27.1	0	3	E	27.7	0
4	A ₁	199.8	1	4	A ₁	191.2	2
5	E	231.1	18	5	E	223.6	20
6	E	231.1	18	6	E	223.6	20
7	A ₂	712.4	0	7	A ₂	743.0	0
8	E	728.0	46	8	E	758.1	47
9	E	728.0	46	9	E	758.1	47
10	A ₁	764.5	228	10	A ₁	786.2	259
11	E	788.9	73	11	E	809.4	87
12	E	788.9	73	12	E	809.4	87
13	E	3349.5	2284	13	E	3513.6	2100
14	E	3349.5	2284	14	E	3513.6	2100
15	A ₁	3439.7	399	15	A ₁	3594.0	308

Table S 41. [Br(HF)₃]⁻.

B3LYP(D3BJ)/def2-TZVPP				SCS-MP2/def2-TZVPP			
Nr.	Symmetry	Wavenumber [cm ⁻¹]	IR intensity [km mol ⁻¹]	Nr.	Symmetry	Wavenumber [cm ⁻¹]	IR intensity [km mol ⁻¹]
1	A ₁	18.8	2	1	A ₁	16.5	1
2	E	23.0	1	2	E	22.8	1
3	E	23.0	1	3	E	22.8	1
4	A ₁	168.6	1	4	A ₁	163.8	1
5	E	181.0	7	5	E	177.4	8
6	E	181.0	7	6	E	177.4	8
7	A ₂	654.6	0	7	A ₂	683.0	0
8	E	664.8	43	8	E	694.5	44
9	E	664.8	43	9	E	694.5	44
10	A ₁	694.3	196	10	A ₁	715.3	222
11	E	718.2	56	11	E	739.3	67
12	E	718.2	56	12	E	739.3	67
13	E	3434.6	2193	13	E	3593.9	2005
14	E	3434.6	2193	14	E	3593.9	2005
15	A ₁	3497.6	445	15	A ₁	3649.7	326

Table S 42. [(HF)₃]⁻.

B3LYP(D3BJ)/def2-TZVPP				SCS-MP2/def2-TZVPP			
Nr.	Symmetry	Wavenumber [cm ⁻¹]	IR intensity [km mol ⁻¹]	Nr.	Symmetry	Wavenumber [cm ⁻¹]	IR intensity [km mol ⁻¹]
1	A ₁	17.0	2	1	A ₁	17.7	1
2	E	19.8	1	2	E	20.7	1
3	E	19.8	1	3	E	20.7	1
4	A ₁	146.0	1	4	A ₁	139.8	1
5	E	152.2	3	5	E	145.8	4
6	E	152.2	3	6	E	145.8	4
7	A ₂	589.1	0	7	A ₂	621.9	0
8	E	595.3	41	8	E	628.2	51
9	E	595.3	41	9	E	628.2	51
10	A ₁	624.8	171	10	A ₁	650.6	197
11	E	643.3	46	11	E	666.3	56
12	E	643.3	46	12	E	666.3	56
13	E	3511.4	2131	13	E	3690.7	1799
14	E	3511.4	2131	14	E	3690.7	1799
15	A ₁	3552.8	587	15	A ₁	3725.7	461

Table S 43. [F(HF)₄]⁻.

B3LYP(D3BJ)/def2-TZVPP				SCS-MP2/def2-TZVPP			
Nr.	Symmetry	Wavenumber [cm ⁻¹]	IR intensity [km mol ⁻¹]	Nr.	Symmetry	Wavenumber [cm ⁻¹]	IR intensity [km mol ⁻¹]
1	E	39.4	0	1	E	38.1	0
2	E	39.4	0	2	E	38.1	0
3	T ₂	55.4	2	3	T ₂	55.7	1
4	T ₂	55.4	2	4	T ₂	55.7	1
5	T ₂	55.4	2	5	T ₂	55.7	1
6	A ₁	247.7	0	6	A ₁	240.7	0
7	T ₂	310.8	26	7	T ₂	299.2	28
8	T ₂	310.8	26	8	T ₂	299.2	28
9	T ₂	310.8	26	9	T ₂	299.2	28
10	T ₁	800.1	0	10	T ₁	838.0	0
11	T ₁	800.1	0	11	T ₁	838.0	0
12	T ₁	800.1	0	12	T ₁	838.0	0
13	E	946.8	0	13	E	970.7	0
14	E	946.8	0	14	E	970.7	0
15	T ₂	955.9	335	15	T ₂	989.1	348
16	T ₂	955.9	335	16	T ₂	989.1	348
17	T ₂	955.9	335	17	T ₂	989.1	348
18	T ₂	3291.0	1857	18	T ₂	3390.4	1830
19	T ₂	3291.0	1857	19	T ₂	3390.4	1830
20	T ₂	3291.0	1857	20	T ₂	3390.4	1830
21	A ₁	3529.2	0	21	A ₁	3618.2	0

Table S 44. [Cl(HF)₄]⁻.

B3LYP(D3BJ)/def2-TZVPP				SCS-MP2/def2-TZVPP			
Nr.	Symmetry	Wavenumber [cm ⁻¹]	IR intensity [km mol ⁻¹]	Nr.	Symmetry	Wavenumber [cm ⁻¹]	IR intensity [km mol ⁻¹]
1	<i>E</i>	23.2	0	1	<i>E</i>	19.6	0
2	<i>E</i>	23.2	0	2	<i>E</i>	19.6	0
3	<i>T</i> ₂	26.4	1	3	<i>T</i> ₂	25.5	1
4	<i>T</i> ₂	26.4	1	4	<i>T</i> ₂	25.5	1
5	<i>T</i> ₂	26.4	1	5	<i>T</i> ₂	25.5	1
6	<i>A</i> ₁	171.1	0	6	<i>A</i> ₁	164.9	0
7	<i>T</i> ₂	211.2	11	7	<i>T</i> ₂	202.3	12
8	<i>T</i> ₂	211.2	11	8	<i>T</i> ₂	202.3	12
9	<i>T</i> ₂	211.2	11	9	<i>T</i> ₂	202.3	12
10	<i>T</i> ₁	646.2	0	10	<i>T</i> ₁	677.3	0
11	<i>T</i> ₁	646.2	0	11	<i>T</i> ₁	677.3	0
12	<i>T</i> ₁	646.2	0	12	<i>T</i> ₁	677.3	0
13	<i>T</i> ₂	705.9	214	13	<i>T</i> ₂	733.2	242
14	<i>T</i> ₂	705.9	214	14	<i>T</i> ₂	733.2	242
15	<i>T</i> ₂	705.9	214	15	<i>T</i> ₂	733.2	242
16	<i>E</i>	726.3	0	16	<i>E</i>	747.5	0
17	<i>E</i>	726.3	0	17	<i>E</i>	747.5	0
18	<i>T</i> ₂	3499.2	1899	18	<i>T</i> ₂	3648.7	1682
19	<i>T</i> ₂	3499.2	1899	19	<i>T</i> ₂	3648.7	1682
20	<i>T</i> ₂	3499.2	1899	20	<i>T</i> ₂	3648.7	1682
21	<i>A</i> ₁	3593.3	0	21	<i>A</i> ₁	3730.8	0

Table S 45. [Br(HF)₄]⁻.

B3LYP(D3BJ)/def2-TZVPP				SCS-MP2/def2-TZVPP			
Nr.	Symmetry	Wavenumber [cm ⁻¹]	IR intensity [km mol ⁻¹]	Nr.	Symmetry	Wavenumber [cm ⁻¹]	IR intensity [km mol ⁻¹]
1	<i>E</i>	21.2	0	1	<i>E</i>	20.4	0
2	<i>E</i>	21.2	0	2	<i>E</i>	20.4	0
3	<i>T</i> ₂	21.8	2	3	<i>T</i> ₂	21.6	1
4	<i>T</i> ₂	21.8	2	4	<i>T</i> ₂	21.6	1
5	<i>T</i> ₂	21.8	2	5	<i>T</i> ₂	21.6	1
6	<i>A</i> ₁	152.9	0	6	<i>A</i> ₁	148.2	0
7	<i>T</i> ₂	168.8	5	7	<i>T</i> ₂	163.6	5
8	<i>T</i> ₂	168.8	5	8	<i>T</i> ₂	163.6	5
9	<i>T</i> ₂	168.8	5	9	<i>T</i> ₂	163.6	5
10	<i>T</i> ₁	601.9	0	10	<i>T</i> ₁	631.2	0
11	<i>T</i> ₁	601.9	0	11	<i>T</i> ₁	631.2	0
12	<i>T</i> ₁	601.9	0	12	<i>T</i> ₁	631.2	0
13	<i>T</i> ₂	645.9	179	13	<i>T</i> ₂	673.8	203
14	<i>T</i> ₂	645.9	179	14	<i>T</i> ₂	673.8	203
15	<i>T</i> ₂	645.9	179	15	<i>T</i> ₂	673.8	203
16	<i>E</i>	672.2	0	16	<i>E</i>	693.9	0
17	<i>E</i>	672.2	0	17	<i>E</i>	693.9	0
18	<i>T</i> ₂	3545.5	1897	18	<i>T</i> ₂	3693.7	1667
19	<i>T</i> ₂	3545.5	1897	19	<i>T</i> ₂	3693.7	1667
20	<i>T</i> ₂	3545.5	1897	20	<i>T</i> ₂	3693.7	1667
21	<i>A</i> ₁	3615.8	0	21	<i>A</i> ₁	3754.5	0

Table S 46. $[(\text{HF})_4]^-$.

B3LYP(D3BJ)/def2-TZVPP				SCS-MP2/def2-TZVPP			
Nr.	Symmetry	Wavenumber [cm ⁻¹]	IR intensity [km mol ⁻¹]	Nr.	Symmetry	Wavenumber [cm ⁻¹]	IR intensity [km mol ⁻¹]
1	T_2	18.1	2	1	E	10.6	0
2	T_2	18.1	2	2	E	10.6	0
3	T_2	18.1	2	3	T_2	13.0	2
4	E	18.6	0	4	T_2	13.0	2
5	E	18.6	0	5	T_2	13.0	2
6	A_1	135.9	0	6	A_1	129.2	0
7	T_2	145.1	2	7	T_2	138.1	3
8	T_2	145.1	2	8	T_2	138.1	3
9	T_2	145.1	2	9	T_2	138.1	3
10	T_1	548.2	0	10	T_1	583.9	0
11	T_1	548.2	0	11	T_1	583.9	0
12	T_1	548.2	0	12	T_1	583.9	0
13	T_2	582.9	154	13	T_2	614.2	184
14	T_2	582.9	154	14	T_2	614.2	184
15	T_2	582.9	154	15	T_2	614.2	184
16	E	609.7	0	16	E	632.1	0
17	E	609.7	0	17	E	632.1	0
18	T_2	3590.5	1954	18	T_2	3757.2	1613
19	T_2	3590.5	1954	19	T_2	3757.2	1613
20	T_2	3590.5	1954	20	T_2	3757.2	1613
21	A_1	3640.2	0	21	A_1	3798.0	0

Table S 47. Vibrational frequencies for $[\text{F}(\text{HF})_4]^-$ and $[\text{Cl}(\text{HF})_4]^-$ calculated on SCS-MP2(COSMO)/def2-TZVPP.

$[\text{F}(\text{HF})_4]^-$				$[\text{Cl}(\text{HF})_4]^-$			
Nr.	Symmetry	Wavenumber [cm ⁻¹]	IR intensity [km mol ⁻¹]	Nr.	Symmetry	Wavenumber [cm ⁻¹]	IR intensity [km mol ⁻¹]
1	E	34.2	0	1	T_2	19.6	1
2	E	34.2	0	2	T_2	19.6	1
3	T_2	49.6	3	3	T_2	19.6	1
4	T_2	49.6	3	4	E	20.1	0
5	T_2	49.6	3	5	E	20.1	0
6	A_1	252.3	0	6	A_1	169.4	0
7	T_2	300.3	42	7	T_2	202.1	19
8	T_2	300.3	42	8	T_2	202.1	19
9	T_2	300.3	42	9	T_2	202.1	19
10	T_1	806.7	0	10	T_1	585.2	0
11	T_1	806.7	0	11	T_1	585.2	0
12	T_1	806.7	0	12	T_1	585.2	0
13	T_2	897.9	490	13	T_2	609.5	389
14	T_2	897.9	490	14	T_2	609.5	389
15	T_2	897.9	490	15	T_2	609.5	389
16	E	911.7	0	16	E	631.6	0
17	E	911.7	0	17	E	631.6	0
18	T_2	3312.5	2257	18	T_2	3595.0	2261
19	T_2	3312.5	2257	19	T_2	3595.0	2261
20	T_2	3312.5	2257	20	T_2	3595.0	2261
21	A_1	3573.4	0	21	A_1	3683.7	0

Table S 48. Vibrational frequencies for $[\text{Br}(\text{HF})_4]^-$ and $[\text{I}(\text{HF})_4]^-$ calculated on SCS-MP2(COSMO)/def2-TZVPP.

$[\text{Br}(\text{HF})_4]^-$				$[\text{I}(\text{HF})_4]^-$			
Nr.	Symmetry	Wavenumber [cm^{-1}]	IR intensity [km mol^{-1}]	Nr.	Symmetry	Wavenumber [cm^{-1}]	IR intensity [km mol^{-1}]
1	E	16.7	0	1	E	5.9	0
2	E	16.7	0	2	E	5.9	0
3	T_2	21.9	2	3	T_2	16.7	2
4	T_2	21.9	2	4	T_2	16.7	2
5	T_2	21.9	2	5	T_2	16.7	2
6	A_1	151.0	0	6	A_1	130.5	0
7	T_2	164.8	10	7	T_2	139.2	6
8	T_2	164.8	10	8	T_2	139.2	6
9	T_2	164.8	10	9	T_2	139.2	6
10	T_1	526.5	0	10	T_2	457.9	356
11	T_1	526.5	0	11	T_2	457.9	356
12	T_1	526.5	0	12	T_2	457.9	356
13	T_2	536.0	363	13	T_1	458.5	0
14	T_2	536.0	363	14	T_1	458.5	0
15	T_2	536.0	363	15	T_1	458.5	0
16	E	561.6	0	16	E	483.0	0
17	E	561.6	0	17	E	483.0	0
18	T_2	3647.7	2354	18	T_2	3714.2	2336
19	T_2	3647.7	2354	19	T_2	3714.2	2336
20	T_2	3647.7	2354	20	T_2	3714.2	2336
21	A_1	3712.3	0	21	A_1	3753.4	0

Table S 49. $[\text{Cl}(\text{HF})_2(\text{HCl})]^-$.

B3LYP(D3BJ)/def2-TZVPP				SCS-MP2/def2-TZVPP			
Nr.	Symmetry	Wavenumber [cm^{-1}]	IR intensity [km mol^{-1}]	Nr.	Symmetry	Wavenumber [cm^{-1}]	IR intensity [km mol^{-1}]
1	A'	23.0	0	1	A'	15.0	0
2	A''	23.3	0	2	A''	17.3	0
3	A'	26.1	0	3	A'	20.3	0
4	A'	174.6	29	4	A'	159.0	26
5	A'	209.8	27	5	A'	201.7	27
6	A''	227.0	18	6	A''	221.3	21
7	A'	631.9	11	7	A'	632.3	16
8	A''	635.6	5	8	A''	636.1	10
9	A''	711.6	43	9	A''	750.5	46
10	A'	742.2	155	10	A'	772.8	179
11	A''	748.6	11	11	A''	775.4	9
12	A'	772.6	93	12	A'	801.5	110
13	A'	2082.1	2970	13	A'	2370.8	2480
14	A''	3379.2	2162	14	A''	3524.8	2051
15	A'	3437.2	1031	15	A'	3577.7	904

Table S 50. [Br(HF)₂(HBr)]⁻.

B3LYP(D3BJ)/def2-TZVPP				SCS-MP2/def2-TZVPP			
Nr.	Symmetry	Wavenumber [cm ⁻¹]	IR intensity [km mol ⁻¹]	Nr.	Symmetry	Wavenumber [cm ⁻¹]	IR intensity [km mol ⁻¹]
1	A'	18.2	1	1	A'	-19.1	0
2	A''	18.4	0	2	A''	-15.4	0
3	A'	21.8	1	3	A'	20.9	1
4	A'	115.2	28	4	A'	102.9	24
5	A'	167.8	7	5	A'	165.0	8
6	A''	175.2	6	6	A''	174.7	8
7	A'	574.0	3	7	A'	564.8	5
8	A''	577.2	0	8	A''	581.4	2
9	A''	639.3	36	9	A''	680.9	38
10	A'	666.1	113	10	A'	710.7	146
11	A''	676.1	6	11	A''	719.3	4
12	A'	692.3	76	12	A'	725.7	83
13	A'	1711.4	3728	13	A'	2007.8	3015
14	A''	3481.7	1977	14	A''	3616.9	1902
15	A'	3520.1	1109	15	A'	3651.9	953

Table S 51. [(HF)₂(HI)]⁻.

B3LYP(D3BJ)/def2-TZVPP				SCS-MP2/def2-TZVPP			
Nr.	Symmetry	Wavenumber [cm ⁻¹]	IR intensity [km mol ⁻¹]	Nr.	Symmetry	Wavenumber [cm ⁻¹]	IR intensity [km mol ⁻¹]
1	A''	15.2	0	1	A'	8.7	1
2	A'	15.4	2	2	A''	15.6	0
3	A'	18.9	1	3	A'	15.7	2
4	A'	86.4	26	4	A'	70.7	21
5	A'	142.8	4	5	A'	137.0	4
6	A''	147.0	3	6	A''	141.8	4
7	A'	495.0	0	7	A'	483.9	0
8	A''	499.5	1	8	A''	489.7	0
9	A''	567.5	31	9	A''	616.5	37
10	A'	591.0	78	10	A'	627.1	111
11	A''	600.1	3	11	A''	631.4	3
12	A'	614.1	68	12	A'	652.4	84
13	A'	1395.2	4818	13	A'	1775.0	3594
14	A''	3561.5	1902	14	A''	3710.3	1694
15	A'	3585.7	1233	15	A'	3731.7	1015

Table S 52. $[\text{Cl}(\text{HF})_2(\text{HCl})_2]^-$.

B3LYP(D3BJ)/def2-TZVPP				SCS-MP2/def2-TZVPP			
Nr.	Symmetry	Wavenumber [cm ⁻¹]	IR intensity [km mol ⁻¹]	Nr.	Symmetry	Wavenumber [cm ⁻¹]	IR intensity [km mol ⁻¹]
1	A ₁	14.8	0	1	A ₁	15.4	0
2	A ₂	18.4	0	2	A ₂	19.8	0
3	B ₂	20.5	0	3	B ₂	22.3	0
4	B ₁	21.7	1	4	A ₁	23.6	0
5	A ₁	24.0	1	5	B ₁	23.8	1
6	A ₁	138.1	6	6	A ₁	129.6	6
7	B ₁	159.5	38	7	B ₁	151.7	33
8	A ₁	195.4	17	8	A ₁	188.8	16
9	B ₂	210.5	12	9	B ₂	203.9	14
10	B ₁	533.5	2	10	B ₁	546.6	5
11	A ₂	547.8	0	11	A ₂	569.7	0
12	B ₂	554.2	16	12	B ₂	576.7	24
13	A ₁	576.5	25	13	A ₁	580.0	28
14	B ₂	660.9	63	14	B ₂	695.1	70
15	B ₁	686.6	147	15	A ₂	718.8	0
16	A ₂	688.9	0	16	B ₁	721.8	174
17	A ₁	710.6	95	17	A ₁	742.0	112
18	B ₁	2314.4	2928	18	B ₁	2557.7	2332
19	A ₁	2399.6	1365	19	A ₁	2619.8	1092
20	B ₂	3508.4	1837	20	B ₂	3637.6	1662
21	A ₁	3554.8	978	21	A ₁	3679.5	892

Table S 53. $[\text{Br}(\text{HF})_2(\text{HBr})_2]^-$.

B3LYP(D3BJ)/def2-TZVPP				SCS-MP2/def2-TZVPP			
Nr.	Symmetry	Wavenumber [cm ⁻¹]	IR intensity [km mol ⁻¹]	Nr.	Symmetry	Wavenumber [cm ⁻¹]	IR intensity [km mol ⁻¹]
1	A ₁	8.7	0	1	A ₁	9.1	0
2	B ₂	14.9	0	2	B ₂	15.1	0
3	A ₂	15.3	0	3	A ₂	16.7	0
4	B ₁	16.7	2	4	B ₁	18.8	2
5	A ₁	20.2	2	5	A ₁	20.2	1
6	A ₁	92.8	7	6	A ₁	85.8	7
7	B ₁	99.1	26	7	B ₁	94.5	22
8	A ₁	156.7	6	8	A ₁	155.7	6
9	B ₂	165.2	5	9	B ₂	163.3	6
10	B ₁	480.8	0	10	B ₁	487.2	1
11	A ₂	495.6	0	11	A ₂	499.1	0
12	B ₂	497.1	2	12	B ₂	501.4	7
13	A ₁	515.9	6	13	A ₁	512.0	8
14	B ₂	598.1	45	14	B ₂	638.5	48
15	B ₁	615.5	97	15	B ₁	669.7	127
16	A ₂	624.5	0	16	A ₂	671.6	0
17	A ₁	640.2	75	17	A ₁	679.3	93
18	B ₁	1966.6	3701	18	B ₁	2213.9	2761
19	A ₁	2061.7	1554	19	A ₁	2278.4	1162
20	B ₂	3578.0	1752	20	B ₂	3700.4	1571
21	A ₁	3609.8	1058	21	A ₁	3729.0	951

Table S 54. [(HF)₂(HI)₂]⁻.

B3LYP(D3BJ)/def2-TZVPP				SCS-MP2/def2-TZVPP			
Nr.	Symmetry	Wavenumber [cm ⁻¹]	IR intensity [km mol ⁻¹]	Nr.	Symmetry	Wavenumber [cm ⁻¹]	IR intensity [km mol ⁻¹]
1	A ₁	4.6	0	1	A ₁	6.6	1
2	B ₂	11.5	0	2	B ₂	8.0	0
3	A ₂	13.0	0	3	A ₁	11.3	1
4	B ₁	13.8	3	4	A ₂	17.9	0
5	A ₁	17.7	2	5	B ₁	18.6	2
6	A ₁	68.6	6	6	A ₁	59.5	6
7	B ₁	71.4	26	7	B ₁	64.1	19
8	A ₁	135.3	4	8	A ₁	132.0	3
9	B ₂	140.8	2	9	B ₂	137.1	3
10	B ₁	410.4	2	10	B ₁	416.6	0
11	B ₂	424.7	1	11	B ₂	430.2	0
12	A ₂	426.2	0	12	A ₂	430.7	0
13	A ₁	436.8	0	13	A ₁	433.7	0
14	B ₂	535.9	34	14	B ₂	587.4	39
15	B ₁	549.4	57	15	B ₁	596.9	98
16	A ₂	559.9	0	16	A ₂	601.0	0
17	A ₁	574.1	63	17	A ₁	619.3	83
18	B ₁	1646.8	4998	18	B ₁	1965.4	3226
19	A ₁	1746.5	1817	19	A ₁	2022.3	1243
20	B ₂	3628.1	1752	20	B ₂	3763.5	1513
21	A ₁	3648.9	1210	21	A ₁	3781.8	986

Table S 55. HCN.

B3LYP(D3BJ)/def2-TZVPP				SCS-MP2/def2-TZVPP			
Nr.	Symmetry	Wavenumber [cm ⁻¹]	IR intensity [km mol ⁻¹]	Nr.	Symmetry	Wavenumber [cm ⁻¹]	IR intensity [km mol ⁻¹]
1	Π	767.8	37	1	Π	731.9	37
2	Π	767.8	37	2	Π	731.9	37
3	Σ ⁺	2201.1	1	3	Σ ⁺	2066.2	0
4	Σ ⁺	3443.5	65	4	Σ ⁺	3467.4	72

Table S 56. [Br(HCN)]⁻.

B3LYP(D3BJ)/def2-TZVPP				SCS-MP2/def2-TZVPP			
Nr.	Symmetry	Wavenumber [cm ⁻¹]	IR intensity [km mol ⁻¹]	Nr.	Symmetry	Wavenumber [cm ⁻¹]	IR intensity [km mol ⁻¹]
1	Σ ⁺	159.1	16	1	Σ ⁺	158.7	16
2	Π	166.1	20	2	Π	194.5	20
3	Π	166.1	20	3	Π	194.5	20
4	Π	982.5	16	4	Π	1010.6	17
5	Π	982.5	16	5	Π	1010.6	17
6	Σ ⁺	2092.5	555	6	Σ ⁺	2013.6	223
7	Σ ⁺	2834.1	1339	7	Σ ⁺	2945.9	1398

Table S 57. [ClO₄]⁻.

B3LYP(D3BJ)/def2-TZVPP				SCS-MP2/def2-TZVPP			
Nr.	Symmetry	Wavenumber [cm ⁻¹]	IR intensity [km mol ⁻¹]	Nr.	Symmetry	Wavenumber [cm ⁻¹]	IR intensity [km mol ⁻¹]
1	<i>E</i>	449.5	0	1	<i>E</i>	470.2	0
2	<i>E</i>	449.5	0	2	<i>E</i>	470.2	0
3	<i>T</i> ₂	617.4	23	3	<i>T</i> ₂	647.3	29
4	<i>T</i> ₂	617.4	23	4	<i>T</i> ₂	647.3	29
5	<i>T</i> ₂	617.4	23	5	<i>T</i> ₂	647.3	29
6	<i>A</i> ₁	918.4	0	6	<i>A</i> ₁	1001.7	0
7	<i>T</i> ₂	1103.0	384	7	<i>T</i> ₂	1175.3	429
8	<i>T</i> ₂	1103.0	384	8	<i>T</i> ₂	1175.3	429
9	<i>T</i> ₂	1103.0	384	9	<i>T</i> ₂	1175.3	429

Table S 58. [ClO₄(HF)₂]⁻.

B3LYP(D3BJ)/def2-TZVPP				SCS-MP2/def2-TZVPP			
Nr.	Symmetry	Wavenumber [cm ⁻¹]	IR intensity [km mol ⁻¹]	Nr.	Symmetry	Wavenumber [cm ⁻¹]	IR intensity [km mol ⁻¹]
1	<i>B</i> ₁	10.1	1	1	<i>B</i> ₁	12.0	1
2	<i>A</i> ₂	15.0	0	2	<i>A</i> ₂	20.5	0
3	<i>A</i> ₁	42.3	2	3	<i>A</i> ₁	39.2	1
4	<i>B</i> ₂	79.1	0	4	<i>B</i> ₂	73.1	0
5	<i>A</i> ₁	178.0	0	5	<i>A</i> ₁	168.6	0
6	<i>B</i> ₂	258.9	50	6	<i>B</i> ₂	242.9	48
7	<i>A</i> ₂	439.5	0	7	<i>A</i> ₂	463.8	0
8	<i>A</i> ₁	470.6	3	8	<i>A</i> ₁	489.0	3
9	<i>B</i> ₁	605.6	14	9	<i>B</i> ₁	637.5	15
10	<i>B</i> ₂	607.5	24	10	<i>B</i> ₂	640.0	33
11	<i>A</i> ₁	636.2	6	11	<i>A</i> ₁	663.1	6
12	<i>A</i> ₂	767.1	0	12	<i>A</i> ₂	772.3	0
13	<i>B</i> ₁	770.5	190	13	<i>B</i> ₁	775.7	205
14	<i>B</i> ₂	847.5	10	14	<i>B</i> ₂	842.8	5
15	<i>A</i> ₁	847.7	138	15	<i>A</i> ₁	843.9	164
16	<i>A</i> ₁	919.3	19	16	<i>A</i> ₁	1001.6	18
17	<i>B</i> ₂	1042.2	659	17	<i>B</i> ₂	1116.0	710
18	<i>A</i> ₁	1113.9	359	18	<i>A</i> ₁	1185.4	394
19	<i>B</i> ₁	1166.8	363	19	<i>B</i> ₁	1237.2	406
20	<i>B</i> ₂	3451.8	3239	20	<i>B</i> ₂	3615.2	2882
21	<i>A</i> ₁	3488.4	33	21	<i>A</i> ₁	3646.4	27

Table S 59. $[(\text{HBr})_2]^-$.

B3LYP(D3BJ)/def2-TZVPP				SCS-MP2/def2-TZVPP			
Nr.	Symmetry	Wavenumber [cm ⁻¹]	IR intensity [km mol ⁻¹]	Nr.	Symmetry	Wavenumber [cm ⁻¹]	IR intensity [km mol ⁻¹]
1	A_1	10.3	0	1	A_1	10.1	0
2	A_1	98.2	9	2	A_1	85.9	9
3	B_1	98.8	39	3	B_1	88.2	34
4	B_1	526.1	3	4	B_1	525.1	0
5	B_2	533.6	4	5	B_2	531.2	7
6	A_2	542.7	0	6	A_2	537.8	0
7	A_1	580.1	1	7	A_1	558.9	2
8	B_1	1610.6	6297	8	B_1	1939.9	5161
9	A_1	1749.2	2345	9	A_1	2036.4	1831

g) Raman Spectra of Samples Cooled to $-196\text{ }^{\circ}\text{C}$

Method for low temperature Raman spectroscopy of single crystals:

- 1) Transfer of the sample from the reaction flask into a cool nitrogen stream where a crystal can be selected (Figure S 23).
- 2) Transfer of the selected crystal onto a Teflon plate which is cooled by a copper block which is cooled by liquid nitrogen (Figure S 24, Figure S 25). By evaporation of the nitrogen a layer of cool gaseous nitrogen protects the sample from moisture.
- 3) Measuring of the Raman spectra using a Raman microscope (Figure S 26).

As often rather big needle shaped crystals were obtained often a crystal was split with a scalpel and one part was used for XRD while the other part was used for Raman spectroscopy.

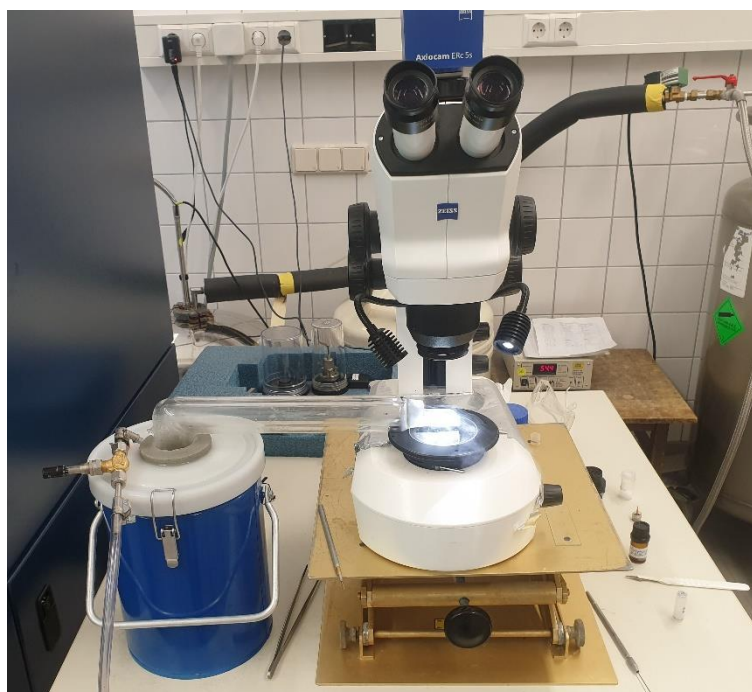


Figure S 23. Setting for preparing a single crystal for x-ray diffraction or low temperature Raman spectroscopy.

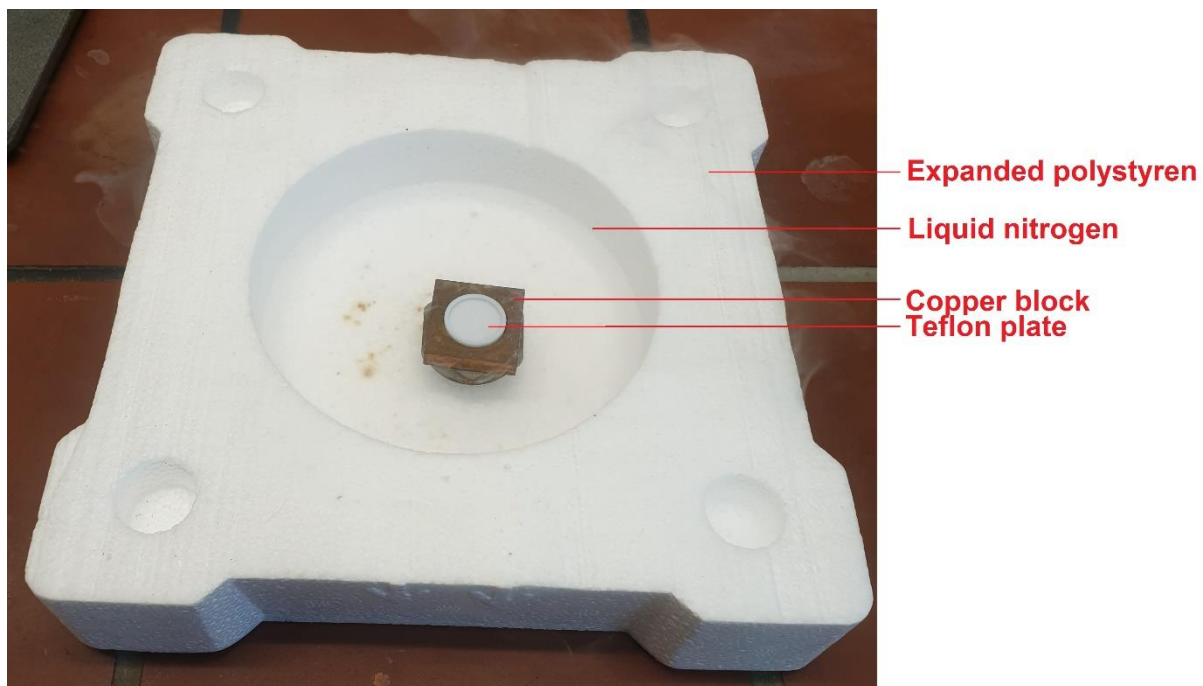


Figure S 24. Setting for cooling a sample to $-196\text{ }^{\circ}\text{C}$ for low temperature Raman spectroscopy.

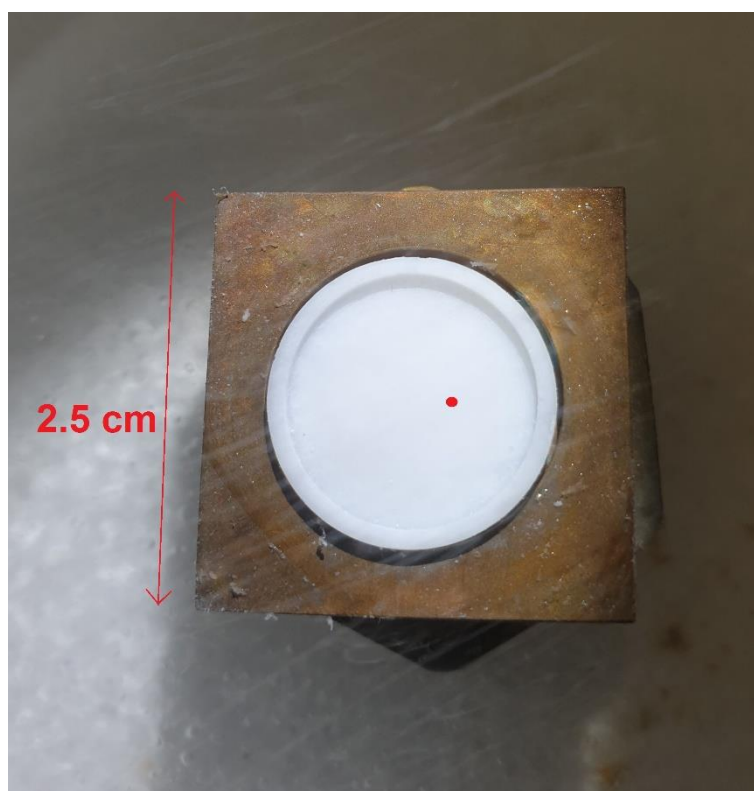


Figure S 25. Prepared crystal (red dot) on the Teflon plate for low temperature Raman spectroscopy.

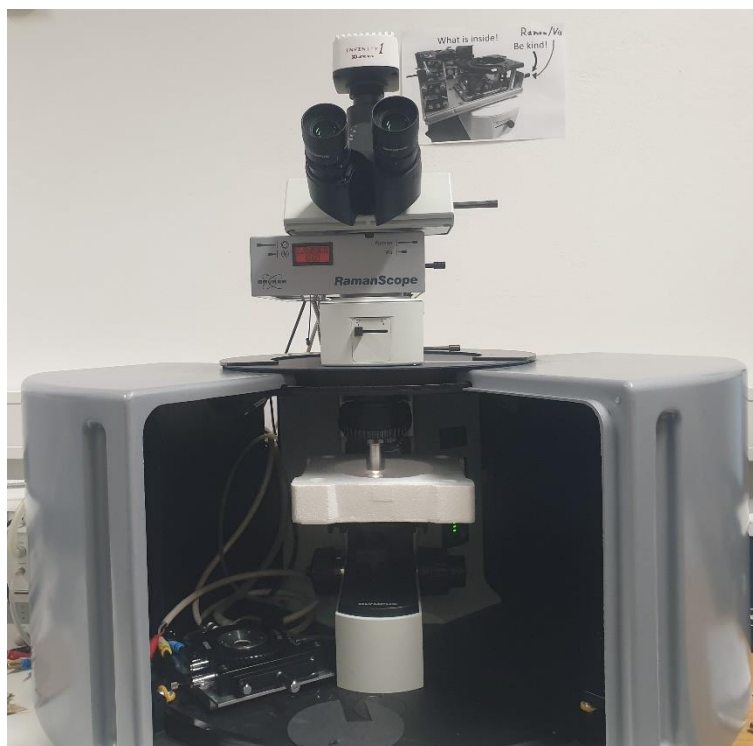


Figure S 26. Assembly in the RamanScope.

8.2 SI of From Missing Links to New Records: A Series of Novel Polychlorine Anions

Patrick Voßnacker, Thomas Keilhack, Nico Schwarze, Karsten Sonnenberg, Konrad Seppelt, Moritz Malischewski*, Sebastian Riedel*

Eur. J. Inorg. Chem. **2021**, 2021, 1034.

<https://doi.org/10.1002/ejic.202001072>

© 2020 The Authors. *European Journal of Inorganic Chemistry* published by Wiley-VCH GmbH

European Journal of Inorganic Chemistry

Supporting Information

From Missing Links to New Records: A Series of Novel Polychlorine Anions

Patrick Voßnacker, Thomas Keilhack, Nico Schwarze, Karsten Sonnenberg, Konrad Seppelt,
Moritz Malischewski,* and Sebastian Riedel*

Table of Contents

a) Molecular Structures Including Cations and Disorders	2
a1. [CCl(NMe ₂) ₂][Cl(Cl ₂) ₃]	2
a2. [NPr ₄][Cl(Cl ₂) ₄].....	3
a3. [Cp* ₂ Fe][Cl(Cl ₂) ₄ (HF)]	5
a4. [Cp* ₂ Fe] ₂ [Cl ₂₀].....	6
b) Experimental and Calculated Raman Spectra	8
c) Optimized Structures	13
d) Calculated Energies and Free Reaction Energies.....	17
d1) B3LYP(D3BJ)/def2-TZVPP Energies	17
d2) SCS-MP2/def2-TZVPP Energies	19
d3) Free Reaction Energy Calculation	20
d4) Comparison Between Different Structures	22
e) Coordinates of Optimized Structures	23
f) Calculated Vibrational Spectra.....	47
g) Raman Spectra of Samples Cooled to –196 °C.....	69
h) Crystal Data	72
i) Pictures of Samples	74

a) Molecular Structures Including Cations and Disorders

a1. $[\text{CCl}(\text{NMe}_2)_2][\text{Cl}(\text{Cl}_2)_3]$

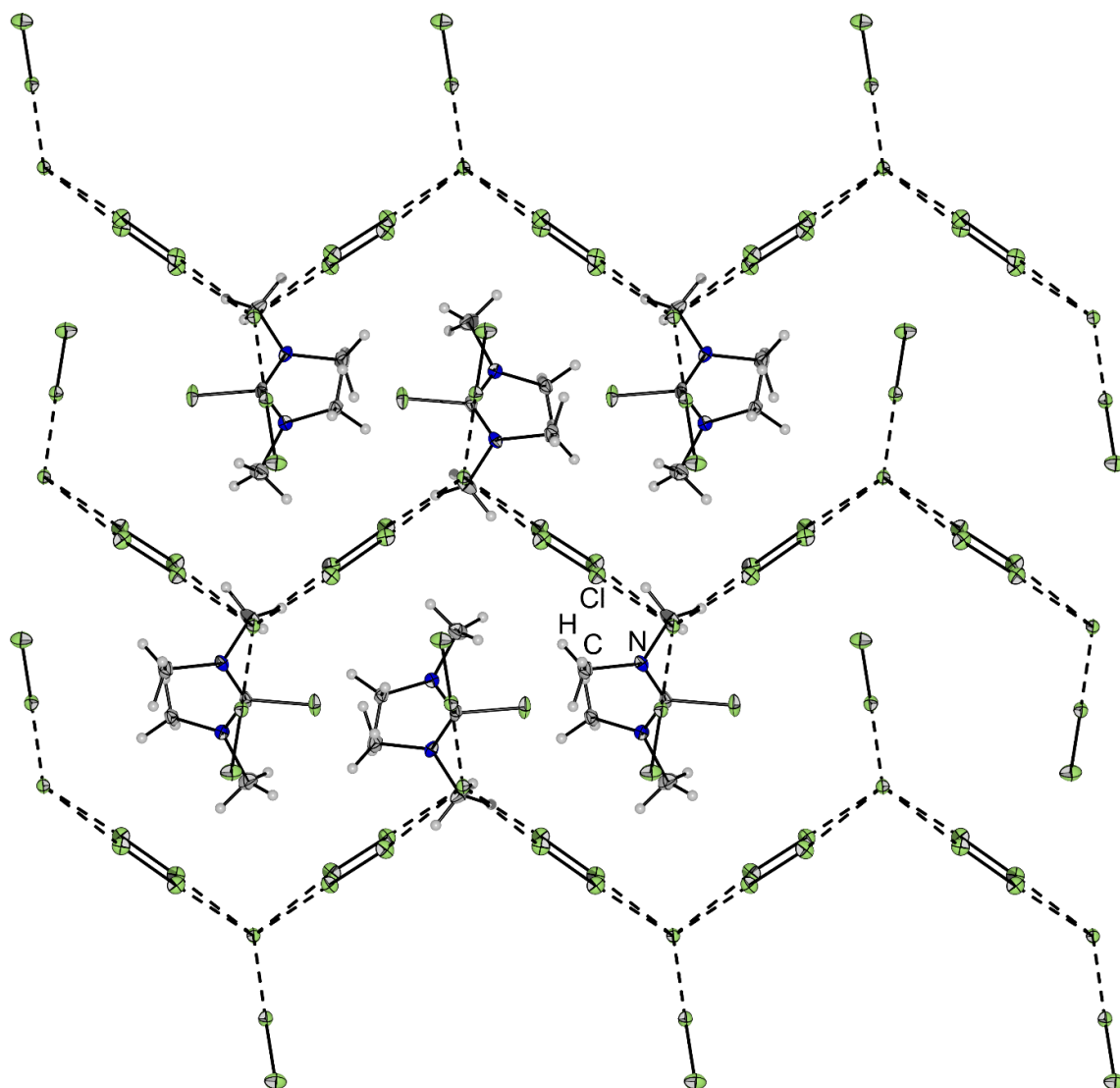


Figure S1. Arrangement of the ions within the solid state structure of $[\text{NPr}_3\text{Me}][\text{Cl}(\text{Cl}_2)_3]$. Thermal ellipsoids are shown at 50 % probability.

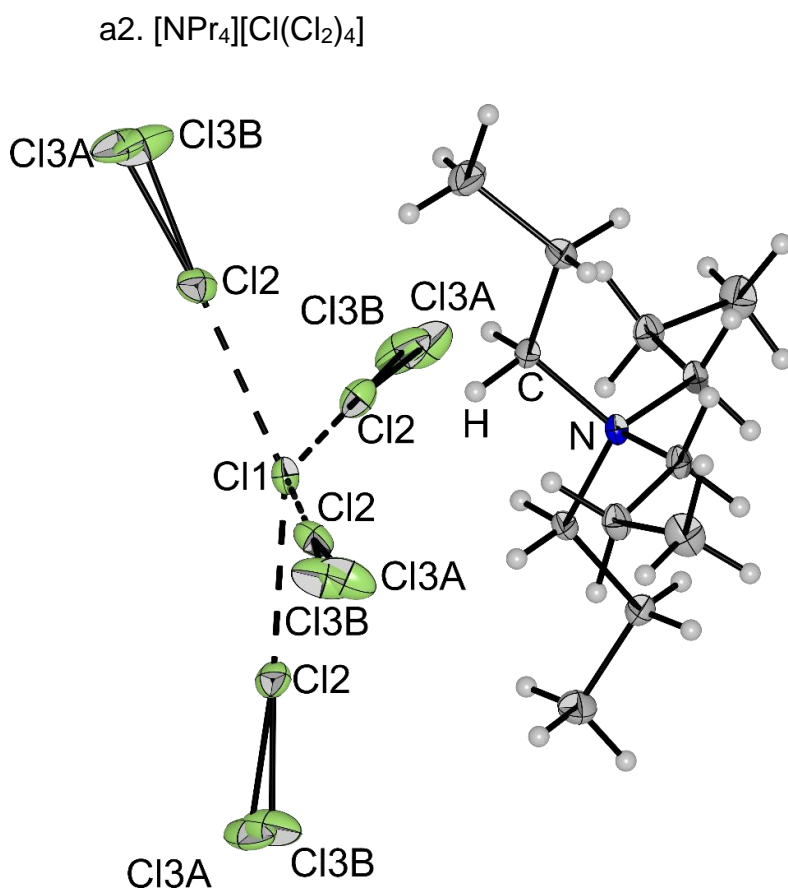


Figure S2. Molecular structure of $[\text{NPr}_4][\text{Cl}(\text{Cl}_2)_4]$ in the solid state including disorders with thermal ellipsoids shown at 50 % probability. The occupation number of Cl3A is 70(4) % while the occupation number of Cl3B is 30(4) %.

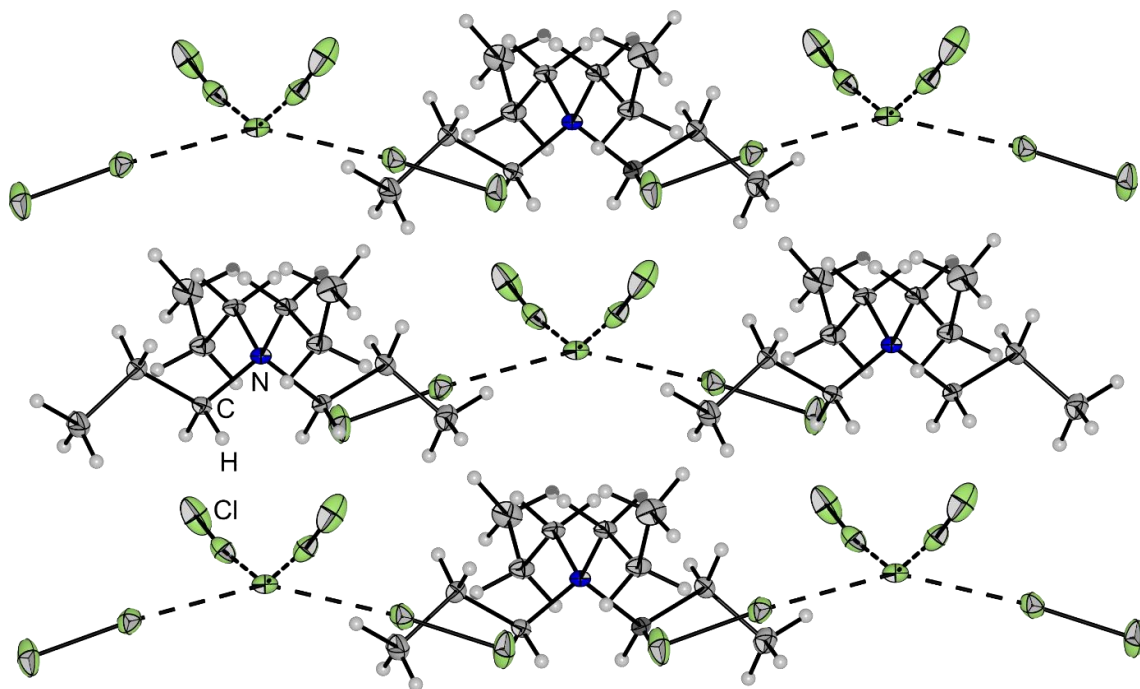


Figure S3. Arrangement of the ions within the solid state structure of $[\text{NPr}_4][\text{Cl}(\text{Cl}_2)_4]$. Thermal ellipsoids are shown at 50 % probability. Disorder is omitted for clarity.

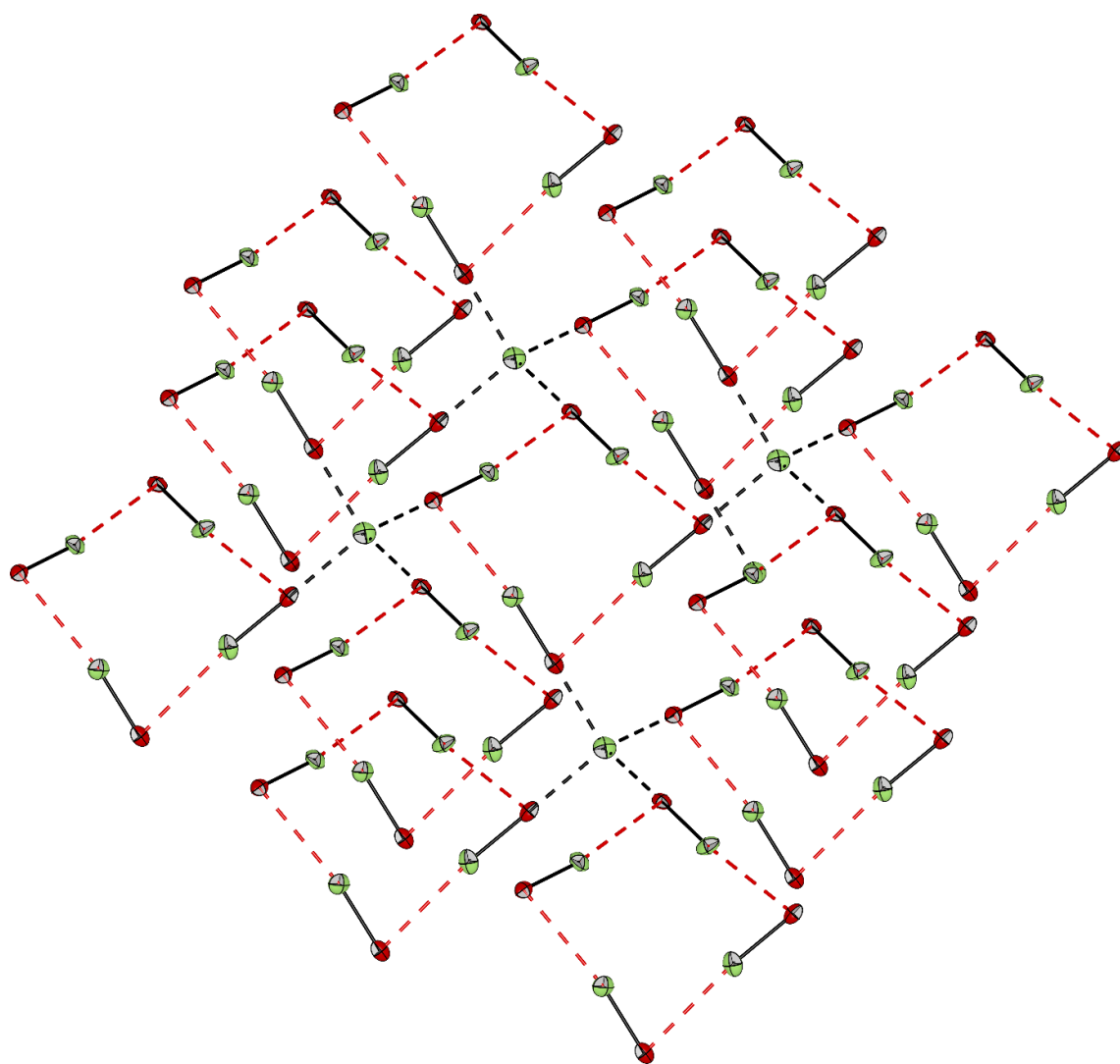


Figure S4. Structure of the anion within the solid state structure of [NPr₄][Cl(BrCl)₄]. The [Cl(BrCl)₄]⁻ anions are connected via Br1-Cl2 distances of 350.8(2) pm (dotted red lines). Thermal ellipsoids are shown at 50 % probability.

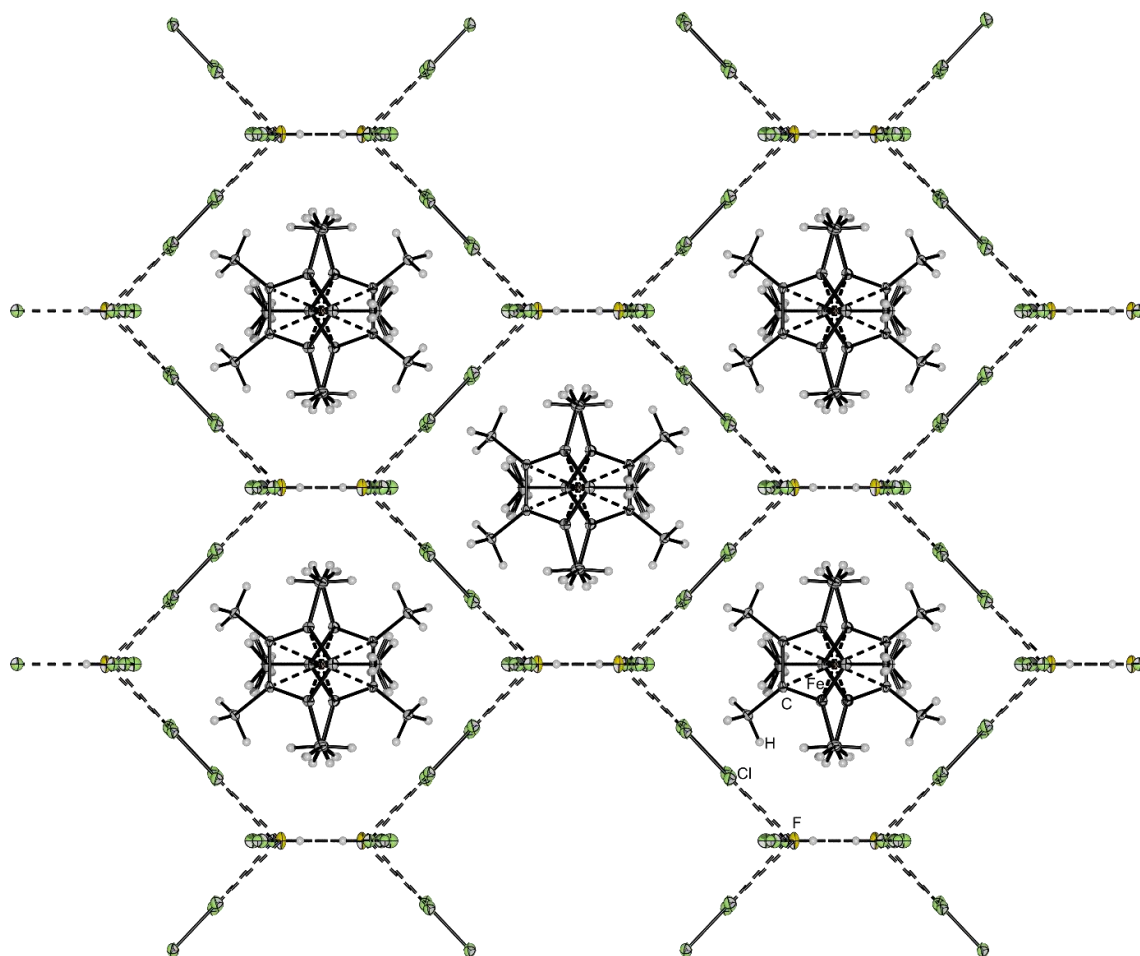
a3. $[\text{Cp}^*_2\text{Fe}][\text{Cl}(\text{Cl}_2)_4(\text{HF})]$ 

Figure S5. Arrangement of the ions within the solid state structure of $[\text{Cp}^*_2\text{Fe}][\text{Cl}(\text{Cl}_2)_4(\text{HF})]$ (viewing along the crystallographic a axes). Thermal ellipsoids are shown at 50 % probability.

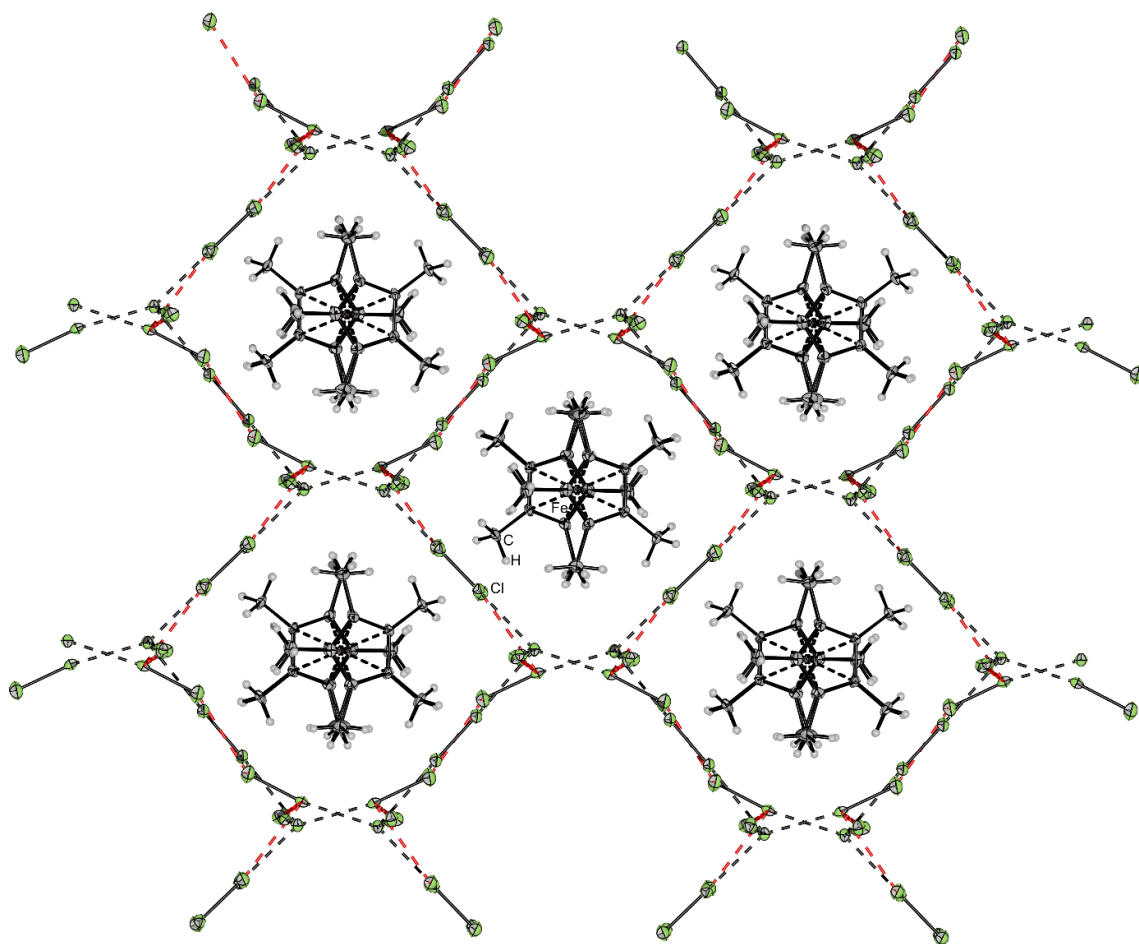
a4. $[\text{Cp}^*_2\text{Fe}]_2[\text{Cl}_{20}]$ 

Figure S6. Arrangement of the ions within the solid state structure of $[\text{Cp}^*_2\text{Fe}]_2[\text{Cl}_{20}]$ (viewing along the crystallographic *a* axes). Thermal ellipsoids are shown at 50 % probability. Intermolecular interactions are indicated with red dotted lines.

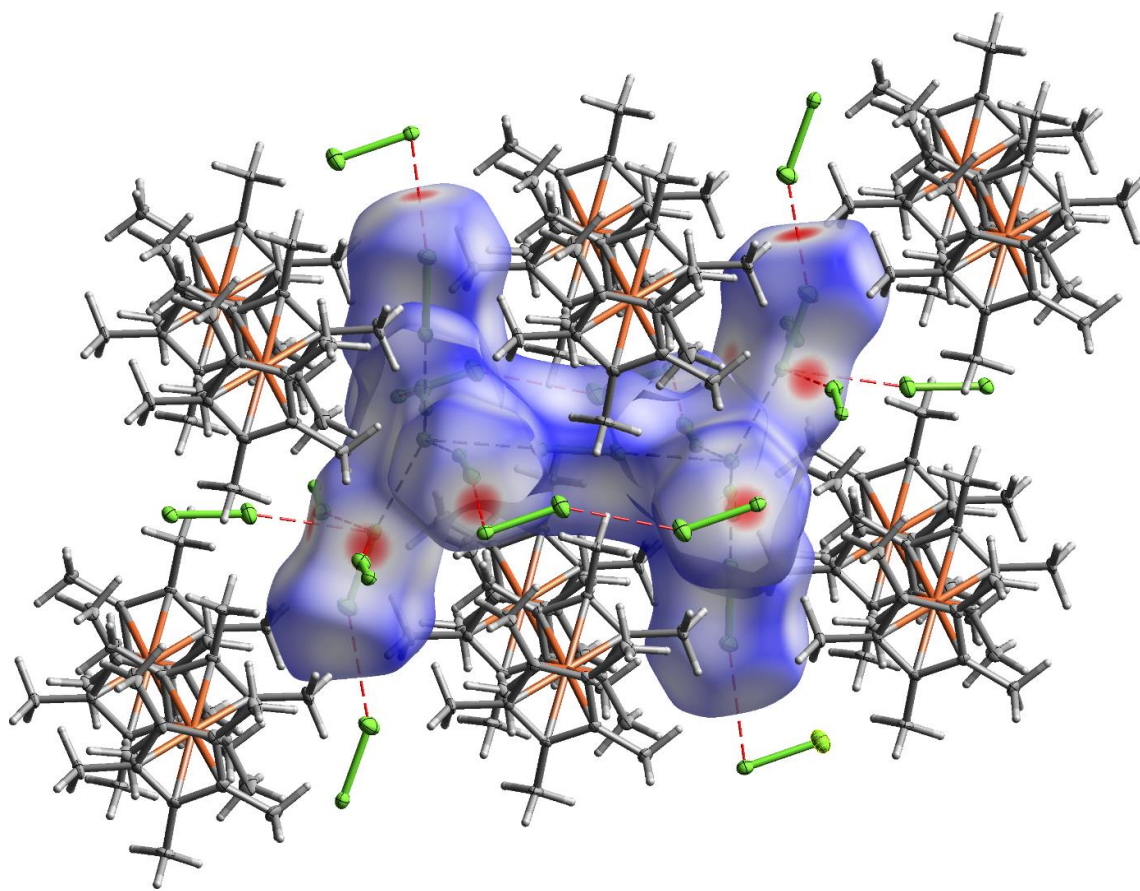
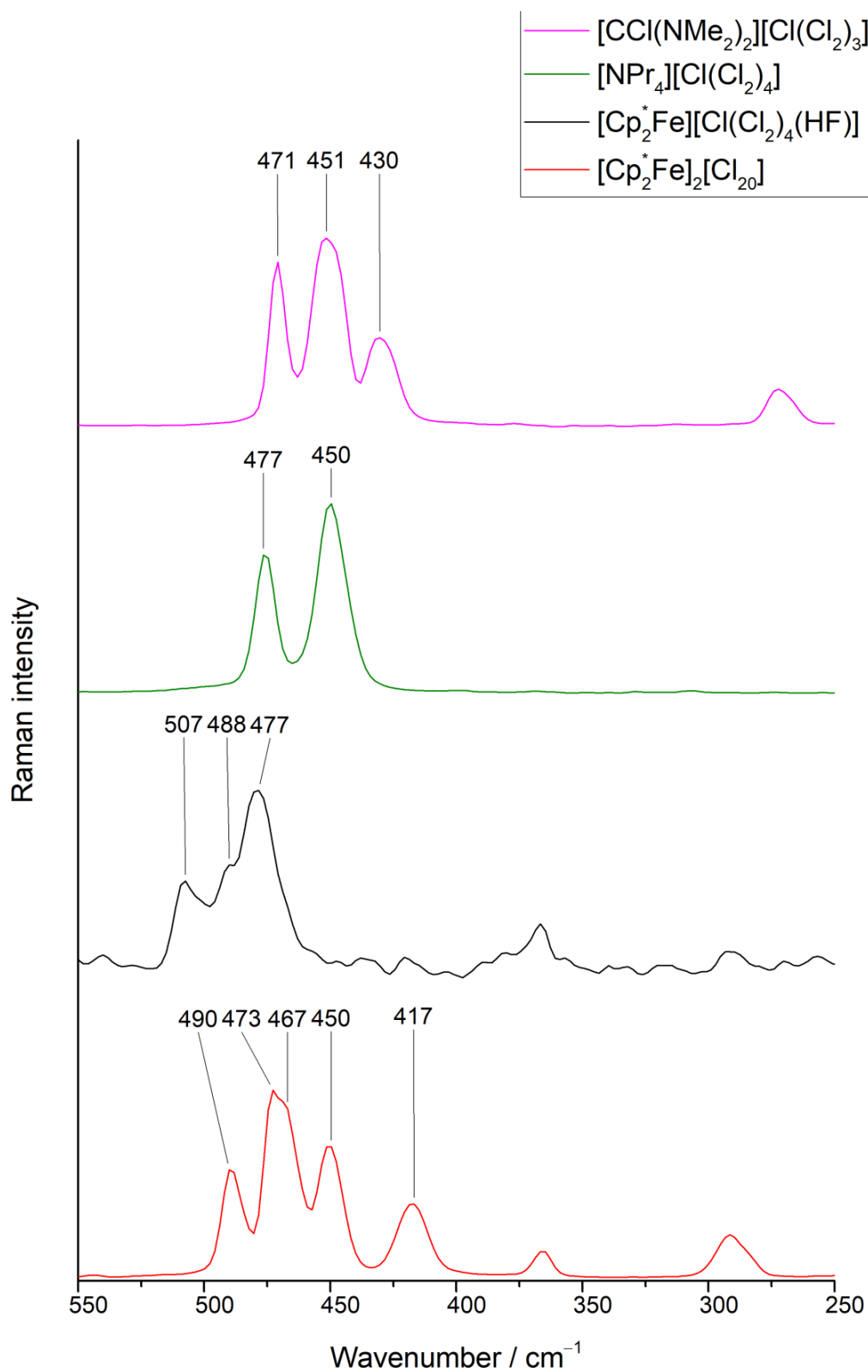


Figure S7. Hirshfeld surface of the $[\text{Cl}_{20}]^{2-}$ anion in $[\text{Cp}^*_2\text{Fe}]_2[\text{Cl}_{20}]$. Color code: grey = C, white = H, green = chlorine, orange = iron. Dashed red line displays halogen bonding.

b) Experimental and Calculated Raman Spectra

**Figure S8.** Experimental Raman spectrum of the single crystals of $[\text{Cat}][\text{Cl}_x]$ recorded at $-196\text{ }^\circ\text{C}$.

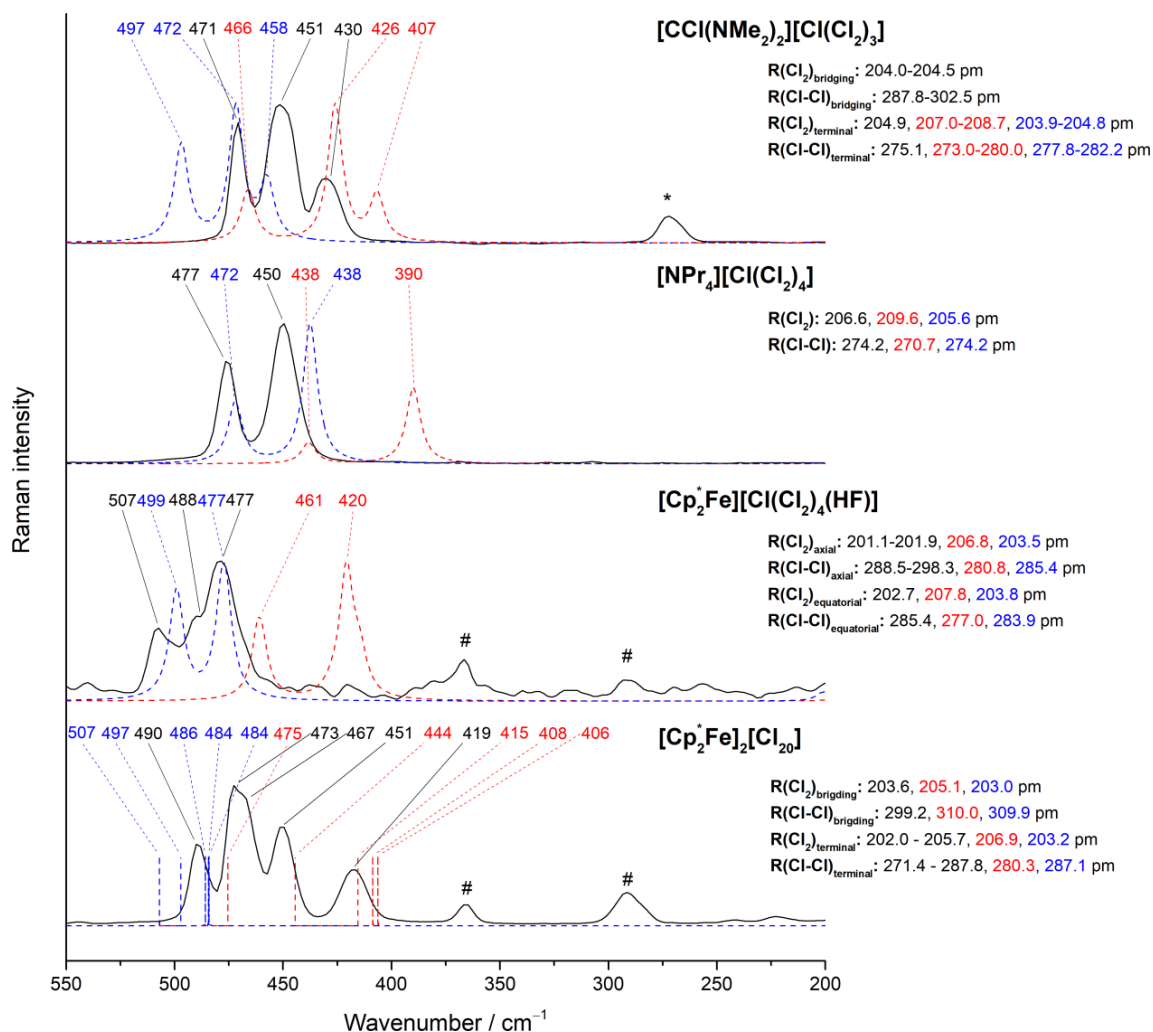


Figure S9. Experimental Raman spectra of the single crystals recorded at $-196\text{ }^{\circ}\text{C}$ (black) and calculated Raman spectra (B3LYP(D3BJ)/def2-TZVPP (red) and SCS-MP2/def2-TZVPP (blue)) as well as calculated (B3LYP(D3BJ)/def2-TZVPP (red) and SCS-MP2/def2-TZVPP (blue)) and experimental bond length from the molecular structure in the solid state. For the $[\text{Cl}_{20}]^{2-}$ anion a Cosmo model for solvation correction was used in the calculations. Therefore, no Raman intensities could be calculated for this molecule. The Raman spectrum of $[\text{CCl}(\text{NMe}_2)_2][\text{Cl}(\text{Cl}_2)_3]$ is compared to the calculated spectra of a $[\text{Cl}(\text{Cl}_2)_5]^-$ (C_{4v}) ion since the coordination number of the central halide is five. Bands marked with an asterisk are due to small amounts of $[\text{Cl}_3]^-$ present on the surface of the single crystals. Bands marked with hash belong to the ferrocenium cation.

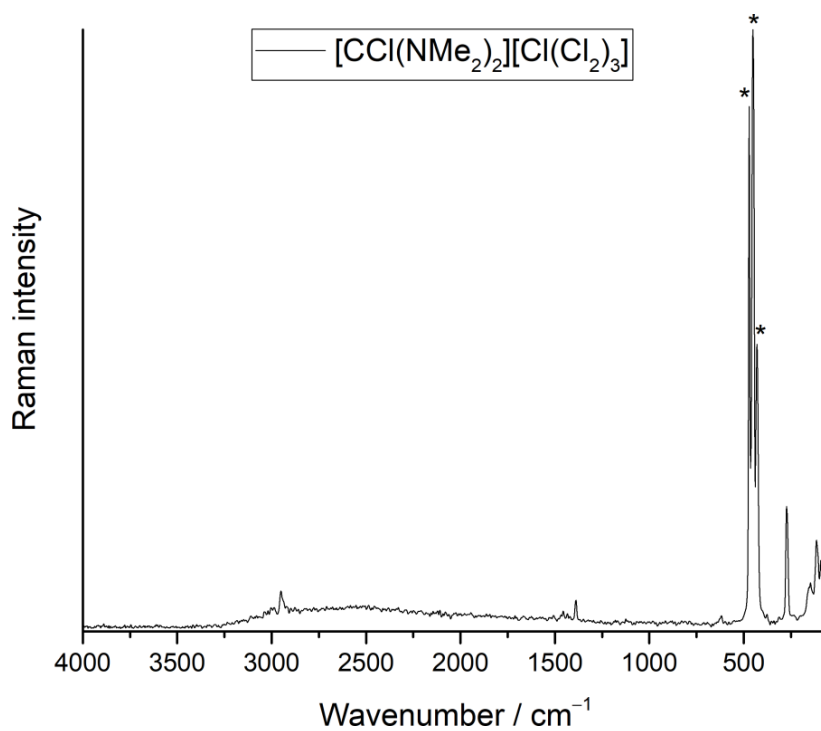


Figure S10. Experimental Raman spectrum of a single crystal of $[\text{CCl}(\text{NMe}_2)_2][\text{Cl}(\text{Cl}_2)_3]$ recorded at -196 °C. Bands highlighted with asterisk are associated to the $[\text{Cl}(\text{Cl}_2)_3]^-$.

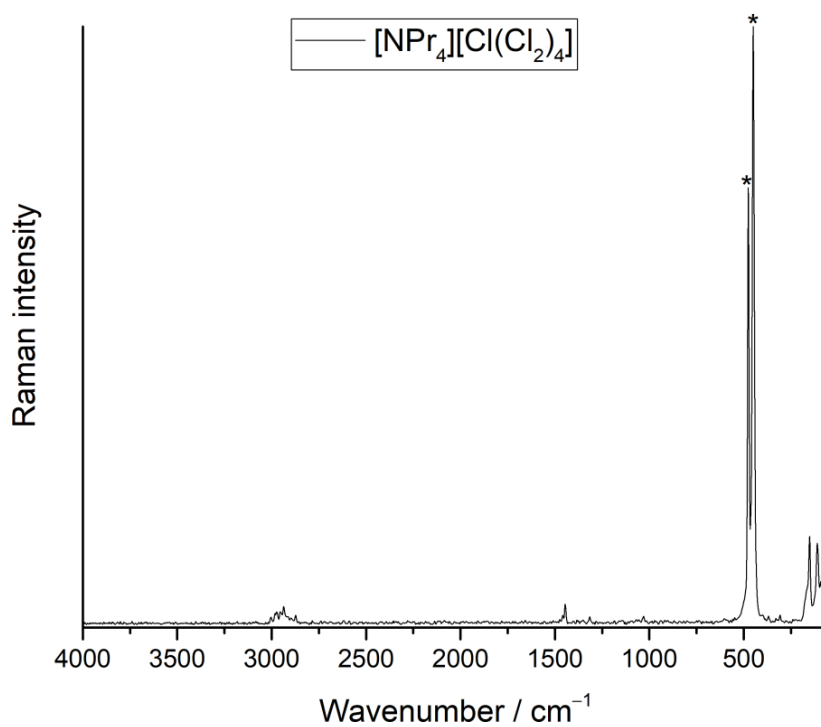


Figure S11. Experimental Raman spectrum of a single crystal of $[\text{NPr}_4][\text{Cl}(\text{Cl}_2)_4]$ recorded at -196 °C. Bands highlighted with asterisk are associated to the $[\text{Cl}(\text{Cl}_2)_4]^-$.

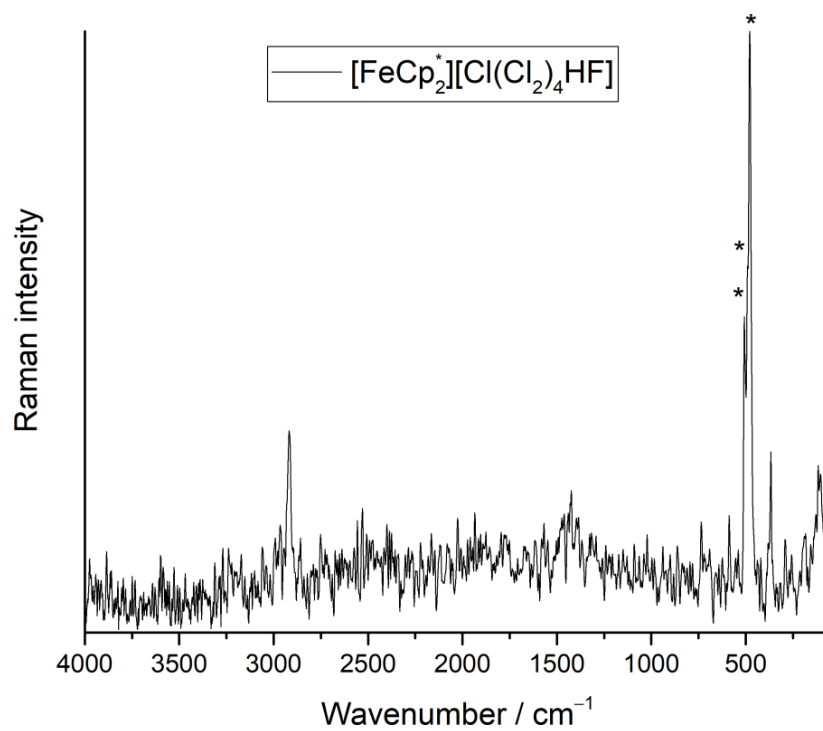


Figure S12. Experimental Raman spectrum of a single crystal of $[\text{FeCp}_2^*][\text{Cl}(\text{Cl}_2)_4(\text{HF})]$ recorded at $-196\text{ }^\circ\text{C}$. Bands highlighted with asterisk are associated to the $[\text{Cl}(\text{Cl}_2)_4(\text{HF})]^-$.

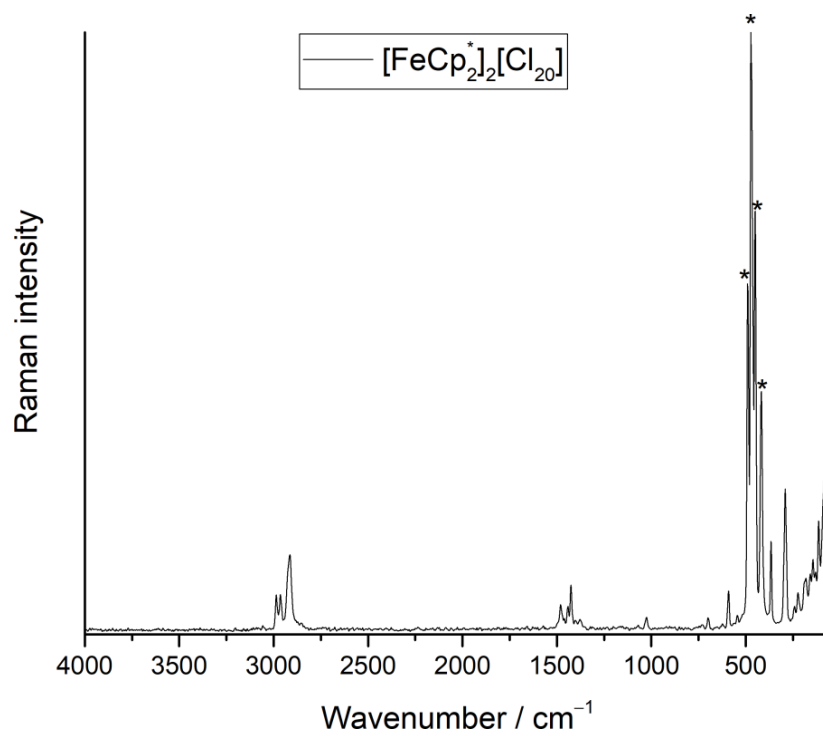


Figure S13. Experimental Raman spectrum of a single crystal of $[\text{FeCp}^*_2][\text{Cl}_{20}]$ recorded at $-196\text{ }^\circ\text{C}$. Bands highlighted with asterisk are associated to the $[\text{Cl}_{20}]^{2-}$.

c) Optimized Structures

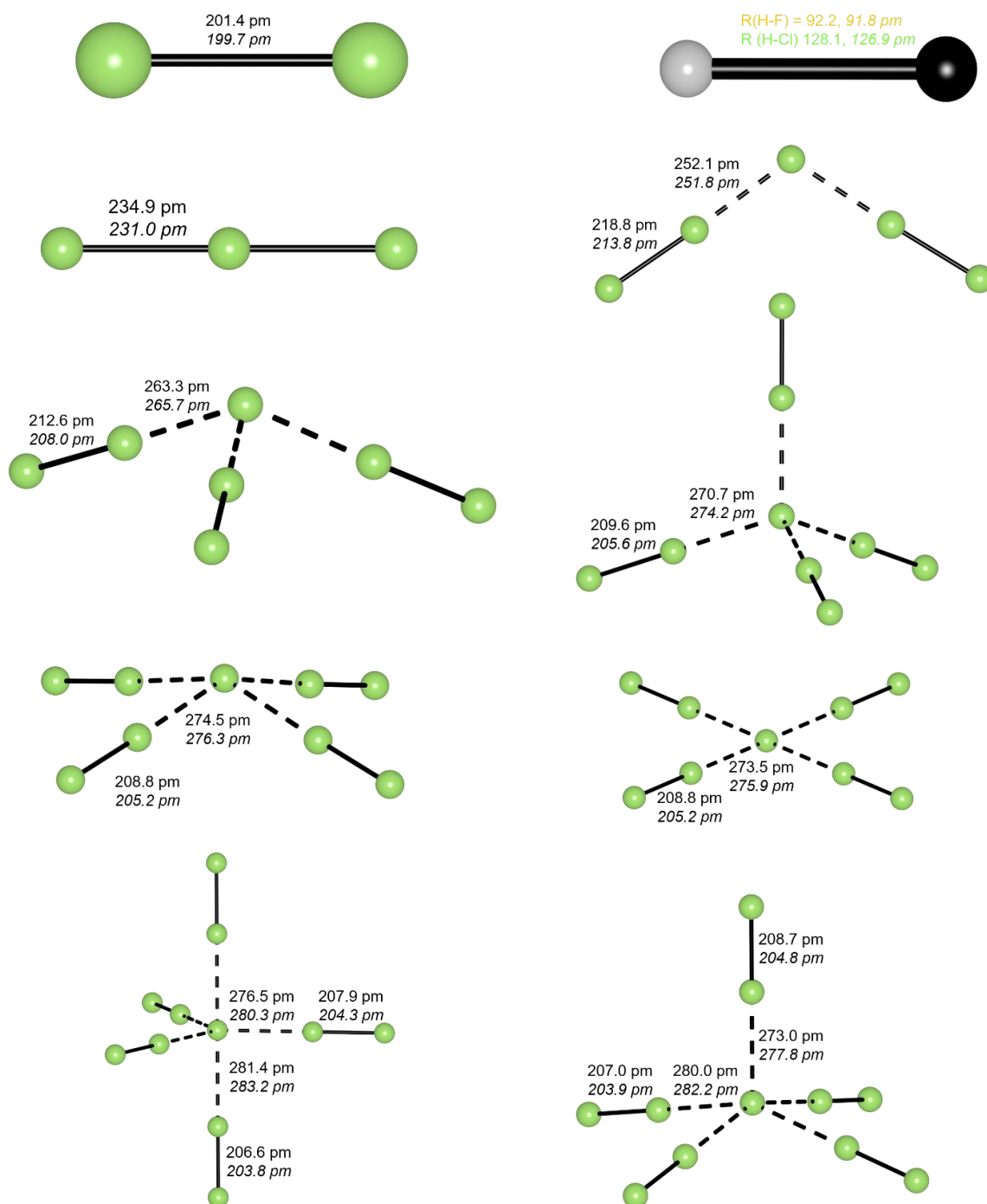


Figure S14. Optimized structures calculated on the B3LYP(D3BJ)/def2-TZVPP and SCS-MP2/def2-TZVPP (*italics*) level of theory. Structures for HCl and HF were taken from P. Vořnacker, S. Steinhauer, J. Bader, S. Riedel, *Chem. Eur. J.* **2020**.

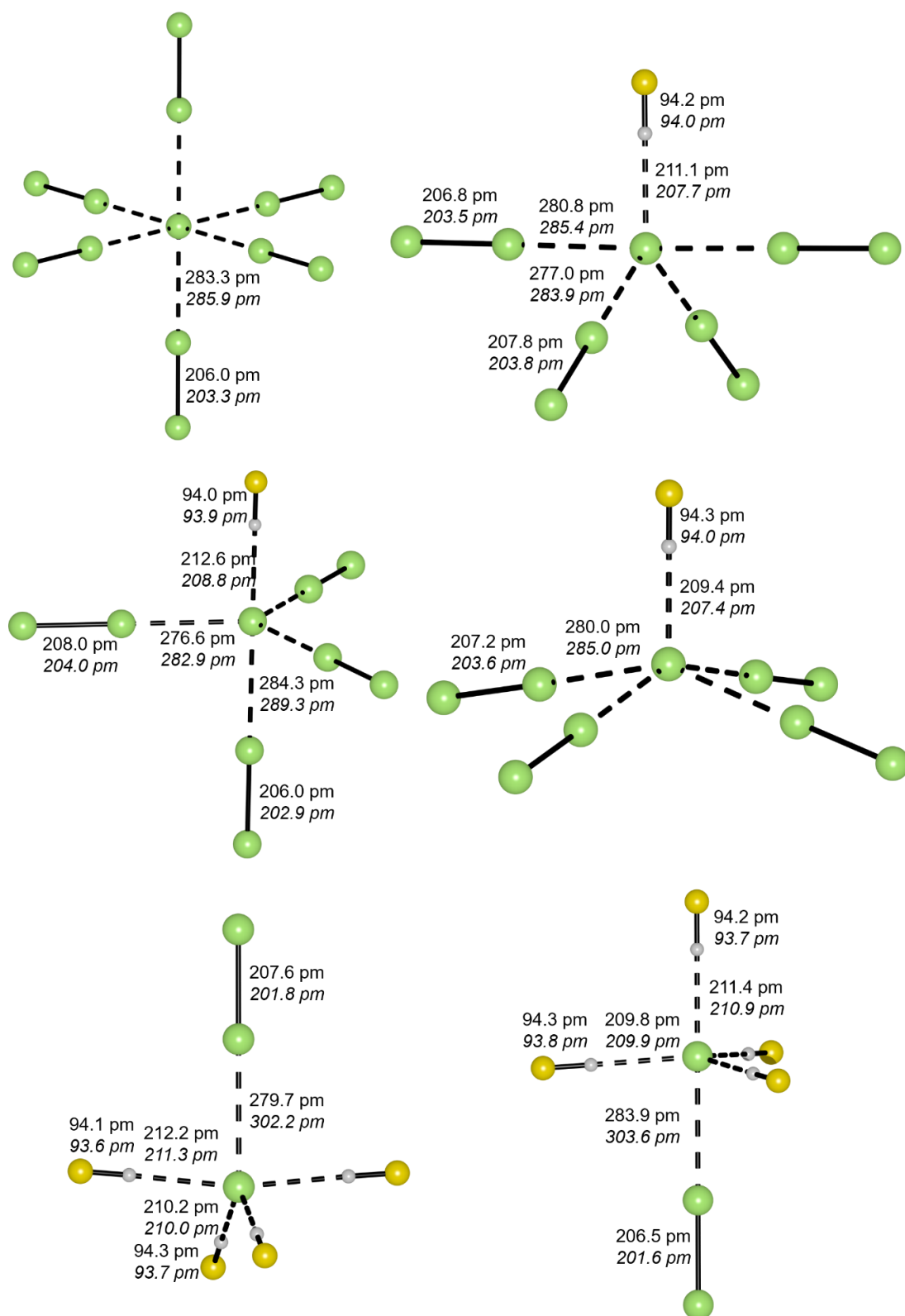


Figure S15. Optimized structures calculated on the B3LYP(D3BJ)/def2-TZVPP and SCS-MP2/def2-TZVPP (*italics*) level of theory.

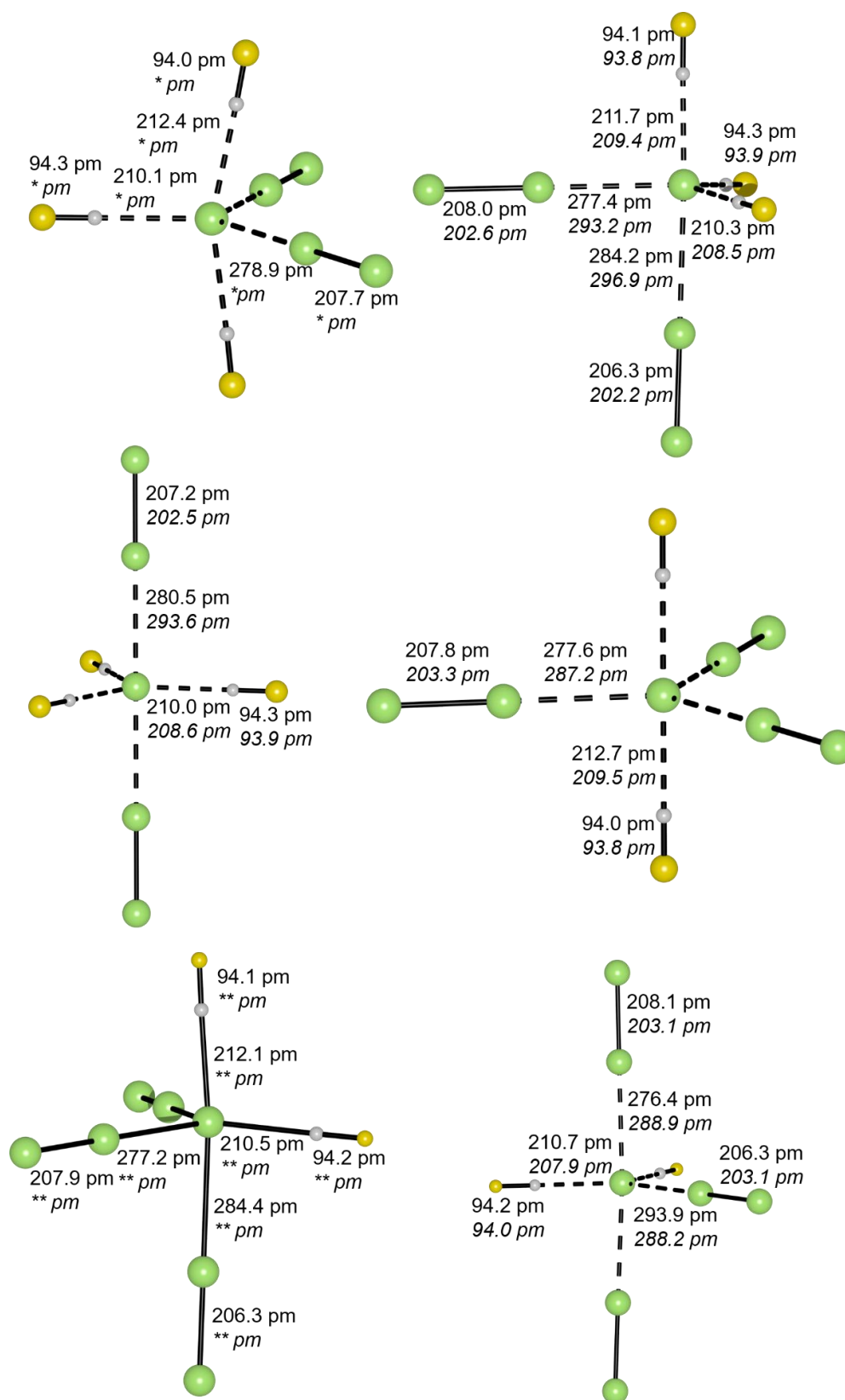


Figure S16. Optimized structures calculated on the B3LYP(D3BJ)/def2-TZVPP and SCS-MP2/def2-TZVPP (*italics*) level of theory. * Optimization on SCS-MP2/def2-TZVPP level of theory yields D_{3h} symmetric structure. ** Optimization on SCS-MP2/def2-TZVPP level of theory yields C_{2v} symmetric structure.

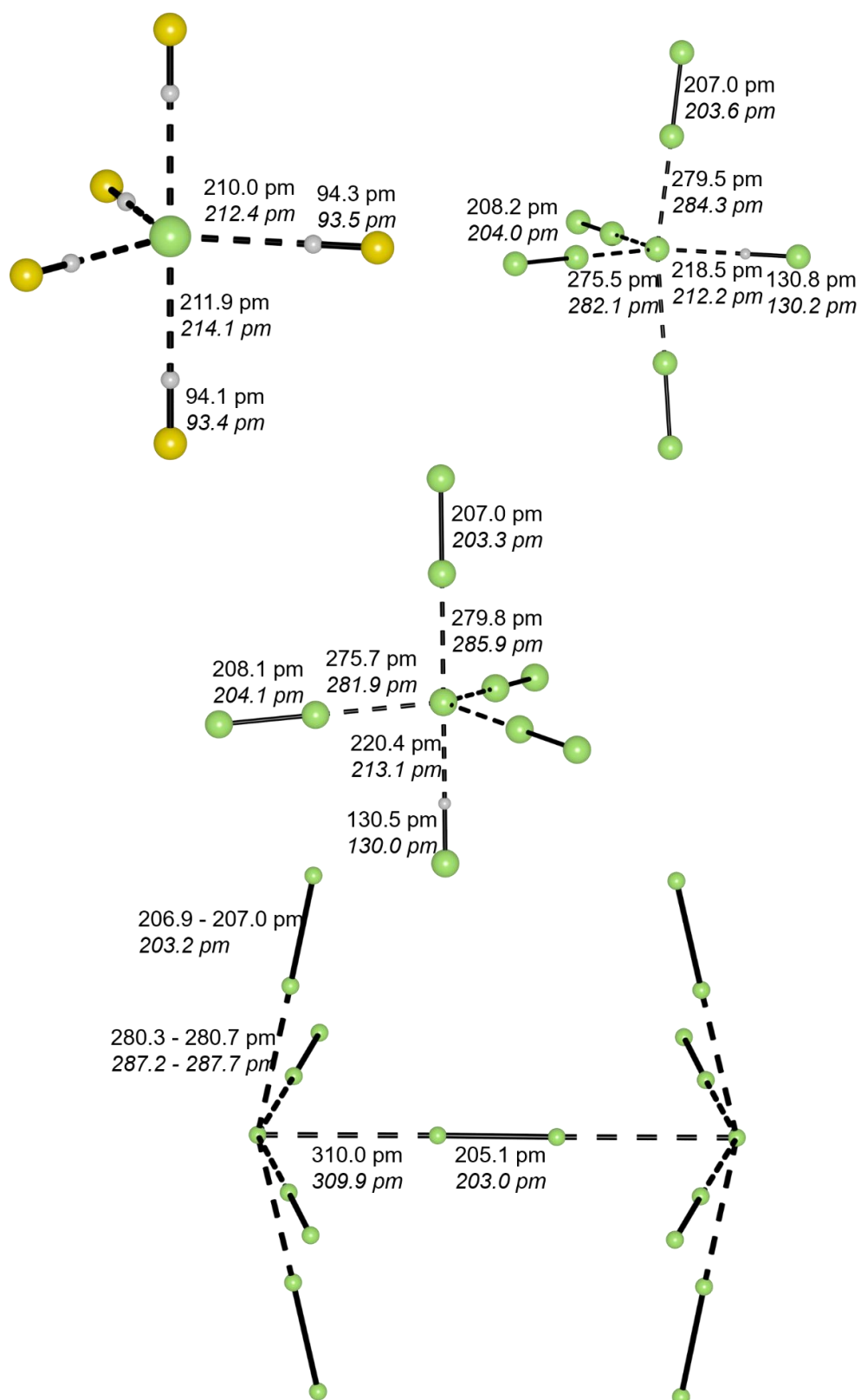


Figure S17. Optimized structures calculated on the B3LYP(D3BJ)/def2-TZVPP and SCS-MP2/def2-TZVPP (*italics*) level of theory.

d) Calculated Energies and Free Reaction Energies

d1) B3LYP(D3BJ)/def2-TZVPP Energies

All Free Energy calculations were carried out for $T = 298.15$ K and $p = 1.0$ bar.

Table S1. Calculated energies on B3LYP(D3BJ)/def2-TZVPP level of theory.

Compound	E_{tot} / E_H	$E_{tot} / \text{kJ mol}^{-1}$	$G / \text{kJ mol}^{-1}$
HF ^a	-100.45529924	-263745.39	-263764.34
HCl ^a	-460.76800069	-1209746.39	-1209775.98
Cl ₂	-920.29315162	-2416229.67	-2416283.93
[Cl ₃] ⁻	-1380.56949107	-3624685.20	-3624748.27
[Cl(Cl ₂) ₂] ⁻	-2300.88575524	-6040975.55	-6041061.91
[Cl(Cl ₂) ₃] ⁻	-3221.19485926	-8457247.10	-8457354.23
[Cl(Cl ₂) ₄] ⁻ (<i>T_d</i>)	-4141.50072815	-10873510.16	-10873640.85
[Cl(Cl ₂) ₄] ⁻ (<i>C_{4v}</i>)	-4141.49747584	-10873501.62	-
[Cl(Cl ₂) ₄] ⁻ (<i>D_{4h}</i>)	-4141.49704232	-10873444.34	-
[Cl(Cl ₂) ₅] ⁻ (<i>D_{3h}</i>)	-5061.80354389	-13289765.20	-13289916.16
[Cl(Cl ₂) ₅] ⁻ (<i>C_{4v}</i>)	-5061.80337649	-13289764.76	-
[Cl(Cl ₂) ₆] ⁻	-5982.10669046	-15706021.12	-15706190.26
[Cl(Cl ₂) ₄ (HF)] ⁻ (<i>C_{2v}</i>)	-4241.97122699	-11137295.46	-11137413.77
[Cl(Cl ₂) ₄ (HF)] ⁻ (<i>C_{3v}</i>)	-4241.97113667	-11137295.22	-11137416.92
[Cl(Cl ₂) ₄ (HF)] ⁻ (<i>C_{4v}</i>)	-4241.97104492	-11137294.98	-
[Cl(Cl ₂)(HF) ₄] ⁻ (<i>C_{2v}</i>)	-1782.47591911	-4679890.53	-4679901.85
[Cl(Cl ₂)(HF) ₄] ⁻ (<i>C_{3v}</i>)	-1782.47596990	-4679890.66	-4679901.05
[Cl(Cl ₂) ₂ (HF) ₃] ⁻ (<i>C_s</i>)	-2602.30736550	-6832357.99	-6832407.07
[Cl(Cl ₂) ₂ (HF) ₃] ⁻ (<i>D_{3h}</i>)	-2602.30769004	-6832358.84	-6832405.65
[Cl(Cl ₂) ₂ (HF) ₃] ⁻ (<i>C_{2v}</i>)	-2602.30746903	-6832358.26	-6832405.68
[Cl(Cl ₂) ₃ (HF) ₂] ⁻ (<i>D_{3h}</i>)	-3422.13923548	-8984826.56	-8984909.06
[Cl(Cl ₂) ₃ (HF) ₂] ⁻ (<i>C_s</i>)	-3422.13907952	-8984826.15	-8984911.37
[Cl(Cl ₂) ₃ (HF) ₂] ⁻ (<i>C_{2v}</i>)	-3422.13918497	-8984826.43	-8984911.20
[Cl(HF) ₅] ⁻ (<i>D_{3h}</i>)	-962.64466138	-2527423.56	-2527396.31

Compound	E_{tot} / E_H	$E_{tot} / \text{kJ mol}^{-1}$	$G / \text{kJ mol}^{-1}$
$[\text{Cl}(\text{Cl}_2)_4(\text{HCl})]^- (C_{2v})$	-4602.28086551	-12083288.41	-12083421.16
$[\text{Cl}(\text{Cl}_2)_4(\text{HCl})]^- (C_{3v})$	-4602.28113975	-12083289.13	-12083420.95

^a Taken from P. Voßnacker, S. Steinhauer, J. Bader, S. Riedel, *Chem. Eur. J.* **2020**, *26*, 13256-13263.

d2) SCS-MP2/def2-TZVPP Energies

Table S2. Calculated energies on SCS-MP2/def2-TZVPP level of theory.

Compound	E_{tot} / E_H	E_{MP2} / E_H	$E_{tot+MP2} / \text{kJ mol}^{-1}$	$G / \text{kJ mol}^{-1}$
HF ^a	-100.06531033	-0.28555788	-263471.20	-263489.53
HCl ^a	-460.09919729	-0.35546237	-1208923.71	-1208952.42
Cl ₂	-918.98287941	-0.67866826	-2414571.39	-2414625.41
[Cl ₃] ⁻	-1378.55619763	-1.04983123	-3622155.63	-3622217.46
[Cl(Cl ₂) ₂] ⁻	-2297.54169047	-1.73983891	-6036763.66	-6036850.78
[Cl(Cl ₂) ₃] ⁻	-3216.53341317	-2.42204810	-8451367.56	-8451475.38
[Cl(Cl ₂) ₄] ⁻ (<i>T_d</i>)	-4135.52436491	-3.10389122	-10865968.49	-10866098.21
[Cl(Cl ₂) ₄] ⁻ (<i>C_{4v}</i>)	-4135.52296467	-3.10365679	-10865964.19	-
[Cl(Cl ₂) ₄] ⁻ (<i>D_{4h}</i>)	-4135.52300416	-3.10358430	-10865964.11	-
[Cl(Cl ₂) ₅] ⁻ (<i>D_{3h}</i>)	-5054.51231842	-3.78730409	-13280565.66	-13280704.97
[Cl(Cl ₂) ₅] ⁻ (<i>C_{4v}</i>)	-5054.51203097	-3.78757235	-13280565.61	-13280713.19
[Cl(Cl ₂) ₆] ⁻	-5973.49899525	-4.47208983	-15695163.08	-15695322.89
[Cl(Cl ₂) ₄ (HF)] ⁻ (<i>C_{2v}</i>)	-4235.61244195	-3.38565621	-11129489.51	-11129601.05
[Cl(Cl ₂) ₄ (HF)] ⁻ (<i>C_{3v}</i>)	-4235.61215233	-3.38551263	-11129488.37	-11129601.09
[Cl(Cl ₂) ₄ (HF)] ⁻ (<i>C_{4v}</i>)	-4235.61246606	-3.38563591	-11129489.52	-11129598.70
[Cl(Cl ₂)(HF) ₄] ⁻ (<i>C_{2v}</i>)	-1778.90628191	-2.18862475	-4676264.68	-4676267.30
[Cl(Cl ₂)(HF) ₄] ⁻ (<i>C_{3v}</i>)	-1778.90677984	-2.18859323	-4676265.90	-4676270.10
[Cl(Cl ₂) ₂ (HF) ₃] ⁻ (<i>C_s</i>)	-2597.80989230	-2.58610225	-6827339.68	-6827381.97
[Cl(Cl ₂) ₂ (HF) ₃] ⁻ (<i>D_{3h}</i>)	-2597.81010268	-2.58612230	-6827340.29	-6827379.49
[Cl(Cl ₂) ₂ (HF) ₃] ⁻ (<i>C_{2v}</i>) ^b	-	-	-	-

Compound	E_{tot} / E_H	E_{MP2} / E_H	$E_{tot+MP2} / \text{kJ mol}^{-1}$	$G / \text{kJ mol}^{-1}$
$[\text{Cl}(\text{Cl}_2)_3(\text{HF})_2]^-$ (D_{3h})	-3416.71095790	-2.98515020	-8978412.13	-8978490.52
$[\text{Cl}(\text{Cl}_2)_3(\text{HF})_2]^-$ (C_s) ^c	-	-	-	-
$[\text{Cl}(\text{Cl}_2)_3(\text{HF})_2]^-$ (C_{2v})	-3416.71177538	-2.98523055	-8978414.49	-8978490.64
$[\text{Cl}(\text{HF})_5]^-$ (D_{3h})	-960.00108684	-1.79270510	-2525189.60	-2525153.36
$[\text{Cl}(\text{Cl}_2)_4(\text{HCl})]^-$ (C_{2v})	-4595.63934112	-3.45891969	-12074932.48	-12075054.46
$[\text{Cl}(\text{Cl}_2)_4(\text{HCl})]^-$ (C_{3v})	-4595.63912520	-3.45901564	-12074932.17	-12075053.07

^a Taken from P. Voßnacker, S. Steinhauer, J. Bader, S. Riedel, *Chem. Eur. J.* **2020**, *26*, 13256-13263.

^b Structure converges into D_{3h} symmetric structure. ^c Structure converges into a C_{2v} symmetric structure.

d3) Free Reaction Energy Calculation

Table S3. ΔE and ΔG for the reaction of $[\text{Cl}(\text{Cl})_n]^- + \text{Cl}_2 \rightarrow [\text{Cl}(\text{Cl}_2)_{n+1}]^-$ calculated on the B3LYP(D3BJ)/def2-TZVPP and SCS-MP2/def2-TZVPP level of theory.

n	$\Delta E_{B3LYP} / \text{kJ mol}^{-1}$	$\Delta G_{B3LYP} / \text{kJ mol}^{-1}$	$\Delta E_{MP2} / \text{kJ mol}^{-1}$	$\Delta G_{MP2} / \text{kJ mol}^{-1}$
1	-60.7	-29.7	-36.6	-7.9
2	-41.9	-8.4	-32.5	0.8
3	-33.4	-2.7	-29.5	2.6
4	-25.4	8.6	-25.8	18.7
5	-26.2	9.8	-26.0	7.5

Table S4. ΔE and ΔG for the reaction of $[\text{Cl}(\text{Cl}_2)_4]^- + \text{HF} \rightarrow [\text{Cl}(\text{Cl}_2)_4(\text{HF})]^-$ calculated on B3LYP(D3BJ)/def2-TZVPP and SCS-MP2/def-TZVPP level of theory.

$\Delta E_{\text{B3LYP}} / \text{kJ mol}^{-1}$	$\Delta G_{\text{B3LYP}} / \text{kJ mol}^{-1}$	$\Delta E_{\text{MP2}} / \text{kJ mol}^{-1}$	$\Delta G_{\text{MP2}} / \text{kJ mol}^{-1}$
-39.9	-8.6	-49.8	-13.3

Table S5. ΔE and ΔG for the reaction of $[\text{Cl}(\text{Cl}_2)_5]^- + \text{HF} \rightarrow [\text{Cl}(\text{Cl}_2)_4(\text{HF})]^- + \text{Cl}_2$ calculated on B3LYP(D3BJ)/def2-TZVPP and SCS-MP2/def-TZVPP level of theory.

$\Delta E_{\text{B3LYP}} / \text{kJ mol}^{-1}$	$\Delta G_{\text{B3LYP}} / \text{kJ mol}^{-1}$	$\Delta E_{\text{MP2}} / \text{kJ mol}^{-1}$	$\Delta G_{\text{MP2}} / \text{kJ mol}^{-1}$
-14.5	-17.2	-24.0	-32.0

Table S6. ΔE and ΔG for the reaction of $[\text{Cl}(\text{Cl})_{5-n}(\text{HF})_n]^- + \text{HF} \rightarrow [\text{Cl}(\text{Cl}_2)_{5-n-1}(\text{HF})_{n+1}]^- + \text{Cl}_2$ calculated on the B3LYP(D3BJ)/def2-TZVPP and SCS-MP2/def2-TZVPP level of theory.

n	$\Delta E_{\text{B3LYP}} / \text{kJ mol}^{-1}$	$\Delta G_{\text{B3LYP}} / \text{kJ mol}^{-1}$	$\Delta E_{\text{MP2}} / \text{kJ mol}^{-1}$	$\Delta G_{\text{MP2}} / \text{kJ mol}^{-1}$
0	-14.5	-17.2	-24.0	-32.0
1	-15.4	-14.9	-22.8	-25.4
2	-16.6	-16.2	-28.3	-24.8
3	-16.1	-15.0	-25.8	-26.5
4	-17.2	-14.9	-23.9	-19.1

Table S7. ΔE and ΔG for the reaction of $[\text{Cl}(\text{Cl}_2)_5]^- (D_{3h}) + \text{HCl} \rightarrow [\text{Cl}(\text{Cl}_2)_4(\text{HCl})]^- (C_{2v}) + \text{Cl}_2$ calculated on B3LYP(D3BJ)/def2-TZVPP and SCS-MP2/def-TZVPP level of theory.

$\Delta E_{\text{B3LYP}} / \text{kJ mol}^{-1}$	$\Delta G_{\text{B3LYP}} / \text{kJ mol}^{-1}$	$\Delta E_{\text{MP2}} / \text{kJ mol}^{-1}$	$\Delta G_{\text{MP2}} / \text{kJ mol}^{-1}$
-6.5	-13.0	-14.5	-22.5

d4) Comparison Between Different Structures

Table S8. Comparison of different geometries for the $[\text{Cl}(\text{Cl}_2)_n]^-$ ($n = 4, 5$) $[\text{Cl}(\text{Cl}_2)_{5-n}(\text{HF})_n]^-$ ($n = 1 - 4$) and $[\text{Cl}(\text{Cl}_2)_4(\text{HCl})]^-$ anion calculated on the B3LYP(D3BJ)/def2-TZVPP and SCS-MP2/def-TZVPP level of theory.

Compound	Structure	$\Delta E_{\text{B3LYP}} / \text{kJ mol}^{-1}$	$\Delta E_{\text{MP2}} / \text{kJ mol}^{-1}$
$[\text{Cl}(\text{Cl}_2)_4]^-$	T_d	0.0	0.0
$[\text{Cl}(\text{Cl}_2)_4]^-$	C_{4v}	8.5	4.3
$[\text{Cl}(\text{Cl}_2)_4]^-$	D_{4h}	9.7	4.4
$[\text{Cl}(\text{Cl}_2)_5]^-$	D_{3h}	0.0	0.0
$[\text{Cl}(\text{Cl}_2)_5]^-$	C_{4v}	0.4	0.1
$[\text{Cl}(\text{Cl}_2)_4(\text{HF})]^-$	C_{2v}	0.0	0.0
$[\text{Cl}(\text{Cl}_2)_4(\text{HF})]^-$	C_{3v}	0.2	1.1
$[\text{Cl}(\text{Cl}_2)_4(\text{HF})]^-$	C_{4v}	0.5	0.0
$[\text{Cl}(\text{Cl}_2)(\text{HF})_4]^-$	C_{2v}	0.1	1.2
$[\text{Cl}(\text{Cl}_2)(\text{HF})_4]^-$	C_{3v}	0.0	0.0
$[\text{Cl}(\text{Cl}_2)_2(\text{HF})_3]^-$	C_s	0.6	0.6
$[\text{Cl}(\text{Cl}_2)_2(\text{HF})_3]^-$	C_{2v}	0.6	–
$[\text{Cl}(\text{Cl}_2)_2(\text{HF})_3]^-$	D_{3h}	0.0	0.0
$[\text{Cl}(\text{Cl}_2)_3(\text{HF})_2]^-$	C_s	0.4	–
$[\text{Cl}(\text{Cl}_2)_3(\text{HF})_2]^-$	C_{2v}	0.1	–2.4
$[\text{Cl}(\text{Cl}_2)_3(\text{HF})_2]^-$	D_{3h}	0	0
$[\text{Cl}(\text{Cl}_2)_4(\text{HCl})]^-$	C_{2v}	0.7	-0.3
$[\text{Cl}(\text{Cl}_2)_4(\text{HCl})]^-$	C_{3v}	0	0

e) Coordinates of Optimized Structures

Cl₂

B3LYP

Cl	0.000000	0.000000	-1.007067
----	----------	----------	-----------

Cl	0.000000	0.000000	1.007067
----	----------	----------	----------

MP2

Cl	0.000000	0.000000	-0.998719
----	----------	----------	-----------

Cl	0.000000	0.000000	0.998719
----	----------	----------	----------

HF

B3LYP(D3BJ)/def2-TZVPP

H	0.000000	0.000000	-0.461179
---	----------	----------	-----------

F	0.000000	0.000000	0.461179
---	----------	----------	----------

SCS-MP2/def2-TZVPP

H	0.000000	0.000000	-0.458911
---	----------	----------	-----------

F	0.000000	0.000000	0.458911
---	----------	----------	----------

[Cl₃]⁻

B3LYP

Cl	0.000000	0.000000	0.000000
----	----------	----------	----------

Cl	0.000000	0.000000	2.349407
----	----------	----------	----------

Cl	0.000000	0.000000	-2.349407
----	----------	----------	-----------

MP2

Cl	0.000000	0.000000	0.000000
----	----------	----------	----------

Cl	0.000000	0.000000	2.309539
----	----------	----------	----------

Cl	0.000000	0.000000	-2.309539
----	----------	----------	-----------

[Cl(Cl₂)₂]⁻

B3LYP

Cl	0.000000	0.000000	1.622314
Cl	-2.073816	0.000000	0.188549
Cl	-3.910600	0.000000	-0.999701
Cl	2.073816	0.000000	0.188549
Cl	3.910600	0.000000	-0.999701

MP2

Cl	0.000000	0.000000	1.675646
Cl	-2.035771	0.000000	0.194206
Cl	-3.787579	0.000000	-1.032024
Cl	2.035771	0.000000	0.194206
Cl	3.787579	0.000000	-1.032024

[Cl(Cl₂)₃]⁻

B3LYP

Cl	0.000000	0.000000	-1.172398
Cl	-1.217987	2.109616	-0.172702
Cl	-1.217987	-2.109616	-0.172702
Cl	2.435975	0.000000	-0.172702
Cl	-2.210211	3.828197	0.590098
Cl	-2.210211	-3.828197	0.590098
Cl	4.420421	0.000000	0.590098

MP2

Cl	0.000000	0.000000	-1.352348
Cl	-1.197595	2.074295	-0.203260
Cl	-1.197595	-2.074295	-0.203260
Cl	2.395190	0.000000	-0.203260
Cl	-2.139171	3.705153	0.680639
Cl	-2.139171	-3.705153	0.680639
Cl	4.278343	0.000000	0.680639

[Cl(Cl₂)₄]⁻ (T_d)

B3LYP

Cl	0.000000	0.000000	0.000000
Cl	-1.562657	1.562657	1.562657
Cl	1.562657	-1.562657	1.562657
Cl	1.562657	1.562657	-1.562657
Cl	-2.772668	2.772668	2.772668
Cl	-1.562657	-1.562657	-1.562657
Cl	-2.772668	-2.772668	-2.772668
Cl	2.772668	2.772668	-2.772668
Cl	2.772668	-2.772668	2.772668

MP2

Cl	0.000000	0.000000	0.000000
Cl	-1.583094	1.583094	1.583094
Cl	1.583094	-1.583094	1.583094
Cl	1.583094	1.583094	-1.583094
Cl	-2.770238	2.770238	2.770238
Cl	-1.583094	-1.583094	-1.583094
Cl	-2.770238	-2.770238	-2.770238
Cl	2.770238	2.770238	-2.770238
Cl	2.770238	-2.770238	2.770238

[Cl(Cl₂)₄]⁻ (C_{4v})

B3LYP

Cl	0.000000	0.000000	0.840397
Cl	1.875613	1.875613	0.133658
Cl	1.875613	-1.875613	0.133658
Cl	-1.875613	-1.875613	0.133658
Cl	3.312616	3.312616	-0.343757
Cl	3.312616	-3.312616	-0.343757
Cl	-3.312616	-3.312616	-0.343757
Cl	-1.875613	1.875613	0.133658
Cl	-3.312616	3.312616	-0.343757

MP2

Cl	0.000000	0.000000	0.606293
Cl	1.920789	1.920789	0.100995
Cl	1.920789	-1.920789	0.100995
Cl	-1.920789	-1.920789	0.100995
Cl	3.349803	3.349803	-0.252568
Cl	3.349803	-3.349803	-0.252568
Cl	-3.349803	-3.349803	-0.252568
Cl	-1.920789	1.920789	0.100995
Cl	-3.349803	3.349803	-0.252568

[Cl(Cl₂)₄]⁻ (D_{4h})

B3LYP

Cl	0.000000	0.000000	0.000000
Cl	1.934028	-1.934028	0.000000
Cl	1.934028	1.934028	0.000000
Cl	-1.934028	-1.934028	0.000000
Cl	-1.934028	1.934028	0.000000
Cl	3.410378	-3.410378	0.000000
Cl	3.410378	3.410378	0.000000
Cl	-3.410378	-3.410378	0.000000
Cl	-3.410378	3.410378	0.000000

MP2

Cl	0.000000	0.000000	0.000000
Cl	1.950780	-1.950780	0.000000
Cl	1.950780	1.950780	0.000000
Cl	-1.950780	-1.950780	0.000000
Cl	-1.950780	1.950780	0.000000
Cl	3.401627	-3.401627	0.000000
Cl	3.401627	3.401627	0.000000
Cl	-3.401627	-3.401627	0.000000
Cl	-3.401627	3.401627	0.000000

[Cl(Cl₂)₅]⁻ (D_{3h})

B3LYP

Cl	0.000000	0.000000	0.000000
Cl	0.000000	0.000000	2.814077
Cl	-1.382381	2.394355	0.000000
Cl	0.000000	0.000000	-2.814077
Cl	-1.382381	-2.394355	0.000000
Cl	2.764763	0.000000	0.000000
Cl	0.000000	0.000000	-4.880091
Cl	-2.421684	4.194480	0.000000
Cl	0.000000	0.000000	4.880091
Cl	4.843368	0.000000	0.000000
Cl	-2.421684	-4.194480	0.000000

MP2

Cl	0.000000	0.000000	0.000000
Cl	-1.401556	2.427566	0.000000
Cl	0.000000	0.000000	2.831512
Cl	0.000000	0.000000	4.869122
Cl	-1.401556	-2.427566	0.000000
Cl	2.803111	0.000000	0.000000
Cl	0.000000	0.000000	-2.831512
Cl	-2.423208	-4.197120	0.000000
Cl	0.000000	0.000000	-4.869122
Cl	-2.423208	4.197120	0.000000
Cl	4.846416	0.000000	0.000000

[Cl(Cl₂)₅]⁻ (C_{4v})

B3LYP

Cl	0.000000	0.000000	-0.054051
Cl	1.927571	1.927571	-0.695179
Cl	1.927571	-1.927571	-0.695179
Cl	-1.927571	-1.927571	-0.695179
Cl	3.355209	3.355209	-1.150918
Cl	3.355209	-3.355209	-1.150918
Cl	-3.355209	-3.355209	-1.150918
Cl	0.000000	0.000000	2.675453
Cl	0.000000	0.000000	4.762984
Cl	-1.927571	1.927571	-0.695179
Cl	-3.355209	3.355209	-1.150918

MP2

Cl	0.000000	0.000000	-0.297079
Cl	1.975156	1.975156	-0.698690
Cl	1.975156	-1.975156	-0.698690
Cl	-1.975156	-1.975156	-0.698690
Cl	3.403401	3.403401	-0.979342
Cl	3.403401	-3.403401	-0.979342
Cl	-3.403401	-3.403401	-0.979342
Cl	0.000000	0.000000	2.480736
Cl	0.000000	0.000000	4.528469
Cl	-1.975156	1.975156	-0.698690
Cl	-3.403401	3.403401	-0.979342

[Cl(Cl₂)₆]⁻

B3LYP

Cl	0.000000	0.000000	0.000000
Cl	0.000000	-2.833453	0.000000
Cl	0.000000	0.000000	2.833453
Cl	2.833453	0.000000	0.000000
Cl	-2.833453	0.000000	0.000000
Cl	0.000000	0.000000	-2.833453
Cl	0.000000	2.833453	0.000000
Cl	0.000000	4.893870	0.000000
Cl	0.000000	0.000000	4.893870
Cl	4.893870	0.000000	0.000000
Cl	0.000000	-4.893870	0.000000
Cl	-4.893870	0.000000	0.000000
Cl	0.000000	0.000000	-4.893870

MP2

Cl	0.000000	0.000000	0.000000
Cl	0.000000	-2.859341	0.000000
Cl	0.000000	0.000000	2.859341
Cl	2.859341	0.000000	0.000000
Cl	-2.859341	0.000000	0.000000
Cl	0.000000	0.000000	-2.859341
Cl	0.000000	2.859341	0.000000
Cl	0.000000	4.891937	0.000000
Cl	0.000000	0.000000	4.891937
Cl	4.891937	0.000000	0.000000
Cl	0.000000	-4.891937	0.000000
Cl	-4.891937	0.000000	0.000000
Cl	0.000000	0.000000	-4.891937

[Cl(Cl₂)₄(HF)]⁻ (C_{2v})

B3LYP

F	0.000000	0.000000	-3.333265
Cl	0.000000	0.000000	-0.280739
H	0.000000	0.000000	-2.391682
Cl	0.000000	2.808001	-0.320531
Cl	0.000000	-2.808001	-0.320531
Cl	-2.309510	0.000000	1.247935
Cl	2.309510	0.000000	1.247935
Cl	0.000000	4.876328	-0.342270
Cl	0.000000	-4.876328	-0.342270
Cl	-4.039088	0.000000	2.400329
Cl	4.039088	0.000000	2.400329

MP2

F	0.000000	0.000000	-3.284122
Cl	0.000000	0.000000	-0.267362
H	0.000000	0.000000	-2.344106
Cl	0.000000	2.840383	0.009950
Cl	0.000000	-2.840383	0.009950
Cl	-2.575640	0.000000	0.927170
Cl	2.575640	0.000000	0.927170
Cl	0.000000	4.865849	0.207065
Cl	0.000000	-4.865849	0.207065
Cl	-4.423275	0.000000	1.786231
Cl	4.423275	0.000000	1.786231

[Cl(Cl₂)₄(HF)]⁻ (C_{3v})

B3LYP

Cl	0.000000	0.000000	0.269161
Cl	-1.382580	2.394698	0.221942
Cl	-2.422227	4.195421	0.180958
Cl	-1.382580	-2.394698	0.221942
Cl	-2.422227	-4.195421	0.180958
Cl	2.765159	0.000000	0.221942
Cl	4.844455	0.000000	0.180958
Cl	0.000000	0.000000	-2.574319
Cl	0.000000	0.000000	-4.634738
H	0.000000	0.000000	2.395588
F	0.000000	0.000000	3.335634

MP2

Cl	0.000000	0.000000	0.354702
Cl	-1.412610	2.446712	0.209756
Cl	-2.430906	4.210453	0.099174
Cl	-1.412610	-2.446712	0.209756
Cl	-2.430906	-4.210453	0.099174
Cl	2.825220	0.000000	0.209756
Cl	4.861812	0.000000	0.099174
Cl	0.000000	0.000000	-2.538190
Cl	0.000000	0.000000	-4.566922
H	0.000000	0.000000	2.442483
F	0.000000	0.000000	3.381163

[Cl(Cl₂)₄(HF)]⁻ (C_{4v})

B3LYP

Cl	0.000000	0.000000	0.217131
Cl	1.917460	1.917460	-0.479160
Cl	1.917460	-1.917460	-0.479160
Cl	-1.917460	-1.917460	-0.479160
Cl	3.341214	3.341214	-0.966605
Cl	3.341214	-3.341214	-0.966605
Cl	-3.341214	-3.341214	-0.966605
Cl	-1.917460	1.917460	-0.479160
Cl	-3.341214	3.341214	-0.966605
H	0.000000	0.000000	2.311369
F	0.000000	0.000000	3.254562

MP2

Cl	0.000000	0.000000	0.237000
Cl	1.951299	1.951299	-0.472636
Cl	1.951299	-1.951299	-0.472636
Cl	-1.951299	-1.951299	-0.472636
Cl	3.346071	3.346071	-0.977088
Cl	3.346071	-3.346071	-0.977088
Cl	-3.346071	-3.346071	-0.977088
Cl	-1.951299	1.951299	-0.472636
Cl	-3.346071	3.346071	-0.977088
H	0.000000	0.000000	2.310785
F	0.000000	0.000000	3.251111

[Cl(Cl₂)(HF)₄]⁻ (C_{2v})

B3LYP

Cl	-0.000627	-0.000660	-0.307486
H	-0.008658	-1.864638	-1.279844
F	-0.012271	-2.697661	-1.721205
H	0.000476	1.866198	-1.274304
F	0.000945	2.700528	-1.713189
H	-2.111676	0.004195	-0.087673
F	-3.049703	0.006392	-0.016683
H	2.111938	-0.006145	-0.102762
F	3.050449	-0.008543	-0.038476
Cl	0.009365	-0.004813	2.489358
Cl	0.016782	-0.007896	4.565502

MP2

Cl	0.000000	0.000000	-0.389967
H	0.000000	-1.734601	-1.574597
F	0.000000	-2.511710	-2.099374
H	0.000000	1.734601	-1.574597
F	0.000000	2.511710	-2.099374
H	-2.072648	0.000000	0.022346
F	-2.990781	0.000000	0.205577
H	2.072648	0.000000	0.022346
F	2.990781	0.000000	0.205577
Cl	0.000000	0.000000	2.632217
Cl	0.000000	0.000000	4.649848

[Cl(Cl₂)(HF)₄]⁻ (C_{3v})

B3LYP

Cl	0.000000	0.000000	0.332937
H	1.046127	1.811945	0.180356
F	1.516799	2.627174	0.122533
H	1.046127	-1.811945	0.180356
F	1.516799	-2.627174	0.122533
Cl	0.000000	0.000000	-2.506273
Cl	0.000000	0.000000	-4.571701
H	-2.092253	0.000000	0.180356
F	-3.033599	0.000000	0.122533
H	0.000000	0.000000	2.447358
F	0.000000	0.000000	3.389010

MP2

Cl	0.000000	0.000000	0.430669
H	1.042338	1.805383	0.186601
F	1.507679	2.611377	0.073177
H	1.042338	-1.805383	0.186601
F	1.507679	-2.611377	0.073177
Cl	0.000000	0.000000	-2.605325
Cl	0.000000	0.000000	-4.621232
H	-2.084677	0.000000	0.186601
F	-3.015358	0.000000	0.073177
H	0.000000	0.000000	2.539788
F	0.000000	0.000000	3.476764

[Cl(Cl₂)(HF)₃]⁻ (C_{2v})

B3LYP

Cl	0.000000	0.000000	0.354082
Cl	0.000000	2.447303	-0.984192
Cl	0.000000	4.271688	-1.975889
H	-2.093367	0.000000	-0.005283
F	-3.024375	0.000000	-0.138108
H	2.093367	0.000000	-0.005283
F	3.024375	0.000000	-0.138108
Cl	0.000000	-2.447303	-0.984192
Cl	0.000000	-4.271688	-1.975889
H	0.000000	0.000000	2.455039
F	0.000000	0.000000	3.397824

MP2

Structure converges into a D_{3h} symmetric minimum. See below.

[Cl(Cl₂)₂(HF)₃]⁻ (D_{3h})

B3LYP

Cl	0.000000	0.000000	0.000000
H	-1.049929	-1.818531	0.000000
F	-1.521252	-2.634886	0.000000
H	-1.049929	1.818531	0.000000
F	-1.521252	2.634886	0.000000
Cl	0.000000	0.000000	2.804970
Cl	0.000000	0.000000	4.876920
Cl	0.000000	0.000000	-2.804970
Cl	0.000000	0.000000	-4.876920
H	2.099859	0.000000	0.000000
F	3.042505	0.000000	0.000000

MP2

Cl	0.000000	0.000000	0.000000
H	-1.043105	-1.806710	0.000000
F	-1.512440	-2.619623	0.000000
H	-1.043105	1.806710	0.000000
F	-1.512440	2.619623	0.000000
Cl	0.000000	0.000000	2.936165
Cl	0.000000	0.000000	4.961530
Cl	0.000000	0.000000	-2.936165
Cl	0.000000	0.000000	-4.961530
H	2.086209	0.000000	0.000000
F	3.024880	0.000000	0.000000

[Cl(Cl₂)(HF)₃]⁻ (C_s)

B3LYP

Cl	0.296757	0.324191	0.000000
Cl	-2.475662	0.235583	0.000000
Cl	-4.554853	0.164557	0.000000
H	0.237875	2.440826	0.000000
F	0.226764	3.381932	0.000000
H	1.224826	0.167497	1.880672
F	1.648129	0.108325	2.720657
H	1.224826	0.167497	-1.880672
F	1.648129	0.108325	-2.720657
Cl	0.272042	-2.517698	0.000000
Cl	0.251167	-4.581035	0.000000

MP2

Cl	0.348746	0.393888	0.000000
Cl	-2.577098	0.210876	0.000000
Cl	-4.598730	0.079552	0.000000
H	0.082722	2.471069	0.000000
F	-0.043378	3.400795	0.000000
H	1.435592	0.196535	1.768831
F	1.917898	0.099082	2.568640
H	1.435592	0.196535	-1.768831
F	1.917898	0.099082	-2.568640
Cl	0.117196	-2.565854	0.000000
Cl	-0.036439	-4.581560	0.000000

[Cl(Cl₂)₃(HF)₂]⁻ (D_{3h})

B3LYP

Cl	0.000000	0.000000	0.000000
Cl	1.387910	2.403930	0.000000
Cl	2.426984	4.203659	0.000000
Cl	1.387910	-2.403930	0.000000
Cl	2.426984	-4.203659	0.000000
H	0.000000	0.000000	2.127087
F	0.000000	0.000000	3.066948
H	0.000000	0.000000	-2.127087
F	0.000000	0.000000	-3.066948
Cl	-2.775819	0.000000	0.000000
Cl	-4.853967	0.000000	0.000000

MP2

Cl	0.000000	0.000000	0.000000
Cl	1.435941	2.487123	0.000000
Cl	2.452670	4.248149	0.000000
Cl	1.435941	-2.487123	0.000000
Cl	2.452670	-4.248149	0.000000
H	0.000000	0.000000	2.094581
F	0.000000	0.000000	3.032140
H	0.000000	0.000000	-2.094581
F	0.000000	0.000000	-3.032140
Cl	-2.871882	0.000000	0.000000
Cl	-4.905340	0.000000	0.000000

[Cl(Cl₂)₃(HF)₂]⁻ (C_s)

B3LYP

Cl	-0.284656	0.307674	0.000000
Cl	-0.205269	-2.534867	0.000000
Cl	1.118716	0.224078	-2.389378
H	-2.384535	0.166620	0.000000
F	-3.325342	0.113382	0.000000
Cl	-0.144851	-4.595805	0.000000
Cl	2.162648	0.154509	-4.186083
Cl	1.118716	0.224078	2.389378
Cl	2.162648	0.154509	4.186083
H	-0.132879	2.423172	0.000000
F	-0.085196	3.362651	0.000000

MP2

Structure converges into a C_{2v} symmetric minimum. See below.

[Cl(Cl₂)₃(HF)₂]⁻ (C_{2v})

B3LYP

Cl	0.000000	0.000000	-0.238489
Cl	0.000000	2.803940	-0.367190
Cl	0.000000	-2.803940	-0.367190
Cl	0.000000	0.000000	2.525593
H	1.915770	0.000000	-1.115844
H	-1.915770	0.000000	-1.115844
F	2.769714	0.000000	-1.513113
F	-2.769714	0.000000	-1.513113
Cl	0.000000	-4.872103	-0.450551
Cl	0.000000	4.872103	-0.450551
Cl	0.000000	0.000000	4.606291

MP2

Cl	0.000000	0.000000	-0.343170
Cl	0.000000	2.880413	-0.124941
Cl	0.000000	-2.880413	-0.124941
Cl	0.000000	0.000000	2.538760
H	1.785698	0.000000	-1.408655
H	-1.785698	0.000000	-1.408655
F	2.595825	0.000000	-1.884543
F	-2.595825	0.000000	-1.884543
Cl	0.000000	-4.904862	0.035242
Cl	0.000000	4.904862	0.035242
Cl	0.000000	0.000000	4.570204

[Cl(HF)₅]⁻ (D_{3h})

B3LYP

Cl	0.000000	0.000000	0.000000
H	-1.050233	-1.819058	0.000000
F	-1.521699	-2.635660	0.000000
H	-1.050233	1.819058	0.000000
F	-1.521699	2.635660	0.000000
H	2.100467	0.000000	0.000000
F	3.043398	0.000000	0.000000
H	0.000000	0.000000	2.119383
F	0.000000	0.000000	3.060396
H	0.000000	0.000000	-2.119383
F	0.000000	0.000000	-3.060396

MP2

Cl	0.000000	0.000000	0.000000
H	-1.062067	-1.839555	0.000000
F	-1.529777	-2.649652	0.000000
H	-1.062067	1.839555	0.000000
F	-1.529777	2.649652	0.000000
H	2.124135	0.000000	0.000000
F	3.059554	0.000000	0.000000
H	0.000000	0.000000	2.141407
F	0.000000	0.000000	3.075357
H	0.000000	0.000000	-2.141407
F	0.000000	0.000000	-3.075357

[Cl₂₀]²⁻ (C_i)

B3LYP

Cl	0.010581	-0.005774	-1.025459
Cl	-0.010581	0.005774	1.025459
Cl	-0.029310	-0.017723	4.125454
Cl	0.029310	0.017723	-4.125454
Cl	-1.919745	1.941871	-3.510105
Cl	-1.886940	-1.951833	-3.568305
Cl	1.964564	-1.936481	-3.583798
Cl	1.919745	-1.941871	3.510105
Cl	-1.994744	-1.922143	3.510095
Cl	-1.964564	1.936481	3.583798
Cl	1.994744	1.922143	-3.510095
Cl	1.886940	1.951833	3.568305
Cl	-3.395502	3.381403	3.200611
Cl	-3.447374	-3.330744	3.078076
Cl	3.354795	-3.366324	3.073986
Cl	3.304750	3.407203	3.176276
Cl	3.447374	3.330744	-3.078076
Cl	-3.354795	3.366324	-3.073986
Cl	-3.304750	-3.407203	-3.176276
Cl	3.395502	-3.381403	-3.200611

MP2

Cl	-0.009705	-0.017091	-1.014670
Cl	0.009705	0.017091	1.014670
Cl	0.006496	0.009021	4.113648
Cl	-0.006496	-0.009021	-4.113648
Cl	-1.990812	1.975535	-3.487445
Cl	-1.962661	-2.031585	-3.538715
Cl	1.977741	-2.013551	-3.567490
Cl	1.990812	-1.975535	3.487445
Cl	-1.998942	-1.956242	3.488889
Cl	-1.977741	2.013551	3.567490
Cl	1.998942	1.956242	-3.488889
Cl	1.962661	2.031585	3.538715
Cl	-3.377406	3.439543	3.198444
Cl	-3.414442	-3.350092	3.063315
Cl	3.393265	-3.383911	3.066049
Cl	3.350144	3.465280	3.152714
Cl	3.414442	3.350092	-3.063315
Cl	-3.393265	3.383911	-3.066049
Cl	-3.350144	-3.465280	-3.152714
Cl	3.377406	-3.439543	-3.198444

[Cl(Cl₂)₄(HCl)]⁻ (C_{2v})

B3LYP

Cl	0.000000	0.000000	-3.622155
Cl	0.000000	0.000000	-0.129925
H	0.000000	0.000000	-2.314436
Cl	0.000000	2.780696	-0.409001
Cl	0.000000	-2.780696	-0.409001
Cl	-2.274010	0.000000	1.426031
Cl	2.274010	0.000000	1.426031
Cl	0.000000	4.842265	-0.598793
Cl	0.000000	-4.842265	-0.598793
Cl	-3.994569	0.000000	2.597641
Cl	3.994569	0.000000	2.597641#

MP2

Cl	0.000000	0.000000	-3.724147
Cl	0.000000	0.000000	-0.299642
H	0.000000	0.000000	-2.422008
Cl	0.000000	2.843036	-0.292795
Cl	0.000000	-2.843036	-0.292795
Cl	-2.319740	0.000000	1.306444
Cl	2.319740	0.000000	1.306444
Cl	0.000000	4.879090	-0.285606
Cl	0.000000	-4.879090	-0.285606
Cl	-3.990364	0.000000	2.477476
Cl	3.990364	0.000000	2.477476

[Cl(Cl₂)₄(HCl)]⁻ (C_{3v})

B3LYP

Cl	0.000000	0.000000	-0.036780
Cl	1.375189	2.381897	-0.224892
Cl	2.413152	4.179702	-0.364859
Cl	1.375189	-2.381897	-0.224892
Cl	2.413152	-4.179702	-0.364859
Cl	-2.750378	0.000000	-0.224892
Cl	-4.826304	0.000000	-0.364859
Cl	0.000000	0.000000	2.760953
Cl	0.000000	0.000000	4.830793
H	0.000000	0.000000	-2.240600
Cl	0.000000	0.000000	-3.545136

MP2

Cl	0.000000	0.000000	-0.210262
Cl	1.409524	2.441368	-0.195497
Cl	2.429866	4.208651	-0.183525
Cl	1.409524	-2.441368	-0.195497
Cl	2.429866	-4.208651	-0.183525
Cl	-2.819049	0.000000	-0.195497
Cl	-4.859731	0.000000	-0.183525
Cl	0.000000	0.000000	2.648543
Cl	0.000000	0.000000	4.681966
H	0.000000	0.000000	-2.341431
Cl	0.000000	0.000000	-3.641777

f) Calculated Vibrational Spectra

Table S9. Cl₂

B3LYP-D3BJ/def2-TZVPP				SCS-MP2/def2-TZVPP			
Nr.	Symmetry	Wavenumber / cm ⁻¹	IR intensity / km mol ⁻¹	Nr.	Symmetry	Wavenumber / cm ⁻¹	IR intensity / km mol ⁻¹
1	Σ_g^+	537.1	0	1	Σ_g^+	561.2	0

Table S10. HF

B3LYP-D3BJ/def2-TZVPP				SCS-MP2/def2-TZVPP			
Nr.	Symmetry	Wavenumber / cm ⁻¹	IR intensity / km mol ⁻¹	Nr.	Symmetry	Wavenumber / cm ⁻¹	IR intensity / km mol ⁻¹
1	Σ^+	4081.2	106	1	Σ^+	4146.9	111

Table S11. [Cl₃]⁻

B3LYP-D3BJ/def2-TZVPP				SCS-MP2/def2-TZVPP			
Nr.	Symmetry	Wavenumber / cm ⁻¹	IR intensity / km mol ⁻¹	Nr.	Symmetry	Wavenumber / cm ⁻¹	IR intensity / km mol ⁻¹
1	Π_u	154.5	1	1	Π_u	169.0	1
2	Π_u	154.5	1	2	Π_u	169.0	1
3	Σ_g^+	247.4	0	3	Σ_g^+	270.5	0
4	Σ_u^-	261.7	410	4	Σ_u^-	295.3	568

Table S12. [Cl(Cl₂)₂]⁻

B3LYP-D3BJ/def2-TZVPP				SCS-MP2/def2-TZVPP			
Nr.	Symmetry	Wavenumber / cm ⁻¹	IR intensity / km mol ⁻¹	Nr.	Symmetry	Wavenumber / cm ⁻¹	IR intensity / km mol ⁻¹
1	A_1	19.4	0	1	A_1	16.5	0
2	B_1	128.7	33	2	B_1	91.2	760
3	A_2	135.0	0	3	A_1	139.3	18
4	A_1	136.7	7	4	A_2	144.2	0
5	B_2	149.5	1	5	B_1	151.1	187
6	B_1	187.3	445	6	B_2	161.8	1
7	A_1	201.0	19	7	A_1	203.0	45
8	B_1	304.3	374	8	B_1	325.5	269
9	A_1	353.3	93	9	A_1	374.3	124

Table S13. $[\text{Cl}(\text{Cl}_2)_3]^-$

B3LYP-D3BJ/def2-TZVPP				SCS-MP2/def2-TZVPP			
Nr.	Symmetry	Wavenumber / cm^{-1}	IR intensity / km mol^{-1}	Nr.	Symmetry	Wavenumber / cm^{-1}	IR intensity / km mol^{-1}
1	<i>E</i>	12.6	0	1	<i>E</i>	11.8	0
2	<i>E</i>	12.6	0	2	<i>E</i>	11.8	0
3	<i>A</i> ₁	16.3	0	3	<i>A</i> ₁	14.8	0
4	<i>E</i>	112.0	45	4	<i>E</i>	92.2	169
5	<i>E</i>	112.0	45	5	<i>E</i>	92.2	169
6	<i>A</i> ₁	112.4	3	6	<i>A</i> ₁	112.3	7
7	<i>A</i> ₂	118.5	0	7	<i>A</i> ₂	123.3	0
8	<i>E</i>	127.2	14	8	<i>E</i>	128.1	6
9	<i>E</i>	127.2	14	9	<i>E</i>	128.1	6
10	<i>A</i> ₁	169.4	5	10	<i>E</i>	155.4	125
11	<i>E</i>	176.3	166	11	<i>E</i>	155.4	125
12	<i>E</i>	176.3	166	12	<i>A</i> ₁	170.0	15
13	<i>E</i>	355.3	364	13	<i>E</i>	393.2	286
14	<i>E</i>	355.3	364	14	<i>E</i>	393.2	286
15	<i>A</i> ₁	407.6	34	15	<i>A</i> ₁	438.2	50

Table S14. $[\text{Cl}(\text{Cl}_2)_4]^- (T_d)$

B3LYP-D3BJ/def2-TZVPP				SCS-MP2/def2-TZVPP			
Nr.	Symmetry	Wavenumber / cm^{-1}	IR intensity / km mol^{-1}	Nr.	Symmetry	Wavenumber / cm^{-1}	IR intensity / km mol^{-1}
1	<i>E</i>	7.4	0	1	<i>E</i>	6.9	0
2	<i>E</i>	7.4	0	2	<i>E</i>	6.9	0
3	<i>T</i> ₂	8.5	0	3	<i>T</i> ₂	9.5	0
4	<i>T</i> ₂	8.5	0	4	<i>T</i> ₂	9.5	0
5	<i>T</i> ₂	8.5	0	5	<i>T</i> ₂	9.5	0
6	<i>A</i> ₁	90.2	0	6	<i>A</i> ₁	83.5	0
7	<i>T</i> ₂	98.6	40	7	<i>T</i> ₂	90.4	61
8	<i>T</i> ₂	98.6	40	8	<i>T</i> ₂	90.4	61
9	<i>T</i> ₂	98.6	40	9	<i>T</i> ₂	90.4	61
10	<i>T</i> ₁	107.6	0	10	<i>T</i> ₁	111.4	0
11	<i>T</i> ₁	107.6	0	11	<i>T</i> ₁	111.4	0
12	<i>T</i> ₁	107.6	0	12	<i>T</i> ₁	111.4	0
13	<i>E</i>	120.7	0	13	<i>E</i>	119.3	0
14	<i>E</i>	120.7	0	14	<i>E</i>	119.3	0
15	<i>T</i> ₂	172.4	100	15	<i>T</i> ₂	158.2	97
16	<i>T</i> ₂	172.4	100	16	<i>T</i> ₂	158.2	97
17	<i>T</i> ₂	172.4	100	17	<i>T</i> ₂	158.2	97
18	<i>T</i> ₂	389.9	309	18	<i>T</i> ₂	437.5	220
19	<i>T</i> ₂	389.9	309	19	<i>T</i> ₂	437.5	220
20	<i>T</i> ₂	389.9	309	20	<i>T</i> ₂	437.5	220
21	<i>A</i> ₁	438.3	0	21	<i>A</i> ₁	472.1	0

Table S15. $[\text{Cl}(\text{Cl}_2)_4]^-$ (C_{4v})

B3LYP-D3BJ/def2-TZVPP				SCS-MP2/def2-TZVPP			
Nr.	Symmetry	Wavenumber / cm^{-1}	IR intensity / km mol^{-1}	Nr.	Symmetry	Wavenumber / cm^{-1}	IR intensity / km mol^{-1}
1	B_2	-8.6	0	1	B_2	-4.0	0
2	A_1	18.2	0	2	A_1	17.3	1
3	E	20.2	2	3	E	19.3	0
4	E	20.2	2	4	E	19.3	0
5	B_1	23.0	0	5	B_1	20.3	0
6	B_2	64.9	0	6	B_2	56.9	0
7	A_1	94.4	1	7	A_1	86.8	1
8	B_2	99.7	0	8	E	99.3	70
9	E	100.3	24	9	E	99.3	70
10	E	100.3	24	10	B_2	105.6	0
11	A_2	102.0	0	11	A_2	107.5	0
12	E	108.1	0	12	E	111.3	0
13	E	108.1	0	13	E	111.3	0
14	B_1	119.4	0	14	B_1	120.8	0
15	A_1	139.8	2	15	A_1	135.2	2
16	E	148.4	247	16	E	143.4	217
17	E	148.4	247	17	E	143.4	217
18	B_2	396.2	0	18	B_2	444.4	0
19	E	400.4	403	19	E	445.3	291
20	E	400.4	403	20	E	445.3	291
21	A_1	448.2	10	21	A_1	479.4	5

Table S16. $[\text{Cl}(\text{Cl}_2)_4]^-$ (D_{4h})

B3LYP-D3BJ/def2-TZVPP				SCS-MP2/def2-TZVPP			
Nr.	Symmetry	Wavenumber / cm^{-1}	IR intensity / km mol^{-1}	Nr.	Symmetry	Wavenumber / cm^{-1}	IR intensity / km mol^{-1}
1	B_{1u}	-16.2	0	1	B_{1u}	-1.9	0
2	A_{2u}	-10.8	0	2	E_u	17.3	0
3	E_u	16.5	1	3	E_u	17.3	0
4	E_u	16.5	1	4	B_{1g}	18.4	0
5	B_{1g}	19.6	0	5	A_{2u}	23.5	1
6	B_{2g}	70.1	0	6	B_{2g}	57.5	0
7	A_{1g}	88.5	0	7	A_{1g}	81.7	0
8	B_{1u}	91.5	0	8	E_u	100.0	69
9	E_u	101.8	36	9	E_u	100.0	69
10	E_u	102.3	36	10	B_{1u}	105.2	0
11	A_{2g}	102.3	0	11	A_{2g}	107.6	0
12	E_g	105.4	0	12	E_g	112.0	0
13	E_g	105.4	0	13	E_g	112.0	0
14	A_{2u}	111.3	1	14	B_{1g}	120.1	0
15	B_{1g}	118.2	0	15	A_{2u}	129.1	1
16	E_u	151.5	270	16	E_u	144.1	245
17	E_u	151.5	270	17	E_u	144.1	245
18	E_u	398.5	437	18	E_u	444.6	304
19	E_u	398.5	437	19	E_u	444.6	304
20	B_{2g}	401.1	0	20	B_{2g}	445.3	0
21	A_{1g}	447.6	0	21	A_{1g}	479.1	0

Table S17. $[\text{Cl}(\text{Cl}_2)_5]^- (D_{3h})$

B3LYP-D3BJ/def2-TZVPP				SCS-MP2/def2-TZVPP			
Nr.	Symmetry	Wavenumber / cm^{-1}	IR intensity / km mol^{-1}	Nr.	Symmetry	Wavenumber / cm^{-1}	IR intensity / km mol^{-1}
1	E'	5.9	0	1	E'	12.7	0
2	E'	5.9	0	2	E'	12.7	0
3	E'	12.9	0	3	E''	19.4	0
4	E'	12.9	0	4	E''	19.4	0
5	E''	15.2	0	5	E'	21.1	0
6	E''	15.2	0	6	E'	21.1	0
7	A_2''	15.5	1	7	A_2''	23.3	0
8	A_1'	64.1	0	8	A_1'	57.2	0
9	A_1'	83.8	0	9	A_1'	77.3	0
10	E'	89.7	14	10	E'	89.3	39
11	E'	89.7	14	11	E'	89.3	39
12	E''	93.9	0	12	A_2''	100.2	48
13	E''	93.9	0	13	A_2'	103.1	0
14	A_2''	97.6	28	14	E'	107.6	0
15	E'	97.9	19	15	E'	107.6	0
16	E'	97.9	19	16	E''	108.9	0
17	A_2'	100.8	0	17	E''	108.9	0
18	E''	110.2	0	18	E''	118.6	0
19	E''	110.2	0	19	E''	118.6	0
20	A_2''	148.2	161	20	A_2''	149.8	125
21	E'	160.3	95	21	E'	151.4	84
22	E'	160.3	95	22	E'	151.4	84
23	E'	414.5	278	23	E'	463.8	172
24	E'	414.5	278	24	E'	463.8	172
25	A_1'	423.2	0	25	A_1'	468.9	0
26	A_2''	432.2	311	26	A_2''	474.9	196
27	A_1'	466.2	0	27	A_1'	496.8	0

Table S18. $[\text{Cl}(\text{Cl}_2)_5]^-$ (C_{4v})

B3LYP-D3BJ/def2-TZVPP				SCS-MP2/def2-TZVPP			
Nr.	Symmetry	Wavenumber / cm^{-1}	IR intensity / km mol^{-1}	Nr.	Symmetry	Wavenumber / cm^{-1}	IR intensity / km mol^{-1}
1	B_2	-3.6	0	1	B_2	5.3	0
2	E	8.8	0	2	E	12.2	0
3	E	8.8	0	3	E	12.2	0
4	A_1	12.1	0	4	A_1	13.6	0
5	E	16.3	1	5	B_1	16.6	0
6	E	16.3	1	6	E	17.2	0
7	B_1	18.8	0	7	E	17.2	0
8	B_2	62.3	0	8	B_2	57.5	0
9	A_1	82.2	3	9	A_1	73.9	7
10	A_1	89.5	16	10	A_1	86.5	19
11	E	93.5	17	11	E	93.2	34
12	E	93.5	17	12	E	93.2	34
13	A_2	93.8	0	13	A_2	99.4	0
14	B_2	94.8	0	14	B_2	100.2	0
15	E	98.2	1	15	E	103.3	0
16	E	98.2	1	16	E	103.3	0
17	E	106.0	22	17	B_1	109.9	0
18	E	106.0	22	18	E	111.4	13
19	B_1	108.1	0	19	E	111.4	13
20	E	154.3	137	20	A_1	144.1	57
21	E	154.3	137	21	E	151.3	129
22	A_1	157.9	74	22	E	151.3	129
23	A_1	406.7	233	23	A_1	457.4	132
24	B_2	425.9	0	24	E	471.4	203
25	E	426.6	314	25	E	471.4	203
26	E	426.6	314	26	B_2	471.7	0
27	A_1	466.2	2	27	A_1	496.9	0

Table S19. $[\text{Cl}(\text{Cl}_2)_6]^-$

B3LYP-D3BJ/def2-TZVPP				SCS-MP2/def2-TZVPP			
Nr.	Symmetry	Wavenumber / cm^{-1}	IR intensity / km mol^{-1}	Nr.	Symmetry	Wavenumber / cm^{-1}	IR intensity / km mol^{-1}
1	T_{2u}	8.8	0	1	T_{2u}	11.3	0
2	T_{2u}	8.8	0	2	T_{2u}	11.3	0
3	T_{2u}	8.8	0	3	T_{2u}	11.3	0
4	T_{1u}	12.7	1	4	T_{1g}	15.0	0
5	T_{1u}	12.7	1	5	T_{1g}	15.0	0
6	T_{1u}	12.7	1	6	T_{1g}	15.0	0
7	T_{2g}	13.7	0	7	T_{1u}	18.4	0
8	T_{2g}	13.7	0	8	T_{1u}	18.4	0
9	T_{2g}	13.7	0	9	T_{1u}	18.4	0
10	E_g	63.3	0	10	E_g	57.8	0
11	E_g	63.3	0	11	E_g	57.8	0
12	A_{1g}	79.0	0	12	A_{1g}	73.0	0
13	T_{1u}	87.9	14	13	T_{1u}	89.5	23
14	T_{1u}	87.9	14	14	T_{1u}	89.5	23
15	T_{1u}	87.9	14	15	T_{1u}	89.5	23
16	T_{1g}	88.9	0	16	T_{1g}	97.1	0
17	T_{1g}	88.9	0	17	T_{1g}	97.1	0
18	T_{1g}	88.9	0	18	T_{1g}	97.1	0
19	T_{2u}	88.9	0	19	T_{2u}	98.1	0
20	T_{2u}	88.9	0	20	T_{2u}	98.1	0
21	T_{2u}	88.9	0	21	T_{2u}	98.1	0
22	T_{2g}	100.5	0	22	T_{2g}	105.8	0
23	T_{2g}	100.5	0	23	T_{2g}	105.8	0
24	T_{2g}	100.5	0	24	T_{2g}	105.8	0
25	T_{1u}	144.0	144	25	T_{1u}	147.4	110
26	T_{1u}	144.0	144	26	T_{1u}	147.4	110
27	T_{1u}	144.0	144	27	T_{1u}	147.4	110
28	T_{1u}	441.8	270	28	T_{1u}	485.8	156
29	T_{1u}	441.8	270	29	T_{1u}	485.8	156
30	T_{1u}	441.8	270	30	T_{1u}	485.8	156
31	E_g	443.8	0	31	E_g	486.5	0
32	E_g	443.8	0	32	E_g	486.5	0
33	A_{1g}	480.7	0	33	A_{1g}	509.3	0

Table S20. $[\text{Cl}(\text{Cl}_2)_4(\text{HF})]^- (\text{C}_{2v})$

B3LYP-D3BJ/def2-TZVPP				SCS-MP2/def2-TZVPP			
Nr.	Symmetry	Wavenumber / cm^{-1}	IR intensity / km mol^{-1}	Nr.	Symmetry	Wavenumber / cm^{-1}	IR intensity / km mol^{-1}
1	A_1	6.5	0	1	A_1	7.1	0
2	B_1	8.4	2	2	B_1	14.3	2
3	A_1	13.4	0	3	A_1	17.2	1
4	A_2	14.9	0	4	A_2	17.6	0
5	B_2	15.2	0	5	B_2	18.4	1
6	B_1	17.1	1	6	B_1	20.7	0
7	B_2	21.9	0	7	B_2	22.6	1
8	A_1	67.8	4	8	A_1	56.7	1
9	A_1	90.2	3	9	A_1	79.3	4
10	B_1	91.4	9	10	B_1	92.4	27
11	B_2	95.9	9	11	B_2	95.8	27
12	A_2	95.9	0	12	A_2	99.9	0
13	A_1	98.3	3	13	A_1	102.6	0
14	B_1	99.5	8	14	B_1	103.1	0
15	B_2	103.5	18	15	B_2	103.2	7
16	A_2	110.7	0	16	A_2	112.3	0
17	A_1	118.4	1	17	A_1	115.0	1
18	B_1	145.7	91	18	B_1	137.1	84
19	B_2	146.8	166	19	B_2	137.8	112
20	A_1	192.6	33	20	A_1	200.8	24
21	B_1	414.6	243	21	B_1	476.0	152
22	A_1	420.8	66	22	A_1	477.6	12
23	B_2	428.2	324	23	B_2	480.6	175
24	A_1	460.9	10	24	A_1	499.1	9
25	B_2	595.8	101	25	B_2	708.9	95
26	B_1	599.2	58	26	B_1	710.2	68
27	A_1	3659.4	1423	27	A_1	3672.1	1428

Table S21. $[\text{Cl}(\text{Cl}_2)_4(\text{HF})]^- (\text{C}_{3v})$

B3LYP-D3BJ/def2-TZVPP				SCS-MP2/def2-TZVPP			
Nr.	Symmetry	Wavenumber / cm^{-1}	IR intensity / km mol^{-1}	Nr.	Symmetry	Wavenumber / cm^{-1}	IR intensity / km mol^{-1}
1	<i>E</i>	3.9	0	1	<i>E</i>	7.7	0
2	<i>E</i>	3.9	0	2	<i>E</i>	7.7	0
3	<i>E</i>	13.4	0	3	<i>E</i>	15.4	1
4	<i>E</i>	13.4	0	4	<i>E</i>	15.4	1
5	<i>A</i> ₁	13.5	0	5	<i>E</i>	19.5	0
6	<i>E</i>	17.7	0	6	<i>E</i>	19.5	0
7	<i>E</i>	17.7	0	7	<i>A</i> ₁	20.4	1
8	<i>A</i> ₁	73.2	9	8	<i>A</i> ₁	63.1	5
9	<i>E</i>	90.3	12	9	<i>A</i> ₁	84.4	12
10	<i>E</i>	90.3	12	10	<i>E</i>	88.5	30
11	<i>A</i> ₁	90.8	7	11	<i>E</i>	88.5	30
12	<i>E</i>	96.5	21	12	<i>E</i>	100.0	1
13	<i>E</i>	96.5	21	13	<i>E</i>	100.0	1
14	<i>A</i> ₂	99.6	0	14	<i>A</i> ₂	101.2	0
15	<i>E</i>	107.4	0	15	<i>E</i>	111.2	0
16	<i>E</i>	107.4	0	16	<i>E</i>	111.2	0
17	<i>A</i> ₁	113.8	3	17	<i>A</i> ₁	118.1	3
18	<i>E</i>	158.2	92	18	<i>E</i>	141.9	70
19	<i>E</i>	158.2	92	19	<i>E</i>	141.9	70
20	<i>A</i> ₁	183.0	53	20	<i>A</i> ₁	196.4	48
21	<i>E</i>	412.3	278	21	<i>E</i>	471.6	153
22	<i>E</i>	412.3	278	22	<i>E</i>	471.6	153
23	<i>A</i> ₁	430.0	61	23	<i>A</i> ₁	483.4	15
24	<i>A</i> ₁	462.3	50	24	<i>A</i> ₁	503.3	39
25	<i>E</i>	568.6	94	25	<i>E</i>	679.3	95
26	<i>E</i>	568.6	94	26	<i>E</i>	679.3	95
27	<i>A</i> ₁	3689.8	1402	27	<i>A</i> ₁	3699.3	1496

Table S22. $[\text{Cl}(\text{Cl}_2)_4(\text{HF})]^-$ (C_{4v})

B3LYP-D3BJ/def2-TZVPP				SCS-MP2/def2-TZVPP			
Nr.	Symmetry	Wavenumber / cm^{-1}	IR intensity / km mol^{-1}	Nr.	Symmetry	Wavenumber / cm^{-1}	IR intensity / km mol^{-1}
1	B_2	-4.5	0	1	B_2	6.4	0
2	A_1	14.4	0	2	A_1	18.4	1
3	E	15.6	2	3	E	18.7	2
4	E	15.6	2	4	E	18.7	2
5	E	19.1	0	5	B_1	21.7	0
6	E	19.1	0	6	E	22.4	0
7	B_1	19.4	0	7	E	22.4	0
8	B_2	62.2	0	8	B_2	54.3	0
9	A_1	86.0	1	9	A_1	77.2	3
10	E	93.7	17	10	E	91.9	28
11	E	93.7	17	11	E	91.9	28
12	A_2	94.5	0	12	A_2	98.2	0
13	B_2	94.9	0	13	B_2	99.2	0
14	E	100.3	0	14	E	102.4	0
15	E	100.3	0	15	E	102.4	0
16	B_1	109.2	0	16	B_1	109.0	0
17	A_1	112.5	0	17	A_1	113.6	1
18	E	142.0	160	18	E	135.6	108
19	E	142.0	160	19	E	135.6	108
20	A_1	195.9	14	20	A_1	201.8	19
21	B_2	422.5	0	21	B_2	478.3	0
22	E	423.5	314	22	E	478.8	168
23	E	423.5	314	23	E	478.8	168
24	A_1	461.8	13	24	A_1	499.3	10
25	E	625.3	71	25	E	707.6	80
26	E	625.3	71	26	E	707.6	80
27	A_1	3628.1	1403	27	A_1	3665.9	1411

Table S23. $[\text{Cl}(\text{Cl}_2)(\text{HF})_4]^-$ (C_{2v})

B3LYP-D3BJ/def2-TZVPP				SCS-MP2/def2-TZVPP			
Nr.	Symmetry	Wavenumber / cm^{-1}	IR intensity / km mol^{-1}	Nr.	Symmetry	Wavenumber / cm^{-1}	IR intensity / km mol^{-1}
1	B_2	8.2	0	1	B_2	8.5	0
2	A_1	14.3	0	2	A_1	18.6	1
3	B_1	22.1	0	3	B_2	27.2	0
4	B_2	22.3	0	4	B_1	29.4	0
5	A_1	25.4	2	5	A_2	29.4	0
6	B_1	27.2	1	6	A_1	30.8	2
7	A_2	28.7	0	7	B_1	32.6	1
8	B_2	106.5	0	8	A_1	72.8	10
9	B_1	108.1	0	9	B_2	88.8	0
10	A_1	108.7	21	10	B_1	94.7	0
11	A_1	147.0	0	11	A_1	150.5	0
12	A_1	168.4	30	12	A_1	174.5	14
13	B_1	199.4	15	13	B_2	193.7	10
14	B_2	200.4	9	14	B_1	202.9	18
15	A_1	430.9	117	15	A_1	521.8	28
16	A_2	537.1	0	16	A_2	625.3	0
17	B_2	562.9	92	17	B_2	628.1	14
18	B_1	563.0	51	18	B_1	635.0	22
19	A_1	568.2	114	19	A_1	649.7	147
20	B_2	609.2	115	20	B_2	668.7	220
21	A_1	636.4	192	21	A_1	694.6	196
22	B_1	639.7	131	22	B_1	717.9	179
23	A_2	675.3	0	23	A_2	730.4	0
24	B_2	3624.5	1805	24	B_2	3705.5	1532
25	A_1	3643.2	708	25	A_1	3720.3	893
26	B_1	3662.7	2136	26	B_1	3734.9	2014
27	A_1	3719.5	400	27	A_1	3795.4	140

Table S24. $[\text{Cl}(\text{Cl}_2)(\text{HF})_4]^-$ (C_{3v})

B3LYP-D3BJ/def2-TZVPP				SCS-MP2/def2-TZVPP			
Nr.	Symmetry	Wavenumber / cm^{-1}	IR intensity / km mol^{-1}	Nr.	Symmetry	Wavenumber / cm^{-1}	IR intensity / km mol^{-1}
1	E	9.7	0	1	E	11.1	1
2	E	9.7	0	2	E	11.1	1
3	E	24.6	0	3	E	24.1	0
4	E	24.6	0	4	E	24.1	0
5	A_1	27.0	1	5	A_1	26.8	2
6	E	27.0	1	6	E	29.0	1
7	E	27.0	1	7	E	29.0	1
8	A_1	94.9	19	8	A_1	68.1	10
9	E	97.4	0	9	E	81.8	0
10	E	97.4	0	10	E	81.8	0
11	A_1	153.7	1	11	A_1	155.0	0
12	A_1	180.5	44	12	A_1	181.0	21
13	E	198.0	9	13	E	197.4	11
14	E	198.0	9	14	E	197.4	11
15	A_1	445.5	110	15	A_1	525.8	26
16	E	553.5	32	16	E	623.9	13
17	E	553.5	32	17	E	623.9	13
18	A_2	586.9	0	18	A_2	645.3	0
19	A_1	626.3	295	19	A_1	671.1	333
20	E	644.6	68	20	E	696.8	49
21	E	644.6	68	21	E	696.8	49
22	E	655.8	105	22	E	708.2	163
23	E	655.8	105	23	E	708.2	163
24	E	3617.9	1711	24	E	3710.0	1612
25	E	3617.9	1711	25	E	3710.0	1612
26	A_1	3638.3	722	26	A_1	3718.9	1056
27	A_1	3691.0	1114	27	A_1	3780.9	368

Table S25. $[\text{Cl}(\text{Cl}_2)_2(\text{HF})_3]^-$ (C_{2v})

B3LYP-D3BJ/def2-TZVPP				SCS-MP2/def2-TZVPP			
Nr.	Symmetry	Wavenumber / cm^{-1}	IR intensity / km mol^{-1}	Nr.	Symmetry	Wavenumber / cm^{-1}	IR intensity / km mol^{-1}
1	A_1	4.9	1	1	*	*	*
2	B_2	14.3	1	2	*	*	*
3	B_1	18.7	0	3	*	*	*
4	A_1	20.9	0	4	*	*	*
5	B_2	24.1	1	5	*	*	*
6	A_2	25.1	0	6	*	*	*
7	B_1	25.2	1	7	*	*	*
8	A_1	85.3	6	8	*	*	*
9	B_2	97.9	15	9	*	*	*
10	A_2	106.3	0	10	*	*	*
11	B_1	108.4	0	11	*	*	*
12	A_1	113.6	0	12	*	*	*
13	B_2	139.1	101	13	*	*	*
14	A_1	144.2	0	14	*	*	*
15	A_1	192.7	18	15	*	*	*
16	B_1	200.2	16	16	*	*	*
17	B_2	416.9	263	17	*	*	*
18	A_1	440.5	41	18	*	*	*
19	B_1	554.2	18	19	*	*	*
20	B_2	570.6	150	20	*	*	*
21	A_1	576.4	170	21	*	*	*
22	A_2	587.8	0	22	*	*	*
23	B_2	619.3	122	23	*	*	*
24	B_1	648.8	71	24	*	*	*
25	A_1	3633.4	1475	25	*	*	*
26	B_1	3669.2	1999	26	*	*	*
27	A_1	3710.1	120	27	*	*	*

* Structure converges into a D_{3h} symmetric minimum. See table S24

Table S26. $[\text{Cl}(\text{Cl}_2)_2(\text{HF})_3]^- (D_{3h})$

B3LYP-D3BJ/def2-TZVPP				SCS-MP2/def2-TZVPP			
Nr.	Symmetry	Wavenumber / cm^{-1}	IR intensity / km mol^{-1}	Nr.	Symmetry	Wavenumber / cm^{-1}	IR intensity / km mol^{-1}
1	E'	5.8	1	1	E'	11.2	3
2	E'	5.8	1	2	E'	11.2	3
3	E''	22.4	0	3	E''	20.5	0
4	E''	22.4	0	4	E''	20.5	0
5	E'	22.9	1	5	A_2''	21.7	2
6	E'	22.9	1	6	E'	24.7	0
7	A_2''	23.3	1	7	E'	24.7	0
8	A_1'	72.6	0	8	A_1'	56.2	0
9	E'	96.8	0	9	E''	92.4	0
10	E'	96.8	0	10	E''	92.4	0
11	E''	98.8	0	11	E'	94.8	0
12	E''	98.8	0	12	E'	94.8	0
13	A_2''	136.7	192	13	A_2''	111.0	84
14	A_1'	150.5	0	14	A_1'	156.4	0
15	E'	198.8	10	15	E'	205.5	14
16	E'	198.8	10	16	E'	205.5	14
17	A_2''	421.7	346	17	A_2''	502.4	113
18	A_1'	446.2	0	18	A_1'	509.4	0
19	A_2'	582.2	0	19	A_2'	658.8	0
20	E''	618.2	0	20	E''	680.8	0
21	E''	618.2	0	21	E''	680.8	0
22	A_2''	619.5	294	22	A_2''	681.1	342
23	E'	639.3	111	23	E'	710.6	118
24	E'	639.3	111	24	E'	710.6	118
25	E'	3627.7	1647	25	E'	3686.9	1665
26	E'	3627.7	1647	26	E'	3686.9	1665
27	A_1'	3672.6	0	27	A_1'	3738.7	0

Table S27. $[\text{Cl}(\text{Cl}_2)_2(\text{HF})_3]^- (\text{C}_3)$

B3LYP-D3BJ/def2-TZVPP				SCS-MP2/def2-TZVPP			
Nr.	Symmetry	Wavenumber / cm^{-1}	IR intensity / km mol^{-1}	Nr.	Symmetry	Wavenumber / cm^{-1}	IR intensity / km mol^{-1}
1	A''	9.3	0	1	A''	8.8	0
2	A'	10.1	1	2	A'	13.8	1
3	A'	17.5	0	3	A''	16.8	0
4	A''	19.1	0	4	A'	21.1	1
5	A'	21.4	2	5	A'	25.4	1
6	A'	25.0	1	6	A'	28.7	1
7	A''	26.5	0	7	A''	31.0	0
8	A'	85.3	21	8	A'	68.4	12
9	A'	96.5	4	9	A'	89.9	9
10	A''	96.7	0	10	A''	95.6	0
11	A''	109.4	0	11	A'	98.1	6
12	A'	110.8	4	12	A''	101.6	0
13	A'	122.9	16	13	A'	106.8	5
14	A'	167.5	34	14	A'	173.9	18
15	A'	182.2	48	15	A'	190.6	29
16	A''	202.7	11	16	A''	203.4	14
17	A'	419.5	153	17	A'	504.6	44
18	A'	452.2	91	18	A'	515.3	36
19	A''	548.5	38	19	A''	640.1	15
20	A'	565.2	74	20	A'	654.7	84
21	A''	601.1	36	21	A''	673.2	60
22	A'	621.4	148	22	A'	703.3	203
23	A'	630.6	171	23	A'	708.4	142
24	A''	647.1	44	24	A''	718.3	56
25	A''	3629.4	1761	25	A''	3675.7	1644
26	A'	3646.3	875	26	A'	3688.0	1225
27	A'	3683.9	1729	27	A'	3732.9	1192

Table S28. $[\text{Cl}(\text{Cl}_2)_3(\text{HF})_2]^- (D_{3h})$

B3LYP-D3BJ/def2-TZVPP				SCS-MP2/def2-TZVPP			
Nr.	Symmetry	Wavenumber / cm^{-1}	IR intensity / km mol^{-1}	Nr.	Symmetry	Wavenumber / cm^{-1}	IR intensity / km mol^{-1}
1	E'	6.6	0	1	E'	8.1	1
2	E'	6.6	0	2	E'	8.1	1
3	A_2''	14.5	1	3	E'	16.1	1
4	E'	16.6	1	4	E'	16.1	1
5	E'	16.6	1	5	A_2''	16.9	2
6	E''	20.2	0	6	E''	19.5	0
7	E''	20.2	0	7	E''	19.5	0
8	A_1'	78.5	0	8	A_1'	64.8	0
9	E'	95.5	32	9	E'	86.8	26
10	E'	95.5	32	10	E'	86.8	26
11	A_2'	100.4	0	11	A_2'	97.3	0
12	E''	106.0	0	12	E''	101.2	0
13	E''	106.0	0	13	E''	101.2	0
14	A_2''	108.1	0	14	A_2''	105.6	0
15	A_1'	140.7	0	15	E'	130.2	52
16	E'	154.3	83	16	E'	130.2	52
17	E'	154.3	83	17	A_1'	151.2	0
18	A_2''	203.2	19	18	A_2''	218.5	28
19	E'	414.7	268	19	E'	484.9	120
20	E'	414.7	268	20	E'	484.9	120
21	A_1'	446.5	0	21	A_1'	498.1	0
22	E'	562.3	194	22	E'	643.2	204
23	E'	562.3	194	23	E'	643.2	204
24	E''	580.6	0	24	E''	664.1	0
25	E''	580.6	0	25	E''	664.1	0
26	A_2''	3681.1	1971	26	A_2''	3706.8	2120
27	A_1'	3716.9	0	27	A_1'	3749.5	0

Table S29. $[\text{Cl}(\text{Cl}_2)_3(\text{HF})_2]^- (\text{C}_3)$

B3LYP-D3BJ/def2-TZVPP				SCS-MP2/def2-TZVPP			
Nr.	Symmetry	Wavenumber / cm^{-1}	IR intensity / km mol^{-1}	Nr.	Symmetry	Wavenumber / cm^{-1}	IR intensity / km mol^{-1}
1	A'	5.2	0	1	**	**	**
2	A''	11.2	1	2	**	**	**
3	A'	15.3	0	3	**	**	**
4	A'	17.0	0	4	**	**	**
5	A''	18.0	0	5	**	**	**
6	A''	20.3	1	6	**	**	**
7	A'	24.0	1	7	**	**	**
8	A'	78.2	18	8	**	**	**
9	A''	92.6	6	9	**	**	**
10	A'	95.5	1	10	**	**	**
11	A'	97.2	6	11	**	**	**
12	A''	99.0	12	12	**	**	**
13	A''	109.2	0	13	**	**	**
14	A'	112.1	2	14	**	**	**
15	A'	120.3	1	15	**	**	**
16	A''	144.2	103	16	**	**	**
17	A'	180.8	46	17	**	**	**
18	A'	193.5	29	18	**	**	**
19	A''	413.1	264	19	**	**	**
20	A'	426.3	96	20	**	**	**
21	A'	458.1	70	21	**	**	**
22	A'	555.3	82	22	**	**	**
23	A''	573.0	59	23	**	**	**
24	A''	612.0	96	24	**	**	**
25	A'	627.9	99	25	**	**	**
26	A'	3642.3	1379	26	**	**	**
27	A'	3681.7	1659	27	**	**	**

** Structure converges into a C_{2v} minimum. See table S28.

Table S30. $[\text{Cl}(\text{Cl}_2)_3(\text{HF})_2]^- (\text{C}_{2v})$

B3LYP-D3BJ/def2-TZVPP				SCS-MP2/def2-TZVPP			
Nr.	Symmetry	Wavenumber / cm^{-1}	IR intensity / km mol^{-1}	Nr.	Symmetry	Wavenumber / cm^{-1}	IR intensity / km mol^{-1}
1	A_1	6.6	1	1	B_1	6.6	1
2	B_1	7.5	1	2	A_1	12.8	2
3	B_2	12.4	0	3	B_2	20.4	1
4	B_1	15.1	0	4	A_1	21.3	1
5	A_1	18.6	1	5	A_2	22.1	0
6	B_2	22.5	0	6	B_2	24.0	1
7	A_2	23.2	0	7	B_1	25.8	1
8	A_1	70.5	3	8	A_1	58.0	1
9	A_1	91.2	4	9	A_1	85.3	10
10	B_1	95.4	0	10	B_2	94.7	10
11	B_2	96.2	3	11	B_2	103.3	15
12	A_2	98.4	0	12	B_1	103.8	0
13	B_2	105.8	21	13	A_2	106.0	0
14	B_1	109.4	0	14	B_1	109.3	0
15	A_1	121.5	20	15	A_1	110.5	11
16	B_2	143.7	165	16	B_2	126.3	90
17	A_1	166.7	37	17	A_1	179.3	26
18	B_1	204.1	13	18	B_1	211.2	17
19	A_1	417.3	141	19	A_1	489.6	40
20	B_2	427.5	333	20	B_2	490.1	147
21	A_1	455.9	7	21	A_1	503.3	17
22	B_1	593.3	25	22	B_1	675.2	36
23	B_2	600.5	203	23	A_2	697.9	0
24	A_2	605.5	0	24	B_2	698.2	210
25	A_1	614.9	107	25	A_1	712.3	109
26	B_1	3645.0	1734	26	B_1	3666.3	1678
27	A_1	3674.2	710	27	A_1	3698.8	962

Table S31. $[\text{Cl}(\text{HF})_5]^-$ (D_{3h})

B3LYP-D3BJ/def2-TZVPP				SCS-MP2/def2-TZVPP			
Nr.	Symmetry	Wavenumber / cm^{-1}	IR intensity / km mol^{-1}	Nr.	Symmetry	Wavenumber / cm^{-1}	IR intensity / km mol^{-1}
1	E'	11.1	0	1	E'	11.9	0
2	E'	11.1	0	2	E'	11.9	0
3	E'	27.5	1	3	E'	30.4	1
4	E'	27.5	1	4	E'	30.4	1
5	A_2''	28.6	1	5	E''	32.8	0
6	E''	30.0	0	6	E''	32.8	0
7	E''	30.0	0	7	A_2''	33.1	1
8	A_1'	138.2	0	8	A_1'	131.4	0
9	A_1'	157.5	0	9	A_1'	151.6	0
10	E'	195.1	7	10	E'	186.7	8
11	E'	195.1	7	11	E'	186.7	8
12	A_2''	198.1	13	12	A_2''	191.1	14
13	E''	535.5	0	13	E''	581.4	0
14	E''	535.5	0	14	E''	581.4	0
15	E'	563.8	91	15	E'	610.9	67
16	E'	563.8	91	16	E'	610.9	67
17	A_2'	583.7	0	17	A_2'	615.8	0
18	A_2''	622.8	280	18	A_2''	664.4	307
19	E'	648.6	212	19	E'	676.8	270
20	E'	648.6	212	20	E'	676.8	270
21	E''	682.6	0	21	E''	716.7	0
22	E''	682.6	0	22	E''	716.7	0
23	E'	3620.5	1771	23	E'	3754.0	1558
24	E'	3620.5	1771	24	E'	3754.0	1558
25	A_1'	3643.1	0	25	A_1'	3772.4	0
26	A_2''	3654.7	2267	26	A_2''	3781.4	1998
27	A_1'	3736.3	0	27	A_1'	3852.1	0

Table S32. $[\text{Cl}_{20}]^{2-}(\text{C})$.

B3LYP-D3BJ/def2-TZVPP				SCS-MP2/def2-TZVPP			
Nr.	Symmetry	Wavenumber / cm^{-1}	IR intensity / km mol^{-1}	Nr.	Symmetry	Wavenumber / cm^{-1}	IR intensity / km mol^{-1}
1	A_u	-4.8	0	1	A_u	7.5	0
2	A_u	-1.9	0	2	A_u	8.9	0
3	A_u	-1.5	0	3	A_u	11.6	0
4	A_g	10.0	0	4	A_g	13.2	0
5	A_g	10.2	0	5	A_g	14.1	0
6	A_g	12.5	0	6	A_u	14.4	0
7	A_u	12.8	1	7	A_g	14.5	0
8	A_u	13.0	1	8	A_g	15.1	0
9	A_g	13.1	0	9	A_u	15.2	1
10	A_u	13.6	1	10	A_u	16.4	1
11	A_u	16.1	7	11	A_g	18.2	0
12	A_g	16.8	0	12	A_g	19.2	0
13	A_u	17.4	0	13	A_u	19.9	0
14	A_g	18.5	0	14	A_g	20.1	0
15	A_g	18.8	0	15	A_u	24.2	9
16	A_g	41.8	0	16	A_g	44.0	0
17	A_u	45.2	0	17	A_u	44.9	0
18	A_u	45.8	0	18	A_u	45.9	0
19	A_u	55.8	12	19	A_u	52.2	0
20	A_g	57.6	0	20	A_g	52.3	0
21	A_u	57.7	0	21	A_u	55.5	3
22	A_g	82.8	0	22	A_g	77.2	0
23	A_g	83.0	0	23	A_g	84.5	0
24	A_u	86.1	246	24	A_g	85.1	0
25	A_u	86.5	246	25	A_u	85.5	106
26	A_g	89.0	0	26	A_u	86.1	100
27	A_g	91.2	0	27	A_u	87.5	33
28	A_g	91.5	0	28	A_g	95.2	0
29	A_g	94.2	0	29	A_u	95.3	0
30	A_u	94.2	0	30	A_g	97.4	0
31	A_g	94.9	0	31	A_u	98.0	0
32	A_u	94.9	0	32	A_g	98.0	0
33	A_u	98.8	13	33	A_g	98.1	0
34	A_u	102.1	1	34	A_u	100.7	0
35	A_u	102.1	1	35	A_u	101.0	0
36	A_g	105.7	0	36	A_g	102.4	0
37	A_g	105.8	0	37	A_u	102.4	0
38	A_g	107.5	0	38	A_g	112.9	0
39	A_u	107.6	0	39	A_g	113.9	0
40	A_g	122.0	0	40	A_u	121.5	34
41	A_u	122.1	574	41	A_g	125.1	0
42	A_g	122.4	0	42	A_u	125.8	293
43	A_u	122.5	568	43	A_u	126.8	302
44	A_u	124.3	29	44	A_g	128.0	0
45	A_g	128.1	0	45	A_g	129.1	0
46	A_u	406.0	1019	46	A_g	484.1	0
47	A_u	406.2	1015	47	A_u	484.2	327

48	A_g	408.5	0	48	A_g	484.4	0
49	A_g	408.7	0	49	A_u	484.4	354
50	A_g	415.5	0	50	A_g	485.8	0
51	A_u	416.1	3	51	A_u	485.8	31
52	A_g	444.5	0	52	A_g	497.1	0
53	A_u	453.7	2	53	A_u	499.9	7
54	A_g	475.4	0	54	A_g	507.0	0

Table S33. $[\text{Cl}(\text{Cl}_2)_4(\text{HCl})]^- (\text{C}_{2v})$

B3LYP-D3BJ/def2-TZVPP				SCS-MP2/def2-TZVPP			
Nr.	Symmetry	Wavenumber / cm^{-1}	IR intensity / km mol^{-1}	Nr.	Symmetry	Wavenumber / cm^{-1}	IR intensity / km mol^{-1}
1	B_1	3.0	0	1	B_1	7.7	0
2	A_1	6.9	0	2	A_1	9.8	0
3	B_1	11.4	0	3	B_2	16.3	0
4	A_1	12.1	0	4	A_2	17.2	0
5	A_2	12.6	0	5	B_1	19.4	0
6	B_2	13.2	0	6	A_1	19.7	0
7	B_2	18.9	0	7	B_2	20.3	0
8	A_1	68.5	2	8	A_1	59.1	2
9	A_1	89.1	2	9	A_1	82.2	7
10	B_1	91.3	11	10	B_1	90.4	26
11	A_1	96.2	2	11	B_2	99.4	33
12	A_2	97.0	0	12	B_1	103.0	0
13	B_2	98.1	7	13	A_1	104.1	3
14	B_1	100.7	8	14	A_2	104.6	0
15	B_2	103.2	24	15	A_1	105.2	0
16	A_1	104.9	7	16	B_2	108.6	4
17	A_2	111.9	0	17	A_2	113.5	0
18	B_1	147.9	97	18	B_1	137.0	63
19	B_2	152.5	167	19	B_2	142.9	116
20	A_1	164.3	54	20	A_1	166.6	64
21	B_1	408.5	231	21	B_1	470.1	132
22	A_1	416.8	93	22	A_1	473.5	42
23	B_2	424.7	315	23	B_2	478.0	185
24	B_2	446.9	50	24	B_1	496.0	13
25	B_1	451.6	37	25	B_2	541.6	30
26	A_1	457.1	10	26	B_1	541.7	17
27	A_1	2579.6	1527	27	A_1	2612.0	1875

Table S34. $[\text{Cl}(\text{Cl}_2)_4(\text{HCl})]^- (\text{C}_{3v})$

B3LYP-D3BJ/def2-TZVPP				SCS-MP2/def2-TZVPP			
Nr.	Symmetry	Wavenumber / cm^{-1}	IR intensity / km mol^{-1}	Nr.	Symmetry	Wavenumber / cm^{-1}	IR intensity / km mol^{-1}
1	E	4.8	0	1	E	9.4	0
2	E	4.8	0	2	E	9.4	0
3	E	10.6	0	3	E	15.2	0
4	E	10.6	0	4	E	15.2	0
5	A_1	13.2	0	5	E	19.1	0
6	E	15.1	0	6	E	19.1	0
7	E	15.1	0	7	A_1	19.4	0
8	A_1	72.9	5	8	A_1	63.3	4
9	A_1	87.4	3	9	A_1	81.4	8
10	E	93.4	25	10	E	89.7	35
11	E	93.4	25	11	E	89.7	35
12	E	100.0	8	12	A_2	102.1	0
13	E	100.0	8	13	E	106.0	0
14	A_2	100.7	0	14	E	106.0	0
15	A_1	101.3	8	15	A_1	107.4	4
16	E	110.5	0	16	E	112.7	0
17	E	110.5	0	17	E	112.7	0
18	A_1	159.0	90	18	E	144.5	75
19	E	161.6	94	19	E	144.5	75
20	E	161.6	94	20	A_1	165.5	86
21	E	410.5	226	21	E	469.2	158
22	E	410.5	226	22	E	469.2	158
23	E	420.5	83	23	A_1	478.2	35
24	E	420.5	83	24	A_1	496.1	41
25	A_1	421.6	123	25	E	549.7	25
26	A_1	454.3	36	26	E	549.7	25
27	A_1	2619.0	1354	27	A_1	2635.5	1772

g) Raman Spectra of Samples Cooled to $-196\text{ }^{\circ}\text{C}$

Method for low temperature Raman spectroscopy of single crystals:

- 1) Transfer of the sample from the reaction flask into a cool nitrogen stream where a crystal can be selected (Figure S18).
- 2) Transfer of the selected crystal onto a Teflon plate which is cooled by a copper block which is cooled by liquid nitrogen (Figure S19, Figure S20). By evaporation of the nitrogen a layer of cool gaseous nitrogen protects the sample from moisture.
- 3) Measuring of the Raman spectra using a Raman microscope (Figure S21).

As often rather big needle shaped crystals were obtained often a crystal was split with a scalpel and one part was used for XRD while the other part was used for Raman spectroscopy.

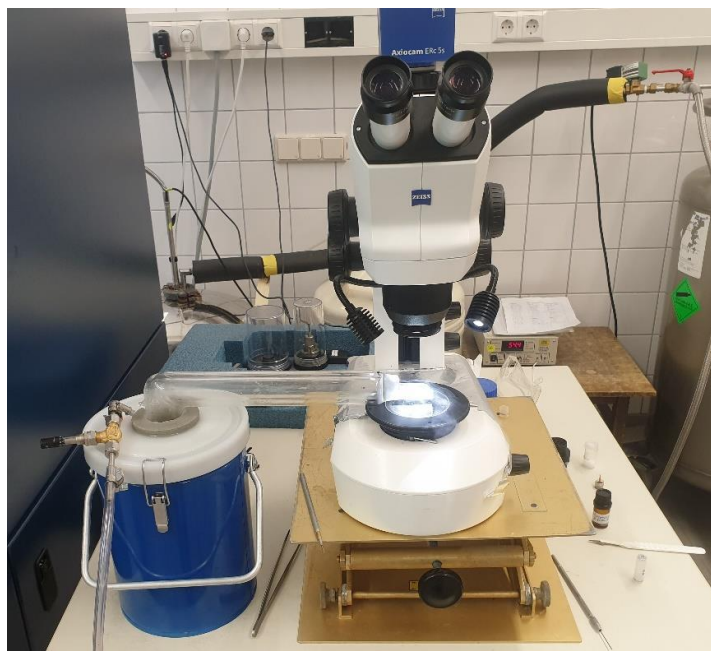


Figure S18. Setting for preparing a single crystal for x-ray diffraction or low temperature Raman spectroscopy.

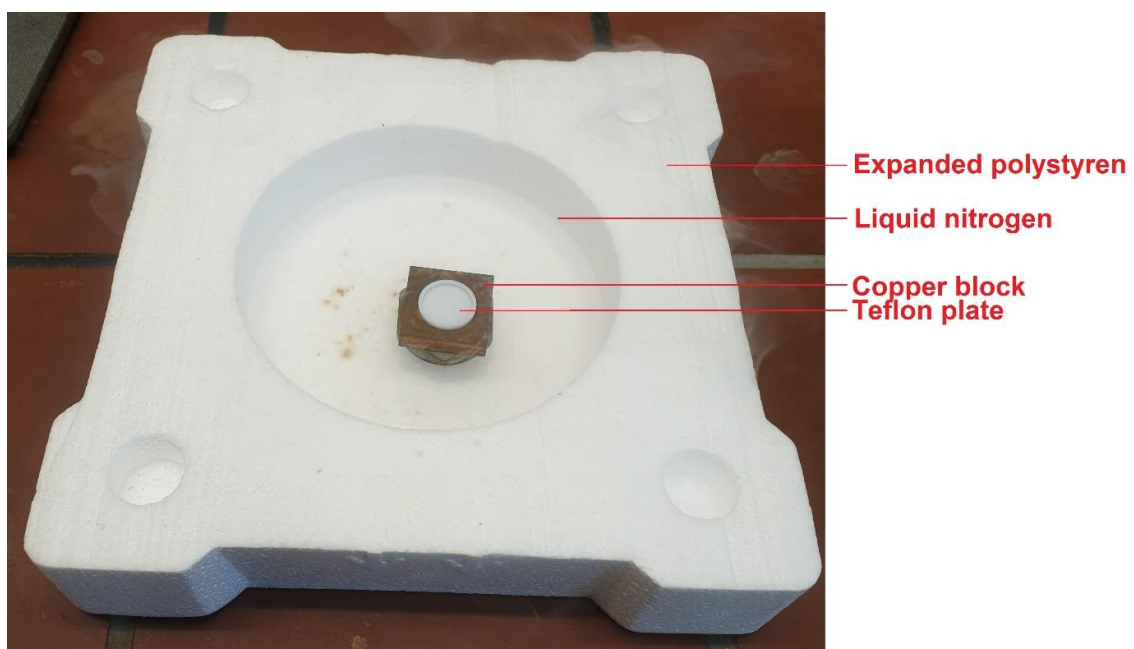


Figure S19. Setting for cooling a sample to $-196\text{ }^{\circ}\text{C}$ for low temperature Raman spectroscopy.

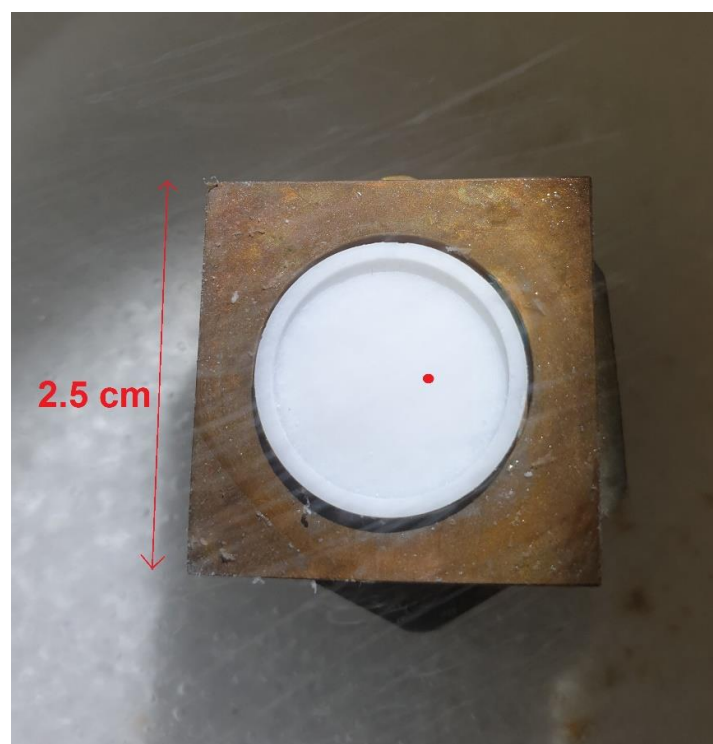


Figure S20. Prepared crystal (red dot) on the Teflon plate for low temperature Raman spectroscopy.

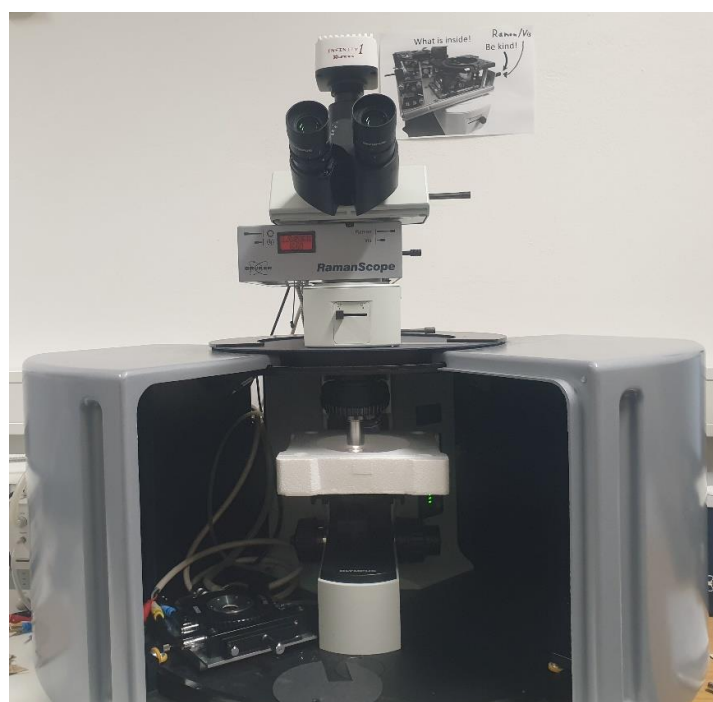


Figure S21. Assembly in the RamanScope.

h) Crystal Data

Table S35. Crystal data of the synthesized compounds

Empirical formula	C ₅ H ₁₂ Cl ₈ N ₂	C ₂₀ H ₃₁ Cl ₉ FFe	C ₂₀ H ₃₀ Cl ₁₀ Fe
Formula weight	383.785	665.35	680.79
Temperature/K	100.8	100.05	104.01
Crystal system	orthorhombic	monoclinic	monoclinic
Space group	P2 ₁ 2 ₁ 2 ₁	C2/m	C2/c
a/Å	9.4032(6)	16.218(2)	15.9249(13)
b/Å	10.4318(6)	11.1516(14)	22.7897(18)
c/Å	15.3683(9)	15.612(2)	15.8496(13)
α/°	90	90	90
β/°	90	92.468(6)	91.107(3)
γ/°	90	90	90
Volume/Å ³	1507.51(16)	2820.9(7)	5751.1(8)
Z	4	4	8
ρ _{calc} /cm ³	1.691	1.567	1.573
μ/mm ⁻¹	1.467	1.403	1.463
F(000)	772.9	1356.0	2768.0
Crystal size/mm ³	0.42 × 0.22 × 0.08	0.4 × 0.3 × 0.15	0.228 × 0.178 × 0.172
Radiation	Mo Kα (λ = 0.71073)	MoKα (λ = 0.71073)	MoKα (λ = 0.71073)
2θ range for data collection/°	4.72 to 56.66	5.028 to 62.044	5.116 to 61.122
Reflections collected	28044	47723	42418
Independent reflections	3748 [R _{int} = 0.0255, R _{sigma} = 0.0147]	4622 [R _{int} = 0.0641, R _{sigma} = 0.0407]	8515 [R _{int} = 0.0460, R _{sigma} = 0.0395]
Data/restraints/parameters	3748/0/140	4622/0/168	8515/0/401
Goodness-of-fit on F ²	1.032	1.053	1.019
Final R indexes [I ≥ 2σ(I)]	R ₁ = 0.0151, wR ₂ = 0.0374	R ₁ = 0.0405, wR ₂ = 0.0707	R ₁ = 0.0405, wR ₂ = 0.0876
Final R indexes [all data]	R ₁ = 0.0158, wR ₂ = 0.0378	R ₁ = 0.0765, wR ₂ = 0.0793	R ₁ = 0.0691, wR ₂ = 0.0978
Largest diff. peak/hole / e Å ⁻³	0.18/-0.35	0.47/-0.47	1.25/-0.61
Flack parameter	0.07(5)	-	-
CCDC deposition numbers	2031714	2031710	2031711

Table S36. Crystal data of the synthesized compounds

Empirical formula	C ₁₂ H ₂₈ Cl ₉ N
Formula weight	505.40
Temperature/K	100.01
Crystal system	tetragonal
Space group	I-4
a/Å	11.7904(8)
b/Å	11.7904(8)
c/Å	8.5436(6)
α/°	90
β/°	90
γ/°	90
Volume/Å ³	1187.68(18)
Z	2
ρ _{calc} /cm ³	1.413
μ/mm ⁻¹	1.057
F(000)	520.0
Crystal size/mm ³	0.45 × 0.38 × 0.25
Radiation	MoKα (λ = 0.71073)
2θ range for data collection/°	4.886 to 60.986
Reflections collected	15575
Independent reflections	1827 [R _{int} = 0.0302, R _{sigma} = 0.0166]
Data/restraints/parameters	1827/0/61
Goodness-of-fit on F ²	1.085
Final R indexes [I ≥ 2σ(I)]	R ₁ = 0.0175, wR ₂ = 0.0413
Final R indexes [all data]	R ₁ = 0.0185, wR ₂ = 0.0418
Largest diff. peak/hole / e Å ⁻³	0.18/-0.25
Flack parameter	0.01(2)
CCDC deposition numbers	2031713

i) Pictures of Samples



Figure S22. Picture of a sample of $[\text{Cp}^*_2\text{Fe}][\text{Cl}(\text{Cl}_2)_4(\text{HF})]$.



Figure S23. Picture of a sample of $[\text{Cp}^*_2\text{Fe}][\text{Cl}_2]$.

8.3 SI of Alkyl Ammonium Chloride Salts for Efficient Chlorine Storage at Ambient Conditions

Patrick Voßnacker, Nico Schwarze, Thomas Keilhack, Merlin Kleoff, Simon Steinhauer, Yuliya Schiesser, Maxime Paven, Sivathmeehan Yogendra, Rainer Weber, Sebastian Riedel*

ACS Sustainable Chem. Eng. **2022**, 29, 9525.

<https://doi.org/10.1021/acssuschemeng.2c02186>

© 2022 The Authors. Published by American Chemical Society

Supplementary Information

Alkyl Ammonium Chloride Salts for Efficient Chlorine Storage at Ambient Conditions

Patrick Voßnacker,[†] Nico Schwarze,[†] Thomas Keilhack,[†] Merlin Kleoff,[†] Simon Steinhauer,[†] Yuliya Schiesser,[‡] Maxime Paven,[‡] Sivathmeehan Yogendra,[‡] Rainer Weber,[‡] Sebastian Riedel^{†}*

[†] P. Voßnacker, Dr. N. Schwarze, T. Keilhack, Dr. M. Kleoff, Dr. S. Steinhauer, Prof. Dr. S. Riedel, Institut für Chemie und Biochemie, Freie Universität Berlin, Fabeckstr. 34/36, Berlin D-14195, Germany, E-mail: s.riedel@fu-berlin.de,

[‡] Dr. Y. Schiesser, Dr. M. Paven, Dr. S. Yogendra, Dr. R. Weber, Covestro Deutschland AG, Leverkusen D-51365, Germany

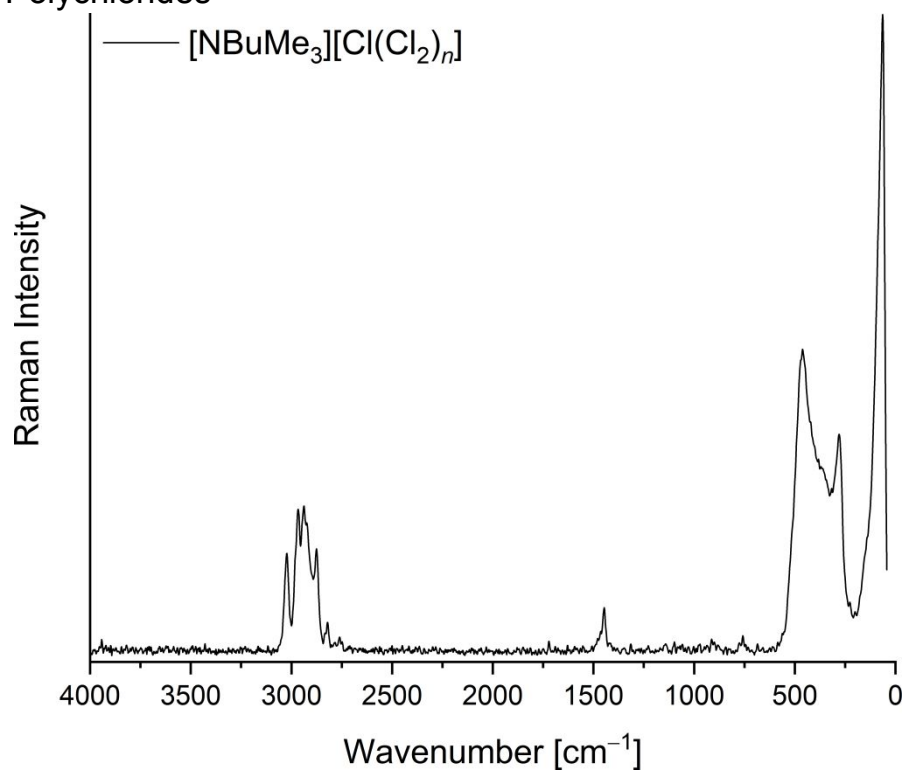
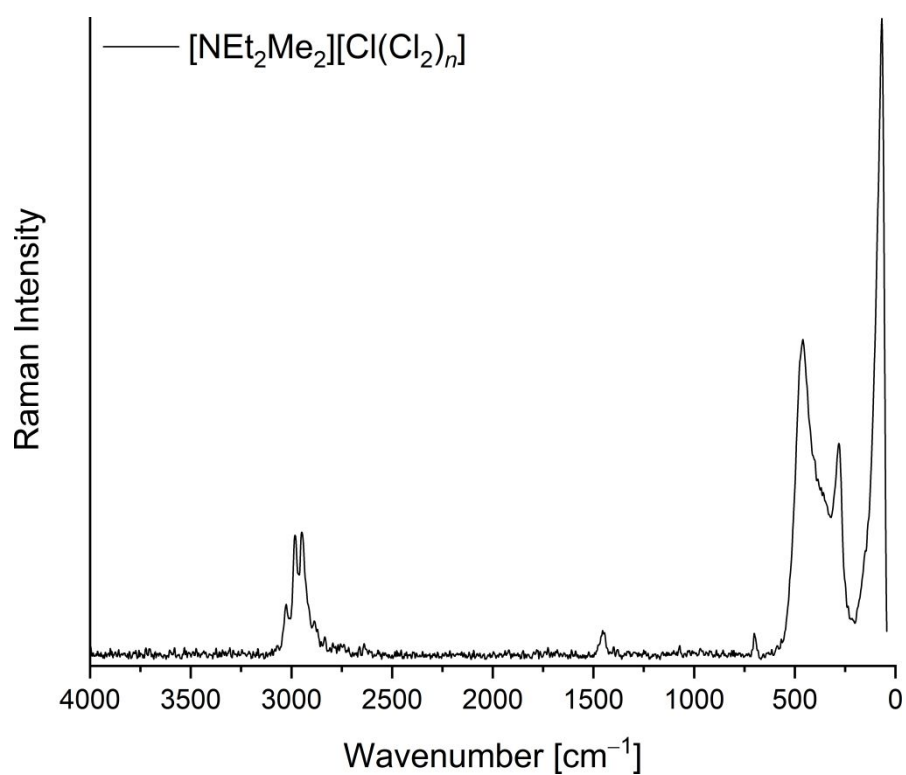
Number of Pages: 38
Number of Figures: 38
Number of Schemes: 0
Number of Tables: 74

Table of Contents

a) Raman Spectra.....	3
a1. Polychlorides	3
a2. Long Term Stability	6
b) Mass Spectra.....	12
c) Chlorine Release Experiments.....	13
c1. Setup for Chlorine Release Experiments.....	13
c2. Vapor Pressure Curves for $[\text{NEt}_3\text{Me}][\text{Cl}(\text{Cl}_2)_n]$	14
c3. Kinetic of Chlorine Release Experiments under Different Conditions	16
c4. Chlorine Release by Water Addition	17
d) Chlorine Storage Capacities and Physical Properties	19
e) Calorimetric Measurements.....	20
e1. Setup.....	20
e2. Hydration Energy of $[\text{NEt}_3\text{Me}]\text{Cl}$	21
e3. Reaction of $[\text{NEt}_3\text{Me}][\text{Cl}(\text{Cl}_2)_{1.18}]$ with 5 Equivalents H_2O	27
e4. Reaction of $[\text{NEt}_3\text{Me}][\text{Cl}(\text{Cl}_2)_{1.68}]$ with 5 Equivalents H_2O	33

a) Raman Spectra

a1. Polychlorides

Figure S 1. Raman Spectrum of $[\text{NBuMe}_3][\text{Cl}(\text{Cl}_2)_n]$.Figure S 2. Raman Spectrum of $[\text{NEt}_2\text{Me}_2][\text{Cl}(\text{Cl}_2)_n]$.

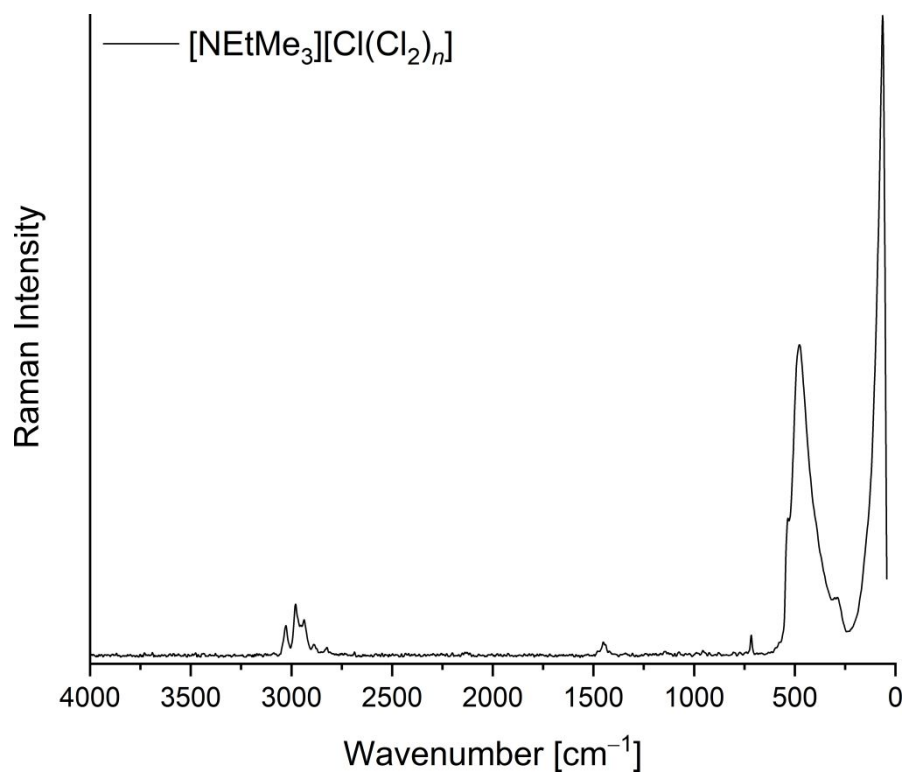


Figure S 3. Raman Spectrum of $[\text{NEtMe}_3][\text{Cl}(\text{Cl}_2)_n]$.

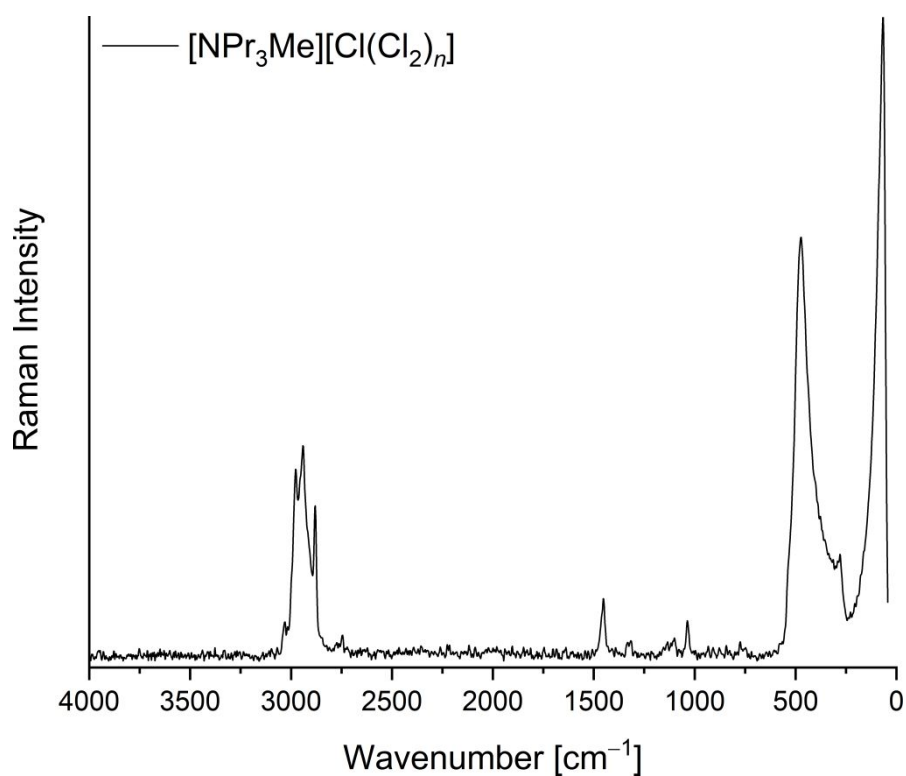


Figure S 4. Raman Spectrum of $[\text{NPr}_3\text{Me}][\text{Cl}(\text{Cl}_2)_n]$.

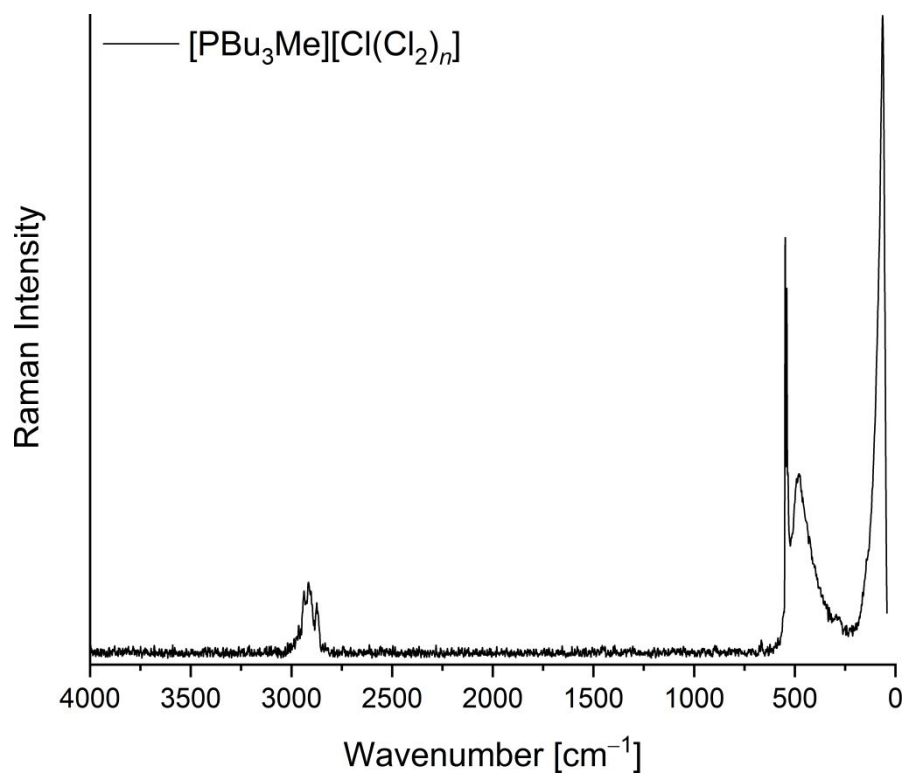


Figure S 5. Raman Spectrum of $[\text{PBu}_3\text{Me}][\text{Cl}(\text{Cl}_2)_n]$.

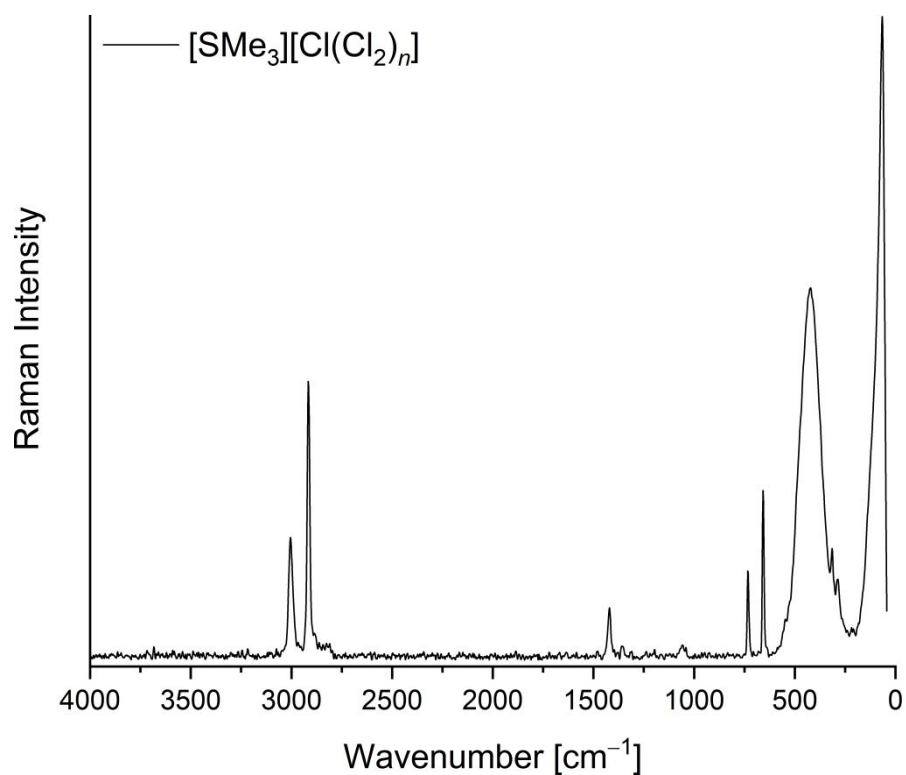
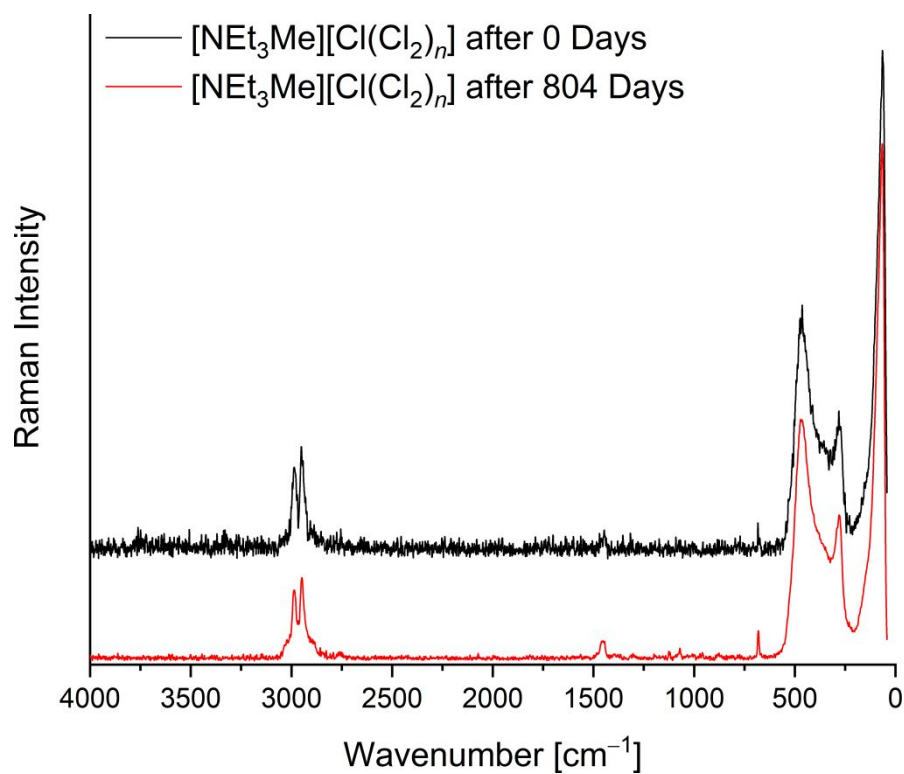
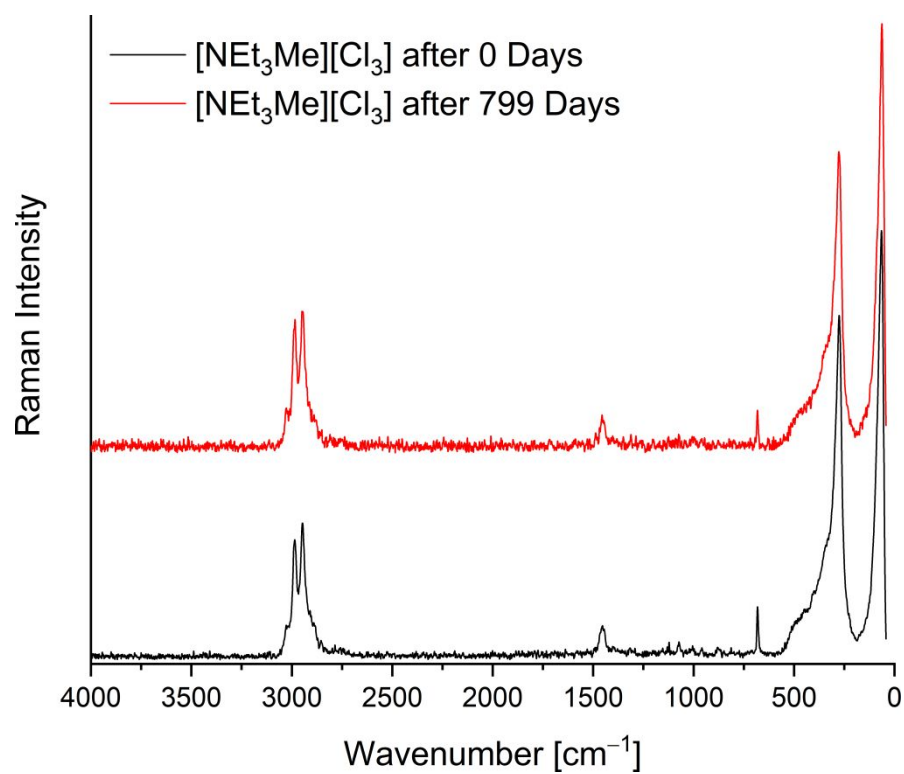


Figure S 6. Raman Spectrum of $[\text{SMe}_3][\text{Cl}(\text{Cl}_2)_n]$.

a2. Long Term Stability

**Figure S 7.** Raman Spectrum of $[\text{NEt}_3\text{Me}][\text{Cl}(\text{Cl}_2)_n]$ after 0 and 804 days.**Figure S 8.** Raman Spectrum of $[\text{NEt}_3\text{Me}][\text{Cl}_3]$ after 0 and 799 days.

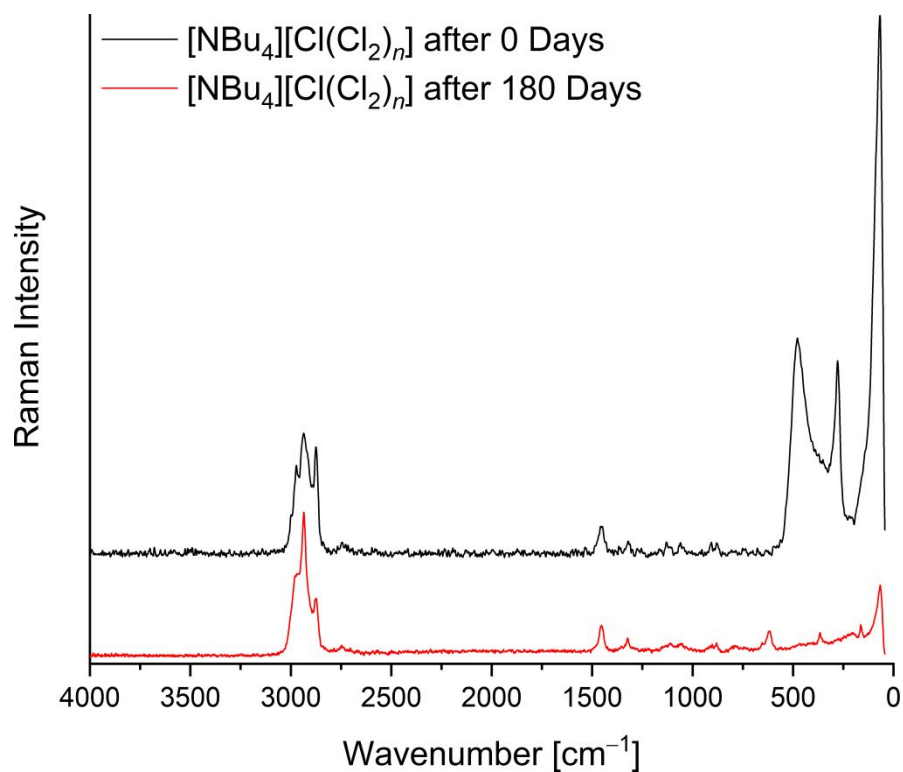


Figure S 9. Raman Spectrum of $[\text{NBu}_4][\text{Cl}(\text{Cl}_2)_n]$ after 0 and 180 days.

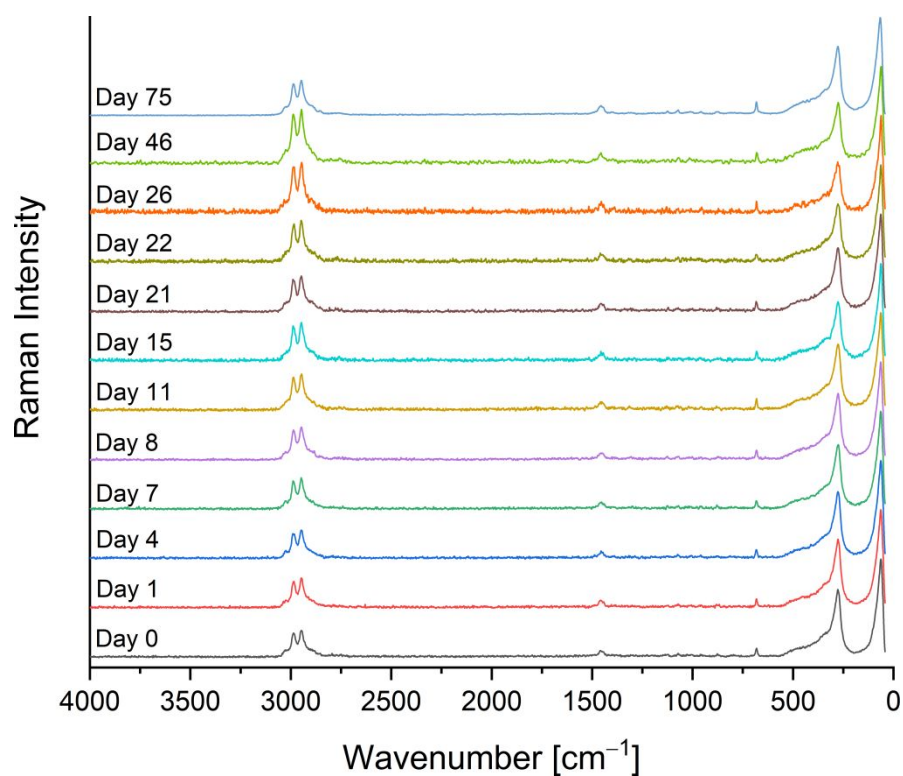


Figure S 10. Raman Spectra of $[\text{NEt}_3\text{Me}][\text{Cl}_3]$ after storing at room temperature in the presence of light for 0 to 75 days.

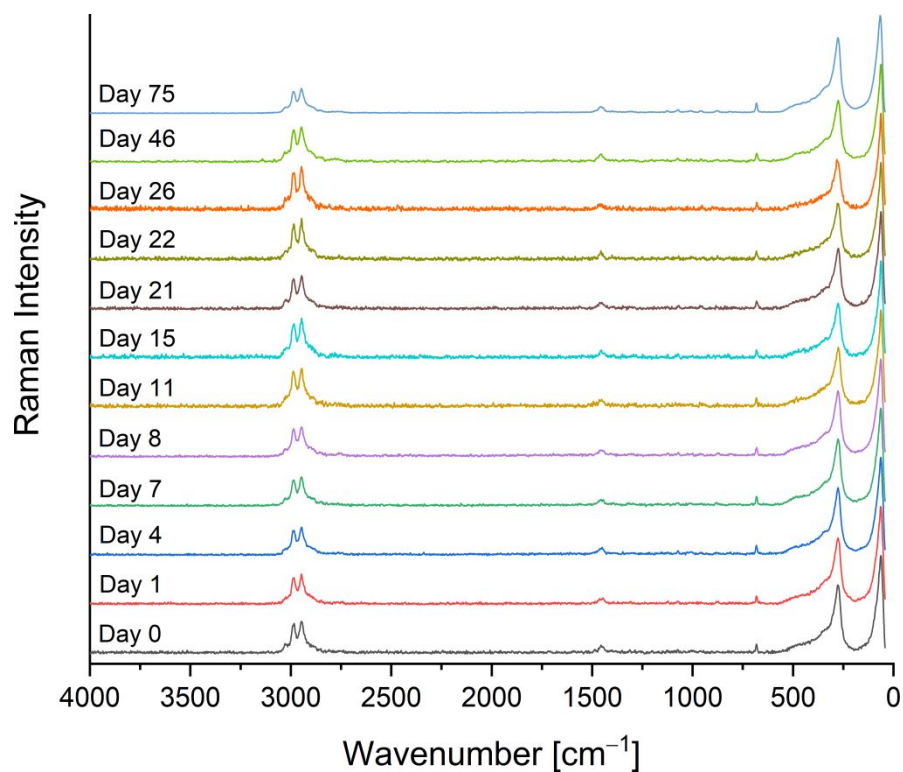


Figure S 11. Raman Spectra of $[\text{NEt}_3\text{Me}][\text{Cl}_3]$ after storing at room temperature in the absence of light for 0 to 75 days.

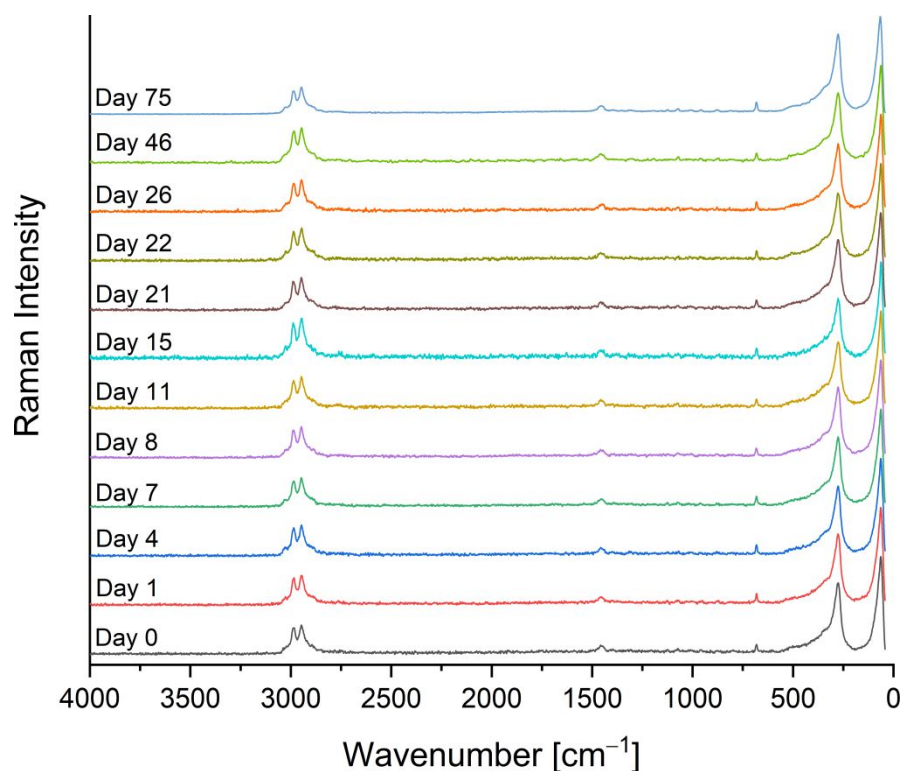


Figure S 12. Raman Spectra of $[\text{NEt}_3\text{Me}][\text{Cl}_3]$ after storing at 0 °C in the absence of light for 0 to 75 days.

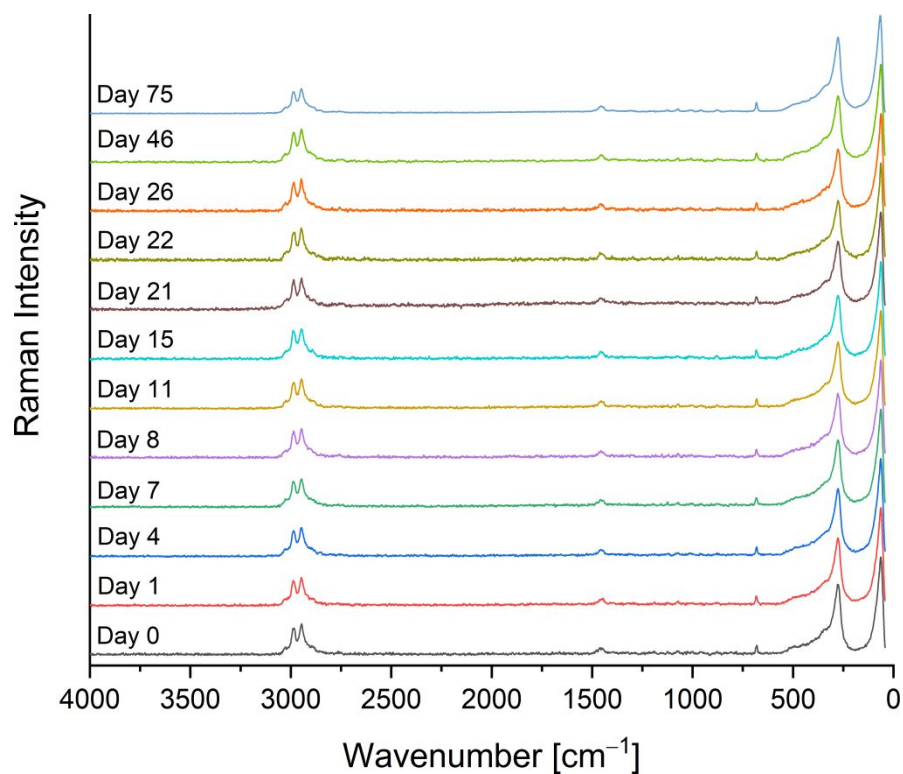


Figure S 13. Raman Spectra of $[\text{NEt}_3\text{Me}][\text{Cl}_3]$ after storing at 50 °C in the absence of light for 0 to 75 days.

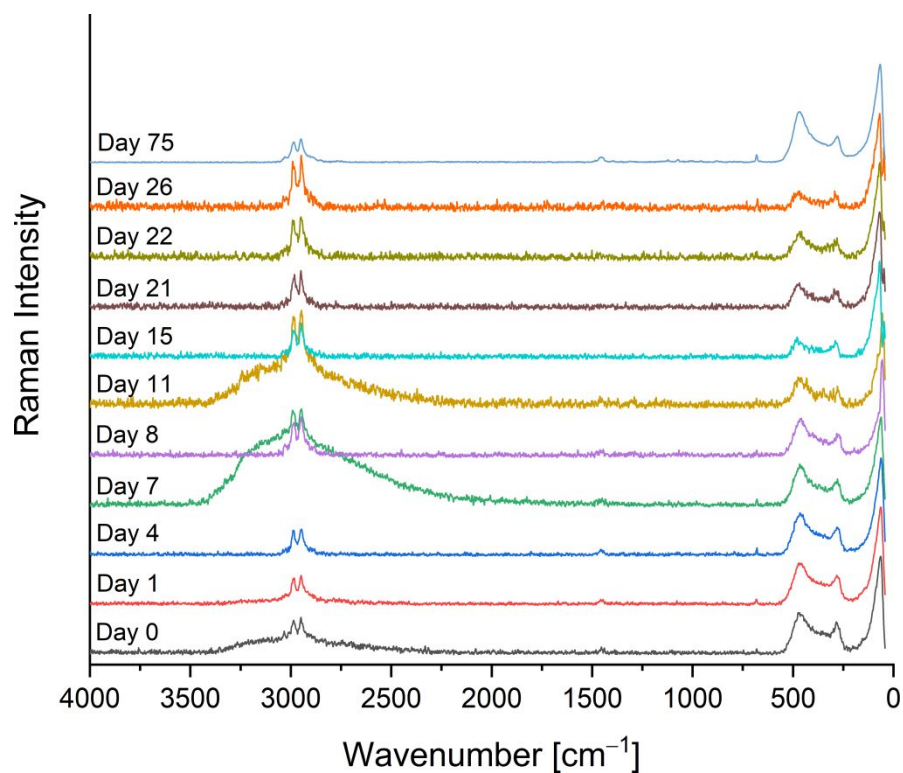


Figure S 14. Raman Spectra of $[\text{NEt}_3\text{Me}][\text{Cl}(\text{Cl}_2)_n]$ after storing at room temperature in the presence of light for 0 to 75 days.

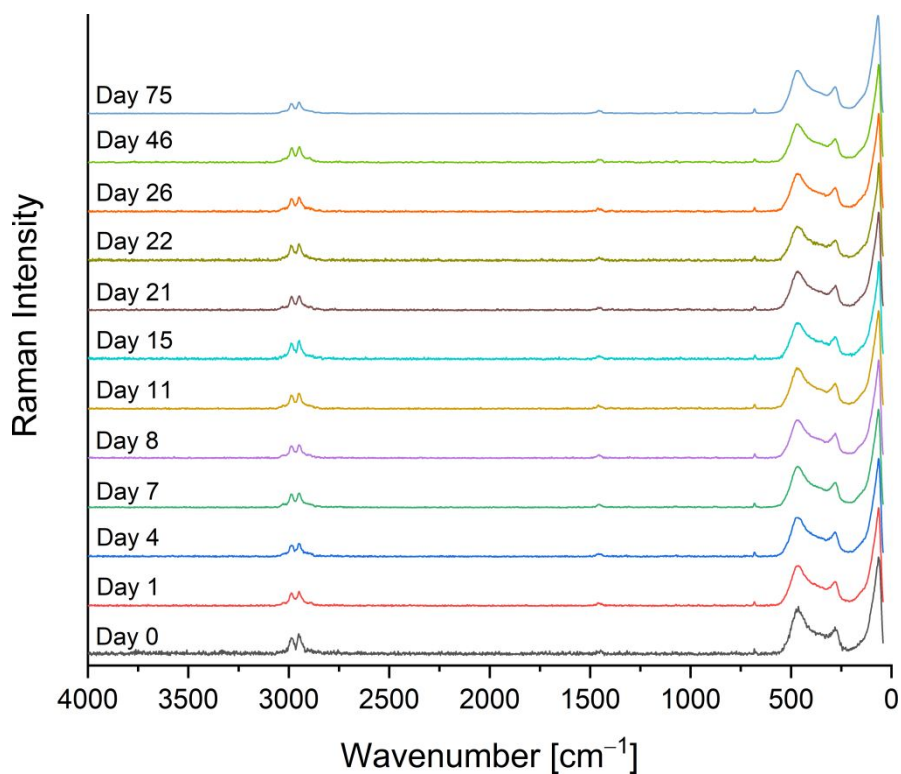


Figure S 15. Raman Spectra of $[\text{NEt}_3\text{Me}][\text{Cl}(\text{Cl}_2)_n]$ after storing at room temperature in the absence of light for 0 to 75 days.

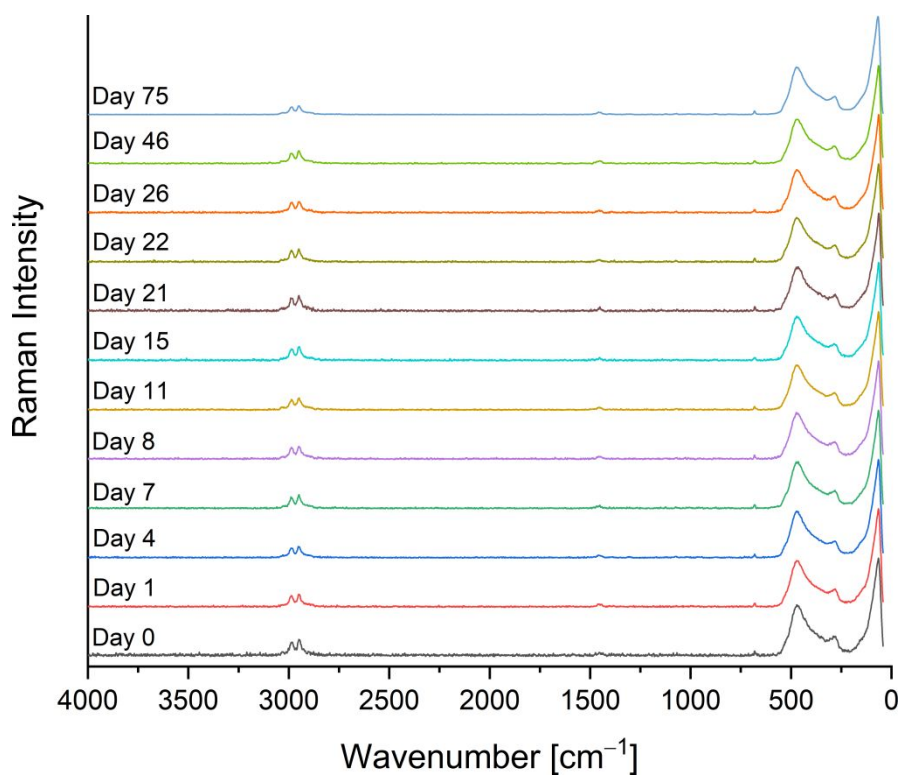


Figure S 16. Raman Spectra of $[\text{NEt}_3\text{Me}][\text{Cl}(\text{Cl}_2)_n]$ after storing at 0°C in the absence of light for 0 to 75 days.

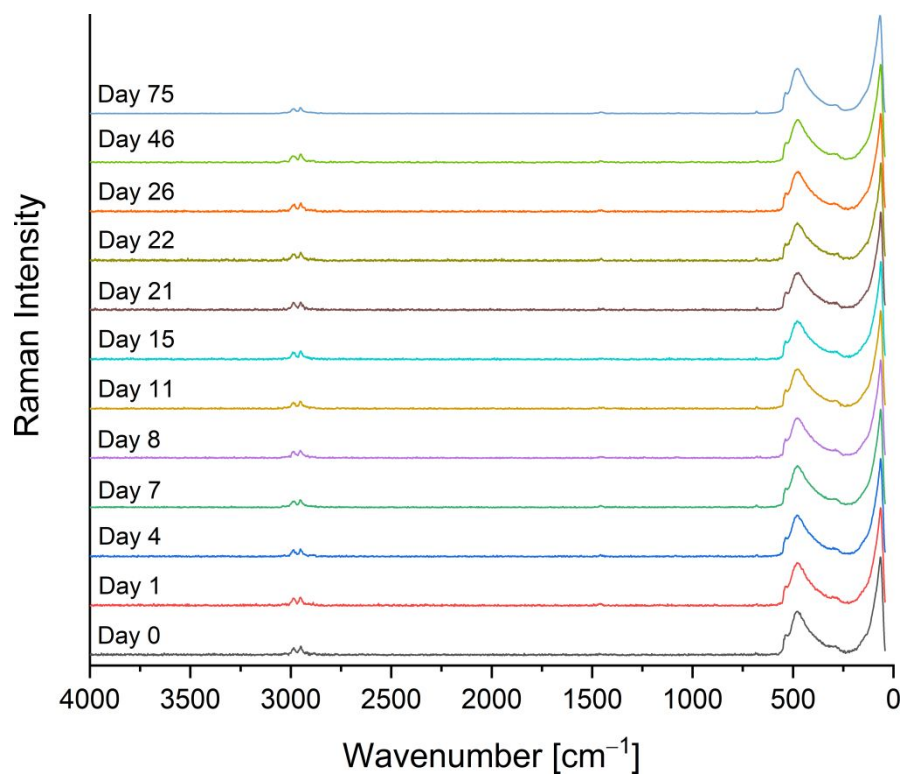


Figure S 17. Raman Spectra of $[\text{NEt}_3\text{Me}][\text{Cl}(\text{Cl}_2)_n]$ after storing at 50 °C in the absence of light for 0 to 75 days.

b) Mass Spectra

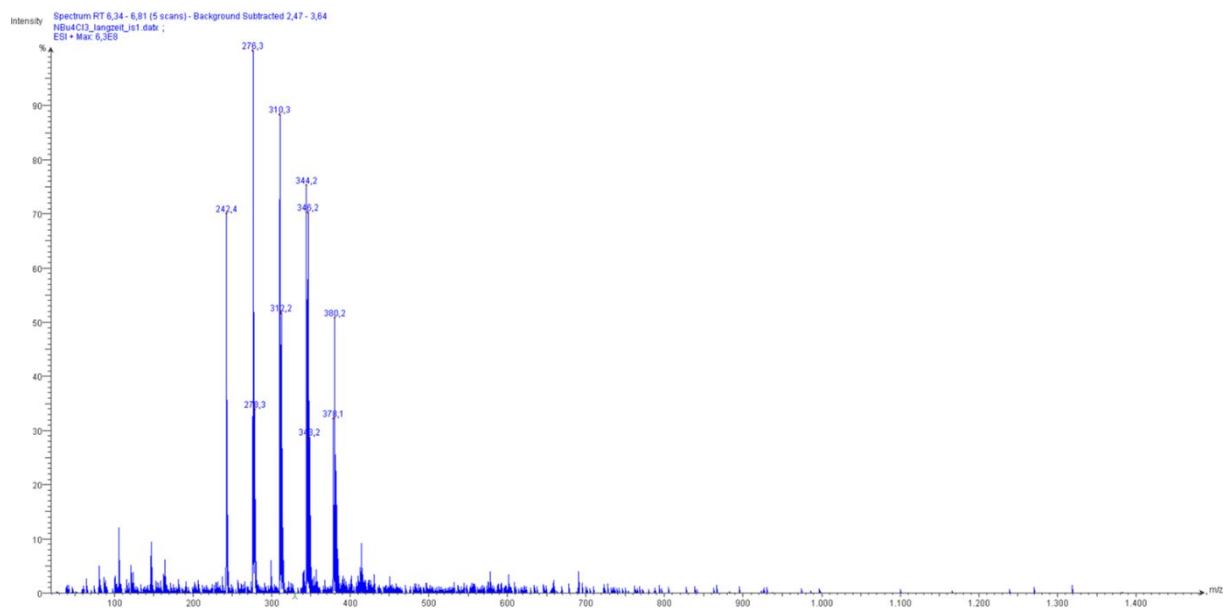


Figure S 18. ESI (pos) mass spectrum of $[\text{NBu}_4][\text{Cl}_3]$ after 6 months.

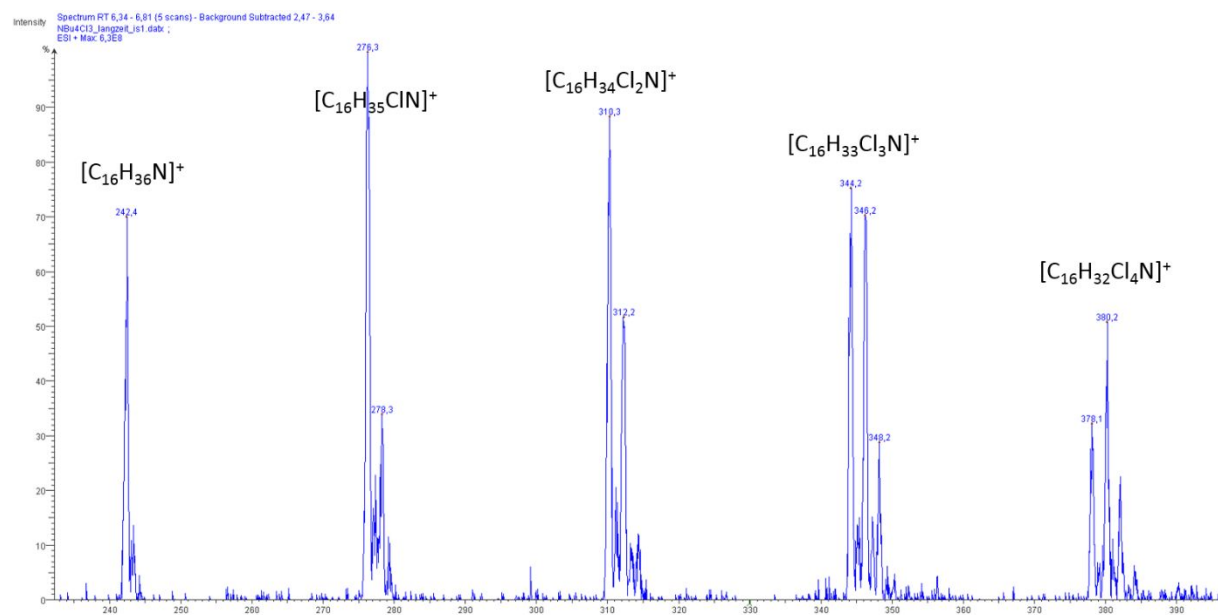


Figure S 19. Detailed excerpt of the ESI (pos) mass spectrum of $[\text{NBu}_4][\text{Cl}_3]$ after 6 months and assignments of the characteristic signals.

c) Chlorine Release Experiments

c1. Setup for Chlorine Release Experiments

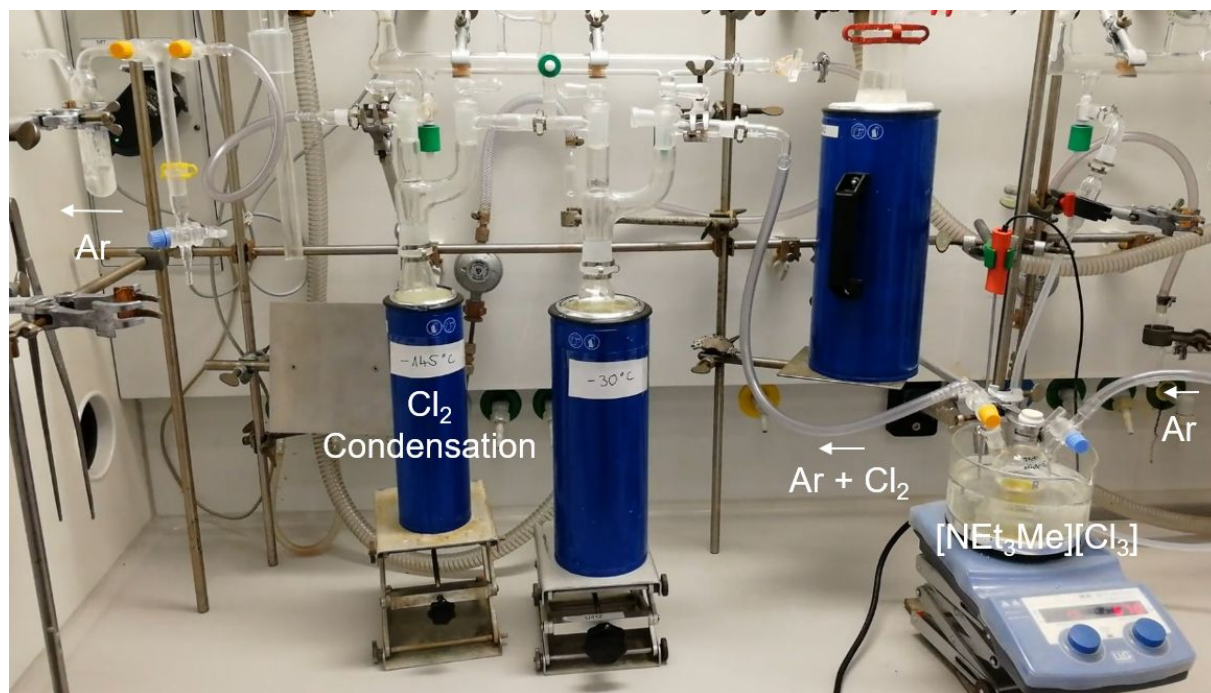


Figure S 20. Setup for chlorine release.

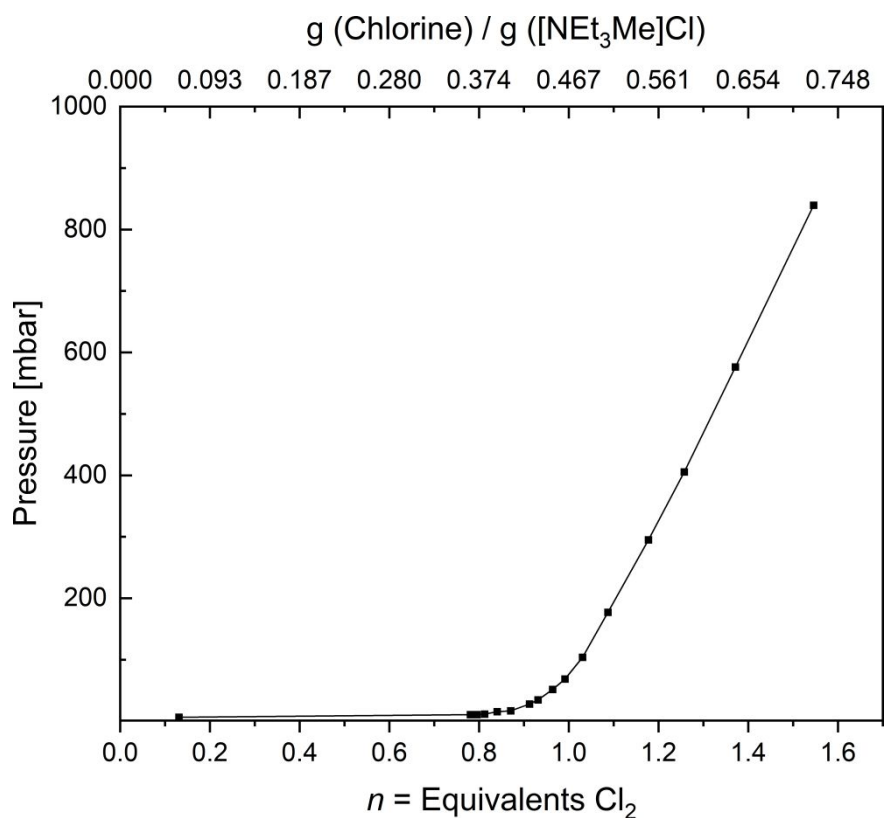
c2. Vapor Pressure Curves for $[\text{NEt}_3\text{Me}][\text{Cl}(\text{Cl}_2)_n]$ 

Figure S 21. Vapor pressure curve of $[\text{NEt}_3\text{Me}][\text{Cl}(\text{Cl}_2)_n]$ depending on different values of n determined by gravimetric determination of Cl_2 equivalents.

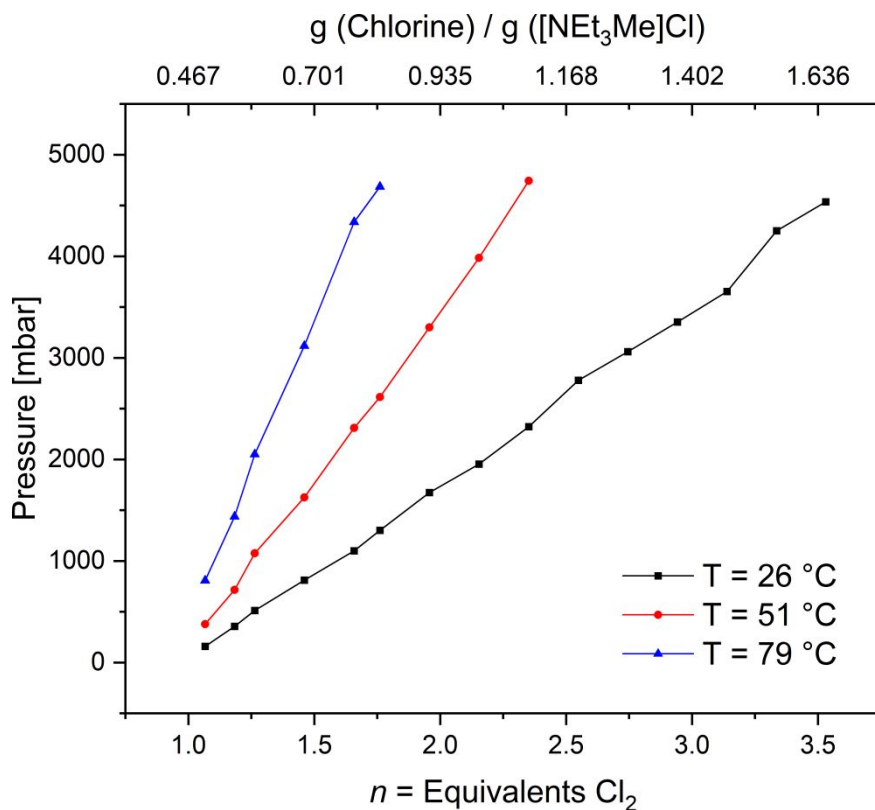


Figure S 22. Vapor pressure curve of $[\text{NEt}_3\text{Me}][\text{Cl}(\text{Cl}_2)_n]$ depending on n determined by volumetric determination (by mass flow controller) of Cl_2 equivalents.

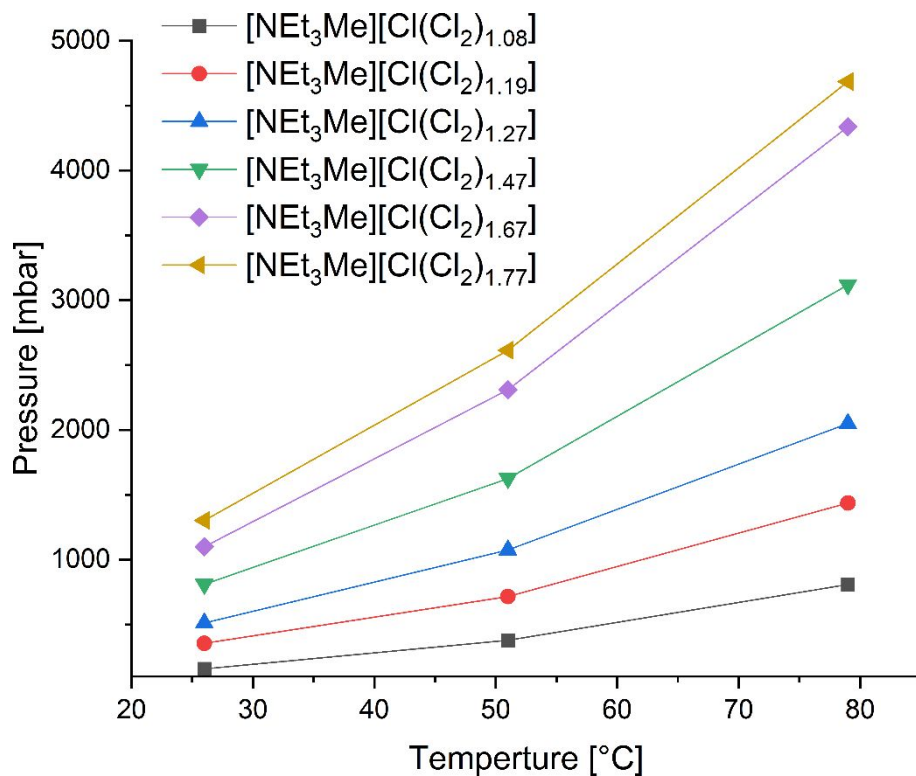


Figure S 23. p-T diagram of $[\text{NEt}_3\text{Me}][\text{Cl}(\text{Cl}_2)_n]$ for various values of n .

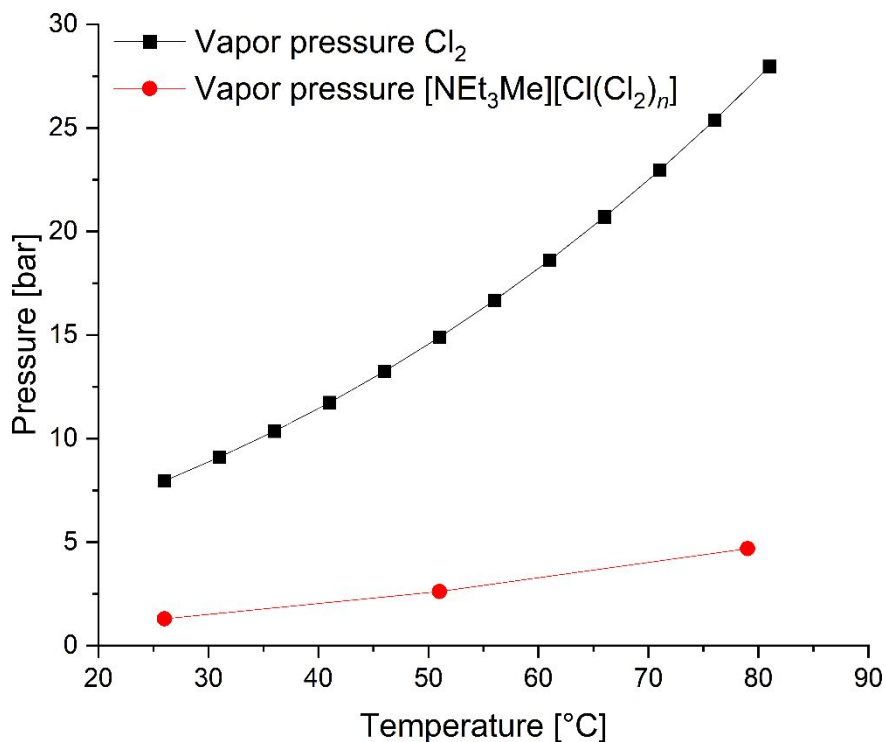


Figure S 24. Comparison of the vapor pressures of Cl_2 (Stull, D. R. Vapor Pressure of Pure Substances. Organic and Inorganic Compounds, *Ind. Eng. Chem.*, **1947**, 39, 517-540, <https://doi.org/10.1021/ie50448a022>) and $[\text{NEt}_3\text{Me}][\text{Cl}(\text{Cl}_2)_{1.77}]$ at different temperatures.

c3. Kinetic of Chlorine Release Experiments under Different Conditions

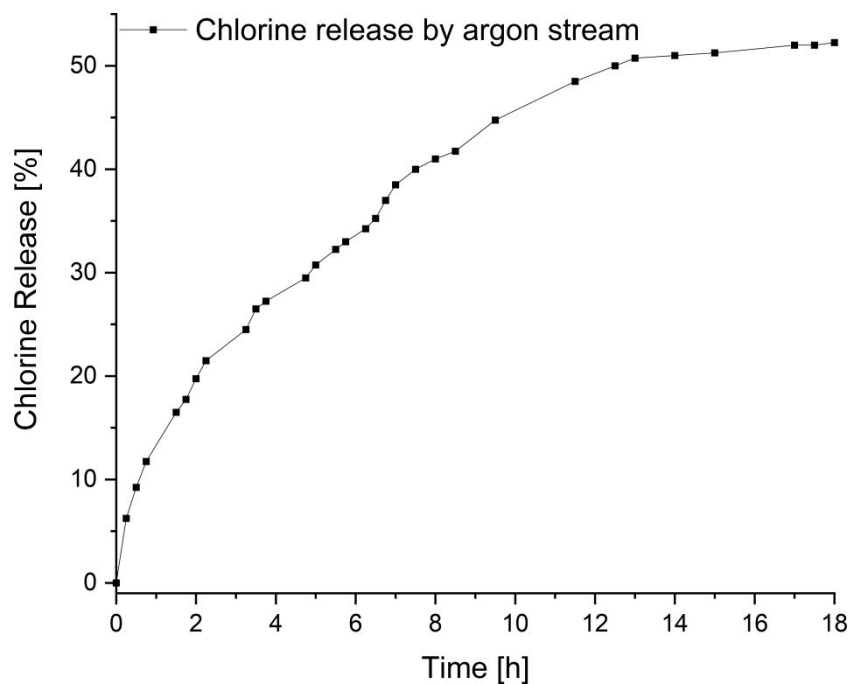


Figure S 25. Chlorine release by an argon stream at room temperature.

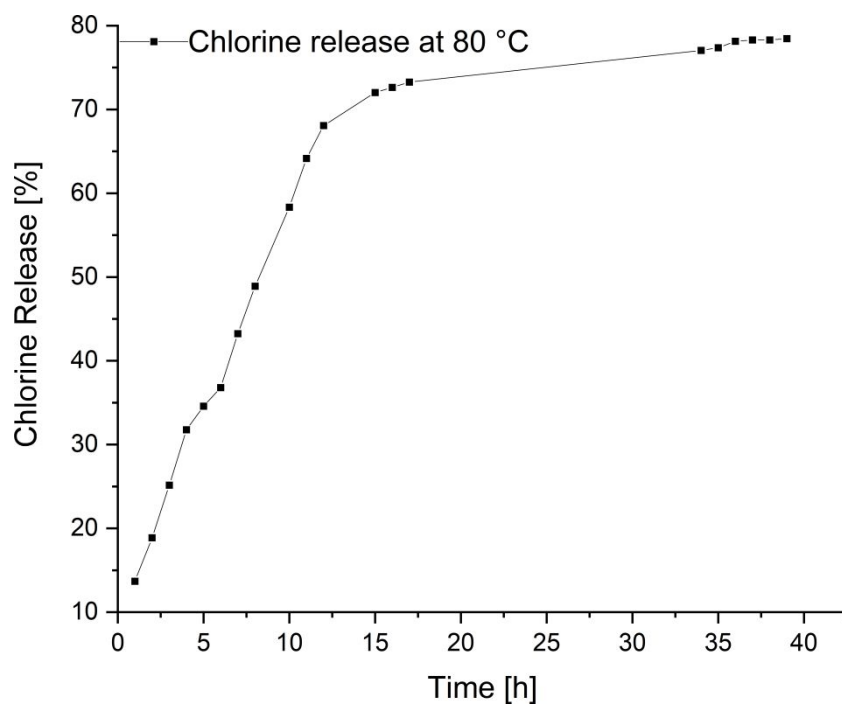


Figure S 26. Chlorine release at 80 °C.

c4. Chlorine Release by Water Addition

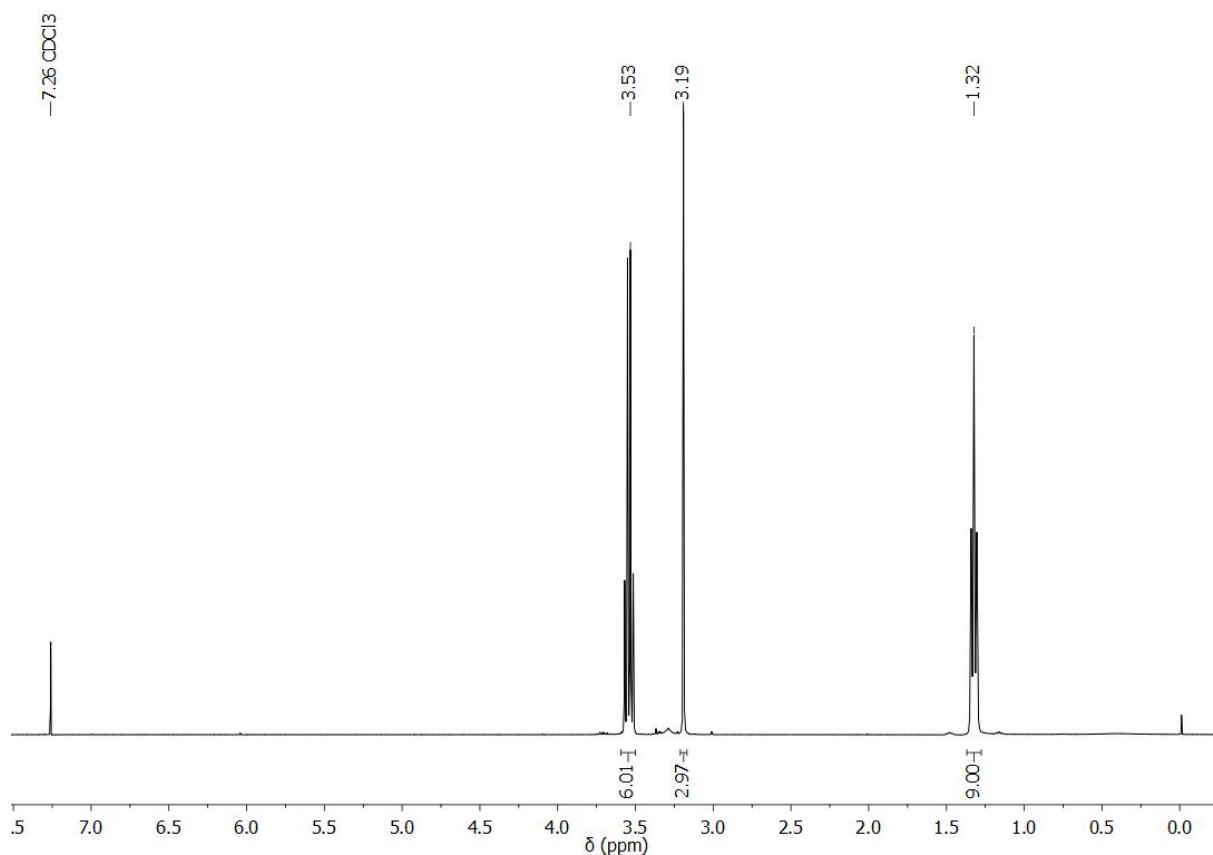


Figure S 27. ^1H NMR spectrum (400 MHz, CDCl_3 , 20 $^\circ\text{C}$) of the recycled $[\text{NEt}_3\text{Me}]\text{Cl}$.

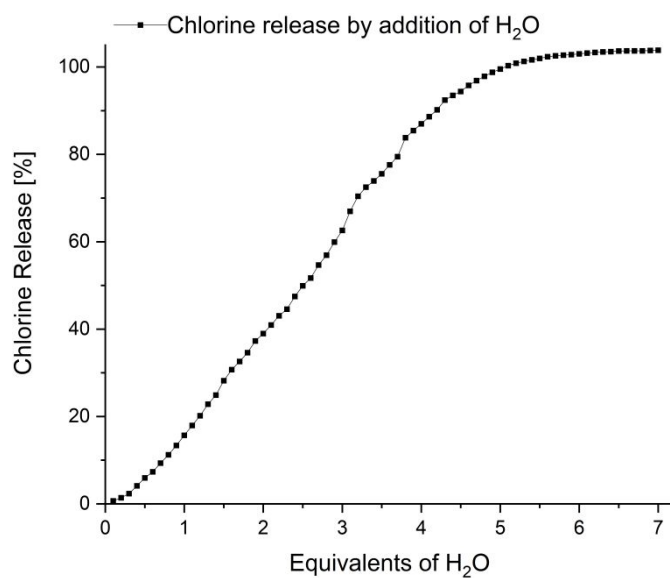


Figure S 28. Optimization of the amount of H_2O needed for chlorine release.

Table S 1. Chlorine release by addition of polar solvents.

Method	Chlorine Release
Addition of 5 equiv. H ₂ O at r.t.	97 %
Addition of 10 equiv. H ₂ O at r.t.	70 %
Addition of 10 equiv. H ₂ O at 40 °C	76 %
Addition of 10 equiv. 5 % sodium chloride solution at r.t.	82 %
Addition of 10 equiv. saturated sodium chloride solution at r.t.	89 %

d) Chlorine Storage Capacities and Physical Properties

Table S 2. Storage capacities of [Cat]Cl and physical properties of [Cat][Cl(Cl₂)_n].

Substrate	Melting point poly-chloride [°C]	Density at 25 °C [g ml ⁻¹]	dyn. viscosity [mPa s]	Storage capacity by amount of substance [mol mol ⁻¹] ^[a]	Storage capacity by mass [g g ⁻¹] ^[b]	Storage capacity by volume [g mL ⁻¹] ^[c]
Cl ₂ ^[d]	-101, (-34) ^[e]	1.38			-	1.38
[NMe ₄]Cl	decomposition	-	solid	1.06	0.68	-
[NEt ₄]Cl	60	1.10	solid	1.51	0.64	0.43
[NPr ₄]Cl	65–70	1.00	solid	1.23	0.39	0.39
[NBu ₄]Cl	5	1.30	684	2.18	0.55	0.46
[NEtMe ₃]Cl	8	1.24	low viscosity	1.44	0.82	0.56
[NEt ₂ Me ₂]Cl	-19	1.20	16	1.57	0.8	0.54
[NEt ₃ Me]Cl	1(-10) ^[f]	1.21	19	1.68	0.79	0.53
[NBuMe ₃]Cl	21	1.25	low viscosity	2.57	1.19	0.68
[NBuEt ₂ Me]Cl	-19	1.30	46	2.72	1.06	0.67
[NMePr ₃]Cl	9	1.23	141	2.13	0.77	0.54
[NBu ₂ Me ₂]Cl	-27	1.17	low viscosity	2.29	0.83	0.53
[NBu ₃ Me]Cl	8	1.19	low viscosity	2.46	0.73	0.51
[PEt ₃ Me]Cl	5	1.60	low viscosity	1.85	0.77	0.70
[PBu ₃ Me]Cl	-1	1.05	low viscosity	2.2	0.61	0.40
[SMe ₃]Cl	45	1.36	high viscosity	0.94	0.59	0.51

[a] Storage capacity by amount of substance is equal to the amount of substance of Cl₂ which can be stored on 1 mol of the chloride salt. [b] Storage capacity by mass is equal to the mass of Cl₂ which can be stored on 1 g of the chloride salt. [c] Storage capacity by volume is equal to the mass of Cl₂ which is stored in 1 mL of the [Cat][Cl(Cl₂)_n]. [d] Values taken from P. Schmittinger, T. Florkiewicz, L. C. Curlin, B. Lüke, R. Scannell, T. Navin, E. Zelfel, R. Bartsch, Chlorine. In Ullmann's Encyclopedia of Industrial Chemistry. Wiley-VCH, Weinheim, **2000**. [e] b.p. of elemental chlorine. [f] Determined by cooling liquid [NEt₃Me][Cl(Cl₂)_{1.68}].

e) Calorimetric Measurements

e1. Setup

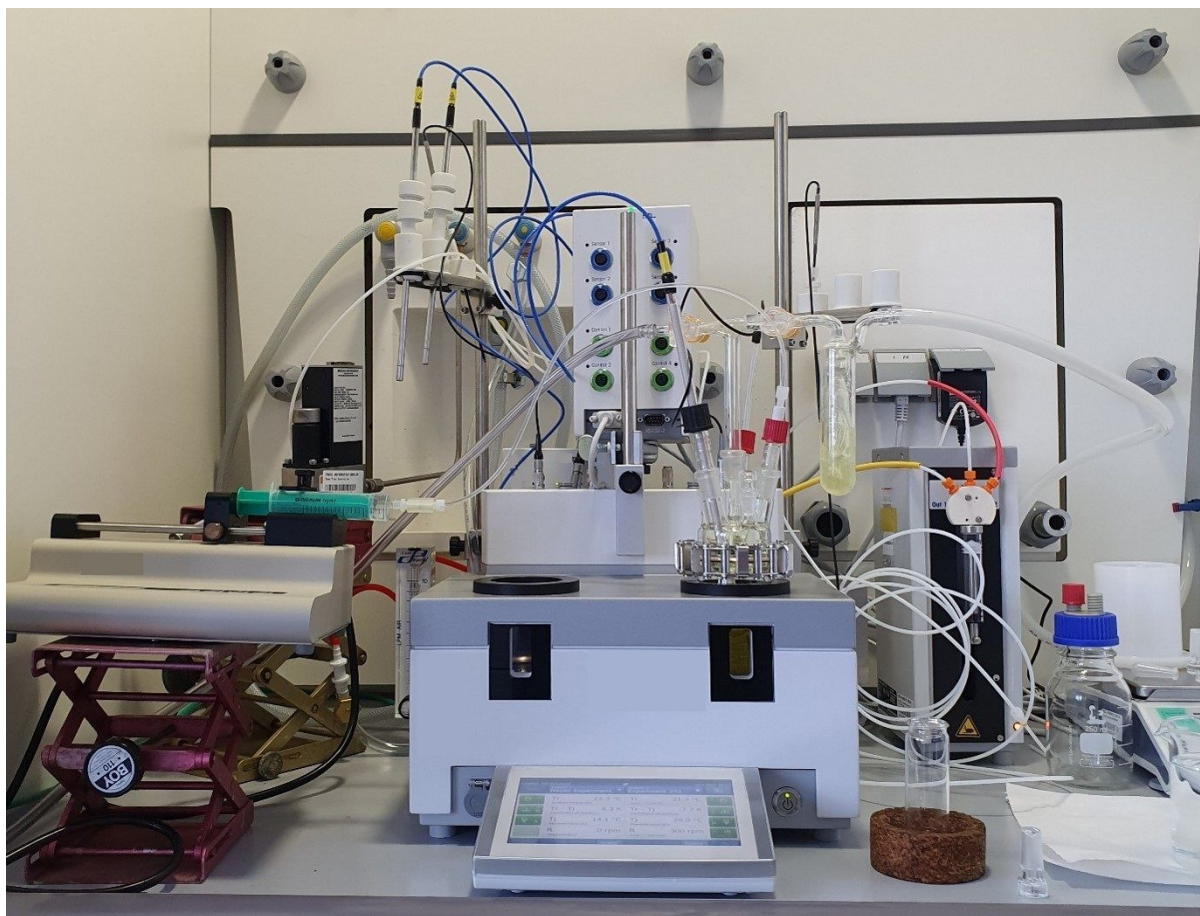


Figure S 29. Setup for calorimetric measurements.

e2. Hydration Energy of [NEt₃Me]Cl**Table S 3.** Recipe for determination of Hydration Energy of [NEt₃Me]Cl

#	Action / Note / Sample	Start Time	End Time
1	Start of experiment with thermostat off and stirrer off, Water=50 ml Details:	00:00:00	00:00:05
2	Ramp stirrer speed to 300 rpm over 10 sec	00:00:05	00:00:17
3	Heat Tr to 25 (22) °C as fast as possible	00:00:05	00:01:53
4	Wait 10 min	00:00:17	00:10:17
5	Record virtual volume in reactor	00:03:11	
6	U - cpr - U determination with 15 min waiting time and Δ Tr of 3 K	00:10:17	01:55:24
7	Add 10 g of [NEt ₃ Me]Cl over 10 min	01:55:24	01:57:42
8	Wait 10 min	01:57:42	02:07:42
9	Record virtual volume in reactor	02:09:08	
10	U - cpr - U determination with 15 min waiting time and Δ Tr of 3 K	02:09:08	03:54:14
11	End of experiment	03:56:01	03:56:01





Obtained Values

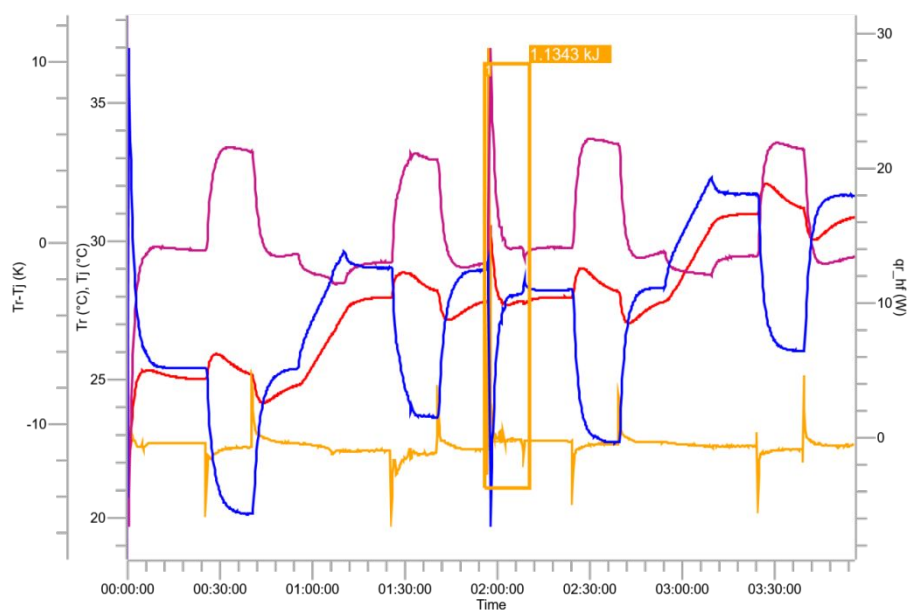
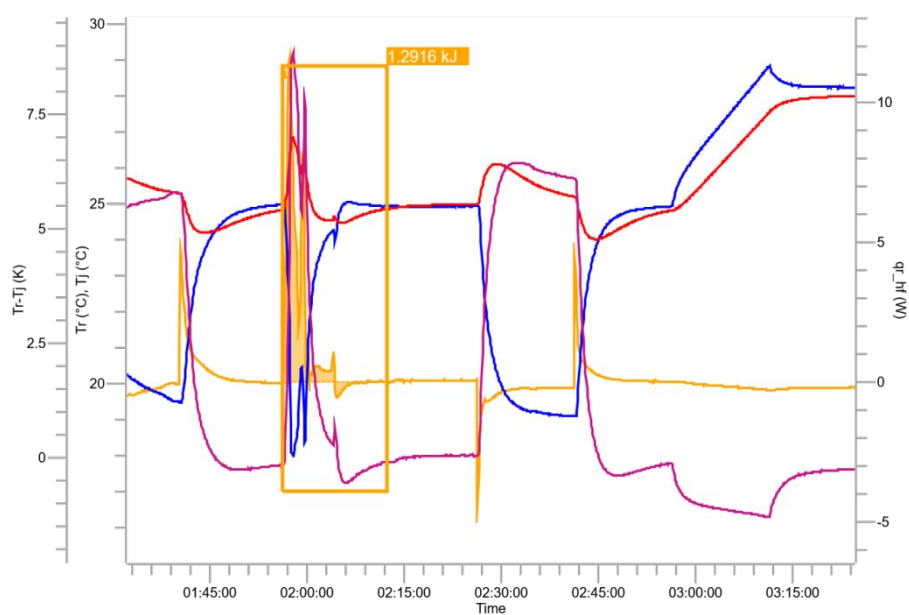
Table S 4. Determined values for the solvation energy of [NEt₃Me]Cl in water.

Measurement	m [NEt ₃ Me]Cl [g]	n [NEt ₃ Me]Cl [mol]	E [kJ]	E_{solv} [kJ mol ⁻¹]
1	10.003	0.066	-1.134	-17.18
2	10.003	0.066	-1.292	-19.58
3	10.003	0.066	-1.247	-18.89
Average	10.003	0.066	-1.224	-18.55

Trends

Table S 5. Color code for measured data.

Trend	Color	Units
Tr		°C
Tj		°C
Tr-Tj		K
qr_hf		W

**Figure S 30.** Temperature curves and heat flow for the addition of 10 g of [NEt₃Me]Cl in 50 mL of water (Measurement 1).**Figure S 31.** Temperature curves and heat flow for the addition of 10 g of [NEt₃Me]Cl in 50 mL of water (Measurement 2).

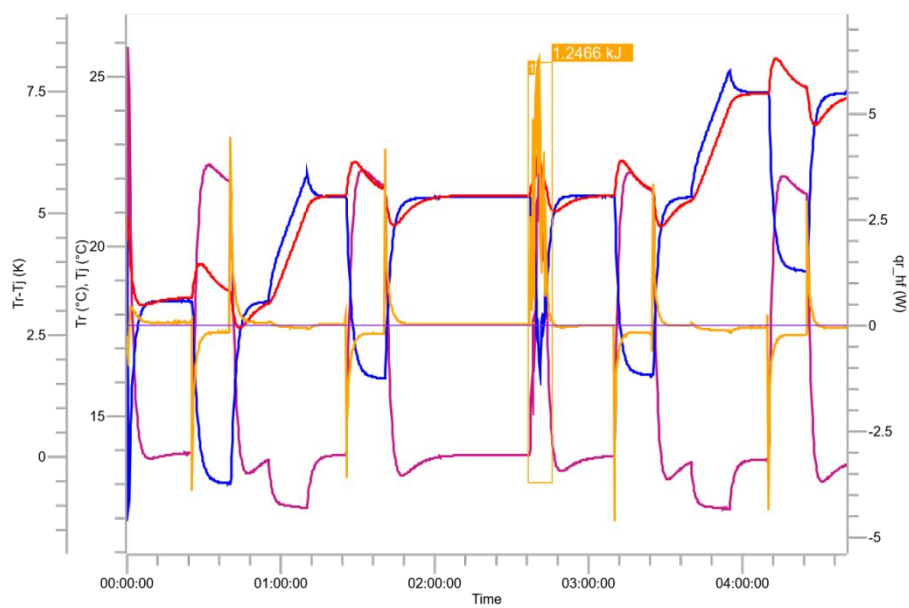


Figure S 32. Temperature curves and heat flow for the addition of 10 g of $[\text{NEt}_3\text{Me}]\text{Cl}$ in 50 mL of water (Measurement 3 using a glass covered Pt100 and a glass cover calibration heater).

Calorimetric Calculations Raw Data

Measurement 1

Table S 6. Integral Results.

Trend	Name	Start Time	End Time	Integral	Baseline Type	ΔT_{ad}
qr_hf	1	01:56:01	02:10:32	1.1343 kJ	Proportional To Conversion	5.2326 K

Table S 7. Virtual Volume (Vv).

Time	Vv (used)	Interpolation
00:00:06	50 ml	Proportional to Vr
00:03:12	64 ml	Proportional to Vr
02:09:08	72 ml	Constant offset

Table S 8. Heat Transfer Coefficient (U).

Time	U (used)	UA	Calculated by	Tr	Interpolation
00:32:50	136.58 W/K*m ²	0.89142 W/K	Standard method	25.66 °C	Proportional to Vv_observed
01:32:54	135.53 W/K*m ²	0.88455 W/K	Standard method	28.73 °C	Proportional to Vv_observed
02:31:40	121.72 W/K*m ²	0.86932 W/K	Standard method	28.65 °C	Proportional to Vv_observed
03:31:42	117.31 W/K*m ²	0.83781 W/K	Standard method	31.67 °C	Hold value

Table S 9. Specific Heat (cpr).

Time	cpr (used)	Calculated by	Tr	Interpolation
01:02:50	4.9888 J/g*K	Standard method	26.01 °C	Proportional to Mr
03:01:40	3.6180 J/g*K	Standard method	29.05 °C	Hold value

Table S 10. Selected reactor inserts.

EasyMax calibration heater, C22, 10W
Pt100 temperature sensor, EasyMax, FEP-coated, 175mm
Magnetic stir bar, cross-shaped, PTFE coated, 38mm

Table S 11. Specific Heat of Reactor Inserts (Cpi).

	Cpi at Min. Working Vol.	Cpi per cm
At start of experiment	10.92 J/K	1.079 J/K*cm
Total	10.92 J/K	1.079 J/K*cm

Table S 12. Various Parameters.

qr definition	$qr_{hf} = q_{flow_hf} - q_c + q_{accu} + q_{dos}$
qdos averaged	yes
Reactor Time Constant	15 s
ΔT_{ad} calculation	Use mr and cpr at the end of the integral

Measurement 2

Table S 13. Integral Results.

Trend	Name	Start Time	End Time	Integral	Baseline Type	ΔT_{ad}
qr_hf	1	01:56:18	02:12:28	1.2916 kJ	Proportional To Conversion	7.0231 K

Table S 14. Virtual Volume (Vv).

Time	Vv (used)	Interpolation
00:00:06	40 ml	Proportional to Vr
00:00:50	52 ml	Proportional to Vr
02:11:14	62 ml	Constant offset

Table S 15. Heat Transfer Coefficient (U).

Time	U (used)	UA	Calculated by	Tr	Interpolation
00:32:50	153.69 W/K*m ²	0.86122 W/K	Standard method	22.70 °C	Proportional to Vv_observed
01:32:52	157.77 W/K*m ²	0.88406 W/K	Standard method	25.67 °C	Proportional to Vv_observed
02:33:44	127.44 W/K*m ²	0.81215 W/K	Standard method	25.69 °C	Proportional to Vv_observed
03:33:46	124.53 W/K*m ²	0.79360 W/K	Standard method	28.70 °C	Hold value

Table S 16. Specific Heat (cpr).

Time	cpr (used)	Calculated by	Tr	Interpolation
01:02:50	4.5769 J/g*K	Standard method	23.05 °C	Proportional to Mr
03:03:46	3.6831 J/g*K	Standard method	26.06 °C	Hold value

Table S 17. Selected reactor inserts.

EasyMax calibration heater, C22, 10W
Pt100 temperature sensor, EasyMax, FEP-coated, 175mm
Magnetic stir bar, cross-shaped, PTFE coated, 38mm

Table S 18. Specific Heat of Reactor Inserts (Cpi).

	Cpi at Min. Working Vol.	Cpi per cm
At start of experiment	10.92 J/K	1.079 J/K*cm
Total	10.92 J/K	1.079 J/K*cm

Table S 19. Various Parameters.

qr definition	$qr_{hf} = q_{flow_{hf}} - q_c + q_{accu} + q_{dos}$
qdos averaged	yes
Reactor Time Constant	15 s
ΔT_{ad} calculation	Use mr and cpr at the end of the integral

Measurement 3

Table S 20. Integral Results.

Trend	Name	Start Time	End Time	Integral	Baseline Type	ΔT_{ad}
qr_hf	1	02:36:35	02:45:38	1.2466 kJ	Proportional To Conversion	6.5174 K

Table S 21. Virtual Volume (Vv).

Time	Vv (used)	Interpolation
00:00:06	50 ml	Proportional to Vr
00:05:04	62 ml	Proportional to Vr
02:54:44	72 ml	Constant offset

Table S 22. Heat Transfer Coefficient (U).

Time	U (used)	UA	Calculated by	Tr	Interpolation
00:32:50	134.13 W/K*m ²	0.85474 W/K	Standard method	19.16 °C	Proportional to Vv_observed
01:32:52	135.55 W/K*m ²	0.86379 W/K	Standard method	22.16 °C	Proportional to Vv_observed
03:17:16	123.17 W/K*m ²	0.87965 W/K	Standard method	22.12 °C	Proportional to Vv_observed
04:17:20	123.23 W/K*m ²	0.88009 W/K	Standard method	25.12 °C	Hold value

Table S 23. Specific Heat (cpr).

Time	cpr (used)	Calculated by	Tr	Interpolation
01:02:50	3.9705 J/g*K	Standard method	19.59 °C	Proportional to Mr
03:47:18	3.1924 J/g*K	Standard method	22.61 °C	Hold value

Table S 24. Selected reactor inserts.

EasyMax calibration heater, C22, 10W
Pt100 temperature sensor, EasyMax, glass
Magnetic stir bar, cross-shaped, PTFE coated, 38mm

Table S 25. Specific Heat of Reactor Inserts (Cpi).

	Cpi at Min. Working Vol.	Cpi per cm
At start of experiment	11.43 J/K	1.413 J/K*cm
Total	11.43 J/K	1.413 J/K*cm

Table S 26. Various Parameters.

qr definition	qr_hf = qflow_hf - qc + qaccu + qdos
qdos averaged	yes
Reactor Time Constant	15 s
ΔT_{ad} calculation	Use mr and cpr at the end of the integral

e3. Reaction of $[\text{NEt}_3\text{Me}][\text{Cl}(\text{Cl}_2)_{1.18}]$ with 5 Equivalents H_2O **Table S 27.** Recipe for determination of reaction energy of $[\text{NEt}_3\text{Me}][\text{Cl}(\text{Cl}_2)_{1.18}]$ with 5 Equivalents H_2O .

#	Action / Note / Sample	Start Time	End Time
1	Start of experiment with Tr set to 25 C and R set to 300 rpm, $[\text{NEt}_3\text{Me}][\text{Cl}(\text{Cl}_2)_n]=40$ ml	00:00:00	00:00:05
2	Ramp stirrer speed to 300 rpm over 10 sec	00:00:05	00:00:17
3	Cool Tr to 22 °C as fast as possible	00:00:05	00:01:28
4	Wait 10 min	00:00:18	00:10:18
5	Record virtual volume in reactor	00:19:46	
6	U - cpr - U determination with 15 min waiting time and Δ Tr of 3 K	00:19:46	02:04:53
7	Cool Tr to 22 °C as fast as possible	02:04:53	02:06:12
8	Wait 20 min	02:06:12	02:26:12
9	Add 19 ml of Water at once	02:26:12	02:56:53
10	Wait 10 min	02:56:53	03:06:55
11	Record virtual volume in reactor	03:07:37	





Obtained Values

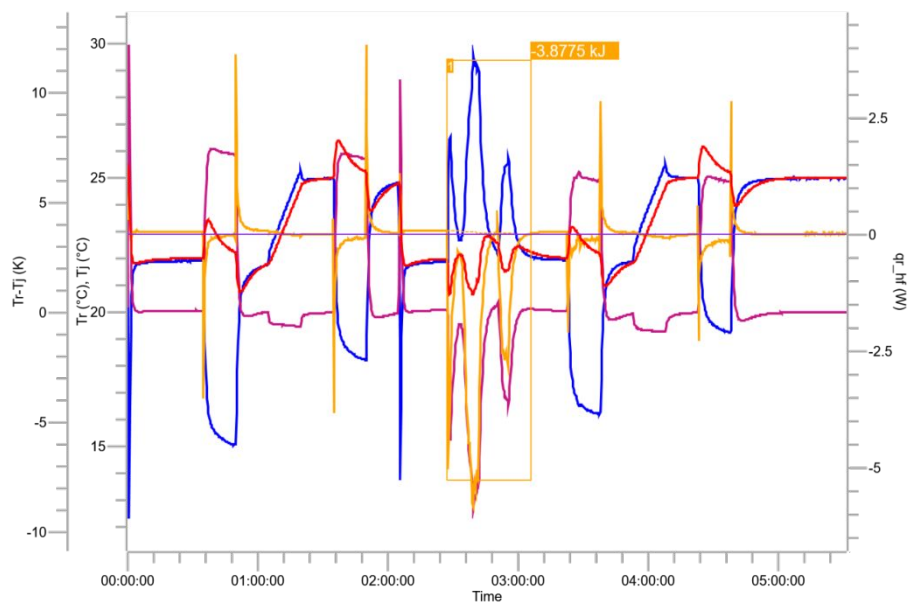
Table S 28. Determined values for the reaction energy of $[\text{NEt}_3\text{Me}][\text{Cl}(\text{Cl}_2)_n]$ with 5 equivalents of water.

Measurement	n	mass [g]	Amount of substance [mol]	E [kJ]	E_{Solv} [kJ mol ⁻¹]
1	1.16	48.532	0.207	3.878	18.73
2	1.19	48.378	0.207	3.755	18.14
3	1.19	50.486	0.214	4.275	19.98
Average	1.18	49.131	0.209	3.969	18.99

Trends

Table S 29. Color code for measured data.

Trend	Color	Units
Tr		°C
Tj		°C
Tr-Tj		K
qr_hf		W

**Figure S 33.** Temperature curves and heat flow for the addition of 19 g Water to $[\text{NEt}_3\text{Me}][\text{Cl}(\text{Cl}_2)_{1.16}]$ (Measurement 1).

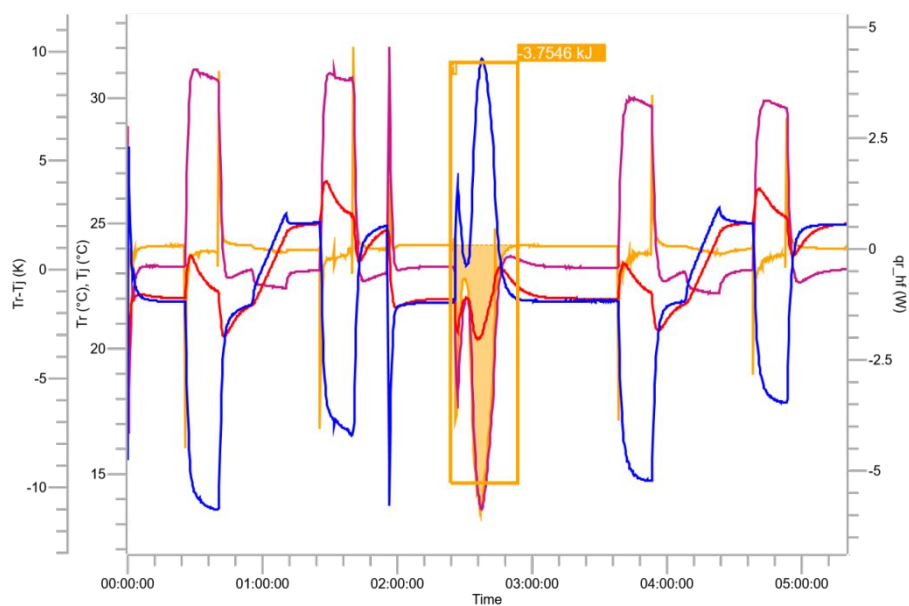


Figure S 34. Temperature curves and heat flow for the addition of 19 g Water to $[\text{NEt}_3\text{Me}][\text{Cl}(\text{Cl}_2)_{1.16}]$ (Measurement 2).

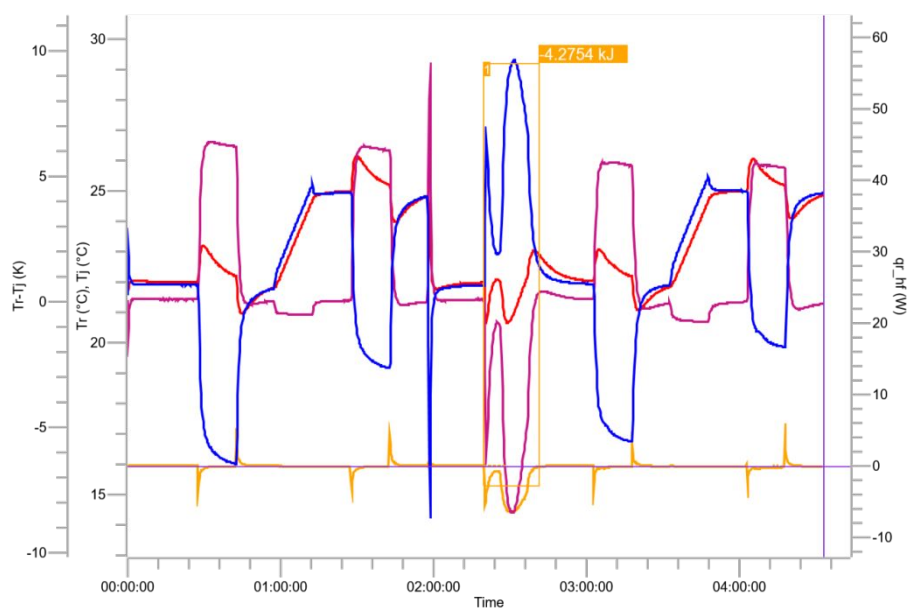


Figure S 35. Temperature curves and heat flow for the addition of 19 g Water to $[\text{NEt}_3\text{Me}][\text{Cl}(\text{Cl}_2)_{1.16}]$ (Measurement 3).

Calorimetric Calculations

Measurement 1

Table S 30. Integral Results.

Trend	Name	Start Time	End Time	Integral	Baseline Type	ΔT_{ad}
qr_hf	1	02:26:58	03:05:36	-3.8775 kJ	Proportional To Conversion	-27.174 K

Table S 31. Virtual Volume (Vv).

Time	Vv (used)	Interpolation
00:00:06	40 ml	Proportional to Vr
00:19:46	42 ml	Proportional to Vr
03:07:38	60 ml	Constant offset

Table S 32. Heat Transfer Coefficient (U).

Time	U (used)	UA	Calculated by	Tr	Interpolation
00:42:18	141.52 W/K*m ²	0.68413 W/K	Standard method	22.73 °C	Proportional to Vv_observed
01:42:22	143.24 W/K*m ²	0.69245 W/K	Standard method	25.73 °C	Proportional to Vv_observed
03:30:10	130.96 W/K*m ²	0.81444 W/K	Standard method	22.61 °C	Proportional to Vv_observed
04:30:12	130.83 W/K*m ²	0.81360 W/K	Standard method	25.63 °C	Hold value

Table S 33. Specific Heat (cpr).

Time	cpr (used)	Calculated by	Tr	Interpolation
01:12:18	1.5105 J/g*K	Standard method	23.14 °C	Proportional to Mr
04:00:10	2.0394 J/g*K	Standard method	23.14 °C	Hold value

Table S 34. Selected reactor inserts.

EasyMax calibration heater, C22, 10W
Pt100 temperature sensor, EasyMax, glass
Magnetic stir bar, cross-shaped, PTFE coated, 38mm

Table S 35. Specific Heat of Reactor Inserts (Cpi).

	Cpi at Min. Working Vol.	Cpi per cm
At start of experiment	11.43 J/K	1.413 J/K*cm
Total	11.43 J/K	1.413 J/K*cm

Table S 36. Various Parameters.

qr definition	qr_hf = qflow_hf - qc + qaccu + qdos
qdos averaged	yes
Reactor Time Constant	15 s
ΔT_{ad} calculation	Use mr and cpr at the end of the integral

Measurement 2

Table S 37. Integral Results.

Trend	Name	Start Time	End Time	Integral	Baseline Type	ΔT_{ad}
qr_hf	1	02:23:52	02:53:27	-3.7546 kJ	Proportional To Conversion	-25.811 K

Table S 38. Virtual Volume (Vv).

Time	Vv (used)	Interpolation
00:00:06	36.92 ml	Proportional to Vr
00:10:22	48 ml	Proportional to Vr
03:22:54	59 ml	Constant offset

Table S 39. Heat Transfer Coefficient (U).

Time	U (used)	UA	Calculated by	Tr	Interpolation
00:32:52	106.24 W/K*m ²	0.56261 W/K	Standard method	22.93 °C	Proportional to Vv_observed
01:33:00	105.77 W/K*m ²	0.56013 W/K	Standard method	25.90 °C	Proportional to Vv_observed
03:45:26	105.80 W/K*m ²	0.64983 W/K	Standard method	22.84 °C	Proportional to Vv_observed
04:45:28	106.41 W/K*m ²	0.65358 W/K	Standard method	25.83 °C	Hold value

Table S 40. Specific Heat (cpr).

Time	cpr (used)	Calculated by	Tr	Interpolation
01:02:56	1.7326 J/g*K	Standard method	23.05 °C	Proportional to Mr
04:15:24	2.2050 J/g*K	Standard method	23.05 °C	Hold value

Table S 41. Selected reactor inserts.

EasyMax calibration heater, C22, 10W
Pt100 temperature sensor, EasyMax, glass
Magnetic stir bar, cross-shaped, PTFE coated, 38mm

Table S 42. Specific Heat of Reactor Inserts (Cpi).

	Cpi at Min. Working Vol.	Cpi per cm
At start of experiment	11.43 J/K	1.413 J/K*cm
Total	11.43 J/K	1.413 J/K*cm

Table S 43. Various Parameters.

qr definition	qr_hf = qflow_hf - qc + qaccu + qdos
qdos averaged	yes
Reactor Time Constant	15 s
ΔT_{ad} calculation	Use mr and cpr at the end of the integral

Measurement 3

Table S 44. Integral Results.

Trend	Name	Start Time	End Time	Integral	Baseline Type	ΔT_{ad}
qr_hf	1	02:19:26	02:41:36	-4.2754 kJ	Proportional To Conversion	-29.055 K

Table S 45. Virtual Volume (Vv).

Time	Vv (used)	Interpolation
00:00:06	38.77 ml	Proportional to Vr
00:12:30	49 ml	Proportional to Vr
02:47:32	60 ml	Constant offset

Table S 46. Heat Transfer Coefficient (U).

Time	U (used)	UA	Calculated by	Tr	Interpolation
00:35:02	147.83 W/K*m ²	0.79426 W/K	Standard method	22.63 °C	Proportional to Vv_observed
01:35:06	150.41 W/K*m ²	0.80811 W/K	Standard method	25.62 °C	Proportional to Vv_observed
03:10:04	146.15 W/K*m ²	0.90888 W/K	Standard method	22.57 °C	Proportional to Vv_observed
04:10:06	145.98 W/K*m ²	0.90782 W/K	Standard method	25.55 °C	Hold value

Table S 47. Specific Heat (cpr).

Time	cpr (used)	Calculated by	Tr	Interpolation
01:05:02	1.5571 J/g*K	Standard method	23.18 °C	Proportional to Mr
03:40:04	2.1523 J/g*K	Standard method	23.16 °C	Hold value

Table S 48. Selected reactor inserts.

EasyMax calibration heater, C22, 10W
Pt100 temperature sensor, EasyMax, glass
Magnetic stir bar, cross-shaped, PTFE coated, 38mm

Table S 49. Specific Heat of Reactor Inserts (Cpi).

	Cpi at Min. Working Vol.	Cpi per cm
At start of experiment	11.43 J/K	1.413 J/K*cm
Total	11.43 J/K	1.413 J/K*cm

Table S 50. Various Parameters.

qr definition	$qr_{hf} = q_{flow_hf} - q_c + q_{accu} + q_{dos}$
qdos averaged	yes
Reactor Time Constant	15 s
ΔT_{ad} calculation	Use mr and cpr at the end of the integral

e4. Reaction of $[\text{NEt}_3\text{Me}][\text{Cl}(\text{Cl}_2)_{1.68}]$ with 5 Equivalents H_2O **Table S 51.** Recipe for determination of the reaction energy for the reaction of $[\text{NEt}_3\text{Me}][\text{Cl}(\text{Cl}_2)_{1.68}]$ with 5 Equivalents H_2O





#	Action / Note / Sample	Start Time	End Time
1	Start of experiment with thermostat off and stirrer off, $[\text{NEt}_3\text{Me}][\text{Cl}(\text{Cl}_2)_n]=40$ ml	00:00:00	00:00:05
2	Ramp stirrer speed to 300 rpm over 10 sec	00:00:05	00:00:17
3	Heat Tr to 18.5 °C as fast as possible	00:00:06	00:00:10
4	Wait 10 min	00:00:17	00:10:17
5	Record virtual volume in reactor	00:11:06	
6	U - cpr - U determination with 15 min waiting time and Δ Tr of 3 K	00:11:07	01:56:13
7	Add 19 g of Water at once	01:56:13	02:47:06
8	Wait 10 min	03:18:58	03:28:58
9	Record virtual volume in reactor	03:29:45	
10	U - cpr - U determination with 15 min waiting time and Δ Tr of 3 K	03:29:45	05:14:54
11	End of experiment	05:53:49	05:53:49

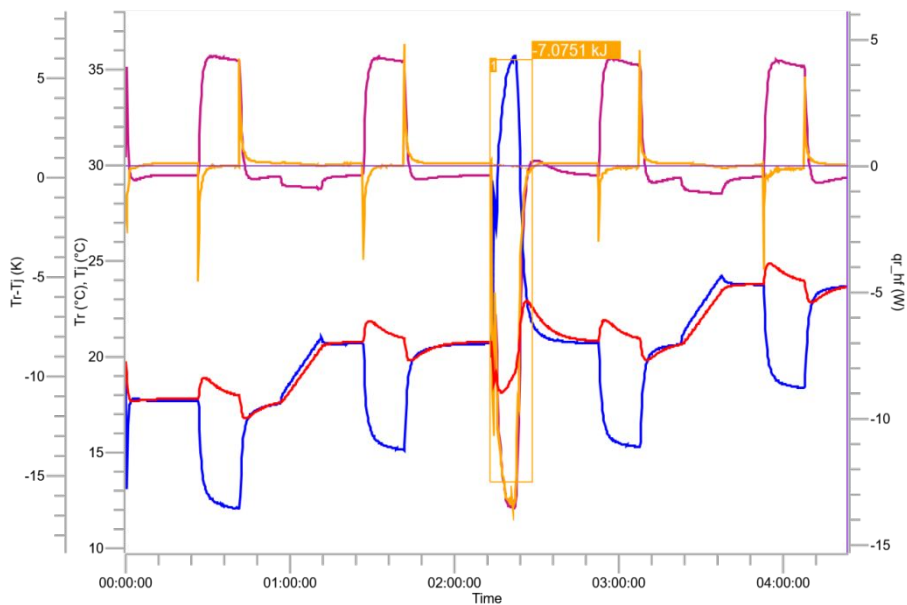
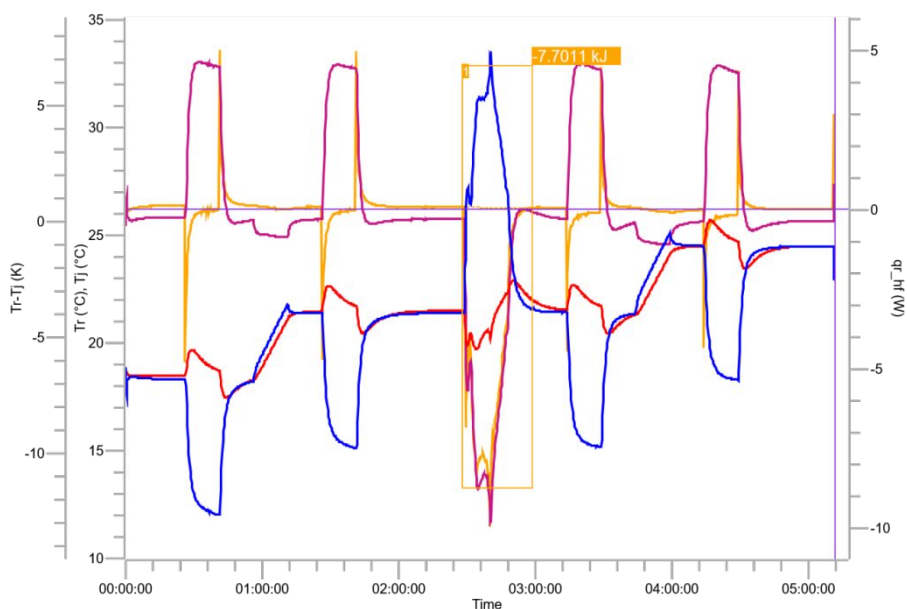
Obtained Values

Table S 52. Determined values for the reaction energy of $[\text{NEt}_3\text{Me}][\text{Cl}(\text{Cl}_2)_n]$ with 5 equivalents of water.

Measurement	n	mass [g]	Amount of substance [mol]	E [kJ]	E_{solv} [kJ mol ⁻¹]
1	1.68	56.405	0.208	7.075	34.01
2	1.67	56.292	0.208	7.701	37.02
3	1.69	56.597	0.209	7.325	35.05
Average	1.68	56.431	0.208	7.367	35.36

Table S 53. Color code for measured data.

Trend	Color	Units
Tr		°C
Tj		°C
Tr-Tj		K
qr_hf		W

**Figure S 36.** Temperature curves and heat flow for the addition of 19 g Water to $[\text{NEt}_3\text{Me}][\text{Cl}(\text{Cl}_2)_{1.68}]$ (Measurement 1).**Figure S 37.** Temperature curves and heat flow for the addition of 19 g Water to $[\text{NEt}_3\text{Me}][\text{Cl}(\text{Cl}_2)_{1.68}]$ (Measurement 2).

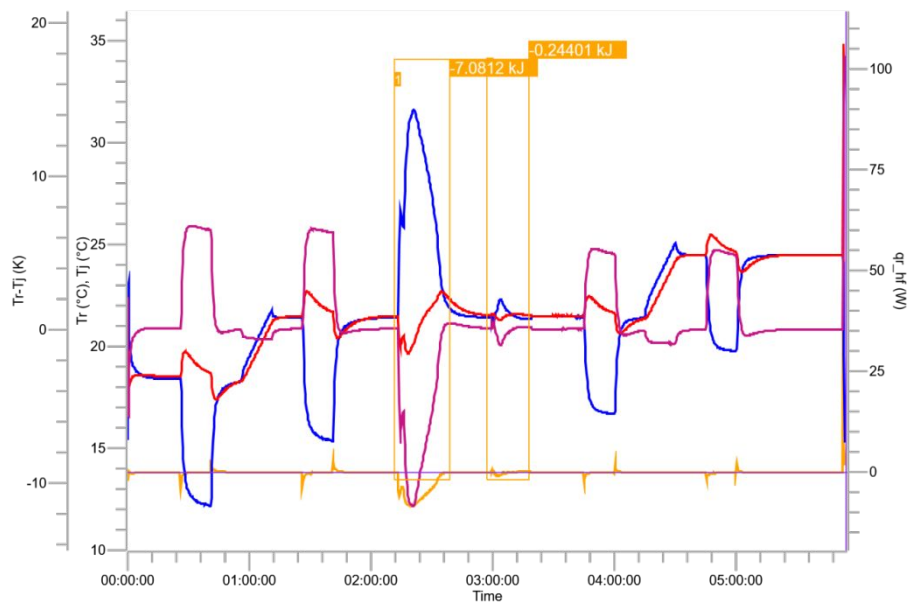


Figure S 38. Temperature curves and heat flow for the addition of 19 g Water to $[\text{NEt}_3\text{Me}][\text{Cl}(\text{Cl}_2)_{1.68}]$ (Measurement 3).

Calorimetric Calculations

Measurement 1

Table S 54. Integral Results.

Trend	Name	Start Time	End Time	Integral	Baseline Type	ΔT_{ad}
qr_hf	1	02:12:50	02:28:23	-7.0751 kJ	Proportional To Conversion	-47.296 K

Table S 55. Virtual Volume (Vv).

Time	Vv (used)	Interpolation
00:00:06	40 ml	Proportional to Vr
00:01:28	55 ml	Proportional to Vr
02:37:20	61 ml	Constant offset

Table S 56. Heat Transfer Coefficient (U).

Time	U (used)	UA	Calculated by	Tr	Interpolation
00:34:00	143.38 W/K*m ²	0.83650 W/K	Standard method	18.40 °C	Proportional to Vv_observed
01:34:02	144.87 W/K*m ²	0.84522 W/K	Standard method	21.40 °C	Proportional to Vv_observed
02:59:50	137.40 W/K*m ²	0.86502 W/K	Standard method	21.40 °C	Proportional to Vv_observed
03:59:54	137.72 W/K*m ²	0.86703 W/K	Standard method	24.39 °C	Hold value

Table S 57. Specific Heat (cpr).

Time	cpr (used)	Calculated by	Tr	Interpolation
01:04:00	1.7848 J/g*K	Standard method	18.99 °C	Proportional to Mr
03:29:52	2.1370 J/g*K	Standard method	21.95 °C	Hold value

Table S 58. Selected reactor inserts.

EasyMax calibration heater, C22, 10W
Pt100 temperature sensor, EasyMax, glass
Magnetic stir bar, cross-shaped, PTFE coated, 38mm

Table S 59. Specific Heat of Reactor Inserts (Cpi).

	Cpi at Min. Working Vol.	Cpi per cm
At start of experiment	11.43 J/K	1.413 J/K*cm
Total	11.43 J/K	1.413 J/K*cm

Table S 60. Various Parameters.

qr definition	$qr_{hf} = q_{flow_hf} - q_c + q_{accu} + q_{dos}$
qdos averaged	yes
Reactor Time Constant	15 s
ΔT_{ad} calculation	Use mr and cpr at the end of the integral

Measurement 2

Table S 61. Integral Results.

Trend	Name	Start Time	End Time	Integral	Baseline Type	ΔT_{ad}
qr_hf	1	02:27:43	02:58:21	-7.7011 kJ	Proportional To Conversion	-49.297 K

Table S 62. Virtual Volume (Vv).

Time	Vv (used)	Interpolation
00:00:06	40 ml	Proportional to Vr
00:11:12	52 ml	Proportional to Vr
02:58:40	61 ml	Constant offset

Table S 63. Heat Transfer Coefficient (U).

Time	U (used)	UA	Calculated by	Tr	Interpolation
00:33:44	132.12 W/K*m ²	0.74033 W/K	Standard method	19.22 °C	Proportional to Vv_observed
01:33:48	133.58 W/K*m ²	0.74851 W/K	Standard method	22.22 °C	Proportional to Vv_observed
03:21:12	118.84 W/K*m ²	0.74818 W/K	Standard method	22.24 °C	Proportional to Vv_observed
04:21:14	118.97 W/K*m ²	0.74899 W/K	Standard method	25.22 °C	Hold value

Table S 64. Specific Heat (cpr).

Time	cpr (used)	Calculated by	Tr	Interpolation
01:03:44	2.1065 J/g*K	Standard method	19.61 °C	Proportional to Mr
03:51:10	2.2317 J/g*K	Standard method	22.58 °C	Hold value

Table S 65. Selected reactor inserts.

EasyMax calibration heater, C22, 10W
Pt100 temperature sensor, EasyMax, glass
Magnetic stir bar, cross-shaped, PTFE coated, 38mm

Table S 66. Specific Heat of Reactor Inserts (Cpi).

	Cpi at Min. Working Vol.	Cpi per cm
At start of experiment	11.43 J/K	1.413 J/K*cm
Total	11.43 J/K	1.413 J/K*cm

Table S 67. Various Parameters.

qr definition	$qr_{hf} = q_{flow_hf} - q_c + q_{accu} + q_{dos}$
qdos averaged	yes
Reactor Time Constant	15 s
ΔT_{ad} calculation	Use mr and cpr at the end of the integral

Measurement 3

Table S 68. Integral Results.

Trend	Name	Start Time	End Time	Integral	Baseline Type	ΔT_{ad}
qr_hf	1	02:11:47	02:38:52	-7.0812 kJ	Proportional To Conversion	-72.517 K
qr_hf	2	02:57:22	03:17:41	-0.24401 kJ	Proportional To Conversion	-1.737 K

Table S 69. Virtual Volume (Vv).

Time	Vv (used)	Interpolation
00:00:06	40 ml	Proportional to Vr
00:11:06	55 ml	Proportional to Vr
03:29:46	82 ml	Constant offset

Table S 70. Heat Transfer Coefficient (U).

Time	U (used)	UA	Calculated by	Tr	Interpolation
00:33:38	129.38 W/K*m ²	0.75482 W/K	Standard method	19.18 °C	Proportional to Vv_observed
01:33:42	131.90 W/K*m ²	0.76952 W/K	Standard method	22.16 °C	Proportional to Vv_observed
03:52:18	124.17 W/K*m ²	0.98235 W/K	Standard method	22.03 °C	Proportional to Vv_observed
04:52:20	124.60 W/K*m ²	0.98577 W/K	Standard method	25.03 °C	Hold value

Table S 71. Specific Heat (cpr).

Time	cpr (used)	Calculated by	Tr	Interpolation
01:03:40	1.8779 J/g*K	Standard method	19.65 °C	Proportional to Mr
04:22:20	2.1359 J/g*K	Standard method	22.66 °C	Hold value

Table S 72. Selected reactor inserts.

EasyMax calibration heater, C22, 10W
Pt100 temperature sensor, EasyMax, glass
Magnetic stir bar, cross-shaped, PTFE coated, 38mm

Table S 73. Specific Heat of Reactor Inserts (Cpi).

	Cpi at Min. Working Vol.	Cpi per cm
At start of experiment	11.43 J/K	1.413 J/K*cm
Total	11.43 J/K	1.413 J/K*cm

Table S 74. Various Parameters.

qr definition	qr_hf = qflow_hf - qc + qaccu + qdos
qdos averaged	yes
Reactor Time Constant	15 s
ΔT_{ad} calculation	Use mr and cpr at the end of the integral

8.4 SI of Novel Synthetic Pathway for the Production of Phosgene

Patrick Voßnacker, Alisa Wüst, Thomas Keilhack, Carsten Müller, Simon Steinhauer, Helmut Beckers, Sivathmeehan Yogendra, Yuliya Schiesser, Rainer Weber, Marc Reimann, Robert Müller, Martin Kaupp, Sebastian Riedel*

Sci. Adv. **2021**, 7, eabj5186.

<https://doi.org/10.1126/sciadv.abj5186>

© 2021 The Authors, some rights reserved; exclusive licensee American Association for the Advancement of Science. No claim to original U.S. Government Works. Distributed under a Creative Commons Attribution License 4.0 (CC BY).



Supplementary Materials for

Novel synthetic pathway for the production of phosgene

Patrick Voßnacker, Alisa Wüst, Thomas Keilhack, Carsten Müller, Simon Steinhauer, Helmut Beckers, Sivathmeehan Yogendra, Yuliya Schiesser, Rainer Weber, Marc Reimann, Robert Müller, Martin Kaupp, Sebastian Riedel*

*Corresponding author. Email: s.riedel@fu-berlin.de

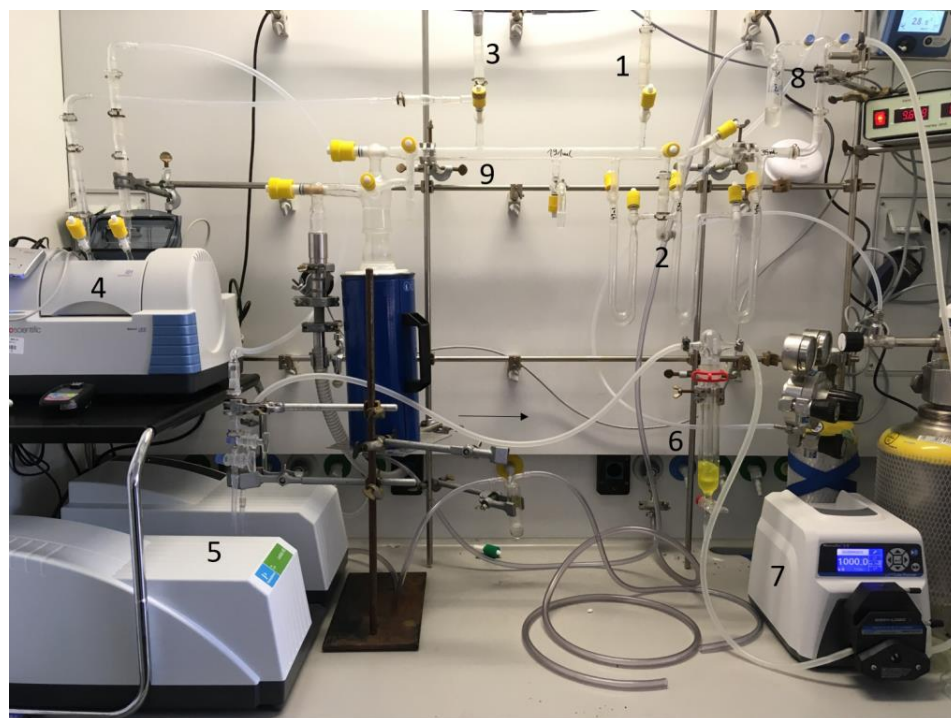
Published 29 September 2021, *Sci. Adv.* **7**, eabj5186 (2021)

DOI: 10.1126/sciadv.abj5186

This PDF file includes:

Electronic Supporting Information
Supplementary Text
Figs. S1 to S27
Tables S1 to S4
Movie S1
References

Experimental Setup



- 1 CO inlet
- 2 Cl₂ inlet
- 3 Pressure sensor
- 4 IR spectrometer
- 5 UV/Vis spectrometer
- 6 Gas wash bottle with diffuser and stopcock
- 7 Peristaltic pump
- 8 Bubbler with stopcock
- 9 Vacuum line

Fig. S1. Experimental setup for the investigation of the reaction of Cl₂ with CO.
Photo Credit: Patrick Voßnacker, FU Berlin

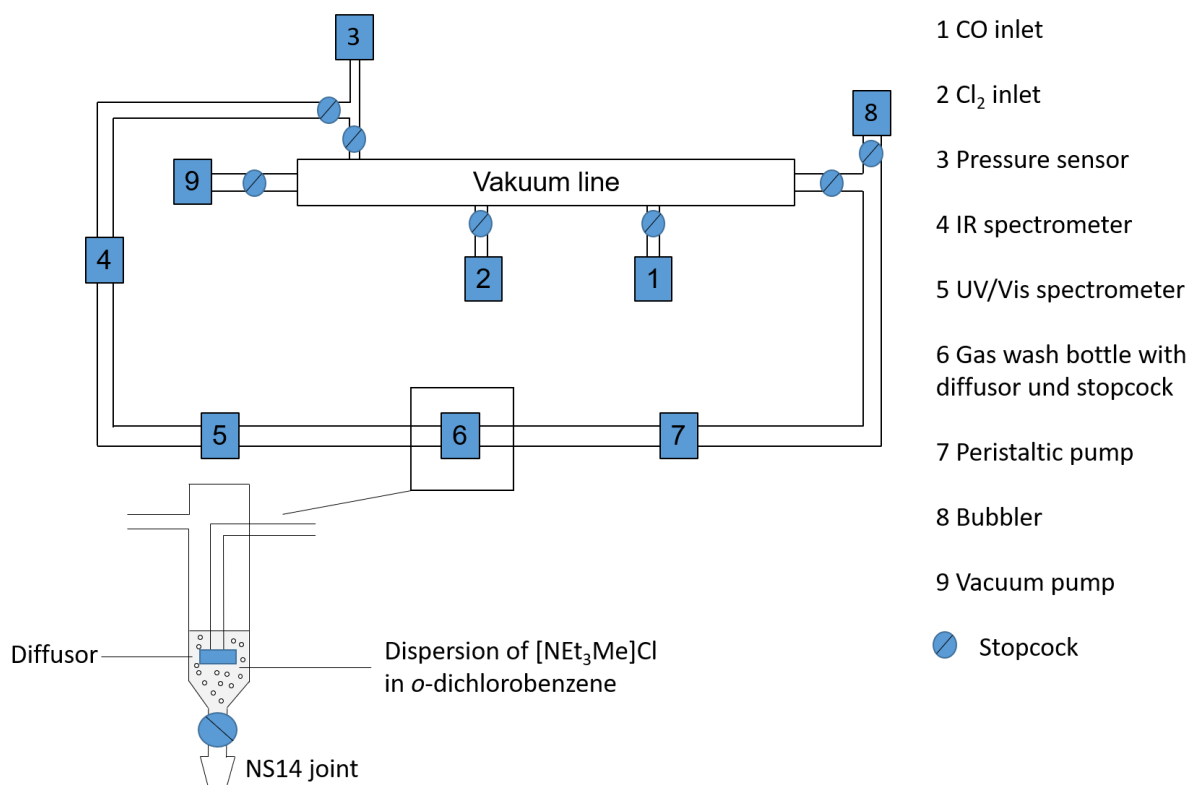


Fig. S2. Schematic representation of the experimental setup for the investigation of the reaction of Cl₂ with CO.



Fig. S3. Experimental setup for the investigation of the dark reaction of Cl₂ with CO. Photo Credit: Patrick Voßnacker, FU Berlin

Detailed Quantum-Chemical Results

A first method assessment, summarized in Table S1, showed that SCS-MP2 results deviate by less than 5% from high-level single-point CCSD(T)//SCS-MP2 relative energies for the intermediate complex ($[\text{IC}]^-$) with respect to free and separated CO and $[\text{Cl}_3]^-$, and for the overall electronic reaction energy (ΔE). MP2 single-point calculations, on the other hand, overestimate the formation energy of the $[\text{IC}]^-$ and the reaction energy of the products by about 10%. DFT results with several different functionals vary appreciably. M06-2X agrees best with the SCS-MP2 results and was hence applied subsequently in the ONIOM calculations with $[\text{NEt}_3\text{Me}]^+$. Addition of D3 dispersion corrections⁽⁵⁵⁾ was considered for B3LYP, M06, and M06-2X but had no appreciable impact on any value. Neglecting solvent effects completely at SCS-MP2 level has a dramatic destabilizing effect, reducing the relative electronic energy of the IC to -60.6 kJ/mol and the reaction energy to -16.0 kJ/mol. The corresponding Gibbs free energies at SCS-MP2 level (including solvent effects) are -72.8 and -81.2 kJ/mol, respectively. This means, the character of the final Cl^- -abstraction step is endothermic but becomes exergonic once entropic contributions are considered. Consequently, we will focus the main discussion in the following on free energies in oDCB but provide also electronic energies and enthalpies for comparison.

Table S1. Calculated relative electronic energies (ΔE^{0K}) for the intermediate complex $[\text{COCl}_2][\text{Cl}^-]$ ($[\text{IC}]^-$) and the **total reaction** energy for the formation of C(O)Cl_2 and Cl^- . Energies are given with respect to free separated CO and $[\text{Cl}_3]^-$ and were calculated at different levels of theory. All energies (in kJ/mol) were calculated from full structure optimizations at the indicated levels, except for those at MP2 and CCSD(T) levels, which were obtained from single point calculations at SCS-MP2 optimized structures. For B3LYP, M06 and M06-2X, values in parenthesis were calculated including Grimme's D3 dispersion correction. Implicit solvent effects by *ortho*-dichlorobenzene were considered through the use of a polarizable continuum model (PCM).

	SCS-MP2	spMP2	spCCSD(T)	B3LYP-D3
$[\text{IC}]^-$	-99.8	-112.8	-97.4	-76.4(-81.2)
total reaction	-94.0	-104.9	-90.3	-74.0(-75.7)
	M06-D3	M06-2X-D3	PBE0	
$[\text{IC}]^-$	-106.3(-106.4)	-101.3(-101.5)	-121.4	
total reaction	-100.5(-100.3)	-93.8 (-93.7)	-116.5	

Table S2 and Fig. S4 show characteristic energies and free energies along the reaction path, calculated with different models. Considering only energies or enthalpies ($\Delta E_{\text{SCS-MP2}}^{0K}$ or $\Delta H_{\text{CCSD(T)-F12}}^{298.15K}$), CO and $[\text{Cl}_3]^-$ form a weakly bound encounter complex ($[\text{EC}]^-$) at a C-Cl distance of about 3.4 Å, which is, however, not stable on the free energy surface at room temperature ($\Delta G_{\text{CCSD(T)-F12}}^{298.15K, \text{oDCB}}$). When CO and $[\text{Cl}_3]^-$ get closer, one Cl-Cl bond is cleaved, forming a transition state ($[\text{TS}]^-$) with a relative free energy ($\Delta G_{\text{CCSD(T)-F12}}^{298.15K, \text{oDCB}}$) of +57 kJ/mol (omitting the counter-ion) or +78 kJ/mol (including one explicit cation). From there, energies would suggest formation of a stable $[\text{COCl}_2][\text{Cl}^-]$ intermediate complex ($[\text{IC}]^-$), with a structure very similar to that of the products, namely one chloride ion weakly bound to a phosgene molecule. In the phosgene moiety the C-O and C-Cl distances deviate by less than 0.012 Å from the equilibrium structure of isolated COCl_2 . However, due to entropic reasons, this $[\text{IC}]^-$ dissociates without any free-energy barrier into the final products COCl_2 and $[\text{Cl}]^-$, and in total, the reaction is favorable by about 60 kJ/mol ($\Delta G_{\text{CCSD(T)-F12}}^{298.15K, \text{oDCB}}$).

Both the encounter complex $[\text{EC}]^-$ and the intermediate complex $[\text{IC}]^-$ are stable on the potential-energy surface, even after adding ZPE. But they are disfavored entropically and by solvent effects and do not exist on the free-energy surface in solution.

Table S2. Calculated characteristic energies and free energies along the reaction path. Relative energies (in kJ/mol) with respect to isolated CO and $[\text{Cl}_3]^-$ of the $[\text{CO}][\text{Cl}_3]^-$ encounter complex ($[\text{EC}]^-$), the transition state ($[\text{TS}]^-$), the intermediate $[\text{COCl}_2][\text{Cl}]^-$ complex ($[\text{IC}]^-$), and the overall **total reaction** energy are given. Where indicated, complexes of the anions $[\text{EC}]^-$, $[\text{TS}]^-$, $[\text{IC}]^-$, $[\text{Cl}_3]^-$ and Cl^- with the $[\text{NEt}_3\text{Me}]^+$ cation were modeled. All calculations were performed for isolated anions/ion pairs; solvent effects were included a posteriori. The energy contributions are the total electronic energies at SCS-MP2 level ($\Delta E_{\text{SCS-MP2}}^{0\text{K}}$); the correction for higher order electron correlation effects at CCSD(T)-F12 level ($\Delta E_{\text{CCSD(T)-F12}}$); the zero point energy correction (ΔE_{ZPE}); thermal corrections for 298.15 K ($\Delta E_{\text{therm.}}^{298.15\text{K}}$); the enthalpy at 298.15 K ($\Delta H_{\text{CCSD(T)-F12}}^{298.15\text{K}} = \Delta E_{\text{SCS-MP2}}^{0\text{K}} + \Delta E_{\text{CCSD(T)-F12}} + \Delta E_{\text{ZPE}} + \Delta E_{\text{therm.}}^{298.15\text{K}}$); entropic contributions at 298.15 K ($-T\Delta S$); the free energy of solvation contribution ($\Delta G_{\text{COSMO-RS}}$), and the resulting Gibbs free energy for 298.15 K ($\Delta G_{\text{CCSD(T)-F12}}^{298.15\text{K},\text{oDCB}} = \Delta H_{\text{CCSD(T)-F12}}^{298.15\text{K}} + \Delta G_{\text{COSMO-RS}}$) when summing up all terms.

	$\Delta E_{\text{SCS-MP2}}^{0\text{K}}$	$\Delta E_{\text{CCSD(T)-F12}}$	ΔE_{ZPE}	$\Delta E_{\text{therm.}}^{298.15\text{K}}$
$[\text{EC}]^-$	-11.3	+1.0	+0.5	-3.0
$[\text{TS}]^-$	+67.3	-3.3	+2.4	-2.1
$[\text{IC}]^-$	-68.5	+8.6	+10.3	-4.0
total reaction	-21.8	+9.5	+9.3	-3.9
	$\Delta H_{\text{CCSD(T)-F12}}^{298.15\text{K}}$	$-T\Delta S$	$\Delta G_{\text{COSMO-RS}}$	$\Delta G_{\text{CCSD(T)-F12}}^{298.15\text{K},\text{oDCB}}$
$[\text{EC}]^-$	-12.8	+29.5	-14.7	+2.0
$[\text{TS}]^-$	+64.3	+28.8	-36.2	+56.9
$[\text{IC}]^-$	-53.6	+34.9	-33.8	-52.5
total reaction	-6.9	+8.6	-61.1	-59.4
	$\Delta E_{\text{SCS-MP2}}^{0\text{K}}$	$\Delta E_{\text{CCSD(T)-F12}}$	ΔE_{ZPE}	$\Delta E_{\text{therm.}}^{298.15\text{K}}$
$[\text{EC}]^-[\text{NEt}_3\text{Me}]^+$	-9.7	+0.6	+1.0	-1.8
$[\text{TS}]^-[\text{NEt}_3\text{Me}]^+$	+37.1	-4.1	+3.4	-3.7
$[\text{IC}]^-[\text{NEt}_3\text{Me}]^+$	-95.1	+8.8	+9.5	-2.1
total reaction	-61.3	+9.3	+7.1	-5.5
	$\Delta H_{\text{CCSD(T)-F12}}^{298.15\text{K}}$	$-T\Delta S$	$\Delta G_{\text{COSMO-RS}}$	$\Delta G_{\text{CCSD(T)-F12}}^{298.15\text{K},\text{oDCB}}$
$[\text{EC}]^-[\text{NEt}_3\text{Me}]^+$	-9.9	+37.5	-8.0	+19.6
$[\text{TS}]^-[\text{NEt}_3\text{Me}]^+$	+32.7	+44.8	+0.1	+77.6
$[\text{IC}]^-[\text{NEt}_3\text{Me}]^+$	-78.9	+24.1	-12.0	-56.8
total reaction	-50.4	-2.2	-10.4	-63.0

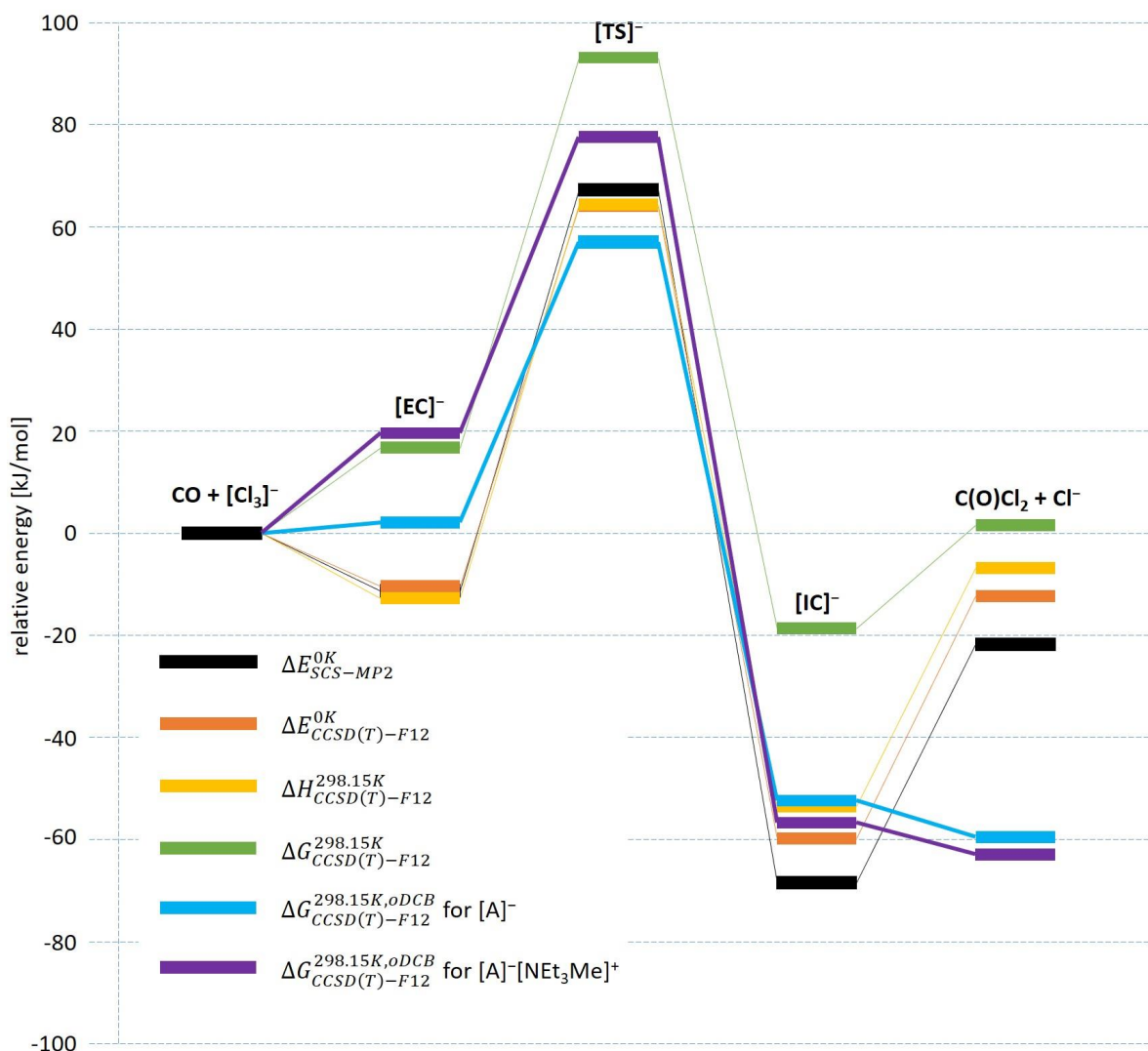


Fig. S4. Calculated reaction path for the reaction of CO and [Cl₃]⁻. Relative energies and free energies (in kJ/mol) with respect to isolated CO and [Cl₃]⁻ of the [CO][Cl₃]⁻ encounter complex ([EC]⁻), the transition state ([TS]⁻), the intermediate [COCl₂][Cl]⁻ complex ([IC]⁻), and the products C(O)Cl₂ and Cl⁻. All calculations were performed for isolated anions/ion pairs; solvent effects were included a posteriori. Reaction profiles are derived from the total electronic energy at SCS-MP2 level ($\Delta E_{SCS-MP2}^{0K}$; black), including higher-order electron correlation effects at CCSD(T)-F12 level ($\Delta E_{CCSD(T)-F12}^{0K} = \Delta E_{SCS-MP2}^{0K} + \Delta \epsilon_{CCSD(T)-F12}$; orange), including zero point energy correction and thermal corrections for 298.15 K ($\Delta H_{CCSD(T)-F12}^{298.15K} = \Delta E_{CCSD(T)-F12}^{0K} + \Delta \epsilon_{ZPE} + \Delta \epsilon_{therm.}^{298.15K}$; yellow), including entropic contributions to the Gibbs free energy for 298.15 K ($\Delta G_{CCSD(T)-F12}^{0K} = \Delta H_{CCSD(T)-F12}^{298.15K} - T\Delta S$; green), including solvent effects for orthodichlorobenzene calculated with COSMO-RS but no cations ($\Delta G_{CCSD(T)-F12}^{298.15K, oDCB}$ for [A]⁻; blue), and including one explicit [NEt₃Me]⁺ cation for each anion ($\Delta G_{CCSD(T)-F12}^{298.15K, oDCB}$ for [A]⁻[NEt₃Me]⁺; violet).

The cation and the solvent complement each other in stabilizing the anionic species. That is, solvent effects are diminished when a cation is included in the computations, as one might expect. The cation reduces the electronic contribution to the barrier by about 30 kJ mol⁻¹ but at the same time increases the entropic barrier by about 15 kJ mol⁻¹ and the solvent contribution by about 24

kJ mol^{-1} . A moderate overall increase of the free-energy barrier by about 20 kJ mol^{-1} results. We note, however, that these reaction steps likely do not occur in the organic phase but in the IL phase or at the interface between the two phases (see below). In that sense, the employed solvent model and the single counter-ion only approximate the true environmental effects.

The distribution of the involved stable species between the oDCB and the IL phase was investigated by COSMO-RS calculations of the equilibrium mole fractions (Table S3). While the gaseous compounds (CO , Cl_2 , COCl_2) have a decent to clear preference for the organic phase, all ionic species, including the chloride ion, prefer almost exclusively the IL phase. Even contact ion pairs of $[\text{NEt}_3\text{Me}][\text{Cl}_3]$ clearly prefer the IL phase. Since the $[\text{IC}]^-$ intermediate shows a very clear preference for the IL phase as well, the reaction most likely takes place in the IL or at the interface between both phases, while gaseous CO and COCl_2 move to or from the IL through the organic phase. This is in agreement with the experimental finding that the reaction takes place in the pure ionic liquid as well.

Table S3. Equilibrium mole fractions of various compounds in the organic (phase 1) and the IL phase (phase 2), calculated at the COSMO-RS level, as well as the ratio of the two molar fractions. The equilibrium was calculated starting from a pure oDCB phase and an IL phase containing equal parts of $[\text{NEt}_3\text{Me}]^+$ and $[\text{Cl}_3]^-$ ($x_0=0.49455984$) and all other compounds, respectively ($x_0=0.00098912$).

Compound	x in phase 1 (oDCB)	x in phase 2 (IL)	x_1/x_2
CO	0.00089679	0.00018638	4.8
Cl₂	0.00093889	0.00012016	7.8
COCl₂	0.00096326	0.00008484	11.4
Cl⁻	0.00000001	0.00073359	$1.4 \cdot 10^{-5}$
[Cl₃]⁻	0.00019333	0.47089775	$4.1 \cdot 10^{-4}$
[NEt₃Me]⁺	0.00019421	0.47283414	$4.1 \cdot 10^{-4}$
[NEt₃Me]⁺ [Cl₃]⁻	0.00012376	0.00130763	$9.5 \cdot 10^{-2}$
IC	0.00000087	0.00120280	$7.2 \cdot 10^{-4}$
oDCB	0.99668887	0.05263270	18.9

Molecular Structures

Cartesian coordinates (in Ångström) from optimizations at SCS-MP2/aug-cc-pVTZ level for all systems without $[\text{NEt}_3\text{Me}]^+$ or with ONIOM (SCS-MP2/aug-cc-pVTZ:M06-2X/cc-pVTZ) for all systems with $[\text{NEt}_3\text{Me}]^+$. No solvent models were applied during the optimizations. Each line refers to one atom, containing: a continuous number, the atomic number and the x, y, and z coordinate in an arbitrary three-dimensional Cartesian coordinate system.

```

carbon monoxide --- CO
  1  6  0.000000    0.000000    0.000000
  2  8  1.136400    0.000000    0.000000

trichloride --- [Cl3]-
  1 17  0.000000    0.000000    0.000000
  2 17  2.317300    0.000000    0.000000
  3 17 -2.317300    0.000000    0.000000

phosgene --- C(O)Cl2
  1 17  1.447090   -0.483050   -0.000002
  2 17 -1.447090   -0.483050   -0.000002
  3  6 -0.000000    0.496780    0.000023
  4  8  0.000000    1.680375   -0.000008

encounter complex ([EC]-) --- CO[Cl3]-
  1  6  1.686805    2.061250    0.656033
  2  8  1.773912    2.215708   -0.467011
  3 17 -2.597394    0.335838   -0.002855
  4 17 -0.483791   -0.596151   -0.003088
  5 17  1.651060   -1.509874   -0.005828

transition state ([TS]-) --- [ClO(C)Cl2]-
  1  6  1.237324   -1.039218   -0.000000
  2  8  2.261997   -1.549988   -0.000000
  3 17 -0.940758    2.941711    0.000000
  4 17 -0.000000    1.078018    0.000000
  5 17 -0.560414   -2.923539   -0.000000

intermediate complex ([IC]-) --- C(O)Cl2[Cl]-
  1 17 -0.453801   -2.450094    0.000000
  2 17  0.000000    0.435316    0.000000
  3  6 -1.186389   -0.802977    0.000000
  4  8 -2.369686   -0.678641    0.000000
  5 17  1.987673    2.617542    0.000000

```

cation-chloride-pair --- [NEt₃Me]⁺Cl⁻

1	7	0.828370	-0.001430	0.004410
2	6	2.310567	-0.007764	0.017571
3	1	2.676670	-0.321818	-0.955356
4	1	2.657979	-0.698760	0.780010
5	1	2.671099	0.992367	0.239271
6	6	0.308666	-1.373336	-0.390532
7	6	0.451447	-1.703856	-1.862555
8	1	1.464027	-1.580218	-2.247698
9	1	-0.240954	-1.121262	-2.465490
10	1	0.182066	-2.751679	-1.984362
11	1	0.858873	-2.083194	0.224156
12	1	-0.749858	-1.363844	-0.118664
13	6	0.323391	1.026045	-0.994239
14	6	0.452825	2.465889	-0.540635
15	1	1.458761	2.741932	-0.222942
16	1	-0.255388	2.692415	0.252518
17	1	0.195714	3.094491	-1.391564
18	1	0.890078	0.851180	-1.906697
19	1	-0.731940	0.783425	-1.140890
20	6	0.302489	0.349277	1.385770
21	6	0.413291	-0.764488	2.407172
22	1	-0.299978	-1.558773	2.200699
23	1	0.151509	-0.339521	3.374822
24	1	1.414309	-1.187044	2.496767
25	1	0.866426	1.225537	1.699764
26	1	-0.750160	0.599678	1.233668
27	17	-2.684346	0.004970	-0.013776

cation-trichloride-pair --- [NEt ₃ Me] ⁺ [Cl ₃] ⁻				
1	7	1.856939	0.000276	-0.174425
2	6	3.285138	0.000570	-0.582528
3	1	3.771014	-0.885670	-0.186217
4	1	3.770808	0.886697	-0.185717
5	1	3.340061	0.000883	-1.668021
6	6	1.804613	-0.000041	1.333555
7	6	0.407493	-0.000186	1.911838
8	1	-0.163296	0.881507	1.620913
9	1	0.500623	-0.000510	2.997188
10	1	-0.163339	-0.881675	1.620375
11	1	2.365566	-0.877965	1.648299
12	1	2.365548	0.877763	1.648670
13	6	1.157793	1.214337	-0.759100
14	6	1.566320	2.547804	-0.174305
15	1	1.017410	3.309273	-0.725768
16	1	2.630654	2.761369	-0.268191
17	1	1.261040	2.642805	0.865848
18	1	1.362143	1.170174	-1.828378
19	1	0.092277	1.063894	-0.613535
20	6	1.158160	-1.213757	-0.759684
21	6	1.566524	-2.547317	-0.174991
22	1	2.631008	-2.760557	-0.267968
23	1	1.018300	-3.308733	-0.727206
24	1	1.260267	-2.642760	0.864837
25	1	0.092547	-1.063489	-0.614589
26	1	1.363060	-1.169333	-1.828845
27	17	-2.055815	2.302612	-0.099079
28	17	-2.195042	-0.000183	-0.149172
29	17	-2.054468	-2.303257	-0.098775

cation-encounter-complex-pair --- [NEt ₃ Me] ⁺ [EC] ⁻				
1	6	1.816408	1.025532	-1.123072
2	7	1.823485	0.033561	-0.004280
3	6	0.977803	0.561889	1.140960
4	6	1.345285	1.951596	1.617253
5	6	1.194809	-1.237828	-0.540549
6	6	1.015353	-2.345338	0.472978
7	6	3.223839	-0.203534	0.488392
8	6	4.148006	-0.884039	-0.502045
9	17	-1.886340	0.395388	-0.932461
10	17	-1.346852	2.642290	-0.585514
11	17	-2.200836	-1.846225	-1.160288
12	1	2.429812	1.878493	-0.847905
13	1	0.789403	1.347988	-1.289782
14	1	2.215136	0.550500	-2.013978
15	1	1.952347	-2.662952	0.932099
16	1	0.591912	-3.194481	-0.060652
17	1	0.297561	-2.074910	1.244234
18	1	0.230660	-0.945332	-0.946266
19	1	1.825773	-1.556319	-1.366835
20	1	4.200753	-0.352675	-1.450637
21	1	3.862536	-1.916699	-0.689910
22	1	5.149668	-0.891451	-0.075610
23	1	3.615570	0.772967	0.760947
24	1	3.135944	-0.793304	1.398612
25	1	1.169392	2.698631	0.847276
26	1	2.363583	2.024753	1.997153
27	1	0.669782	2.190182	2.437483
28	1	-0.047383	0.550752	0.779190
29	1	1.073363	-0.165028	1.943566
30	6	-2.084603	-0.804885	2.292375
31	8	-3.216642	-0.791388	2.360462

cation-transition state-pair				---	[NEt ₃ Me] ⁺ [TS] ⁻
1	6	-0.994615	-0.808380	-1.493237	
2	7	0.068441	-0.415770	-0.519753	
3	6	0.121861	1.099510	-0.418132	
4	6	0.276936	1.829650	-1.736117	
5	6	-0.339283	-0.965895	0.834967	
6	6	0.681158	-0.764936	1.935334	
7	6	1.407971	-0.935465	-0.953234	
8	6	1.529155	-2.446556	-0.976242	
9	17	-0.786860	2.625886	2.517084	
10	17	-3.248863	0.962484	0.454727	
11	17	1.372789	2.932226	2.476965	
12	1	-0.676573	-0.532128	-2.494410	
13	1	-1.910683	-0.289258	-1.209052	
14	1	-1.144075	-1.881978	-1.435376	
15	1	1.604317	-1.318124	1.762974	
16	1	0.240329	-1.144066	2.856238	
17	1	0.919449	0.282997	2.104905	
18	1	-1.284888	-0.471186	1.062253	
19	1	-0.539456	-2.024418	0.679963	
20	1	0.810929	-2.908206	-1.650833	
21	1	1.416221	-2.884793	0.013090	
22	1	2.524932	-2.698817	-1.337003	
23	1	1.584926	-0.528859	-1.945818	
24	1	2.140610	-0.497954	-0.278044	
25	1	-0.603398	1.723973	-2.366529	
26	1	1.165521	1.543747	-2.297414	
27	1	0.374528	2.887139	-1.494426	
28	1	-0.817631	1.384253	0.052429	
29	1	0.945098	1.332214	0.252712	
30	6	-2.914772	2.355341	2.558150	
31	8	-3.925002	2.555809	3.042568	

cation-intermediate complex-pair --- [NEt₃Me]⁺[IC]⁻

1	6	-2.584915	-2.121630	-0.072786
2	7	-2.046890	-0.741211	-0.023410
3	6	-3.049250	0.183269	0.644590
4	6	-4.248097	0.542401	-0.209746
5	6	-1.769945	-0.241610	-1.430947
6	6	-0.544908	-0.845974	-2.087505
7	6	-0.751645	-0.714366	0.766831
8	6	-0.910406	-0.872015	2.264996
9	17	-0.784120	2.584984	0.079077
10	1	-2.738850	-2.482563	0.939762
11	1	-1.875851	-2.764257	-0.586090
12	1	-3.530225	-2.118421	-0.607412
13	1	-1.469038	-1.760870	2.558723
14	1	-1.364884	0.008371	2.712959
15	1	0.091952	-0.965606	2.681078
16	1	-0.135621	-1.511337	0.356089
17	1	-0.310376	0.258655	0.544706
18	1	-4.775562	-0.321582	-0.614610
19	1	-3.968693	1.211674	-1.019856
20	1	-4.947243	1.081676	0.427270
21	1	-3.357869	-0.327791	1.554521
22	1	-2.486681	1.087861	0.885151
23	1	0.371686	-0.488100	-1.623562
24	1	-0.536857	-0.509989	-3.123184
25	1	-0.541875	-1.936227	-2.097708
26	1	-2.668223	-0.463559	-2.003645
27	1	-1.637513	0.837809	-1.328595
28	17	2.263094	1.233042	-0.017966
29	6	3.539237	0.072422	-0.011595
30	17	2.905561	-1.587926	0.032101
31	8	4.699054	0.303255	-0.032419

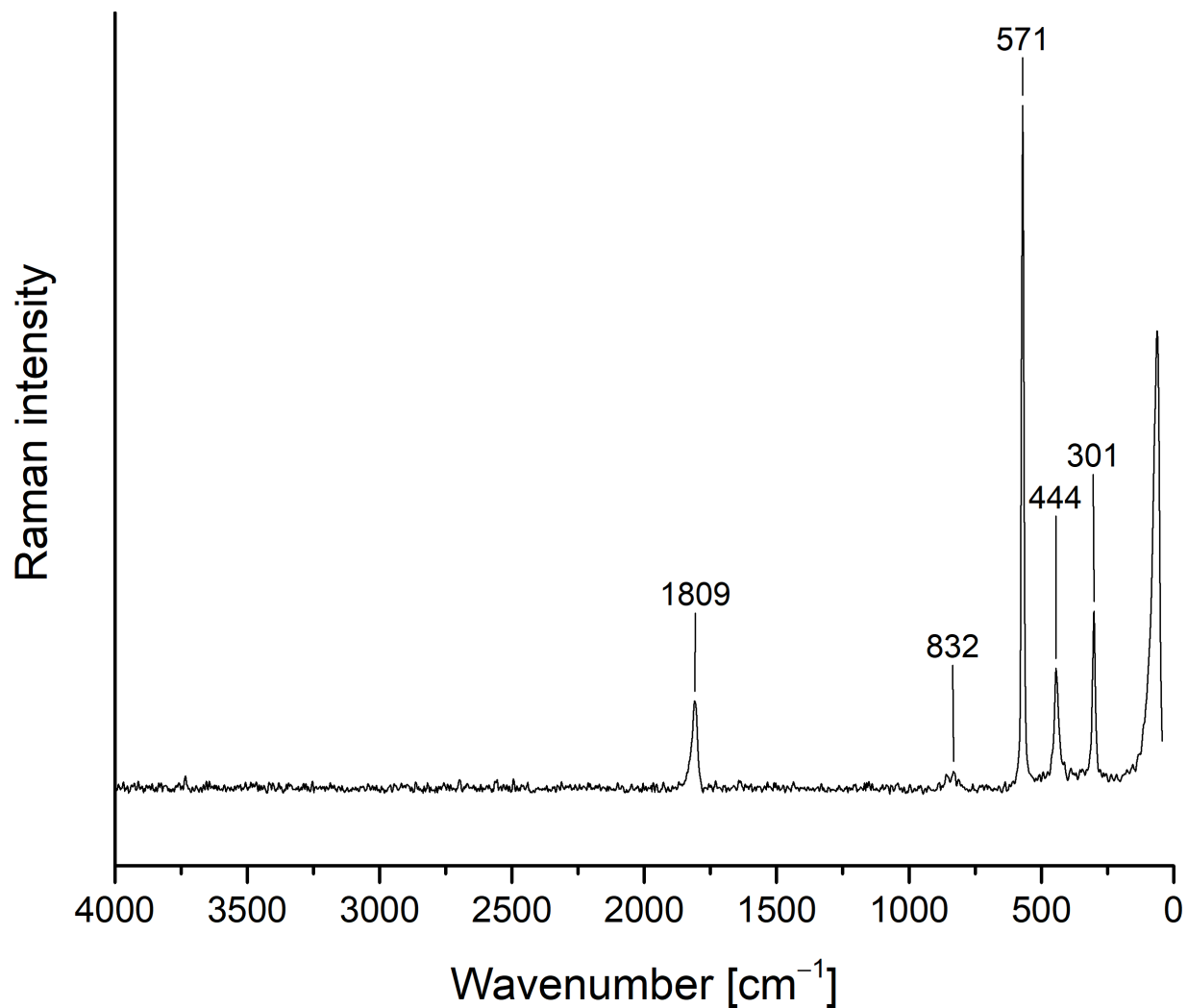
Spectra[NEt₃Me][Cl₃] + CO (bulk)

Fig. S5. Raman spectrum of purified COCl₂ obtained from the reaction of [NEt₃Me][Cl₃] + CO in *o*DCB.

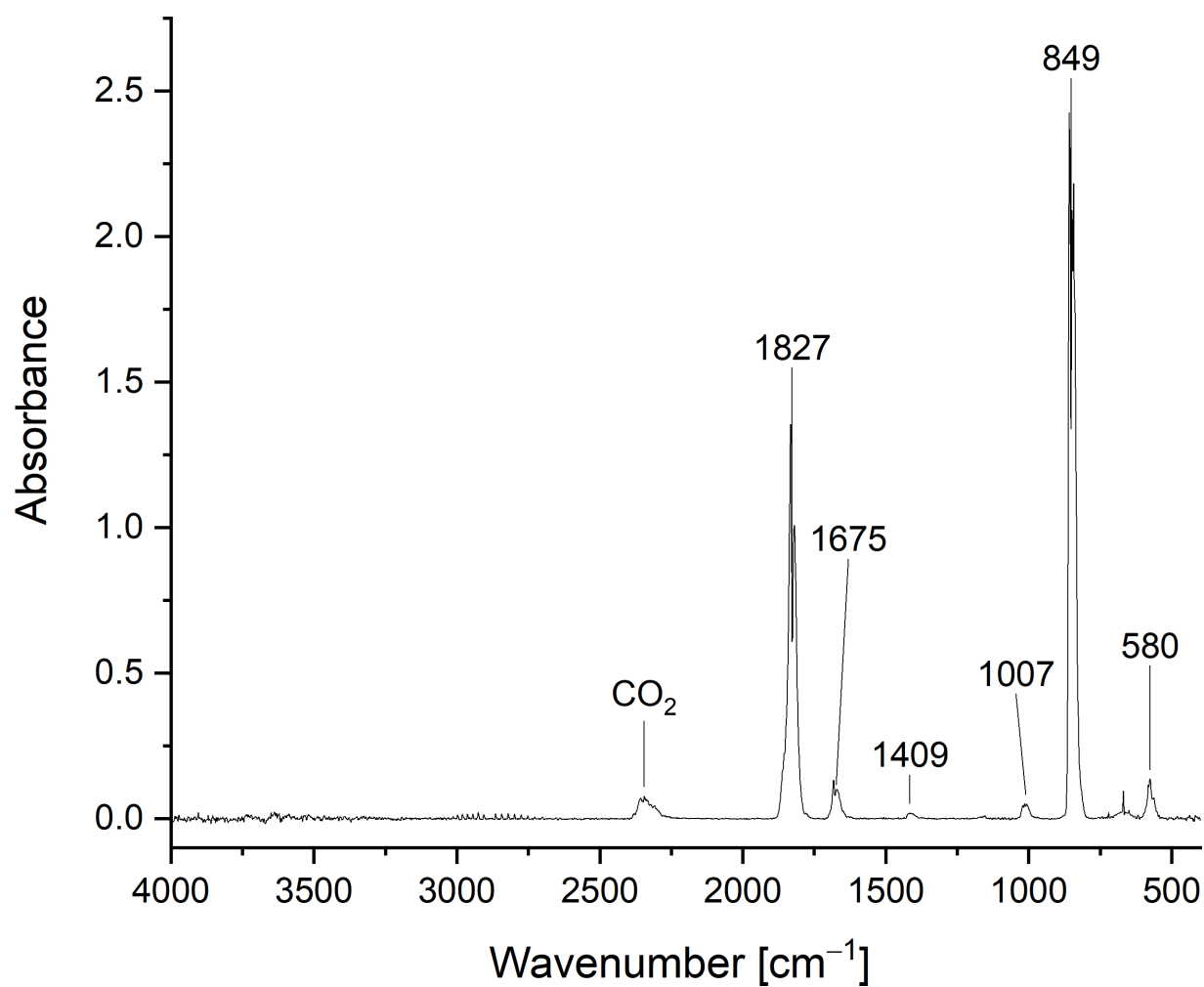


Fig. S6. Gas-phase IR spectrum of purified COCl₂ obtained from the reaction of [NEt₃Me][Cl₃] + CO in *o*DCB.

3.5 mol% [NEt₃Me]Cl + Cl₂ + CO (bulk)

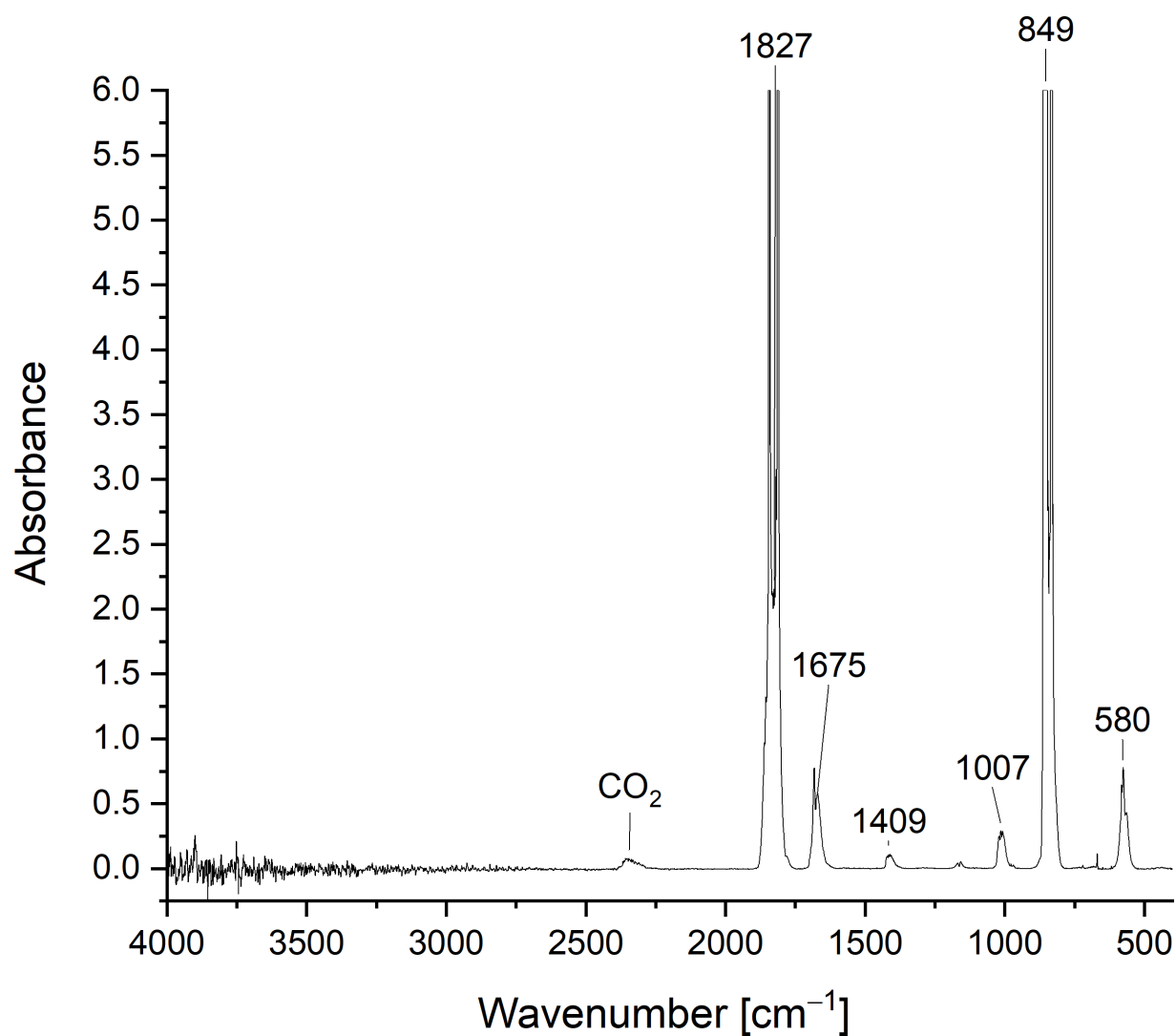


Fig. S7. Gas-phase IR spectrum of purified COCl₂ obtained from the reaction of Cl₂ + CO in *o*DCB catalyzed by 3.5 mol% [NEt₃Me]Cl.

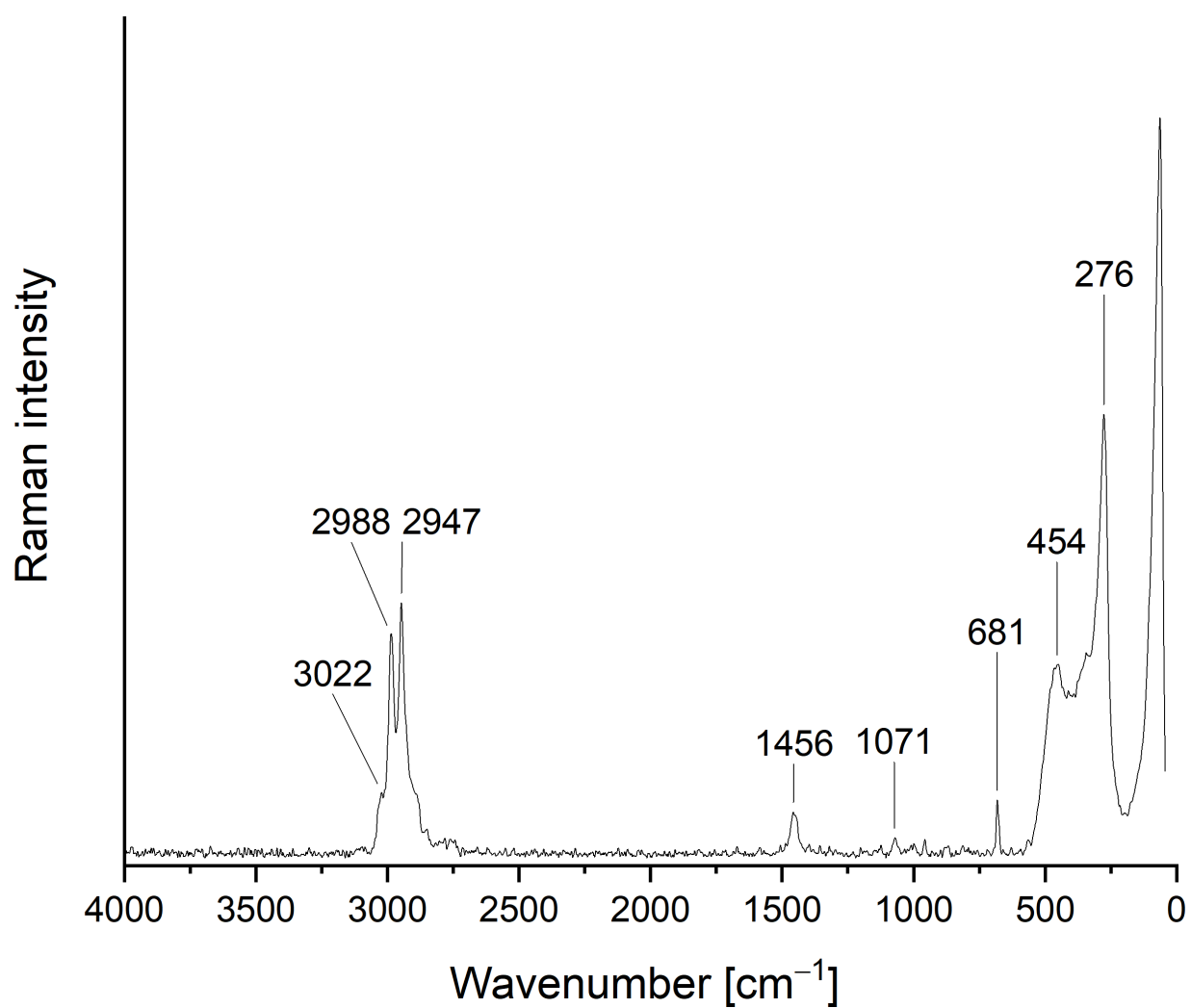


Fig. S8. Raman spectrum of $[\text{NEt}_3\text{Me}][\text{Cl}(\text{Cl}_2)_{1.45}]$

[NEt₃Me]Cl + CO + Cl₂ (flow)

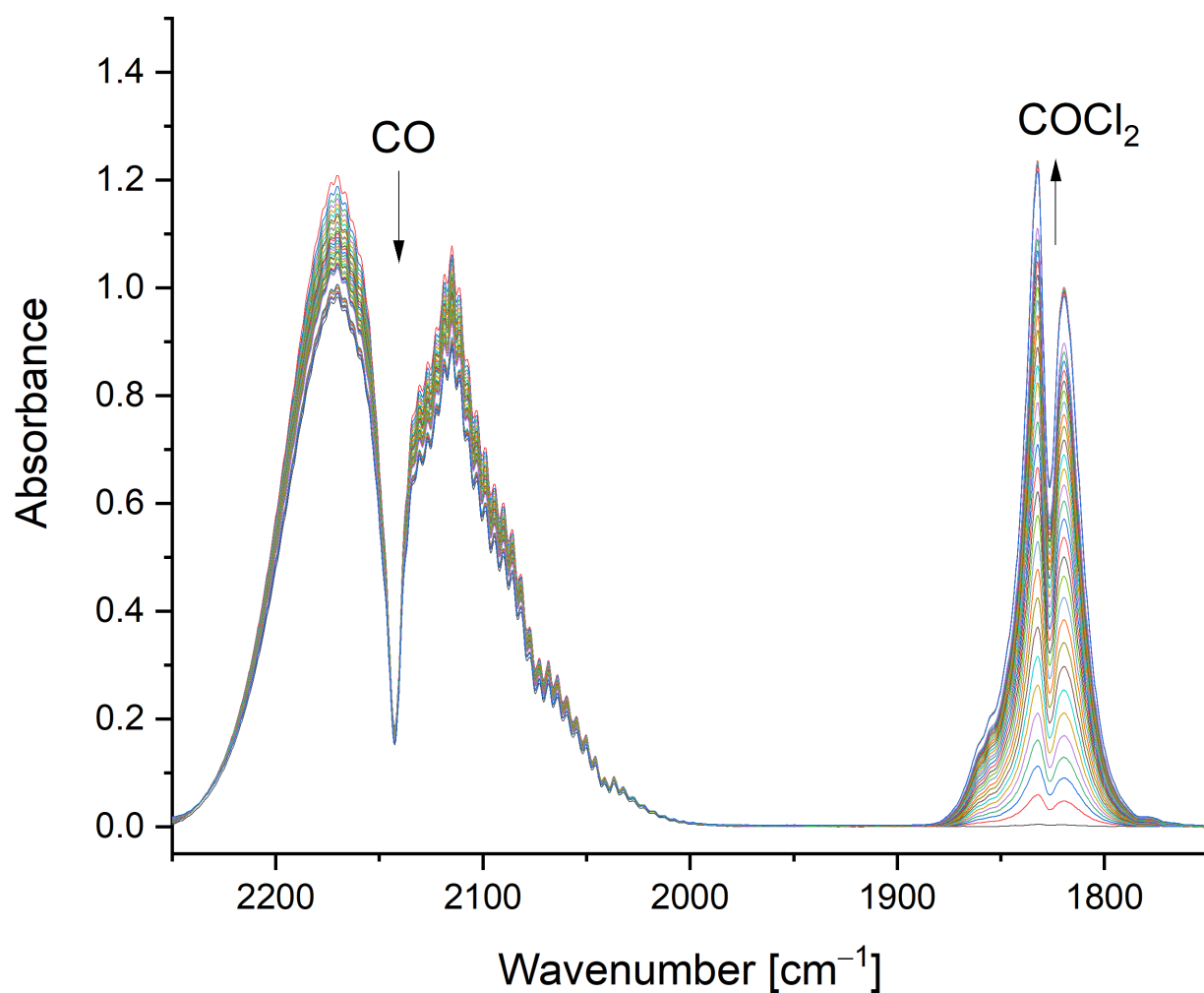


Fig. S9. Time-dependent gas-phase IR spectra of the gaseous constituents obtained from the reaction of [NEt₃Me]Cl + CO + Cl₂. Spectra were recorded after 0, 6, 11, 16, 21, 26, 31, 36, 41, 46, 51, 56, 61, 66, 71, 76, 81, 86, 91, 96, 101, 106, 111, 116, 121, 126, 131, 136, 141, 184, 191, 196, 201, 206, 211, 216, 221, 226 min.

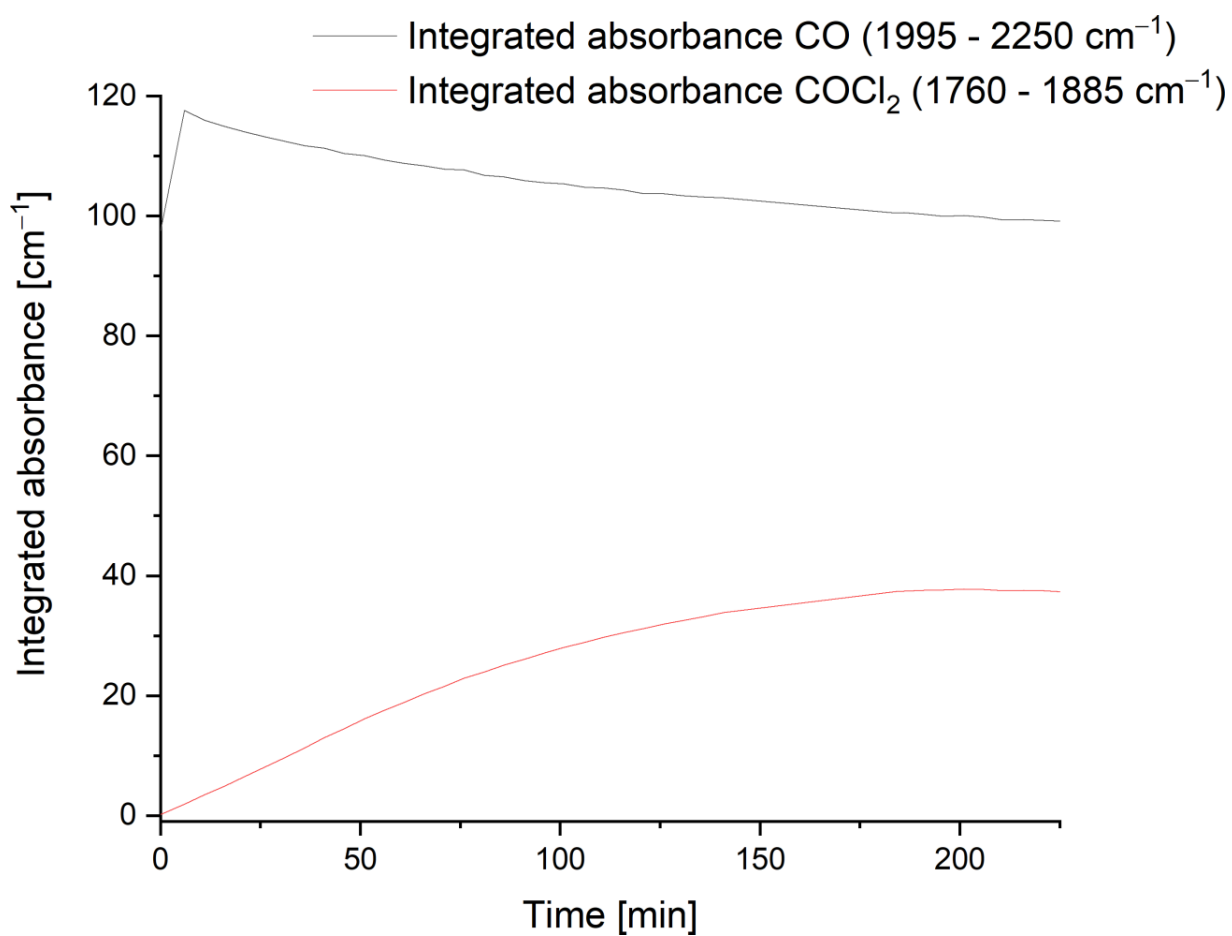


Fig. S10. Time-dependent integrated gas-phase IR absorbances for the CO stretching bands of CO (black line, 1995 – 2250 cm^{-1}) and COCl_2 (red line, 1760 – 1885 cm^{-1}) taken for the reaction of $[\text{NEt}_3\text{Me}]\text{Cl} + \text{CO} + \text{Cl}_2$ at reaction times between 0 and 226 min.

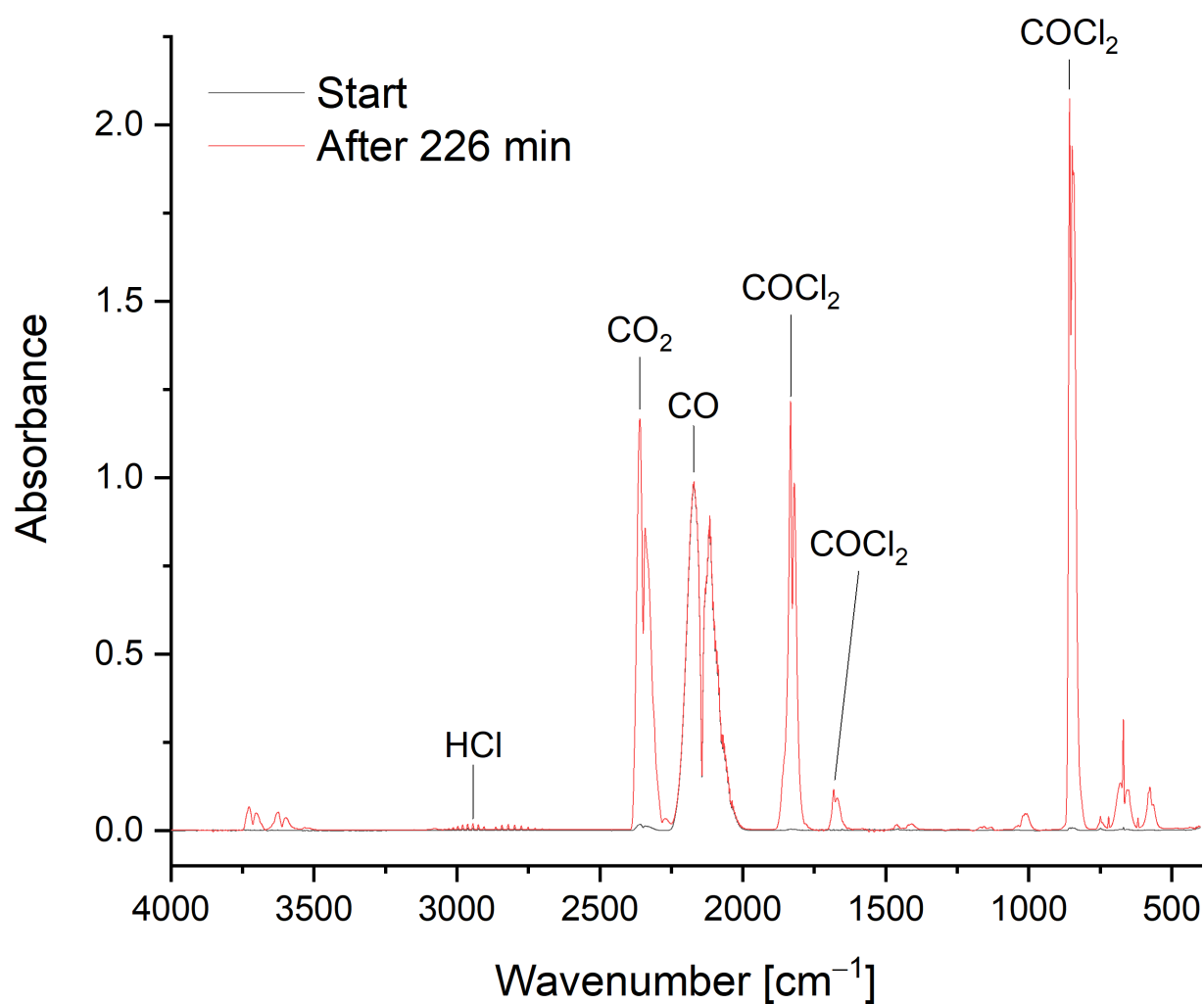


Fig. S11. Gas-phase IR spectra of the gaseous constituents obtained in the reaction of $[\text{NEt}_3\text{Me}]\text{Cl} + \text{CO} + \text{Cl}_2$ after a reaction time of 0 (black spectrum) and 226 min (red spectrum), respectively.

[NEt₃Me][Cl₃] + CO (flow)

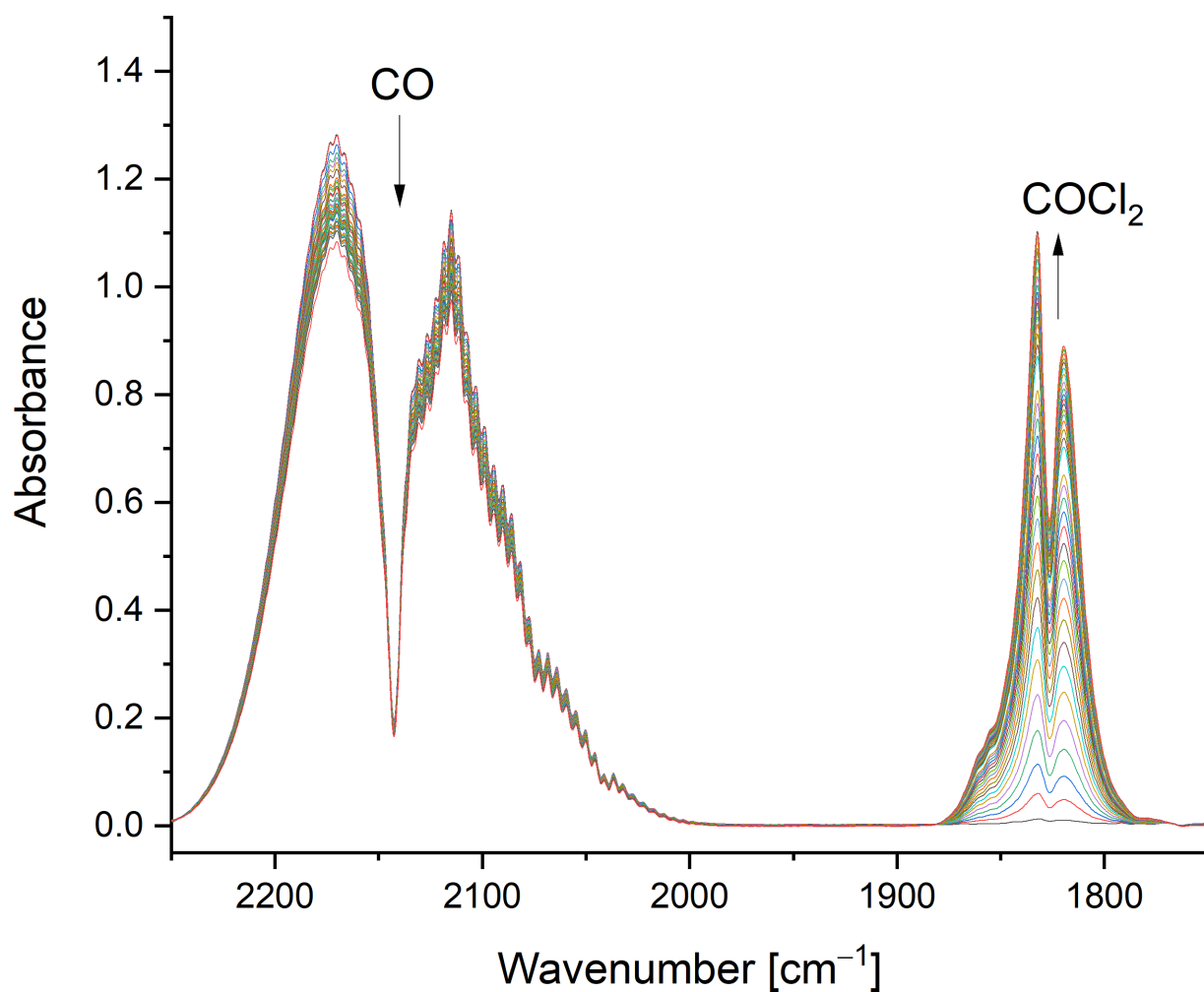


Fig. S12. Time-dependent gas-phase IR spectra of the gaseous constituents obtained from the reaction of [NEt₃Me][Cl₃] + CO. Spectra were recorded after 0, 5, 10, 15, 20, 25, 30, 35, 40, 45, 50, 55, 60, 65, 70, 75, 80, 85, 98, 103, 108, 113, 123, 128, 133, 138, 144, 154, 164, 174, 184, 194, 204, 214, 224 min.

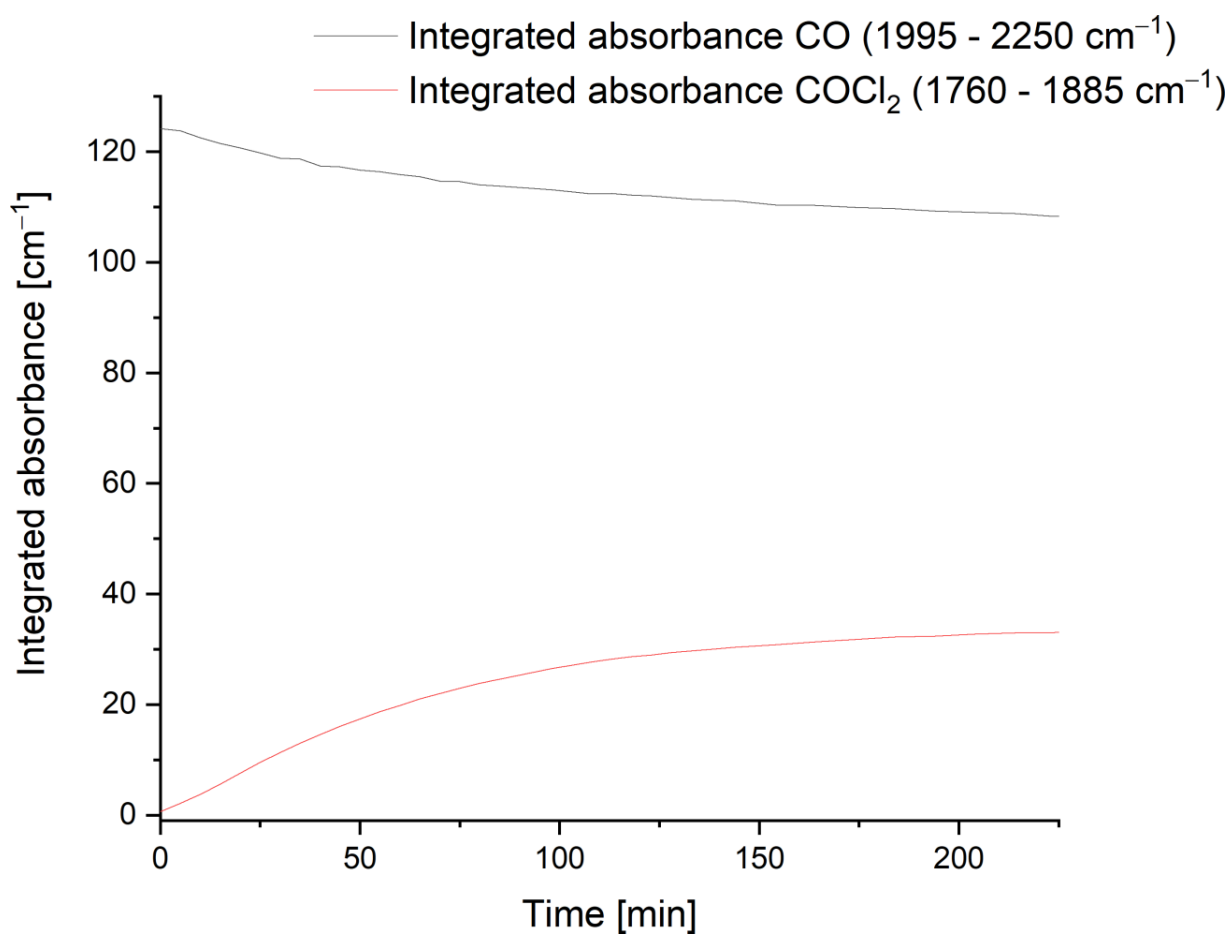


Fig. S13. Time-dependent integrated gas-phase IR absorbances for the CO stretching bands of CO (black line, 1995 – 2250 cm^{-1}) and COCl_2 (red line, 1760 – 1885 cm^{-1}) taken for the reaction of $[\text{NET}_3\text{Me}][\text{Cl}_3] + \text{CO}$ at reaction times between 0 and 224 min.

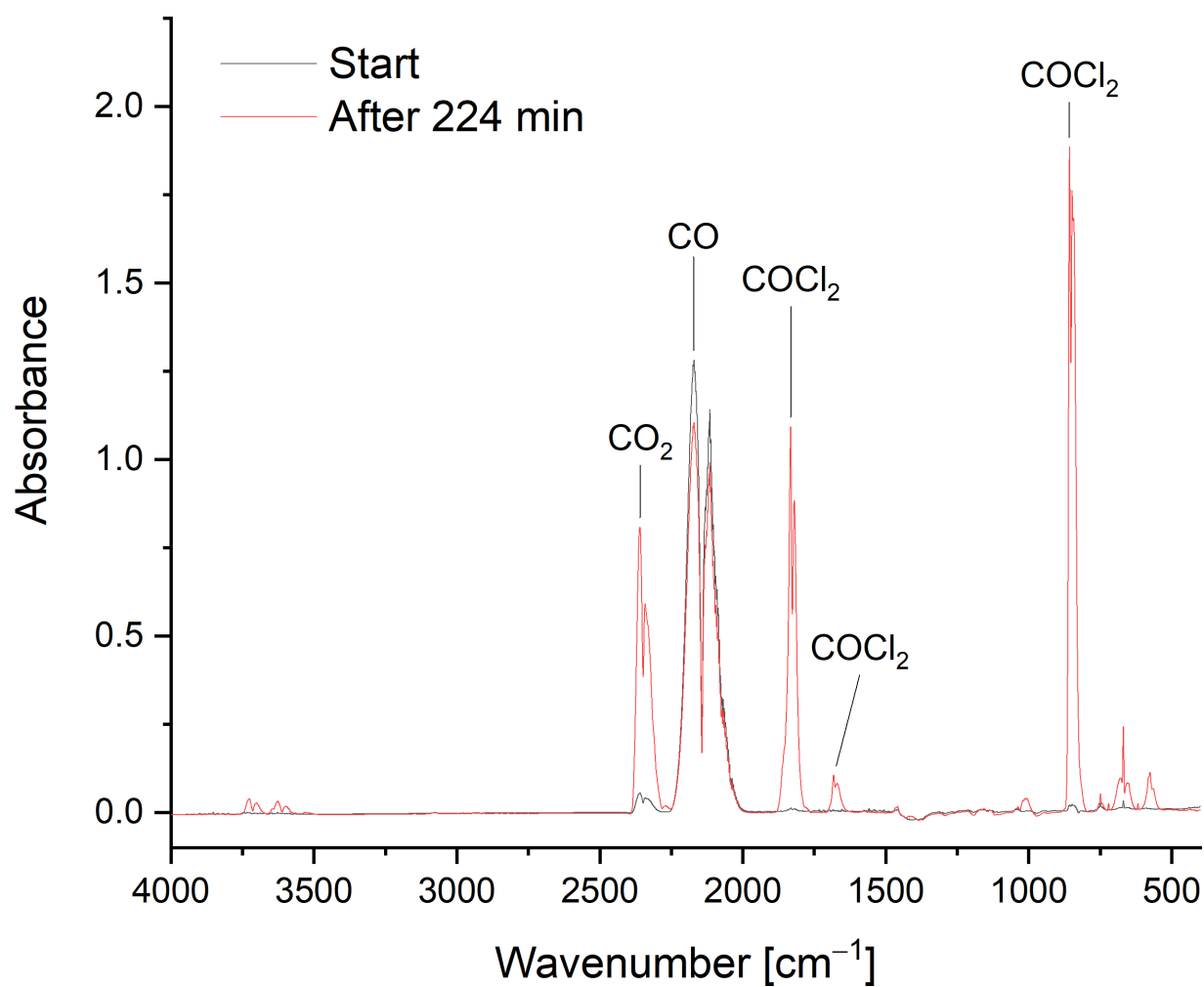


Fig. S14. Gas-phase IR spectra of the gaseous constituents obtained from the reaction of $[\text{NEt}_3\text{Me}][\text{Cl}_3] + \text{CO}$ and at reaction times of 0 (black spectrum) and 224 min (red spectrum), respectively.

[NEt₄]Cl + CO + Cl₂ (flow)

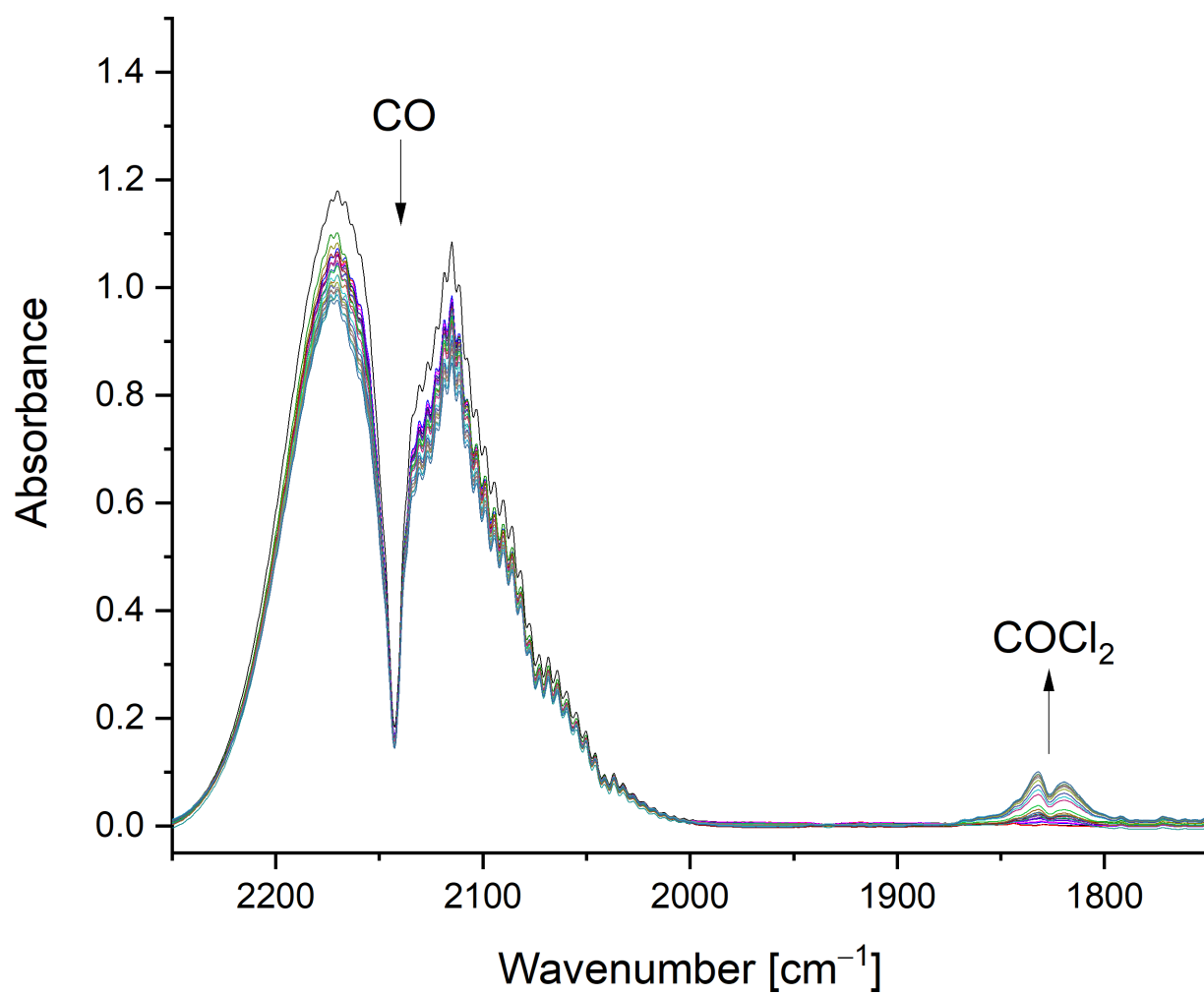


Fig. S15. Time-dependent gas-phase IR spectra of the gaseous constituents obtained from the reaction of [NEt₄]Cl + CO + Cl₂. Spectra were recorded after 0, 1, 6, 11, 21, 27, 32, 37, 42, 47, 52, 65, 77, 137, 197, 257, 317, 377, 437, 497, 558, 628 min.

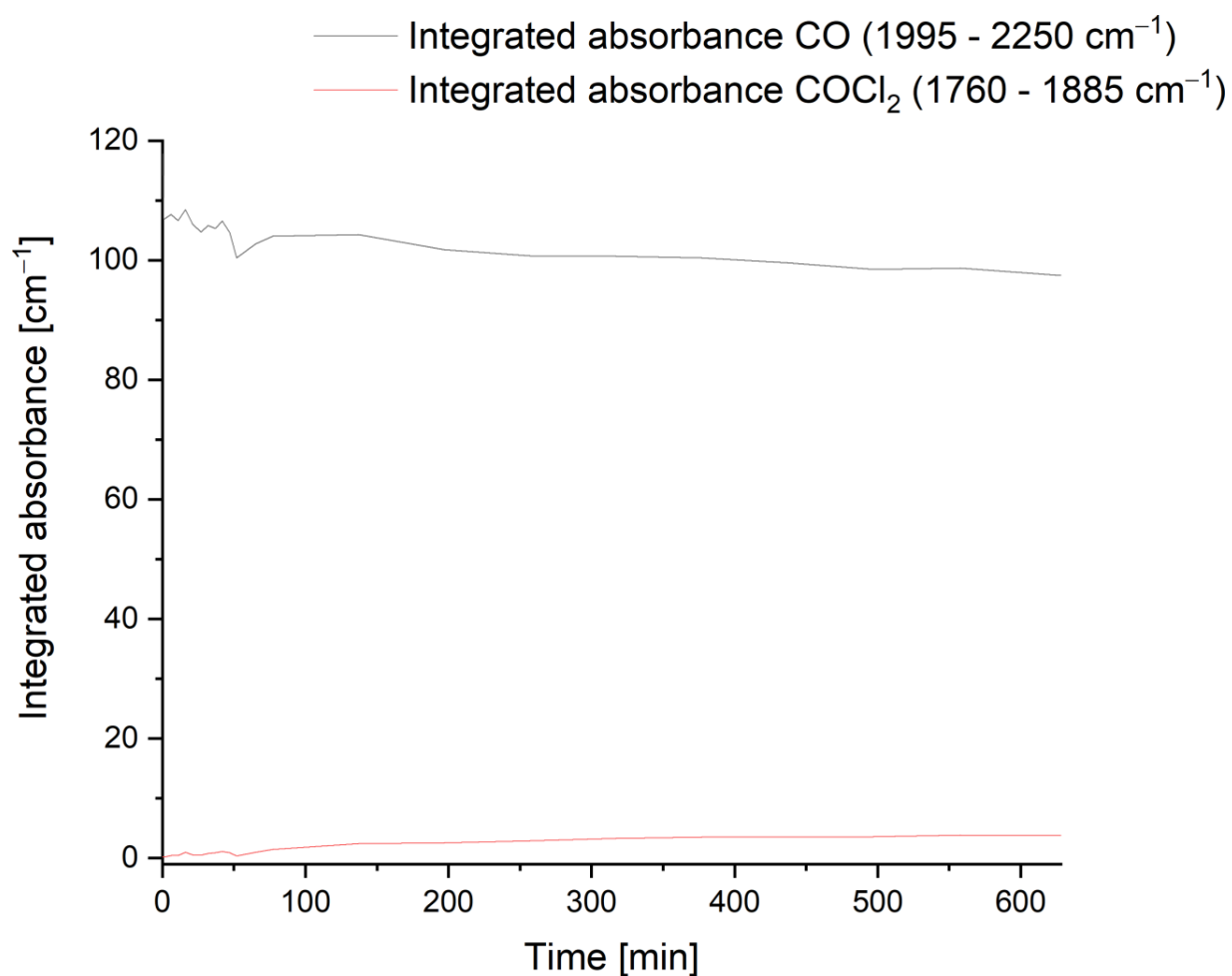


Fig. S16. Time-dependent integrated gas-phase IR absorbances for the CO stretching bands of CO (black line, 1995 – 2250 cm⁻¹) and COCl₂ (red line, 1760 – 1885 cm⁻¹) taken for the reaction of [NEt₄]Cl + CO + Cl₂ at reaction times 0 and 628.

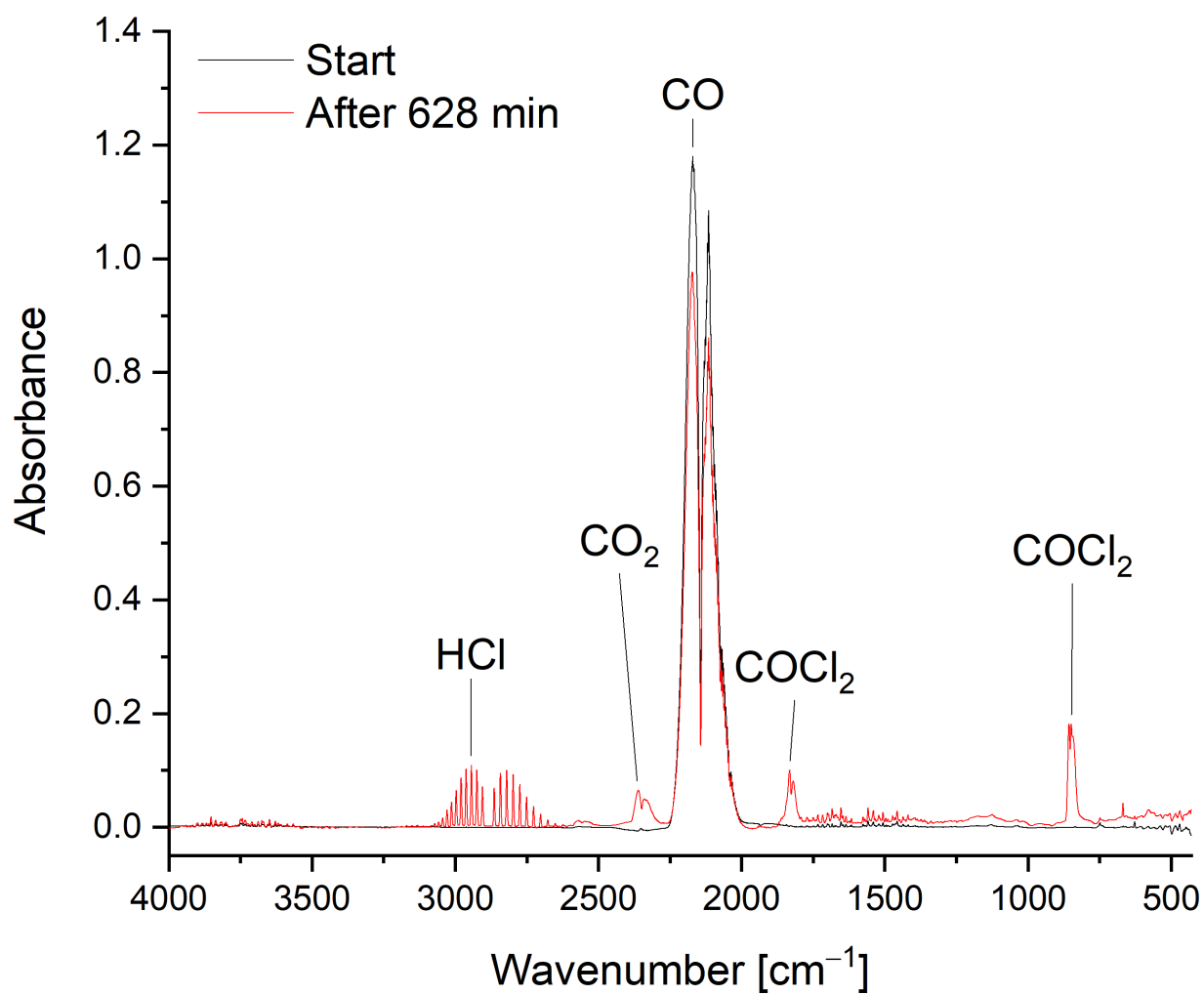


Fig. S17. Gas-phase IR spectra of the gaseous constituents obtained in the reaction of [NEt₄]Cl + CO + Cl₂ at reaction times of 0 and 628, respectively.

CO + Cl₂ (under exclusion of light, flow)

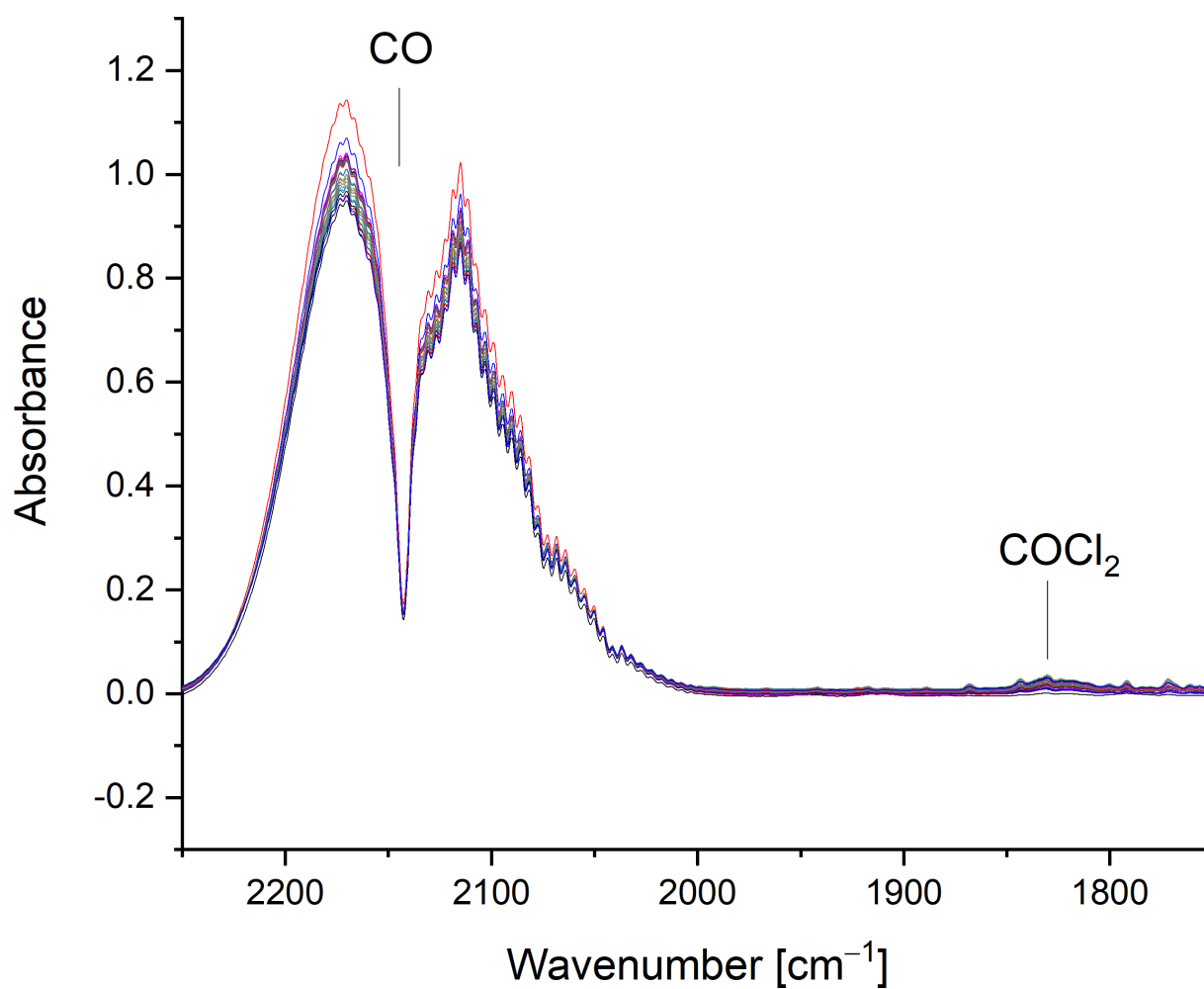


Fig. S18. Time-dependent gas-phase IR spectra of the gaseous constituents obtained from the reaction of Cl₂ + CO. Spectra were recorded after 0, 4, 9, 14, 18, 19, 34, 49, 64, 79, 94, 109, 124, 139, 154, 261, 262, 323, 384, 445, 506, 567, 628, 689, 750, 811 min.

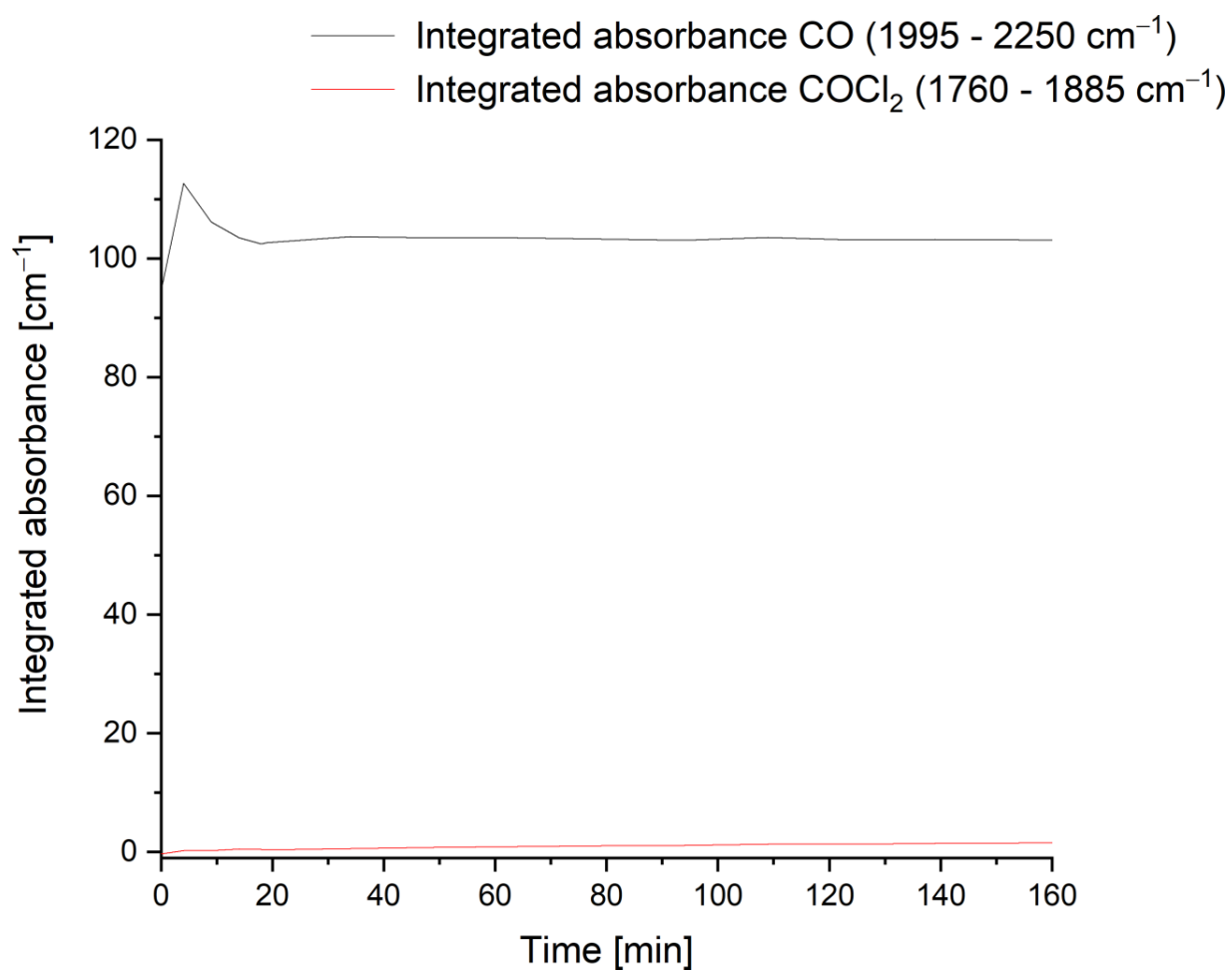


Fig. S19. Time-dependent integrated gas-phase IR absorbances for the CO stretching bands of CO (black line, 1995 – 2250 cm^{-1}) and COCl_2 (red line, 1760 – 1885 cm^{-1}) taken for the reaction $\text{CO} + \text{Cl}_2$ at reaction times 0 and 628.

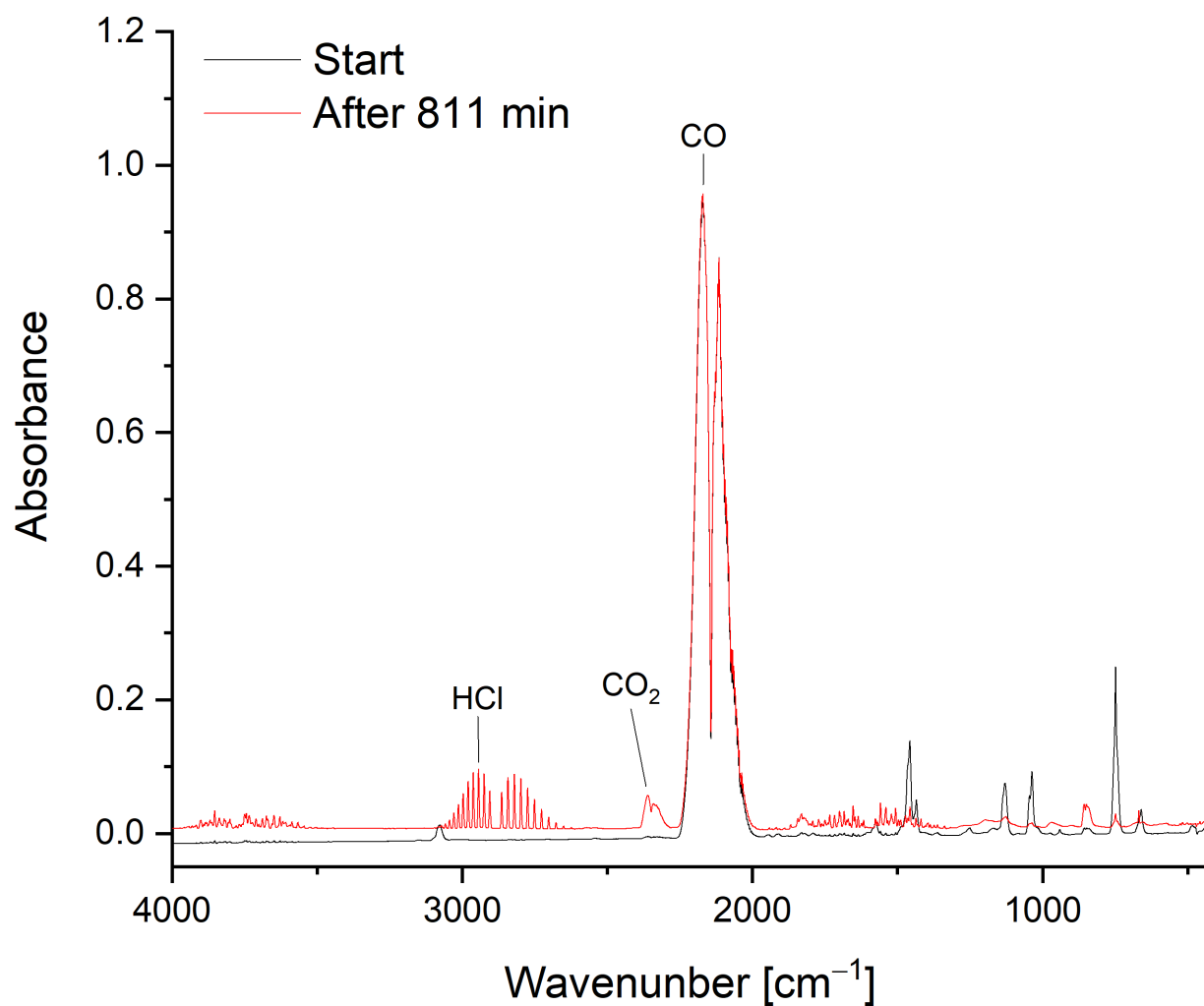


Fig. S20. Gas-phase IR spectra of the gaseous constituents obtained in the reaction of CO + Cl₂ at reaction times of 0 and 811 min, respectively.

CO + Cl₂ (without exclusion of light, flow)

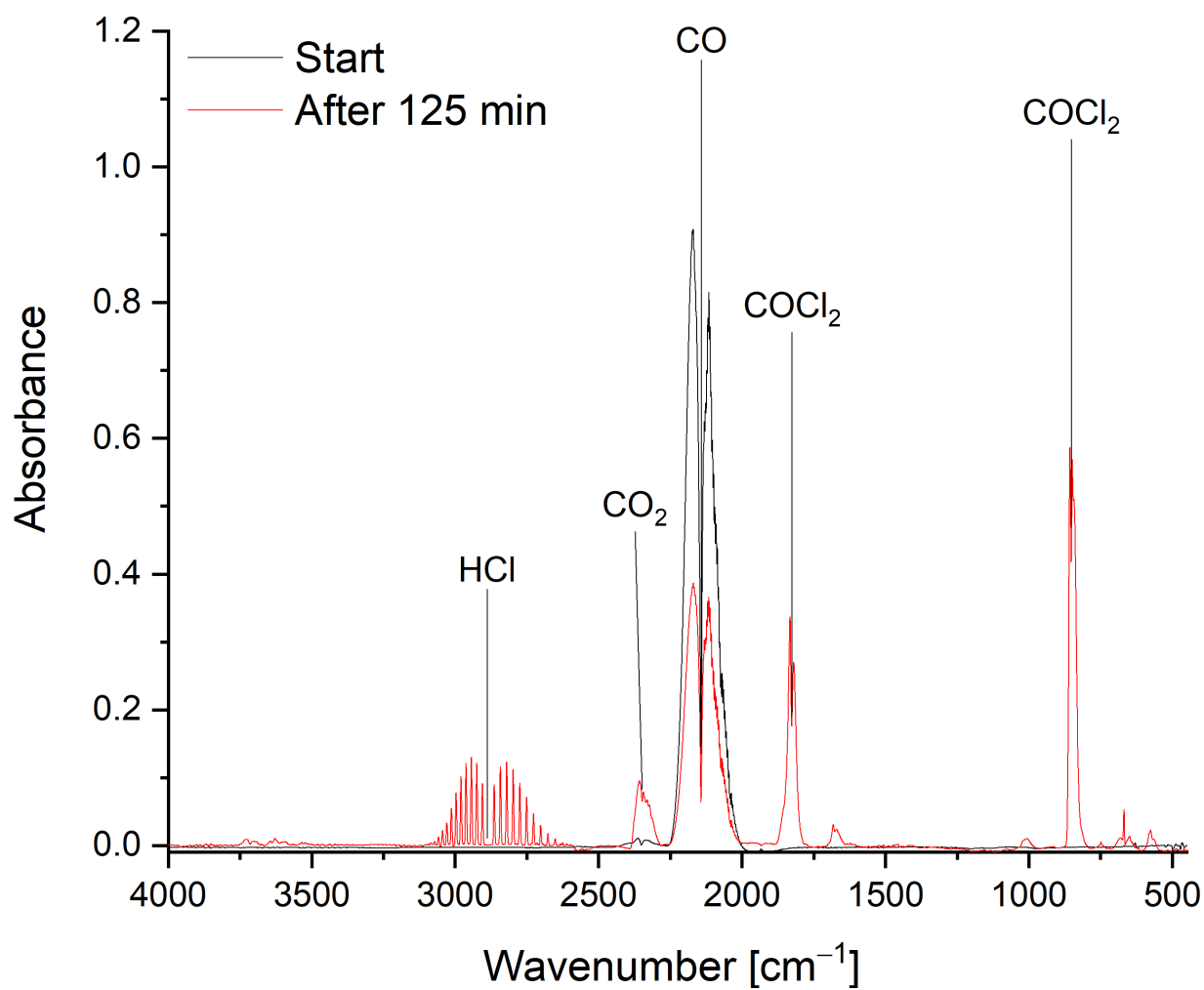


Fig. S21. Gas-phase IR spectra of the gaseous constituents obtained in the reaction of CO + Cl₂ at reaction times of 0 and 125 min, respectively, with continuous UV/Vis measurements.

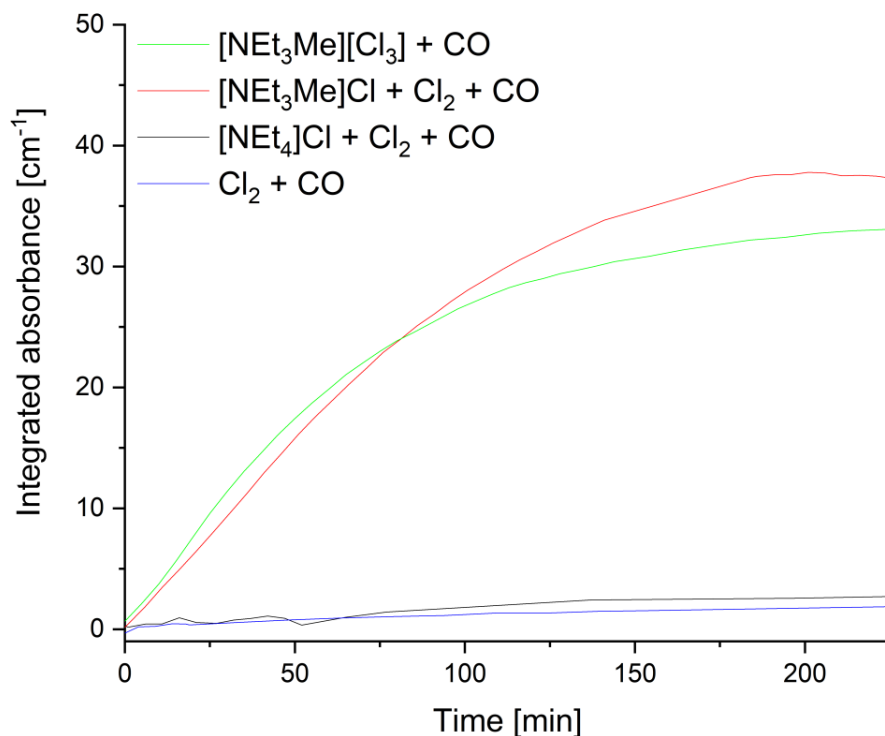
Comparison of the COCl₂ formation using different catalyst systems as well as the uncatalysed reaction

Fig. S22. Comparison of the COCl₂ formation using different catalyst systems. The concentration of COCl₂ is estimated by integrating the IR absorbance of the carbonyl stretching vibration of COCl₂ (1760 – 1885 cm⁻¹). The following conditions were used: dashed - dotted line: [NEt₃Me][Cl(Cl₂)_{1.50}] (0.783 g, 3.033 mmol [NEt₃Me]Cl + 4.555 mmol Cl₂), 20 mL *o*DCB, 1000 mbar CO (22.32 mmol); dashed line: [NEt₃Me]Cl (0.460 g, 3.033 mmol), 20 mL *o*DCB, 1000 mbar CO (22.32 mmol), and 208 mbar Cl₂ (4.65 mmol); dotted line: [NEt₄]Cl (0.230 g, 1.393 mmol), 850 mbar CO (20.20 mmol), 150 mbar Cl₂ (3.530 mmol); continuous line: 850 mbar CO (20.20 mmol), 150 mbar Cl₂ (3.53 mmol) in 20 mL *o*DCB (under exclusion of light). See Materials and Methods for detailed description.

[NEt₃Me]Cl + Cl₂ + CH₄

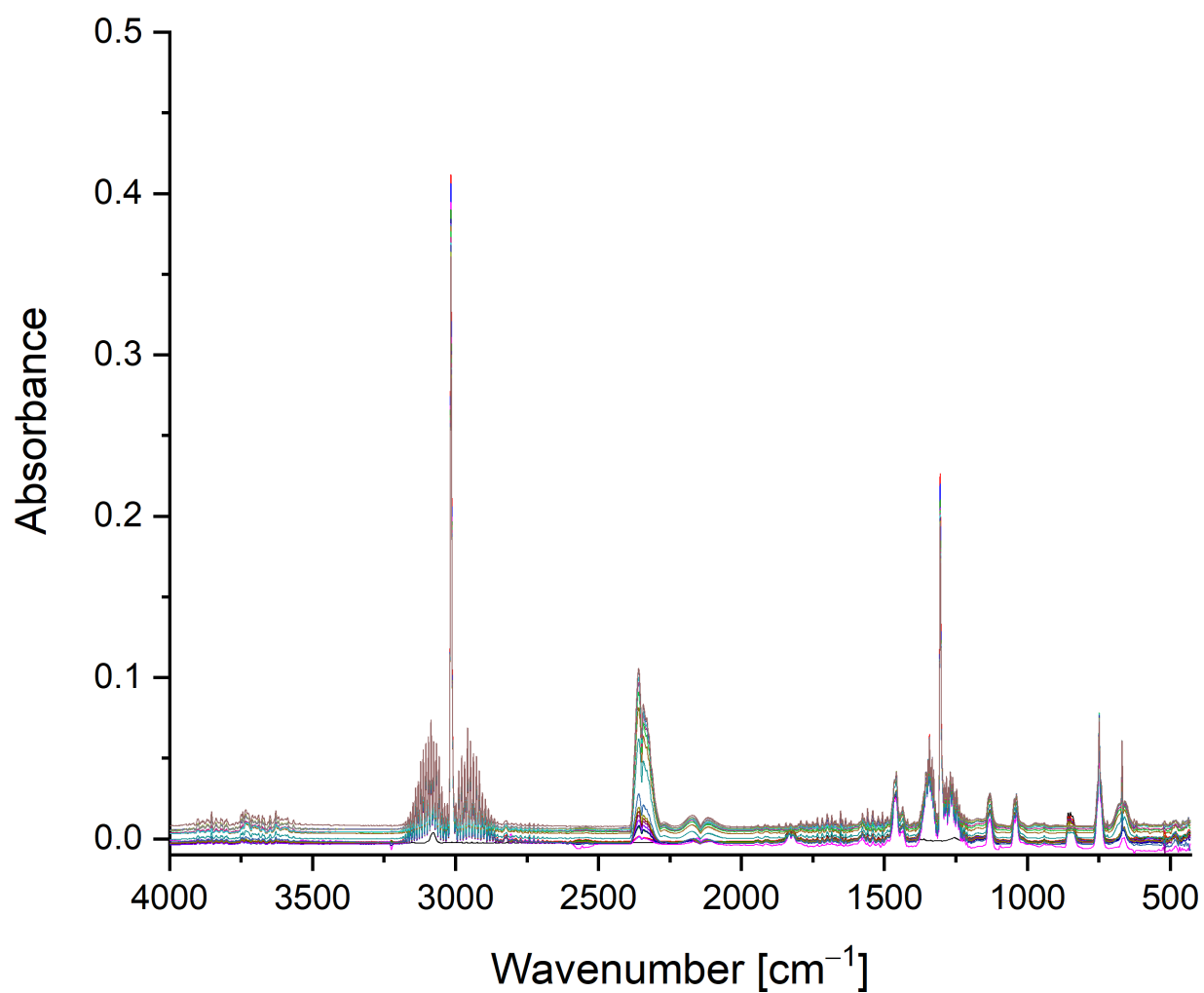


Fig. S23. Gas-phase IR spectra of the gaseous constituents obtained during the reaction of [NEt₃Me]Cl + Cl₂ + CH₄. Spectra were recorded after 0, 3, 6, 9, 12, 15, 19, 22, 25, 28, 39, 40, 100, 161, 221, 282, 342, 403, 363, 524 min.

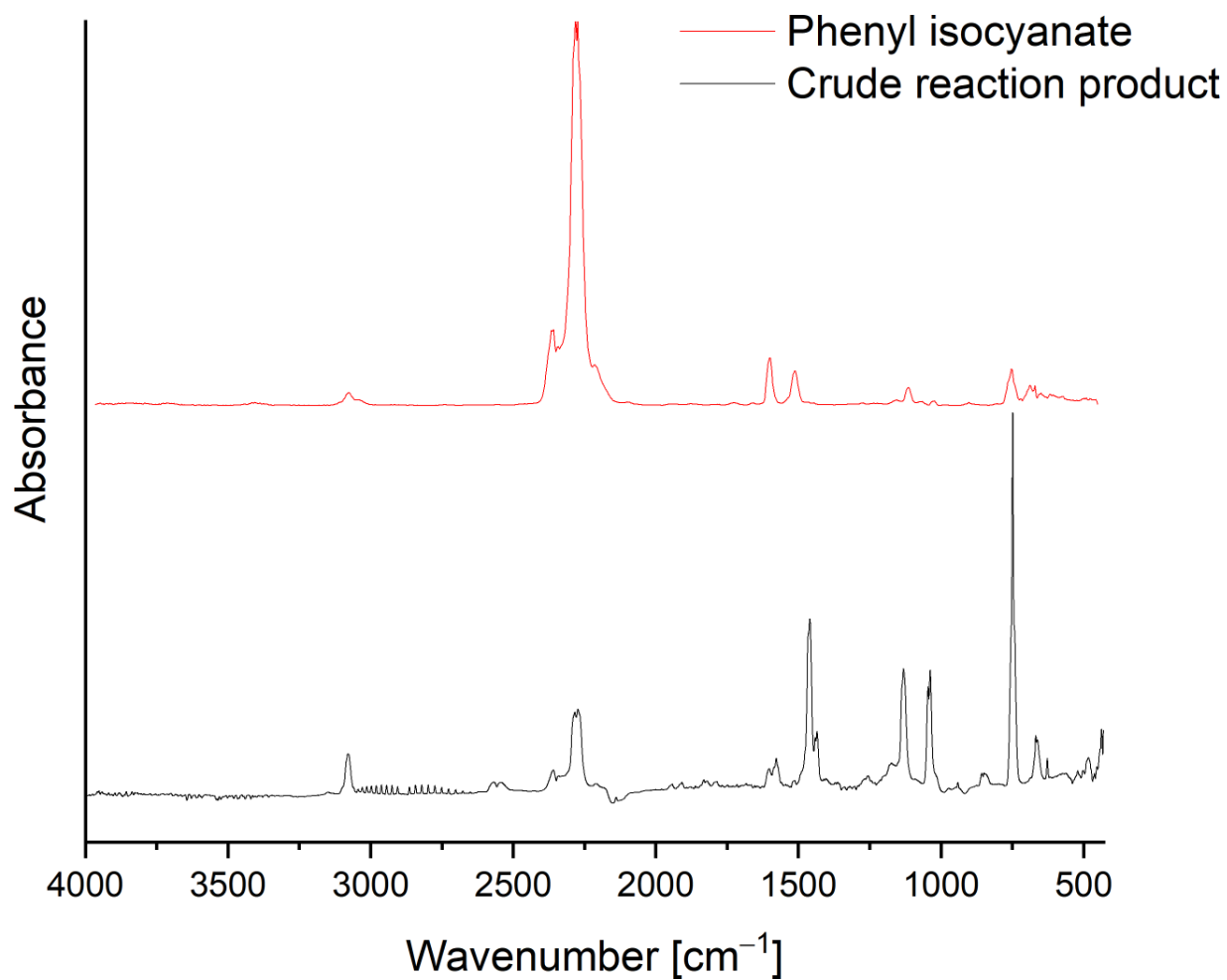
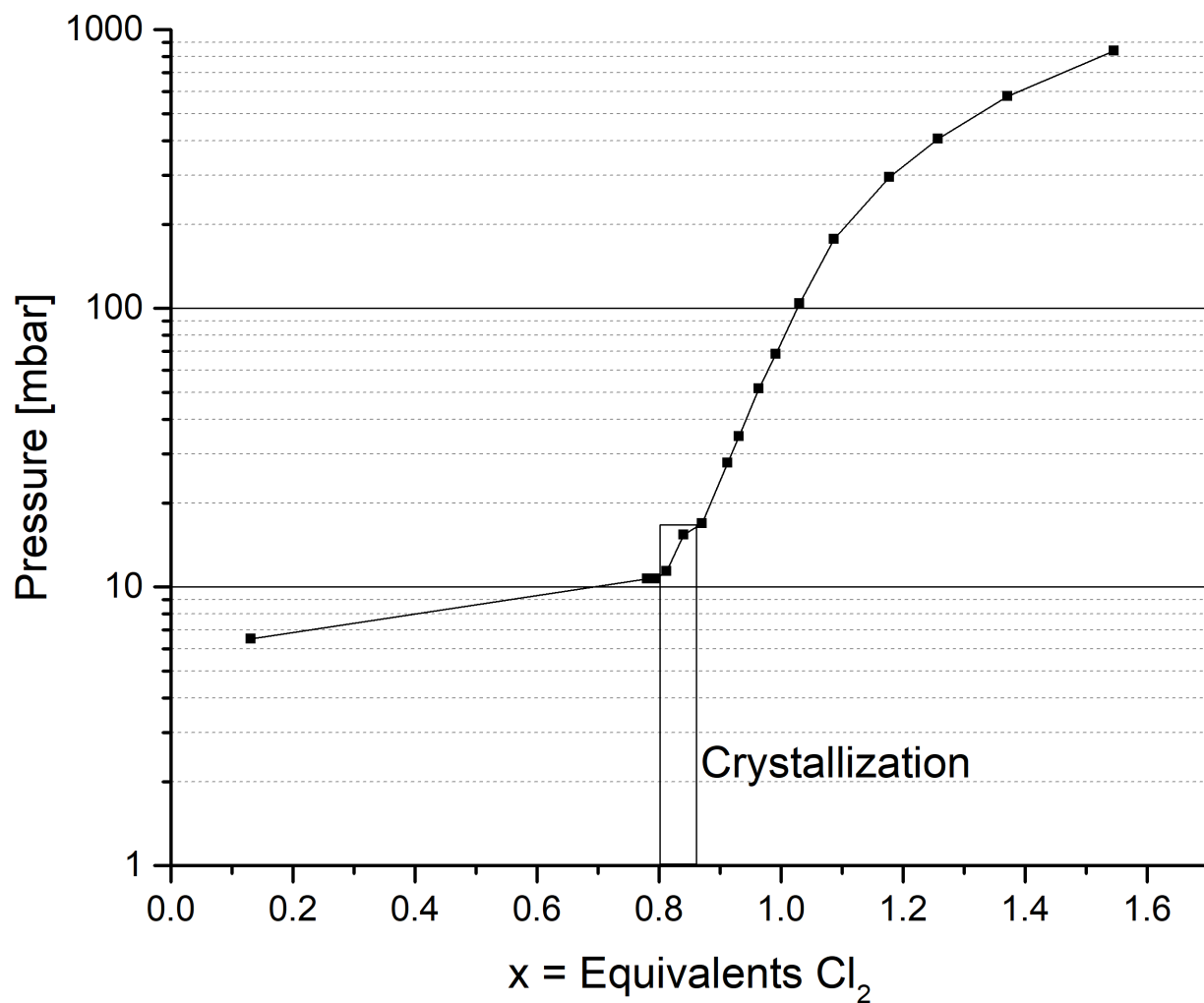


Fig. S24. Comparison of the gas-phase IR spectrum of the crude reaction product obtained from the reaction $\text{PhNH}_2 + \text{COCl}_2$ (black) with the gas-phase IR spectrum of neat phenyl isocyanate (red). (56)

Vapor Pressure Curve of pristine $[\text{NEt}_3\text{Me}][\text{Cl}(\text{Cl}_2)_x]$ **Fig. S25.** Vapor pressure of pristine $[\text{NEt}_3\text{Me}][\text{Cl}(\text{Cl}_2)_x]$ depending on x.

Half-life time estimation for the reaction of [NEt₃Me]Cl₃ and CO in oDCBDescription of the procedure

The half-life time for the CO consumption of the reaction of [NEt₃Me]Cl₃ with CO in oDCB, was estimated in three different experiments, carried out under similar conditions and amount of starting materials (see table S1), but different reaction times. The reaction was carried out as followed:

[NEt₃Me]Cl was loaded into a 250 mL Schlenk flask, dried *in vacuo* at 150 °C for 1 hour and suspended in 10 mL dry *o*-Dichlorobenzene (*o*DCB). The solution was degassed and chlorine was added until the system retained a pressure of 200 mbar. 800 mbar of CO were added to the flask and the reaction mixture was stirred, under the exclusion of light, for 62, 202 and 1000 min, respectively. CO was then removed from the reaction mixture by freeze-pump-thaw-degassing (CO is the only reactant with a residual vapor pressure at a temperature of -196 °C). To determine the amount of consumed CO the flask was weighted befor and after the degassing.

Table S4. Amount of chemicals used in the reactions.

Batch	1	2	3
<i>m</i>([NEt₃Me]Cl) [mg]	369	363	360
<i>n</i>([NEt₃Me]Cl) [mmol]	2.43	2.39	2.37
<i>m</i>(Cl₂) [mg]	551	560	567
<i>n</i>(Cl₂) [mmol]	7.77	7.90	8.00
<i>m</i>(CO) [mg]	241	248	247
<i>n</i>(CO) [mmol]	8.60	8.85	8.82
<i>m</i>(CO (used)) [mg]	27	94	190
<i>m</i>(CO (left)) [mg]	214	154	57
<i>n</i>(CO (left)) [mmol]	7.64	5.50	2.04
reaction time [min]	62	202	1000

The uncertainties of measured masses and reaction times are estimated to be ±5 mg (due to residual grease from the joints) and ±5 min, respectively. The following error propagation is assumed:

$$\delta m = \delta n = \delta \left(\frac{1}{n} \right) \quad (1)$$

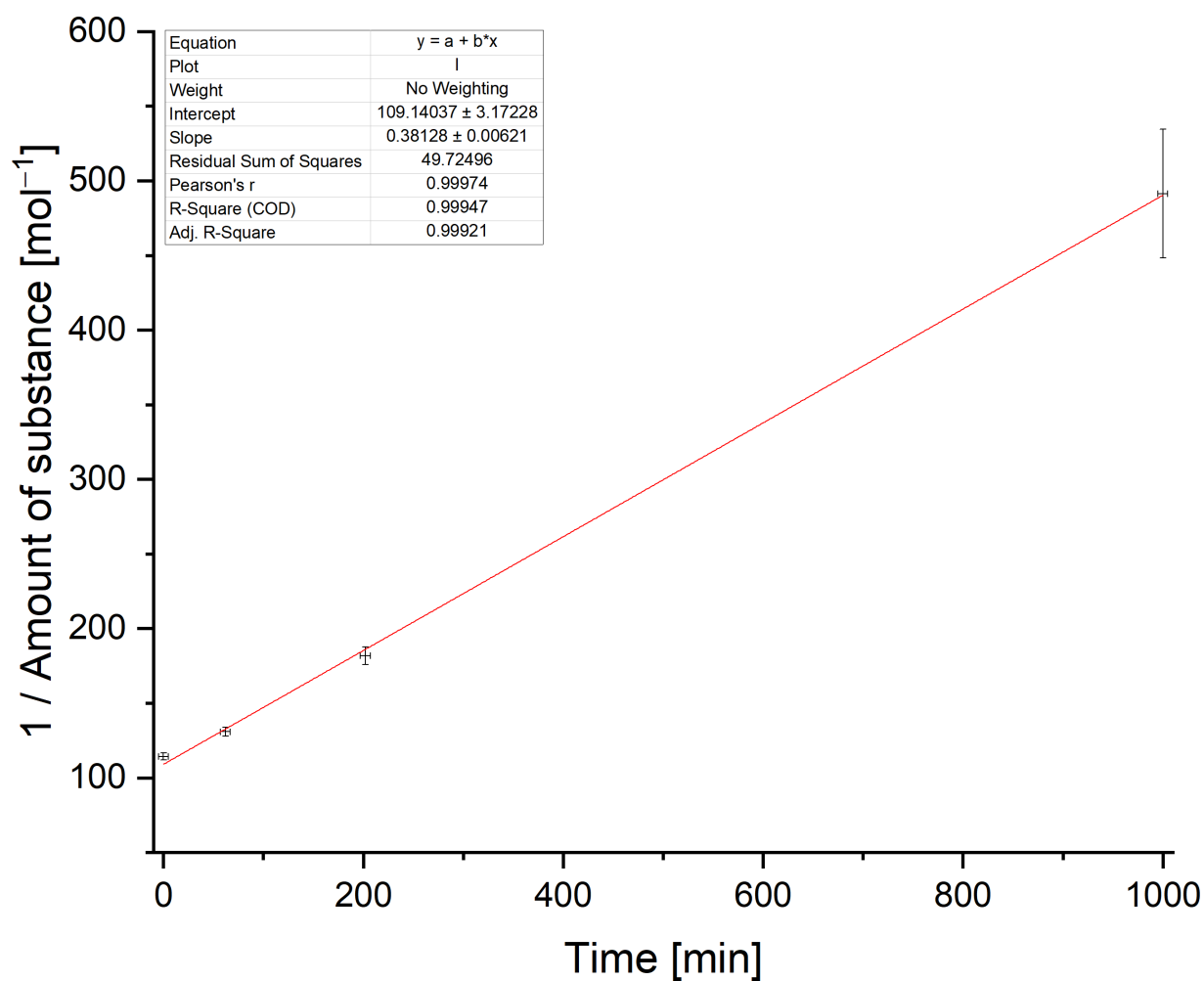
For plotting 1/ amount of substance vs. time a linear correlation was obtained indicating a second order reaction. Therefore the expression for the time dependence of the concentration for a second order reaction was used (assuming that $[\text{CO}]_0 = [\text{Cl}_2]_0$):

$$\frac{1}{[\text{CO}]} = \frac{1}{[\text{CO}]_0} + kt \quad (2)$$

The half-life of a second order reaction is given by:

$$t_{1/2} = \frac{1}{[\text{CO}]_0 \cdot k} \quad (3)$$

and using a linear fit (see Fig. S25) k was determined to be $(0.38 \pm 0.01) \text{ mol}^{-1} \text{ min}^{-1}$ and $t_{1/2}$ was determined to be $(287 \pm 14) \text{ min}$.

Plots**Fig. S26.** Plot of $1 / n(\text{CO})$ vs time.

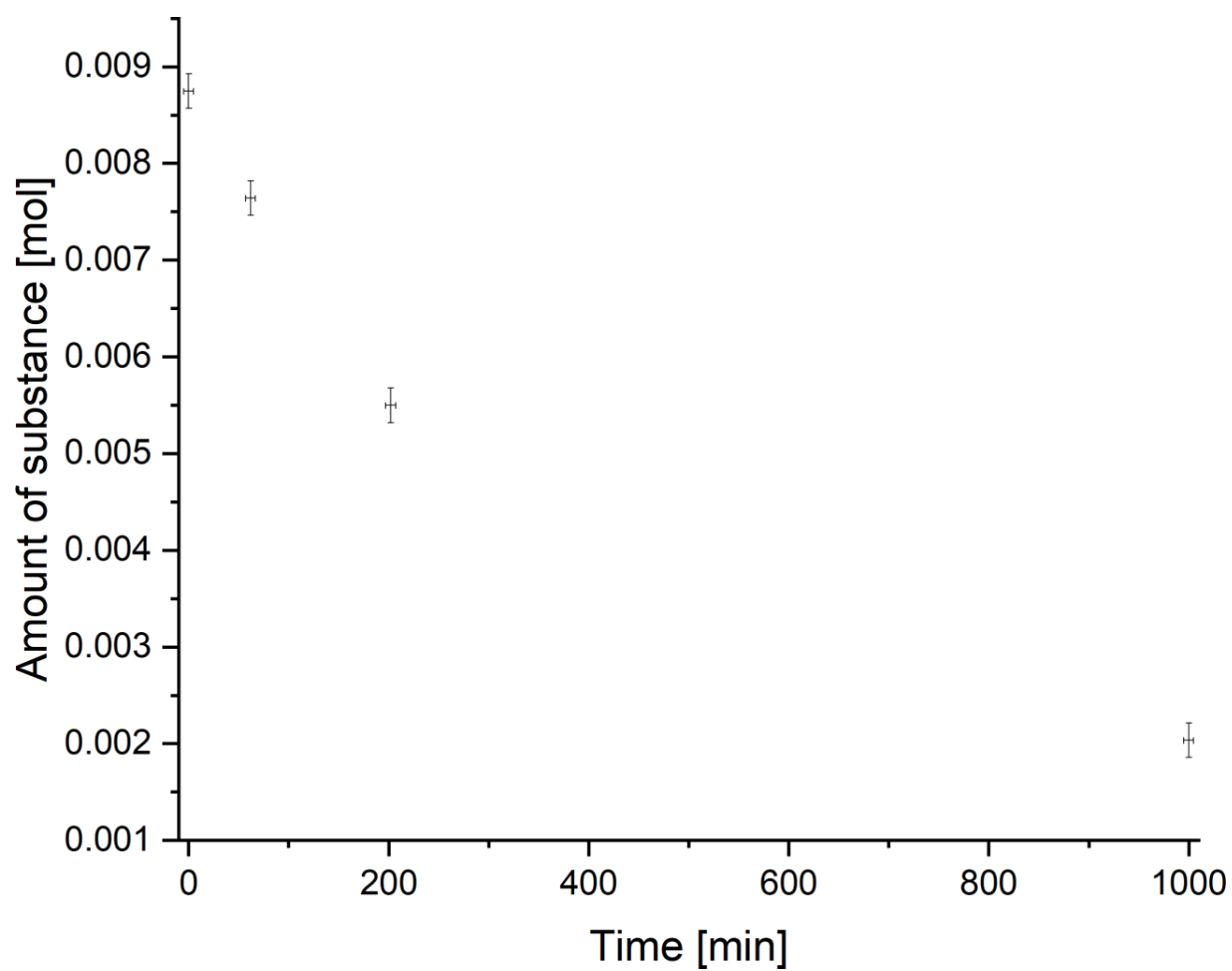


Fig. S27. Plot of $n(\text{CO})$ vs time

Interpretation of the obtained values

Some rather harsh assumption had to be made to obtain the values described above. The reaction between $[\text{NEt}_3\text{Me}][\text{Cl}_3]$ and CO takes place in a rather complicated reaction media consisting of three phase (gas phase (Cl_2 and CO), *o*DCB solution (solved Cl_2 , maybe small amounts of $[\text{Cl}_3]^-$ and CO) and the $[\text{NEt}_3\text{Me}][\text{Cl}_3]$ ionic liquid phase). It is not completely clear in which phase the reaction takes place but it is most likely that small amounts of CO dissolve in $[\text{NEt}_3\text{Me}][\text{Cl}_3]$ and react there. In this system the $[\text{Cl}_3]^-$ will be in large excess over the CO which makes the assumption that $n(\text{CO}) \approx n(\text{Cl}_2)$ rather unprecise. If the mixing of the reactants is fast the concentration of CO in $[\text{NEt}_3\text{Me}][\text{Cl}_3]$ should be nearly constant and should only slowly decrease when the partial pressure of CO in the gas phase decreases. Additionally, the concentration of $[\text{Cl}_3]^-$ will also stay rather constant since consumed Cl_2 will be replaced by Cl_2 from dissolved Cl_2 from the *o*DCB phase or from the gas phase. Due to this many equilibria between the phases a rather complex kinetic can be expected. Nevertheless, the plot of $1/n(\text{CO})$ vs t shows a rather good linear behavior and at least the determined $t_{1/2}$ of (287 ± 14) min (for this defined system) can be used as a good estimate for the speed of the reaction. A half-life of ca. 5 h also correlates well to the observed reaction time of ca. 2 days for a full conversion of the Cl_2 to COCl_2 .

Movie S1. Synthesis and handling of $[\text{NEt}_3\text{Me}][\text{Cl}(\text{Cl}_2)_{1.45}]$

REFERENCES AND NOTES

1. J. Davy, VI. On a gaseous compound of carbonic oxide and chlorine. *Phil. Trans. R. Soc.* **102**, 144–151 (1812).
2. L. Cotarca, C. Lange, K. Meurer, J. Pauluhn, *Ullmann's Encyclopedia of Industrial Chemistry* (Phosgene, 2019), pp. 1–30.
3. G. E. Rossi, J. M. Winfield, N. Meyer, D. H. Jones, R. H. Carr, D. Lennon, Phosgene formation via carbon monoxide and dichlorine reaction over an activated carbon catalyst: Towards a reaction model. *Appl. Catal. Gen.* **609**, 117900 (2021).
4. N. K. Gupta, A. Pashigreva, E. A. Pidko, E. J. M. Hensen, L. Mleczko, S. Roggan, E. E. Ember, J. A. Lercher, Bent carbon surface moieties as active sites on carbon catalysts for phosgene synthesis. *Angew. Chem. Int. Ed.* **55**, 1728–1732 (2016).
5. N. K. Gupta, B. Peng, G. L. Haller, E. E. Ember, J. A. Lercher, Nitrogen modified carbon nano-materials as stable catalysts for phosgene synthesis. *ACS Catal.* **6**, 5843–5855 (2016).
6. G. E. Rossi, J. M. Winfield, C. J. Mitchell, N. Meyer, D. H. Jones, R. H. Carr, D. Lennon, Phosgene formation via carbon monoxide and dichlorine reaction over an activated carbon catalyst: Reaction kinetics and mass balance relationships. *Appl. Catal. Gen.* **602**, 117688 (2020).
7. C. J. Mitchell, W. van der Borden, K. van der Velde, M. Smit, R. Scheringa, K. Ahrika, D. H. Jones, Selection of carbon catalysts for the industrial manufacture of phosgene. *Cat. Sci. Technol.* **2**, 2109 (2012).
8. S. K. Ajmera, M. W. Losey, K. F. Jensen, M. A. Schmidt, Microfabricated packed-bed reactor for phosgene synthesis. *AIChE J.* **47**, 1639–1647 (2001).
9. L. Khachatryan, B. Dellinger, Formation of chlorinated hydrocarbons from the reaction of chlorine atoms and activated carbon. *Chemosphere* **52**, 709–716 (2003).
10. K. Sonnenberg, L. Mann, F. A. Redeker, B. Schmidt, S. Riedel, Polyhalogen and polyinterhalogen anions from fluorine to iodine. *Angew. Chem. Int. Ed.* **59**, 5464–5493 (2020).

11. H. Keil, D. Sonnenberg, C. Müller, R. Herbst-Irmer, H. Beckers, S. Riedel, D. Stalke, Insights in the topology and the formation of a genuine $\text{pp}\sigma$ bond: Experimental and computed electron densities in mono anionic trichlorine $[\text{Cl}_3]^-$. *Angew. Chem.* **60**, 2569–2573 (2020).
12. M. Paven, Y. Schiesser, R. Weber, G. Langstein, V. Trieu, S. Hasenstab-Riedel, N. Schwarze, S. Steinhauer, Storage medium and a method of separating, storage and transportation of chlorine derived from chlorine-containing gases, WO2019215037A1 (2018).
13. S. Grimme, Improved second-order Møller–Plesset perturbation theory by separate scaling of parallel- and antiparallel-spin pair correlation energies. *J. Chem. Phys.* **118**, 9095–9102 (2003).
14. S. Dapprich, I. Komáromi, K.S. Byun, K. Morokuma, M. J. Frisch, A new ONIOM implementation in Gaussian98. Part I. The calculation of energies, gradients, vibrational frequencies and electric field derivatives. *J. Mol. Struct.* **461–462**, 1–21 (1999).
15. M. J. Frisch, G. W. Trucks, H. B. Schlegel, G. E. Scuseria, M. A. Robb, J. R. Cheeseman, G. Scalmani, V. Barone, G. A. Petersson, H. Nakatsuji, X. Li, M. Caricato, A. V. Marenich, J. Bloino, B. G. Janesko, R. Gomperts, B. Mennucci, H. P. Hratchian, J. V. Ortiz, A. F. Izmaylov, J. L. Sonnenberg, D. Williams-Young, F. Ding, F. Lipparini, F. Egidi, J. Goings, B. Peng, A. Petrone, T. Henderson, D. Ranasinghe, V. G. Zakrzewski, J. Gao, N. Rega, G. Zheng, W. Liang, M. Hada, M. Ehara, K. Toyota, R. Fukuda, J. Hasegawa, M. Ishida, T. Nakajima, Y. Honda, O. Kitao, H. Nakai, T. Vreven, K. Throssell, J. A. Montgomery, Jr., J. E. Peralta, F. Ogliaro, M. J. Bearpark, J. J. Heyd, E. N. Brothers, K. N. Kudin, V. N. Staroverov, T. A. Keith, R. Kobayashi, J. Normand, K. Raghavachari, A. P. Rendell, J. C. Burant, S. S. Iyengar, J. Tomasi, M. Cossi, J. M. Millam, M. Klene, C. Adamo, R. Cammi, J. W. Ochterski, R. L. Martin, K. Morokuma, O. Farkas, J. B. Foresman, and D. J. Fox, *Gaussian 16* (Gaussian Inc., 2016).
16. H.-J. Werner, P. J. Knowles, G. Knizia, F. R. Manby, M. Schütz, Molpro: A general-purpose quantum chemistry program package. *WIREs Comput. Mol. Sci.* **2**, 242–253 (2012).
17. H.-J. Werner, P. J. Knowles, G. Knizia, F. R. Manby, M. Schütz, P. Celani, W. Györffy, D. Kats, T. Korona, R. Lindh, A. Mitrushenkov, G. Rauhut, K. R. Shamasundar, T. B. Adler, R. D. Amos, S. J. Bennie, A. Bernhardsson, A. Berning, D. L. Cooper, M. J. O. Deegan, A. J. Dobbyn, F. Eckert, E.

Goll, C. Hampel, A. Hesselmann, G. Hetzer, T. Hrenar, G. Jansen, C. Köppl, S. J. R. Lee, Y. Liu, A. W. Lloyd, Q. Ma, R. A. Mata, A. J. May, S. J. McNicholas, W. Meyer, T. F. Miller III, M. E. Mura, A. Nicklass, D. P. O'Neill, P. Palmieri, D. Peng, K. Pflüger, R. Pitzer, M. Reiher, T. Shiozaki, H. Stoll, A. J. Stone, R. Tarroni, T. Thorsteinsson, M. Wang, M. Welborn, *MOLPRO, version 2019.2, a package of ab initio programs*.

18. T. H. Dunning Jr, Gaussian basis sets for use in correlated molecular calculations. I. The atoms boron through neon and hydrogen. *J. Chem. Phys.* **90**, 1007–1023 (1989).
19. R. A. Kendall, T. H. Dunning, R. J. Harrison, Electron affinities of the first-row atoms revisited. Systematic basis sets and wave functions. *J. Chem. Phys.* **96**, 6796–6806 (1992).
20. D. E. Woon, T. H. Dunning Jr, Gaussian basis sets for use in correlated molecular calculations. III. The atoms aluminum through argon. *J. Chem. Phys.* **98**, 1358–1371 (1993).
21. F. Weigend, A fully direct RI-HF algorithm: Implementation, optimised auxiliary basis sets, demonstration of accuracy and efficiency. *Phys. Chem. Chem. Phys.* **4**, 4285–4291 (2002).
22. S. Miertuš, E. Scrocco, J. Tomasi, Electrostatic interaction of a solute with a continuum. A direct utilization of AB initio molecular potentials for the prevision of solvent effects. *Chem. Phys.* **55**, 117–129 (1981).
23. S. Miertuš, J. Tomasi, Approximate evaluations of the electrostatic free energy and internal energy changes in solution processes. *Chem. Phys.* **65**, 239–245 (1982).
24. J. L. Pascual-ahuir, E. Silla, I. Tuñon, GEPOL: An improved description of molecular surfaces. III. A new algorithm for the computation of a solvent-excluding surface. *J. Comput. Chem.* **15**, 1127–1138 (1994).
25. M. Cossi, V. Barone, R. Cammi, J. Tomasi, Ab initio study of solvated molecules: A new implementation of the polarizable continuum model. *Chem. Phys. Lett.* **255**, 327–335 (1996).

26. E. Cancès, B. Mennucci, J. Tomasi, A new integral equation formalism for the polarizable continuum model: Theoretical background and applications to isotropic and anisotropic dielectrics. *J. Chem. Phys.* **107**, 3032–3041 (1997).
27. V. Barone, M. Cossi, J. Tomasi, A new definition of cavities for the computation of solvation free energies by the polarizable continuum model. *J. Chem. Phys.* **107**, 3210–3221 (1997).
28. B. Mennucci, J. Tomasi, Continuum solvation models: A new approach to the problem of solute's charge distribution and cavity boundaries. *J. Chem. Phys.* **106**, 5151–5158 (1997).
29. B. Mennucci, E. Cancès, J. Tomasi, Evaluation of solvent effects in isotropic and anisotropic dielectrics and in ionic solutions with a unified integral equation method: Theoretical bases, computational implementation, and numerical applications. *J. Phys. Chem. B* **101**, 10506–10517 (1997).
30. V. Barone, M. Cossi, Quantum calculation of molecular energies and energy gradients in solution by a conductor solvent model. *J. Phys. Chem. A* **102**, 1995–2001 (1998).
31. M. Cossi, V. Barone, B. Mennucci, J. Tomasi, Ab initio study of ionic solutions by a polarizable continuum dielectric model. *Chem. Phys. Lett.* **286**, 253–260 (1998).
32. V. Barone, M. Cossi, J. Tomasi, Geometry optimization of molecular structures in solution by the polarizable continuum model. *J. Comput. Chem.* **19**, 404–417 (1998).
33. R. Cammi, B. Mennucci, J. Tomasi, Second-order Møller–Plesset analytical derivatives for the polarizable continuum model using the relaxed density approach. *J. Phys. Chem. A* **103**, 9100–9108 (1999).
34. J. Tomasi, B. Mennucci, E. Cancès, The IEF version of the PCM solvation method: An overview of a new method addressed to study molecular solutes at the QM ab initio level. *J. Mol. Struct. (THEOCHEM)* **464**, 211–226 (1999).
35. M. Cossi, N. Rega, G. Scalmani, V. Barone, Polarizable dielectric model of solvation with inclusion of charge penetration effects. *J. Chem. Phys.* **114**, 5691–5701 (2001).

36. M. Cossi, G. Scalmani, N. Rega, V. Barone, New developments in the polarizable continuum model for quantum mechanical and classical calculations on molecules in solution. *J. Chem. Phys.* **117**, 43–54 (2002).
37. M. Cossi, N. Rega, G. Scalmani, V. Barone, Energies, structures, and electronic properties of molecules in solution with the C-PCM solvation model. *J. Comput. Chem.* **24**, 669–681 (2003).
38. G. Scalmani, M. J. Frisch, Continuous surface charge polarizable continuum models of solvation. I. General formalism. *J. Chem. Phys.* **132**, 114110 (2010).
39. F. Lipparini, G. Scalmani, B. Mennucci, E. Cancès, M. Caricato, M. J. Frisch, A variational formulation of the polarizable continuum model. *J. Chem. Phys.* **133**, 014106 (2010).
40. F. Eckert, A. Klamt, Fast solvent screening via quantum chemistry: COSMO-RS approach. *AIChE J.* **48**, 369–385 (2002).
41. A. Klamt, The COSMO and COSMO-RS solvation models. *Wiley Interdiscip. Rev. Comput. Mol. Sci.* **1**, 699–709 (2011).
42. A. Klamt, M. Diedenhofen, Calculation of solvation free energies with DCOSMO-RS. *J. Phys. Chem. A* **119**, 5439–5445 (2015).
43. A. Hellweg, F. Eckert, Brick by brick computation of the gibbs free energy of reaction in solution using quantum chemistry and COSMO-RS. *AIChE J.* **63**, 3944–3954 (2017).
44. R. Ahlrichs, M. Bär, M. Häser, H. Horn, C. Kölmel, Electronic structure calculations on workstation computers: The program system turbomole. *Chem. Phys. Lett.* **162**, 165–169 (1989).
45. O. Treutler, R. Ahlrichs, Efficient molecular numerical integration schemes. *J. Chem. Phys.* **102**, 346–354 (1995).
46. M. V. Arnim, R. Ahlrichs, Performance of parallel TURBOMOLE for density functional calculations. *J. Comput. Chem.* **19**, 1746–1757 (1998).

47. A. D. Becke, Density-functional exchange-energy approximation with correct asymptotic behavior. *Phys. Rev. A* **38**, 3098–3100 (1988).
48. J. P. Perdew, Density-functional approximation for the correlation energy of the inhomogeneous electron gas. *Phys. Rev. B.* **33**, 8822–8824 (1986).
49. F. Weigend, R. Ahlrichs, Balanced basis sets of split valence, triple zeta valence and quadruple zeta valence quality for H to Rn: Design and assessment of accuracy, *Phys. Chem. Chem. Phys.* **7**, 3297–3305 (2005).
50. K. Eichkorn, O. Treutler, H. Öhm, M. Häser, R. Ahlrichs, Auxiliary basis sets to approximate Coulomb potentials. *Chem. Phys. Lett.* **242**, 652–660 (1995).
51. K. Eichkorn, F. Weigend, O. Treutler, R. Ahlrichs, Auxiliary basis sets for main row atoms and transition metals and their use to approximate Coulomb potentials. *Theor. Chem. Acc.* **97**, 119–124 (1997).
52. F. Weigend, Accurate Coulomb-fitting basis sets for H to Rn. *Phys. Chem. Chem. Phys.* **8**, 1057–1065 (2006).
53. M. Sierka, A. Hogekamp, R. Ahlrichs, Fast evaluation of the Coulomb potential for electron densities using multipole accelerated resolution of identity approximation. *J. Chem. Phys.* **118**, 9136–9148 (2003).
54. A. Klamt, M. Diedenhofen, A refined cavity construction algorithm for the conductor-like screening model. *J. Comput. Chem.* **39**, 1648–1655 (2018).
55. S. Grimme, J. Antony, S. Ehrlich, H. Krieg, A consistent and accurate ab initio parametrization of density functional dispersion correction (DFT-D) for the 94 elements H-Pu. *J. Chem. Phys.* **132**, 154104 (2010).
56. NIST Chemistry WebBook, Sadtler Research Labs Under US-EPA Contract (10 February 2021); <https://webbook.nist.gov/cgi/cbook.cgi?ID=C103719&Type=IR-SPEC&Index=0#IR-SPEC>.

8.5 SI of Synthesis of a Hexachloro Sulfate(IV) Dianion Enabled by Polychloride Chemistry

Patrick Voßnacker, Alisa Wüst, Carsten Müller, Merlin Kleoff, Sebastian Riedel*

Angew. Chem. Int. Ed. **2022**, *61*, e202209684.

Angew. Chem. **2022**, *134*, e202209684.

<https://doi.org/10.1002/anie.202209684>

<https://doi.org/10.1002/ange.202209684>

© 2022 The Authors. *Angewandte Chemie International Edition* published by Wiley-VCH GmbH.



Supporting Information

Synthesis of a Hexachloro Sulfate(IV) Dianion Enabled by Polychloride Chemistry

*P. Voßnacker, A. Wüst, C. Müller, M. Kleoff, S. Riedel**

Table of Contents

a) Experimental Section	2
a1. Apparatus and Materials	2
a2. Synthesis of $[\text{NEt}_3\text{Me}]_2[\text{SCl}_6]$	2
a3. Synthesis of $[\text{NEt}_3\text{Me}]_2[\text{SCl}_6] \cdot 4\text{CH}_2\text{Cl}_2$	3
a4. Stability of $[\text{NEt}_3\text{Me}]_2[\text{SCl}_6]$	3
b) Molecular Structures in Solid State Including Intermolecular Interactions	4
b1. $[\text{NEt}_3\text{Me}]_2[\text{SCl}_6]$	4
b2. $[\text{NEt}_3\text{Me}]_2[\text{SCl}_6] \cdot 4 \text{CH}_2\text{Cl}_2$	5
c) Crystal Data.....	6
d) Experimental and Calculated Raman and IR Spectra.....	7
e) Stereochemically Active Lone Pair in AB_6E Systems.....	10
f) NBO Analysis of Symmetric and Asymmetric $[\text{SCl}_6]^{2-}$	11
g) Relaxed Surface Scan of $[\text{SCl}_6]^{2-}$	13
h) Solid State Calculations	16
i) Optimized Structures	19
j) Calculated Energies and Free Reaction Energies	21
j1) B3LYP(D4)/def2-TZVPP Energies	21
j2) SCS-MP2/def2-TZVPP Energies	22
j3) Free Reaction Energy Calculation.....	23
k) Calculated Vibrational Frequencies	25
l) Coordinates of Optimized Structures	34
m) References.....	44

a) Experimental Section

a1. Apparatus and Materials

All substances sensitive to water and oxygen were handled under an argon atmosphere using standard Schlenk techniques and oil pump vacuum up to 10^{-3} mbar. Commercially available $[\text{NEt}_3\text{Me}]\text{Cl}$, sulfur, and chlorine were used without further purification. All salts were dried *in vacuo* at $100\text{ }^\circ\text{C}$ for 1 h to 1 day prior to use. Dry DCM was obtained by storage over activated 3 \AA molecular sieves. Raman spectra were recorded at room temperature on a Bruker (Karlsruhe, Germany) MultiRAM II equipped with a low-temperature Ge detector (1064 nm, 100-180 mW, resolution of 4 cm^{-1}). Spectra of single crystals were recorded at $-196\text{ }^\circ\text{C}$ using the Bruker RamanScope III (See *Chem.Eur.J.* **2020**, *26*, 13256–13263 for detailed description) ^[1] X-ray diffraction data were collected on a Bruker D8 Venture CMOS area detector (Photon 100) diffractometer with $\text{MoK}\alpha$ radiation. Single crystals were coated with perfluoroether oil at low temperature ($-40/-80\text{ }^\circ\text{C}$) and mounted on a 0.1-0.2 mm Micromount. The structures were solved with the ShelXT^[2] structure solution program using intrinsic phasing and refined with the ShelXL^[3] refinement package using least squares on weighted F_2 values for all reflections using OLEX2^[4]. Hydrogen atoms were treated using the HFIX 23 (CH_2 groups) and HFIX 137 (for CH_3 groups) restraints as implemented in ShelXL. For structure optimization (with and without solvent model COSMO^[5]), and frequency calculations (including Raman intensities) the program package TURBOMOLE 7.3^[6] was used. Relaxed surface scans were performed using orca 5.0.3^[7] and NBO^[8] analyses were performed with Gaussain G16^[9] software package. Functionals (B3LYP(D4)^[10,11] and SCS-MP2^[12]) and the basis set (def2-TZVPP^[13], aug-cc-pVTZ^[14]) were used as implemented. Minima on the potential energy surface were characterized by harmonic vibrational frequency analysis. Thermochemistry was provided for ΔG values calculated at 298.15 K and 1.0 bar. Representations of Hirshfeld surfaces were generated using CrystalExplorer21^[15]

a2. Synthesis of $[\text{NEt}_3\text{Me}]_2[\text{SCl}_6]$

270 mg (1.06 mmol, 1.35 equiv. (1.54 mmol Cl_2 , 1.97 equiv.)) $[\text{NEt}_3\text{Me}][\text{Cl}(\text{Cl}_2)_{1.45}]$ was dissolved in 1.5 mL CH_2Cl_2 and 25 mg (0.78 mmol, 1 equiv.) sulfur was added. A clear solution was obtained which was stirred overnight. Yellow single crystals of $[\text{NEt}_3\text{Me}]_2[\text{SCl}_6]$ were obtained within several days by slowly cooling to $-40\text{ }^\circ\text{C}$.

$[\text{NEt}_3\text{Me}]_2[\text{SCl}_6]$ Raman ($-196\text{ }^\circ\text{C}$): $\tilde{\nu} = 3023$ (w), 2994 (m), 2941 (m), 1446 (w), 680 (w), 3016 (w), 2973 (w), 1076 (w), 877 (vw), 281 (vs), 242 (vs), 168 (vs) cm^{-1} .

CCDC number: 2156516

a3. Synthesis of [NEt₃Me]₂[SCl₆]·4CH₂Cl₂

75 mg (1.06 mmol, 2 equiv.) Cl₂ was condensed onto 160 mg (1.06 mmol, 2 equiv. [NEt₃Me]Cl and 16 mg (0.53 mmol, 1 equiv.) sulfur. Addition of 2 mL CH₂Cl₂ yields a clear solution. Yellow single crystals of [NEt₃Me]₂[SCl₆]·4CH₂Cl₂ were obtained by slowly cooling to -80 °C.

[NEt₃Me]₂[SCl₆] Raman (-196 °C): $\tilde{\nu}$ = 3043 (w), 2987 (m), 2976 (m), 2958 (w), 2936 (w), 1474 (w), 1144 (w), 699 (m), 345 (w), 277 (vs), 239 (vs), 177 (m), 166 (w) cm⁻¹.

CCDC number: 2156517

a4. Stability of [NEt₃Me]₂[SCl₆]

0.466 g (6.57 mmol, 1.93 equiv.) Cl₂ was condensed onto 1.035 g (6.82 mmol, 2 equiv.) [NEt₃Me]Cl and 0.109 g (3.40 mmol, 1 equiv.) sulfur. The reaction mixture was warmed to 40 °C and a clear orange solution was obtained. Cooling to room temperature yields an orange solid. The reaction mixture was characterized by Raman spectroscopy at room temperature and 40 °C and by IR spectroscopy at -80 °C.

Raman (RT): $\tilde{\nu}$ = 3016 (w), 2991 (m), 2945 (m), 2885 (vw), 1448 (w), 1129 (vw), 1075 (vw), 1027 (vw), 1009 (vw), 956 (vw), 877 (vw), 680 (w), 451 (vw), 278 (vs), 237 (vs), 166 (vs) cm⁻¹.

Raman (40 °C): $\tilde{\nu}$ = 2985 (m), 2946 (m), 1455 (vw), 1124 (vw), 1072 (vw), 1011 (vw), 961 (vw), 875 (vw), 682 (w), 499 (m), 534 (vw), 429 (m), 275 (vs), 210 (w) cm⁻¹.

IR (-80 °C): $\tilde{\nu}$ = 3024 (vw), 2983 (w), 2946 (vw), 1486 (w), 1444 (m), 1402 (m), 1393 (w), 1379 (w), 1379 (w), 1370 (w), 1350 (w), 1317 (w), 1305 (vw), 1213 (w), 1205 (w), 1205 (w), 1191 (w), 1151 (vw), 1127 (w), 1071 (vw), 1024 (m), 1007 (w), 954 (w), 873 (vw), 808 (w), 791 (m), 305 (vs), 264 (s), 126 (vs) cm⁻¹.

b) Molecular Structures in Solid State Including Intermolecular Interactions

b1. $[\text{NEt}_3\text{Me}]_2[\text{SCl}_6]$

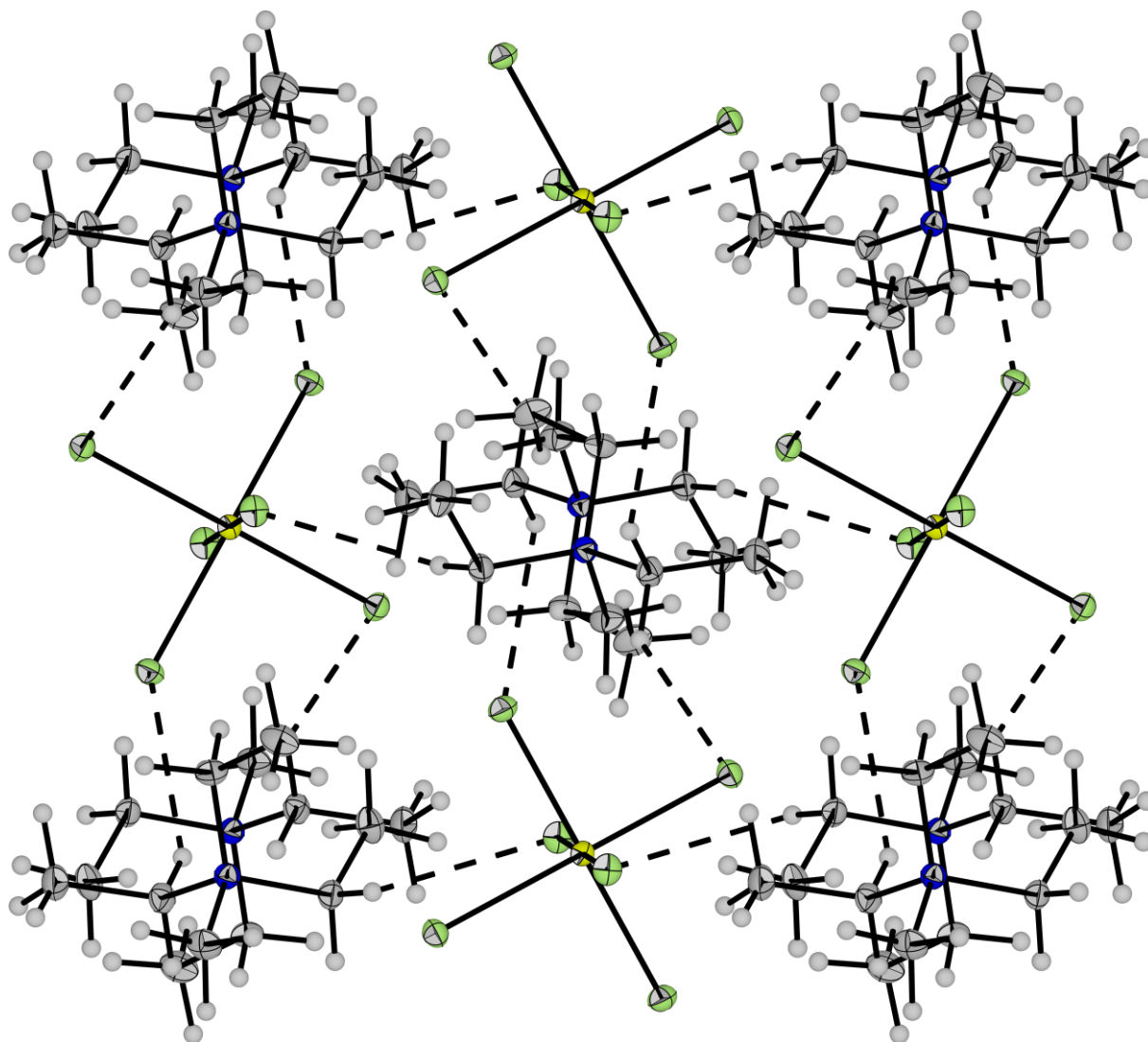


Figure S 1. Arrangement of the molecules within the unit cell of $[\text{NEt}_3\text{Me}]_2[\text{SCl}_6]$. Thermal ellipsoids are shown at 50 % probability. Cl-H hydrogen bonds are displayed by dashed lines.

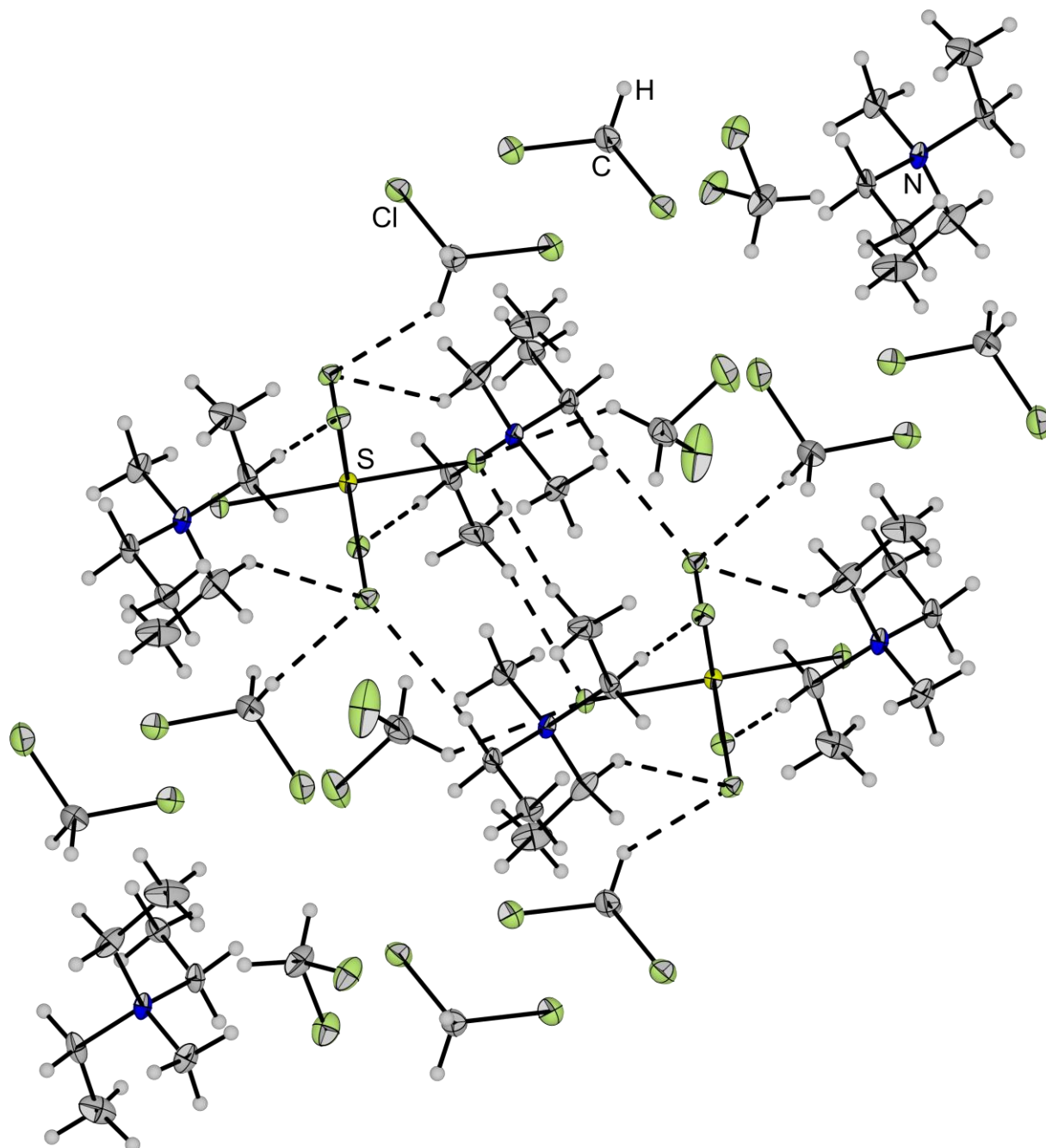
b2. $[\text{NEt}_3\text{Me}]_2[\text{SCl}_6] \cdot 4 \text{CH}_2\text{Cl}_2$ 

Figure S 2. Arrangement of the molecules within the unit cell of $[\text{NEt}_3\text{Me}]_2[\text{SCl}_6] \cdot 4 \text{CH}_2\text{Cl}_2$. Thermal ellipsoids are shown at 50 % probability. Cl-H hydrogen bonds are displayed by dashed lines. Disorder is omitted for clarity.

c) Crystal Data

Table S 1. Crystal data of the synthesized compounds.

Empirical formula	C ₁₄ H ₃₆ Cl ₆ N ₂ S	C ₁₈ H ₄₄ Cl ₁₄ N ₂ S
Formula weight	477.21	816.91
Temperature/K	104.4	100.0
Crystal system	monoclinic	triclinic
Space group	P2 ₁ /n	P-1
a/Å	9.7726(4)	10.1220(10)
b/Å	9.0349(5)	13.5938(9)
c/Å	13.1501(6)	14.6209(15)
α/°	90	116.305(3)
β/°	90.136(2)	90.917(3)
γ/°	90	91.176(3)
Volume/Å ³	1161.08(10)	1802.4(3)
Z	2	2
ρ _{calc} /cm ³	1.365	1.505
μ/mm ⁻¹	0.831	1.143
F(000)	504.0	840.0
Crystal size/mm ³	0.387 × 0.312 × 0.242	0.502 × 0.452 × 0.335
Radiation	MoKα (λ = 0.71073)	MoKα (λ = 0.71073)
2θ range for data collection/°	5.2 to 61.024	4.026 to 56.608
Reflections collected	47821	122213
Independent reflections	3496 [R _{int} = 0.0291, R _{sigma} = 0.0125]	8950 [R _{int} = 0.0602, R _{sigma} = 0.0264]
Data/restraints/parameters	3496/0/110	8950/12/373
Goodness-of-fit on F ²	1.129	1.024
Final R indexes [I] ≥ 2σ (I)]	R ₁ = 0.0173, wR ₂ = 0.0425	R ₁ = 0.0252, wR ₂ = 0.0579
Final R indexes [all data]	R ₁ = 0.0202, wR ₂ = 0.0443	R ₁ = 0.0336, wR ₂ = 0.0610
Largest diff. peak/hole / e Å ⁻³	0.40/-0.22	0.38/-0.29
CCDC deposition numbers	2156516	2156517

d) Experimental and Calculated Raman and IR Spectra

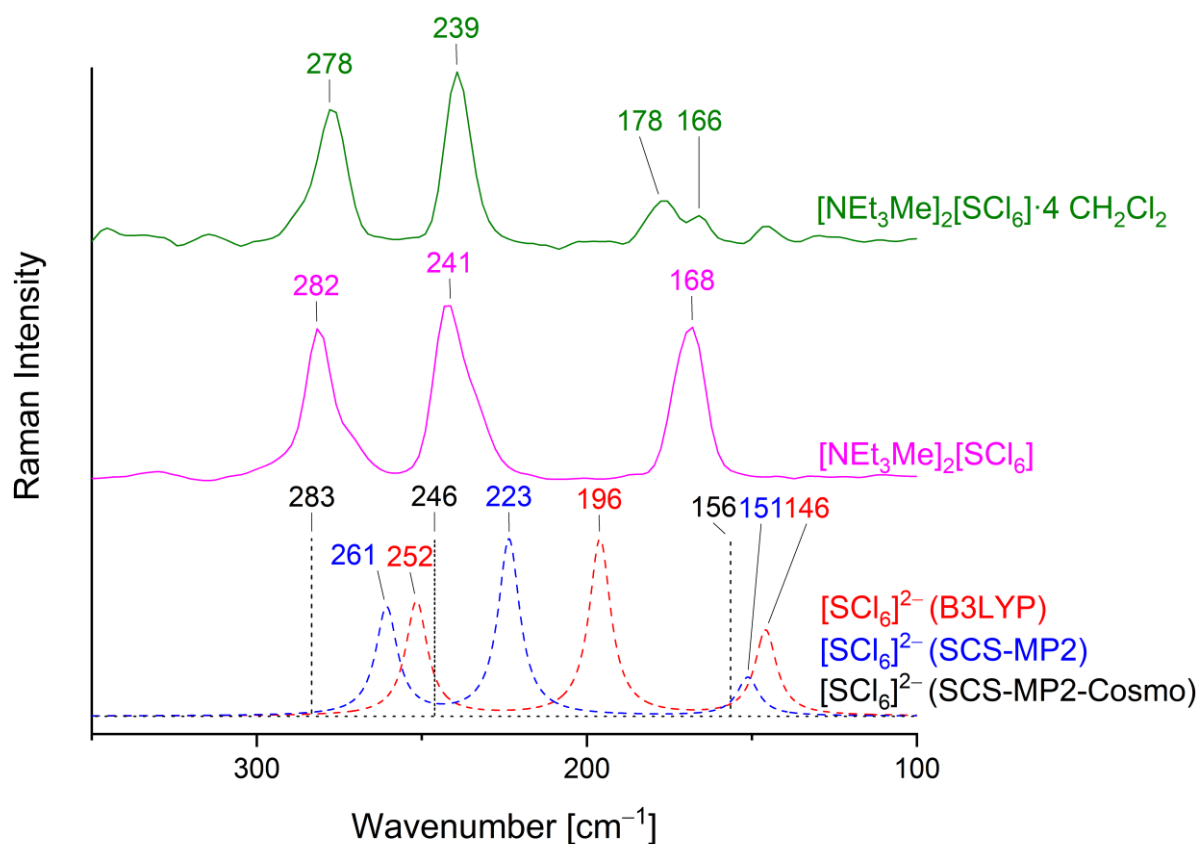


Figure S 3. Experimental Raman spectrum of a single crystal of [NEt₃Me]₂[SCl₆] and [NEt₃Me]₂[SCl₆]·4 CH₂Cl₂ recorded at -196 °C and comparison to the calculated spectra (B3LYP/def2-TZVPP, SCS-MP2/def2-TZVPP and SCS-MP2-Cosmo/def2-TZVPP ($\epsilon_r = 100$) level of theory).

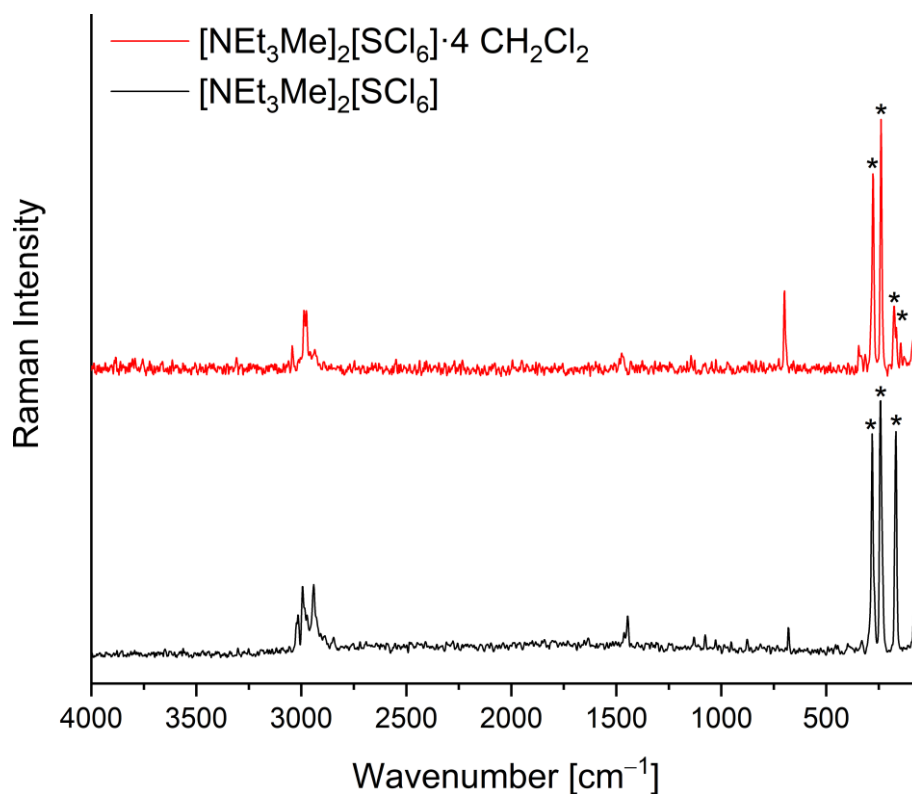


Figure S 4. Experimental Raman spectrum of a single crystal of [NEt₃Me]₂[SCl₆] and [NEt₃Me]₂[SCl₆]·4 CH₂Cl₂ recorded at -196 °C. Bands highlighted with asterisk are associated to the [SCl₆]²⁻.

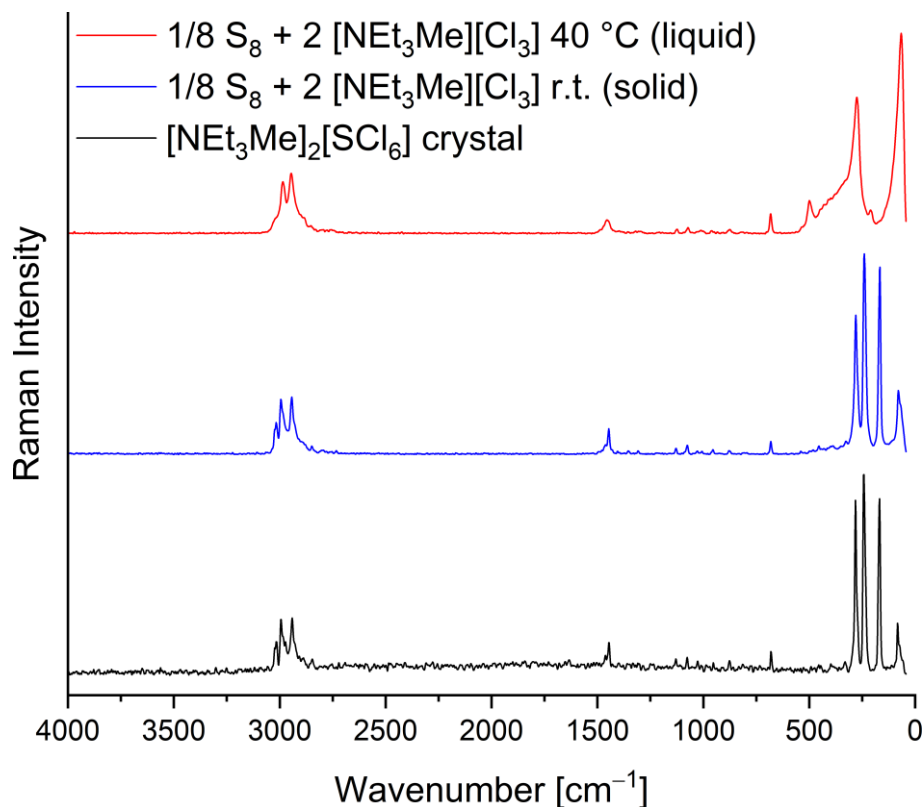


Figure S 5. Raman spectrum of the reaction mixture of sulfur and [NEt₃Me][Cl₃] at 40 °C (red) and room temperature (blue) and comparison to the Raman spectrum of the single crystal of [NEt₃Me]₂[SCl₆] (black).

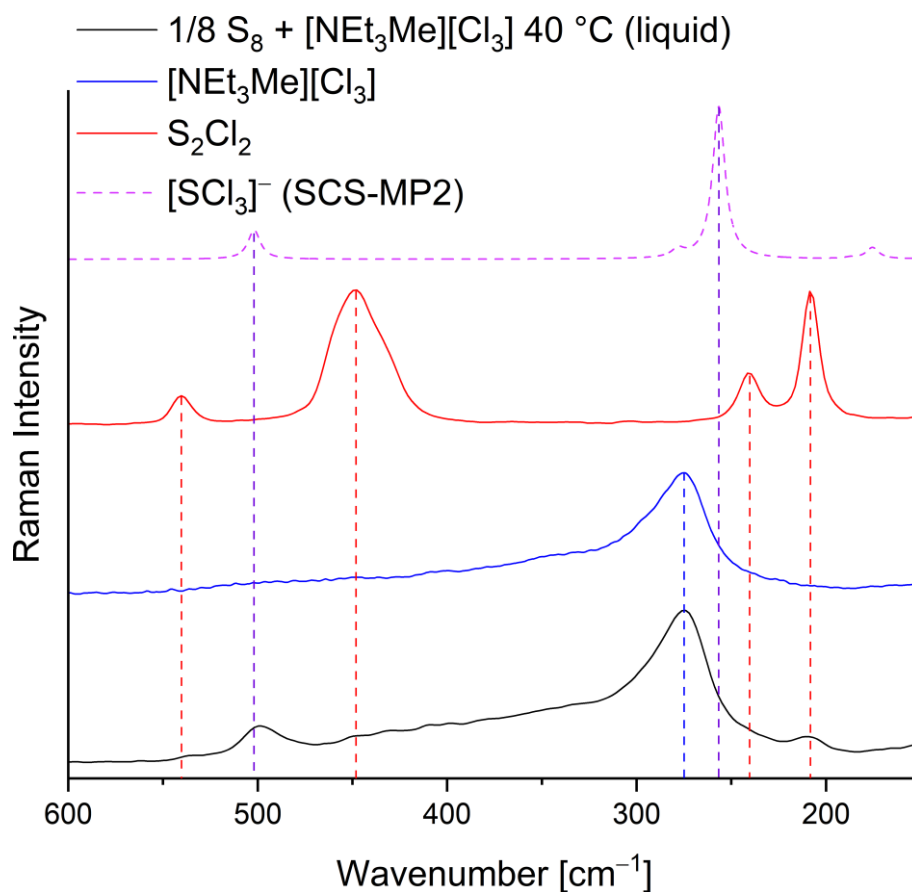


Figure S 6. Raman spectra of the reaction mixture of sulfur and [NEt₃Me][Cl₃] at 40 °C as well as reference spectra of [NEt₃Me][Cl₃], S₂Cl₂ and the calculated spectrum of [SCl₃]⁻ (SCS-MP2/def2-TZVPP).

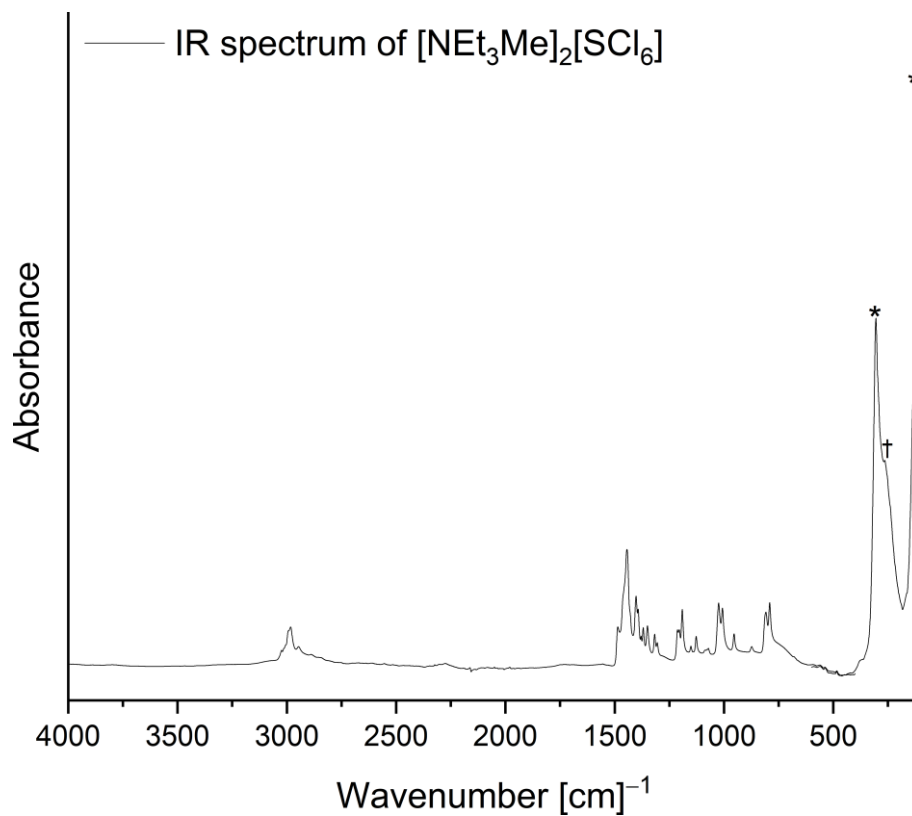


Figure S 7. IR spectrum of the reaction mixture of sulfur and [NEt₃Me][Cl₃] recorded at -80 °C. Bands highlighted with an asterisk belong to the [SCl₆]²⁻ anion while the band highlighted with a dagger presumably corresponds to [SCl₃]⁻.

e) Stereochemically Active Lone Pair in AB_6E Systems

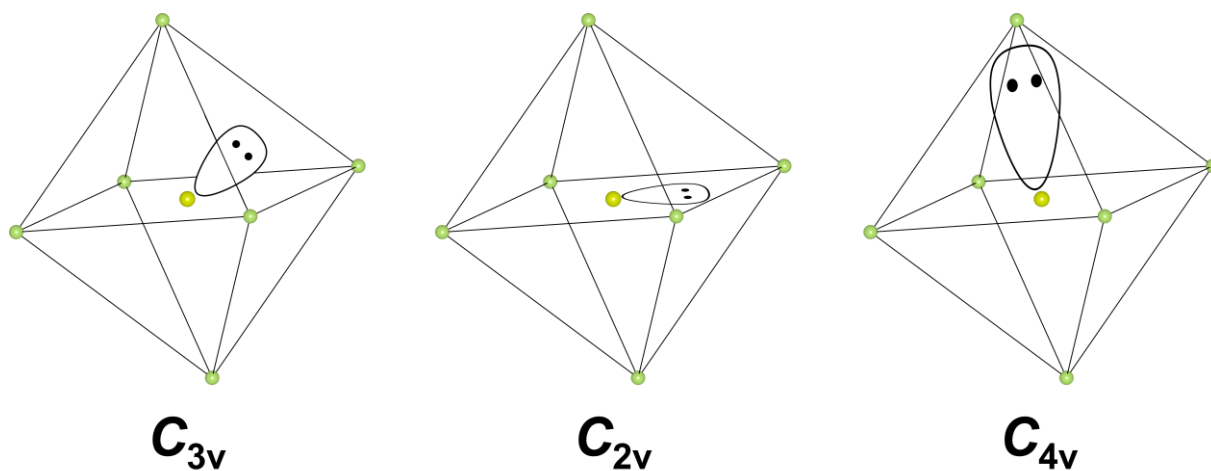


Figure S 8. Possible orientations of the stereochemically active lone pair in AB_6E systems.

f) NBO Analysis of Symmetric and Asymmetric $[\text{SCl}_6]^{2-}$

NBO analysis for $[\text{SCl}_6]^{2-}$ was performed on B3LYP/aug-cc-pVTZ level of theory using the NBO 7.0.4 program as implemented in Gaussian 16. The NBO analysis was performed on geometries of $[\text{SCl}_6]^{2-}$ taken from the solid state structures of $[\text{NEt}_3\text{Me}]_2[\text{SCl}_6]$ and $[\text{NEt}_3\text{Me}]_2[\text{SCl}_6] \cdot 4\text{CH}_2\text{Cl}_2$. For the symmetric $[\text{SCl}_6]^{2-}$ ($[\text{NEt}_3\text{Me}]_2[\text{SCl}_6]$) the lone pair has a s-character of 100% while for the asymmetric $[\text{SCl}_6]^{2-}$ ($[\text{NEt}_3\text{Me}]_2[\text{SCl}_6] \cdot 4\text{CH}_2\text{Cl}_2$) the lone pair has a s-character of 99.67 % and a p-character of 0.33 %.

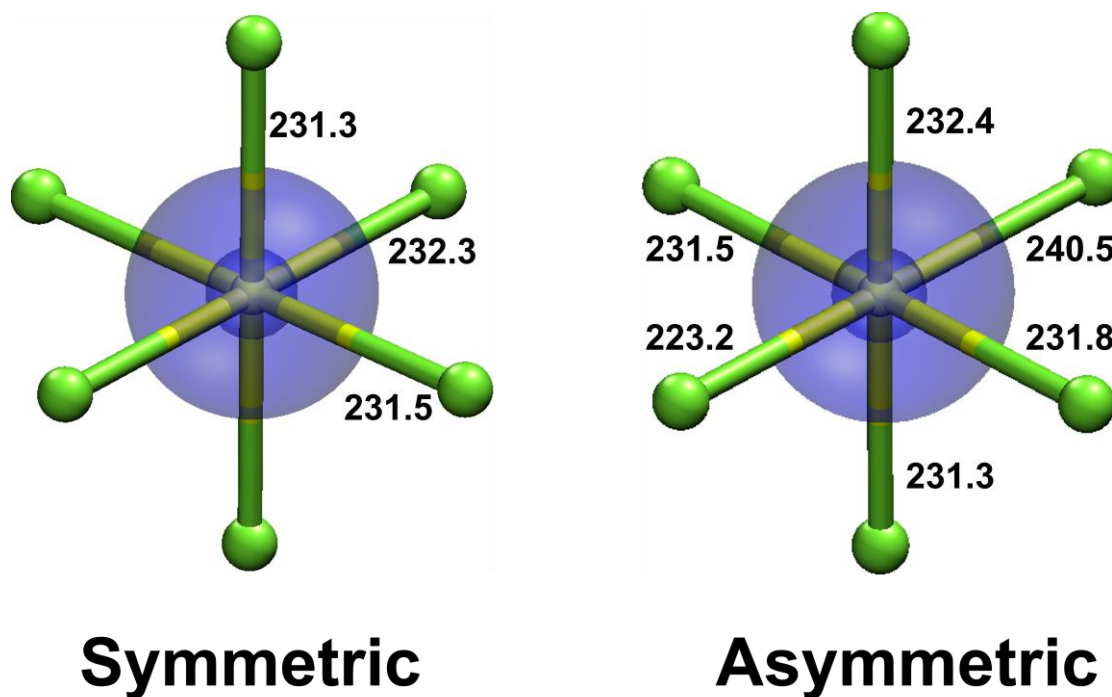


Figure S 9. NBOs showing the lone pair located at the sulfur atom for the symmetric $[\text{SCl}_6]^{2-}$ ($[\text{NEt}_3\text{Me}]_2[\text{SCl}_6]$, left) and the asymmetric $[\text{SCl}_6]^{2-}$ ($[\text{NEt}_3\text{Me}]_2[\text{SCl}_6] \cdot 4\text{CH}_2\text{Cl}_2$, right). Isosurface value 0.1 a.u., bond lengths are given in pm.

Table S 2. Summary of Natural Population Analysis for the symmetric $[\text{SCl}_6]^{2-}$.

Atom	No	Natural Charge	Natural Population			
			Core	Valence	Rydberg	Total
S	1	0.56732	9.99999	5.29113	0.14156	15.43268
Cl	2	-0.42760	9.99999	7.41535	0.01226	17.42760
Cl	3	-0.42696	9.99999	7.41461	0.01236	17.42696
Cl	4	-0.42910	9.99999	7.41706	0.01204	17.42910
Cl	5	-0.42760	9.99999	7.41535	0.01226	17.42760
Cl	6	-0.42696	9.99999	7.41461	0.01236	17.42696
Cl	7	-0.42910	9.99999	7.41706	0.01204	17.42910
Total	-	-2	69.99996	49.78516	0.21487	120

Table S 3. Summary of Natural Population Analysis for the asymmetric $[\text{SCl}_6]^{2-}$.

Atom	No	Natural Charge	Natural Population			
			Core	Valence	Rydberg	Total
Cl	1	-0.42877	9.99999	7.41662	0.01215	17.42877
S	2	0.57218	9.99999	5.2858	0.14202	15.42782
Cl	3	-0.42451	9.99999	7.41213	0.01238	17.42451
Cl	4	-0.36797	9.99999	7.35176	0.01621	17.36797
Cl	5	-0.42673	9.99999	7.41446	0.01228	17.42673
Cl	6	-0.49245	10.00000	7.48344	0.00901	17.49245
Cl	7	-0.43176	9.99999	7.41984	0.01193	17.43176
Total	-	-2	69.99996	49.78405	0.21599	120

Coordinates for the symmetric $[\text{SCl}_6]^{2-}$

S -4.88630 9.03490 0.00000
 Cl -3.78193 7.03123 -0.35558
 Cl -4.54947 8.81282 2.27654
 Cl -6.92342 7.93165 0.17161
 Cl -5.99067 11.03857 0.35558
 Cl -5.22313 9.25698 -2.27654
 Cl -2.84918 10.13815 -0.17161

Coordinates for the asymmetric $[\text{SCl}_6]^{2-}$

Cl 4.36174 2.94997 3.48244
 S 2.35235 1.80829 3.30268
 Cl 2.37056 1.41420 5.58199
 Cl 3.44747 -0.11057 2.97750
 Cl 0.35165 0.65522 3.13551
 Cl 1.15929 3.86980 3.63757
 Cl 2.32435 2.21746 1.01486

g) Relaxed Surface Scan of $[\text{SCl}_6]^{2-}$

The relaxed surface scan for $[\text{SCl}_6]^{2-}$ was performed on B3LYP/def2-TZVPP level of theory using a CPCM model for CH_2Cl_2 as implemented in orca 5.0.3. The scan was started at the equilibrium structure of $[\text{SCl}_6]^{2-}$ and one S-Cl bond was elongated in 5 pm increments while all other degrees of freedom were optimizing freely.

Table S 4. Calculated Energies for the relaxed surface scan of $[\text{SCl}_6]^{2-}$.

R (S-Cl)	E (Hartree)	ΔE (kJ mol ⁻¹)
237.63	-3159.43917236	0.00
242.63	-3159.43910991	0.16
247.63	-3159.43894456	0.60
252.63	-3159.43869710	1.25
257.63	-3159.43838824	2.06
262.63	-3159.43804388	2.96
267.63	-3159.43767931	3.92
272.63	-3159.43729111	4.94
277.63	-3159.43686877	6.05
282.63	-3159.43640691	7.26
287.63	-3159.43591142	8.56
292.63	-3159.43539777	9.91
297.63	-3159.43488392	11.26
302.63	-3159.43438382	12.57
307.63	-3159.43390545	13.83
312.63	-3159.43345178	15.02
317.63	-3159.43302258	16.15
322.63	-3159.43261865	17.21
327.63	-3159.43224617	18.18
332.63	-3159.43191625	19.05
337.63	-3159.43163663	19.79
342.63	-3159.43140226	20.40
347.63	-3159.43119659	20.94
352.63	-3159.43100297	21.45
357.63	-3159.43081470	21.94
362.63	-3159.43063880	22.40
367.63	-3159.43048405	22.81
372.63	-3159.43033711	23.20
377.63	-3159.43018948	23.58
382.63	-3159.43006028	23.92
387.63	-3159.42996910	24.16
392.63	-3159.42990485	24.33
397.63	-3159.42984703	24.48
402.63	-3159.42979206	24.63
407.63	-3159.42974122	24.76
412.63	-3159.42969771	24.88
417.63	-3159.42967816	24.93
422.63	-3159.42970806	24.85
427.63	-3159.42975366	24.73
432.63	-3159.42977422	24.67
437.63	-3159.42978394	24.65

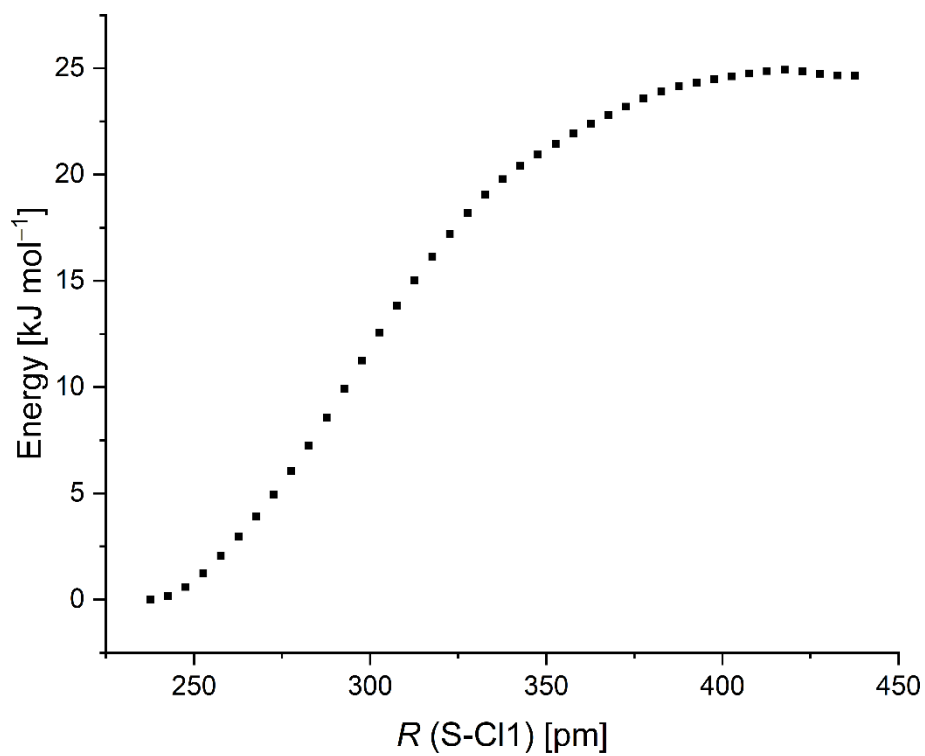


Figure S 10. Relaxed surface scan for $[\text{SCl}_6]^{2-}$ (complete).

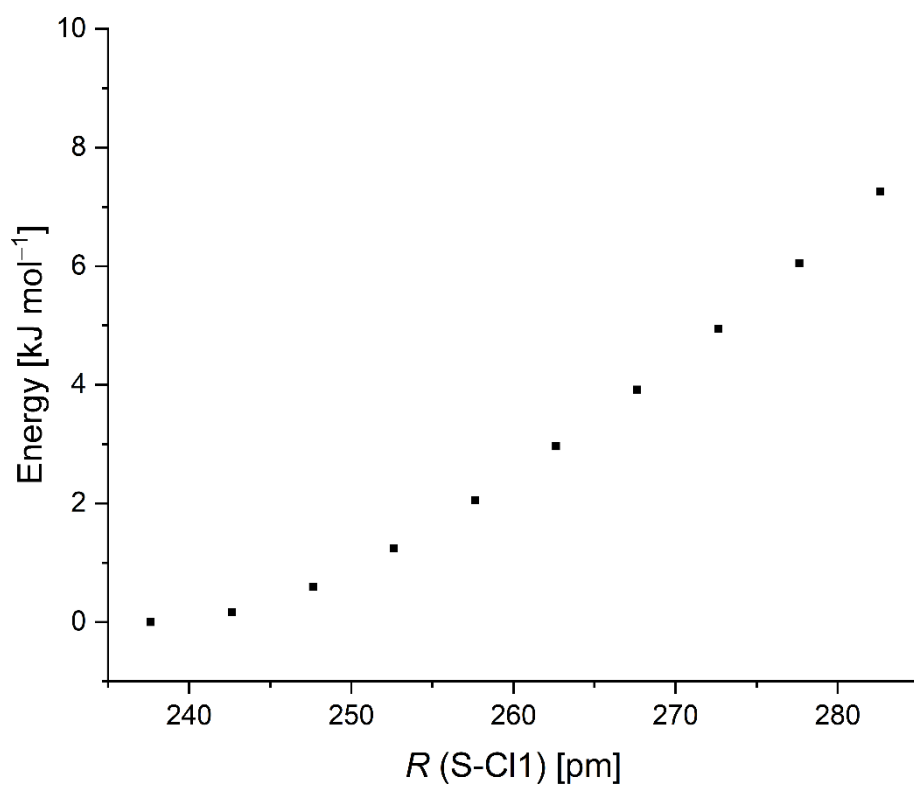


Figure S 11. Relaxed surface scan for $[\text{SCl}_6]^{2-}$ (part).

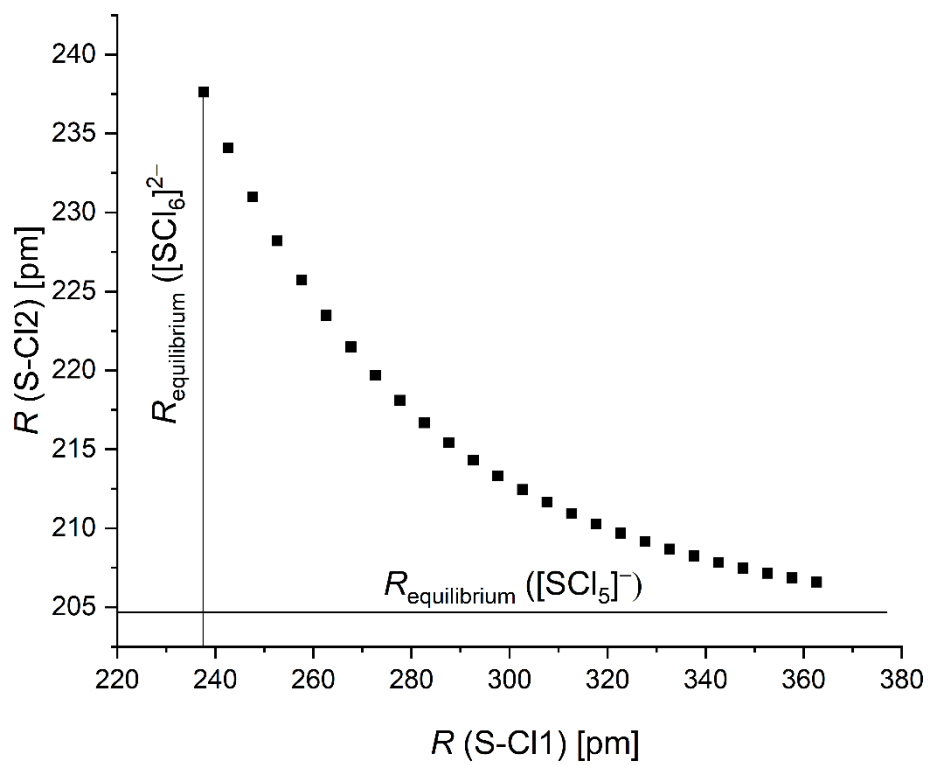


Figure S 12. Correlation between $R(\text{S-Cl2})$ and $R(\text{S-Cl1})$.

h) Solid State Calculations

Periodic density functional theory (DFT) calculations with the B3LYP functional and cc-pVDZ basis set^[16] were performed with the CRYSTAL17 program^[17]. Electron dispersion effects were included via the empirical D3 scheme^[11,18]. The first Brillouin zone was sampled using an 6×6×6 Monkhorst-Pack grid. To facilitate convergence, the Coulomb and exchange integral thresholds were sufficiently tightened with the TOLINTEG keyword to values of 8, 8, 8, 16 and 32. AIM analysis was performed with the TOPOND code developed by Gatti^[19] and recently implemented in CRYSTAL17. The estimated stabilization energy for one [SCl₆]²⁻ molecule in the solid was calculated as

$$\Delta E = 0.5 \cdot (E_{\text{bulk}} - 2 \cdot E_{\text{dianion}} - E_{\text{cation-lattice}}),$$

where E_{bulk} is the total energy of the periodic [NEt₃Me]₂[SCl₆] per unit cell, E_{dianion} is the total energy of one isolated [SCl₆]²⁻ ion, and $E_{\text{cation-lattice}}$ the total energy of the cation sub-lattice per unit cell. All three energies were calculated based on the experimental crystal structure.

Table S 5. Properties for all 52 symmetry-inequivalent bond critical points (BCP) found in the unit cell of the periodic [NEt₃Me]₂[SCl₆] structure. Columns A1 and A2 list the two bound atoms; $r_{\text{A1-A2}}$ the bond distance; ρ_{BCP} , $\nabla^2\rho_{\text{BCP}}$, ELF_{BCP} the values of the electron density, Laplacian of the electron density and electron localization function at the BCP, and G_{BCP} , V_{BCP} , $|V_{\text{BCP}}|/G_{\text{BCP}}$ the values for the potential and kinetic energy density as well as there ratio at the BCP.

#	A1	A2	$r_{\text{A1-A2}}$ [Å]	ρ_{BCP} [e/Å ³]	$\nabla^2\rho_{\text{BCP}}$ [e/Å ⁵]	ELF_{BCP}	G_{BCP} a.u.	V_{BCP} a.u.	$ V_{\text{BCP}} /G_{\text{BCP}}$
1	1 S	7 Cl	2.3120	0.584	1.737	0.556	4.3341E-02	-6.8662E-02	1.58
2	1 S	3 Cl	2.3153	0.580	1.750	0.555	4.3064E-02	-6.7972E-02	1.58
3	1 S	11 Cl	2.3232	0.571	1.786	0.550	4.2302E-02	-6.6079E-02	1.56
5	2 Cl	66 H	2.7936	0.056	0.633	0.028	5.6361E-03	-4.7054E-03	0.83
6	2 Cl	54 H	2.9112	0.046	0.506	0.025	4.5013E-03	-3.7515E-03	0.83
7	2 Cl	68 H	3.0730	0.036	0.432	0.016	3.6537E-03	-2.8247E-03	0.77
11	3 Cl	55 H	2.7364	0.065	0.724	0.035	6.5395E-03	-5.5720E-03	0.85
12	3 Cl	88 H	2.8692	0.048	0.511	0.027	4.5879E-03	-3.8780E-03	0.85
13	3 Cl	68 H	2.9875	0.041	0.444	0.020	3.9400E-03	-3.2785E-03	0.83
14	3 Cl	107 H	3.0003	0.045	0.564	0.021	4.6468E-03	-3.4448E-03	0.74
15	3 Cl	60 H	3.0308	0.037	0.412	0.019	3.5849E-03	-2.9001E-03	0.81
16	3 Cl	52 H	3.1388	0.025	0.310	0.010	2.6051E-03	-1.9952E-03	0.77
17	4 Cl	68 H	2.7983	0.058	0.638	0.031	5.7683E-03	-4.9194E-03	0.85
18	4 Cl	47 H	2.8678	0.049	0.537	0.027	4.7975E-03	-4.0211E-03	0.84
23	5 N	35 C	1.5005	1.603	-11.841	0.806	1.2820E-01	-3.7924E-01	2.96
24	5 N	19 C	1.5144	1.556	-11.103	0.809	1.2105E-01	-3.5729E-01	2.95
25	5 N	27 C	1.5195	1.538	-10.738	0.806	1.1974E-01	-3.5088E-01	2.93
26	5 N	23 C	1.5210	1.536	-10.704	0.811	1.1774E-01	-3.4653E-01	2.94
27	6 C	47 H	0.9900	2.344	-38.054	0.986	5.7850E-02	-5.1048E-01	8.82
28	6 C	51 H	0.9900	2.351	-38.377	0.988	5.5288E-02	-5.0869E-01	9.20
29	6 C	39 C	1.5161	1.656	-12.626	0.950	6.3120E-02	-2.5722E-01	4.08
30	7 C	55 H	0.9900	2.353	-38.375	0.987	5.5826E-02	-5.0974E-01	9.13
31	7 C	59 H	0.9900	2.344	-38.165	0.987	5.7015E-02	-5.0995E-01	8.94
32	7 C	31 C	1.5160	1.656	-12.621	0.950	6.3150E-02	-2.5723E-01	4.07
33	8 C	63 H	0.9900	2.344	-38.025	0.986	5.8321E-02	-5.1112E-01	8.76
34	8 C	67 H	0.9880	2.356	-38.621	0.988	5.3666E-02	-5.0798E-01	9.47

#	A1	A2	Γ_{A1-A2} [Å]	ρ_{BCP} [e/Å ³]	$\nabla^2 \rho_{BCP}$ [e/Å ⁵]	ELF _{BCP}	G _{BCP} a.u.	V _{BCP} a.u.	V _{BCP} /G _{BCP}
35	8 C	43 C	1.5136	1.664	-12.725	0.951	6.3510E-02	-2.5903E-01	4.08
36	9 C	71 H	0.9800	2.318	-36.835	0.977	7.4074E-02	-5.3027E-01	7.16
37	9 C	75 H	0.9800	2.319	-12.750	0.978	7.3145E-02	-5.2909E-01	7.23
38	9 C	79 H	0.9800	2.299	-36.401	0.976	7.5138E-02	-5.2790E-01	7.03
39	9 C	15 N	2.5579	0.071	1.343	0.019	1.0485E-02	-7.0415E-03	0.67
40	10 C	87 H	0.9800	2.364	-38.806	0.986	6.0136E-02	-5.2285E-01	8.69
41	11 C	95 H	0.9760	2.314	-36.674	0.976	7.5541E-02	-5.3253E-01	7.05
42	12 C	115 H	0.9760	2.316	-36.731	0.976	7.5297E-02	-5.3164E-01	7.06
44	15 H	83 H	2.2872	0.021	0.278	0.008	2.1638E-03	-1.4457E-03	0.67
45	16 H	104 H	2.4182	0.028	0.406	0.009	3.2553E-03	-2.2958E-03	0.71
46	17 H	75 H	2.1191	0.071	1.204	0.022	9.7410E-03	-6.9932E-03	0.72
52	24 H	107 H	2.1834	0.016	0.210	0.006	1.6042E-03	-1.0255E-03	0.64

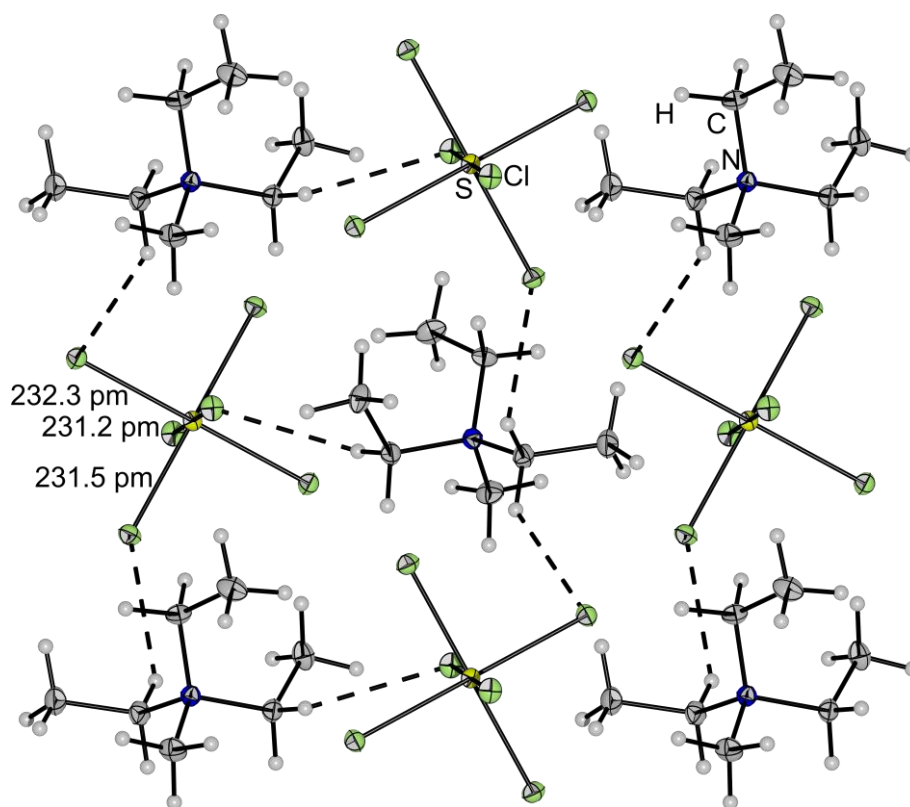


Figure S 13. Molecular structure in the solid state of [NEt₃Me]₂[SCl₆] for comparison to the periodic calculation.

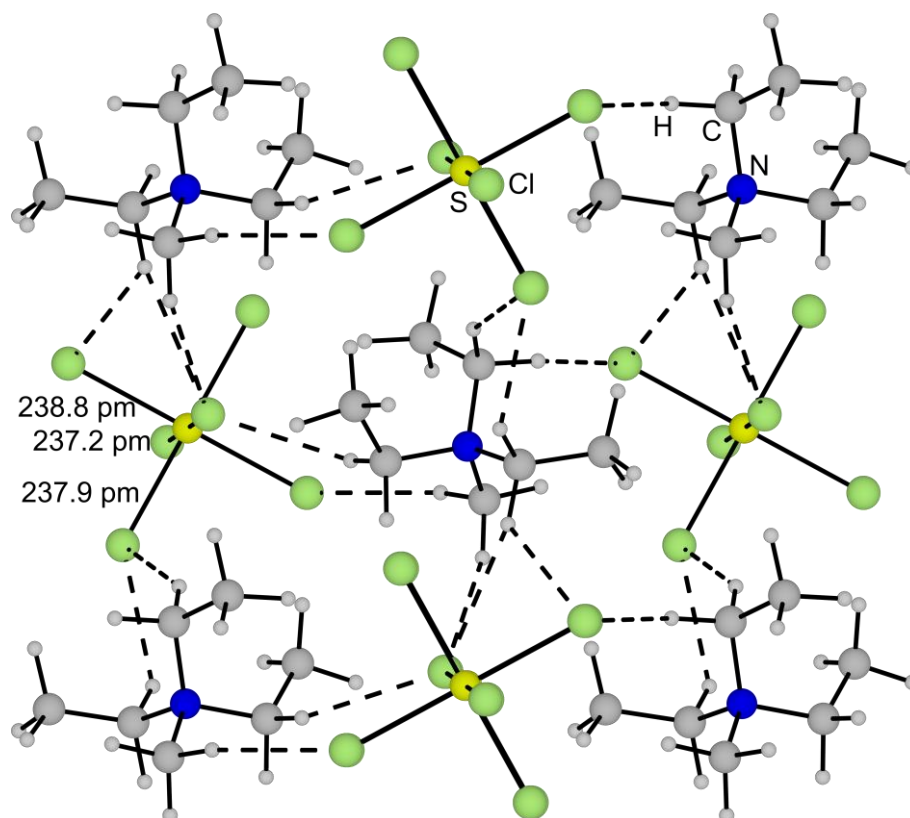


Figure S 14. Optimized structure using a periodic model for [NEt₃Me]₂[SCl₆]

i) Optimized Structures

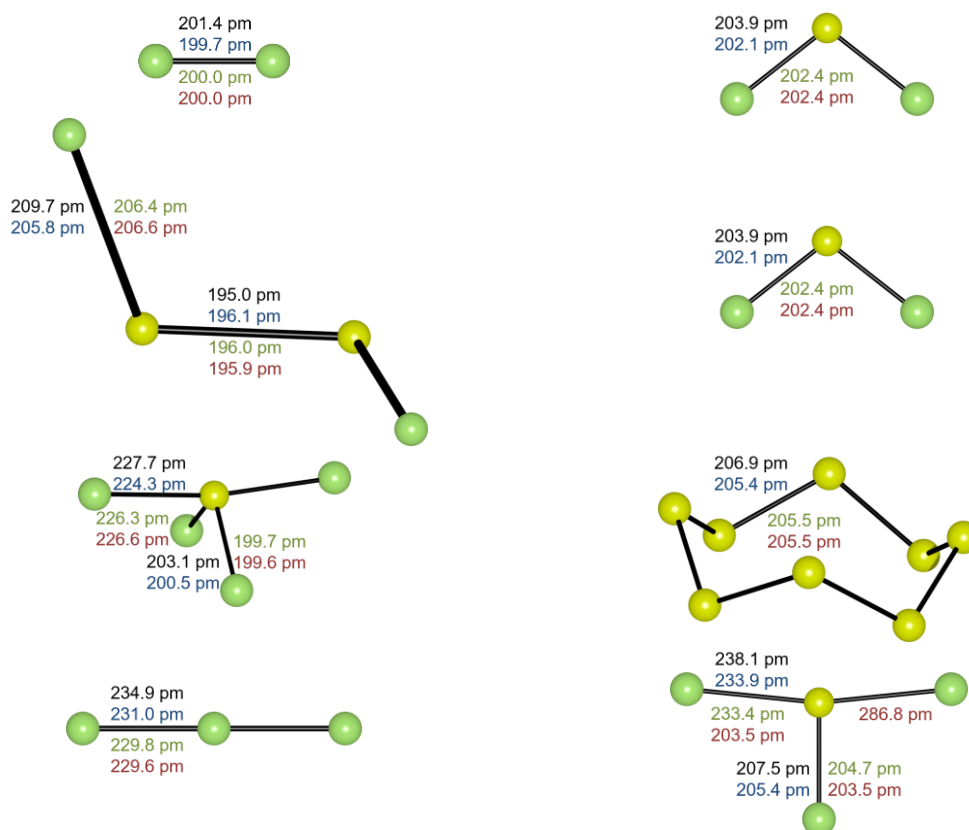


Figure S 15. Optimized structures calculated on the B3LYP(D4)/def2-TZVPP (black), SCS-MP2/def2-TZVPP (blue), Cosmo-SCS-MP2/def2-TZVPP with ($\epsilon_r = 10$) (green) and Cosmo-SCS-MP2/def2-TZVPP with ($\epsilon_r = 100$) (red) level of theory.

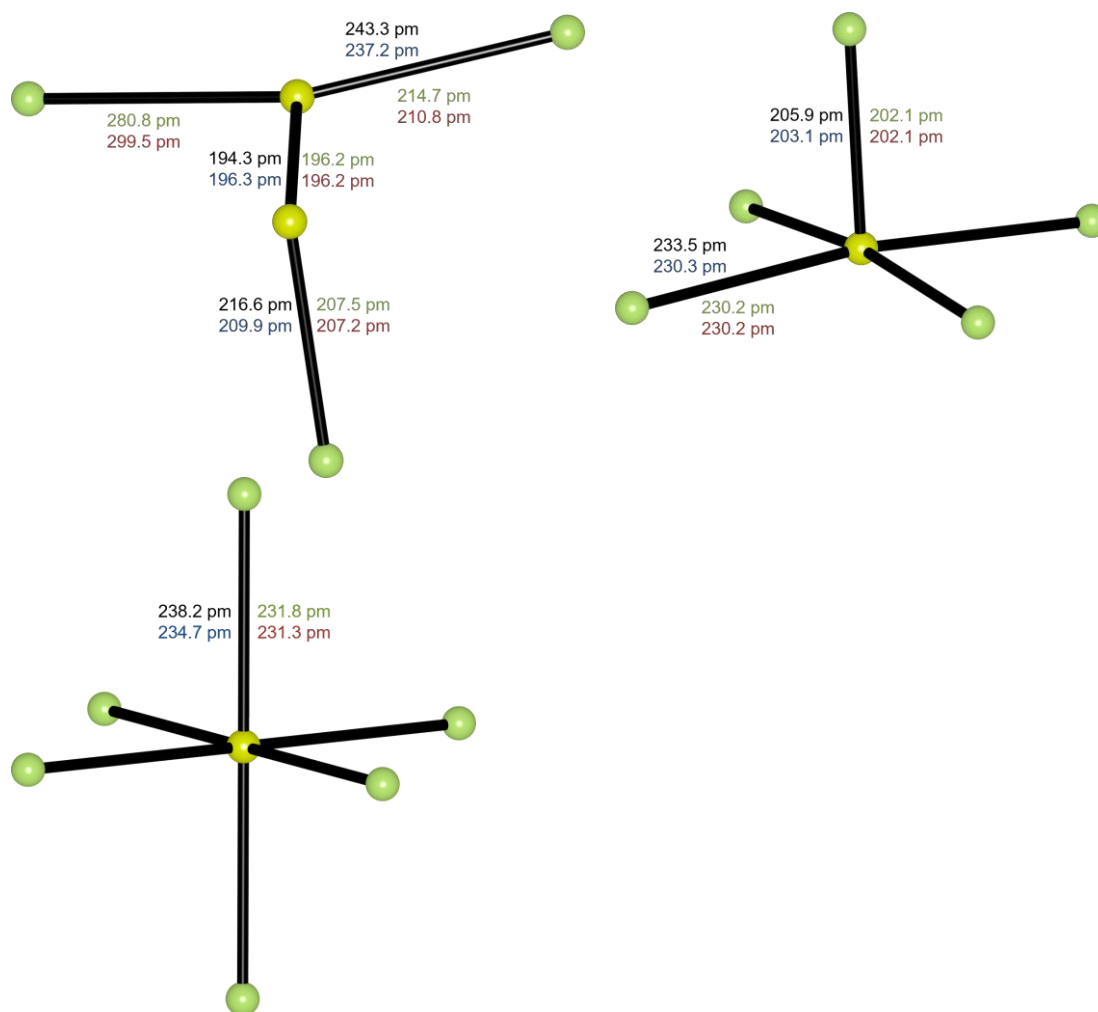


Figure S 16. Optimized structures calculated on the B3LYP(D4)/def2-TZVPP (black), SCS-MP2/def2-TZVPP (blue), Cosmo-SCS-MP2/def2-TZVPP with ($\epsilon_r = 10$) (green) and Cosmo-SCS-MP2/def2-TZVPP with ($\epsilon_r = 100$) (red) level of theory.

j) Calculated Energies and Free Reaction Energies

j1) B3LYP(D4)/def2-TZVPP Energies

All Free Energy calculations were carried out for $T = 298.15$ K and $p = 1.0$ bar.

Table S 6. Calculated energies on B3LYP(D4)/def2-TZVPP level of theory.

Compound	E_{tot} / E_H	$E_{tot} / \text{kJ mol}^{-1}$	$G / \text{kJ mol}^{-1}$
Cl ⁻	-460.22009153	-1208307.9	-1208347.3
Cl ₂	-920.29295228	-2416229.1	-2416283.4
[Cl ₃] ⁻	-1380.56911826	-3624684.2	-3624747.3
[Cl ₅] ⁻	-2300.88506425	-6040973.7	-6041061.9
S ₈	-3185.38469	-8363227.5	-8363292.6
S ₂ Cl ₂	-1716.66099442	-4507093.4	-4507161.5
SCl ₂	-1318.47707733	-3461661.6	-3461726.2
SCl ₄	-2238.77338942	-5877899.5	-5877970.8
[S ₂ Cl ₃] ⁻	-2176.934085	-5715540.4	-5715620.6
[SCl ₃] ⁻	-1778.74899354	-4670105.5	-4670181.2
[SCl ₅] ⁻	-2699.06736670	-7086401.4	-7086478.6
[SCl ₆] ²⁻	-3159.21730437	-8294525.0	-8294606.0

j2) SCS-MP2/def2-TZVPP Energies

Table S 7. Calculated energies on SCS-MP2/def2-TZVPP level of theory.

Compound	E_{tot} / E_H	E_{MP2} / E_H	$E_{tot+MP2} / \text{kJ mol}^{-1}$	$G / \text{kJ mol}^{-1}$
Cl ⁻	-459.55562242	-0.346212077	-1207472.27	-1207511.75
Cl ₂	-918.98287991	-0.67866770	-2414571.39	-2414625.42
[Cl ₃] ⁻	-1378.55619762	-1.04983132	-3622155.63	-3622217.50
[Cl ₅] ⁻	-2297.54169011	-1.73983938	-6036763.66	-6036852.28
S ₈	-3180.36529468	-2.53454576	-8356703.53	-8356765.52
S ₂ Cl ₂	-1714.09391978	-1.31117234	-4503796.07	-4503862.97
SCl ₂	-1316.54256107	-0.99272865	-3459188.90	-3459252.84
SCl ₄	-2235.48081451	-1.70958138	-5873743.38	-5873811.61
[S ₂ Cl ₃] ⁻	-2173.66974220	-1.67968992	-5711379.93	-5711457.62
[SCl ₃] ⁻	-1776.11860560	-1.36104112	-4666772.81	-4666846.56
[SCl ₅] ⁻	-2695.06746152	-2.09289076	-7081394.50	-7081467.87
[SCl ₆] ²⁻	-3154.51139576	-2.47971458	-8288680.16	-8288752.86

Table S 8. Calculated energies on Cosmo-SCS-MP2/def2-TZVPP ($\epsilon_r = 10$) level of theory.

Compound	E_{tot} / E_H	E_{MP2} / E_H	$E_{tot+MP2} / \text{kJ mol}^{-1}$	$G / \text{kJ mol}^{-1}$
Cl ⁻	-459.6633456	-0.34613543	-1207754.893	-1207794.381
Cl ₂	-918.9842183	-0.678549984	-2414574.598	-2414628.688
[Cl ₃] ⁻	-1378.62918	-1.049801827	-3622347.166	-3622410.036
[Cl ₅] ⁻	-2297.622704	-1.72535081	-6036938.319	-6037030.549
S ₈	-3180.368375	-2.533420838	-8356708.665	-8356771.545
S ₂ Cl ₂	-1714.096259	-1.310756176	-4503801.119	-4503868.529
SCl ₂	-1316.544514	-0.992405961	-3459193.182	-3459257.372
SCl ₄	-2235.489494	-1.707635175	-5873761.061	-5873830.591
[S ₂ Cl ₃] ⁻	-2173.752312	-1.668086776	-5711566.256	-5711647.546
[SCl ₃] ⁻	-1776.191788	-1.360170229	-4666962.667	-4667038.997
[SCl ₅] ⁻	-2695.136970	-2.091107879	-7081572.319	-7081646.659
[SCl ₆] ²⁻	-3154.752235	-2.480096521	-8289313.487	-8289388.007

Table S 9. Calculated energies on Cosmo-SCS-MP2/def2-TZVPP ($\epsilon_r = 100$) level of theory.

Compound	E_{tot} / E_H	E_{MP2} / E_H	$E_{tot+MP2} / \text{kJ mol}^{-1}$	$G / \text{kJ mol}^{-1}$
Cl ⁻	-459.6794238	-0.346124185	-1207797.076	-1207836.565
Cl ₂	-918.9844248	-0.67853317	-2414575.096	-2414629.196
[Cl ₃] ⁻	-1378.642319	-1.049811384	-3622381.689	-3622445.039
[Cl ₅] ⁻	-2297.638332	-1.721391767	-6036968.955	-6037061.055
S ₈	-3180.368853	-2.533246899	-8356709.463	-8356772.383
S ₂ Cl ₂	-1714.096651	-1.310697273	-4503801.994	-4503869.474
SCl ₂	-1316.544829	-0.992352347	-3459193.87	-3459258.09
SCl ₄	-2235.491051	-1.707287039	-5873764.236	-5873834.086
[S ₂ Cl ₃] ⁻	-2173.769121	-1.664525301	-5711601.039	-5711682.859
[SCl ₃] ⁻	-1776.217233	-1.347866492	-4666997.17	-4667074.33
[SCl ₅] ⁻	-2695.147504	-2.090806612	-7081599.185	-7081673.785
[SCl ₆] ²⁻	-3154.788322	-2.480188857	-8289408.476	-8289482.736

j3) Free Reaction Energy Calculation

Table S 10. ΔE for the reactions between sulfur and chlorine containing compounds calculated on the B3LYP(D4)/def2-TZVPP, SCS-MP2/def2-TZVPP, Cosmo-SCS-MP2/def2-TZVPP with ($\epsilon_r = 10$) (Cosmo1) and Cosmo-SCS-MP2/def2-TZVPP with ($\epsilon_r = 100$) (Cosmo2) level of theory.

Reaction	$\Delta E_{B3LYP} / \text{kJ mol}^{-1}$	$\Delta E_{MP2} / \text{kJ mol}^{-1}$	$\Delta E_{\text{Cosmo1-MP2}} / \text{kJ mol}^{-1}$	$\Delta E_{\text{Cosmo2-MP2}} / \text{kJ mol}^{-1}$
$\frac{1}{4} \text{S}_8 + \text{Cl}_2 \rightarrow \text{S}_2\text{Cl}_2$	-57.4	-48.8	-49.4	-49.5
$\frac{1}{8} \text{S}_8 + \text{Cl}_2 \rightarrow \text{SCl}_2$	-29.0	0.0	-30.0	-30.1
$\frac{1}{8} \text{S}_8 + 2 \text{Cl}_2 \rightarrow \text{SCl}_4$	-37.8	-12.7	-23.3	-25.4
$\text{S}_2\text{Cl}_2 + \text{Cl}_2 \rightarrow 2 \text{SCl}_2$	-0.5	-10.3	-10.6	-10.6
$\text{SCl}_2 + \text{Cl}_2 \rightarrow 2 \text{SCl}_4$	-8.8	16.9	6.7	4.7
$\frac{1}{4} \text{S}_8 + [\text{Cl}_3]^- \rightarrow [\text{S}_2\text{Cl}_3]^-$	-49.3	-48.4	-41.9	-42.0
$\frac{1}{8} \text{S}_8 + [\text{Cl}_3]^- \rightarrow [\text{SCl}_3]^-$	-17.8	-29.2	-26.9	-26.8
$\frac{1}{8} \text{S}_8 + [\text{Cl}_5]^- \rightarrow [\text{SCl}_5]^-$	-24.2	-42.9	-45.4	-41.5
$[\text{S}_2\text{Cl}_3]^- + [\text{Cl}_3]^- \rightarrow 2 [\text{SCl}_3]^-$	13.7	-10.1	-11.9	-11.6
$[\text{SCl}_3]^- + \text{Cl}_2 \rightarrow [\text{SCl}_5]^-$	-66.7	-50.3	-35.1	-26.9

Table S 11. ΔG for the reactions between sulfur and chlorine containing compounds calculated on the B3LYP(D4)/def2-TZVPP, SCS-MP2/def2-TZVPP, Cosmo-SCS-MP2/def2-TZVPP with ($\epsilon_r = 10$) (Cosmo1) and Cosmo-SCS-MP2/def2-TZVPP with ($\epsilon_r = 100$) (Cosmo2) level of theory.

Reaction	$\Delta G_{B3LYP}/$ kJ mol ⁻¹	$\Delta G_{MP2}/$ kJ mol ⁻¹	$\Delta G_{Cosmo1-MP2}/$ kJ mol ⁻¹	$\Delta G_{Cosmo2-MP2}/$ kJ mol ⁻¹
$\frac{1}{4} S_8 + Cl_2 \rightarrow S_2Cl_2$	-55.0	-46.2	-47.0	-47.2
$\frac{1}{8} S_8 + Cl_2 \rightarrow SCl_2$	-31.2	-31.7	-32.2	-32.3
$\frac{1}{8} S_8 + 2 Cl_2 \rightarrow SCl_4$	7.6	34.9	23.2	20.9
$S_2Cl_2 + Cl_2 \rightarrow 2 SCl_2$	-7.5	-17.3	-17.5	-17.5
$SCl_2 + Cl_2 \rightarrow 2 SCl_4$	38.8	66.7	55.5	53.2
$\frac{1}{4} S_8 + [Cl_3]^- \rightarrow [S_2Cl_3]^-$	-50.1	-48.7	-44.6	-44.7
$\frac{1}{8} S_8 + [Cl_3]^- \rightarrow [SCl_3]^-$	-22.4	-33.4	-32.5	-32.7
$\frac{1}{8} S_8 + [Cl_5]^- \rightarrow [SCl_5]^-$	-5.1	-19.9	-19.7	-16.2
$[S_2Cl_3]^- + [Cl_3]^- \rightarrow 2 [SCl_3]^-$	5.4	-18.0	-20.4	-20.8
$[SCl_3]^- + Cl_2 \rightarrow [SCl_5]^-$	-14.0	4.1	21.0	29.7

k) Calculated Vibrational Frequencies

Table S 12. Cl₂

B3LYP(D4)/def2-TZVPP				SCS-MP2/def2-TZVPP			
Nr.	Symmetry	Wavenumber / cm ⁻¹	IR intensity / km mol ⁻¹	Nr.	Symmetry	Wavenumber / cm ⁻¹	IR intensity / km mol ⁻¹
1	Σ_g^+	537.0	0	1	Σ_g^+	560.6	0

SCS-MP2/def2-TZVPP-Cosmo ($\epsilon_r = 10$)				SCS-MP2/def2-TZVPP-Cosmo ($\epsilon_r = 100$)			
Nr.	Symmetry	Wavenumber / cm ⁻¹	IR intensity / km mol ⁻¹	Nr.	Symmetry	Wavenumber / cm ⁻¹	IR intensity / km mol ⁻¹
1	Σ_g^+	557.0	0	1	Σ_g^+	556.4	0

Table S 13. [Cl₃]⁻

B3LYP(D4)/def2-TZVPP				SCS-MP2/def2-TZVPP			
Nr.	Symmetry	Wavenumber / cm ⁻¹	IR intensity / km mol ⁻¹	Nr.	Symmetry	Wavenumber / cm ⁻¹	IR intensity / km mol ⁻¹
1	Π_u	154.5	1	1	Π_u	167.9	1
2	Π_u	154.5	1	2	Π_u	167.9	1
3	Σ_g^+	247.3	0	3	Σ_g^+	270.5	0
4	Σ_u^-	261.6	410	4	Σ_u^-	295.1	569

SCS-MP2/def2-TZVPP-Cosmo ($\epsilon_r = 10$)				SCS-MP2/def2-TZVPP-Cosmo ($\epsilon_r = 100$)			
Nr.	Symmetry	Wavenumber / cm ⁻¹	IR intensity / km mol ⁻¹	Nr.	Symmetry	Wavenumber / cm ⁻¹	IR intensity / km mol ⁻¹
1	Π_u	168.8	1	1	Π_u	168.5	1
2	Π_u	168.8	1	2	Π_u	168.5	1
3	Σ_u^-	202.8	1392	3	Σ_u^-	168.7	1657
4	Σ_g^+	277.8	0	4	Σ_g^+	278.9	0

Table S 14. $[\text{Cl}(\text{Cl}_2)_2]^-$

B3LYP(D4)/def2-TZVPP				SCS-MP2/def2-TZVPP			
Nr.	Symmetry ¹	Wavenumber / cm^{-1}	IR intensity / km mol^{-1}	Nr.	Symmetry	Wavenumber / cm^{-1}	IR intensity / km mol^{-1}
1	A	18.8	0	1	A	17.7	0
2	A	128.3	33	2	A	92.4	743
3	A	134.9	0	3	A	140.0	17
4	A	135.9	7	4	A	143.4	0
5	A	148.8	1	5	A	152.2	192
6	A	187.8	452	6	A	160.4	1
7	A	200.5	18	7	A	203.3	45
8	A	304.3	376	8	A	326.3	270
9	A	353.0	91	9	A	374.5	125

SCS-MP2/def2-TZVPP-Cosmo ($\epsilon_r = 10$)				SCS-MP2/def2-TZVPP-Cosmo ($\epsilon_r = 100$)			
Nr.	Symmetry	Wavenumber / cm^{-1}	IR intensity / km mol^{-1}	Nr.	Symmetry	Wavenumber / cm^{-1}	IR intensity / km mol^{-1}
1	A	17.1	2	1	A	18.2	3
2	A	58.4	223	2	A	74.1	105
3	A	104.5	99	3	A	97.4	81
4	A	118.0	0	4	A	108.7	0
5	A	124.8	35	5	A	116.5	36
6	A	133.0	4	6	A	120.4	10
7	A	135.8	57	7	A	122.5	41
8	A	419.0	232	8	A	457.9	143
9	A	440.5	162	9	A	469.9	121

¹ $[\text{Cl}(\text{Cl}_2)_2]^-$ was optimized in C_1 symmetries because conversion issues for Cosmo calculations arise at higher symmetries

Table S 15. S₈

B3LYP(D4)/def2-TZVPP				SCS-MP2/def2-TZVPP			
Nr.	Symmetry	Wavenumber / cm ⁻¹	IR intensity / km mol ⁻¹	Nr.	Symmetry	Wavenumber / cm ⁻¹	IR intensity / km mol ⁻¹
1	E ₂	68.9	0	1	E ₂	68.0	0
2	E ₂	68.9	0	2	E ₂	68.0	0
3	E ₂	146.0	0	3	E ₂	154.0	0
4	E ₂	146.0	0	4	E ₂	154.0	0
5	E ₁	191.2	4	5	E ₁	195.2	3
6	E ₁	191.2	4	6	E ₁	195.2	3
7	A ₁	215.1	0	7	A ₁	219.0	0
8	B ₂	243.2	3	8	E ₃	252.3	0
9	E ₃	248.4	0	9	E ₃	252.3	0
10	E ₃	248.4	0	10	B ₂	253.2	4
11	B ₁	389.8	0	11	B ₁	452.4	0
12	E ₃	415.7	0	12	E ₃	465.6	0
13	E ₃	415.7	0	13	E ₃	465.6	0
14	E ₂	461.8	0	14	E ₁	485.8	1
15	E ₂	461.8	0	15	E ₁	485.8	1
16	E ₁	466.8	2	16	E ₂	489.7	0
17	E ₁	466.8	2	17	E ₂	489.7	0
18	A ₁	475.3	0	18	A ₁	490.2	0

SCS-MP2/def2-TZVPP-Cosmo (ε _r = 10)				SCS-MP2/def2-TZVPP-Cosmo (ε _r = 100)			
Nr.	Symmetry	Wavenumber / cm ⁻¹	IR intensity / km mol ⁻¹	Nr.	Symmetry	Wavenumber / cm ⁻¹	IR intensity / km mol ⁻¹
1	E ₂	65.8	0	1	E ₂	65.7	0
2	E ₂	65.8	0	2	E ₂	65.7	0
3	E ₂	153.2	0	3	E ₂	153.1	0
4	E ₂	153.2	0	4	E ₂	153.1	0
5	E ₁	193.4	7	5	E ₁	193.1	8
6	E ₁	193.4	7	6	E ₁	193.1	8
7	A ₁	217.2	0	7	A ₁	216.8	0
8	E ₃	249.9	0	8	E ₃	249.4	0
9	E ₃	249.9	0	9	E ₃	249.4	0
10	B ₂	251.2	7	10	B ₂	250.8	8
11	B ₁	453.0	0	11	B ₁	453.1	0
12	E ₃	465.2	0	12	E ₃	465.2	0
13	E ₃	465.2	0	13	E ₃	465.2	0
14	E ₁	483.8	2	14	E ₁	483.5	3
15	E ₁	483.8	2	15	E ₁	483.5	3
16	A ₁	487.1	0	16	A ₁	486.6	0
17	E ₂	488.2	0	17	E ₂	488.0	0
18	E ₂	488.2	0	18	E ₂	488.0	0

Table S 16. S₂Cl₂

B3LYP(D4)/def2-TZVPP				SCS-MP2/def2-TZVPP			
Nr.	Symmetry	Wavenumber / cm ⁻¹	IR intensity / km mol ⁻¹	Nr.	Symmetry	Wavenumber / cm ⁻¹	IR intensity / km mol ⁻¹
1	A	93.6	0	1	A	95.5	0
2	A	205.2	1	2	A	208.7	0
3	B	236.3	7	3	B	247.5	5
4	B	424.4	129	4	B	476.3	92
5	A	438.9	38	5	A	487.1	33
6	A	545.2	7	6	A	537.9	5

SCS-MP2/def2-TZVPP-Cosmo ($\epsilon_r = 10$)				SCS-MP2/def2-TZVPP-Cosmo ($\epsilon_r = 100$)			
Nr.	Symmetry	Wavenumber / cm ⁻¹	IR intensity / km mol ⁻¹	Nr.	Symmetry	Wavenumber / cm ⁻¹	IR intensity / km mol ⁻¹
1	A	94.6	0	1	A	94.4	0
2	A	208.0	0	2	A	207.8	0
3	B	244.3	12	3	B	243.7	14
4	B	458.1	163	4	B	454.2	182
5	A	471.4	65	5	A	467.8	73
6	A	534.5	6	6	A	534.2	6

Table S 17. SCl₂

B3LYP(D4)/def2-TZVPP				SCS-MP2/def2-TZVPP			
Nr.	Symmetry	Wavenumber / cm ⁻¹	IR intensity / km mol ⁻¹	Nr.	Symmetry	Wavenumber / cm ⁻¹	IR intensity / km mol ⁻¹
1	A ₁	199.6	0	1	A ₁	209.9	0
2	B ₁	493.9	77	2	B ₁	531.0	65
3	A ₁	508.2	10	3	A ₁	532.8	11

SCS-MP2/def2-TZVPP-Cosmo ($\epsilon_r = 10$)				SCS-MP2/def2-TZVPP-Cosmo ($\epsilon_r = 100$)			
Nr.	Symmetry	Wavenumber / cm ⁻¹	IR intensity / km mol ⁻¹	Nr.	Symmetry	Wavenumber / cm ⁻¹	IR intensity / km mol ⁻¹
1	A ₁	208.7	1	1	A ₁	208.6	1
2	B ₁	517.3	110	2	B ₁	514.7	121
3	A ₁	526.6	20	3	A ₁	525.6	21

Table S 18. SCl₄

B3LYP(D4)/def2-TZVPP				SCS-MP2/def2-TZVPP			
Nr.	Symmetry	Wavenumber / cm ⁻¹	IR intensity / km mol ⁻¹	Nr.	Symmetry	Wavenumber / cm ⁻¹	IR intensity / km mol ⁻¹
1	A ₁	100.4	2	1	A ₁	114.5	3
2	B ₂	151.2	2	2	B ₂	175.0	3
3	A ₂	187.2	0	3	A ₂	208.3	0
4	B ₁	225.0	13	4	B ₁	246.3	8
5	A ₁	228.0	0	5	A ₁	254.0	0
6	A ₁	256.4	6	6	A ₁	272.4	4
7	B ₁	370.8	521	7	B ₁	416.5	536
8	B ₂	479.7	105	8	A ₁	520.3	27
9	A ₁	484.4	31	9	B ₂	529.6	92

SCS-MP2/def2-TZVPP-Cosmo (ε _r = 10)				SCS-MP2/def2-TZVPP-Cosmo (ε _r = 100)			
Nr.	Symmetry	Wavenumber / cm ⁻¹	IR intensity / km mol ⁻¹	Nr.	Symmetry	Wavenumber / cm ⁻¹	IR intensity / km mol ⁻¹
1	A ₁	115.6	5	1	A ₁	115.4	6
2	B ₂	171.9	7	2	B ₂	171.2	8
3	A ₂	204.8	0	3	A ₂	204.1	0
4	B ₁	239.3	85	4	B ₁	235.7	186
5	A ₁	250.8	1	5	A ₁	250.1	1
6	A ₁	264.9	8	6	A ₁	263.6	9
7	B ₁	329.1	1153	7	B ₁	306.4	1270
8	A ₁	519.8	47	8	A ₁	519.4	52
9	B ₂	522.6	165	9	B ₂	521.0	183

Table S 19. $[\text{S}_2\text{Cl}_3]^-$

B3LYP(D4)/def2-TZVPP				SCS-MP2/def2-TZVPP			
Nr.	Symmetry ¹	Wavenumber / cm^{-1}	IR intensity / km mol^{-1}	Nr.	Symmetry	Wavenumber / cm^{-1}	IR intensity / km mol^{-1}
1	A	65.8	1	1	A	64.7	2
2	A	80.4	1	2	A	96.9	1
3	A	130.5	6	3	A	149.9	6
4	A	185.2	71	4	A	200.0	82
5	A	207.7	9	5	A	237.8	2
6	A	226.2	25	6	A	244.0	19
7	A	258.8	373	7	A	270.0	553
8	A	369.8	109	8	A	428.0	92
9	A	545.0	5	9	A	524.3	2

SCS-MP2/def2-TZVPP-Cosmo ($\epsilon_r = 10$)				SCS-MP2/def2-TZVPP-Cosmo ($\epsilon_r = 100$)			
Nr.	Symmetry	Wavenumber / cm^{-1}	IR intensity / km mol^{-1}	Nr.	Symmetry	Wavenumber / cm^{-1}	IR intensity / km mol^{-1}
1	A	51.4	29	1	A	44.8	12
2	A	79.4	207	2	A	79.8	92
3	A	92.4	9	3	A	84.1	13
4	A	111.8	11	4	A	99.7	7
5	A	214.6	1	5	A	212.8	1
6	A	242.4	14	6	A	242.3	14
7	A	345.5	359	7	A	397.5	279
8	A	451.0	120	8	A	454.1	123
9	A	521.6	2	9	A	524.9	2

¹ $[\text{S}_2\text{Cl}_3]^-$ was optimized in C_1 symmetries because conversion issues for Cosmo calculations arise at higher symmetries

Table S 20. [SCl₃]⁻

B3LYP(D4)/def2-TZVPP				SCS-MP2/def2-TZVPP			
Nr.	Symmetry ¹	Wavenumber / cm ⁻¹	IR intensity / km mol ⁻¹	Nr.	Symmetry	Wavenumber / cm ⁻¹	IR intensity / km mol ⁻¹
1	A	106.5	2	1	A	129.3	2
2	A	156.9	44	2	A	175.4	61
3	A	175.0	2	3	A	186.1	2
4	A	231.0	5	4	A	256.7	3
5	A	261.3	447	5	A	278.2	604
6	A	466.3	40	6	A	501.5	33

SCS-MP2/def2-TZVPP-Cosmo ($\epsilon_r = 10$)				SCS-MP2/def2-TZVPP-Cosmo ($\epsilon_r = 100$)			
Nr.	Symmetry	Wavenumber / cm ⁻¹	IR intensity / km mol ⁻¹	Nr.	Symmetry	Wavenumber / cm ⁻¹	IR intensity / km mol ⁻¹
1	A	92.1	1256	1	A	78.3	99
2	A	134.4	5	2	A	94.8	62
3	A	182.5	4	3	A	130.5	4
4	A	199.8	147	4	A	206.2	8
5	A	258.6	4	5	A	426.1	289
6	A	504.0	50	6	A	512.0	57

¹ [SCl₃]⁻ was optimized in C₁ symmetries because conversion issues for Cosmo calculations arise at higher symmetries

Table S 21. [SCl₅]⁻

B3LYP(D4)/def2-TZVPP				SCS-MP2/def2-TZVPP			
Nr.	Symmetry	Wavenumber / cm ⁻¹	IR intensity / km mol ⁻¹	Nr.	Symmetry	Wavenumber / cm ⁻¹	IR intensity / km mol ⁻¹
1	<i>B</i> ₂	79.0	0	1	<i>B</i> ₂	94.4	0
2	<i>E</i>	128.3	11	2	<i>E</i>	137.7	6
3	<i>E</i>	128.3	11	3	<i>E</i>	137.7	6
4	<i>B</i> ₁	160.5	0	4	<i>B</i> ₁	163.3	0
5	<i>A</i> ₁	162.7	1	5	<i>A</i> ₁	187.4	3
6	<i>E</i>	186.3	38	6	<i>E</i>	205.4	23
7	<i>E</i>	186.3	38	7	<i>E</i>	205.4	23
8	<i>B</i> ₂	214.7	0	8	<i>B</i> ₂	238.8	0
9	<i>A</i> ₁	252.7	7	9	<i>A</i> ₁	264.9	3
10	<i>E</i>	348.2	442	10	<i>E</i>	407.2	457
11	<i>E</i>	348.2	442	11	<i>E</i>	407.2	457
12	<i>A</i> ₁	459.9	62	12	<i>A</i> ₁	503.1	53

SCS-MP2/def2-TZVPP-Cosmo (ε _r = 10)				SCS-MP2/def2-TZVPP-Cosmo (ε _r = 100)			
Nr.	Symmetry	Wavenumber / cm ⁻¹	IR intensity / km mol ⁻¹	Nr.	Symmetry	Wavenumber / cm ⁻¹	IR intensity / km mol ⁻¹
1	<i>B</i> ₂	97.2	0	1	<i>B</i> ₂	97.5	0
2	<i>E</i>	136.7	18	2	<i>E</i>	136.2	26
3	<i>E</i>	136.7	18	3	<i>E</i>	136.2	26
4	<i>B</i> ₁	163.0	0	4	<i>B</i> ₁	162.9	0
5	<i>A</i> ₁	189.4	9	5	<i>A</i> ₁	189.3	11
6	<i>E</i>	205.4	78	6	<i>E</i>	204.5	108
7	<i>E</i>	205.4	78	7	<i>E</i>	204.5	108
8	<i>B</i> ₂	242.6	0	8	<i>B</i> ₂	243.2	0
9	<i>A</i> ₁	266.7	5	9	<i>A</i> ₁	267.0	6
10	<i>E</i>	357.5	1016	10	<i>E</i>	343.9	1177
11	<i>E</i>	357.5	1016	11	<i>E</i>	343.9	1177
12	<i>A</i> ₁	504.5	88	12	<i>A</i> ₁	504.5	97

Table S 22. [SCl₆]²⁻

B3LYP(D4)/def2-TZVPP				SCS-MP2/def2-TZVPP			
Nr.	Symmetry	Wavenumber / cm ⁻¹	IR intensity / km mol ⁻¹	Nr.	Symmetry	Wavenumber / cm ⁻¹	IR intensity / km mol ⁻¹
1	T _{2u}	103.6	0	1	T _{2u}	112.5	0
2	T _{2u}	103.6	0	2	T _{2u}	112.5	0
3	T _{2u}	103.6	0	3	T _{2u}	112.5	0
4	T _{1u}	127.9	82	4	T _{2g}	151.2	0
5	T _{1u}	127.9	82	5	T _{2g}	151.2	0
6	T _{1u}	127.9	82	6	T _{2g}	151.2	0
7	T _{2g}	145.8	0	7	T _{1u}	160.2	32
8	T _{2g}	145.8	0	8	T _{1u}	160.2	32
9	T _{2g}	145.8	0	9	T _{1u}	160.2	32
10	E _g	196.0	0	10	E _g	223.6	0
11	E _g	196.0	0	11	E _g	223.6	0
12	A _{1g}	251.6	0	12	A _{1g}	260.7	0
13	T _{1u}	333.9	372	13	T _{1u}	404.3	371
14	T _{1u}	333.9	372	14	T _{1u}	404.3	371
15	T _{1u}	333.9	372	15	T _{1u}	404.3	371

SCS-MP2/def2-TZVPP-Cosmo (ε _r = 10)				SCS-MP2/def2-TZVPP-Cosmo (ε _r = 100)			
Nr.	Symmetry	Wavenumber / cm ⁻¹	IR intensity / km mol ⁻¹	Nr.	Symmetry	Wavenumber / cm ⁻¹	IR intensity / km mol ⁻¹
1	T _{2u}	113.8	0	1	T _{2u}	114.9	0
2	T _{2u}	113.8	0	2	T _{2u}	114.9	0
3	T _{2u}	113.8	0	3	T _{2u}	114.9	0
4	T _{2g}	155.6	0	4	T _{2g}	156.4	0
5	T _{2g}	155.6	0	5	T _{2g}	156.4	0
6	T _{2g}	155.6	0	6	T _{2g}	156.4	0
7	T _{1u}	167.8	62	7	T _{1u}	166.4	75
8	T _{1u}	167.8	62	8	T _{1u}	166.4	75
9	T _{1u}	167.8	62	9	T _{1u}	166.4	75
10	E _g	243.3	0	10	E _g	246.1	0
11	E _g	243.3	0	11	E _g	246.1	0
12	A _{1g}	280.7	0	12	A _{1g}	283.4	0
13	T _{1u}	392.0	875	13	T _{1u}	396.5	948
14	T _{1u}	392.0	875	14	T _{1u}	396.5	948
15	T _{1u}	392.0	875	15	T _{1u}	396.5	948

I) Coordinates of Optimized Structures

Cl₂

B3LYP

Cl 0.000000 0.000000 -1.007079

Cl 0.000000 0.000000 1.007079

MP2

Cl 0.000000 0.000000 -0.998704

Cl 0.000000 0.000000 0.998704

MP2 Cosmo ($\epsilon_r = 10$)

Cl 0.000000 0.000000 -0.999952

Cl 0.000000 0.000000 0.999952

MP2 Cosmo ($\epsilon_r = 100$)

Cl 0.000000 0.000000 -1.000157

Cl 0.000000 0.000000 1.000157

[Cl₃]⁻

B3LYP

Cl 0.000000 0.000000 0.000000

Cl 0.000000 0.000000 2.349427

Cl 0.000000 0.000000 -2.349427

MP2

Cl 0.000000 0.000000 0.000000

Cl 0.000000 0.000000 2.309542

Cl 0.000000 0.000000 -2.309542

MP2 Cosmo ($\epsilon_r = 10$)

Cl 0.000000 0.000000 0.000000

Cl 0.000000 0.000000 2.298025

Cl 0.000000 0.000000 -2.298025

MP2 Cosmo ($\epsilon_r = 100$)

Cl	0.000000	0.000000	0.000000
Cl	0.000000	0.000000	2.296380
Cl	0.000000	0.000000	-2.296380

[Cl(Cl₂)₂]⁻

B3LYP

Cl	0.222258	0.514373	-0.000000
Cl	2.678007	-0.057822	0.000000
Cl	4.790828	-0.624876	-0.000000
Cl	-0.148794	3.008114	-0.000000
Cl	-0.542299	5.160211	0.000000

MP2

Cl	0.165632	0.462139	0.000000
Cl	2.635412	-0.027498	-0.000001
Cl	4.725038	-0.481047	0.000000
Cl	-0.121860	2.963389	0.000001
Cl	-0.404222	5.083018	-0.000000

MP2 Cosmo ($\epsilon_r = 10$)

Cl	-0.170316	0.150464	0.000004
Cl	2.554754	0.053896	-0.000022
Cl	4.613609	-0.012314	0.000013
Cl	-0.048356	2.875282	0.000016
Cl	0.050309	4.932672	-0.000010

MP2 Cosmo ($\epsilon_r = 100$)

Cl	-0.250981	0.075830	0.000008
Cl	2.557894	0.069397	-0.000049
Cl	4.600761	0.065456	0.000029
Cl	-0.033255	2.876317	0.000032
Cl	0.125582	4.912999	-0.000021

S₈

B3LYP

S	2.189522	-0.906930	0.497590
S	2.189522	0.906930	-0.497590
S	0.906930	-2.189522	-0.497590
S	0.906930	2.189522	0.497590
S	-0.906930	-2.189522	0.497590
S	-0.906930	2.189522	-0.497590
S	-2.189522	-0.906930	-0.497590
S	-2.189522	0.906930	0.497590

MP2

S	2.162388	-0.895691	0.502364
S	2.162388	0.895691	-0.502364
S	0.895691	-2.162388	-0.502364
S	0.895691	2.162388	0.502364
S	-0.895691	-2.162388	0.502364
S	-0.895691	2.162388	-0.502364
S	-2.162388	-0.895691	-0.502364
S	-2.162388	0.895691	0.502364

MP2 Cosmo ($\epsilon_r = 10$)

S	2.162390	-0.895691	0.503380
S	2.162390	0.895691	-0.503380
S	0.895691	-2.162390	-0.503380
S	0.895691	2.162390	0.503380
S	-0.895691	-2.162390	0.503380
S	-0.895691	2.162390	-0.503380
S	-2.162390	-0.895691	-0.503380
S	-2.162390	0.895691	0.503380

MP2 Cosmo ($\epsilon_r = 100$)

S	2.162342	-0.895671	0.503551
S	2.162342	0.895671	-0.503551
S	0.895671	-2.162342	-0.503551
S	0.895671	2.162342	0.503551
S	-0.895671	-2.162342	0.503551
S	-0.895671	2.162342	-0.503551
S	-2.162342	-0.895671	-0.503551
S	-2.162342	0.895671	0.503551

S₂Cl₂

B3LYP

S	-0.973840	0.049395	-0.723364
S	0.973840	-0.049395	-0.723364
Cl	-1.581697	1.439759	0.723364
Cl	1.581697	-1.439759	0.723364

MP2

S	-0.979500	0.039295	-0.723227
S	0.979500	-0.039295	-0.723227
Cl	-1.527604	1.397023	0.723227
Cl	1.527604	-1.397023	0.723227

MP2 Cosmo ($\epsilon_r = 10$)

S	-0.979202	0.035669	-0.727768
S	0.979202	-0.035669	-0.727768
Cl	-1.522878	1.395018	0.727768
Cl	1.522878	-1.395018	0.727768

MP2 Cosmo ($\epsilon_r = 100$)

S	-0.979013	0.035042	-0.728724
S	0.979013	-0.035042	-0.728724
Cl	-1.522057	1.394663	0.728724
Cl	1.522057	-1.394663	0.728724

SCl₄

B3LYP

S	0.000000	0.000000	0.426710
Cl	0.000000	-1.600417	-0.824394
Cl	2.269667	0.000000	0.611040
Cl	-2.269667	0.000000	0.611040
Cl	0.000000	1.600417	-0.824394

MP2

S	0.000000	0.000000	0.453610
Cl	0.000000	-1.582369	-0.777184
Cl	2.240474	0.000000	0.550379
Cl	-2.240474	0.000000	0.550379
Cl	0.000000	1.582369	-0.777184

MP2 Cosmo ($\epsilon_r = 10$)

S	0.000000	0.000000	0.448367
Cl	0.000000	-1.574174	-0.781131
Cl	2.259939	0.000000	0.556948
Cl	-2.259939	0.000000	0.556948
Cl	0.000000	1.574174	-0.781131

MP2 Cosmo ($\epsilon_r = 100$)

S	0.000000	0.000000	0.447113
Cl	0.000000	-1.572774	-0.781965
Cl	2.263459	0.000000	0.558408
Cl	-2.263459	0.000000	0.558408
Cl	0.000000	1.572774	-0.781965

[S₂Cl₃]⁻

B3LYP

S	-6.555245	-0.434200	0.687801
S	-4.629036	-0.659330	0.570898
Cl	-4.515906	-2.502738	-1.012970
Cl	-3.910196	1.027691	2.169884
Cl	-7.238507	1.005480	-0.778965

MP2

S	-6.530229	-0.449748	0.700441
S	-4.583744	-0.664399	0.567514
Cl	-4.598919	-2.436097	-1.009244
Cl	-4.003520	1.033949	2.119195
Cl	-7.132477	0.953199	-0.741257

MP2 Cosmo ($\epsilon_r = 10$)

S	-6.559995	-0.474354	0.686745
S	-4.639647	-0.802338	0.450173
Cl	-4.628442	-2.377471	-1.008932
Cl	-3.909291	1.196895	2.281446
Cl	-7.111517	0.894171	-0.772783

MP2 Cosmo ($\epsilon_r = 100$)

S	-6.575547	-0.490345	0.671065
S	-4.664618	-0.851051	0.413509
Cl	-4.636801	-2.388835	-1.028633
Cl	-3.858907	1.278334	2.359681
Cl	-7.113018	0.888800	-0.778974

[SCI₃]⁻

B3LYP

S	0.000000	0.000000	-0.398814
Cl	2.369318	-0.000000	-0.637646
Cl	-2.369318	-0.000000	-0.637646
Cl	0.000000	-0.000000	1.675760

MP2

S	-0.000000	-0.000041	-0.438694
Cl	2.333946	0.000019	-0.587457
Cl	-2.333946	0.000019	-0.587457
Cl	0.000000	0.000003	1.615261

MP2 Cosmo ($\epsilon_r = 10$)

S	-0.000026	0.000011	-0.448049
Cl	2.330705	-0.000002	-0.574770
Cl	-2.330675	-0.000002	-0.574764
Cl	-0.000004	-0.000006	1.599237

MP2 Cosmo ($\epsilon_r = 100$)

Cl	-6.546107	-0.479562	0.684356
S	-4.561126	-0.833001	0.411389
Cl	-4.692983	-2.360457	-0.993016
Cl	-3.935656	1.221122	2.312893

[SCl₅]⁻

B3LYP

S	0.000000	0.000000	-0.241552
Cl	1.647899	1.647899	-0.394026
Cl	0.000000	0.000000	1.817658
Cl	1.647899	-1.647899	-0.394026
Cl	-1.647899	1.647899	-0.394026
Cl	-1.647899	-1.647899	-0.394026

MP2

S	0.000000	0.000000	-0.273363
Cl	1.627010	1.627010	-0.371192
Cl	0.000000	0.000000	1.758131
Cl	1.627010	-1.627010	-0.371192
Cl	-1.627010	1.627010	-0.371192
Cl	-1.627010	-1.627010	-0.371192

MP2 Cosmo ($\epsilon_r = 10$)

S	0.000000	0.000000	-0.269513
Cl	1.626260	1.626260	-0.370587
Cl	0.000000	0.000000	1.751861
Cl	1.626260	-1.626260	-0.370587
Cl	-1.626260	1.626260	-0.370587
Cl	-1.626260	-1.626260	-0.370587

MP2 Cosmo ($\epsilon_r = 100$)

S	0.000000	0.000000	-0.268077
Cl	1.626210	1.626210	-0.370823
Cl	0.000000	0.000000	1.751369
Cl	1.626210	-1.626210	-0.370823
Cl	-1.626210	1.626210	-0.370823
Cl	-1.626210	-1.626210	-0.370823

[SCl₆]²⁻

B3LYP

S	0.000000	0.000000	0.000000
Cl	0.000000	2.381674	0.000000
Cl	0.000000	0.000000	2.381674
Cl	2.381674	0.000000	0.000000
Cl	-2.381674	0.000000	0.000000
Cl	0.000000	-2.381674	0.000000
Cl	0.000000	0.000000	-2.381674

MP2

S	0.000000	0.000000	0.000000
Cl	0.000000	2.346834	0.000000
Cl	0.000000	0.000000	2.346834
Cl	2.346834	0.000000	0.000000
Cl	-2.346834	0.000000	0.000000
Cl	0.000000	-2.346834	0.000000
Cl	0.000000	0.000000	-2.346834

MP2 Cosmo ($\epsilon_r = 10$)

S	0.000000	0.000000	0.000000
Cl	0.000000	2.317528	0.000000
Cl	0.000000	0.000000	2.317528
Cl	2.317528	0.000000	0.000000
Cl	-2.317528	0.000000	0.000000
Cl	0.000000	-2.317528	0.000000
Cl	0.000000	0.000000	-2.317528

MP2 Cosmo ($\epsilon_r = 100$)

S	0.000000	0.000000	0.000000
Cl	0.000000	2.313361	0.000000
Cl	0.000000	0.000000	2.313361
Cl	2.313361	0.000000	0.000000
Cl	-2.313361	0.000000	0.000000
Cl	0.000000	-2.313361	0.000000
Cl	0.000000	0.000000	-2.313361

m) References

- [1] P. Voßnacker, S. Steinhauer, J. Bader, S. Riedel, *Chem. Eur. J.* **2020**, *26*, 13256.
- [2] G. M. Sheldrick, *Acta Cryst.* **2008**, *A64*, 112.
- [3] G. M. Sheldrick, *Acta Cryst. C* **2015**, *71*, 3.
- [4] O. V. Dolomanov, L. J. Bourhis, R. J. Gildea, J. A. K. Howard, H. Puschmann, *J. Appl. Cryst.* **2009**, *42*, 339.
- [5] A. Klamt, G. Schüürmann, *J. Chem. Soc., Perkin Trans. 2* **1993**, 799.
- [6] TURBOMOLE GmbH, *TURBOMOLE V7.3. a development of University of Karlsruhe and Forschungszentrum Karlsruhe*, **2018**.
- [7] a) F. Neese, *WIREs Comput. Mol. Sci.* **2012**, *2*, 73; b) F. Neese, *WIREs Comput. Mol. Sci.* **2017**, *2*, e1327.
- [8] E. D. Glendening, J. K. Badenhoop, A. E. Reed, J. E. Carpenter, J. A. Bohmann, C. M. Morales, P. Karafiloglou, C. R. Landis, F. Weinhold, *NBO 7.0*, Theoretical Chemistry Institute, University of Wisconsin, Madison, WI, **2018**.
- [9] M. J. Frisch, G. W. Trucks, H. B. Schlegel, G. E. Scuseria, M. A. Robb, J. R. Cheeseman, G. Scalmani, V. Barone, G. A. Petersson, H. Nakatsuji, X. Li, M. Caricato, A. V. Marenich, J. Bloino, B. G. Janesko, R. Gomperts, B. Mennucci, H. P. Hratchian, J. V. Ortiz, A. F. Izmaylov, J. L. Sonnenberg, D. Williams-Young, F. Ding, F. Lipparini, F. Egidi, J. Goings, B. Peng, A. Petrone, T. Henderson, D. Ranasinghe, V. G. Zakrzewski, J. Gao, N. Rega, G. Zheng, W. Liang, M. Hada, M. Ehara, K. Toyota, R. Fukuda, J. Hasegawa, M. Ishida, T. Nakajima, Y. Honda, O. Kitao, H. Nakai, T. Vreven, K. Throssell, J. A. Montgomery, Jr., J. E. Peralta, F. Ogliaro, M. J. Bearpark, J. J. Heyd, E. N. Brothers, K. N. Kudin, V. N. Staroverov, T. A. Keith, R. Kobayashi, J. Normand, K. Raghavachari, A. P. Rendell, J. C. Burant, S. S. Iyengar, J. Tomasi, M. Cossi, J. M. Millam, M. Klene, C. Adamo, R. Cammi, J. W. Ochterski, R. L. Martin, K. Morokuma, O. Farkas, J. B. Foresman, and D. J. Fox, *Gaussian 16*, Gaussian, Inc., Wallingford CT, **2016**.
- [10] a) A. D. Becke, *J. Chem. Phys.* **1993**, *98*, 5648; b) C. Lee, W. Yang, R. G. Parr, *Phys. Rev. B* **1988**, *37*, 785; c) S. H. Vosko, L. Wilk, M. Nusair, *Can. J. Phys.* **1980**, *58*, 1200; d) P. J. Stephens, F. J. Devlin, C. F. Chabalowski, M. J. Frisch, *J. Phys. Chem.* **1994**, *98*, 11623; e) A. D. Becke, E. R. Johnson, *J. Chem. Phys.* **2005**, *123*, 154101; f) E. R. Johnson, A. D. Becke, *J. Chem. Phys.* **2005**, *123*, 24101; g) E. R. Johnson, A. D. Becke, *J. Chem. Phys.* **2006**, *124*, 174104; h) E. Caldeweyher, S. Ehlert, A. Hansen, H. Neugebauer, S. Spicher, C. Bannwarth, S. Grimme, *J. Chem. Phys.* **2019**, *150*, 154122.
- [11] S. Grimme, J. Antony, S. Ehrlich, H. Krieg, *J. Chem. Phys.* **2010**, *132*, 154104.
- [12] S. Grimme, *J. Chem. Phys.* **2003**, *118*, 9095.
- [13] F. Weigend, R. Ahlrichs, *Phys. Chem. Chem. Phys.* **2005**, *7*, 3297.
- [14] F. Weigend, A. Köhn, C. Hättig, *J. Chem. Phys.* **2002**, *116*, 3175.
- [15] P. R. Spackman, M. J. Turner, J. J. McKinnon, S. K. Wolff, D. J. Grimwood, D. Jayatilaka, M. A. Spackman, *J. Appl. Cryst.* **2021**, *54*, 1006.
- [16] a) D. E. Woon, T. H. Dunning, *J. Chem. Phys.* **1993**, *98*, 1358; b) T. H. Dunning, *J. Chem. Phys.* **1989**, *90*, 1007.
- [17] R. Dovesi, A. Erba, R. Orlando, C. M. Zicovich-Wilson, B. Civalleri, L. Maschio, M. Rérat, S. Casassa, J. Baima, S. Salustro et al., *WIREs Comput Mol Sci* **2018**, *8*, e1360.
- [18] S. Grimme, *J. Comput. Chem.* **2006**, *27*, 1787.
- [19] C. Gatti, *Acta Cryst. A* **1996**, *52*, C555-C556.